# The Synthesis and Coordination Chemistry of Quinoline- and Naphthalene-Based Ligands

Bronte Carr

2024

Department of Chemistry

A thesis submitted to

**Auckland University of Technology**

in fulfilment of the requirements for the degree of

**Doctor of Philosophy**

# Abstract

This thesis details the synthesis and characterisation of several multidentate ligands that contain the aromatic moieties quinoline, naphthalene and pyrene, and their associated transition metal complexes. Chapter One presents an introduction to multidentate ligands containing both pyridine and quinoline units. The synthesis and characterisation of each ligand is described in Chapter Two. This includes the synthesis of nine new 2-quinolyl-based ligands including tri- and tetradentate ligands, and a discussion on these ligands is presented in Chapter Three. In addition, four new multidentate tripodal ligands that contain a 2-methyl-1*H*-naphtho[2,3-*d*]imidazole moiety and one pyrene-based bidentate ligand are described in Chapter Six.

All the new ligands synthesised have been reacted with transition metal ions and their corresponding complexes have been analysed using a number of techniques. The new complexes [Pd(**58**)Cl]Cl.x$H_2O$, [Cu(**55**)$NCCH_3$]$(ClO_4)_2$, [Zn(**55**)$NCCH_3$]$(ClO_4)_2$, [(Mn(**55**))$_2O_2$]$(ClO_4)_2$.2$CH_3CN$ and [(**62**)Co$(OH)_3$Co(**62**)]$(ClO_4)_3$.$CH_3CN$, which contain the new quinoline-containing ligands have been prepared and structurally characterised. The synthesis of each complex is presented in Chapter Two and the structural characterisation is expanded on in Chapter Four. The crystal structure for the complex [Pd(**58**)Cl]Cl.x$H_2O$ showed the species to be mononuclear exhibiting a square planar geometry in which three of the nitrogen donor atoms of the ligand and one chlorido ligand are coordinated to the metal ion. The fourth nitrogen donor atom of the ligand belongs to a quinoline group, and this remains uncoordinated. This Pd(II) complex is the first example of a structurally characterised metal complex that contains a 2-quinolylethyl-containing ligand. The complexes [Cu(**55**)$NCCH_3$]$(ClO_4)_2$ and [Zn(**55**)$NCCH_3$]$(ClO_4)_2$ are isomorphous and are shown to be mononuclear, each exhibiting distorted square-based pyramid geometries about the metal centres ($\tau_5$ = 0.256 and $\tau_5$ = 0.160, respectively). The crystal structures of the complexes [(Mn(**55**))$_2O_2$]$(ClO_4)_2$.2$CH_3CN$ and [(**62**)Co$(OH)_3$Co(**62**)]$(ClO_4)_3$.$CH_3CN$ reveal dimer

species in which the two metal centres are bridged by either two oxido or three hydroxido ligands, respectively.

For those compounds in which crystal structures were not obtained, alternative solution state characterisation methods were employed including mass spectrometry and visible spectroscopy (Job's method). The data obtained from these experiments showed all the ligands to form mononuclear 1:1 complexes in solution. A discussion of these results is presented in Chapter Five and Six.

Chapter Seven presents the work conducted as part of a separate side project that investigated 6-amino-2,3-naphthalimide derivatives. This work describes the synthesis and characterisation of a series of 6-amino-2,3-naphthalimide derivatives. This included the synthesis of the 2,3-naphthalimide moiety in which several derivatives were formed with varying imide functional groups. These compounds have been cross-coupled with a variety of small amine groups to achieve amination at the 6-position on the naphthalimide ring. Preliminary photophysical studies of three compounds has been conducted.

# Contents

# List of Figures

# List of Schemes

# List of Tables

# List of Abbreviations

| | |
|---|---|
| δ | Chemical Shift |
| $\lambda_{Em}$ | Emission wavelength |
| $\lambda_{Ex}$ | Excitation wavelength |
| ACBN | 1,1′-Azobis(cyclohexanecarbonitrile) |
| AR | Analytical reagent |
| br | Broadened |
| calcd | Calculated |
| CSD | Cambridge Structural Database |
| COSY | Correlations spectroscopy |
| d | Doublet |
| dba | Dibenzylideneacetone |
| DBU | 1,8-Diazabicyclo[5.4.0]undec-7-ene |
| dd | Doublet of doublets |
| ddd | Doublet of doublets of doublets |
| DMA | Dimethylacetamide |
| DMF | Dimethylformamide |
| DMSO | Dimethyl sulfoxide |
| DMSO-$d_6$ | Deuterated dimethylsulfoxide |
| DNA | Deoxyribonucleic acid |
| equiv | Equivalents |
| ESI | Electrospray ionisation |
| EtOH | Ethanol |
| HRMS | High-resolution mass spectrometry |
| HSQC | Heteronuclear single quantum coherence |
| ICT | Internal charge transfer |
| *J* | Coupling constant |
| L | Ligand |
| MeOTs | Methyl *p*-toluenesulfonate |
| *m/z* | Mass to charge ratio |
| m | Multiplet |

| | |
|---|---|
| MsCl | Methanesulfonyl chloride |
| NBS | *N*-Bromosuccinimide |
| NMR | Nuclear magnetic resonance |
| PAPh | Polyphosphoric acid |
| pH | –log of $[H_3O]^+$ |
| pKa | –log of the acid dissociation constant |
| ppm | Parts per million |
| $S_NAr$ | Nucleophilic aromatic substitution |
| THF | Tetrahydrofuran |
| TLC | Thin layer chromatography |
| TsCl | *p*-Toluenesulfonyl chloride |
| r.t | Room temperature |
| UV-vis | Ultraviolet-visible |
| VT NMR | Variable temperature nuclear magnetic resonance |
| Xantphos | 4,5-Bis(diphenylphosphino)-9,9-dimethylxanthene |

# Attestation of Authorship

I hereby declare that this submission is my own work and that, to the best of my knowledge and belief, it contains no material previously published or written by another person (except where explicitly defined in the acknowledgements), nor material which to a substantial extent has been submitted for the award of any other degree or diploma of a university or other institution of higher learning.

| | April 9th 2024 |
|---|---|
| Signature | Date |

# Acknowledgements

First and foremost, I would like to thank my supervisor Professor Allan Blackman for all his support, guidance and many chemistry and English lessons throughout this project. Your enthusiasm for chemistry and dedication to your students is the reason I am now a chemist. I have been very lucky to have the best supervisor.

A big thank you to Dr. Cassandra Fleming, for completing the best supervisory team. I am so grateful for all the invaluable advice you have provided in and out of the lab, and for always including me in your group! I will always have fond memories of running columns alongside you while listening to music in the lab.

To the technicians who have gone above and beyond for me. I also would like to thank those a part of the wider AUT community who have helped me along the way.

To the best Ph.D buddies Jess and Rosie. For all the coffees, lunches, advice and laughs. Jess for getting me through to the very end. Your genuine support and care I will always treasure.

To Roma and Callum who have been here from start to finish. I am so lucky to have such supportive and amazing friends!

And finally, to all my family. To Mum and Dad for all your endless care and support through my many years of studying. I could not have accomplished this project without you. To my sisters Elosie and Pippa for keeping me grounded and being my best friends. To Tim for all your support and care that has seen me through to the end. You have all kept the smile on my face. I love you all so much!

# *Chapter One*
# Introduction

## 1.1 Chapter Overview

The development of novel ligands for the complexation of transition metals, lanthanoids and actinoids has been and continues as a rapidly developing field of study within inorganic chemistry. In recent years, quinoline-based metal complexes have gained significant attention. The unique physiochemical properties and steric and electronic arrangements of these complexes have made them attractive towards several applications.[1] Thus, the synthesis and characterisation of quinoline-derived ligands and their corresponding metal complexes is of great interest. The primary focus of this Chapter is to introduce amine ligands with particular emphasis on quinoline-based multidentate ligands and the corresponding coordination chemistry.

## 1.2 Introduction

### 1.2.1 Basics of coordination chemistry

A coordination complex consists of a central metal ion to which a number of atoms or ions, known as ligands, are bound. Majority of these types of compounds are transition metal complexes, in which the central ion is from the d-block of the periodic table.

A Lewis acid is an electron-pair acceptor, and a Lewis base is an electron-pair donor. Products formed from the reaction between a Lewis acid and a Lewis base are often referred to as Lewis adducts, or just adducts. Coordination complexes are products of Lewis acid-base reactions and thus are also considered to be Lewis adducts. The transition metal ion is a Lewis acid that reacts with one or more Lewis base species, otherwise known as ligands, that individually contain a lone pair of electrons. To illustrate, the

reaction between Ni(II) (Lewis acid) and six $NH_3$ ligands (Lewis base), affords the coordination complex $[Ni(NH_3)_6]^{2+}$ (Lewis adduct) (*Figure 1*).

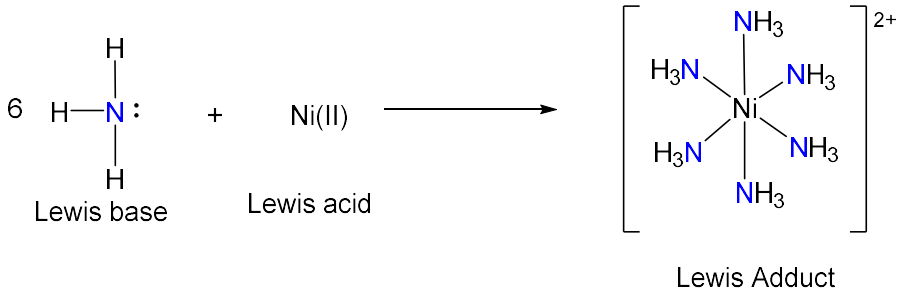


*Figure 1. Lewis acid-base reaction between $NH_3$ and Ni(II).*

The ligand, being the Lewis base, has a lone pair of electrons that it can donate to the Lewis acidic metal ion. In 'classical' coordination complexes, the lone pair is located on a single atom which is referred to as the donor atom, and ligands can have one or more donor atoms. The denticity of a ligand is defined as the number of donor atoms bonded to the metal centre. Ligands that use only one atom to bind with the metal centre are called monodentate ligands, and those that bind via two donor atoms are called bidentate ligands. Polydentate or multidentate is used in reference to ligands that bind via at least two atoms.[2]

### 1.2.2 Ligands

A huge variety of ligands are known, ranging from simple monoatomic ions to large complicated biomolecules. Of particular interest in this work are ligands containing aromatic nitrogen heterocycles. Pyridine is one such example; it is a monodentate ligand, which binds via the nitrogen donor atom to the metal ion. This is illustrated in the copper complex $[Cu(pyridine)_4](HC_2O_4)$, where four monodentate pyridine ligands are bound to the metal centre (*Figure 2*).[3]

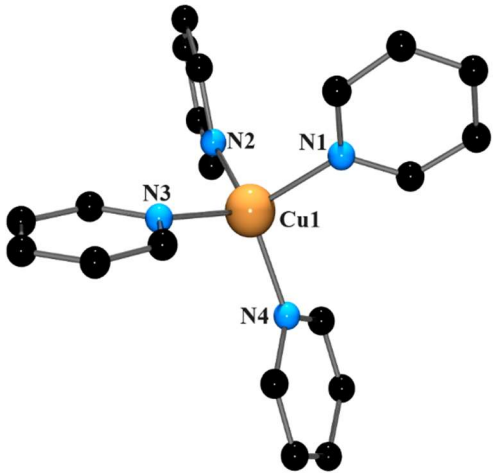


*Figure 2. Structure of the [Cu(pyridine)$_4$](HC$_2$O$_4$) complex. H atoms have been omitted for clarity.*

2,2'-bipyridine is a bidentate ligand, with two N atoms capable of binding to the same metal ion. This can be seen in the Pd(II) complex [Pd(2,2'-bipyridine)$_2$](NO$_3$)$_2$.H$_2$O, where the Pd(II) ion is coordinated by both the available nitrogen donor atoms from each ligand (*Figure 3*).[4]

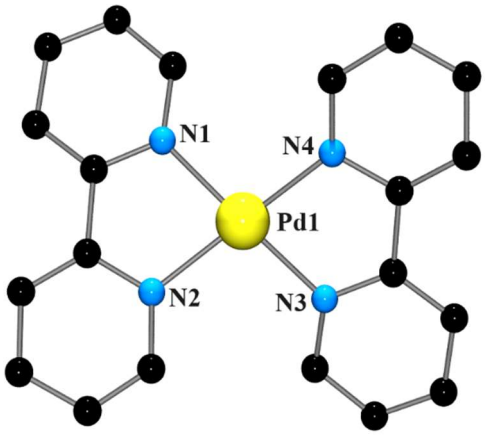


*Figure 3. Structure of the [Pd(2,2'-bipyridine)$_2$](NO$_3$)$_2$.H$_2$O complex. H atoms have been omitted for clarity.*

Tris(2-pyridylmethyl)amine (TPA) is a widely used polydentate ligand that contains four nitrogen donor atoms. The Zn(II) coordination complex, [Zn(TPA)Cl]ClO$_4$, shows the polydentate ligand bound to the metal centre via all four nitrogen donors (*Figure 4*).[5]

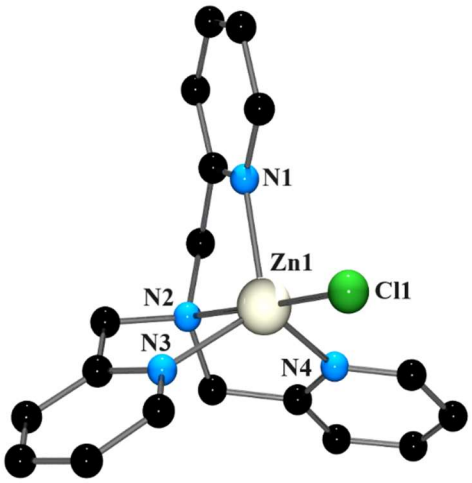


*Figure 4. Structure of the [Zn(TPA)Cl]$^+$ cation. H atoms have been omitted for clarity.*

The coordination of a multidentate ligand through at least two donor atoms results in the formation of a chelate ring, and such complexes are often called chelate complexes, while the ligand is often called a chelating ligand. Chelate rings, by their very nature, are geometrically constrained, and in ligands such as 2,2'-bipyridine that contain $sp^2$-hybridised atoms in the ring, the ligand adopts an essentially planar geometry when coordinated to a metal ion. Multidentate ligands that contain three or more donor atoms have the potential to form one or more chelate rings with the same metal centre and such ligands are often found to have high affinities for metal ions. The ligand TPA is a good example of this and, as can be seen in *Figure 4*, there are three chelate rings present in the [Zn(TPA)Cl]$^+$ cation.

In contrast to organic chemistry, where 6-membered rings have the greatest thermodynamic stability, 5-membered chelate rings are more stable than 6-membered chelate rings, owing to the necessary incorporation of one angle close to 90°.[6–8] Multidentate ligands can form chelate rings of different sizes in the same complex, and this leads to geometric isomers.

### 1.2.3 Tripodal Tetraamine Ligands

Tripodal tetraamine ligands are a group of multidentate ligands that have garnered significant interest in coordination chemistry. They consist of a central nitrogen atom to which three alkyl arms are attached, each of which also contains a nitrogen donor atom (*Figure 5*).

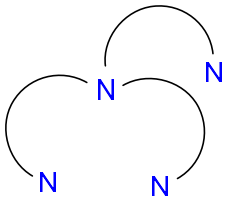


*Figure 5. The general structure of a tripodal tetraamine ligand.*

A wide range of tripodal tetraamine ligands can easily be prepared by altering either the arm length or the nature of the nitrogen donor atom. All three alkyl chains can have the same length (a = b = c), different lengths (a ≠ b ≠ c), and all possibilities in between (*Figure 6*). This can then give rise to a homologous series of ligands through systematic variation of the chain lengths.

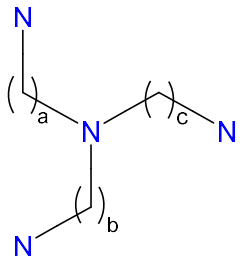


*Figure 6. The possible variations of the alkyl chain lengths of a tripodal tetraamine ligand.*

An example of a homologous series of tripodal ligands (**1**-**4**) is displayed in *Figure 7*.[9] The ligand **1**[10,11] has three ethyl arms, and ligand **2**[12,13] contains one ethyl arm and two propyl arms. Continuing the stepwise insertion of a -$CH_2$ group into each of the ligand arms of **1** leads to the ligands **3**[14,15] and **4**.[16–18]

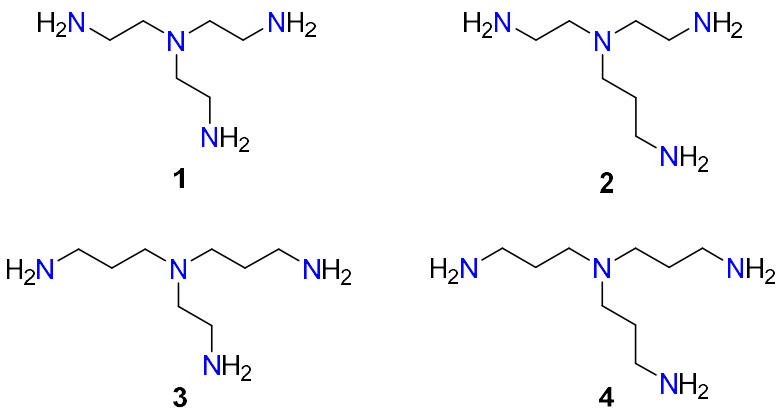


*Figure 7. The homologous series of aliphatic tripodal tetraamine ligands tris(2-aminoethyl)amine **1**, 3-aminopropylbis(2-aminoethyl)amine **2**, 2-aminoethybis(3-aminopropyl)amine **3**, and tris(3-aminopropyl)amine **4**.*

The second feature that can be altered is the nature of the nitrogen donor atom on each of the arms. A wide range of tripodal tetraamine ligands have been prepared that contain aliphatic (primary, secondary and tertiary), pyridyl, pyrazole, imidazole, pyrrole, pyrazine and quinoline nitrogen donors.[19] For example, **1** contains primary aliphatic amine donors, while **5** contains benzimidazole nitrogen donor atoms (*Figure 8*).

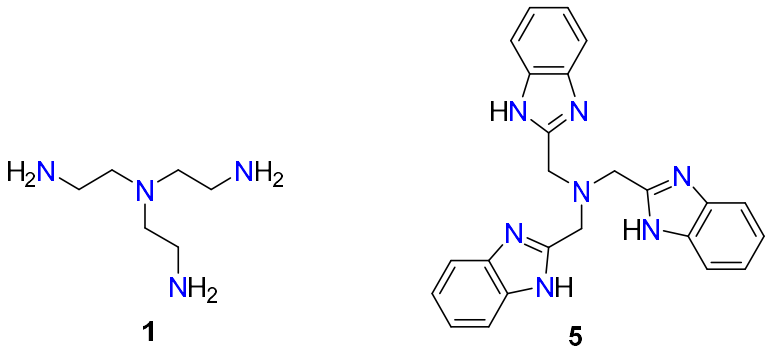


*Figure 8. The tripodal tetraamine ligands tris(2-aminoethyl)amine **1** and tris(benzimdazolylmethyl)amine **5**.*

The nitrogen donor atoms can be varied within the same molecule. For example, the ligand **6** is a tripodal tetraamine ligand that contains two types of nitrogen donor atoms, 1-methyl-1*H*-imidazole and pyridine (*Figure 9*).

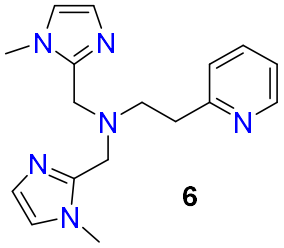


**6**

*Figure 9. Structure of the tripodal tetraamine ligand* ***6*** *containing two different nitrogen donor groups.*

Variation of both the arm length and nitrogen donor atoms can therefore produce a variety of asymmetric ligands, with one such example being the ligand **7** displayed in *Figure 10*.

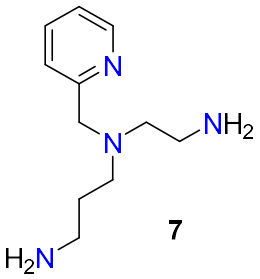


**7**

*Figure 10. Structure of the tripodal tetraamine* ***7*** *containing different nitrogen donor groups and alkyl chain lengths.*

Tripodal tetraamine ligands can be placed into two categories, those that contain three identical arms, and those that contain differing arms in either length or the nature of the nitrogen donor atoms. The latter has effects when the coordination chemistry of these ligands is discussed as the possibility of forming geometric isomers arises when the arms of the ligand are non-identical.

### Tripyridyl Tripodal Tetraamine Ligands

Tripyridyl tripodal ligands are an important class of tripodal tetraamine ligands that contain three 2-pyridyl-appended alkyl arms that are connected to the central nitrogen atom. For example, the ligands **8** ( a = b = c = 1), **9** ( a = b = 1, c = 2), **10** ( a = b = 2, c = 1) and **11** (a = b = c = 2) have a systematic change in the alkyl chain lengths of each arm to make up a homologous series of tripyridyl tripodal tetraamine ligands (*Figure 11*).[20–23]

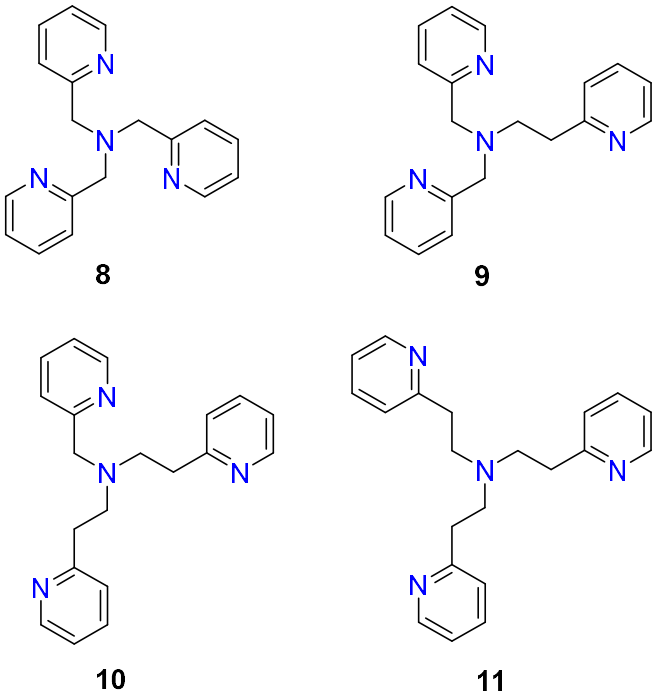


*Figure 11. The tripodal tetraamine ligands **8-11**.*

### 1.2.4 Synthesis of tripodal tetraamine ligands

The first tripodal tetraamine ligand, tris(2-aminoethyl)amine **1**, was prepared in 1896 from the reaction of 2-(2-bromoethyl)-1*H*-isoindole-1,3(2*H*)-dione and dry ammonia followed by the deprotection using HCl (*Scheme 1*). Since then, a variety of methods have been used to prepare tripodal tetraamine ligands.[11,24]

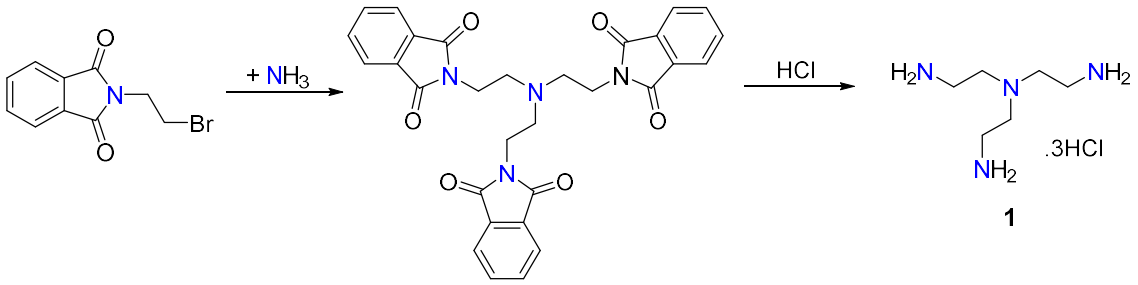


*Scheme 1. Reported synthesis of tris(2-aminoethyl)amine **1**.*[11]

A common feature of all methods is the alkylation of the nitrogen atom of an ammonium ion, or a primary or secondary amine precursor, with this nitrogen atom becoming the tertiary aliphatic N atom of the resulting ligand. Thus, bromo- and chloroalkylphthalimides have been employed in the synthesis of ligands containing aliphatic amine groups, as they can easily alkylate both primary and secondary nitrogen

atoms, and deprotection of the phthaloyl group with acid affords the protonated amine. Similarly, haloalkylpyridines, haloalkylimidazoles and haloalkylpyrazoles are commonly used alkylating agents for the synthesis of ligands containing aromatic N-donor groups. For example, the tripyridyl tripodal ligand **8** can be prepared from the reaction of 2 equivalents of 2-(chloromethyl)pyridine hydrochloride and 1-(pyridin-2-yl)methanamine as seen in *Scheme 2*.[25,26]

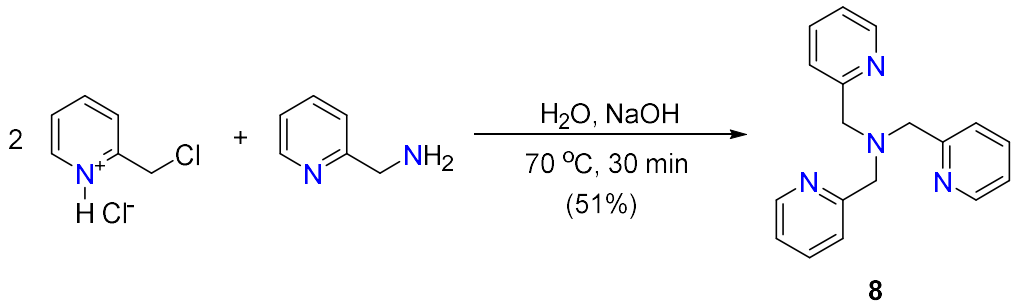


*Scheme 2. Reported synthesis of the ligand **8**.*[25]

In addition, 2-vinylpyridine has been found to be very useful in the synthesis of ligands containing 2-(2-pyridylethyl) arms.[19] For example, the ligand **11** can be synthesised by the reaction of 2-vinylpyridine and ammonium acetate (*Scheme 3*).[25,27–30] Alternative syntheses can include reductive amination between bis(2-pyridyl)alkylamine and pyridine-2-carbaldehyde, or the reaction of an appropriate bis(2-pyridyl)alkylamine with 2-vinylpyridine.[30]

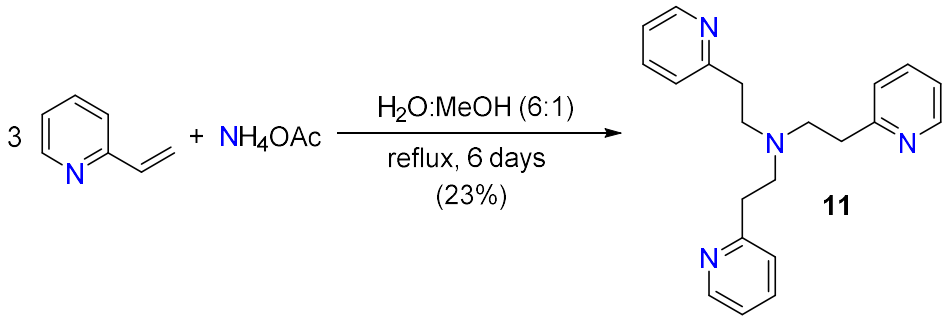


*Scheme 3. Reported synthesis of the ligand **11**.*[30]

Different substituents can also be incorporated into the ligand at the alkyl carbon atoms, aliphatic nitrogen atoms, and the aromatic rings, where present. For the tripyridyl tripodal ligands, once the ligand has been synthesised, the unreactive nature of pyridine means that substituted derivatives are difficult to prepare. As a result, such substituted ligands

are usually prepared using the appropriately substituted precursors.[31] This allows for a vast range of possible ligands; however, to narrow the scope of this work only unsubstituted molecules will be considered.

## 1.3 Quinoline

One of the main aims of this thesis is the synthesis of new quinoline-containing ligands, and therefore a brief review of the chemistry of quinoline is germane at this point.

Quinoline is a planar heterocyclic aromatic organic compound containing a benzene ring fused to a pyridine ring (*Figure 12*).[32] It is a colourless, hygroscopic oily liquid at room temperature and atmospheric pressure, with a boiling point of 237 °C. Quinoline is a weak base with the pKa of the conjugate acid being 4.85 in water at 20 °C. It displays reactivity similar to pyridine and benzene.[33,34]

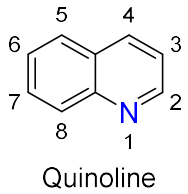


*Figure 12. Chemical structure and numbering of quinoline.*

Runge first isolated quinoline in 1834 from coal tar, giving it the name “leucol”. A few years later, in 1842, Gerhadt isolated quinoline as a degradation product from quinine and cinchonine.[35] Since this time, quinoline and its substituted derivatives have been widely studied, most commonly for use as pharmaceuticals.[36–39]

### 1.3.1 Coordination Chemistry of quinoline

While there is a large number of pyridine-containing ligands known, ligands containing quinoline and its derivatives are much less numerous. As a result, the coordination chemistry of pyridine and its derivatives has been extensively studied, and that of quinoline and its analogues is much less established. A recent review on quinoline-based coordination complexes shows that quinoline itself is not a common ligand; interestingly, there are no crystallographically characterised homoleptic six-coordinate quinoline complexes, and the vast majority of quinoline-containing metal species involve incorporation of quinoline into multidentate ligands.[1]

The most well-studied quinoline-based ligand is quinolin-8-ol **12** (also known as oxine) (*Figure 13*). Metal chelate complexes of this ligand have found use as antimicrobial, antiviral, anti-metastatic and antileukemia agents,[40–43] electroluminescent devices,[44] radiopharmaceuticals,[45] and in PET imaging,[46] amongst many other applications.

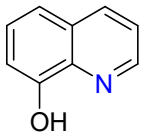


**12**

*Figure 13. The structure of quinolin-8-ol **12**.*

For example, the eight-coordinate zirconium tetrakis(**12**) complex, was first reported in 1974 and consists of a zirconium (IV) centre chelated to four deprotonated quinolin-8-ol **12** moieties (*Figure 14*).[47] This complex has found use in organic light emitting diodes[48] and in PET imaging.[49]

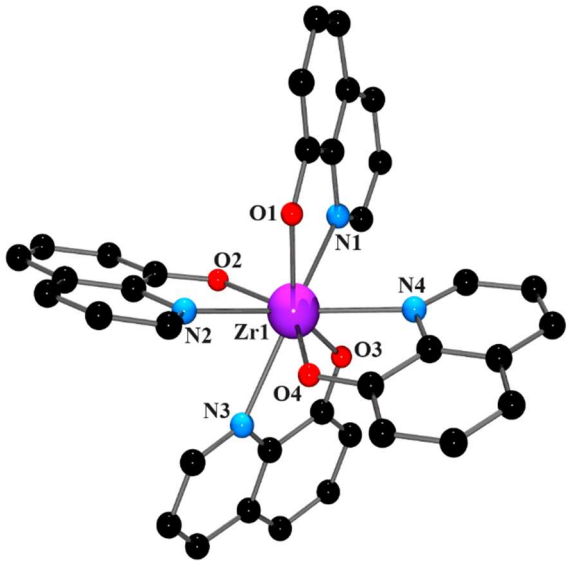


*Figure 14. Structure of the [Zr(**12**)$_4$] complex. H atoms have been omitted for clarity.*

The quinolin-8-amine (**13**) (*Figure 15*) has also been well established in the literature as a ligand and has been demonstrated to be useful in several applications similar to **12**.[50–59]

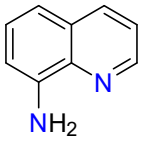


**13**

*Figure 15. The structure of quinolin-8-amine (**13**).*

In particular, there are a number of examples of metal complexes of this ligand that have been developed for their potential in spin crossover (SCO) materials. As an example, Yang and co-workers employed the bidentate ligand **13** for the synthesis of the iron species, $[Fe(\mathbf{13})_3](BPh_4)_2.1.5CH_3COCH_3$ (*Figure 16*).[55]

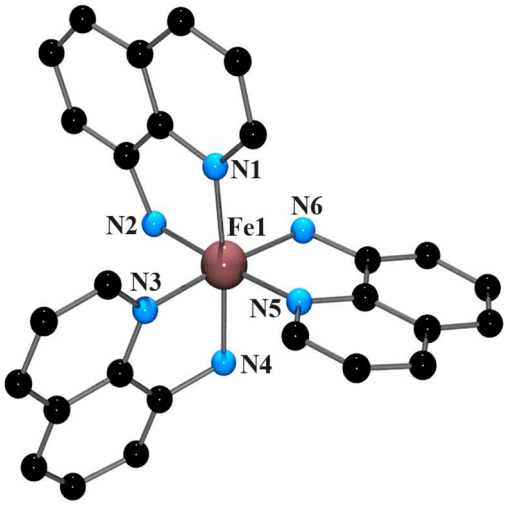


*Figure 16. Structure of the $[Fe(\mathbf{13})_3]^{2+}$ complex. H atoms have been omitted for clarity.*

Quinoline-containing ligands and their corresponding metal complexes have demonstrated great purpose in the development of metallodrugs that can be used in biological systems for the treatment of disease.[60] Several studies have described quinoline analogues as promising compounds that display positive results in preclinical models for the treatment of Alzheimer's.[61–65] For instance, the quinolin-8-ol derivative, clioquinol **14** (*Figure 17*), is a bidentate chelating ligand that binds to Cu(II), and reduces Aβ aggregation and oxidative stress, both contributors to the disease.[66]

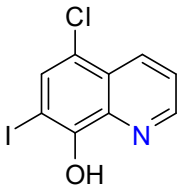


**14**

*Figure 17. Chemical structure of clioquinol (**14**).*

Although there have been no reports of structurally characterised clioquinol-based copper complexes, Vranec *et al.*[67] have reported the X-ray structure of the Pd(II) species, [Pd(**14**)$Cl_2$].2$H_2O$ (*Figure 18*). The preparation of this complex was driven by the aim to develop a potential anticancer agent on the basis of previous square-planar complexes of platinum and palladium chemotherapeutics.[67–69]

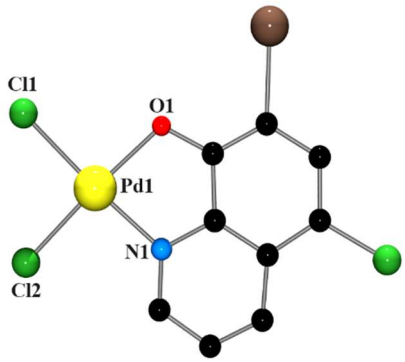


*Figure 18. Structure of the [Pd(**14**)$Cl_2$] complex. H atoms have been omitted for clarity.*

An example of the incorporation of the quinoline moiety into a multidentate ligand is shown in *Scheme 4*. Wang *et al.* reported the synthesis of platinum complexes of tridentate 8-substituted quinoline derived ligands. The ligands were prepared by reaction of equimolar amounts of quinolin-8-amine **13** and pyridine-2-carbaldehyde or (pyridin-2-yl)acetaldehyde and subsequent reaction with *cis*-Pt(DMSO)$_2$$Cl_2$ (*Scheme 4*). However, it should be noted that the synthetic details differ between the experimental section and the results and discussion section of this paper. There is no structural characterisation data reported for these platinum complexes. Both complexes were tested for their anticancer potential and the complex [Pt(**15**)Cl] showed superior activity in comparison to complex [Pt(**16**)Cl].[70]

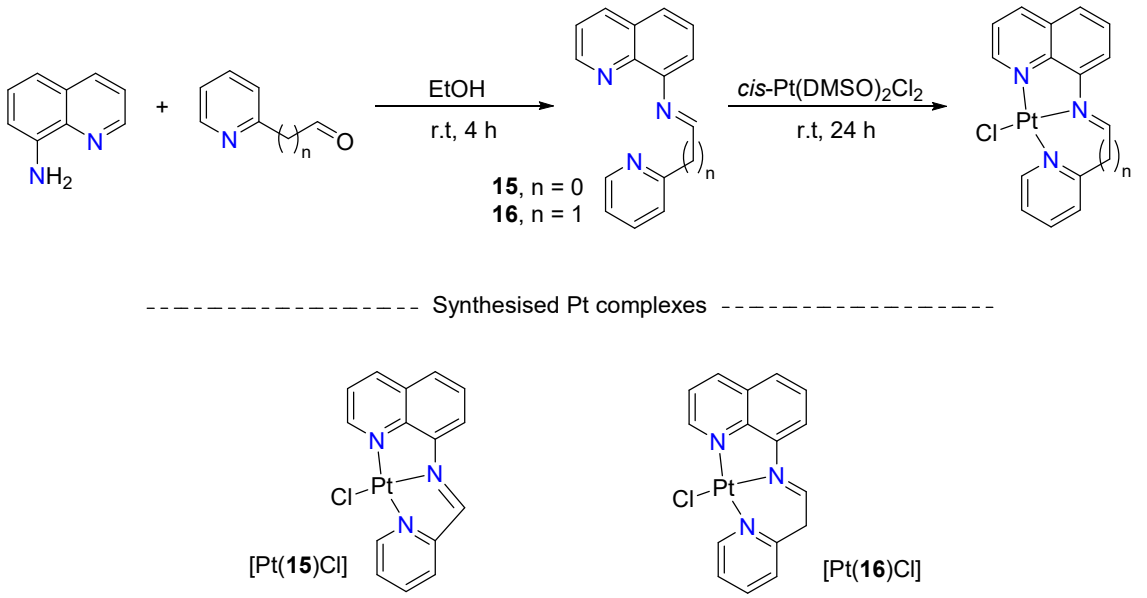


*Scheme 4. Reported synthesis of the ligands **15** and **16** and the corresponding platinum complexes.*[70]

Pavlidis *et al.* have reported the synthesis and characterisation of Cu(II) complexes with the ligands **17** and **18** containing quinoline and pyridine rings, and the ligands **19** and **20**, containing solely quinoline rings (*Figure 19*).

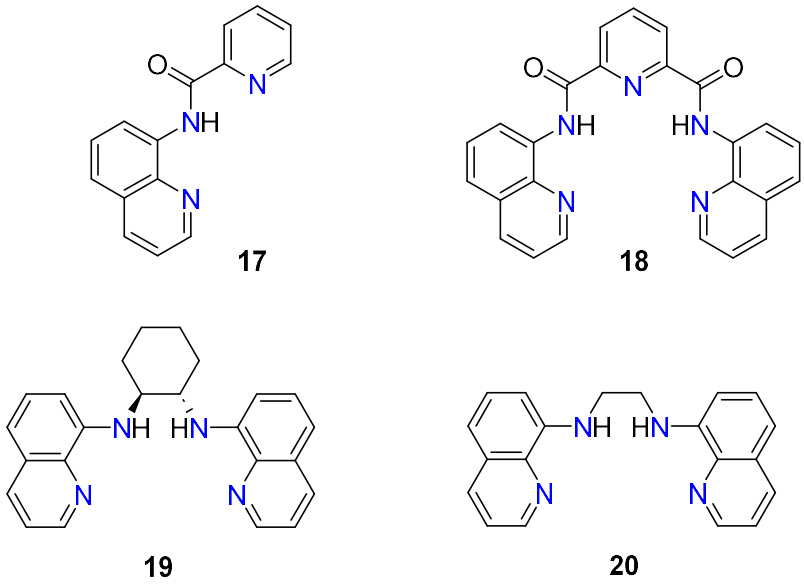


*Figure 19. Structures of the quinoline-based ligands **17-20**.*

This series of ligands and their corresponding copper complexes (*Figure 20*) provided significant insight into the action of quinoline-based metal chelators and their effect against Aβ aggregation and oxidative stress in cells. In particular, the Cu(II) complex [Cu(**19**)$(Cl)_2$].$3H_2O$ revealed an effective protection against oxidative stress in cells. As reported by the authors, X-ray quality crystals of the copper complex containing **19** were not obtained under the reaction conditions established for the other copper complexes. As a result, the ligand was reacted with the starting material $[Cu(OH_2)_6](ClO_4)_2$, and according to the authors these conditions afforded green crystals of *trans*-[Cu(**19**)$(ClO_4)_2$]; however, our attempts to find the X-ray characterisation data were unsuccessful with no entries found on the CSD.[71]

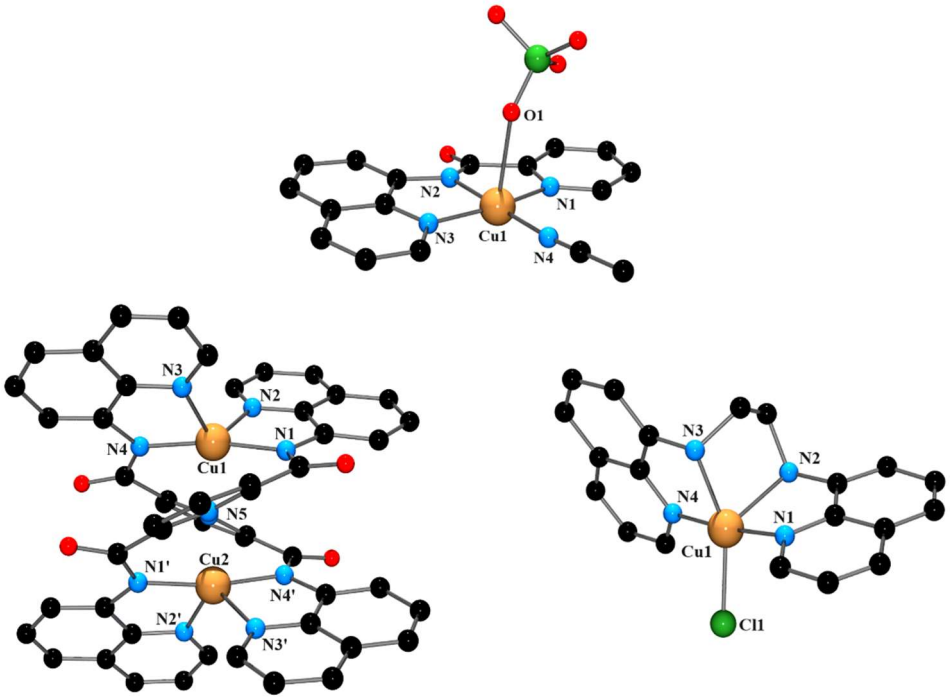


*Figure 20. Structures of the Cu(II) complexes containing the ligands **17** (top), **18** (left) and **20** (right). H atoms have been omitted for clarity.*

Many transition metal complexes containing quinoline-based ligands have been prepared as models for metalloenzymes. The synthesis of enzymatic models has served as a minimalistic approach to understanding the mechanism of enzymes as the focus is on the production of the active site without the recreation of the whole protein scaffold.[72,73] For example, the isolation of bis(μ-oxo) manganese complexes play an important role in the development of research towards modelling the oxygen-evolving complex (OEC) located within the active site of the enzyme photosystem II (*Figure 21*).

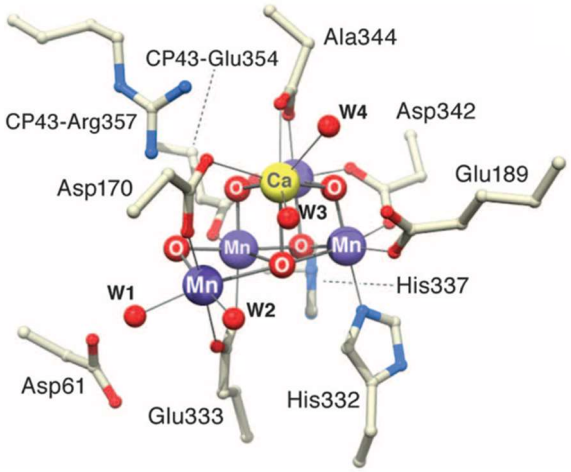


*Figure 21. X-ray crystallographic structure of the oxygen-evolving complex, a $Mn_4O_5Ca$ cofactor.*[74]

The formation of $O_2$ and the photosynthetic oxidation of $H_2O$ are catalysed by a $Mn_4Ca$ complex active site bound within the proteins of photosystem II. This manganese cluster is known as the OEC and there has been a significant amount of attention directed towards solving the structure of the OEC. There has been extensive research on dinuclear manganese complexes for comparative spectroscopic and theoretical studies to elucidate the structure and function of the $Mn_4Ca$ cluster in photosystem II. Therefore, the isolation and characterisation of bis(μ-oxo) manganese complexes is still relevant in the development of this area of research.[75] A quinoline-based bis(μ-oxo) manganese complex is discussed further in chapter four.

The addition of a transition metal catalyst has been well established in achieving many selective organic transformations and has been employed in a number of different reactions such as the development of stereoselective catalysis,[76,77] olefin metathesis,[78] C-H bond activation and functionalisation,[79] cross-coupling reactions,[80] and transesterification reactions, amongst many others.[81–84]

Metal-catalysed transesterification reactions have been well-cited in the literature. Zn(II) complexes have been found to have great potential for these types of reactions due to their relatively low toxicity and stability. The quinoline-based Zn(II) species $[Zn(\mathbf{17})]_2.2CH_3Cl_3$ and $[Zn(\mathbf{18})_2]$ (*Figure 22*) contain the ligands **17** and **18** described above (*Figure 19*) and have been synthesised to investigate their catalytic capabilities

towards transesterification reactions. Both species were analysed against a variety of esters and demonstrated active catalytic activity in the transesterification reactions.[85]

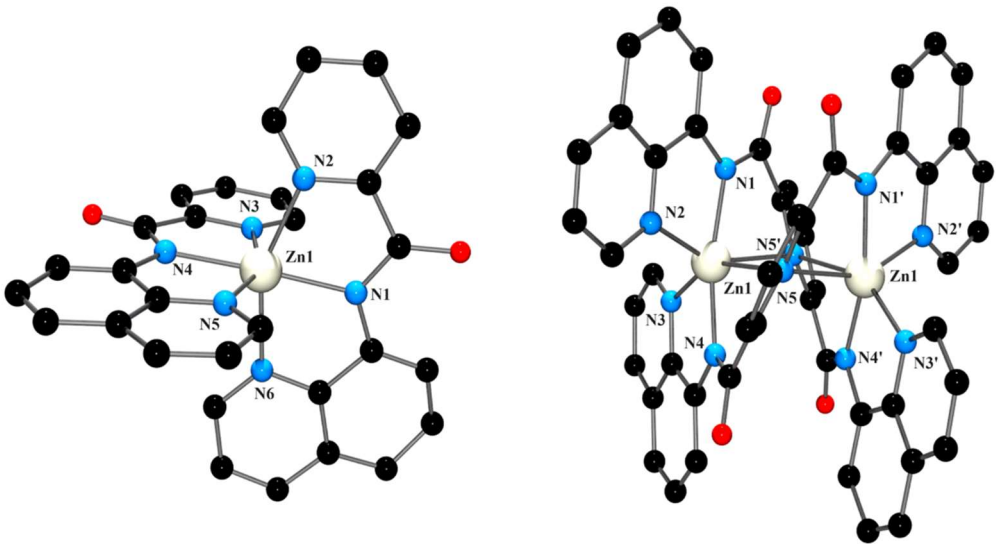


*Figure 22. Structures of the Zn(II) complexes with ligands **17** and **18**. H atoms have been omitted for clarity.*

The application of quinoline-based metal complexes in the field of catalysis has been well established.[86–89] An example of such is the work of Patel *et al*. who reported a series of nickel complexes containing quinoline-based pincer ligands. The ligands have been prepared from the palladium catalysed reaction of quinolin-8-amine and a substituted aniline moiety, followed by the further reaction of the ligand with $(THF)_2NiBr_2$ or $Ni(OAc)_2$ to afford the corresponding nickel complex (*Scheme 5*).[90]

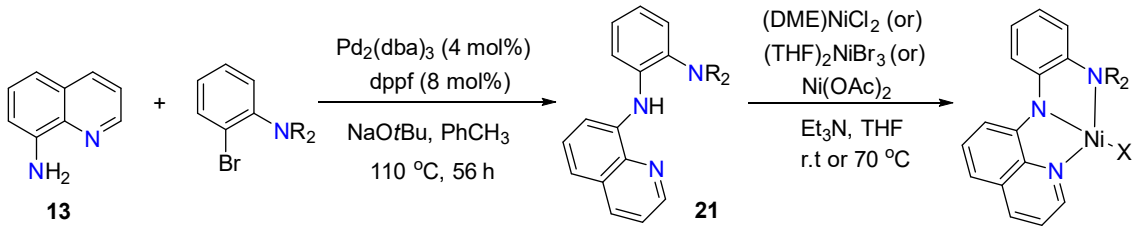


*Scheme 5. Reported synthesis of the ligand **21** and corresponding Ni(II) species.*[90]

The quinoline-based nickel pincer complexes were screened and optimised for the direct C-H bond alkylation of benzothiazole using un-activated alkyl halides such as 1-iodooctane. In particular, the complex [Ni(**21**)Cl] (*Figure 23*) demonstrated excellent activity in the alkylation reaction without the addition of any co-catalysts and under mild

reaction conditions. In addition, excellent functional group tolerance, recyclability, and product formation was observed for this complex.[90]

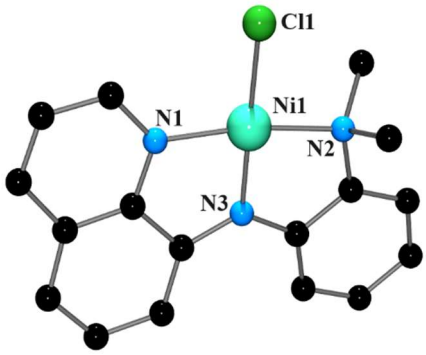


*Figure 23. Structure of the [Ni(**21**)Cl] complex. H atoms have been omitted for clarity.*

Quinoline-based metal complexes have emerged as a promising class of materials for photovoltaic applications. Hsu *et al.* synthesised a series of iridium complexes that contained a quinoline ligand derived from 7-methylquinolin-8-amine (*Scheme 6*). Emission studies showed that Ir(III) complexes of this ligand could be tuned to emit in the range from yellow to red. Thus far, there are no examples of structurally characterised metal complexes of this ligand.[91]

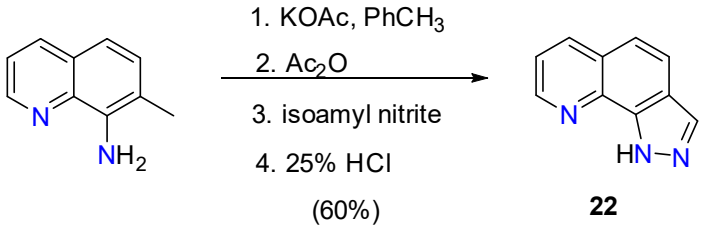


*Scheme 6. Reported synthesis of **22**.*[91]

### 1.3.2 Amine ligands containing 2-quinolylmethyl groups

The incorporation of the unsubstituted quinoline moiety into multidentate ligands is less common than the 8-substituted examples discussed above. The following examples are selected tri- and tetradentate amine ligands containing 2-quinolylmethyl, and metal complexes of such ligands.

**Tridentate ligands**

The general structure of a tridentate amino ligand is given in *Figure 24*; a central N atom is attached to two alkylamino arms.

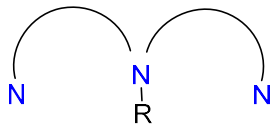


*Figure 24. The general structure of a tridentate amino ligand.*

These ligands can be prepared in a similar manner to the tetraamine ligands discussed above. For example, the ligand **23** can be synthesised from the reaction between quinoline-2-carbaldehyde and N-(2-aminoethyl)acetamide to give the corresponding imine, and borohydride reduction of this affords the desired product.[92] Alternatively, the ligand can be also be prepared by reacting 2-(chloromethyl)quinoline hydrochloride with ethylenediamine (*Scheme 7*).[93]

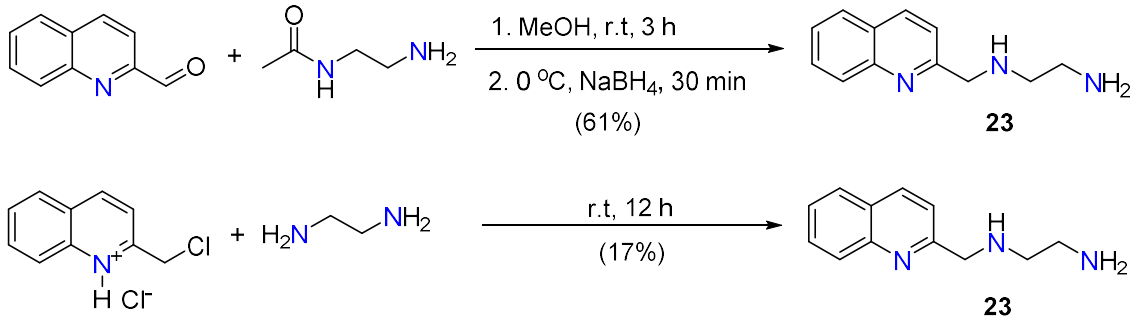


*Scheme 7. Reported syntheses of **23**.*[92,93]

The technetium complex, *fac*-[Tc(**23**)$(CO)_3$]Cl.$H_2O$ (*Figure 25*) is the sole structurally characterised species of this ligand as displayed in *Figure 25*.[94] This metal complex exhibits the coordination of the ligand via all three available nitrogen donor atoms of **23**.

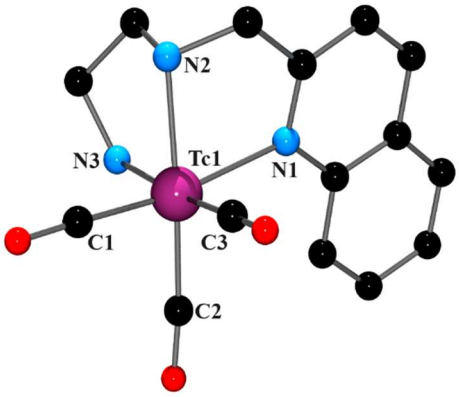


*Figure 25. Structure of the fac-[Tc(**23**)(CO)$_3$]$^+$ cation. H atoms have been omitted for clarity.*

The ligand **24** is another example of a tridentate quinoline-containing ligand. This ligand can be prepared from the reaction of 2-(2-methylaminoethyl)pyridine and 2-(chloromethyl)quinoline hydrochloride in the presence of $Cs_2CO_3$ (*Scheme 8*).[95]

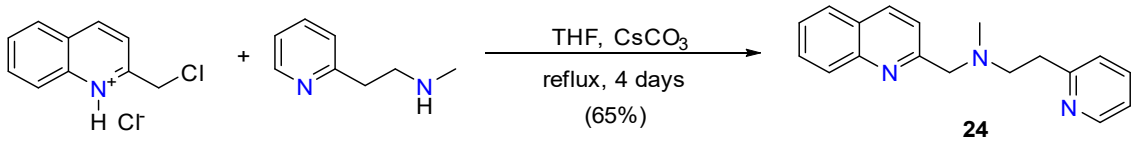


*Scheme 8. Reported synthesis of 2-(2-ethylpyridyl)-(2-methylquinolyl)-methylamine.*[95]

The dinuclear complex *mer*-[Cd$_2$(**24**)$_2$(μ-1,3-N$_3$)$_2$(N$_3$)$_2$] shown in *Figure 26* has been synthesised and structurally characterised. The structure of this complex consists of two *mer*-[Cd(**24**)N$_3$]$^+$ units connected by two bridging azido ligands. The Cd(II) centres are octahedrally coordinated by the three nitrogen donor atoms of **24** in a *mer* configuration, the N atoms from two bridging azido ligands, and a terminal azido ligand (Cd-N = 2.276 Å). Intermolecular π-π interactions of adjacent aromatic rings of **24** are observed, with separation of the pyridyl and quinolyl moieties ranging from 3.510 Å to 3.966 Å.

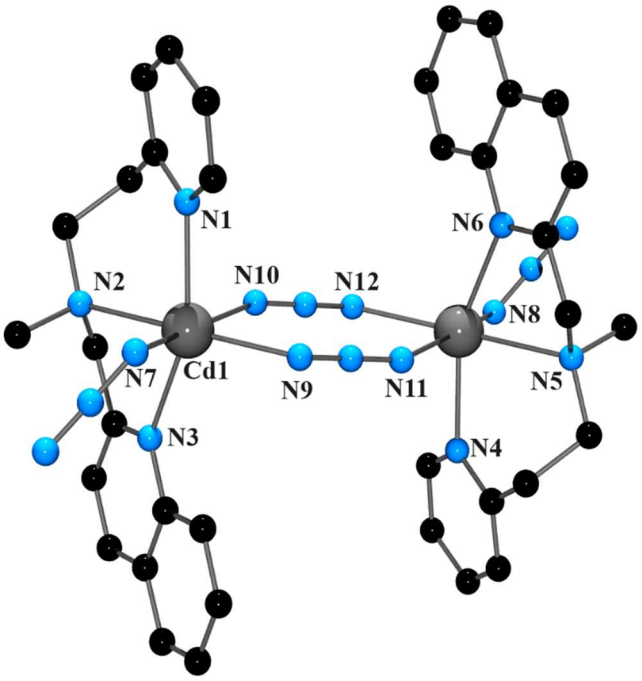


*Figure 26. Structure of the mer-[$Cd_2$(**24**)$_2$($\mu$-1,3-$N_3$)$_2$($N_3$)$_2$] complex. H atoms have been omitted for clarity.*

The ligand 1-(quinol-2-ylmethyl)-1,4-diazacycloheptane (**25**)[96–98] (*Figure 27*) can be prepared from the treatment of 2-(chloromethyl)quinoline hydrochloride with homopiperazine in the presence of $Et_3N$.

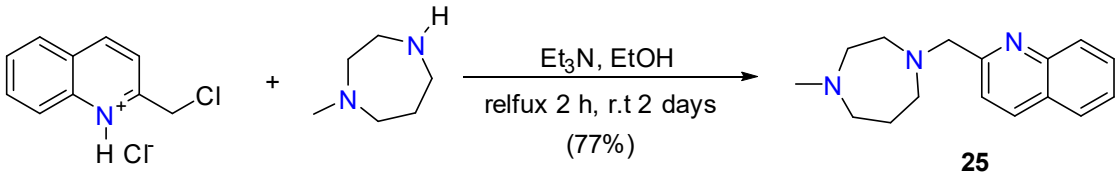


*Figure 27. The structure of 1-(Quinol-2-ylmethyl)-1,4-diazacycloheptane **25**.*[96]

The five coordinate complex, [Cu(**25**)$Cl_2$].$CH_3CN$ (*Figure 28*) was synthesised from the reaction of $CuCl_2.H_2O$ and **25** in MeOH as a possible aziridination catalyst. The geometry of the resulting metal species is square pyramidal ($\tau_5$ = 0.08) with the square planar base consisting of the three ligand N donor atoms. The fourth equatorial position is occupied by a chlorido ligand while the remaining chlorido ligand is axial.[96] In addition, the Cu(II) complex [Cu(**25**)((*p*-$NO_2Ph)_2PO_2)_2$].$H_2O$ was prepared and structurally characterised as part of an investigation into the metal catalysed hydrolysis of phosphate esters.[98]

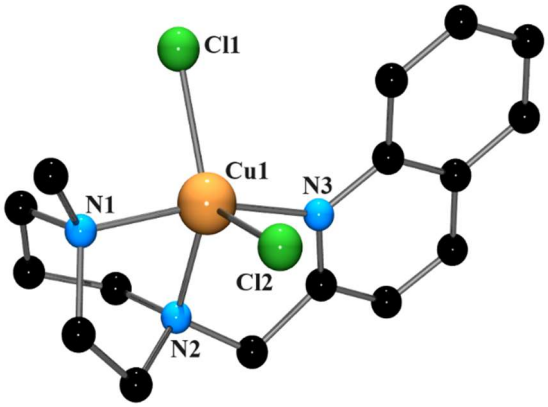


*Figure 28. Structure of the [Cu(**25**)$Cl_2$]$^+$ cation. H atoms have been omitted for clarity.*

The replacement of the quinolyl moiety of the ligand with the less sterically demanding pyridyl group results in the formation of a dicopper complex. In this instance, the two Cu(II) ions are bridged by two bis(*p*-nitrophenyl)phosphate ligands in a μ-1,3 fashion.[98,99]

The ligand **26**[100–103] (*Figure 29*) is an example of a tridentate ligand that contains two quinoline moieties. The reaction of 2-(chloromethyl)quinoline hydrochloride, benzylamine and base ($Na_2CO_3$, $K_2CO_3$, NaOH), affords **26**.

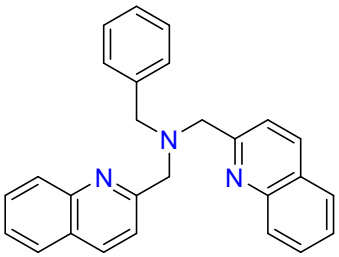


**26**

*Figure 29. Structure of the ligand N-Benzyl-N,N-di(quinolin-2-ylmethyl)amine **26**.*

Several four-, five-, and six-coordinate complexes of **26** have been reported. One example is the five-coordinate copper complex, [Cu(**26**)$Cl_2$].2$CH_3CH_2OH$ (*Figure 30*). In this complex, all three of the nitrogen atoms are bound to the metal centre, and the fourth and fifth positions are occupied by two chlorido ligands affording an overall significantly distorted square-pyramidal geometry ($\tau_5$ = 0.54).

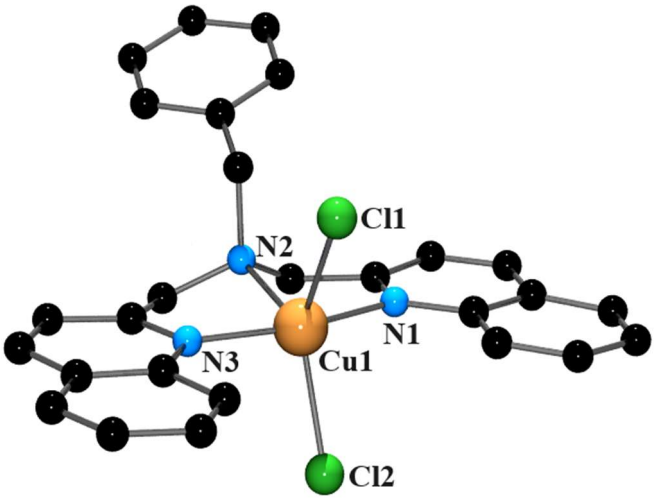


*Figure 30. Structure of the [Cu(**26**)Cl$_2$] complex. H atoms have been omitted for clarity.*

The corresponding pyridine ligand (**26**py) forms the five-coordinate complex [Cu(**26**py)Cl$_2$][104] (*Figure 31*), which adopts a slightly distorted square-pyramidal geometry ($\tau_5$ = 0.11). The major difference between the two structures is the orientation of the aromatic rings relative to the chlorido ligands. In [Cu(**26**py)Cl$_2$], the pyridine ring lies nearly coplanar with a Cu-Cl bond while in [Cu(**26**)Cl$_2$], the phenyl ring of the quinoline moiety essentially bisect the Cl-Cu-Cl bond angle, increasing it significantly compared to the pyridine congener (~108° versus 131.10°, respectively); this arrangement avoids destabilising interactions between H-8 of the quinoline moiety and the Cl ligands, and appears to be a common feature in five coordinate complexes of tridentate quinoline-containing ligands. This behaviour has been termed the quinolyl split[105] and has been observed in several additional quinoline-based five-coordinate metal complexes.[94,106–110]

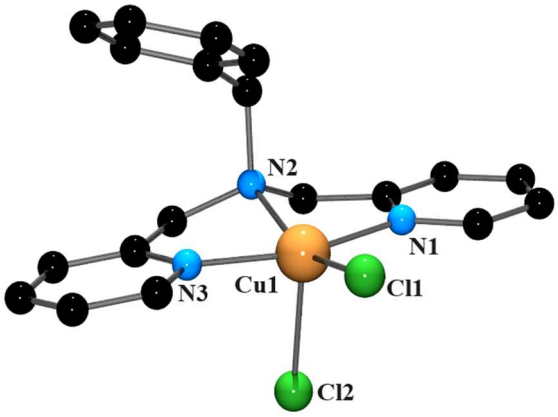


*Figure 31. Structure of the [Cu(**26**py)$Cl_2$] complex. H atoms have been omitted for clarity.*

The tridentate ligand **27**[106,108,111] (*Figure 32*) affords the Zn(II) complex, [Zn(**27**)$(ONO_2)_2$] (*Figure 33*), which is another example of a quinoline-containing five-coordinate species that displays the 'quinolyl split'.

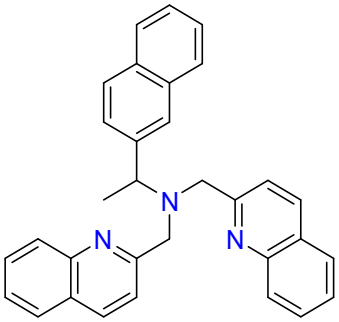


**27**

*Figure 32. Structure of the ligand (1-(1-Naphthylethyl))bis(quinolin-2-ylmethyl)amine **27**.*

The metal ion in [Zn(**27**)$(ONO_2)_2$] is bound by all three nitrogen donor atoms from the ligand **27** and two monodentate nitrato ligands, affording the complex a distorted trigonal bipyramidal geometry ($\tau_5 = 0.30$). As displayed in *Figure 33* the phenyl ring of the quinoline unit bisects the O-Zn-O bond angle (91.62°) and this arrangement is a result of the nitrato ligands avoiding the interaction with the quinoline H-8 atoms.

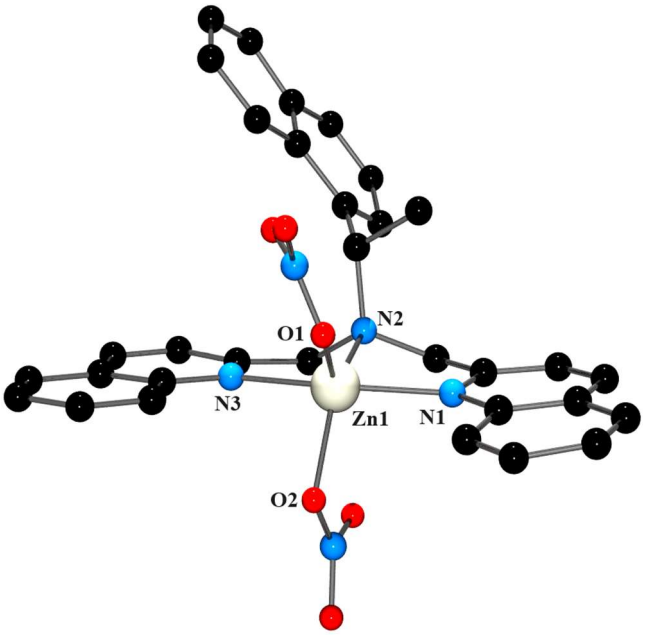


*Figure 33. Structure of the [Zn(**27**)(NO$_3$)$_2$] complex. H atoms have been omitted for clarity.*

**Tetradentate ligands**

Of the numerous examples of quinoline-containing ligands and their corresponding metal complexes, there are 46 tri-, tetra-, penta-, and hexadentate amine ligands that contain unsubstituted quinoline groups.[105] Fifteen of these are tetradentate,[112–125] and four are tetradentate tripodal ligands.[112,117,125]

The first quinolyl-containing tetradentate tripodal ligands were reported in 1993 by Karlin *et al*.[126] Systematic variation of the nitrogen donors from pyridine to quinoline, affords the homologous series comprising the ligands **8**, **28**, **29**, and **30** (*Figure 34*).

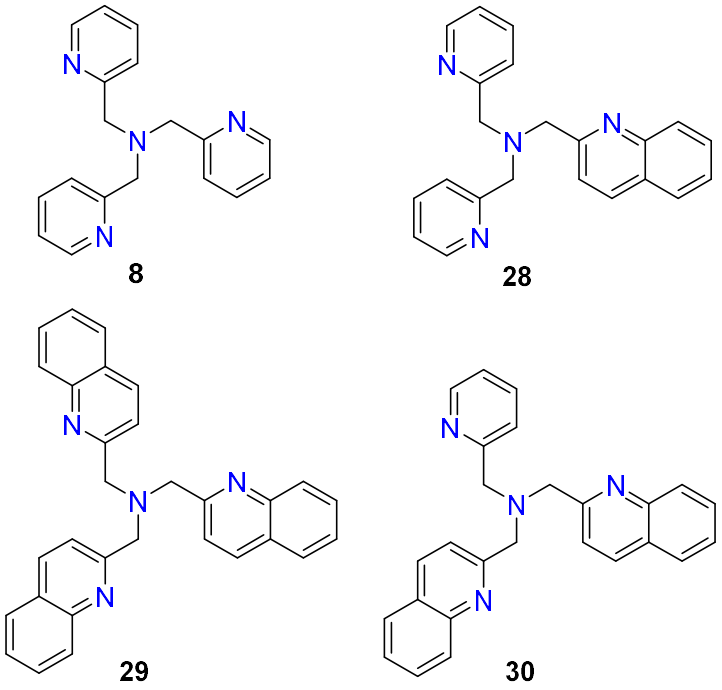


*Figure 34. Structures of a homologous series of quinolyl ligands* ***8-30****.*

The systematic substitution of the pyridyl groups for quinoline allowed the effect of the bulkier quinoline moieties to be examined. Quinoline in comparison to pyridine has a greater hydrophobicity and steric bulk which can have an impact on the steric and electronic properties of resulting metal complexes, and thus investigating the differences in metal complexes of these ligands was of interest.

As discussed in *Chapter One* section 1.2.4, the main methods for the preparation of such ligands are the alkylation of an ammonium ion, or a primary or secondary amine with the appropriate precursors, or alternatively via reductive amination. Commonly employed 2-quinolylmethyl precursors include 2-(chloromethyl)quinoline, 2-(bromomethyl)quinoline and quinoline-2-carbaldehyde.

The ligand **28** was first prepared by Wei and co-workers from the reaction of 1-(pyridin-2-yl)-*N*-[(pyridin-2-yl)methyl]methanamine and 2-(bromomethyl)quinoline in THF, with added $Et_3N$, at room temperature for 3 days (*Scheme 9*).[117] An alternative synthesis of this ligand involves the reaction of 2-(chloromethyl)quinoline hydrochloride and 1-(pyridin-2-yl)-*N*-[(pyridin-2-yl)methyl]methanamine in anhydrous $CH_3CN$ in the presence of anhydrous $K_2CO_3$.[127]

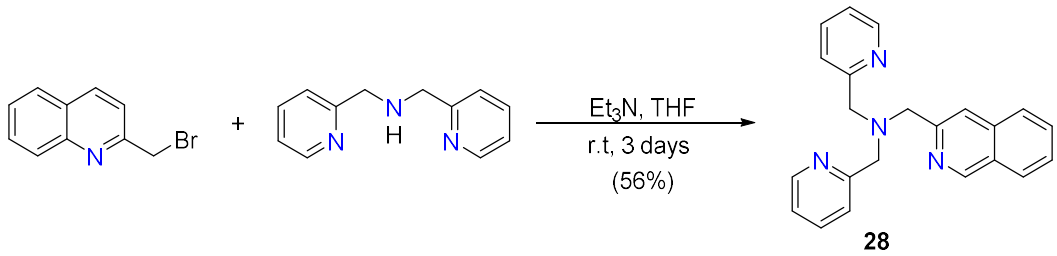


*Scheme 9. Reported synthesis of the ligand **28**.*[117]

Another example is the ligand **29** which consists of two quinolyl and one pyridyl group. The ligand has been synthesised from the reaction of 2-(bromomethyl)quinoline with 1-(pyridin-2-yl)methanamine in THF in the presence of *i*-$Pr_2NEt$. Purification by column chromatography and recrystallisation afforded the ligand as a white crystalline material (*Scheme 10*).[117] An alternative approach reported by Das involves the reaction of 1-(pyridin-2-yl)methanamine and 2-(bromomethyl)quinoline in anhydrous DMF in the presence of $Cs_2CO_3$ in the absence of light.[128]

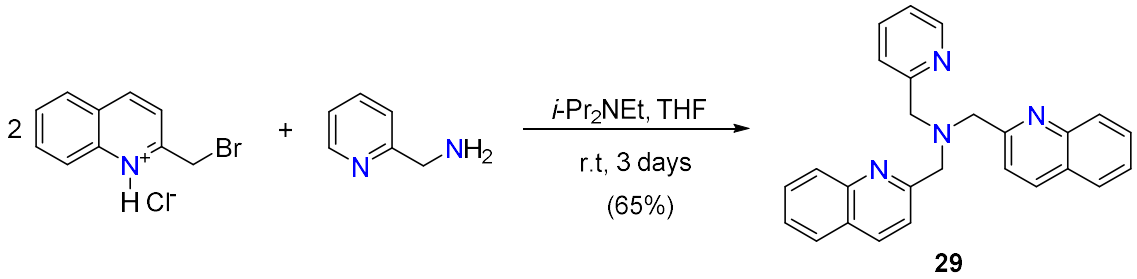


*Scheme 10. Reported synthesis of the ligand **29**.*[117]

2-(chloromethyl)quinoline hydrochloride can also be used in place of the bromoquinoline starting material,[127,129,130] and alternatively, a reductive amination using quinoline-2-carbaldehyde and 1-(pyridin-2-yl)-*N*-[(pyridin-2-yl)methyl]methanamine has been reported for the synthesis of **29**.[131]

The symmetrical ligand **30** in which all the nitrogen donor groups are quinoline, was prepared by the reaction of 2-(bromomethyl)quinoline and $NH_4OH$ in THF (*Scheme 11*).[117]

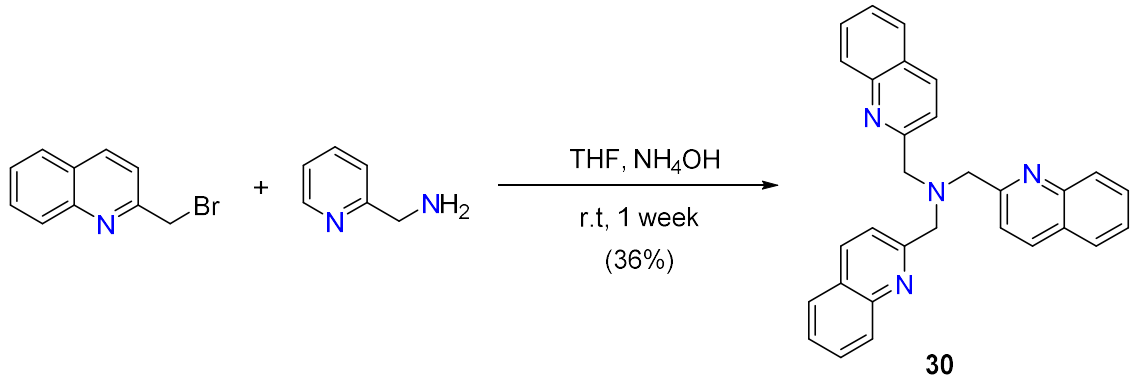


*Scheme 11. Reported synthesis of the ligand **30**.*[117]

Complexes of the three quinoline-containing tripodal ligands described above have been widely studied, the ligands being **28**[127,132–140], **29**[100,102,117,125,127,128,135,136,141–155], and **30**[30,100,125,129,134,141,143–145,154,156–165] (*Figure 35*).

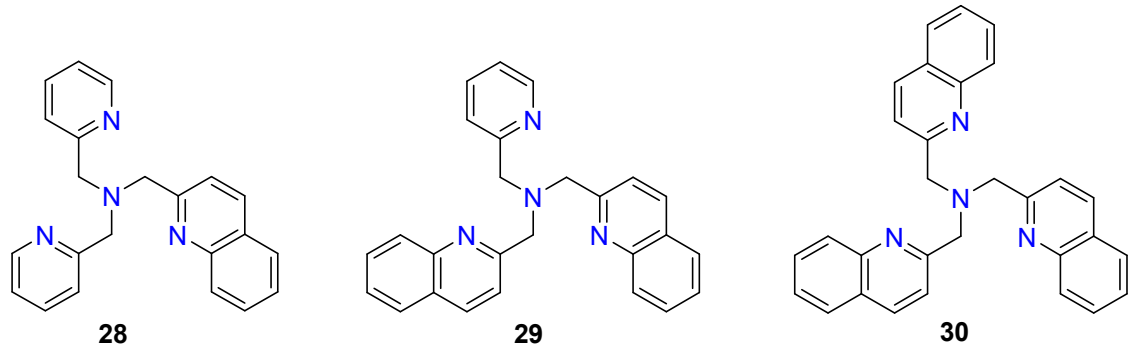


*Figure 35. Structure of the ligands **28**, **29** and **30**.*

Complexes of the ligand **28** with iron, cobalt, copper, and cadmium have been structurally characterised, and are mostly either five- or six-coordinate. The notable exception is the four-coordinate species, [Cu(**28**)][$B(C_6F_5)_4$] (*Figure 36*), which was prepared during an investigation into the reactivity of Cu(I) complexes with CO and $O_2$. In this complex, the central Cu(I) ion is coordinated to all four nitrogen donor atoms of the ligand to give a trigonal pyramidal geometry about the metal centre ($\tau_4 = 0.83$).[139]

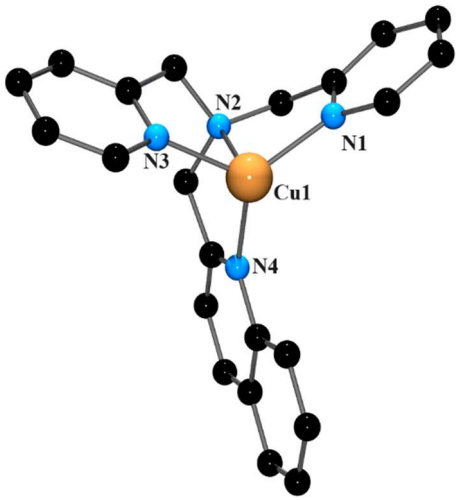


*Figure 36. Structure of the [Cu(**28**)]$^{+}$cation. H atoms have been omitted for clarity.*

The pentacoordinate Cu(II) complex of the ligand **28**, [Cu(**28**)Cl]$ClO_4$, is shown in *Figure 37*. The metal centre is bound to all four N donor atoms of the ligand and one chlorido ligand, affording a square-based pyramidal geometry ($\tau_5$ = 0.157). The quinoline bond length is 2.357 Å suggesting a weak bond between the nitrogen and metal centre, with most Cu-$N_{quinoline}$ bonds ranging from 1.9 Å to 2.2 Å.[166–169] This can be attributed to the Jahn-Teller effect. Interestingly as illustrated in *Figure 37*, the quinoline exhibits a bent coordination with an angle of 154.60° between the Cu-$N_{quinoline}$ bond and the plane of the aromatic ring.

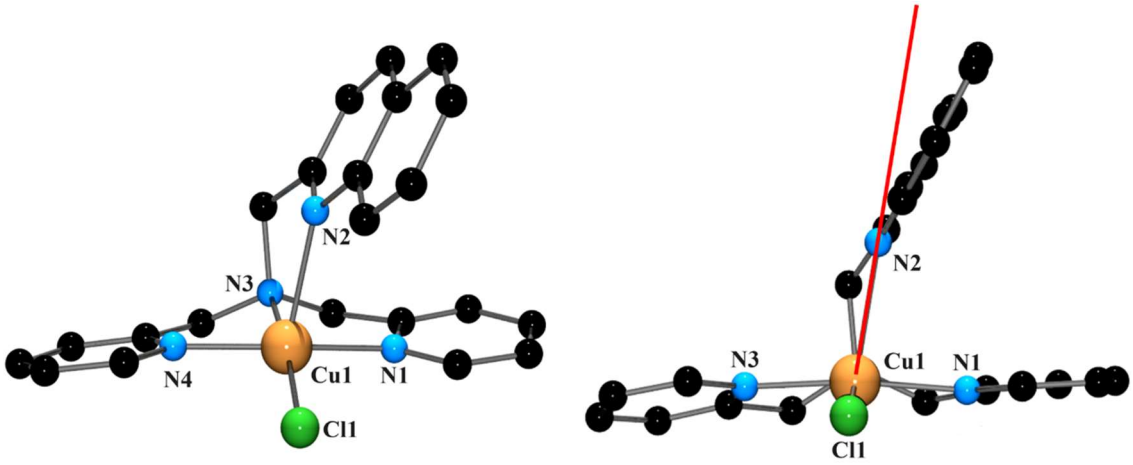


*Figure 37. Structure of the [Cu(**28**)Cl]$^{2+}$cation. H atoms have been omitted for clarity.*

The complex [Cu(**28**)Cl]$ClO_4$ was prepared in series with other Cu(II) compounds that were analysed for their cytotoxicity against various cancer cell lines. The study revealed that this complex cation in particular demonstrated cytotoxicity that is comparable to cisplatin.[135]

The 'bent' coordination feature of the quinoline moiety described above has been observed in several other quinoline-containing complexes.[85,170–173] Another example of this can be seen in the binuclear nickel complex, [(**L**Ni)$_2$(μ-$CO_3$)](Ph$_4$B)$_2$ (**L** = 4-bis[2-(quinoline-2-yl)-methyl]-1,4-diazepane), in which both the quinoline nitrogen atoms display significantly bent geometries, with angles of ~158° between the Ni-N vector and the plane of the quinoline ring (*Figure 38*).[171]

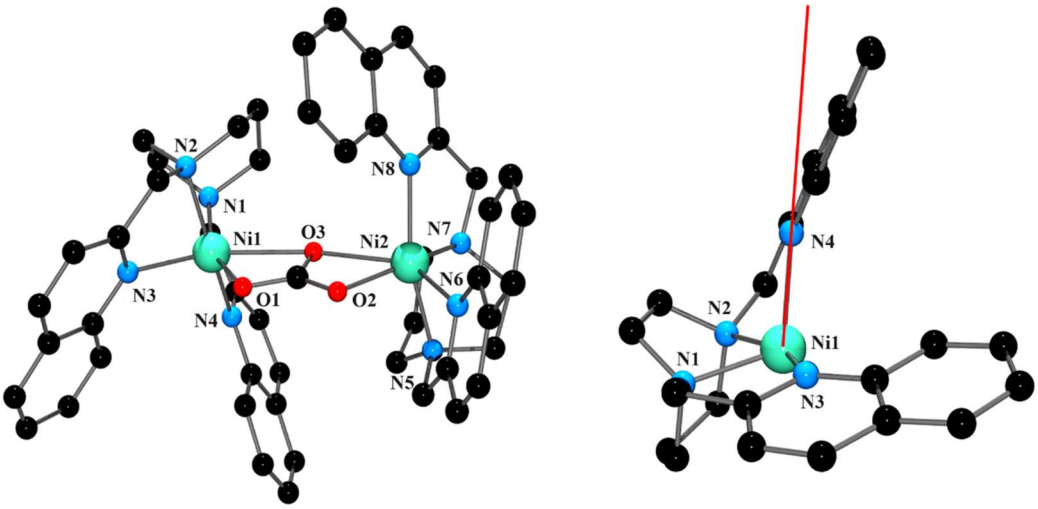


*Figure 38. Structure of the [(**L**Ni)$_2$(μ-CO$_3$)]$^{2+}$cation. H atoms have been omitted for clarity.*

Complexes of **29** with iron, cobalt, cadmium, zinc, and copper have been structurally characterised. The Cd(II) species [Cd(**29**-κ$^3$*N*)$_2$](ClO$_4$)$_2$.2MeOH (*Figure 39*) is an example of a six-coordinate complex that contains two hypodentate ligands bound to one metal ion. Each ligand binds via the tertiary, pyridine and one quinoline nitrogen donor atoms, whilst the second quinoline remains dangling with the N atom situated 3.32 Å from the Cd(II) centre. The complex displays a pseudo-trigonal prismatic geometry, with significant interligand π-π interactions.

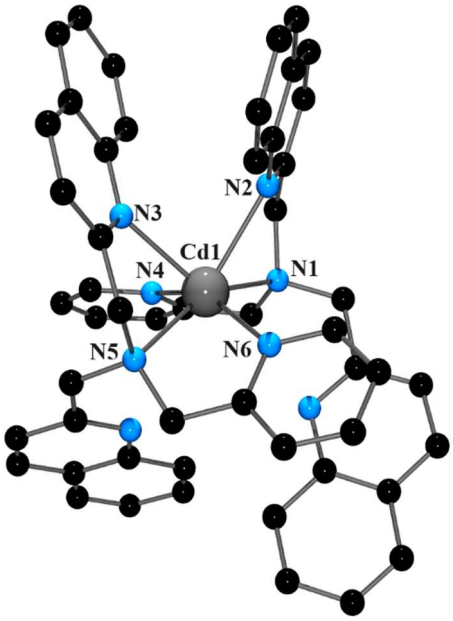


*Figure 39. Structure of the [Cd(**29**)$_2$]$^{2+}$cation. H atoms have been omitted for clarity.*

The six-coordinate Zn(II) complex *cis*-[Zn(**29**)($H_2O$)($ClO_4$)]$ClO_4$.EtOH.$Et_2O$ (*Figure 40*) also contains the ligand **29**. This cation displays a distorted octahedral geometry about the central metal ion afforded by the coordination of all four nitrogen atoms of the ligand, an aqua and perchlorato ligand. According to the authors the perchlorate oxygen interaction with the Zn(II) cation is weak (Zn-O 2.577 Å). Whilst the majority of the reported zinc complexes that contain a coordinated perchlorato ligand have Zn-$O_{perchlorato}$ bond lengths of < 2.4 Å, there are several examples of this bond length being 2.5 Å and greater.[174–180]

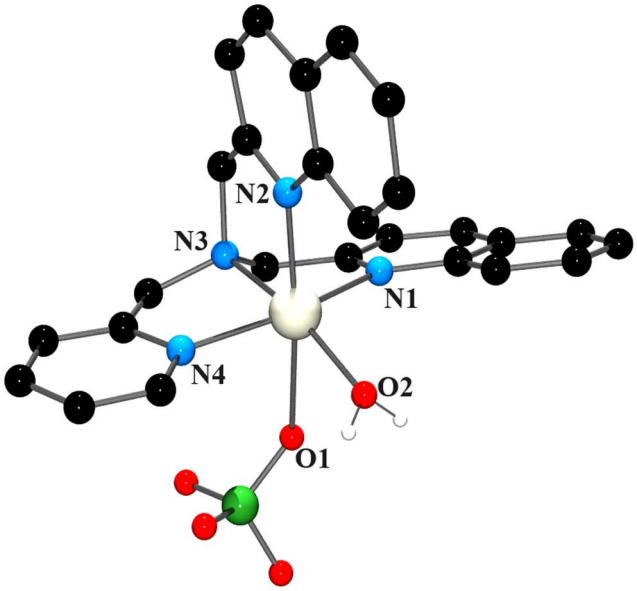


*Figure 40. Structure of the [Zn(**29**)($H_2O$)($ClO_4$)]$^+$cation. H atoms have been omitted for clarity.*

Several five- and six-coordinate metal complexes containing the ligand **30** have been structurally characterised, as have both four-coordinate [Cu(**30**)]$ClO_4$ and eight-coordinate [Pb(**30**)$(NO_3)_2$].$C_2H_5OH$. The [Cu(**30**)]$^+$ cation (*Figure 41*) displays an approximate trigonal pyramidal geometry about the metal ion ($\tau_4 = 0.77$, 0.83), and intermolecular π-π interactions are present (centroid–centroid distances of 3.66 Å).[117]

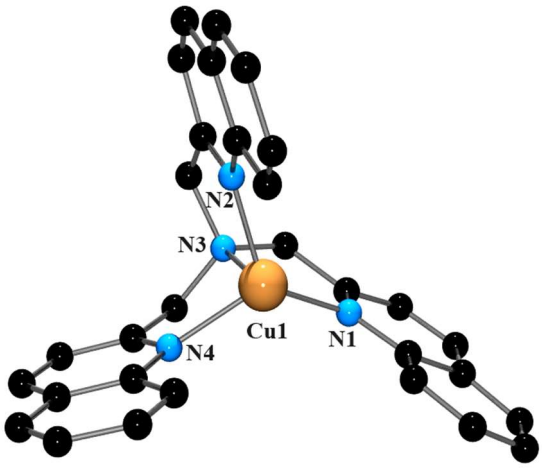


*Figure 41. Structure of the [Cu(**30**)]$^+$ cation. H atoms have been omitted for clarity.*

The Pb(II) complex [Pb(**30**)$(NO_3)_2$].$C_2H_5OH$ (*Figure 42*) has eight coordination sites occupied by four nitrogen donors from the ligand **30** and four oxygen atoms from two

bidentate nitrato ligands, both of which are bound asymmetrically. The structure provides evidence for the presence of a stereochemically active lone pair.[158]

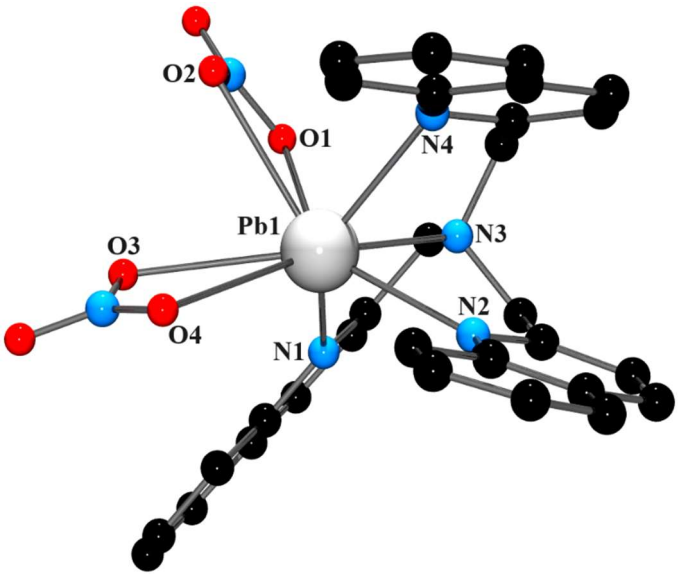


*Figure 42. Structure of the [Pb(**30**)(NO$_2$)$_2$]$^{2+}$cation. H atoms have been omitted for clarity.*

In addition, the Mn(II) complex, *cis*-[Mn(**30**)(NCCH$_3$)(ClO$_4$)]ClO$_4$.CH$_3$CN (*Figure 43*), is another one of the many characterised structures of metal complexes that contain the ligand **30**. Within the asymmetric unit, there are two independent structures that adopt distorted octahedral geometries about the manganese centres. Weak intermolecular offset π-π interactions of 3.663 Å (centroid-centroid) are observed between neighbouring quinolyl moieties. This complex has been prepared in series for the development of manganese catalase models.[163] The study was prompted by the previous work on the oxoiron(IV) complex, [Fe(O)(**30**)(NCCH$_3$)](OTf)$_2$, with the same ligand. The complex demonstrated the ability to oxidise both C-H and C=C bonds making it an excellent model of the oxoiron(IV) unit of the TauD-***J*** enzyme intermediate.[159]

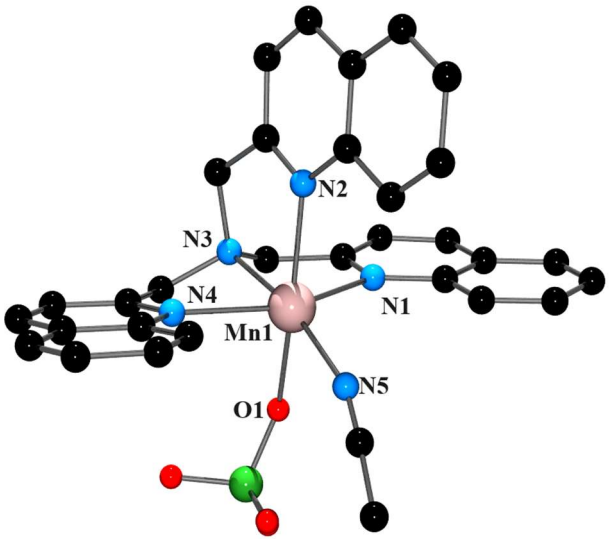


*Figure 43. Structure of the cis-[Mn(**30**)(NCCH$_3$)(ClO$_4$)]$^+$cation. H atoms have been omitted for clarity.*

**Non-tripodal tetra-, penta- and hexadentate quinolyl-containing ligands**

In addition to quinoline-containing tripodal tetradentate ligands, the linear tetradentate tetraamine ligands, **31**[121,181] and **32**[119,120,123,182–187] each of which contain two quinoline moieties (*Figure 44*), have been prepared.

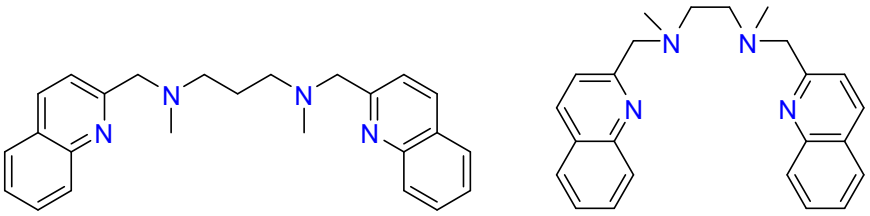


*Figure 44. Structures of the ligands **31** and **32**.*

Only one complex of **31**, the Cu(II) complex *trans*-[Cu(**31**)(ONO$_2$)$_2$] (*Figure 45*), has been structurally characterised. The Cu(II) ion is coordinated to the four nitrogen donor atoms of **31** which exhibits an *mm* configuration, and an oxygen atom of two $NO_3^-$ ligands to give a distorted octahedral geometry. The Cu-O bond lengths of 2.673 Å were thought too long by the authors for coordination of the two nitrate ions, and they described the geometry of the complex as distorted square planar ($\tau_4$ = 0.116). However, Cu-O$_{nitrato}$ bond lengths of > 2.6 Å are not without precedent,[188–194] and a distorted *trans* octahedral geometry appears to be a more appropriate description.

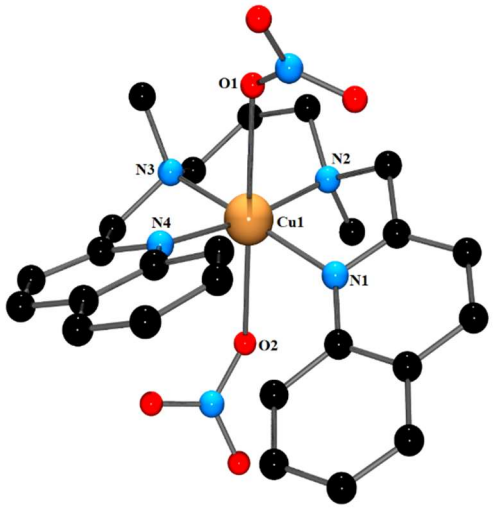


*Figure 45. Structure of the trans-[Cu(**31**)(ONO$_2$)$_2$] complex. H atoms have been omitted for clarity.*

In contrast to the ligand **31**, there are several ligand **32** based metal complexes for which X-ray structural data have been obtained. For example, the six-coordinate complex, *cis*-[Fe(**32**)Cl$_2$].H$_2$O[120] (*Figure 46*), has the tetraamine ligand binding via all four nitrogen donor atoms in an *ff* configuration with the methyl substituents *anti*. Two chlorido ligands occupy the fifth and sixth positions and the Fe(II) ion exhibits a slightly distorted octahedral environment.

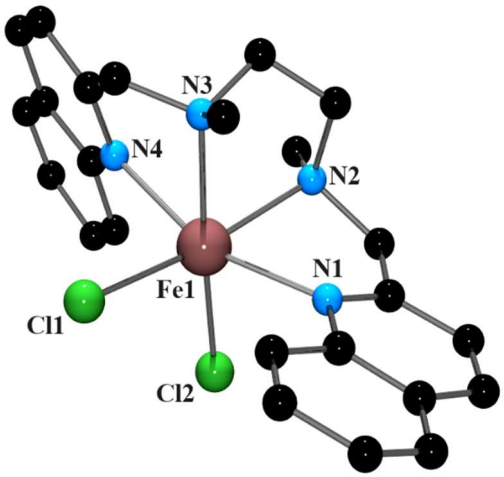


*Figure 46. Structure of the cis-[Fe(**32**)Cl$_2$] complex. H atoms have been omitted for clarity.*

Quinoline-containing multidentate ligands are not restricted to tri- and tetradentate compounds, and several metal complexes of penta- and hexadentate quinoline-containing

ligands have been structurally reported. The ligand **33** exhibits pentacoordination through the five available nitrogen atoms, while **34** and **35** are examples of a hexadentate ligands in which there are six coordinating nitrogen atoms (*Figure 47*). Manganese, iron, copper, and zinc complexes of these three ligands have been structurally characterised.[116,195–202]

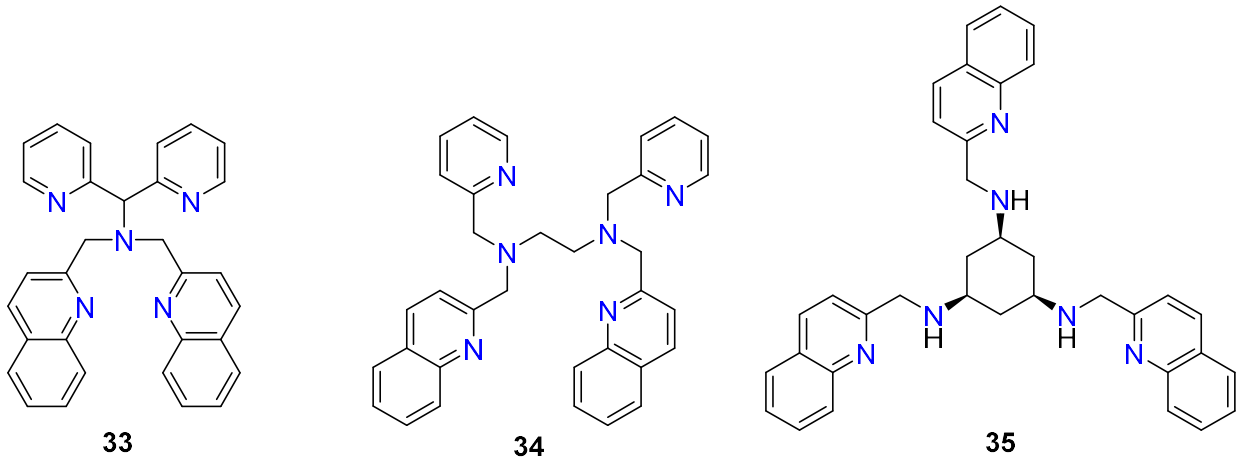


*Figure 47. Structures of the ligands **33**, **34** and **35**.*

Of particular interest amongst these is the iron complex $[Fe(O)(\mathbf{33})](ClO_4)_2.H_2O$, which is a rare example of a crystallographically characterised Fe(IV)-oxo species.[195] The Fe = O bond is, as might be expected, very short, at 1.677 Å, and the oxo ligand is slightly tilted towards the pyridine rings, a structural feature which the authors contend assists the oxidative reactivity of the complex.

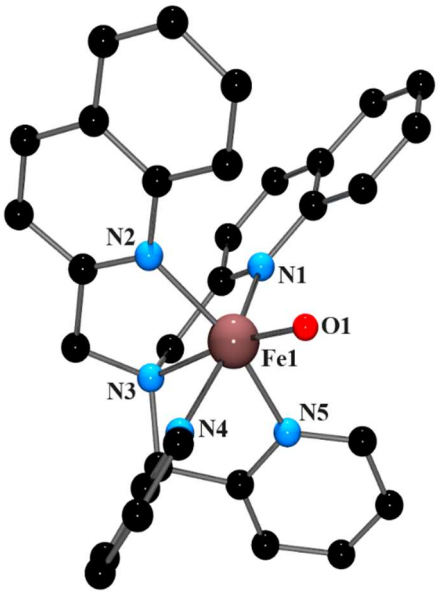


*Figure 48. Structure of the [Fe(**33**)(O)]$^{2+}$ cation. H atoms have been omitted for clarity.*

There is only a single example of a structurally characterised complex of **34**, namely [Zn(**34**)]$(ClO_4)_2.H_2O$ (*Figure 49*). All six nitrogen atoms from the ligand are bound to metal centre affording a distorted octahedral geometry.[197]

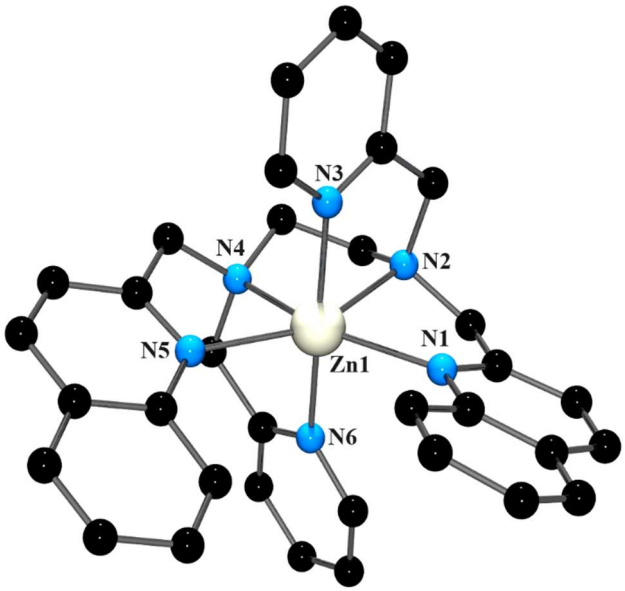


*Figure 49. Structure of the [Zn(**34**)]$^{2+}$ cation. H atoms have been omitted for clarity.*

The ligand **35** also has only one structurally characterised metal complex, [Zn(**35**)]$(ClO_4)_2.H_2O$ (*Figure 50*); the Zn(II) ion is six-coordinate and displays a distorted octahedral geometry. This quinoline-containing species also exhibits bent coordination of the aromatic N atoms with an angle of 149.45° between the Zn-N bond and the plane

of the aromatic ring. In this instance, the bent coordination seemingly indicates substantial chelate ring strain owing to the constrained nature of the ligand. Although it is not unique to quinoline-containing ligands,[203–206] it appears in this case that the steric bulk of the quinoline group is a significant factor in imposing such coordination.[105,170–172,196]

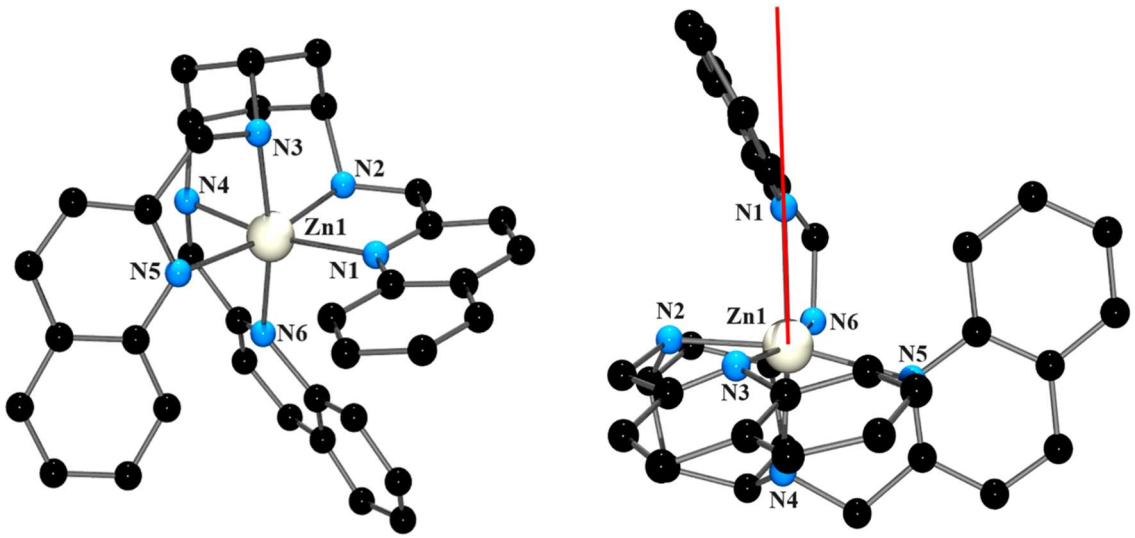


*Figure 50. Structure of the [Zn(**35**)]$^{2+}$ cation. H atoms have been omitted for clarity.*

### 1.3.3 Amine ligands containing 2-quinolylethyl moieties

The literature on 2-quinolylmethyl-containing ligands and resulting coordination chemistry is well established in comparison to the relatively rare 2-quinolylethyl-containing ligands. This appears to be similar to the pyridyl-containing ligands in which there are approximately 8 times the number of pyridylmethyl-containing complexes in comparison to the pyridylethyl-based metal complexes. This difference is also observed for the quinolyl ligands; however, to a much greater extent with only four coordination complexes that contain 2-quinolylethyl-derived ligands that have been structurally characterised. The structural characterisation of the ligands **36**, **37**, and **38** (*Figure 51*) and their corresponding metal complexes have been reported and are discussed below.

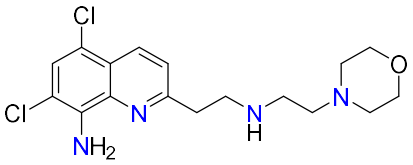


**36**

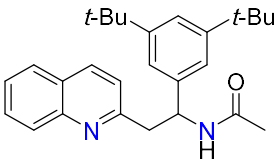


**37**

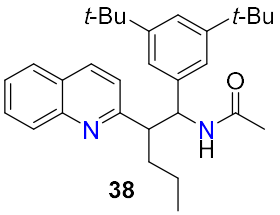


**38**

*Figure 51. Structure of the ligands **36**, **37** and **38**.*

Li *et al.* have reported the structural characterisation of the Cu(II) and Zn(II) metal complexes [Cu(**36**)($OH_2$)Cl]Cl.2$H_2O$ and [Zn(**36**)$Cl_2$]. The two species were isolated during an investigation into the development of chelating ligands to act as potential drug candidates for the treatment of Alzheimer's disease.[207]

The cation [Cu(**36**)($OH_2$)Cl]$^+$ (*Figure 52*) has the Cu(II) metal centre bound by the four nitrogen atoms of the ligand, a chlorido ligand and the oxygen of a water molecule affording a distorted octahedral geometry. Elongation of the Cu-Cl (2.810 Å) and Cu-O (2.730 Å) bonds is observed, a consequence of the Jahn-Teller effect. This feature is consistent with the literature values,[208–210] although these bonds appear to be on the longer side.

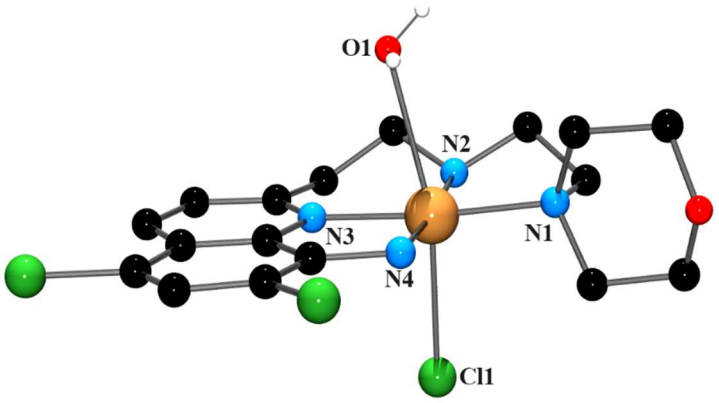


*Figure 52. Structure of the [Cu(**36**)(OH₂)Cl]⁺ cation. H atoms have been omitted for clarity.*

During the UV-vis studies of this complex, the species was found to behave in equilibrium between N3 and N4 chelation of the Cu(II) in solution (*Figure 53*). Whereas, the solid-state analysis of the structure revealed only a N4 chelation of the Cu(II) metal ion.

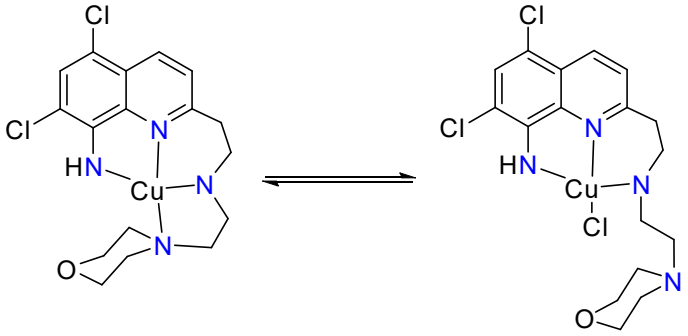


*Figure 53. The possible equilibrium in solution between N4 and N3Cl for the Cu(II) cation [Cu(**36**)(OH₂)Cl]⁺.*

In addition to the Cu(II) complex [Cu(**36**)(OH$_2$)Cl]Cl.2H$_2$O, the authors also reported the structure of the Zn(II) complex, [Zn(**36**)Cl$_2$] (*Figure 54*). In contrast to the Cu(II) complex cation discussed above, [Zn(**36**)Cl$_2$] is a four coordinate species that has the Zn(II) ion bound by the morpholine N atom and the secondary amine nitrogen atom of the ligand and two chlorido ligands. There are two independent structures present in the unit cell with the geometry about the metal centre a distorted tetrahedron ($\tau_4 = 0.88$). Interestingly, in this instance, neither the quinoline nitrogen atom nor the primary amine substituent is coordinated to the Zn(II) metal ion. The bond lengths and angles are consistent with other structurally similar Zn(II) complexes that have been reported.[211–214]

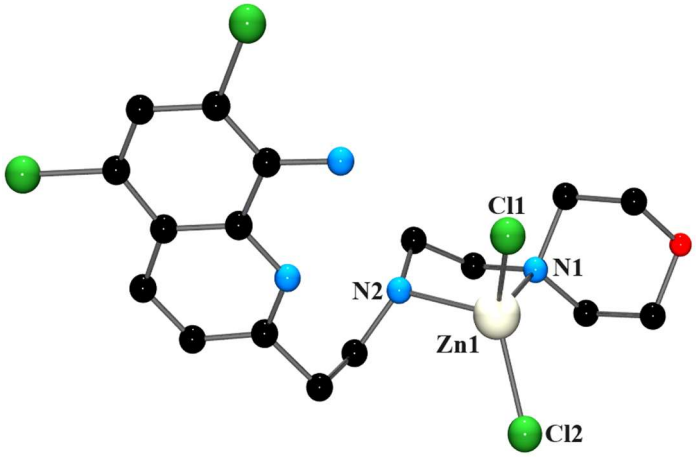


*Figure 54. Structure of the [Zn(**36**)(Cl)$_2$] complex. H atoms have been omitted for clarity.*

Ligands that contain chiral acetyl-protected aminoalkyl quinoline groups have been demonstrated to act as highly efficient enantioselective palladium catalysts for the arylation of methylene C(sp$^3$)-H bonds. The following two Pd(II) metal complexes have been structurally characterised as part of an investigation to further understand the mechanism to which these types of complexes catalyse the arylation reaction.

The reaction between the palladium starting material, [Pd(OAc)$_2$], and the ligands **37** and **38** affords the metal complexes [Pd(**37**)(OAc)]$_2$ and [Pd(**38**)(OAc)]$_2$.C$_6$H$_6$ (*Figure 55*), respectively. Both species exhibit a dimeric amide-bridged bonding motif which displays each Pd(II) centre bound to two nitrogen atoms from the ligand, an acetoxy oxygen atom, and an oxygen from the bridging amide group. The distance between the two Pd(II) metal ions are 3.195 Å and 3.229 Å, respectively. Both distances are in line with the predicted values generated using DFT calculations according to the authors. The two Pd(II) species differ by an ethyl substituent located on the methylene carbon of the quinoline ligand. Despite this structural change, there are no significant distortions in structure between the two complexes.[215]

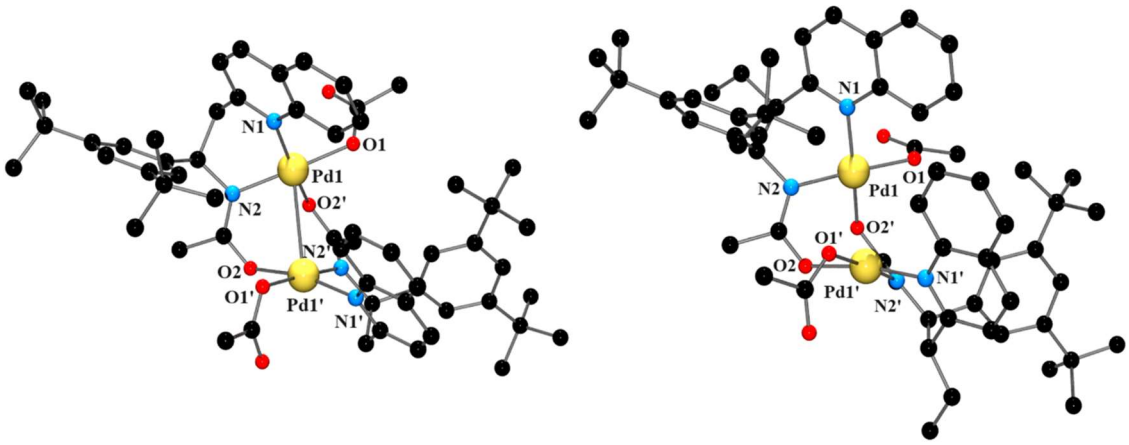


*Figure 55. Structure of the [Pd(**37**)(OAc)]$_2$ (right) and [Pd(**38**)(OAc)]$_2$ (left) complexes. H atoms have been omitted for clarity.*

Interestingly, despite the presence of several metal complexes that contain 2-quinolylethyl derived ligands, there appears to be an absence of simple unsubstituted 2-quinolylethyl-containing compounds presented in the literature. Thus, one of the aims of this thesis was the synthesis and structural characterisation of metal complexes that contain unsubstituted 2-quinolylethyl ligands.

## 1.4 Thesis Overview

The broad objective of this work is to design novel multi-amine ligands and investigate their resulting coordination chemistry. In particular, we are interested in developing the chemistry of tripodal ligands that contain quinoline moieties.

The research presented herein describes the efforts made towards the synthesis of (i) tri- and tetradentate quinoline ligands and their corresponding coordination chemistry and (ii) the synthesis of 1*H*-naphtho[2,3-*d*]imidazole based tripodal ligands and their corresponding coordination chemistry.

Thus far, the chemistry of ligands that contain 2-quinolylethyl and 1*H*-naphtho[2,3-*d*]imidazole motifs has received little attention. Therefore, the chemistry of ligands that contain extended aromatic surfaces is of interest to us. In particular, the extension of the aromatic molecules pyridine and 1,3-benzimidazole is of interest and we have chosen to investigate quinoline and 1*H*-naphtho[2,3-*d*]imidazole for this purpose.

In addition, *Chapter Seven* reports the synthesis and characterisation of several 6-amino-2,3-naphthalimide derivatives. This chapter is separate from the main body of work presented herein and has been completed under the supervision of Dr. Cassandra Fleming.

# *Chapter Two*
# Experimental

*Instrumentation*

All NMR spectra were recorded using a Bruker Ascend 400 NMR spectrometer operating at 400 MHz for $^{1}H$ nuclei and 101 MHz for $^{13}C$ nuclei. Samples were dissolved (0.5 mL) in either deuterated chloroform ($CDCl_3$), deuterated dimethyl sulfoxide (DMSO-$d_6$), or deuterated methanol ($CD_3OD$). The residual solvent peaks specific to that of the deuterated solvents were used as an internal reference; DMSO-$d_6$: 2.50 ppm ($^{1}H$ NMR) and 39.52 ppm ($^{13}C$ NMR), $CD_3OD$: 3.31 ppm ($^{1}H$ NMR) and 49.00 ppm ($^{13}C$ NMR), $CDCl_3$: 7.26 ppm ($^{1}H$ NMR) and 77.16 ppm ($^{13}C$ NMR). All $^{1}H$ NMR spectra are reported as: chemical shift δ (ppm), multiplicity (s = singlet, br = broadened, d = doublet, t = triplet, q = quartet, h = heptet and m = multiplet), *J* (coupling constant in Hz), integral, assignment.

High-resolution mass spectrometry (HRMS) analysis was recorded by Dr. Githal Arachchige on a Thermo Orbitrap Exploris 120 using electrospray ionisation (ESI) in positive mode. All samples were prepared in MeOH at a concentration of less than 1 mg/mL. HRMS data reported as: molecular formula, calculated parent ion (*m/z*), observed parent ion (*m/z*).

Low-resolution mass spectrometry (LRMS) analysis was conducted and recorded on an Agilent 1260 Infinity Quaternary LC System using electrospray ionisation (ESI) in positive mode. All samples were prepared in either MeOH or $CH_3CN$ at a concentration of less than 1 mg/mL. Post-run analyses were done using Qualitative Analysis B.07.00 software. LRMS data reported as: molecular formula, calculated parent ion (*m/z*), observed parent ion (*m/z*).

Absorbance spectra were obtained on a Cary-60 UV-Vis Absorption Spectrometer and samples in $CH_3CN$ were analysed in quartz cuvettes of 1 cm path length.

*Chromatography*

Thin-layer chromatography (TLC) was performed on aluminium backed plates pre-coated (0.25 mm) with Merck Silica Gel 60 F254 or on aluminium backed plates pre-coated (0.2 mm) with Aluminium oxide N with fluorescent indicator $UV_{254}$, with a suitable solvent system. Developed plates were visualised using UV fluorescence (254 nm). Column chromatography was performed using silica gel 60 (70-230 mesh) (Aldrich) or aluminium oxide active basic (70-230 mesh) (LOBA Chemie) and a suitable eluent.

*Reagents*

All chemicals used were of LR or AR grade and were used as received. All syntheses were carried out under aerobic conditions unless stated otherwise.

## 2.1 Experimental: Chapter Three

**Quinoline-2-carbaldehyde (35)**

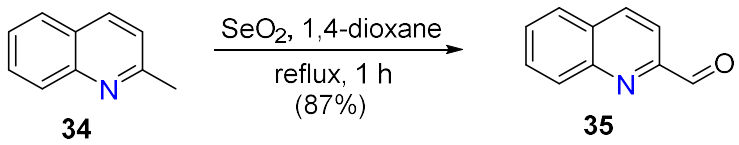


This synthesis was modified from a previously reported procedure.[216] In a 500 mL round bottom flask, a mixture of 2-methylquinoline **34** (5.29 g, 36.9 mmol) and $SeO_2$ (7.41 g, 66.7 mmol) in 1,4-dioxane (150 mL) was refluxed for 1 h. The resulting mixture was filtered, and the solvent removed. The crude residue was triturated with petroleum ether to afford the title compound **35** as a pale brown solid (4.87 g, 87 %); $^1$H NMR (400 MHz, $CDCl_3$) δ 10.23 (d, $J$ = 0.9 Hz, 1H), 8.31 (dt, $J$ = 8.6, 1.0 Hz, 1H), 8.25 (dq, $J$ = 8.5, 0.9 Hz, 1H), 7.91 (dd, $J$ = 8.2, 1.4 Hz, 1H), 7.83 (ddd, $J$ = 8.4, 6.9, 1.5 Hz, 1H), 7.69 (ddd, $J$ = 8.2, 6.9, 1.2 Hz, 1H); $^{13}$C NMR (101 MHz, $CDCl_3$) δ 193.90, 152.75, 148.08, 137.54, 130.64, 130.58, 130.22, 128.01, 117.50; LRMS (ESI, m/z): calculated for $C_{10}H_8NO^+$ $[M + H]^+$ $m/z$ = 158.06; found $m/z$ = 158.0. Data are consistent with the literature.[216]

**2-(Bromomethyl)quinoline (36)**

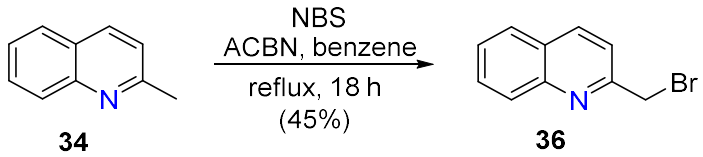


This synthesis was modified from a previously reported procedure.[217] To a solution of 2-methylquinoline **34** (3.07 g, 21.4 mmol) and NBS (4.20 g, 23.6 mmol) in benzene (100 mL) was added ACBN (0.105 g, 0.429 mmol) and the reaction was heated at reflux for 18 h. The resulting solution was washed with saturated $Na_2CO_3$ (2 × 100 mL) and brine (2 × 100 mL), then dried over $MgSO_4$, filtered and the solvent removed (rotavap). Purification by silica gel column chromatography (EtOAc/Hexane 1:1) afforded the title compound **36** (2.15 g, 45%); 1H NMR (400 MHz, CDCl3) δ 8.18 (dd, *J* = 8.5, 0.8 Hz, 1H), 8.07 (dq, *J* = 8.5, 0.9 Hz, $^1$H), 7.82 (dd, *J* = 8.1, 1.5 Hz, 1H), 7.73 (ddd, *J* = 8.5, 6.9, 1.5 Hz, 1H), 7.62 – 7.52 (m, 2H), 4.72 (s, 2H). $^{13}$C NMR (101 MHz, $CDCl_3$) δ 156.75, 147.38, 137.14, 129.80, 129.12, 127.36, 127.18, 126.88, 121.01, 77.16, 76.84, 76.53, 34.22; LRMS (ESI, m/z): calculated for $C_{10}H_9NBr^+$ $[M + H]^+$ *m/z* = 221.99; found *m/z* = 221.9. Data are consistent with the literature.[217]

The compound was converted to the hydrobromide salt by stirring the crude solid in 33% HBr in acetic acid (20 mL) for 5 minutes. The mixture was reduced to dryness (rotavap) and ethanol was added and removed 3 times. Isopropanol (30 mL) was added to the resulting white solid and, following filtration, the solid was washed with isopropanol, diethyl ether and dried in the vacuum desiccator overnight. $^1$H NMR (400 MHz, CDCl3) δ 9.09 (dt, *J* = 8.6, 1.0 Hz, 1H), 8.85 (dd, *J* = 8.7, 0.9 Hz, 1H), 8.17 – 8.07 (m, 2H), 7.96 (d, *J* = 9.0 Hz, 1H), 7.96 – 7.88 (m, 1H), 5.36 (s, 2H). $^{13}$C NMR (101 MHz, $CDCl_3$) δ 154.43, 145.94, 137.92, 135.41, 130.77, 128.21, 128.03, 122.81, 121.87, 77.35, 77.23, 77.03, 76.71, 24.07. Data are consistent with the literature.[217]

***N*-[(*E*)-(quinolin-2-yl)methylidene]hydroxylamine (37)**

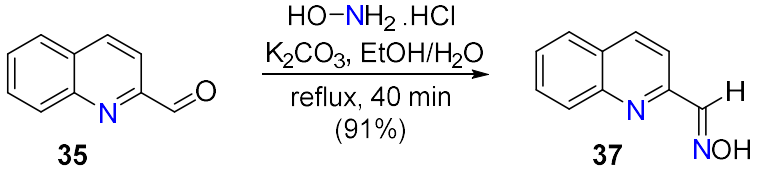

This synthesis was modified from a previously reported procedure.[218] To a solution of quinoline-2-carbaldehyde **35** (0.531 g, 3.37 mmol) in EtOH (15 mL) was added a solution of hydroxylamine hydrochloride (0.235 g, 3.38 mmol) and $K_2CO_3$ (0.541 g, 3.9 mmol) in $H_2O$ (25 mL) and the mixture was heated at reflux for 40 minutes. After cooling to room temperature, the yellow mixture was filtered to remove a white solid and reduced to dryness (rotavap). The crude product **37** was used directly in the next step without further purification (0.532 g, 91%) as a yellow solid; $^1$H NMR (400 MHz, $CDCl_3$) δ 8.45 (d, *J* = 0.6 Hz, 1H), 8.16 (d, *J* = 8.6 Hz, 1H), 8.12 (dq, *J* = 8.5, 0.9 Hz, 1H), 7.96 (d, *J* = 8.6 Hz, 1H), 7.82 (dd, *J* = 8.2, 1.5 Hz, 1H), 7.74 (ddd, *J* = 8.4, 6.9, 1.5 Hz, 1H), 7.57 (ddd, *J* = 8.2, 7.0, 1.2 Hz, 1H); LRMS (ESI, m/z): calculated for $C_{10}H_9N_2O^+$ $[M + H]^+$ *m/z* = 173.07; found *m/z* = 173.1. Data are consistent with the literature.[218]

**2-(Quinolin-2-yl)ethan-1-ol (39)**

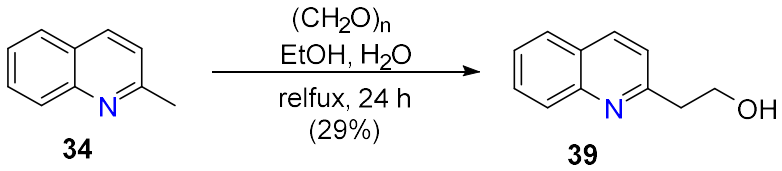


This synthesis was modified from a previously reported procedure.[219] 2-Methylquinoline **34** (4.03 g, 23.1 mmol) and 37% aq. formaldehyde solution (3.4 mL, 41.9 mmol) were dissolved in EtOH (2.5 mL) and $H_2O$ (2.5 mL). The reaction mixture was refluxed for 24 h, and after cooling to room temperature, the reaction was diluted with $H_2O$ (20 ml) and extracted with $CH_2Cl_2$ (3 × 10 mL). The collected organic phases were washed with brine, dried over $Mg_2SO_4$ and, following filtration, the solvent was removed (rotavap). Purification by column chromatography on silica (4% MeOH in $CH_2Cl_2$) afforded the title compound **39** (1.38 g, 29%) as a white solid; $^1$H NMR (400 MHz, $CDCl_3$) δ 8.10 (d, *J* = 8.4 Hz, 1H), 8.00 (d, *J* = 1.1 Hz, 1H), 7.79 (dd, *J* = 8.2, 1.4 Hz, 1H), 7.70 (ddd, *J* = 8.4, 6.9, 1.5 Hz, 1H), 7.51 (ddd, *J* = 8.1, 6.9, 1.2 Hz, 1H), 7.28 (d, *J* = 8.5 Hz, 1H), 4.79 (s, 1H), 4.15 (t, *J* = 5.4 Hz, 2H), 3.24 – 3.17 (m, 2H); $^{13}$C NMR (101 MHz, $CDCl_3$) δ 161.48, 147.29, 136.62, 129.69, 128.79, 127.58, 126.11, 121.86, 76.71, 61.41, 39.21; LSMS (ESI, *m/z*): calculated for $C_{11}H_{12}NO^+$ $[M + H]^+$ *m/z* = 174.09; found 174.0. Data are consistent with the literature.[219]

**2-(Quinoline-2-yl)propane-1,3-diol (40)**

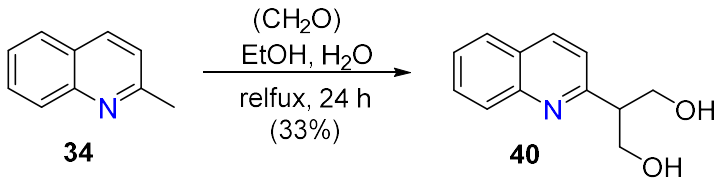


This synthesis was modified from a previously reported procedure.[220] 2-Methylquinoline **34** (4.01 g, 28.0 mmol) and 37% formaldehyde solution (3.4 mL, 41.9 mmol) were dissolved in EtOH (2.5 mL) and $H_2O$ (2.5 mL). The reaction mixture was refluxed for 24 h, and after cooling to room temperature, the reaction was diluted with $H_2O$ (20 ml) and extracted with $CH_2Cl_2$ (3 × 10 mL). The collected organic phases were washed with brine, dried over $Mg_2SO_4$ and, following filtration, the solvent was removed (rotavap). Purification by silica gel column chromatography (4% MeOH in $CH_2Cl_2$) afforded the title compound **40** (1.61 g, 33%); $^1$H NMR (400 MHz, $CDCl_3$) δ 8.15 (dd, *J* = 8.5, 0.9 Hz, 1H), 8.01 (dq, J = 8.5, 0.9 Hz, 1H), 7.81 (dd, J = 8.1, 1.5 Hz, 1H), 7.71 (ddd, *J* = 8.4, 6.9, 1.5 Hz, 1H), 7.53 (ddd, *J* = 8.1, 6.9, 1.2 Hz, 1H), 7.36 (d, *J* = 8.4 Hz, 1H), 4.29 (dd, *J* = 11.1, 4.8 Hz, 2H), 4.16 (dd, *J* = 11.1, 4.4 Hz, 2H), 4.01 (s, 2H), 3.20 (q, *J* = 4.6 Hz, 1H). $^{13}$C NMR (101 MHz, CDCl3) δ 162.62, 147.20, 137.11, 129.97, 129.00, 127.75, 127.20, 126.55, 121.85, 64.40, 49.30. LRMS (ESI, m/z): calculated for $C_{12}H_{14}NO_2^+$ $[M + H]^+$ *m/z* = 204.10; found *m/z* = 204.0. Data are consistent with the literature.[220]

**2-(Chloroethyl)quinoline hydrochloride (41.HCl)**

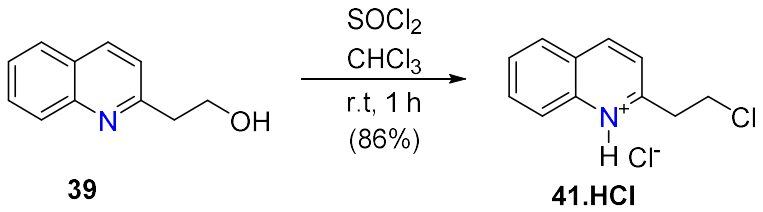


This synthesis was modified from a previously reported procedure.[219] To a round bottom flask containing 2-(quinolin-2-yl)ethan-1-ol **39** (0.588 g, 3.39 mmol) was added anhydrous $CH_2Cl_2$ (16 ml). Repeating this process three times, using a needle connected to the house vacuum and a nitrogen-filled balloon, while stirring the flask was evacuated and nitrogen-filled. $SOCl_2$ (0.54 mL, 7.44 mmol) was added slowly to the flask and the solution turned orange. After stirring at room temperature for 1 h, the solvent was removed (rotavap). To the crude pink residue was added petroleum ether (50 mL) and the

mixture was stirred for 12 h. The cream solid was collected by filtration and dried under vacuum to afford the title compound **41.HCl** (0.553 g, 86%) as a pale brown solid; $^{1}$H NMR (400 MHz, $D_2O$) δ 9.03 (dd, *J* = 8.6, 0.8 Hz, 1H), 8.26 (dt, *J* = 8.3, 1.0 Hz, 1H), 8.22 – 8.08 (m, 2H), 8.01 (d, *J* = 8.6 Hz, 1H), 7.93 (ddd, *J* = 8.2, 6.8, 1.3 Hz, 1H), 4.14 (t, *J* = 6.7, 5.8 Hz, 2H), 3.74 (t, *J* = 6.3 Hz, 2H). $^{13}$C NMR (101 MHz, $D_2O$) δ 156.65, 146.97, 134.89, 129.62, 128.99, 127.73, 122.36, 119.85, 42.09, 36.63. LRMS (ESI, m/z): calculated for $C_{11}H_{11}NCl^+$ $[M + H]^+$ *m/z* = 192.05; found *m/z* = 192.1.

**2-(Quinolin-2-yl)ethyl methanesulfonate (42)**

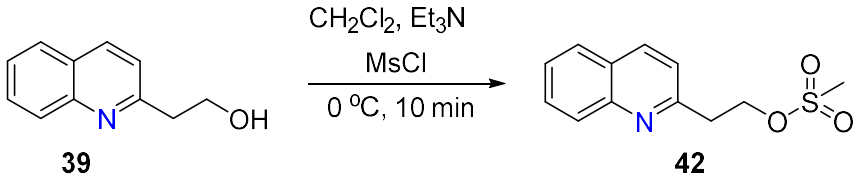


**39** **42**

This synthesis was modified from a previously reported procedure.[221] A solution of 2-(quinolin-2-yl)ethan-1-ol **39** (0.102 g, 0.588 mmol) in anhydrous $CH_2Cl_2$ (4 mL) was cooled to 0 ℃ and to this was added $Et_3N$ (0.25 mL, 1.79 mmol) and $CH_3ClO_2S$ (0.05 mL, 0.704 mmol). After stirring at 0 ℃ for 10 minutes, the reaction mixture was diluted with $CH_2Cl_2$ (20 mL), washed with $H_2O$ (20 mL), brine (5 mL), dried over $Na_2SO_4$, and following filtration, the solvent was removed (rotavap) to afford the title compound **42** as a yellow oil; $^{1}$H NMR (400 MHz, $CDCl_3$) δ 8.12 (d, *J* = 8.4 Hz, 1H), 8.01 (d, *J* = 8.5 Hz, 1H), 7.81 (dd, *J* = 8.2, 1.5 Hz, 1H), 7.72 (ddd, *J* = 8.5, 6.9, 1.5 Hz, 1H), 7.55 – 7.47 (m, 1H), 7.34 (d, *J* = 8.4 Hz, 1H), 4.81 (t, *J* = 6.4 Hz, 2H), 3.42 (t, *J* = 6.5 Hz, 3H), 2.93 (s, 3H). $^{13}$C NMR (101 MHz, $CDCl_3$) δ 157.06, 147.42, 137.40, 130.26, 128.47, 127.85, 127.23, 126.71, 122.11, 68.98, 37.83, 37.38. LRMS (ESI, *m/z*): calculated for $C_{12}H_{14}NO_3S^+$ $[M + H]^+$ *m/z* = 252.06; found *m/z* = 252.1. Data are consistent with the literature.[221]

**2-(Quinolin-2-yl)ethyl-4-methylbenzene-1-sulfonate (43)**

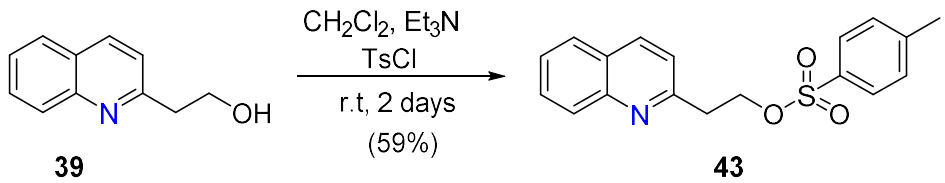


**39** **43**

This synthesis was modified from a previously reported procedure.[222] 2-(Quinolin-2-yl)ethan-1-ol **39** (0.800 g, 4.61 mmol) was dissolved in anhydrous $CH_2Cl_2$ (25 mL). To the solution was added $Et_3N$ (1.3 mL, 9.22 mmol) and then the flask was cooled to 0 ºC, TsCl (1.05 g, 5.53 mmol) was added and the reaction was stirred for 2 days, during which time the solution colour became dark green. The reaction was diluted with $CH_2Cl_2$ (30 mL) and washed with $H_2O$ (20 mL) and brine (10 mL). The organic phase was dried over $Mg_2SO_4$ and following filtration, the solvent was removed (rotavap). The resulting green residue solidified upon standing at room temperature to give a crystalline solid. To this was added petroleum spirits with stirring. The collected petroleum spirits fractions were reduced to dryness (rotavap) to yield an orange residue. To the residue was added additional petroleum spirits and the fine cream precipitate which formed was collected by filtration and air-dried to afford the title compound **43** (0.892 g, 59%); $^1$H NMR (400 MHz, $CDCl_3$) δ 8.06 (d, *J* = 8.4 Hz, 1H), 7.87 (d, *J* = 8.5 Hz, 1H), 7.83 – 7.76 (m, 1H), 7.69 (ddd, *J* = 8.4, 6.7, 1.5 Hz, 1H), 7.63 – 7.58 (m, 2H), 7.52 (ddd, *J* = 7.9, 6.8, 1.1 Hz, 1H), 7.30 – 7.24 (m, 1H), 7.11 (dt, *J* = 7.8, 1.4 Hz, 2H), 4.61 – 4.53 (m, 2H), 3.30 (t, *J* = 6.5 Hz, 2H), 2.33 (d, *J* = 2.1 Hz, 3H). $^{13}$C NMR (101 MHz, $CDCl_3$) δ 157.28, 148.00, 144.64, 136.56, 132.78, 129.71, 129.61, 128.96, 127.89, 127.68, 127.09, 126.30, 122.12, 69.66, 38.09, 21.67. LRMS (ESI, *m/z*): calculated for $C_{18}H_{18}NO_3S^+$ $[M + H]^+$ *m/z* = 328.10; found *m/z* = 328.1. Data are consistent with the literature.[222]

**2-(Bromoethyl)quinoline (44)**

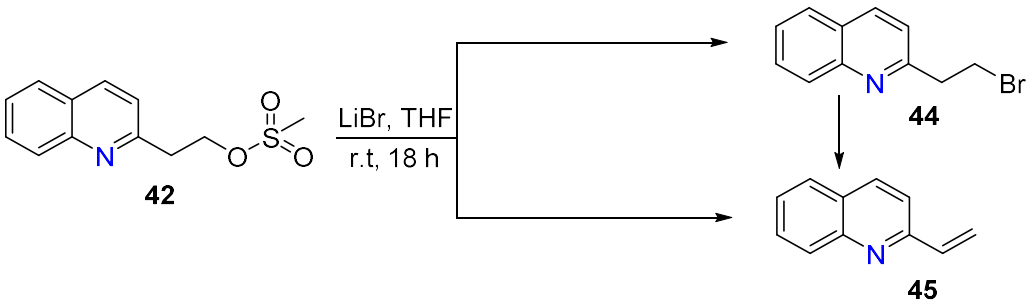


2-(Quinolin-2-yl)ethyl methanesulfonate **42** (0.147, 0.584 mmol) was added to anhydrous THF (4.0 mL) forming a cloudy green mixture. To this was added LiBr (0.203 g, 2.33 mmol) and the reaction mixture became clear and colourless. Over the following 1 h, the solution turned green. The reaction was stirred at room temperature for 18 h. The solvent was removed under reduced pressure without heating. Purification of the crude solid using silica gel column chromatography was attempted by gradient elution starting with

5% EtOAc in $CH_2Cl_2$ + 1% $Et_3N$ and increasing the percentage of EtOAc. However, coelution occurred and attempts at further purification resulted in complete conversion of the material to 2-vinylquinoline. LRMS (ESI, *m/z*): calculated for $C_{11}H_{11}NBr^+$ $[M + H]^+$ *m/z* = 236.00; found *m/z* = 236.0.

**2-Vinylquinoline (45)**

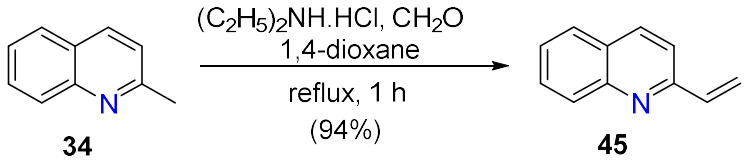


**34** **45**

This synthesis was modified from a previously reported procedure.[223] To a solution of 2-methylquinoline **34** (6.01 g, 41.9 mmol) in 1,4-dioxane (100 mL), was added diethylamine hydrochloride (5.89 g, 54.4 mmol), 37% formaldehyde solution (6.5 mL, 54.5 mmol) and $Et_3N$ (0.88 mL, 6.3 mmol). After stirring at reflux for 1 h, the reaction mixture was cooled to room temperature and the solvent was removed (rotavap). The crude residue was dissolved in $CH_2Cl_2$ (100 mL) and washed with $H_2O$ (100 mL). The organic phase was washed with 10% KOH (2 x 25 mL), $H_2O$ (100 mL), dried over $MgSO_4$ and was reduced to dryness (rotavap) following filtration. Purification by silica gel column chromatography (4% MeOH in $CH_2Cl_2$) afforded the title compound **45** (6.11 g, 94%) as a yellow/brown oil; $^1$H NMR (400 MHz, $CDCl_3$) δ 8.11 (d, *J* = 8.6 Hz, 1H), 8.07 (dd, *J* = 8.5, 0.8 Hz, 1H), 7.78 (dd, *J* = 8.2, 1.5 Hz, 1H), 7.69 (ddd, *J* = 8.4, 6.9, 1.5 Hz, 1H), 7.60 (d, *J* = 8.6 Hz, 1H), 7.50 (ddd, *J* = 8.1, 6.9, 1.2 Hz, 1H), 7.04 (dd, *J* = 17.7, 10.9 Hz, 1H), 6.28 (dd, *J* = 17.7, 0.9 Hz, 1H), 5.67 (dd, *J* = 10.9, 0.9 Hz, 1H). $^{13}$C NMR (101 MHz, $CDCl_3$) δ 156.23, 148.16, 138.13, 136.50, 129.79, 129.52, 127.62, 127.60, 126.46, 119.99, 118.51. LRMS (ESI, m/z): calculated for $C_{11}H_{10}N_1^+$ $[M + H]^+$ *m/z* = 156.08; found *m/z* = 156.1. Data are consistent with the literature.[223]

**2-(2-Azidoethyl)quinoline (47)**

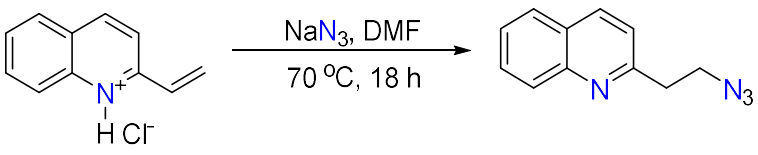


**45.HCl** **47**

A solution of 2-vinylquinoline hydrochloride **45.HCl** (0.220 g, 1.17 mmol) in anhydrous DMF (20 mL) was treated with $NaN_3$ (0.360 g, 5.81 mmol) and the reaction was stirred at 70 ℃ for 18 h. The reaction mixture was cooled to room temperature and $H_2O$ was added (80 mL). The solution was extracted with EtOAc (3 × 100 mL) and washed with $H_2O$ (100 mL) and brine (50 mL). The organic phase was dried over $Mg_2SO_4$, and following filtration, the solvent was removed (rotavap) to afford a 1:1 mixture of 2-(2-azidoethyl)quinoline **47** and 2-vinylquinoline **45** that was used in the following reaction without further purification. Azido: $^1$H NMR (400 MHz, $CDCl_3$) δ 8.12 (d, *J* = 3.8 Hz, 1H), 7.78 (td, *J* = 7.9, 1.5 Hz, 2H), 7.69 (dddd, *J* = 8.4, 6.4, 4.7, 1.5 Hz, 2H), 7.60 (d, *J* = 8.6 Hz, 1H), 7.50 (dddd, *J* = 8.2, 6.8, 5.4, 1.2 Hz, 2H), 7.32 (d, *J* = 8.4 Hz, 1H), 3.84 (t, *J* = 6.9 Hz, 2H), 3.25 (t, *J* = 6.9 Hz, 2H).$^{13}$C NMR (101 MHz, $CDCl_3$) δ 161.47, 147.28, 136.60, 129.68, 128.78, 127.57, 126.09, 121.85, 61.40, 39.20; LRMS (ESI, *m/z*): calculated for $C_{11}H_{11}N_4^+$ $[M + H]^+$ *m/z* = 199.0; found *m/z* = 199.0.

**Click product (49)**

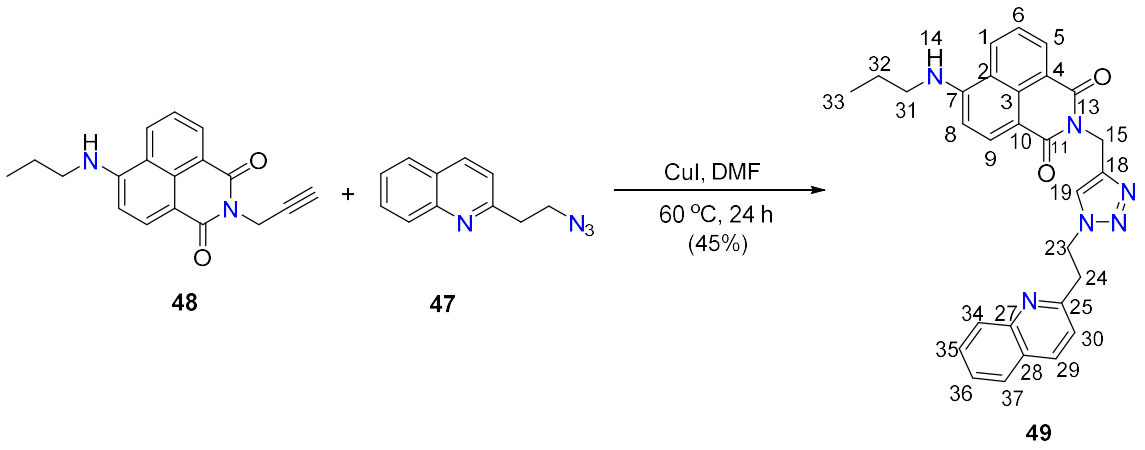


**48** **47** **49**

A mixture of 2-vinylquinoline **45**/2-(2-azidoethyl)quinoline **47** (previously synthesised) (0.098 g) and **48** (0.101 g, 0.322 mmol) were dissolved in anhydrous DMF (10 mL), CuI (0.049 g, 0.257 mmol) was added to the solution. The flask was flushed with $N_2$ and the reaction was stirred at 60 ℃ for 24 h. After cooling to room temperature, the reaction was filtered to remove the brown insoluble solid, and then the solvent was removed (rotavap). Purification by silica gel column chromatography (4% MeOH in $CH_2Cl_2$) afforded the title compound **49** (74 mg, 45%) as an orange solid. H NMR (400 MHz, $CDCl_3$) δ 8.27 (dd, *J* = 11.4, 7.8 Hz, 2H, H-1, H-29), 8.04 – 7.92 (m, 3H, H-5, H-9, H-34), 7.70 – 7.63 (m, 2H, H-35, H-37), 7.61 (s, 1H, H-19), 7.46 (ddd, *J* = 8.2, 7.0, 1.2 Hz, 1H, H-36), 7.30 – 7.21 (m, 1H, H-6), 7.10 (d, *J* = 8.4 Hz, 1H, H-30), 6.57 (d, *J* = 8.5 Hz, 1H, H-8), 5.90

(t, $J$ = 5.2 Hz, 1H, H-14), 5.39 (s, 2H, H-15), 4.91 (t, $J$ = 7.0 Hz, 2H, H-23), 3.55 (t, $J$ = 7.0 Hz, 2H, H-24), 3.33 (td, $J$ = 7.3, 5.1 Hz, 2H, H-31), 1.81 (h, $J$ = 7.3 Hz, 2H, H-32), 1.07 (t, $J$ = 7.4 Hz, 4H, H-33). $^{13}$C NMR (101 MHz, $CDCl_3$) δ 164.38 (C-13), 163.75 (C-11), 157.55 (C-25), 150.23 (C-27), 147.94 (C-7), 136.81 (C-5, C-9), 134.71 (C-29), 131.08 (C-1), 129.78 (C-35, C-37), 129.73 (C-18), 129.16 (C-3), 128.94 (C-34), 128.35 (C-28), 127.67 (C-35, C-37), 127.07 (C-4), 126.61 (C-5, C-9), 126.34 (C-36), 125.42 (C-10), 124.36 (C-6), 124.05 (C-19), 122.43 (C-2), 120.13 (C-30), 104.18 (C-8), 49.17 (C-23), 45.58 (C-31), 38.97 (C-24), 34.94 (C-15), 22.18 (C-32), 11.84 (C-33). HRMS (ESI, *m/z*): calculated for $C_{29}H_{26}N_6O_2Na^+$ $[M + Na]^+$ *m/z* = 513.20095; found 513.2006.

**Click product (50)**

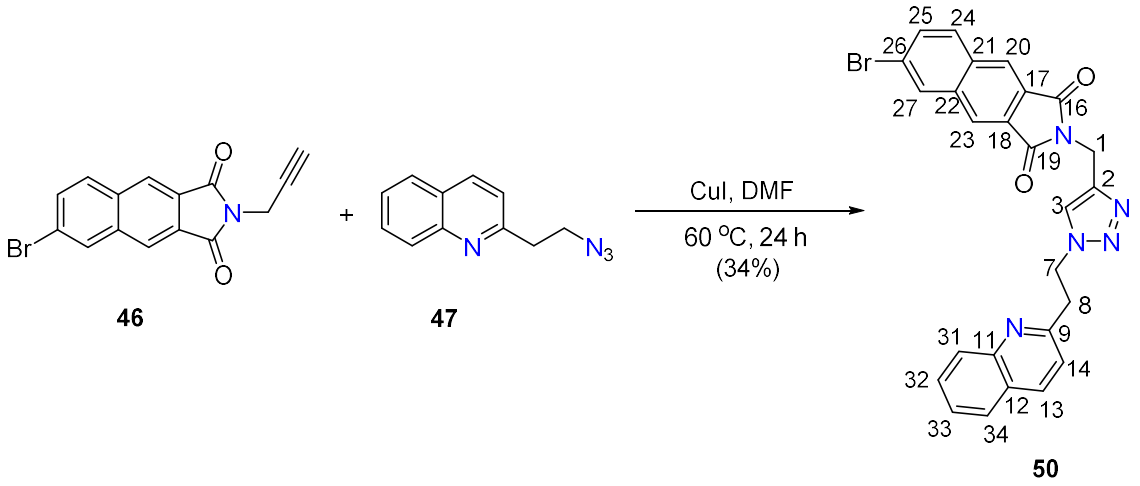


A mixture of 2-vinylquinoline **45**/2-(2-azidoethyl)quinoline **47** (previously synthesised) and **46** (0.151 g, 0.516 mmol) were dissolved in anhydrous DMF (10 mL), CuI (0.079 g, 0.414 mmol) was added to the solution. The flask was flushed with $N_2$ and the reaction was stirred at 60 ℃ for 24 h. After cooling to room temperature, the reaction was filtered to remove the brown insoluble solid, and then the solvent was removed (rotavap). Purification by silica gel column chromatography (4% MeOH in $CH_2Cl_2$) afforded the title compound **50** (87 mg, 34%) as a white solid. $^1$H NMR (400 MHz, $CDCl_3$) δ 8.25 (s, 1H, H-20), 8.21 – 8.16 (m, 2H, H-23, H-24), 8.06 – 7.96 (m, 2H, H-13, H-31), 7.89 (d, $J$ = 8.8 Hz, 1H, H-27), 7.76 (dd, $J$ = 8.7, 1.9 Hz, 1H, H-25), 7.71 (dd, $J$ = 8.2, 1.4 Hz, 1H, H-34), 7.66 (ddd, $J$ = 8.5, 6.9, 1.5 Hz, 1H, H-32), 7.59 (s, 1H, H-3), 7.45 (ddd, $J$ = 8.1, 6.9, 1.2 Hz, 1H, H-33), 7.12 (d, $J$ = 8.4 Hz, 1H, H-14), 4.98 (s, 2H, H-1), 4.94 (t, $J$ = 7.0 Hz, 2H, H-7), 3.56 (t, $J$ = 7.0 Hz, 2H, H-8). $^{13}$C NMR (101 MHz, $CDCl_3$) δ 166.99 (C-

19), 166.93 (C-16), 157.44 (C-9), 147.93 (C-11), 142.32 (C-2), 136.84 (C-13), 136.54 (C-22), 133.96 (C-21), 132.79 (C-25), 132.41 (C-24), 131.69 (C-27), 129.81 (C-32), 128.95 (C-31), 128.87 (C-18), 128.14 (C-17), 127.72 (C-34), 127.09 (C-12), 126.38 (C-33), 124.87 (C-20), 123.92 (C-26), 123.87 (C-3), 123.85 (C-23), 121.8 (C-14)1, 49.10 (C-7), 38.90 (C-8), 33.47 (C-1). HRMS (ESI, *m/z*): calculated for $C_{26}H_{18}BrN_5O_2Na^+$ [M + Na]$^+$ *m/z* = 534.05361; found 534.0535.

**2-(2-Azidoethyl)pyridine (52)**

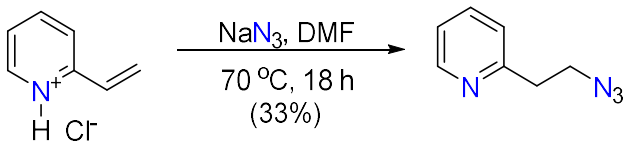


**51.HCl** **52**

A solution of 2-vinylpyridine hydrochloride **51.HCl** (1.137 g, 8.113 mmol) in anhydrous DMF (20 mL) was treated with $NaN_3$ (2.5130 g, 40.565 mmol) and the reaction was stirred at 70 ℃ for 18 h. The reaction mixture was cooled to room temperature and $H_2O$ was added (80 mL). The solution was extracted with EtOAc (3 × 100 mL) and washed with $H_2O$ (100 mL) and brine (50 mL). The organic phase was dried over $Mg_2SO_4$, and following filtration, the solvent was removed (rotavap). The crude residue was washed with saturated $NaHSO_3$ (100 mL), dried over $Mg_2SO_4$, and following filtration, the solvent was removed (rotavap) to afford the title compound **52** (0.401 g, 33%). $^1$H NMR (400 MHz, $CDCl_3$) δ 8.56 (ddt, *J* = 4.9, 1.8, 0.9 Hz, 1H), 7.62 (tdd, *J* = 7.6, 1.9, 0.8 Hz, 1H), 7.29 – 7.11 (m, 3H), 3.71 (t, *J* = 6.9 Hz, 2H), 3.06 (t, *J* = 6.9 Hz, 2H). LRMS (ESI, *m/z*): calculated for $C_7H_9N_4^+$ [M + H]$^+$ *m/z* = 149.08; found *m/z* = 149.0. Data are consistent with the literature.[224]

**Click product (53)**

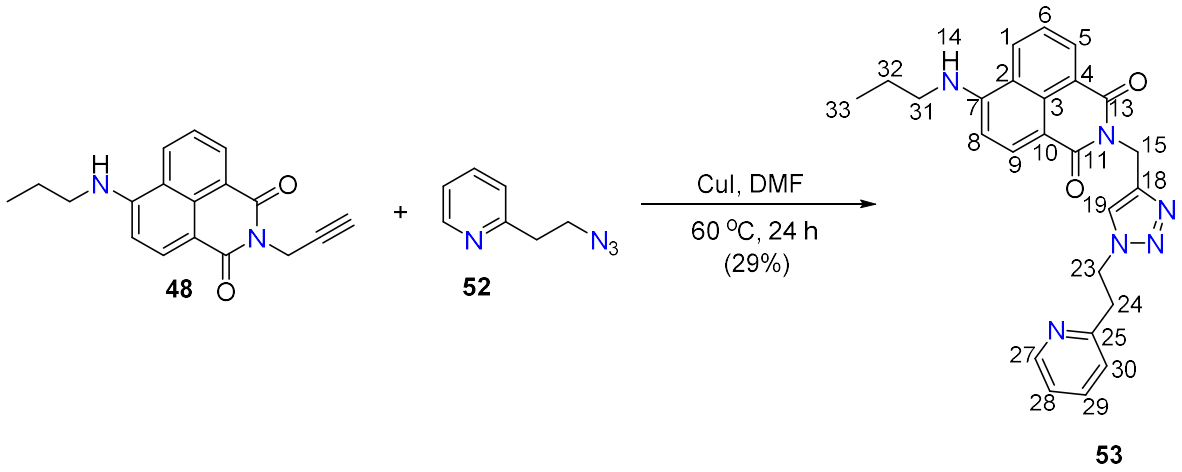


48 52 53

2-(2-Azidoethyl)pyridine **52** (0.349 g, 2.35 mmol) and 6-(propylamino)-2-(prop-2-yn-1-yl)-1*H*-benzo[*de*]isoquinoline-1,3(2*H*)-dione **48** (0.690 g, 2.36 mmol) were dissolved in anhydrous DMF (20 mL), CuI (0.359 g, 1.88 mmol) was added to the solution. The flask was flushed with $N_2$ and the reaction was stirred at 60 ℃ for 24 h. After cooling to room temperature, the reaction was filtered to remove the brown insoluble solid, and then the solvent was removed (rotavap). Purification by silica gel column chromatography (4% MeOH in $CH_2Cl_2$) afforded the title compound **53** (0.300 g, 29%) as a white solid; $^1$H NMR (400 MHz, $CDCl_3$) δ 8.52 (ddd, *J* = 4.9, 1.9, 0.9 Hz, 1H, H-27), 8.43 – 8.31 (m, 2H, H-1, H-9), 8.04 – 7.97 (m, 1H, H-5), 7.46 (td, *J* = 7.7, 1.9 Hz, 1H, H-29), 7.45 (s, 1H, H-19), 7.38 (dd, *J* = 8.4, 7.3 Hz, 1H, H-6), 7.05 (ddd, *J* = 7.6, 4.9, 1.2 Hz, 1H, H-28), 6.96 (dt, *J* = 7.8, 1.1 Hz, 1H, H-30), 6.63 (d, *J* = 8.5 Hz, 1H, H-8), 5.75 (t, *J* = 5.1 Hz, 1H, H-14), 5.40 (s, 2H, H-15), 4.76 (t, *J* = 7.1 Hz, 2H, H-23), 3.34 (t, *J* = 7.0 Hz, 4H, H-24, H-31), 1.82 (h, *J* = 7.4 Hz, 2H, H-32), 1.09 (t, *J* = 7.4 Hz, 3H, H-33). $^{13}$C NMR (101 MHz, $CDCl_3$) δ 164.42 (C-11), 163.78 (C-13), 157.10 (C-25), 150.13 (C-27), 149.69 (C-18), 144.08 (C-29), 136.76 (C-29), 134.78 (C-1), 131.22 (C-9), 129.84 (C-3), 126.46 (C-5), 124.51 (C-6), 123.84 (C-30), 123.74 (C-4), 122.68 (C-2), 122.08 (C-28), 120.19 (C-10), 104.29 (C-8), 49.55 (C-23), 45.61 (C-31), 38.62 (C-24), 34.94 (C-15), 22.24 (C-32), 11.84 (C-33). HRMS (ESI, *m/z*): calculated for $C_{25}H_{24}N_6O_2Na^+$ $[M + Na]^+$ *m/z* = 463.18530; *m/z* = found 463.1850.

**Ligand (55)**

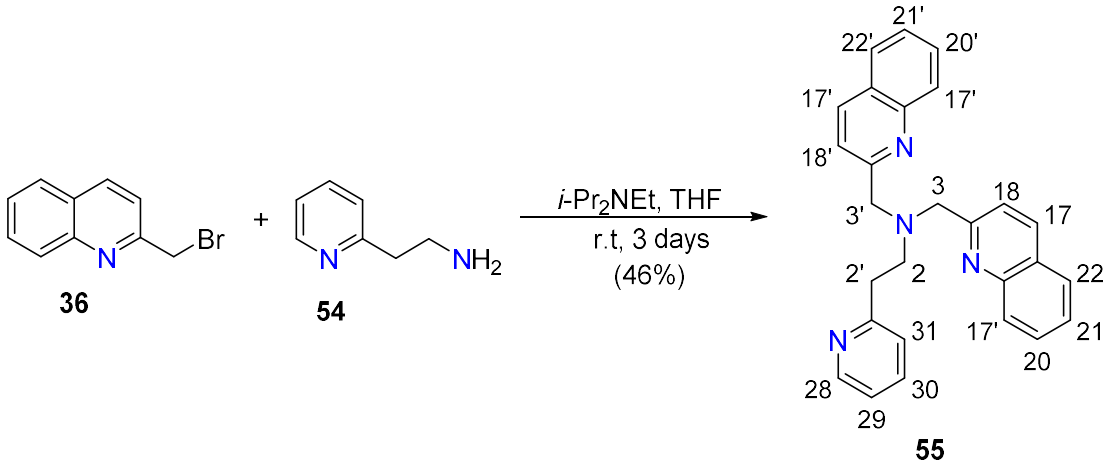


To a solution of 2-(bromomethyl)quinoline **36** (1.13 g, 5.11 mmol) in THF (20 mL), was added *i*-Pr$_2$NEt (1.7 mL, 10.2 mmol) followed by the addition of 2-(pyridin-2-yl)ethan-1-amine **54** (0.312 g, 2.56 mmol). After stirring at room temperature for 3 days, the reaction mixture was filtered through Celite and the solvent removed (rotavap). The crude residue was dissolved in $CH_2Cl_2$ (100 mL) and washed with 1 M NaOH (50 mL), $H_2O$ (100 mL), dried over $MgSO_4$ and concentrated (rotavap). Purification by column chromatography on alumina (10% MeOH in $CH_2Cl_2$ + 1% $NH_4OH$) afforded the title compound **55** (0.951 g, 46%) as a yellow/brown solid; $^1$H NMR (400 MHz, $CDCl_3$) δ 8.46 – 8.39 (m, 1H, H-28), 8.04 (d, *J* = 8.4 Hz, 4H, H-17), 7.76 (dd, *J* = 8.2, 1.6 Hz, 2H, H-22), 7.67 (ddd, *J* = 8.4, 6.8, 1.5 Hz, 2H, H-20), 7.53 (dd, *J* = 8.5, 1.5 Hz, 2H, H-18), 7.51 – 7.45 (m, 3H, H-21,29), 7.08 (ddd, *J* = 7.6, 4.9, 1.2 Hz, 1H, H-29), 7.05 (dt, *J* = 7.8, 1.1 Hz, 1H, H-31), 4.08 (s, *J* = 1.4 Hz, 4H, H-3), 3.08 (s, *J* = 2.2 Hz, 4H, H-2). $^{13}$C NMR (101 MHz, $CDCl_3$) δ 160.52, 160.45, 149.06, 147.55, 136.40, 136.34, 129.46, 129.03, 127.56, 127.45, 126.22, 123.48, 121.23, 121.14, 61.16, 54.78, 35.90. (HRMS) (ESI, m/z): calculated for $C_{27}H_{25}N_4^+$ $[M + H]^+$ *m/z* = 405.2070; found 405.2076.

**Ligand (57)**

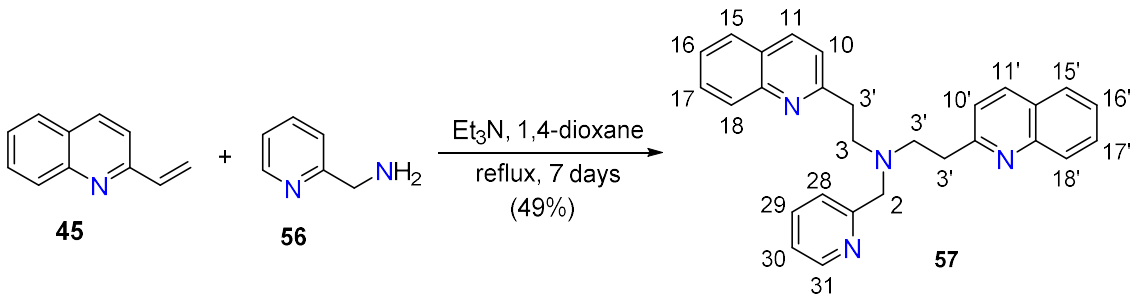

To a stirred solution of 1-(pyridin-2-yl)methanamine **56** (0.802 g, 7.41 mmol) in 1,4-dioxane (100 mL), was added 2-vinylquinoline **45** (2.30 g, 14.8 mmol) and $Et_3N$ (2.3 mL, 16.3 mmol). After stirring at reflux for 7 days, the reaction mixture was cooled to room temperature and 10% KOH solution (50 mL) was added. The mixture was extracted with $CH_2Cl_2$ (3 × 50 mL) and the collected organic fractions were washed with $H_2O$ (100 mL), dried over $MgSO_4$ and concentrated (rotavap) following filtration. Purification by column chromatography on alumina (4% MeOH in $CH_2Cl_2$) afforded the title compound **57** (1.52g, 49 %) as a brown oil; $^1$H NMR (400 MHz, $CDCl_3$) δ 8.44 (ddd, *J* = 4.9, 1.8, 0.9 Hz, 1H, H-31), 7.98 (dq, *J* = 8.5, 0.8 Hz, 2H, H-11), 7.83 (dd, *J* = 8.4, 0.8 Hz, 2H, H-18), 7.73 (dd, *J* = 8.2, 1.4 Hz, 2H, H-15), 7.66 (ddd, *J* = 8.5, 6.9, 1.5 Hz, 2H, H-17), 7.47 (ddd, *J* = 8.1, 6.9, 1.2 Hz, 2H, H-16), 7.18 (td, *J* = 7.6, 1.8 Hz, 1H, H-30), 7.08 (d, *J* = 8.4 Hz, 2H, H-10), 6.99 (ddd, *J* = 7.5, 4.9, 1.2 Hz, 1H, H-29), 6.95 (dt, *J* = 7.8, 1.1 Hz, 1H, H-28), 3.91 (s, 2H, H-2), 3.21 – 3.06 (m, 8H, H-3). $^{13}$C NMR (101 MHz, $CDCl_3$) δ 161.33, 160.14, 148.74, 147.97, 136.19, 135.94, 129.39, 128.90, 127.56, 126.85, 125.81, 122.98, 122.06, 121.81, 60.37, 54.19, 36.89. (HRMS) (ESI, m/z): calculated for $C_{28}H_{27}N_4^+$ $[M + H]^+$ *m/z* = 419.22302; *m/z* = found 419.2228.

**Ligand (58)**

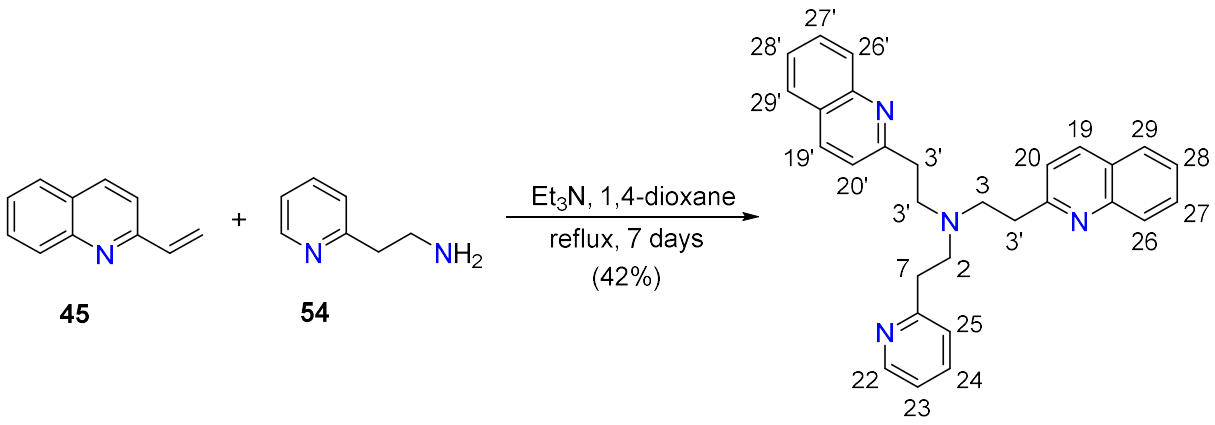


**45** **54** **58**

To a stirred solution of 2-(pyridin-2-yl)ethan-1-amine **54** (1.40 g, 11.4 mmol) in 1,4-dioxane (100 mL), was added 2-vinylquinoline **45** (2.13 g, 13.7 mmol) and $Et_3N$ (3.2 mL, 22.8 mmol). After stirring at reflux for 7 days, the reaction mixture was cooled to room temperature and the solvent was removed (rotavap). The crude residue was dissolved in $CH_2Cl_2$ (100 mL) and washed with $H_2O$ (150 mL). The organic phase was washed with 10% KOH (2 × 20 mL), $H_2O$ (100 mL), dried over $MgSO_4$ and concentrated (rotavap).

Purification by alumina column chromatography (4% MeOH in $CH_2Cl_2$) afforded the title compound **58** (2.06 g, 42%) as a brown oil; $^1$H NMR (400 MHz, $CDCl_3$) δ 8.49 (ddd, *J* = 4.9, 1.9, 0.9 Hz, 1H, H-22, 8.03 (dq, *J* = 8.5, 0.8 Hz, 2H, 26), 7.85 (dd, *J* = 8.4, 0.8 Hz, 2H, H-19), 7.73 (dd, *J* = 7.9, 1.4 Hz, 2H, H-29), 7.67 (ddd, *J* = 8.4, 6.9, 1.5 Hz, 2H, H-27), 7.48 (ddd, *J* = 8.1, 6.9, 1.2 Hz, 2H, H-28), 7.35 (td, *J* = 7.7, 1.9 Hz, 1H, H-24), 7.07 (d, *J* = 8.4 Hz, 2H, H-20), 7.03 (ddd, *J* = 7.6, 4.9, 1.2 Hz, 1H, H-23), 6.90 (dt, *J* = 7.8, 1.1 Hz, 1H, H-25), 3.11 (d, *J* = 1.7 Hz, 8H, H-3), 3.07 – 2.99 (m, 2H, H-2), 2.95 – 2.87 (m, 2H, H-7). $^{13}$C NMR (101 MHz, $CDCl_3$) δ 161.55, 160.77, 149.23, 148.01, 136.16, 135.98, 129.42, 128.92, 127.59, 126.89, 125.81, 123.59, 122.12, 121.11, 54.00, 53.92, 36.99, 36.19. (HRMS) (ESI, m/z): calculated for $C_{29}H_{29}N_4^+$ $[M + H]^+$ *m/z* = 433.23867; *m/z* = found 433.2384.

**1-(Pyridin-2-yl)-*N*-[(pyridin-2-yl)methyl]methanamine (60)**

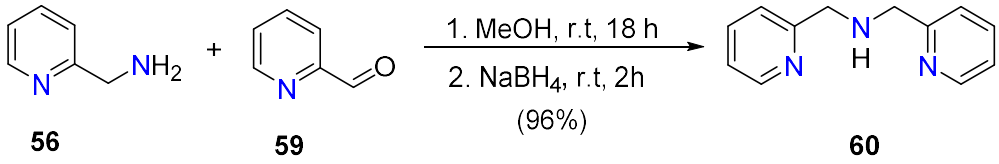


**56** **59** **60**

This synthesis was based on a previously reported procedure.[225] To a stirring solution of 1-(pyridin-2-yl)methanamine **56** (1.01 g, 9.33 mmol) in MeOH (25 mL), was added pyridine-2-carbaldehyde **59** (0.994 g, 9.28 mmol). After stirring at room temperature for 18 h, $NaBH_4$ (0.699 g, 18.4 mmol) was added slowly and stirring was continued for 2 h. The solvent was removed (rotavap) and $H_2O$ (20 mL) was added to the crude brown residue. This was neutralised with concentrated HCl (32%) and extracted with $CH_2Cl_2$ (2 × 50 mL). The combined organic phases were dried over $MgSO_4$ and, following filtration, were concentrated (rotavap) to afford the title compound **60** (1.79 g, 96%) as a brown oil; $^1$H NMR (400 MHz, $CDCl_3$) δ 8.54 (ddd, *J* = 4.9, 1.9, 1.0 Hz, 2H), 7.62 (td, *J* = 7.6, 1.7 Hz, 2H), 7.34 (dt, *J* = 7.8, 1.0 Hz, 2H), 7.13 (ddd, *J* = 7.5, 5.0, 1.3 Hz, 2H), 3.96 (s, 4H). $^{13}$C NMR (101 MHz, $CDCl_3$) δ 159.64, 149.42, 136.63, 122.46, 122.12, 54.81. LRMS (ESI, *m/z*): calculated for $C_{12}H_{14}N_3$ $[M + H]^+$ 200.11; found 200.1. Data are consistent with the literature.[225]

**2-(Pyridin-2-yl)-*N*-[2-pyridin-2-yl)ethyl]ethan-1-amine (62)**

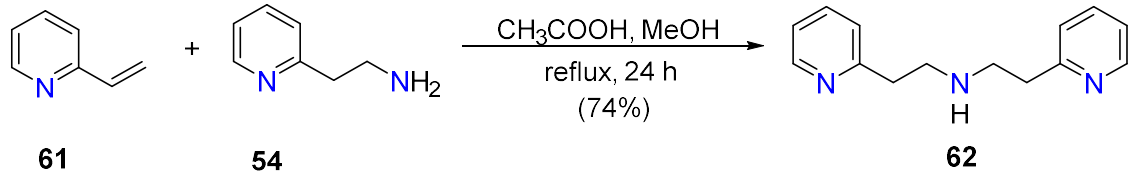


61 54 62

This synthesis was based on a previously reported procedure.[226] To a stirred solution of 2-vinylpyridine **61** (0.531 g, 5.05 mmol) in MeOH (20 mL), was added 2-(pyridin-2-yl)ethan-1-amine **54** (0.617 g, 5.05 mmol) and acetic acid (0.30 mL). After stirring at reflux for 24 hours, the reaction mixture was cooled to room temperature and diluted with $CH_2Cl_2$ (50 mL). The organic phase was washed with $H_2O$ (50 mL), 10% KOH solution (20 mL), dried over $MgSO_4$ and concentrated (rotavap) following filtration. Purification by column chromatography on alumina (4% MeOH in $CH_2Cl_2$) afforded the title compound **62** (0.847 g, 74%) as a brown oil; $^1$H NMR (400 MHz, $CDCl_3$) δ 8.47 – 8.41 (m, 2H), 7.54 (t, *J* = 7.7, 1.7 Hz, 2H), 7.12 (dd, *J* = 7.8, 1.4 Hz, 2H), 7.08 (ddd, *J* = 8.0, 3.8, 2.6 Hz, 2H), 3.08 – 2.99 (m, 4H), 2.96 (dd, *J* = 7.9, 5.8 Hz, 4H). $^{13}$C NMR (101 MHz, $CDCl_3$) δ 160.11, 149.29, 136.50, 123.42, 121.35, 49.14, 38.06, 38.04. LRMS (ESI, *m/z*): calculated for $C_{14}H_{18}N_3^+$ $[M + H]^+$ *m/z* = 228.15; found *m/z* = 228.1. Data are consistent with the literature.[226]

**Ligand (63)**

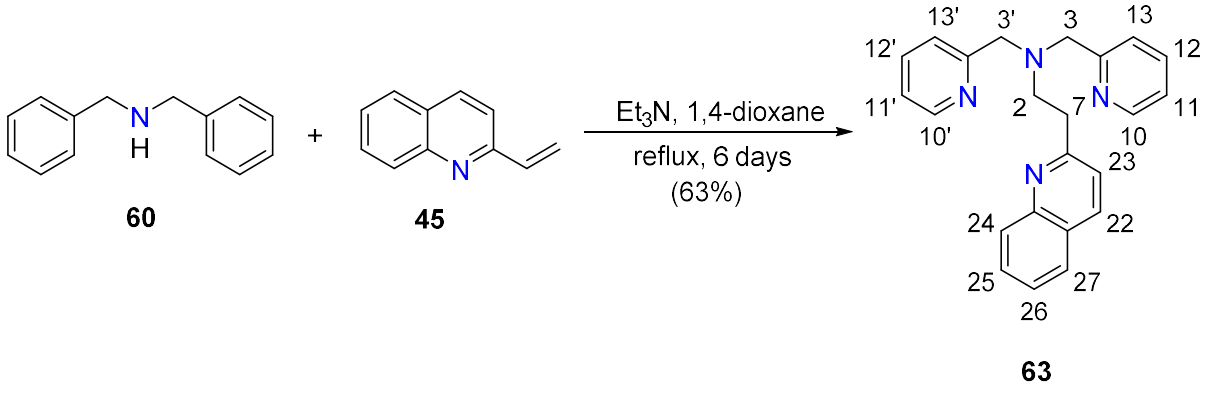


60 45 63

To a stirred solution of 1-(pyridin-2-yl)-*N*-[(pyridin-2-yl)methyl]methanamine **60** (0.501 g, 2.51 mmol) in 1,4-dioxane (50 mL), was added 2-vinylquinoline **45** (0.426 g, 2.74 mmol) and $Et_3N$ (0.38 mL, 2.25 mmol). After stirring at reflux for 6 days, the reaction mixture was cooled to room temperature and the solvent was removed under reduced pressure. The crude residue was dissolved in $CH_2Cl_2$ (50 mL) and washed with $H_2O$ (100

mL). The organic phase was washed with 10% KOH (2 × 10 mL), $H_2O$ (100 mL), dried over $MgSO_4$, and concentrated (rotavap) following filtration. Purification by alumina column chromatography (4% MeOH in $CH_2Cl_2$) afforded the title compound **63** (0.556 g, 63%) as a brown oil; $^1$H NMR (400 MHz, $CDCl_3$) δ 8.48 (ddt, *J* = 4.1, 2.2, 1.1 Hz, 2H, H-10), 8.02 (dd, *J* = 8.5, 0.8 Hz, 1H, H-22), 7.97 (dq, *J* = 8.5, 0.7 Hz, 1H, H-24), 7.78 (dd, *J* = 8.0, 1.4 Hz, 1H, H-27), 7.68 (ddd, *J* = 8.4, 6.9, 1.5 Hz, 1H, H-25), 7.50 (ddd, *J* = 8.1, 6.9, 1.2 Hz, 1H, H-26), 7.44 (td, *J* = 7.7, 1.9 Hz, 2H, H-12), 7.27 (d, *J* = 6.6 Hz, 2H, H-13), 7.21 (d, *J* = 8.4 Hz, 1H, H-23), 7.08 (ddd, *J* = 7.4, 4.9, 1.2 Hz, 2H, H-11), 3.91 (s, 4H, H-3), 3.23 (td, *J* = 6.8, 0.9 Hz, 2H, H-7), 3.13 – 3.03 (m, 2H, H-2). $^{13}$C NMR (101 MHz, $CDCl_3$) δ 161.34, 159.88, 149.01, 148.02, 136.41, 136.09, 129.45, 129.27, 128.99, 127.62, 125.91, 122.99, 122.10, 122.00, 60.42, 54.40, 36.97. LRMS (ESI, *m/z*): calculated for $C_{23}H_{23}N_4^+$ $[M + H]^+$ *m/z* = 355.19; found *m/z* = 355.1.

**Ligand (64)**

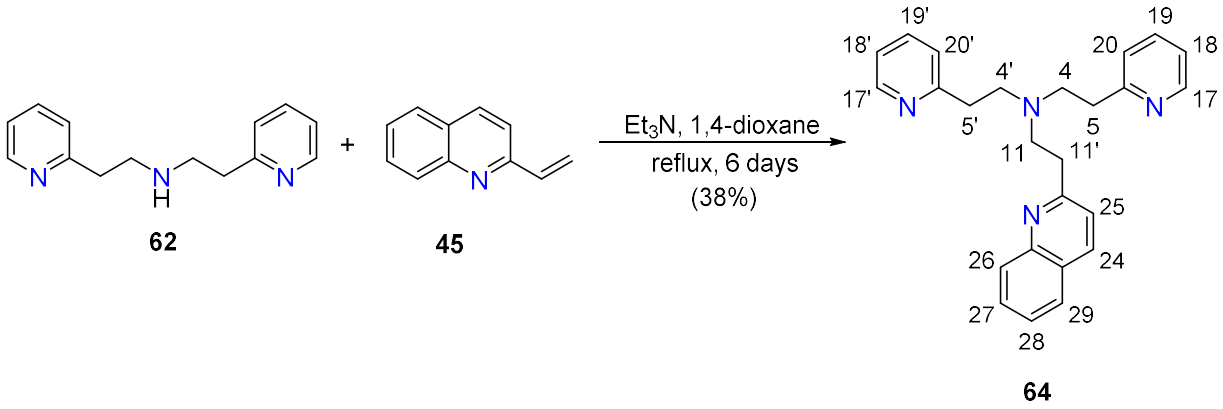


**62** **45** **64**

To a stirred solution of 2-(pyridin-2-yl)-*N*-[2-pyridin-2-yl)ethyl]ethan-1-amine **62** (4.04 g, 17.7 mmol) in 1,4-dioxane (150 mL), was added 2-vinylquinoline **45** (3.31 g, 21.3 mmol) and $Et_3N$ (2.7 mL, 19.5 mmol). After stirring at reflux for 6 days, the reaction mixture was cooled to room temperature and the solvent was removed (rotavap). The crude residue was dissolved in $CH_2Cl_2$ (150 mL) and washed with $H_2O$ (150 mL). The organic phase was washed with 10% KOH (2 × 35 mL), $H_2O$ (150 mL), dried over $MgSO_4$, and concentrated (rotavap) following filtration. Purification by alumina column chromatography (4% MeOH in $CH_2Cl_2$) afforded the title compound **64** (2.55 g, 38%) as a brown oil; $^1$H NMR (400 MHz, $CDCl_3$) δ 8.48 (ddd, *J* = 4.9, 1.9, 0.9 Hz, 2H, H-17), 8.07 – 8.00 (m, 1H, H-24), 7.96 (dd, *J* = 8.5, 0.8 Hz, 1H, H-26), 7.75 (dd, *J* = 8.2, 1.5 Hz, 1H, H-29), 7.66 (ddd, *J* = 8.5, 6.9, 1.5 Hz, 1H, H-28), 7.50 – 7.44 (m, 2H, H-19), 7.42 (dd, *J* = 7.6, 1.9 Hz, 1H, H-27), 7.14 (d, *J* = 8.4 Hz, 1H, H-25), 7.05 (ddd, *J* = 7.6, 4.9,

1.2 Hz, 2H, H-18), 6.95 (dt, *J* = 7.8, 1.1 Hz, 2H, H-20), 3.10 – 3.07 (m, 4H, H-11), 3.05 – 2.96 (m, 4H, H-4), 2.91 (m, 4H, H-5). $^{13}$C NMR (101 MHz, $CDCl_3$) δ 161.40, 160.64, 160.62, 149.18, 147.94, 136.29, 136.27, 136.15, 136.13, 129.45, 128.84, 127.56, 126.88, 125.86, 123.57, 122.06, 121.17, 53.97, 53.88, 36.79, 36.02, 35.99. (HRMS) (ESI, m/z): calculated for $C_{25}H_{27}N_4^+$ $[M + H]^+$ *m/z* = 383.22302; found *m/z* = 383.2229.

**Ligand (65)**

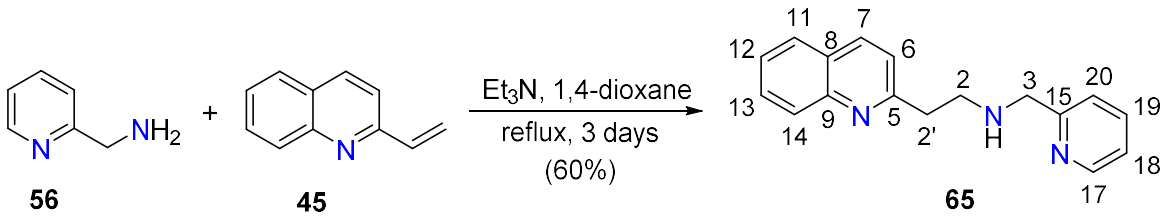


To a stirred solution of 1-(pyridin-2-yl)methanamine **56** (1.40 g, 12.9 mmol) in 1,4-dioxane (100 mL), was added 2-vinylquinoline **45** (2.14 g, 13.8 mmol) and $Et_3N$ (3.5 mL, 25.2 mmol). After stirring at reflux for 3 days, the reaction mixture was cooled to room temperature and the solvent was removed under reduced pressure. The crude residue was dissolved in $CH_2Cl_2$ (100 mL) and washed with $H_2O$ (150 mL). The organic phase was washed with 10% KOH (2 × 20 mL), $H_2O$ (100 mL), dried over $MgSO_4$, and concentrated (rotavap) following filtration. Purification by alumina column chromatography (4% MeOH in $CH_2Cl_2$) afforded the title compound **65** (2.06 g, 60%) as a brown oil; $^1$H NMR (400 MHz, $CDCl_3$) δ 8.52 (ddd, *J* = 4.9, 1.8, 1.0 Hz, 1H, H-17), 8.06 (dd, *J* = 8.3, 0.8 Hz, 1H, H-7), 8.03 (dq, *J* = 8.5, 0.9 Hz, 1H, H-14), 7.77 (dd, *J* = 8.1, 1.5 Hz, 1H, H-11), 7.67 (ddd, *J* = 8.4, 6.9, 1.5 Hz, 1H, H-13), 7.60 (td, *J* = 7.7, 1.8 Hz, 1H, H-19), 7.48 (ddd, *J* = 8.1, 6.9, 1.2 Hz, 1H, H-12), 7.34 – 7.28 (m, 2H, H-6, H-20), 7.16 – 7.10 (m, 1H, H-18), 3.97 (s, 2H, H-3), 3.28 – 3.09 (m, 4H, H-2). $^{13}$C NMR (101 MHz, $CDCl_3$) δ 160.88 (C-5), 159.87 (C-15), 149.37 (C-17), 148.03 (C-9), 136.58 (C-19), 136.46 (C-7), 129.53 (C-13), 129.00 (C-14), 127.64 (C-11), 126.94 (C-8), 125.97 (C-12), 122.35 (C-18), 122.04 (C-20), 121.88 (C-6), 55.26 (C-3), 49.02 (C-2'), 39.34 (C-2). (HRMS) (ESI, m/z): calculated for $C_{17}H_{18}N_3^+$ $[M + H]^+$ *m/z* = 264.14952; found *m/z* = 264.1494.

**Ligand (66)**

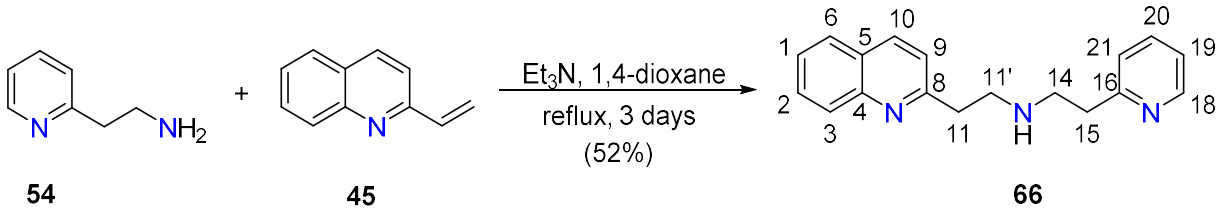


54 45 66

To a stirred solution of 2-(pyridin-2-yl)ethan-1-amine **54** (0.786 g, 6.43 mmol) in 1,4-dioxane (80 mL), was added 2-vinylquinoline **45** (1.00 g, 6.44 mmol) and $Et_3N$ (1.8 mL, 12.8 mmol). After stirring at reflux for 3 days, the reaction mixture was cooled to room temperature and the solvent was removed under reduced pressure. The crude residue was dissolved in $CH_2Cl_2$ (100 mL) and washed with $H_2O$ (100 mL). The organic phase was washed with 10% KOH (2 × 35 mL), $H_2O$ (150 mL), dried over $MgSO_4$, and concentrated (rotavap) following filtration. Purification by alumina column chromatography (4% MeOH in $CH_2Cl_2$) afforded the title compound **66** (0.542 g, 52%) as a brown oil; $^1$H NMR (400 MHz, $CDCl_3$) δ 8.45 (ddd, *J* = 4.9, 1.9, 0.9 Hz, 1H, H-18), 8.04 (dd, *J* = 8.4, 0.8 Hz, 1H, H-10), 7.98 (dq, *J* = 8.6, 0.8 Hz, 1H, H-3), 7.77 (dd, *J* = 8.0, 1.4 Hz, 1H, H-6), 7.67 (ddd, *J* = 8.4, 6.9, 1.5 Hz, 1H, H-2), 7.54 – 7.43 (m, 2H, H-1, H-20, H-1), 7.28 (d, *J* = 8.4 Hz, 1H, H-9), 7.12 (dt, *J* = 7.8, 1.1 Hz, 1H, H-21), 7.05 (ddd, *J* = 7.5, 4.9, 1.2 Hz, 1H, H-19), 3.15 (d, *J* = 1.5 Hz, 4H, H-11), 3.11 – 3.06 (m, 2H, H-14), 2.98 (td, *J* = 6.7, 1.0 Hz, 2H, H-15). $^{13}$C NMR (101 MHz, $CDCl_3$) δ 160.95 (C-8), 160.35 (C-16), 149.42 (C18), 148.04 (C-4), 136.39 (C-20), 136.36 (C-10), 129.46 (C-2), 129.07 (C-3), 127.62 (C-6), 126.91 (C-5), 125.93 (C-1), 123.39 (C-21), 121.88 (C-9), 121.28 (C-19), 49.36 (C-16), 49.23 (C-14'), 39.25 (C-14), 38.54 (C-15). (HRMS) (ESI, m/z): calculated for $C_{18}H_{20}N_3^+$ $[M + H]^+$ *m/z* = 278.16517; found *m/z* = 278.1651.

**1-(Pyridin-2-yl)-*N*-[(quinolin-2-yl)methyl]methanamine (67)**

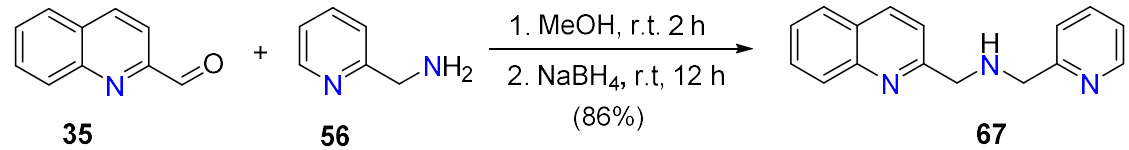


35 56 67

This synthesis was modified from a previously reported procedure.[227] To a stirred solution of 1-(pyridin-2-yl)methanamine **56** (0.688 g, 6.36 mmol) in MeOH (20 mL), was added quinoline-2-carbaldehyde **35** (1.00 g, 6.36 mmol). After stirring at room temperature for 2 h, the reaction mixture was cooled to 0 ℃ and $NaBH_4$ (0.242 g, 6.39 mmol) was added.

After stirring at room temperature for 12 h, the reaction was heated to reflux for 1 h. The reaction mixture was cooled to room temperature, $H_2O$ (50 mL) was added and the pH was adjusted to ~ 1 with 6 M HCl. The mixture was extracted with $CH_2Cl_2$ (3 × 25 mL). The aqueous phase was adjusted to pH 10 by the addition of 10% KOH and the product was extracted with $CH_2Cl_2$ (3 × 50 mL). The organic extracts were washed with $H_2O$ (100 mL), dried over $MgSO_4$ and reduced to dryness to afforded the title compound **67** (1.36 g, 86%) as a brown oil; $^1$H NMR (400 MHz, $CDCl_3$) δ 8.56 (ddd, *J* = 4.9, 1.8, 1.0 Hz, 1H), 8.12 (dd, *J* = 8.6, 0.9 Hz, 1H), 8.05 (dq, *J* = 8.4, 0.9 Hz, 1H), 7.79 (dd, *J* = 8.0, 1.4 Hz, 1H), 7.74 – 7.60 (m, 2H), 7.56 – 7.45 (m, 2H), 7.39 (dt, *J* = 7.8, 1.1 Hz, 1H), 7.22 – 7.14 (m, 1H), 4.29 (s, 2H), 4.17 (s, 2H). $^{13}$C NMR (101 MHz, $CDCl_3$) δ 149.45, 147.60, 137.03, 136.94, 129.84, 129.09, 127.72, 127.57, 126.56, 122.82, 122.67, 120.46, 54.12, 53.89. HRMS (ESI, *m/z*): calculated for $C_{16}H_{16}N_3^+$ $[M + H]^+$ *m/z* = 250.13387; found *m/z* = 250.1338. Data are consistent with the literature.[227]

**2-(Pyridin-2-yl)-*N*-[(quinolin-2-yl)methyl]ethan-1-amine (68)**

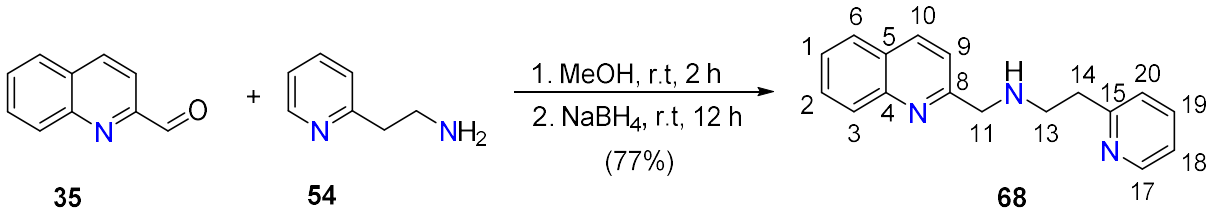


To a stirred solution of 2-(pyridin-2-yl)ethan-1-amine **54** (0.781 g, 6.39 mmol) in MeOH (20 mL), was added quinoline-2-carbaldehyde **35** (1.00 g, 6.36 mmol). After stirring at room temperature for 2 h, the reaction mixture was cooled to 0 ℃ and $NaBH_4$ (0.242 g, 6.39 mmol) was added. After stirring at room temperature for 12 h, the reaction was heated to reflux for 1 h. The reaction mixture was cooled to room temperature, $H_2O$ (50 mL) was added and the pH was adjusted to ~ 1 with 6 M HCl. The mixture was extracted with $CH_2Cl_2$ (3 × 25 mL). The aqueous phase was adjusted to pH 10 by the addition of 10% KOH and the product was extracted with $CH_2Cl_2$ (3 × 50 mL). The organic extracts were washed with $H_2O$ (100 mL), dried over $MgSO_4$ and reduced to dryness to afforded the title compound **68** (1.31 g, 77%) as a brown oil; $^1$H NMR (400 MHz, $CDCl_3$) δ 8.51 (ddd, *J* = 4.9, 1.9, 0.9 Hz, 1H, H-17), 8.07 (dd, *J* = 8.5, 0.8 Hz, 1H, H-10), 8.02 (dq, *J* = 8.5, 0.9 Hz, 1H, H-3), 7.76 (dd, *J* = 8.2, 1.5 Hz, 1H, H-6), 7.66 (ddd, *J* = 8.4, 6.9, 1.5 Hz, 1H, H-2), 7.57 (td, *J* = 7.7, 1.9 Hz, 1H, H-19), 7.48 (ddd, *J* = 8.1, 6.9, 1.2 Hz, 1H, H-1), 7.42 (d, *J* = 8.4 Hz, 1H, H-9), 7.18 (dt, *J* = 7.8, 1.1 Hz, 1H, H-20), 7.10 (ddd, *J* = 7.6, 4.9,

1.2 Hz, 1H, H-18), 4.12 (s, 2H, H-11), 3.16 – 3.08 (m, 2H, H-13), 3.08 – 3.01 (m, 2H, H-14). $^{13}$C NMR (101 MHz, $CDCl_3$) δ 160.38 (C-8), 160.28 (C-15), 149.37 (C-17), 147.77 (C-4), 136.54 (C-19), 136.52 (C-10), 129.52 (C-2), 129.00 (C-3), 127.64 (C-6), 127.38 (C-5), 126.13 (C-1), 123.44 (C-20), 121.38 (C-9), 120.63 (C-18), 55.74 (C-11), 49.34 (C-14), 38.65 (C-13). (HR/LS)MS (ESI, *m/z*): calculated for $C_{17}H_{18}N_3^+$ $[M + H]^+$ *m/z* = 264.14952; found *m/z* = 264.1495

**Ligand (69)**

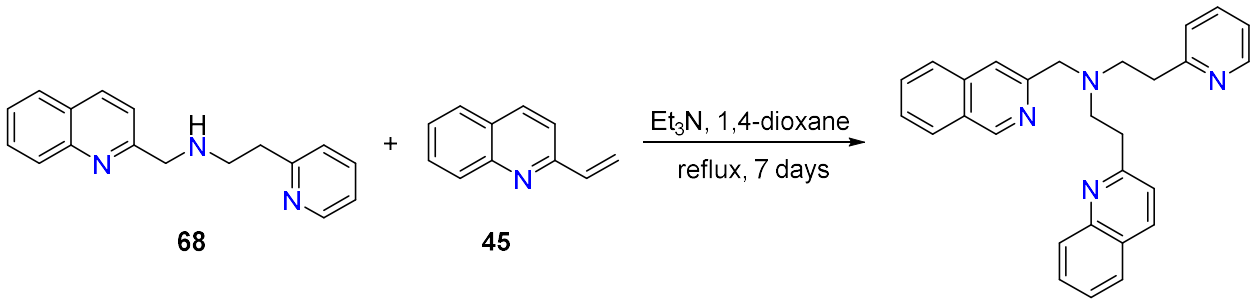


**68** **45** **69**

To a stirred solution of (2-pyridylethyl)(2-quinolylmethyl)amine **68** (1.5415 g, 5.85 mmol) in 1,4-dioxane (80 mL), was added 2-vinylquinoline **45** (1.0090 g, 6.50 mmol) and $Et_3N$ (0.90 mL, 6.50 mmol). After stirring at reflux for 7 days, the reaction mixture was cooled to room temperature and the solvent was removed under reduced pressure. The crude residue was dissolved in $CH_2Cl_2$ (100 mL) and washed with $H_2O$ (100 mL). The organic phase was washed with 10% KOH (2 × 25 mL), $H_2O$ (100 mL), dried over $MgSO_4$, and concentrated (rotavap) following filtration. LRMS of the crude residue indicated the formation of the desired product **69**; however, all attempts at purification failed to yield the desired compound. LRMS (ESI, *m/z*): calculated for $C_{28}H_{27}N_4^+$ $[M + H]^+$ *m/z* = 419.22; found *m/z* = 419.1.

**Ligand (71)**

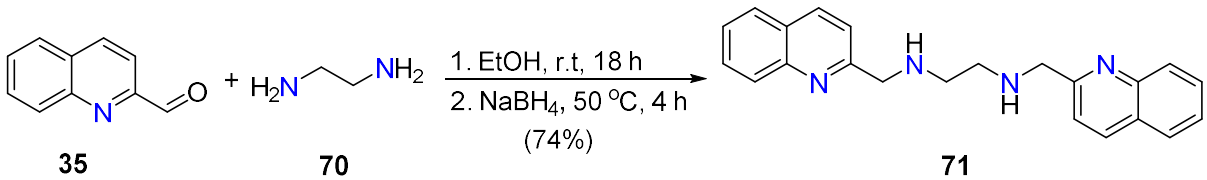


**35** **70** **71**

To a stirred solution of quinoline-2-carbaldehyde **35** (0.505 g, 3.21 mmol) in EtOH (45 mL), was added ethane-1,2-diamine **70** (0.095 g, 1.59 mmol). After stirring at room

temperature for 18 h, $NaBH_4$ (1.08 g, 28.5 mmol) was added and the reaction was heated to 50 ℃ for 4 h. The reaction mixture was cooled to room temperature, and the solvent was removed (rotavap). To the crude residue was added $CH_2Cl_2$ (50 mL) and $H_2O$ (50 mL), and the aqueous phase was extracted with $CH_2Cl_2$ (1 x 30 mL). The combined organic phases were dried over $MgSO_4$ and concentrated (rotavap) following filtration. The brown residue was dissolved in the minimum volume of EtOH (20 mL), and addition of concentrated HCl (3-4 drops) resulted in the precipitation of a brown solid. This was collected by filtration and dried overnight in a vacuum desiccator to afford the title compound **71** (0.843 g, 74%) as a cream solid; $^1$H NMR (400 MHz, DMSO) δ 9.77 (s, 5H), 8.50 (dd, *J* = 8.7, 0.8 Hz, 2H), 8.13 – 8.03 (m, 4H), 7.85 (ddd, *J* = 8.5, 6.9, 1.5 Hz, 2H), 7.73 – 7.62 (m, 4H), 4.67 (s, 4H), 3.63 (s, 4H). 13C NMR (101 MHz, DMSO-d6, TMS): δ = 152.33, 146.08, 137.16, 129.99, 127.96, 127.83, 126.96, 126.77, 120.18, 50.53, 43.20, 40.32. (HRMS (ESI, *m/z*): calculated for $C_{22}H_{23}N_4^+$ $[M + H]^+$ *m/z* = 343.19172; found *m/z* = 343.1915. Data is consistent with the literature.[228]

## 2.2 Experimental: Chapter Four

**[Pd(58)Cl$_2$]Cl.xH$_2$O**

To a stirring solution of $K_2PdCl_4$ (0.078 g, 0.238 mmol) in $H_2O$ (1.5 mL) was added a solution of **58** (0.104 g, 0.248 mmol) in $CH_3CN$ (2 mL) and an instant yellow precipitate was formed. The mixture was heated with stirring at 70 ℃ for 4 hours and during this time the precipitate dissolved. The yellow solution was left to stand under ambient conditions and after 1 week crystals suitable for X-ray analysis were obtained. $^1$H NMR (400 MHz, $CD_3OD$) δ 9.63 (d, *J* = 8.7 Hz, 1H), 9.43 (dd, *J* = 5.9, 1.5 Hz, 1H), 8.67 (d, *J* = 8.3 Hz, 1H), 8.10 (td, *J* = 7.7, 1.6 Hz, 2H), 8.00 (d, *J* = 8.4 Hz, 2H), 7.89 (ddd, *J* = 8.6, 6.8, 1.6 Hz, 1H), 7.82 (d, *J* = 8.2 Hz, 1H), 7.76 (d, *J* = 7.8 Hz, 1H), 7.68 – 7.58 (m, 3H), 7.58 – 7.52 (m, 1H), 7.49 (d, *J* = 7.9 Hz, 2H), 6.86 (d, *J* = 8.4 Hz, 1H), 5.09 (ddd, *J* = 15.1, 12.9, 6.2 Hz, 1H), 4.22 (ddd, *J* = 14.5, 10.7, 4.2 Hz, 1H), 3.87 (ddd, *J* = 16.4, 7.7, 5.0 Hz, 2H), 3.77 (ddd, *J* = 13.8, 6.4, 2.1 Hz, 1H), 3.56 – 3.40 (m, 2H), 3.12 (td, *J* = 13.4, 3.2 Hz, 1H), 3.05 – 2.92 (m, 1H), 2.90 – 2.84 (m, 1H), 2.72 (ddd, *J* = 13.1, 10.7, 5.9 Hz, 1H), 2.46 (ddd, *J* = 13.0, 11.5, 4.2 Hz, 1H). $^{13}$C NMR (101 MHz, MeOD) δ 162.43, 160.22, 158.23, 156.06, 148.30, 147.28, 143.85, 142.22, 138.34, 132.83, 130.91, 129.98, 129.80, 129.71, 129.21, 128.88, 128.76, 128.23, 127.57, 126.67, 124.43, 123.39, 122.25,

64.71, 59.84, 57.88, 42.73, 38.72, 37.14. HRMS (ESI, *m/z*): calculated for $C_{29}H_{28}ClN_4Pd^+$ $[M]^+$ *m/z* = 573.11129; found *m/z* = 573.1115.

**[Cu(55)NCCH$_3$](ClO$_4$)$_2$, [Zn(55)NCCH$_3$](ClO$_4$)$_2$ and [(Mn(55))$_2$O$_2$](ClO$_4$)$_2$.2CH$_3$CN**

*General Procedure 1*: To a stirring solution of metal salt (1 equiv.) dissolved in $CH_3CN$ (1 mL) was added a solution of **55** (1 equiv.) dissolved in $CH_3CN$ (1.5 mL). The resulting solution was stirred at room temperature for 5 minutes. The solution was left to stand under ambient conditions and after three days crystals suitable for X-ray analysis were obtained.

**[Cu(55)NCCH$_3$](ClO$_4$)$_2$**

*General procedure 1:* A solution of **[**$Cu(OH_2)_6](ClO_4)_2$ (51.0 mg, 0.137 mmol) and **55** (50.2 mg, 0.124 mmol) were reacted according to the general procedure. Green crystals suitable for X-ray analysis were obtained. HRMS (ESI, *m/z*): calculated for $C_{27}H_{24}N_4Cu^{2+}$ $[M]^{2+}$ *m/z* = 233.56400; found *m/z* = 233.5643.

**[Zn(55)NCCH$_3$](ClO$_4$)$_2$**

*General procedure 1:* A solution of **[**$Zn(OH_2)_6](ClO_4)_2$ (50.0 mg, 0.134 mmol) and **55** (50.0 mg, 0.123 mmol) were reacted according to the general procedure. Colourless crystals suitable for X-ray analysis were obtained. $^1$H NMR (400 MHz, MeOD) δ 9.45 (d, *J* = 5.4 Hz, 1H), 8.66 (d, *J* = 8.5 Hz, 2H), 8.36 (d, *J* = 8.7 Hz, 2H), 8.10 (d, *J* = 8.2 Hz, 2H), 7.96 (t, *J* = 7.9 Hz, 2H), 7.90 (td, *J* = 7.8, 1.6 Hz, 1H), 7.73 (dd, *J* = 14.5, 7.3 Hz, 5H), 7.28 (d, *J* = 7.9 Hz, 1H), 5.15 – 4.86 (m, 4H), 3.37 (q, *J* = 6.8 Hz, 2H), 2.90 – 2.83 (m, 2H). $^{13}$C NMR (101 MHz, $CD_3OD$) δ 161.77, 150.19, 145.85, 142.99, 142.45, 133.29, 130.41, 130.30, 129.18, 128.69, 126.76, 125.50, 122.04, 63.45, 58.03, 32.91, 0.77. HRMS (ESI, *m/z*): calculated for $C_{27}H_{24}N_4Zn^{2+}$ $[M]^{2+}$ *m/z* = 234.0646; found *m/z* = 234.0641.

**[(Mn(55))$_2$O$_2$](ClO$_4$)$_2$.2CH$_3$CN**

*General procedure 1:* A solution of **[**$Mn(OH_2)_6](ClO_4)_2$ (50.3 mg, 0.138 mmol) and **55** (56 mg, 0.138 mmol) were reacted according to the general procedure. Dark brown crystals suitable for X-ray analysis were obtained. HRMS (ESI, *m/z*): calculated for $C_{54}H_{48}N_8O_2Mn_2^{2+}$ $[M]^{2+}$ *m/z* = 475.13300; found *m/z* = 475.1323.

**[(62)Co(OH)$_3$Co(62)](ClO$_4$)$_3$.CH$_3$CN**

To a stirring solution of **[**Co(OH$_2$)$_6$](ClO$_4$)$_2$ (0.047 g, 0.128 mmol) dissolved in CH$_3$CN (1 mL) was added a solution of **64** (0.051 g, 0.133 mmol) dissolved in CH$_3$CN (1.5 mL). The resulting solution was stirred at room temperature for 5 minutes. The solution was left to stand under ambient conditions and after three days crystals suitable for X-ray analysis were obtained.

## 2.3 Experimental: Chapter Five

### 2.3.1 Mass spectrometry

Solution A: 0.0119 M [M(OH$_2$)$_6$](ClO$_4$)$_2$ (M = Cu, Co and Ni) in CH$_3$CN.

Solution B: 0.0119 M ligand (**57**, **58**, **63**, **64**, **65** and **66**) in CH$_3$CN.

To 20 µL of solution A was added 1, 2 and 3 equivalents of solution B, respectively. The resulting solutions were mixed and left to stand for 30 minutes. Mass spectrometry samples were prepared by the addition of 10 µL of each metal-ligand solution to 0.5 mL of CH$_3$CN followed by the direct injection of each sample into the mass spectrometer.

### 2.3.2 Job's Method

Solution A: 0.0119 M [M(OH$_2$)$_6$](ClO$_4$)$_2$ (M = Cu, Co and Ni) in CH$_3$CN.

Solution B: 0.0119 M ligand (**57**, **58**, **63**, **64**, **65** and **66**) in CH$_3$CN.

0, 0.5, 1.0, 1.5, 2.0, 2.5, 3.0, 3.5, 4.0, 4.5, and 5.0 mL of the metal solution was added into separate 5 mL volumetric flasks using an automatic pipette. Into each flask, respectively, was added 5.0, 4.5, 4.0, 3.5, 3.0, 2.5, 2.0, 1.5, 1.0, 0.5, and 0 mL of the ligand solution. Each flask was mixed thoroughly. After 10 minutes, the UV/vis spectrum of each solution was measured using CH$_3$CN as the reference.

The collected data was plotted using Origin fitting software with the specific absorbance versus mole fraction of the metal.

## 2.4 Experimental: Chapter Six

**2-(Pyridin-2-yl)-*N*-[(quinolin-2-yl)methyl]ethan-1-amine (73.HCl)**

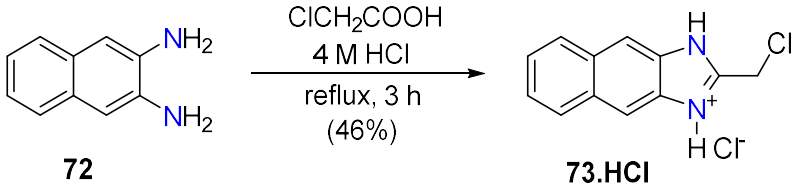


**72** **73.HCl**

Naphthalene-2,3-diamine **72** (0.702 g, 4.43 mmol) and $ClCH_2COOH$ (0.420 g, 4.44 mmol) were dissolved in 4 M HCl (20 mL) and refluxed for 3 h. The resulting mixture was cooled on ice, the solid was collected by vacuum filtration, and washed with ice-cold $H_2O$ (4 × 10 mL). The brown precipitate was recrystallised from hot MeOH to afford the title compound **73.HCl** (0.439 g, 46%); $^1$H NMR (400 MHz, DMSO) δ 8.28 (s, 2H), 8.12 (m, $J$ = 6.2, 3.1 Hz, 2H), 7.51 (m, $J$ = 6.5, 3.3 Hz, 2H), 5.19 (s, 2H); $^{13}$C NMR (101 MHz, DMSO) δ 153.72, 134.09, 130.65, 128.07, 125.04, 111.33, 36.08. (LRMS) (ESI, *m/z*): calculated for $C_{12}H_{10}N_2Cl^+$ $[M + H]^+$ *m/z* = 217.05; found *m/z* = 217.0. Data is consistent with the literature.[229]

**Ligand (74)**

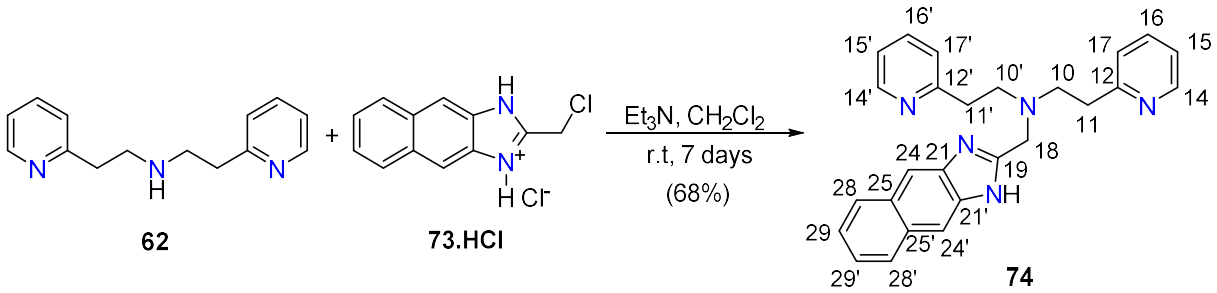


**62** **73.HCl** **74**

To a solution of 2-(chloromethyl)-1*H*-naphtho[2,3-*d*]imidazole hydrochloride **73.HCl** (0.110 g, 0.438 mmol) in $CH_2Cl_2$ (10 mL) cooled to 0 ℃, was added $Et_3N$ (0.12 mL, 0.876 mmol) and 2-(pyridin-2-yl)-*N*-[2-(pyridin-2-yl)ethyl]ethan-1-amine **62** (0.099 g, 0.435 mmol) sequentially. The solution was allowed to warm gradually to room temperature and stirred for 7 days. The reaction mixture was washed with $H_2O$ (50 mL), 10% KOH (25 mL) and $H_2O$ (50 mL), dried over $MgSO_4$, filtered and reduced to dryness (rotavap). Purification by silica gel chromatography (10% MeOH in $CH_2Cl_2$ + 1% $NH_4OH$ ) afforded the title compound **74** (0.120 g, 68%) as a brown oil; $^1$H NMR (400 MHz, $CDCl_3$) δ 8.45 (ddd, $J$ = 5.0, 1.9, 0.9 Hz, 2H, H-14), 7.99 (s, 2H, H-24), 7.96 (dd, $J$ = 6.4,

3.3 Hz, 2H, H-28), 7.49 (td, *J* = 7.7, 1.8 Hz, 2H, H-16), 7.40 (dd, *J* = 6.4, 3.2 Hz, 2H, H-29), 7.10 (ddd, *J* = 7.6, 4.9, 1.2 Hz, 2H, H-15), 6.95 (dt, *J* = 7.8, 1.1 Hz, 2H, H-17), 4.17 (s, 2H, H-18), 3.07 (t, *J* = 6.5 Hz, 4H, H-10), 2.88 (t, *J* = 6.5 Hz, 4H, H-11). $^{13}$C NMR (101 MHz, $CDCl_3$) δ 159.96 (C-19), 159.90 (C-12), 148.40 (C-14), 136.80 (C-16), 130.39 (C-21), 128.01 (C-28), 123.85 (C-29, C-17), 123.77 (C-25), 121.50 (C-15), 111.01 (C-24) 55.21 (C-10), 52.97 (C-18), 35.86 (C-11). HRMS (ESI, *m/z*): calculated for $C_{26}H_{26}N_5^+$ $[M + H]^+$ *m/z* = 408.21827; found *m/z* = 408.2180.

**Ligand (75)**

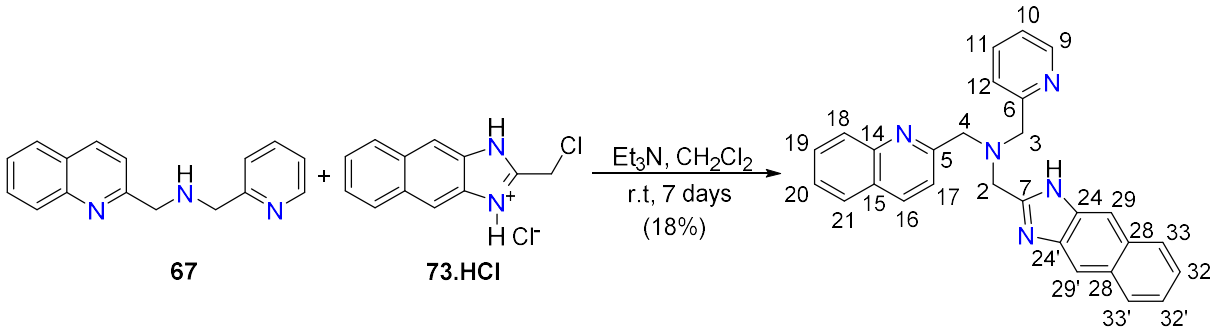


**67** **73.HCl** **75**

To a solution of 2-(chloromethyl)-1*H*-naphtho[2,3-*d*]imidazole hydrochloride **73.HCl** (0.100 g, 0.397 mmol) in $CH_2Cl_2$ (20 mL) cooled to 0 ℃, was added 1-(pyridin-2-yl)-*N*-[(quinolin-2-yl)methyl]methanamine **67** (0.099 g, 0.397 mmol) and $Et_3N$ (0.11 mL, 0.794 mmol) sequentially. The solution was allowed to warm gradually to r.t and stirred for 7 days. The reaction mixture was washed with $H_2O$ (50 mL), 10% KOH (25 mL) and $H_2O$ (50 mL), dried over $MgSO_4$, filtered and concentrated (rotavap). Purification by silica gel chromatography (10% MeOH in $CH_2Cl_2$ + 1% $NH_4OH$) chromatography afforded the title compound **75** (0.031 g, 18%) as a brown oil; $^1$H NMR (400 MHz, $CDCl_3$) δ 8.68 (ddd, *J* = 4.9, 1.9, 0.9 Hz, 1H, H-9), 8.20 (dd, *J* = 8.4, 1.1 Hz, 1H, H-18), 8.10 – 8.03 (m, 3H, H-16, H-29), 7.99 – 7.90 (m, 2H, H-33), 7.81 – 7.73 (m, 2H, H-21, H-19), 7.63 – 7.50 (m, 2H, H-20, H-11), 7.45 (d, *J* = 8.4 Hz, 1H, H-17), 7.38 (dt, *J* = 6.6, 3.3 Hz, 2H, H-32), 7.30 (dt, *J* = 7.9, 1.1 Hz, 1H, H-12), 7.19 (ddd, *J* = 7.6, 4.8, 1.2 Hz, 1H, H-10), 4.20 (s, 2H, H-2), 4.13 (s, 2H, H-4), 3.99 (s, 2H, H-3). $^{13}$C NMR (101 MHz, $CDCl_3$) δ 163.79 (C-24), 159.06 (C-5), 158.26 (C-6), 158.14 (C-7), 149.33 (C-9), 147.63 (C-15), 137.05 (C-16, C-29, C-20), 130.37 (C-28), 130.03 (C-19), 128.76 (C-18), 128.03 (C-33), 127.79 (C-21), 127.56 (C-14), 126.69 (C-11), 124.09 (C-12), 123.63 (C-32), 122.77 (C-

10), 121.61 (C-17), 60.91 (C-2), 60.29 (C-4), 53.01 (C-3). (HRMS) (ESI, *m/z*): calculated for $C_{28}H_{24}N_5^+$ $[M + H]^+$ *m/z* = 430.20262; found *m/z* = 430.2023.

**Ligand (76)**

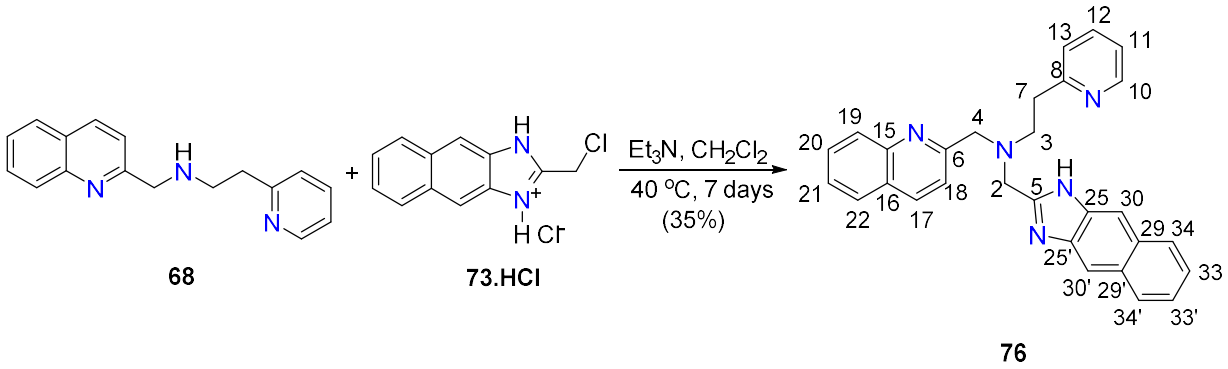


68 73.HCl 76

To a mixture of 2-(chloromethyl)-1*H*-naphtho[2,3-*d*]imidazole hydrochloride **73.HCl** (0.334 g, 1.33 mmol) in $CH_2Cl_2$ (30 mL) was added $Et_3N$ (0.37 mL, 2.66 mmol) with stirring for 1 minute. The solution was then added to a solution of 2-(pyridin-2-yl)-*N*-[(quinolin-2-yl)methyl]ethan-1-amine **68** (0.350 g, 1.33 mmol) in $CH_2Cl_2$ (15 mL). After stirring at 40 ℃ for 7 days, the reaction mixture was washed with $H_2O$ (50 mL), 10% KOH (20 mL) and $H_2O$ (50 mL), dried over $MgSO_4$, filtered and the solvent removed (rotavap). Purification by silica gel chromatography (10% MeOH in $CH_2Cl_2$ + 1% $NH_4OH$) afforded the title compound **76** (0.207 g, 35%) as a brown oil; $^1$H NMR (400 MHz, $CDCl_3$) δ 8.62 (ddd, *J* = 4.9, 1.8, 0.9 Hz, 1H, H-10), 8.12 – 8.07 (m, 1H, H-17), 8.05 (s, 2H, H-30), 7.96 (dd, *J* = 6.4, 3.3 Hz, 2H, H-34), 7.87 (d, *J* = 8.5 Hz, 1H, H-19), 7.77 – 7.66 (m, 2H, H-20, H-21), 7.54 – 7.42 (m, 2H, H-22, H-12), 7.39 (dd, *J* = 6.4, 3.2 Hz, 2H, H-33), 7.16 (ddd, *J* = 7.5, 5.0, 1.2 Hz, 1H, H-11), 7.05 (d, *J* = 8.4 Hz, 1H, H-18), 6.99 (dt, *J* = 7.8, 1.1 Hz, 1H, H-13), 4.19 (s, 2H, H-2), 4.05 (s, 2H, H-4), 3.16 (t, *J* = 6.3 Hz, 2H, H-3), 3.05 (t, *J* = 6.4 Hz, 2H, H-7). $^{13}$C NMR (101 MHz, $CDCl_3$) δ 160.23 (C-5), 159.62 (C-6), 159.30 (C-8), 148.35 (C-10), 147.49 (C-25), 136.89 (C-12), 136.59 (C-19), 129.77 (C-20), 128.82 (C-17, C-30), 128.12 (C-34), 127.70 (C-21), 127.41 (C-29), 126.49 (C-22), 124.05 (C-13), 123.18 (C-33), 121.63 (C-11), 121.02 (C18), 115.76 (C-15), 106.43 (C-16), 61.30 (C-4), 54.75 (C-3), 53.25 (C-2), 36.35 (C-7). (HRMS) (ESI, *m/z*): calculated for $C_{29}H_{26}N_5^+$ $[M + H]^+$ *m/z* = 444.21827; found *m/z* = 444.2180.

**Ligand (77)**

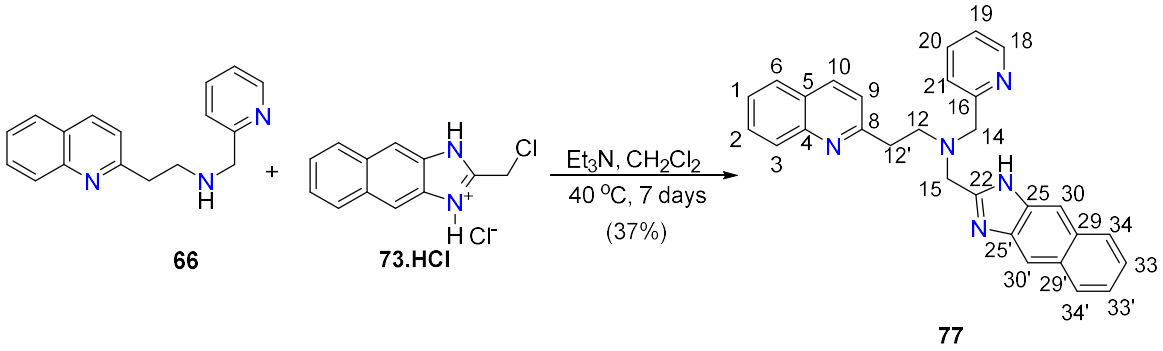


To a mixture of 2-(chloromethyl)-1*H*-naphtho[2,3-*d*]imidazole hydrochloride **73.HCl** (0.400 g, 1.59 mmol) in $CH_2Cl_2$ (40 mL) was added $Et_3N$ (0.44 mL, 3.18 mmol) with stirring for 1 minute. The solution was then added to a solution of *N*-[(pyridin-2-yl)methyl]-2-(quinolin-2-yl)ethan-1-amine **66** (0.421 g, 1.59 mmol) in $CH_2Cl_2$ (20 mL). After stirring at 40 ℃ for 7 days, the reaction mixture was washed with $H_2O$ (50 mL), 10% KOH (20 mL) and $H_2O$ (50 mL), dried over $MgSO_4$, filtered and concentrated (rotavap). Purification by silica gel chromatography (10% MeOH in $CH_2Cl_2$ + 1% $NH_4OH$) afforded the title compound **77** (0.019 g, 37%) as a brown oil; $^1$H NMR (400 MHz, $CDCl_3$) δ 8.41 (ddd, *J* = 4.9, 1.8, 0.9 Hz, 1H, H-21), 8.16 (dq, *J* = 8.4, 0.9 Hz, 1H, H-10), 7.95 (ddd, *J* = 13.0, 7.4, 2.1 Hz, 4H, H-30, H-34), 7.84 – 7.74 (m, 2H, H-3, H-2), 7.57 (ddd, *J* = 8.1, 6.9, 1.2 Hz, 1H, H-1), 7.38 (dd, *J* = 6.5, 3.2 Hz, 2H, H-33), 7.30 – 7.23 (m, 2H, H-6, H-20), 7.13 (d, *J* = 8.4 Hz, 1H, H-9), 7.04 – 6.94 (m, 2H, H-19, H-21), 4.19 (s, 2H, H-15), 3.87 (s, 2H, H-14), 3.19 (h, *J* = 1.4 Hz, 4H, H-12). $^{13}$C NMR (101 MHz, $CDCl_3$) δ 161.12 (C-8), 159.03 (C-22), 158.58 (C-16), 148.85 (C-18), 147.65 (C-25, C-3), 136.67 (C-30), 136.59 (C-20, C-6), 130.29 (C-29), 129.86 (C-2), 128.48 (C-10), 128.01 (C-34), 127.86 (C-3), 126.99 (C-5), 126.25 (C-1), 123.61 (C-33), 123.50 (C-21), 122.32 (C-19), 122.09 (C-9), 60.69 (C-14), 54.88 (C-12), 53.14 (C-15), 37.34 (C-12'). HRMS (ESI, *m/z*): calculated for $C_{29}H_{26}N_5^+$ $[M + H]^+$ *m/z* = 444.21827; *m/z* = 444.2179.

**Pyrene-4,5-dione (79)**

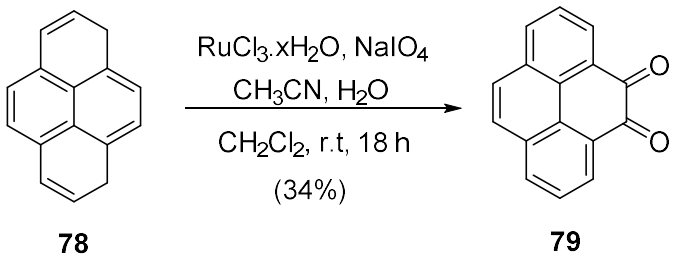

To a mixture of pyrene **78** (0.520 g 2.57 mmol), and $RuCl_3.xH_2O$ (5.12 mg, 0.024 mmol) in $CH_3CN$ (10 mL) was added a solution of $NaIO_4$ dissolved in hot $H_2O$ (12 mL). $CH_2Cl_2$ (10 mL) was added to this and the reaction mixture was stirred vigorously under $N_2$ at room temperature for 18 h. Following filtration through celite, the filtrate was extracted with $CH_2Cl_2$ (3 × 25) and the combined organic phases were washed with $Na_2CO_3$ and $H_2O$ and dried over $MgSO_4$, and the solvent was removed (rotavap). Purification by silica gel chromatography (4% MeOH in $CH_2Cl_2$) afforded the title compound **79** (0.202 g, 34%) as a bright orange solid. $^1$H NMR (400 MHz, $CDCl_3$) δ 8.51 (dd, $J$ = 7.4, 1.3 Hz, 2H), 8.20 (dd, $J$ = 8.0, 1.3 Hz, 2H), 7.87 (s, 2H), 7.77 (dd, $J$ = 8.0, 7.4 Hz, 2H). $^{13}$C NMR (101 MHz, $CDCl_3$) δ 180.69, 135.93, 132.27, 130.39, 130.35, 128.68, 128.18, 127.44. Data is consistent with the literature. [230]

**4,5-Diketopyrene dioxime (80)**

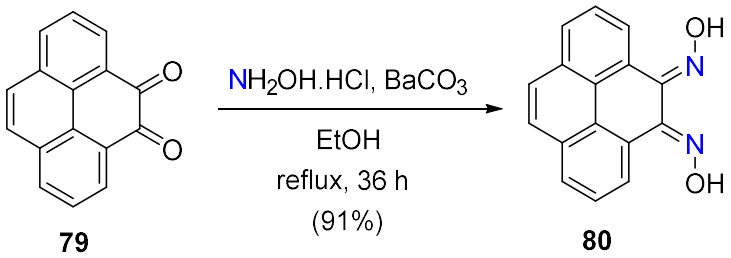


79 80

A mixture of pyrene-4,5-dione **79** (0.169 g, 0.727 mmol), hydroxylamine hydrochloride (0.180 g, 2.59 mmol), and $BaCO_3$ (0.221 g, 1.11 mmol) in EtOH (10 mL) were stirred at reflux for 39 h. After cooling to room temperature, the solvent was removed (rotavap). To the resulting crude yellow residue was added 0.2 M HCl (11.5 mL) and the mixture was stirred at room temperature for 30 minutes. Following filtration, the solid was washed with ice-cold $H_2O$ (10 mL), EtOH (10 mL) and diethyl ether (10 mL) to afford the title compound **80** (0.174 g, 91%). $^1$H NMR (400 MHz, $CDCl_3$) δ 13.80 (d, $J$ = 7.7 Hz, 1H), 12.98 (dd, $J$ = 7.6, 1.2 Hz, 1H), 12.89 (dd, $J$ = 7.9, 1.2 Hz, 1H), 12.85 – 12.78 (m, 2H), 12.58 – 12.44 (m, 3H). LRMS (ESI, *m/z*): calculated for $C_{16}H_{11}N_2O_2^+$ $[M + H]^+$ *m/z* = 263.08; found *m/z* = 263.0. Data is consistent with the literature.[231]

**4,5-Diaminopyrene (81)**

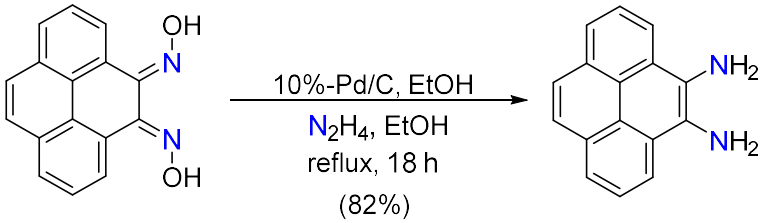


**80** **81**

To a two-neck flask was added **80** (0.174 g, 0.663 mmol) in EtOH (6 mL), followed by the evacuation and $N_2$ filling of the flask, repeated three times. To this was added 10%-Pd/C (0.100 g, 0.939 mmol) and the flask was evacuated, and nitrogen filled again. The mixture was heated to reflux and to this was added $N_2H_4$ (1 mL) in EtOH (1 mL) over two portions separated by 30 minutes. After stirring at reflux for 18 h, the hot reaction mixture was filtered through celite, washed with hot ethanol, and reduced to dryness (rotavap). The crude solid was triturated in $H_2O$ (20 mL) and cooled at 4 °C for 12 h. The resulting green solid was collected by filtration, and dried in a vacuum desiccator, to afford the title compound **81** (0.126 g, 82%). $^1$H NMR (400 MHz, DMSO) δ 8.31 (dd, *J* = 7.8, 1.3 Hz, 2H), 8.07 (s, 2H), 8.02 – 7.93 (m, 4H), 5.21 (s, 4H). $^{13}$C NMR (101 MHz, DMSO) δ 130.57, 127.11, 125.36, 125.33, 123.20, 121.24, 119.15, 117.84. LRMS (ESI, *m/z*): calculated for $C_{16}H_{13}N_2^+$ $[M + H]^+$ *m/z* = 233.10; found *m/z* = 233.0. Data is consistent with the literature.[231]

**Ligand (82)**

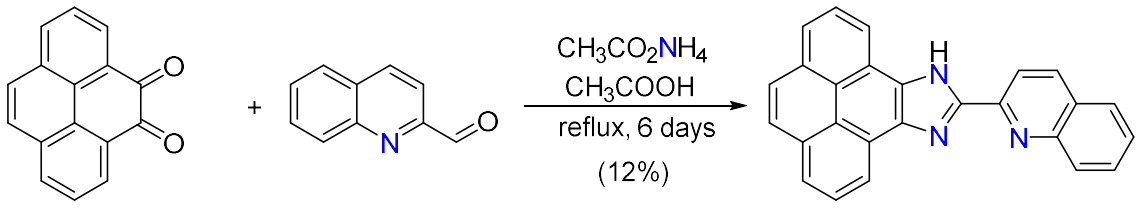


**79** **35** **82**

*Method A*: Pyrene-4,5-dione **79** (0.679 g, 2.92 mmol), quinoline-2-carbaldehyde **35** (0.459 g, 2.92 mmol), and ammonium acetate (4.47 g, 58.0 mmol) were dissolved in acetic acid (50 mL) and the reaction was stirred at reflux for 6 days. The reaction mixture was then cooled to room temperature and the solvent was removed (rotavap). The dark green residue was washed with $H_2O$ (50 mL) and extracted with $CH_2Cl_2$ (3 × 50 mL). The combined organic phases were dried over $MgSO_4$, filtered, and the solvent removed

(rotavap). Purification by silica gel chromatography (EtOAc:Hexane 1:1) afforded the title compound **82** (0.132 g, 12%) as a brown solid.

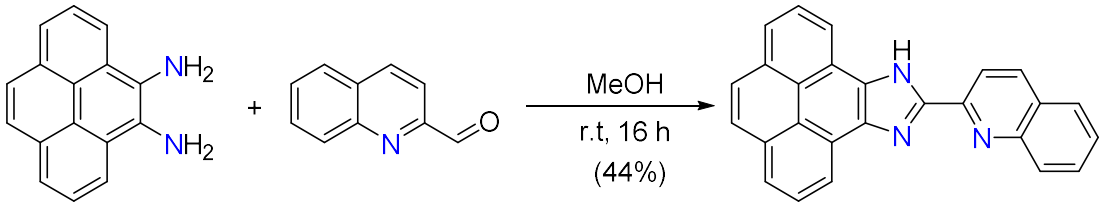


**81** **35** **82**

*Method B*: A solution of 4,5-diaminopyrene **81** (0.074 g, 0.318 mmol) and quinoline-2-carbaldehyde **35** (0.100 g, 0.637 mmol) in MeOH (7 mL) was stirred at room temperature for 16 h. Solid $NaBH_4$ (0.060 g, 1.59 mmol) was added slowly, and the reaction was stirred for a further 3 h at room temperature. To the reaction solution was added $H_2O$, the pH adjusted to pH 7 by the addition of 6 M HCl, and extracted with $CH_2Cl_2$ (3 × 100 mL). The combined organic phases were washed with $H_2O$ (100 mL), dried over $MgSO_4$, and following filtration the solvent was removed (rotavap). The crude residue was triturated in EtOAc (100 mL) and the resulting solid was collected by filtration, dried in a vacuum desiccator, to afford the title compound **82** (0.051 g, 44%) as a bright yellow solid. $^1$H NMR (400 MHz, $CDCl_3$) δ 9.01 (dd, $J$ = 7.6, 1.2 Hz, 1H), 8.81 (dd, $J$ = 7.6, 1.1 Hz, 1H), 8.67 (d, $J$ = 8.5 Hz, 1H), 8.43 (dd, $J$ = 8.4, 1.6 Hz, 2H), 8.27 (dd, $J$ = 7.7, 1.2 Hz, 2H), 8.21 – 8.10 (m, 5H), 7.94 (dd, $J$ = 8.2, 1.5 Hz, 1H), 7.85 (ddd, $J$ = 8.3, 6.8, 1.5 Hz, 1H), 7.66 (ddd, $J$ = 8.0, 6.8, 1.1 Hz, 1H). HRMS (ESI, *m/z*): calculated for $C_{26}H_{16}N_3^+$ $[M + H]^+$ *m/z* = 370.13387; found *m/z* = 370.1339.

# *Chapter Three*

# Synthesis of quinoline-containing starting materials and their corresponding tri- and tetradentate ligands

## 3.1 Chapter Overview

This chapter details an investigation of the synthesis of quinoline-containing starting materials (*Scheme 12*) for the preparation of tridentate and tetradentate tripodal ligands. As mentioned previously, multidentate ligands containing quinoline moieties have thus far been limited to quinolylmethyl moieties, and as yet, no quinolylethyl units have been incorporated into tetradentate tripodal ligands. With this in mind, one of the aims of this chapter is the synthesis of 2-quinolylethyl starting materials and the incorporation of these into tridentate and tetradentate tripodal ligands.

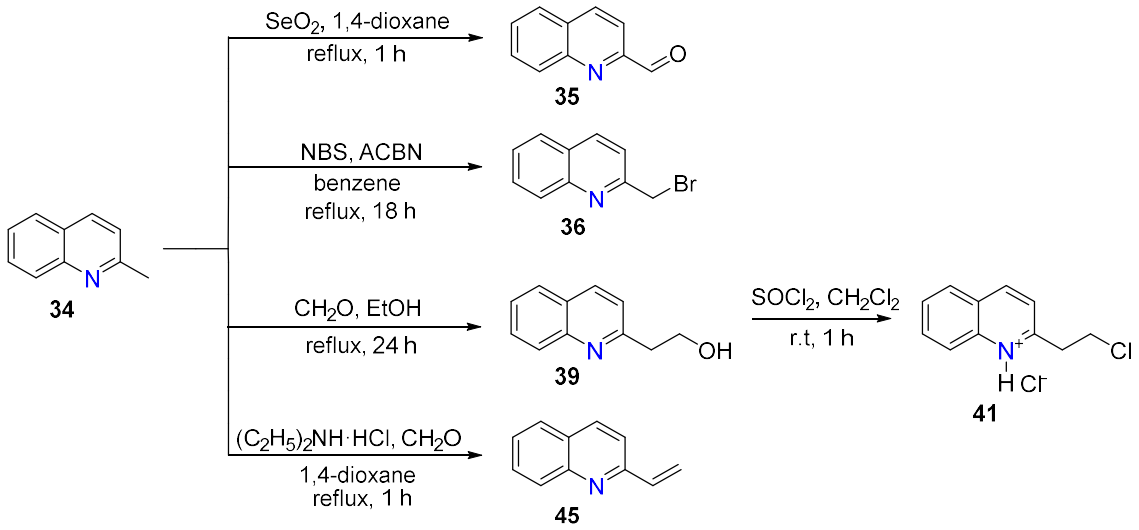


*Scheme 12. General synthetic schemes of quinolyl starting materials derived from 2-methylquinoline.*

## 3.2 Introduction

### 3.2.1 Tetradentate ligands

As previously discussed in *Chapter One* section 1.2.3, a tetradentate tetraamine tripodal ligand consists of a central nitrogen donor atom that is attached to three arms each containing a nitrogen donor (*Figure 56*).

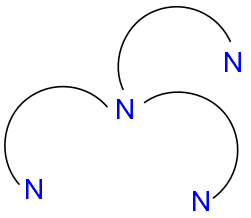

*Figure 56. The general structure of a tripodal tetraamine ligand.*

The synthesis of tripyridyl tripodal ligands, analogous to those reported herein, can be achieved by alkylation of either ammonia or a primary (2-pyridyl)alkylamine with the appropriate pyridine precursor. For example, the symmetrical ligand **11** can be prepared from the reaction of 2 equivalents of 2-vinylpyridine **61** and 2-(pyridin-2-yl)ethan-1-amine **54**,[232,233] or from the reaction of excess 2-vinylpyridine **61** and either ammonium acetate or ammonium chloride (*Scheme 13*).[30,234–236]

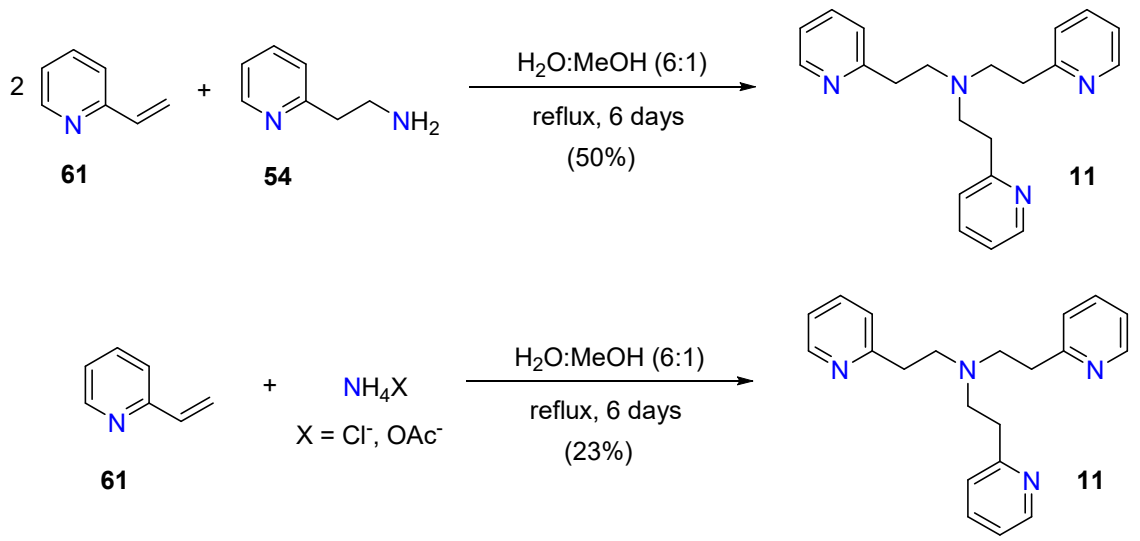


*Scheme 13. Reported syntheses of the ligand **11**.*[28,233]

Reductive amination is another commonly employed method for the preparation of such ligands. To illustrate, **10** can be prepared via reductive amination of 2-(pyridin-2-yl)-*N*-[2-(pyridin-2-yl)ethyl]ethan-1-amine **62** with pyridine-2-carbaldehyde **59** using ($NaBH(OAc)_3$) as the reducing agent. Alternatively, ligand **10** can be synthesised from the reaction of 2 equivalents of 2-vinylpyridine **61** and 1-(pyridin-2-yl)methanamine **56** (*Scheme 14*).[237]

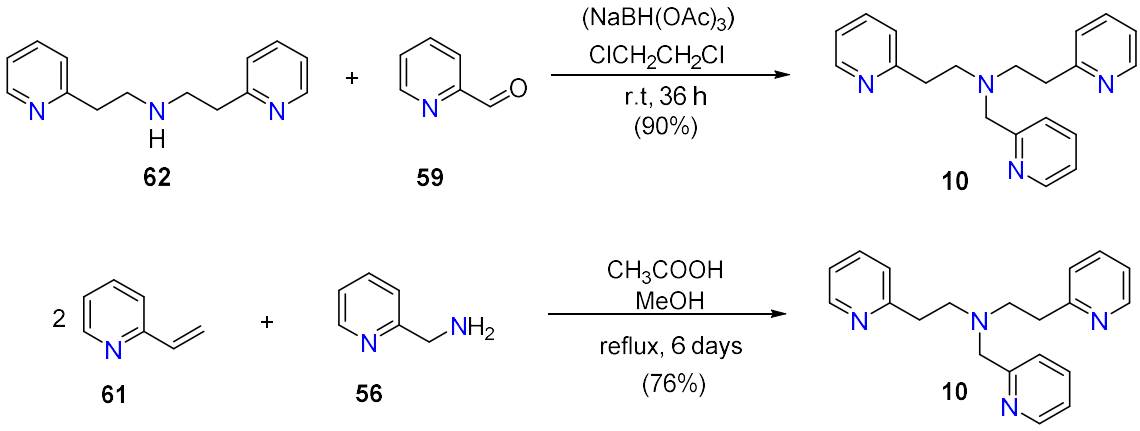


*Scheme 14. Reported syntheses of the ligand **10**.*[237,238]

Another synthetic pathway that utilises a tridentate ligand as a starting material is the synthesis of **9** reported by Lonnon *et al.*[237] The ligand is prepared from the reaction of 1-(pyridin-2-yl)-*N*-[(pyridin-2-yl)methyl]methanamine **60** with 3 equivalents of 2-

vinylpyridine **61** and 1 equivalent of acetic acid refluxed in a MeOH:$H_2O$ mixture (4:1) (*Scheme 15*).[232,237]

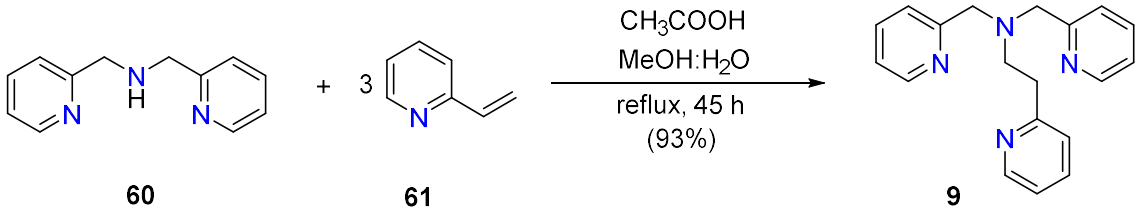


*Scheme 15. Reported synthesis of the ligand **9**.*[237]

The analogous 2-quinolylmethyl-containing tripodal tetradentate ligands are also prepared following similar preparations to the pyridyl ligands described above. The ligand **28** can be prepared from the reaction of 1-(pyridin-2-yl)-*N*-[(pyridin-2-yl)methyl]methanamine **60** and 2-(bromomethyl)quinoline **36** in THF, with added $Et_3N$, at room temperature for 3 days (*Scheme 16*). An alternative synthesis of this ligand involves the reaction of 2-(chloromethyl)quinoline hydrochloride **83** and 1-(pyridin-2-yl)-*N*-[(pyridin-2-yl)methyl]methanamine **60** in anhydrous $CH_3CN$ in the presence of anhydrous $K_2CO_3$.[127]

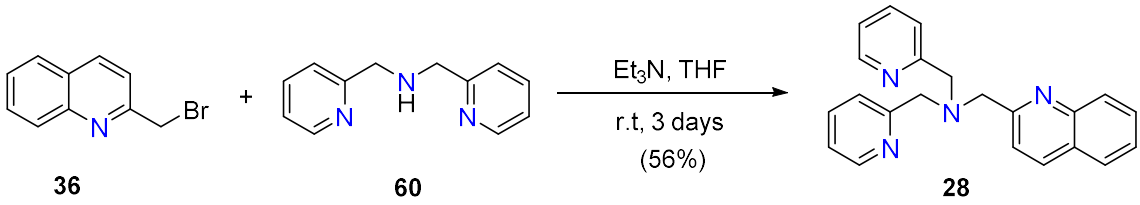


*Scheme 16. Reported synthesis of the ligand **28**.*[125]

The ligand **29** was initially synthesised by Karlin and coworkers[125] by reaction of 2-(bromomethyl)quinoline **36** with 1-(pyridin-2-yl)methanamine **56** in THF in the presence of *i*-$Pr_2NEt$ (*Scheme 17*). An alternative approach reported by Das *et al.*[128] involves the reaction of 1-(pyridin-2-yl)methanamine **56** and 2-(bromomethyl)quinoline **36** in anhydrous DMF in the presence of $Cs_2CO_3$ in the absence of light.

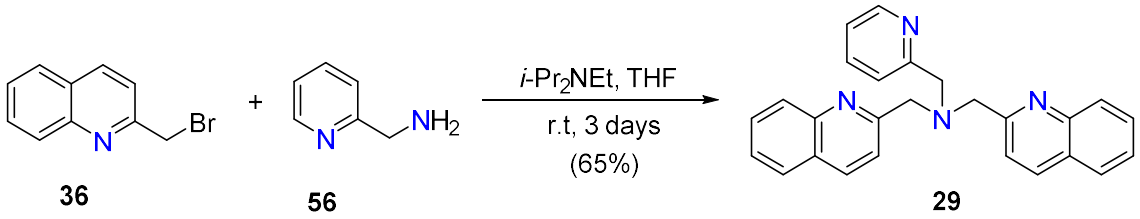


*Scheme 17. Reported synthesis of the ligand **29**.*[125]

As discussed in *Chapter One* section 1.2.3 the chain length of the arms attached to the central nitrogen atom can be the same, in which case the tetradentate tripodal ligands are designated as being symmetric, or different, which gives asymmetric tetradentate tripodal ligands. Utilising such methods gives rise to a plethora of symmetric and asymmetric ligand combinations. Thus, there are four types of starting compounds that are generally used for the synthesis of tetradentate tripodal ligands; alkyl halides, aldehydes, vinylic compounds, and amines.

### 3.2.2 Tridentate ligands

Tridentate ligands contain three donor atoms that have the potential to coordinate to a metal centre (*Figure 57*) (section 1.2.3). The synthesis of such ligands is analogous to that discussed in *Chapter One* section 1.2.4 for the tetradentate ligands. In fact, many of the preparations for the tetradentate tripodal ligands, result in the corresponding tridentate ligand as a byproduct of the reaction.

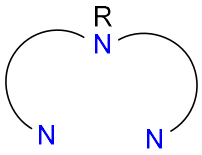


*Figure 57. The general structure of a tridentate amino ligand.*

For example, the tridentate ligand 1-(pyridin-2-yl)-*N*-[(pyridin-2-yl)methyl]methanamine **60** can be prepared from the reaction of 1-(pyridin-2-yl)methanamine **56** and pyridine-2-carbaldehyde **59** following subsequent reduction using $NaBH_4$.[239] Alternatively, the reaction of excess 1-(pyridin-2-yl)methanamine **56** with 2-(chloromethyl)pyridine hydrochloride **84** in the presence of $Na_2CO_3$ affords the same ligand (*Scheme 18*).[240,241] In addition, this methodology also affords the tetradentate analogue **8**.

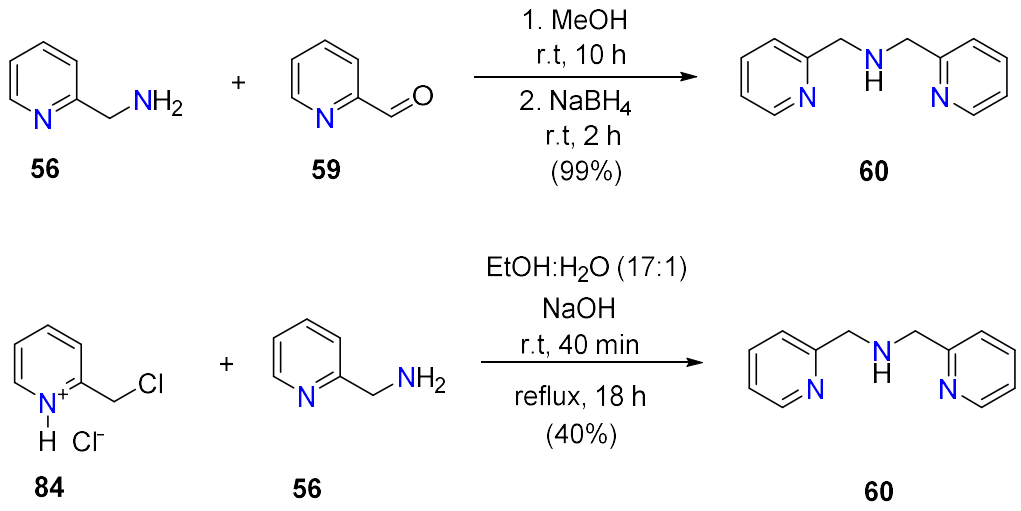


*Scheme 18. Reported syntheses of 1-(pyridin-2-yl)-N-[(pyridin-2-yl)methyl]methanamine* ***60***.[239,241]

There are a handful of tridentate quinolyl-containing ligands reported in the literature that contain unsubstituted quinoline moieties. Again, these compounds are prepared following similar methodologies to those described above.

The reaction between quinoline-2-carbaldehyde **35** and *N*-(2-aminoethyl)acetamide **85** gives the corresponding imine, and $NaBH_4$ reduction of this affords $N^1$-[(quinolin-2-yl)methyl]ethane-1,2-diamine **86**.[92] This ligand can also be prepared by reacting 2-(chloromethyl)quinoline hydrochloride **83** with ethane-1,2-diamine **88** (*Scheme 19*).[93]

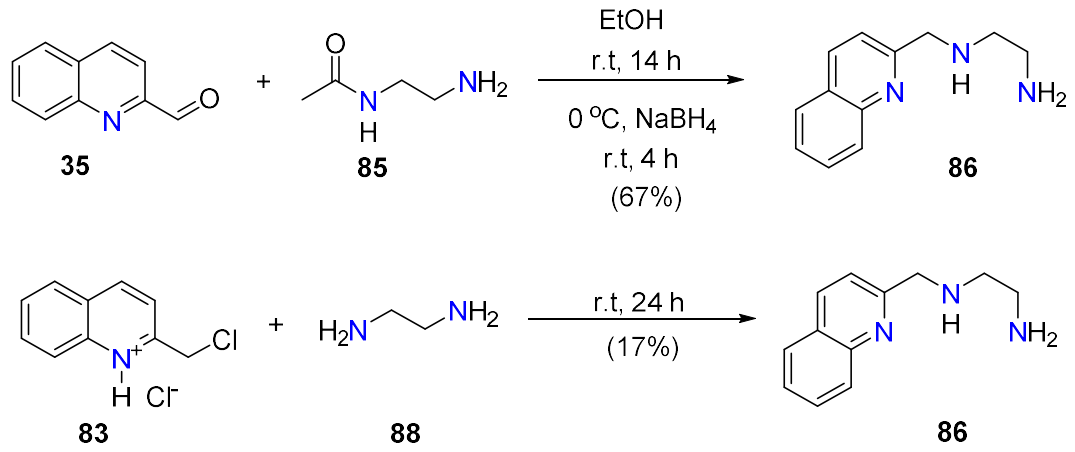


*Scheme 19. Reported syntheses of N[1]-[(quinolin-2-yl)methyl]ethane-1,2-diamine* ***86****.*[92,93]

The ligand *N*-methyl-2-(pyridin-2-yl)-*N*-[(quinolin-2-yl)methyl]ethan-1-amine **89** can be obtained as a viscous yellow oil from the reaction of *N*-methyl-2-(pyridin-2-yl)ethan-1-amine **90** and 2-(chloromethyl)quinoline hydrochloride **83** in the presence of $Cs_2CO_3$ (Scheme 20). It should be noted that the diagram of the ligand given in the original paper is in error, as it contains an isoquinoline, rather than a quinoline unit.[242]

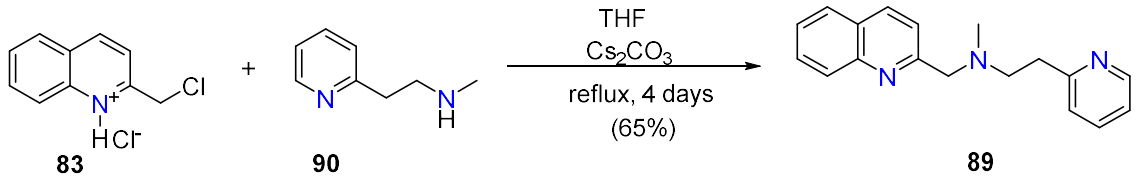


*Scheme 20. Reported synthesis of N-methyl-2-(pyridin-2-yl)-N-[(quinolin-2-yl)methyl]ethan-1-amine* ***89****.*[242]

### 3.2.3 Compounds containing the 2-quinolylethyl moiety

To date it appears that there are only a small handful of compounds that contain 2-ethylquinoline moieties. Two of these are molecules **91** and **92**, derivatives of the more commonly studied phenyl compound lobelane **93**. A study conducted by Vartak *et al.*[243] on improving the water solubility of lobelane **93** (*Figure 58*), afforded the novel quinolyl analogue, quinlobelane **91** (*Figure 58*) from the replacement of the phenyl rings. This compound is most likely the first reported structure to contain a 2-quinolylethyl moiety.

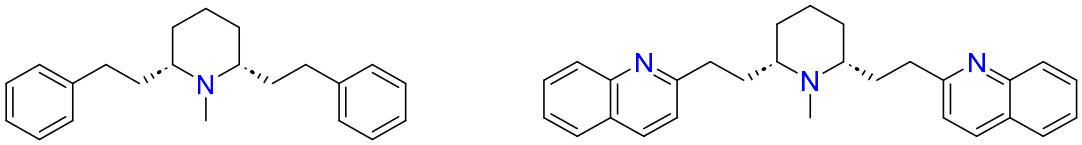

**lobelane 93** **quinlobelane 91**

*Figure 58. Structures of the ligands lobelane (left) and quinlobelane (right).*

The preparation of the quinoline-containing compound was reported from the reaction of 2,6-lutidine **94** with MeOTs to afford compound **95**. In the presence of 2 equivalents of NaOH, **95** is reacted with quinoline-2-carbaldehyde **35** in EtOH followed by sequential reduction of the double bond to afford **91** (*Scheme 21*).[243]

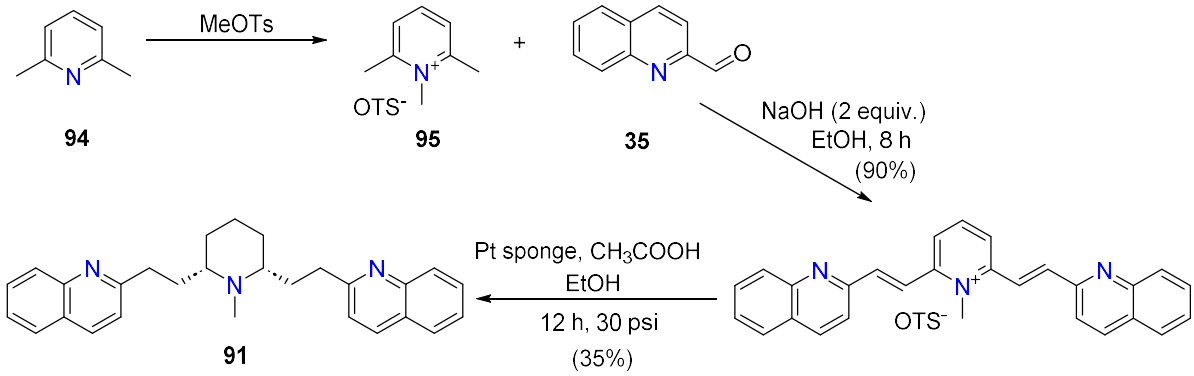


*Scheme 21. Reported synthesis of quinlobelane **91**.*[243]

Subsequently, Ding *et al.*[244] reported an improved synthesis of the piperidine-based compound, **91**. Originally, the N-methylated compounds were synthesised; however, following structure-activity relationship studies on these analogues, it was found that the absence of the N-methyl substituent did not have an impact on their desired properties. With this in mind, the authors continued without the methyl substituent and developed a more efficient synthesis for the formation of **92**. A Wittig reaction of the N-Cbz-protected cis-piperidine-2,6-dicarboxaldehyde **97** with 2-(triphenylphosphinylmethyl)quinoline bromide **98** was employed, followed by sequential deprotection of the *N*-Cbz group and reduction of the alkene groups to afford **92** (*Scheme 22*).

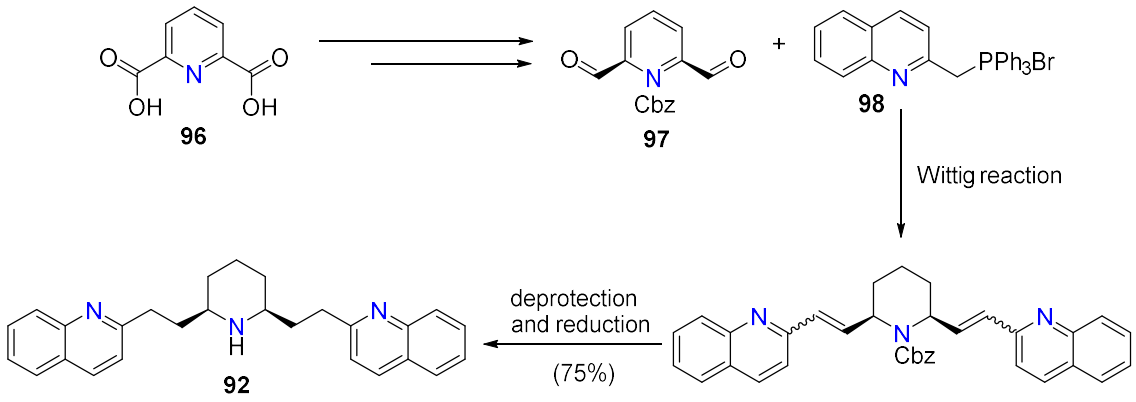


*Scheme 22. Reported modified synthesis of quinlobelane **92**.*[244]

The authors selected the quinoline starting material, 2-(triphenylphosphinyl-methyl)quinoline bromide **98**, which was synthesised via a four step synthetic pathway. The synthesis of the quinoline starting material commenced with the oxidation of 2-methylquinoline **34** to afford quinoline-2-carbaldehyde **35**. The aldehyde was then reduced to the alcohol **99** using $NaBH_4$, followed by a bromination reaction in 33% $HBr/CH_3COOH$ to yield 2-(bromomethyl)quinoline **36**. The final step involved the reaction between the brominated quinoline and triphenylphosphine ($PPh_3$) in toluene to obtain the desired product **98** (*Scheme 23*).[244,245]

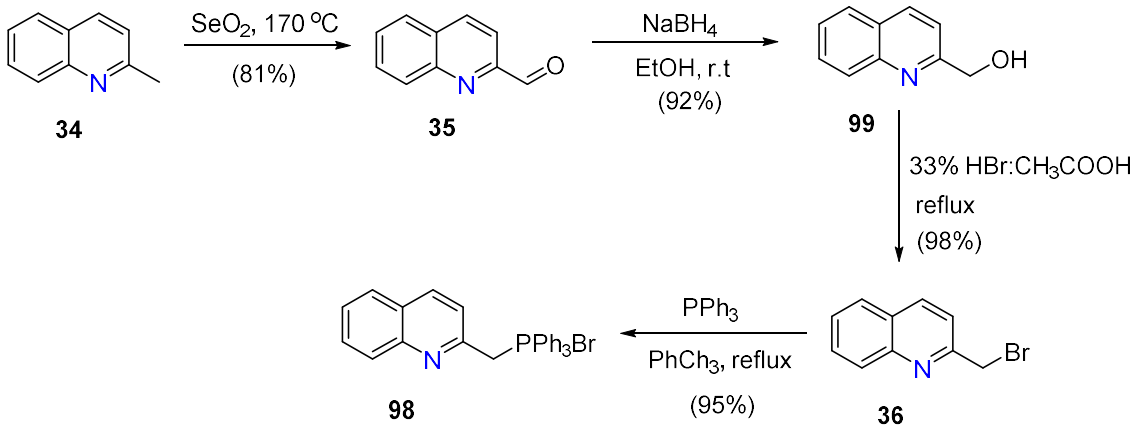


*Scheme 23. Reported synthesis of 2-(triphenylphosphinylmethyl)quinoline bromide **98**.*[244]

The ligand *N*'-{2-[8-amino-6-(trifluoromethyl)quinolin-2-yl]ethyl}-*N*,*N*-dimethylmethanediamine **100** is a mono-quinolylethyl tridentate ligand and has been reported in concert with several other derivatives of the basic skeleton of this compound. The ligand **100** can be prepared via three synthetic steps, commencing with the initial

formation of 8-nitro-6-(trifluoromethyl)-2-vinylquinoline **101** by the treatment of 2-methyl-8-nitro-6-(fluoromethyl)quinoline **102** with $FeCl_3$ and $K_2S_2O_8$ in DMA. Next, the reaction of **101** and N,N-dimethyl-1,2-ethanediamine in the presence of $K_2CO_3$ in 1,4-dioxane, affords **103**. Subsequent reduction of **103**, affords the free ligand **100** (*Scheme 24*).[214] The free ligand was then converted to the hydrochloride salt by the addition of concentrated HCl. This ligand, along with the other derivatives in its series, have been designed to act as chelating compounds for potential use as anti-Alzheimer's agents.[207]

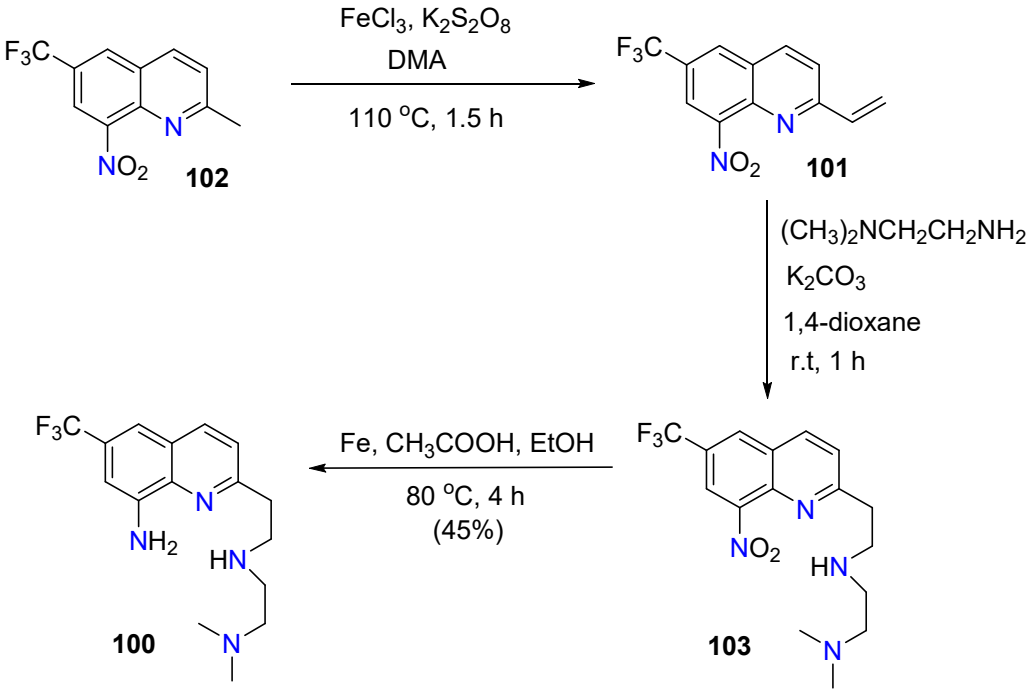


*Scheme 24. Reported synthesis of the ligand **100**.*[214,246]

*N*-(2-(Quinolin-2-yl)ethyl)acetamide **104** can be prepared from the treatment of (quinolin-2-yl)acetonitrile **105** with lithium aluminium hydride in THF at room temperature for 30 minutes. The resulting product is further treated with acetic anhydride in the presence of $Et_3N$ in $CH_2Cl_2$ at room temperature for 2 hours to afford the desired 2-quinolylethyl ligand **104** (*Scheme 25*).

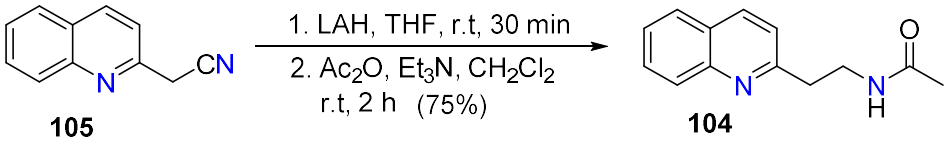


*Scheme 25. Reported synthesis of N-(2-(quinolin-2-yl)ethyl)acetamide **104**.*[215]

Another ligand that is based on the mono-quinolylethyl skeleton is (R)-N-(1-(3,5-di-tert-butylphenyl)-2-(quinolin-2-yl)ethyl)acetamide **106**. The compound **107** is synthesised initially following a preparation similar to that described for **104** above. Sequential treatment with HCl in 1,4-dioxane, $Et_3N$ and acetic anhydride, affords the ligand **106** (*Scheme 26*).[215,246]

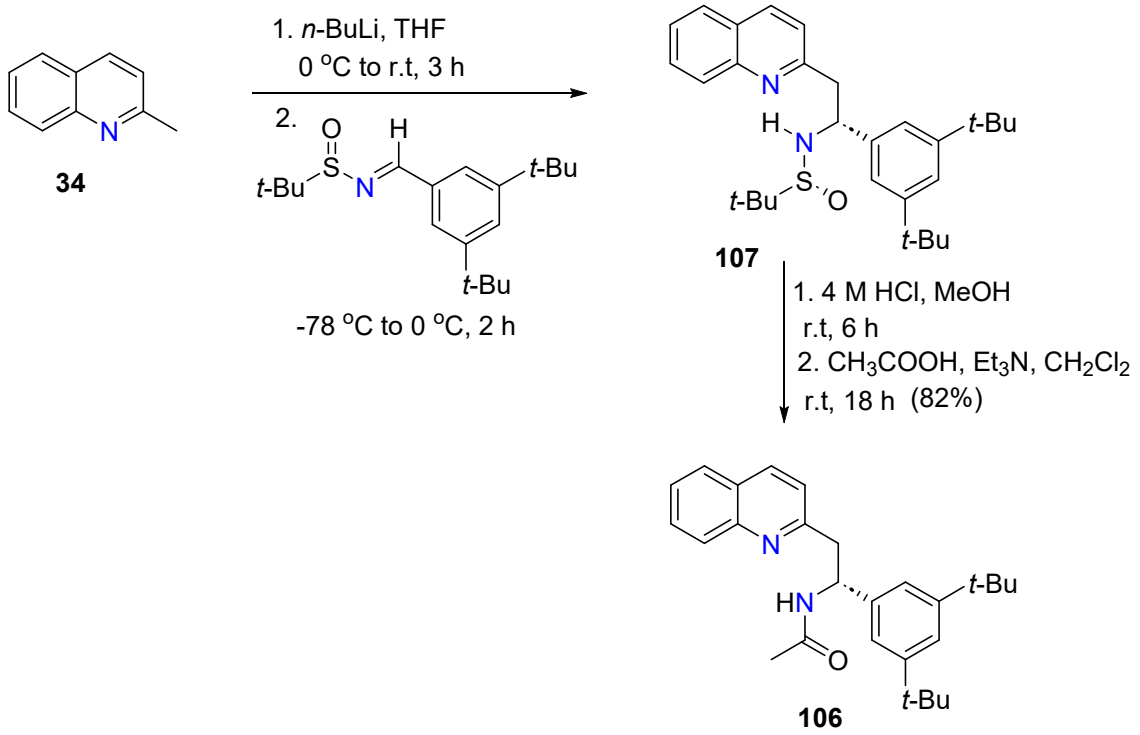


*Scheme 26. Reported synthesis of (R)-N-(1-(3,5-di-tert-butylphenyl)-2-(quinolin-2-yl)ethyl)acetamide **106**.*[215]

### 3.2.4 Aims

This thesis primarily concerns the synthesis and characterisation of new quinoline-containing multidentate ligands. As discussed above, while several derivatives of aminoethylquinoline-containing compounds are known, there is a notable absence of quinolylethyl-containing ligands in which the quinoline unit is unsubstituted. Therefore, in addition to incorporating 2-quinolylmethyl units into multidentate ligands, as reported

elsewhere in this thesis, we are particularly interested in synthesising ligands containing the 2-quinolylethyl moiety.

Using the methods illustrated in *Scheme 12* (section 3.1), the quinoline-containing starting materials quinoline-2-carbaldehyde **35**, 2-(bromomethyl)quinoline **36**, 2-(quinolin-2-yl)ethan-1-ol **39**, 2-(2-chloroethyl)quinoline hydrochloride **41**, 2-(quinolin-2-yl)ethyl methansulfonate **42**, and 2-(quinolin-2-yl)ethyl 4-methylbenzene-1-sulfonate **43** have been synthesised. These compounds have then been used as described below to afford a series of tetradentate and tridentate ligands.

## 3.3 Synthesis of quinoline starting materials

### 3.3.1 The synthesis of 2-quinolylmethyl compounds

The aldehyde-containing starting material, quinoline-2-carbaldehyde **35**, was a necessary starting material for the synthesis of these ligands. Following a modified previously reported preparation,[244] the desired product was prepared from the reaction of 2-methylquinoline **34** and $SeO_2$ in 1,4-dioxane at reflux for 1 hour. After cooling to room temperature, the mixture was filtered to remove a black precipitate, presumably elemental selenium, and the solvent was removed. The crude material was dissolved in $CH_2Cl_2$ followed by an aqueous work-up to afford quinoline-2-carbaldehyde **35** (*Scheme 27*). The identity of the product was confirmed by NMR spectroscopy and mass spectrometry; these data were consistent with the literature.[244,247]

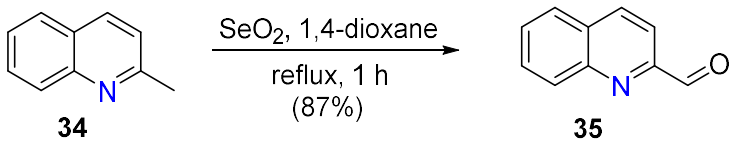


*Scheme 27. The synthesis of quinoline-2-carbaldehyde **35**.*

2-(Bromomethyl)quinoline **36** was prepared by modification of the method reported by Zhao *et al.*[216] A mixture of 2-methylquinoline **34** and N-bromosuccinimide in benzene, in the presence of 1,1-azobis(cyclohexanecarbonitrile) (ACBN), was stirred at reflux for 18 hours. Following aqueous work-up and purification by silica gel column chromatography, the brominated compound **36** was obtained (*Scheme 28*). Analysis by $^1$H NMR spectroscopy revealed the presence of a two proton singlet at $\delta_H$ 4.72 pm, corresponding to the newly installed $CH_2$ group. The synthesis of **36** was further

confirmed by $^{13}C$ NMR spectroscopy and mass spectrometry, data from both of which matched those previously described the literature.[216,217]

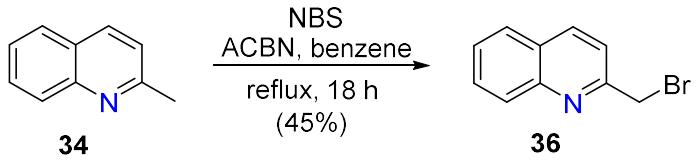


**34** **36**

*Scheme 28. The synthesis of 2-(bromomethyl)quinoline **36**.*

According to the authors, conversion of 2-(bromomethyl)quinoline **36** to the hydrobromide salt is helpful for long term storage to mitigate the polymerisation of the free base.[217] However, in our hands the free base was found to be more useful moving forward. As a result, the free base was synthesised, purified by silica gel chromatography, and carried over to the next step immediately to avoid any polymerisation of the product.

While 2-(bromomethyl)quinoline **36** is useful as an electrophile in formation reactions of multidentate ligands, aminoalkylquinolines will also be useful as nucleophiles in such reactions. The amine provides the central nitrogen atom to which the other arms can easily be attached through reaction with alkylhalides or aldehydes. Therefore, the synthesis of 1-(quinolin-2-yl)methanamine **108** became the next reaction of interest.

Following a previously reported preparation,[216] 2-(bromomethyl)quinoline **36** (described above) and potassium phthalimide in DMF were stirred at room temperature for 5 hours (*Scheme 29*). To the reaction flask was added $H_2O$ and the resultant precipitate was collected by filtration and washed with additional $H_2O$. Recrystallisation from EtOH afforded a white solid. $^1H$ NMR analysis of the solid revealed a spectrum that was not consistent with that reported in the literature for **109**. At this point in time, it was decided not to continue with this reported procedure.

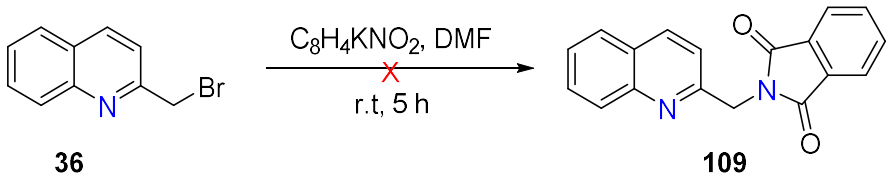


*Scheme 29. Attempted synthesis of 2-[(quinolin-2-yl)methyl]-1H-isoindole-1,3(2H)-dione **109**.*

An alternative method was attempted next involving the synthesis of the corresponding oxime, *N*-[(*E*)-(quinolin-2-yl)methylidene]hydroxylamine **37**, followed by subsequent reaction with acetic acid and zinc dust in EtOH. With slight modifications to the reported preparation,[218] **37** was synthesised from the reaction of quinoline-2-carbaldehyde, hydroxylamine hydrochloride and $K_2CO_3$ in EtOH at reflux for 30 minutes (*Scheme 30*). Following filtration, the solvent was removed (rotavap) to afford a yellow solid **37**. $^1$H NMR analysis of the crude material **37**, revealed a clean spectrum that was consistent with the literature.[218] The solid was used in the next step without further purification.

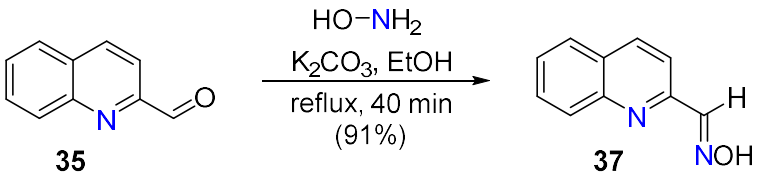


*Scheme 30. The synthesis of the oxime intermediate **37**.*

Following the methodology of Sahu *et al.,*[248] with slight modifications, **37** and acetic acid were dissolved in EtOH. The addition of zinc powder was made in small increments over 1 hour. The mixture was then stirred at room temperature for a further 13 hours (*Scheme 31*). Following filtration, concentration of the filtrate and an aqueous work-up, the residue was obtained as a brown oil.

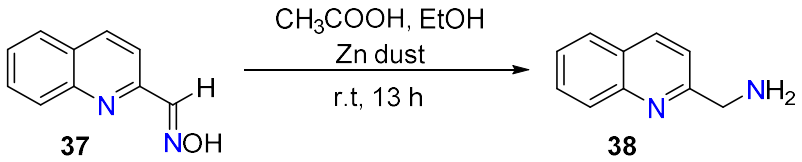


*Scheme 31. The synthesis of 1-(quinolin-2-yl)methanamine **38**.*

The crude material was analysed by mass spectrometry, and a product ion peak at *m/z* = 159.1 was observed in the mass spectrum, consistent with the calculated value for **38** (calcd. for $C_{10}H_{11}N_2^+$ $[M+H]^+$ *m/z* = 159.09; found *m/z* = 159.1). However, this peak was of low relative abundance in comparison to several other signals, with the base peak observed at *m/z* = 291.2. However, this peak could not be sensibly assigned. Further analysis of the crude material by $^1$H NMR spectroscopy revealed a noisy spectrum consistent with the presence of a number of compounds. This was confirmed by TLC analysis which gave a streaky plate with several spots. Purification by silica gel chromatography failed to isolate any of the desired product.

Since we now had several 2-quinolylmethyl starting materials, we decided to use these in reactions with aminomethyl- and aminoethylpyridines for the preparation of tri- and tetradentate ligands.

### 3.3.2 The synthesis of 2-quinolylethyl-containing starting materials

As discussed previously in *Chapter One* section 1.3.3, tripodal ligands that contain 2-quinolylethyl moieties have yet to be reported in the literature. As a result, a series of 2-quinolylethyl derivatives were required for the synthesis of such ligands. 2-(quinolin-2-yl)ethan-1-ol **39** was initially chosen as a useful starting material for the preparation of such derivatives.

Following a previously published method,[219] 2-methylquinoline **34** and 30% formaldehyde in a EtOH:$H_2O$ mixture (1:1) were heated at reflux for 24 hours (*Scheme 32*). Following removal of the reaction solvent, the crude residue was triturated with EtOAc to afford a white precipitate.

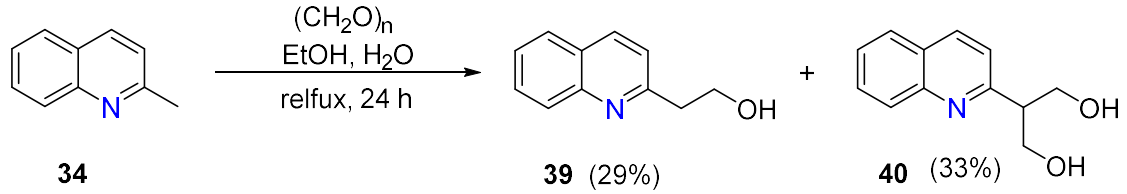


*Scheme 32. The synthesis of 2-(quinolin-2-yl)ethan-1-ol **39** and 2-(quinolin-2-yl)propane-1,3-diol **40**.*

The $^{1}$H NMR spectrum (*Figure 59*) of this exhibited two multiplet signals each integrating for two protons ($\delta_H$ 4.29 and 4.16 ppm), as well as the loss of the resonance assigned to the methyl group of the starting material. In addition, a one proton quintet appearing at $\delta_H$ 3.21 ppm was present, a signal that could not be assigned to the desired product. Further analysis of the sample by mass spectrometry revealed the presence of a single peak, with a molecular weight corresponding to that of 2-(quinolin-2-yl)propane-1,3-diol **40** (calcd. $C_{12}H_{13}NO_2^+$ $[M + H]^+$ *m/z* = 204.0; found *m/z* = 204.0). Upon revisitation of the $^{1}$H NMR spectrum and further 2D NMR analysis, the resonance at $\delta_H$ 3.20 ppm was assigned to the -CH proton from the diol.

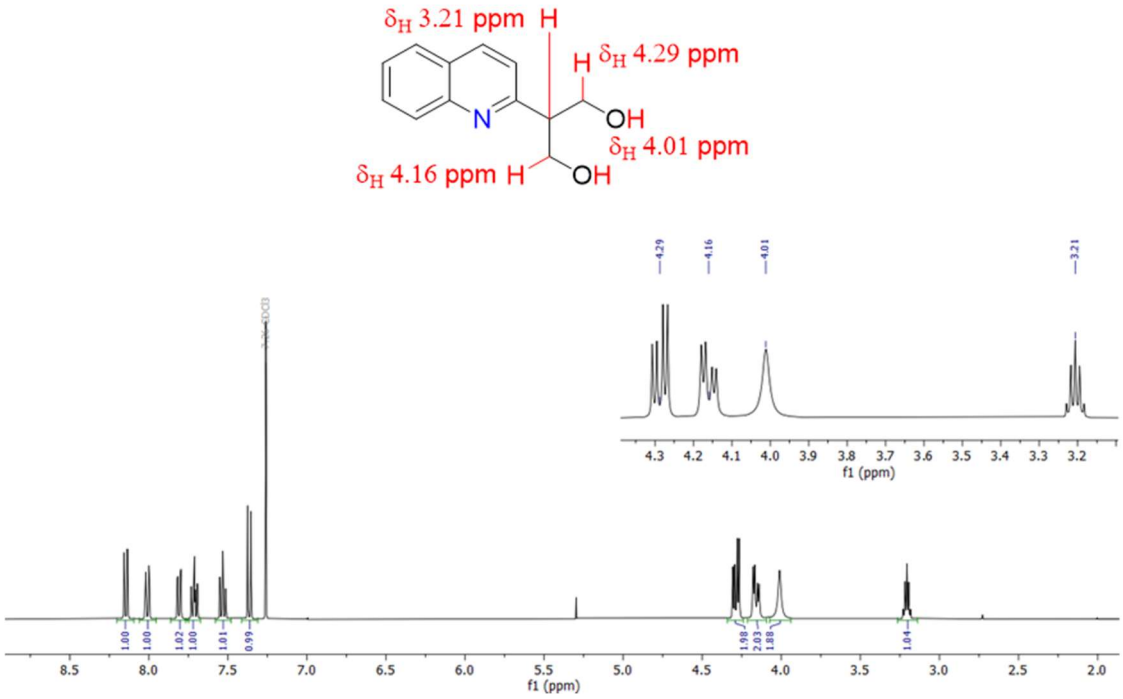


*Figure 59. $^{1}H$ NMR spectrum of 2-(quinolin-2-yl)propane-1,3-diol **40** in $CDCl_3$.*

The presence of 2-(quinolin-2-yl)propane-1,3-diol **40** in the reaction mixture was not reported by the authors of the referenced paper;[219] however, the synthesis of this compound using similar experimental procedures has been previously reported.[220,249] Following the method of Yang *et al.*,[220] we found that the obtained product was identical to the diol **40** we had previously isolated.

The first reaction was then repeated, and 2-(quinolin-2-yl)ethan-1-ol **39** was obtained following silica gel column chromatography of the crude material, separating the desired product from the diol. $^{1}H$ NMR of the product revealed two triplets at $\delta_H$ 4.15 and 3.20 ppm corresponding to the ethyl -$CH_2$ protons (*Figure 60*). Remaining characterisation data ($^{13}C$ and 2D NMR and LRMS) were consistent with those reported in the literature[219] and confirmed the isolation of the correct product.

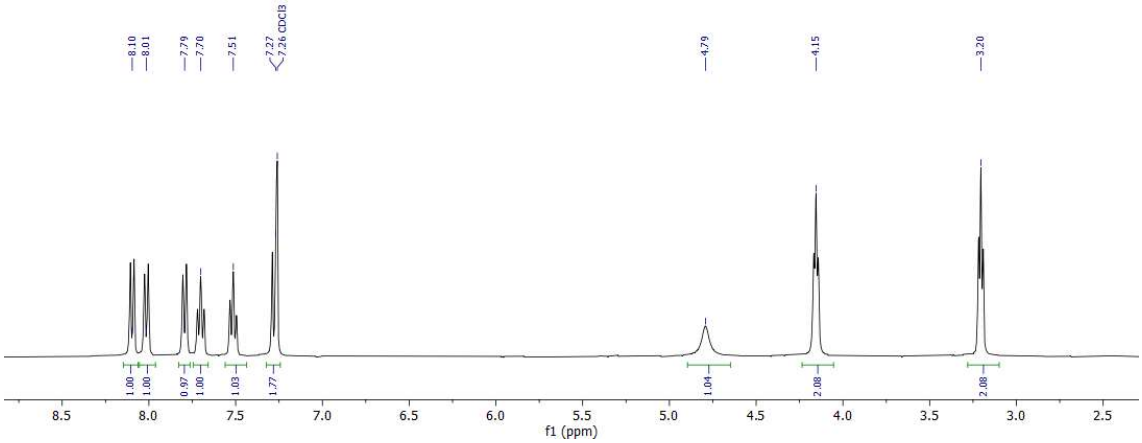


*Figure 60. $^{1}H$ NMR spectrum of 2-(quinolin-2-yl)ethan-1-ol **39** in $CDCl_3$.*

Having successfully prepared 2-(quinolin-2-yl)ethan-1-ol **39**, it was then planned to use this as the starting material for the synthesis of 2-(2-chloroethyl)quinoline **41** following the method of Huang *et al*.[250] This involved the treatment of 2-(quinolin-2-yl)ethan-1-ol **38** with thionyl chloride in anhydrous $CH_2Cl_2$ at room temperature for 1 hour. As per the reported method, after the removal of excess solvent, the subsequent crude product was dissolved in a large volume of ethyl acetate, washed with brine, dried over $MgSO_4$ and excess solvent was removed (rotavap) following filtration. An attempt was then made to analyse the crude material by $^{1}H$ NMR in $CDCl_3$ following the reported method. However, in our hands the addition of $CDCl_3$ only partially dissolved the solid, leaving a cloudy white residue in the flask. The resulting $^{1}H$ NMR spectrum collected was noisy due to the poor solubility of the compound and suggested the presence of a compound that was not the desired molecule. Attempts to purify the crude material by silica gel chromatography resulted in an increased amount of this unknown compound, which was later found to be 2-vinylquinoline **45**.

It was of interest that the obtained material was not very soluble in $CDCl_3$, contrary to the observations of the authors. Given the acidic environment of the reaction mixture and the lack of any basic workup, the $^{1}H$ NMR was re-run in $D_2O$ in which the product was completely dissolved, strongly suggesting the presence of a salt.

The reaction was attempted again under the same conditions, but in this case the crude material was triturated with petroleum ether to afford the desired compound as the hydrochloride salt **41.HCl** in high yield (86%) (*Scheme 33*).

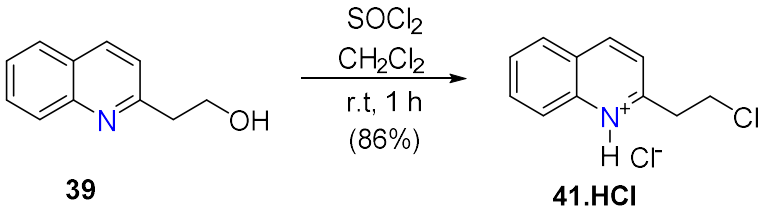


**39** **41.HCl**

*Scheme 33. The synthesis of -(2-chloroethyl)quinoline hydrochloride **41.HCl***

Analysis by mass spectrometry revealed the successful isolation of the clean 2-(2-chloroethyl)quinoline hydrochloride product **41.HCl**. Further confirmation was obtained by $^{1}$H NMR analysis of 2-(quinolin-2-yl)ethan-1-ol hydrochloride **39.HCl** and 2-(2-chloroethyl)quinoline hydrochloride **41.HCl** both in $D_2O$. A sample of 2-(quinolin-2-yl)ethan-1-ol hydrochloride **39.HCl** was prepared *in situ* by the addition of DCl to the free base alcohol **39** in $D_2O$. Comparing the $^{1}$H NMR spectra ($D_2O$) of 2-(2-chloroethyl)quinoline hydrochloride **41.HCl** and 2-(quinolin-2-yl)ethan-1-ol hydrochloride **39.HCl** revealed a shift in ppm of the ethylene triplets from $\delta_H$ 3.97 and 3.31 ppm to $\delta_H$ 4.14 and 3.71 ppm (Figure 61). This shift indicated that the desired product had been formed.

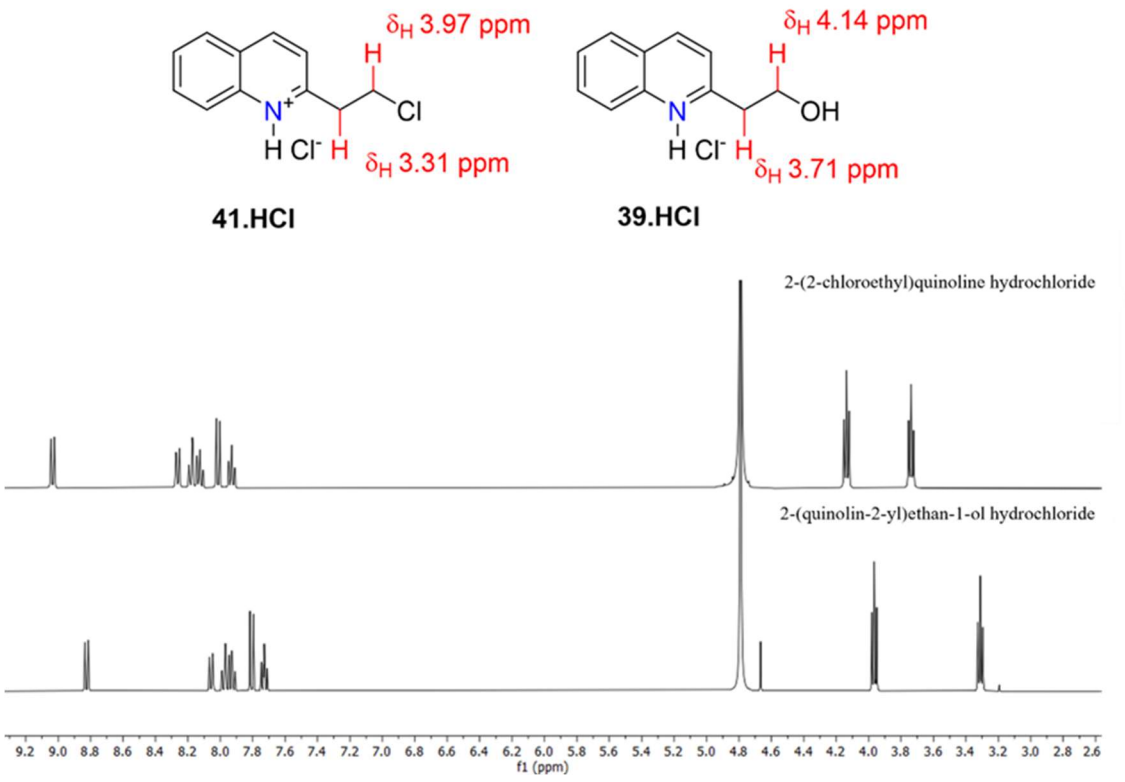


*Figure 61.* $^{1}H$ *NMR spectra of 2-(quinolin-2-yl)ethan-1-ol hydrochloride* ***39.HCl*** *(top) and 2-(2-chloroethyl)quinoline hydrochloride* ***41*** *(bottom) in* $D_2O$.

Following the successful isolation of 2-(2-chloroethyl)quinoline hydrochloride **41.HCl**, it was decided to use this starting material for the preparation of a tetradentate tripodal ligand. Thus, following the methodology of Wei and co-workers,[117] with slight modifications, **41.HCl** and 1-(pyridine-2-yl)methanamine **56**, in the presence of *i*-$Pr_2NEt$, were stirred in THF at room temperature for 5 days (*Scheme 34*). Monitoring the reaction via TLC proved difficult due to the number of streaky spots on the plate. After a base wash and removal of the solvent *in vacuo*, a crude brown residue was obtained. Analysis of the sample by $^{1}H$ NMR spectroscopy revealed a noisy spectrum that was not consistent with that of the desired product. The reaction was attempted several times with modified reaction conditions, none of which afforded the title compound **57**.

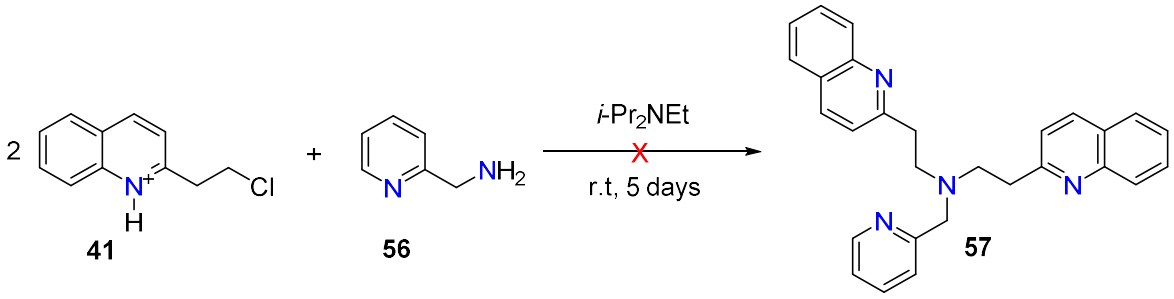


*Scheme 34. Attempted synthesis of the ligand **57**.*

We then considered using 2-(2-bromoethyl)quinoline **44** as the starting material, as we believed that a better leaving group, such as bromide, may be required for the alkylation of the amine to proceed.

The conversion of alcohols to alkyl bromides are well-known substitution reactions with a large number of different reaction conditions having been reported for a wide variety of alcohols.[251–257] Surprisingly, a SciFinder structure search for 2-(bromoethyl)quinoline **44** gave only two hits; one, a Japanese paper from 1944 by Zasshi, which was unavailable, and a paper in which it was reported that 2-(2-bromoethyl)quinoline **44** was commercially obtained.[258]

However, there are several reported methods for the conversion of (quinolin-2-yl)methanol **99** to 2-(bromomethyl)quinoline **36**.[247,259–261] The one step reaction between (quinolin-2-yl)methanol **99** and 33% HBr in acetic acid reported by Ding and co-workers[244] afforded the hydrobromide salt in high yield (98%). Alternatively, a two-step process can be used, in which mesylation of an alcohol is followed by substitution with bromide. Both methods were investigated.

Following the methodology of Schnopp *et al.*,[262] with modifications, a solution of HBr in acetic acid (33%) was added to a solution of 2-(quinolin-2-yl)ethan-1-ol **39** dissolved in acetic acid and the solution was refluxed for 2 hours (*Scheme 35*). The literature preparation reported that the desired product precipitates upon the addition of $Et_2O$ and in our hands a precipitate did form. However, $^1$H NMR analysis of the crude material revealed a noisy spectrum inconsistent with that of the desired product **44.HCl**. As a result, the mesylation reaction was then investigated.

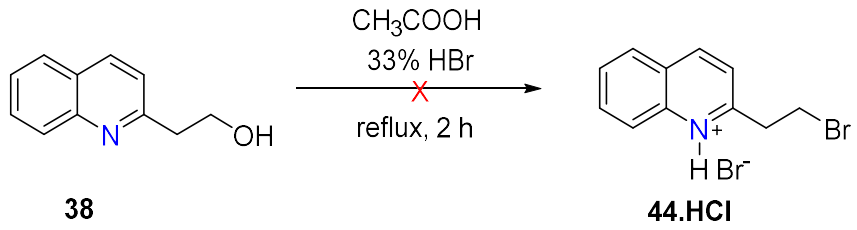


**38** **44.HCl**

*Scheme 35. Attempted synthesis of 2-(2-bromoethyl)quinoline hydrobromide **44.HCl***

With the unsuccessful formation of **44.HCl** the second mesylation method was trialled next. 2-(quinolin-2-yl)ethyl methanesulfonate **42** was prepared from 2-(quinolin-2-yl)ethan-1-ol **38** according to the literature.[221] A mixture of 2-(quinolin-2-yl)ethan-1-ol **39** and methanesulfonyl chloride in anhydrous $CH_2Cl_2$, in the presence of $Et_3N$, was stirred at room temperature for 3 hours. Over this time the reaction solution changed from yellow to green in colour (subsequent results suggest that this may be due to formation of polymerised 2-vinylquinoline). Following aqueous work-up, $^1H$ NMR analysis of the crude material suggested the presence of an equal mix of the mesylated product **42** and another compound that was shown to be 2-vinylquinoline **45**. Purification via silica gel chromatography afforded the mesylated compound in low yield (8.5 %).

In attempts to increase the yield and prevent the formation of 2-vinylquinoline **45**, the reaction was monitored by TLC and revealed that full conversion of the starting material to the mesylated product **42** occurred in under 10 minutes. After this time, TLC monitoring showed the presence of 2-vinylquinoline **45** in the reaction mixture. To slow formation of this byproduct, the reaction was carried out at 0 °C, and this allowed for exclusive isolation of the mesylated quinoline **42**. It was found that once the reaction had been stopped, the crude material was still very reactive, and the following work-up and solvent removal had to be done quickly with no increase in temperature.

To confirm that higher temperatures increase the rate at which the vinyl byproduct is formed, the reaction was repeated at temperatures of 40 °C, 60 °C and 100 °C. In all cases, almost complete conversion to 2-vinylquinoline **45** was observed.

Therefore, following our modified method, a solution of 2-(quinolin-2-yl)ethan-1-ol **39** and mesyl chloride in anhydrous $CH_2Cl_2$, in the presence of $Et_3N$, was stirred at 0 °C for 10 minutes (*Scheme 36*). Following aqueous work-up, 2-(quinolin-2-yl)ethyl methanesulfonate **42** was obtained without further purification.

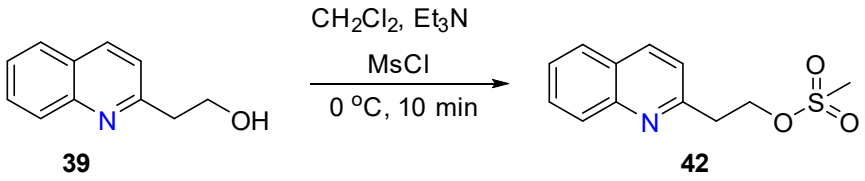


*Scheme 36. The synthesis of 2-(quinolin-2-yl)ethyl methanesulfonate **42**.*

Analysis by $^{1}$H NMR spectroscopy revealed the presence of a three-proton singlet at $\delta_H$ 2.93 ppm in the $^{1}$H NMR spectrum (*Figure 62*), corresponding to the newly installed methanesulfonyl group, consistent with the literature.[221]

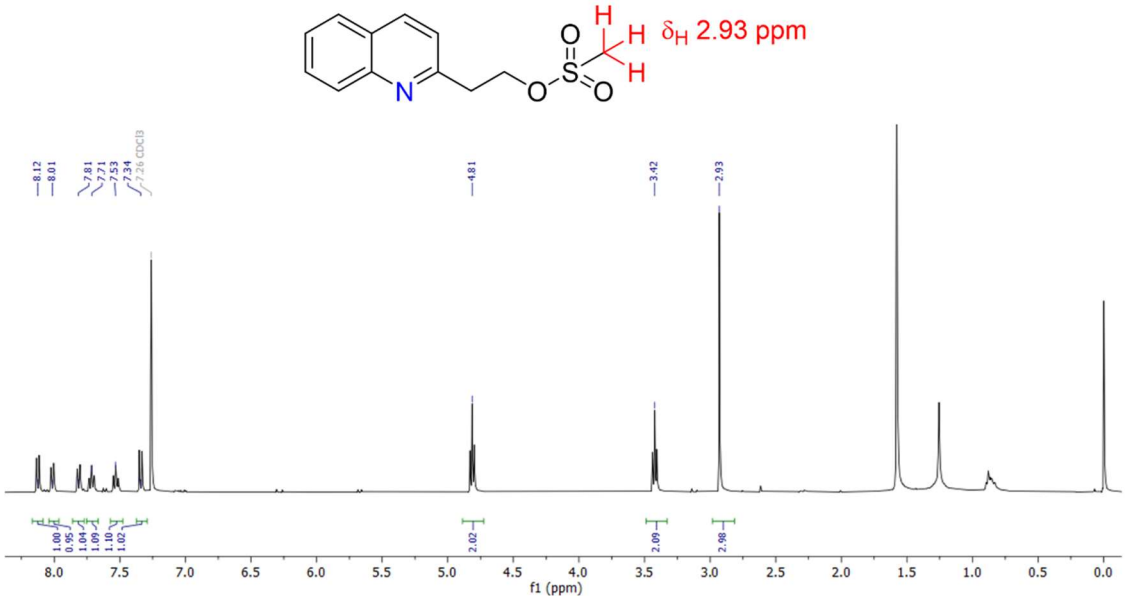


*Figure 62. $^{1}$H NMR spectrum 2-(quinolin-2-yl)ethyl methanesulfonate **42** in $CDCl_3$.*

As mentioned previously, purification of the crude material using silica gel chromatography resulted in a very poor yield of the mesylated product. This can be attributed to an $SiO_2$-catalysed elimination reaction that accelerates the conversion of 2-(quinolin-2-yl)ethyl methanesulfonate **42** to 2-vinylquinoline **45**. This is plausible due to the presence of both hydroxides and oxides on the silica surface that can provide a slightly basic environment to aid the elimination reaction.

The formation of vinylic compounds from the corresponding sulfonate esters is a known reaction. In 2008, Albanese *et al.*[263] reported the preparation of various vinyl heterocyclic

compounds through β-elimination of the corresponding sulfonate ester. The compounds were synthesised in 50% aqueous NaOH solutions at 25 °C to 40 °C with the addition of a phase transfer catalyst. This paper reported the conversion of 2-(pyridin-2-yl)ethan-1-ol **113**, via the sulfonate intermediate **114**, to 2-vinylpyridine **51** (*Scheme 37*). It was noted that the reaction does require a phase transfer catalyst since the reaction is performed under aqueous conditions. It was also demonstrated that the percentage of NaOH was important, with successful conversion requiring at least 40% NaOH.[263]

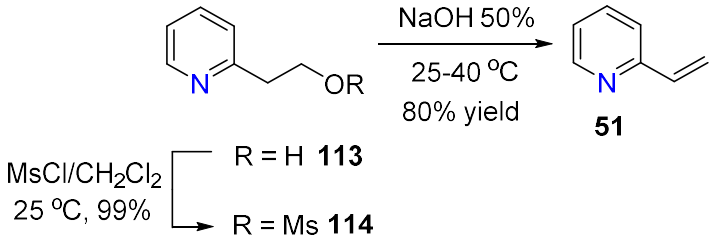


*Scheme 37. Reported synthesis of 2-vinylpyridine **51**.*[263]

In our hands, we were surprised to observe that the formation of 2-vinylquinoline **45** proceeds under very mild conditions in comparison to those reported in the literature. In our hands, 2-vinylquinoline **45** was formed from 2-(quinolin-2-yl)ethylmethanesulfonate **42** in $CH_2Cl_2$ in the presence of only 2 equivalents of $Et_3N$ at room temperature.

Given the ease of this elimination reaction, we wondered if replacement of the mesyl group with a tosyl group might either prevent, or substantially retard, this undesired process, and we therefore set about preparing the tosylated derivative **43**.

Fukata *et al.*[222] reported the preparation of 2-(quinolin-2-yl)ethyl 4-methylbenzene-1-sulfonate **43** from the reaction of the corresponding alcohol with toluene-*p*-sulfonyl chloride and recrystallisation from light petroleum; however, no further details or references were provided.

As was found for 2-(quinolin-2-yl)ethyl methanesulfonate **42**, the synthesis of 2-(quinolin-2-yl)ethyl 4-methylbenzene-1-sulfonate **43** required several attempts to find the best reaction conditions. In contrast to the mesylation reaction described above, formation of the tosylated quinoline **43** required a longer reaction time. However, this also allowed more time for the tosylated product **43** to undergo self-elimination and convert to the vinyl derivative. As a result, **43** could not be obtained in the crude material free from 2-

vinylquinoline **45**. Attempts to mitigate this issue included performing the reaction at 0 °C; although this reduced the amount of 2-vinylquinoline **45** formed, purification of the crude material was still necessary.

Isolation of **43** proved difficult when purification was attempted using silica gel chromatography. TLC analysis of the crude reaction mixture showed equal amounts of 2-(quinolin-2-yl)ethyl 4-methylbenzene-1-sulfonate **43** and 2-vinylquinoline **45**. However, when the crude material was passed through the column, only a small fraction of the desired product **43** was isolated, and the major product obtained was 2-vinylquinoline **45**, as evidenced by $^{1}$H NMR and mass spectrometry. It is suspected that the slightly basic silica gel again facilitated the elimination reaction and as a result the tosylated product **43** was converted to 2-vinylquinoline **45**. Separation of the two compounds could be achieved by triturating the crude material with petroleum spirits to afford the pure compound **43** in a moderate yield. This was achieved by following a literature method, with slight modifications;[221] a solution of 2-(quinolin-2-yl)ethan-1-ol **39** in anhydrous $CH_2Cl_2$ was cooled on ice, $Et_3N$ and *p*-toluenesulfonyl chloride were added and the reaction mixture was stirred for 2 days (*Scheme 38*). Following an aqueous work-up and solvent removal, the crude product was triturated with petroleum ether to afford the title compound **43** as a cream coloured solid.

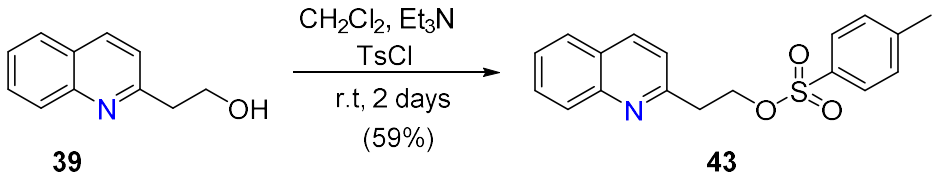


*Scheme 38. The synthesis of 2-(quinolin-2-yl)ethyl 4-methylbenzene-1-sulfonate **43**.*

The structure of the desired product **43** was confirmed by $^{1}$H NMR spectroscopy, with a new diagnostic three proton singlet revealed in the $^{1}$H NMR spectrum at $\delta_H$ 2.32 ppm confirming the introduction of the tosyl group (*Figure 63*).

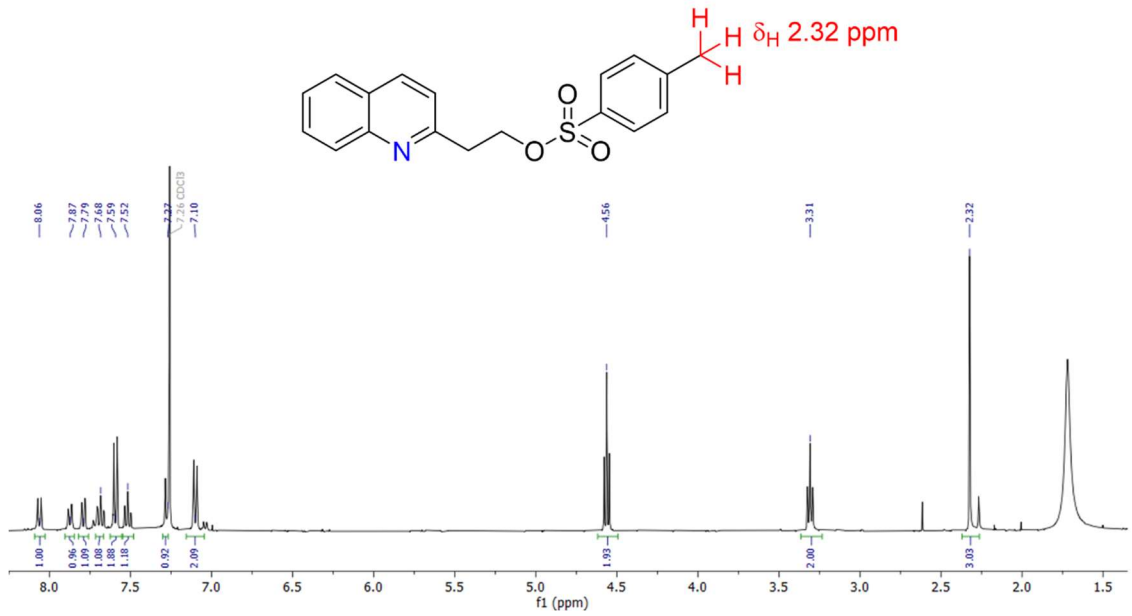


*Figure 63. $^{1}H$ NMR spectrum of 2-(quinolin-2-yl)ethyl 4-methylbenzene-1-sulfonate **43** in $CDCl_3$.*

Over the time the reaction took place there was a change in colour from a pale-yellow solution to a green solution. The change in colour was observed when the product was stored for extended periods of time and was also observed during the longer reaction times for 2-(quinolin-2-yl)ethyl methanesulfonate **42**. The green colour is suspected to be caused by polymerisation of the 2-vinylquinoline that is generated over the longer time periods. Long term storage of such compounds has been studied and similar observations were reported.[264]

While the pure 2-(quinolin-2-yl)ethyl 4-methylbenzene-1-sulfonate **43** that was isolated did prove to be more stable towards elimination in comparison to 2-(quinolin-2-yl)ethyl methanesulfonate **42**, using the mesylated quinoline as the starting material for the formation of 2-(2-bromoethyl)quinoline **44** proved a more convenient option, as **42** could be isolated cleanly from the crude reaction and the reaction time is significantly shorter.

As discussed previously, there are two commonly employed pathways to transformation of an -OH functional group to its brominated analogue. These include direct bromination of the alcohol using HBr, and mesylation of the alcohol followed by substitution with a bromide source. With the successful isolation of 2-(quinolin-2-yl)ethyl methanesulfonate **42**, the mesylation pathway was investigated next in an attempt to synthesise the desired brominated product, 2-(2-bromoethyl)quinoline **44**.

It was envisioned that the synthesis of the quinoline derivative would follow an analogous pathway to that of 2-(2-bromoethyl)pyridine analogue. Following a literature method,[265] with modifications, 2-(quinolin-2-yl)ethyl methanesulfonate **42** and LiBr were refluxed in $(CH_3)_2CO$ for 1 hour (*Scheme 39*). Following aqueous workup and attempted purification by silica gel chromatography, $^1$H NMR analysis revealed a noisy spectrum with the major product being 2-vinylquinoline **45**.

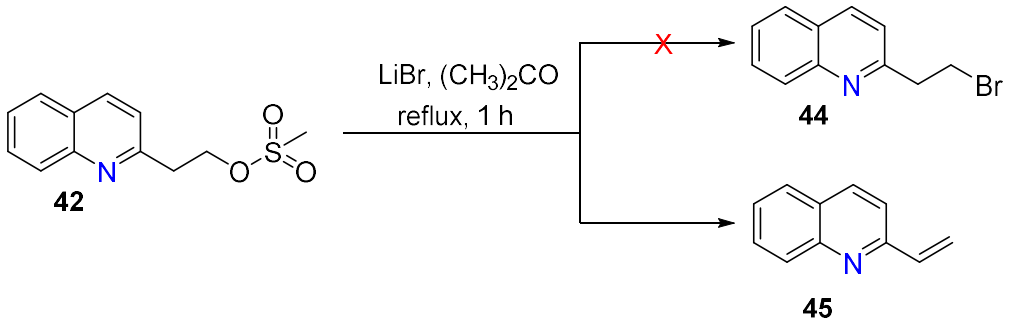


*Scheme 39. Attempted synthesis of 2-(2-bromoethyl)quinoline **44**.*

The reaction was then attempted at room temperature in THF as the solvent (*Scheme 40*).[266] This time the $^1$H NMR spectrum of the crude material showed a relatively clean conversion to 2-vinylquinoline **45**, with no obvious evidence of 2-(2-bromoethyl)quinoline **44** formation. Further investigation by mass spectrometry revealed the presence of 2-(2-bromoethyl)quinoline **44**, albeit in very small amounts; however, all attempts at the isolation of this were unsuccessful.

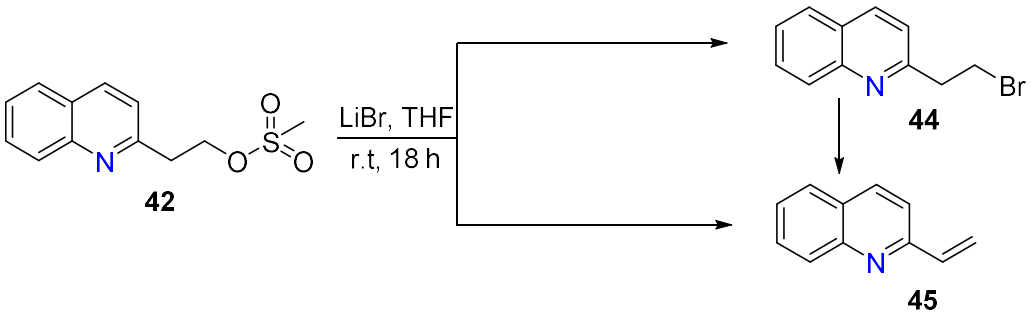


*Scheme 40. Attempted synthesis of 2-(2-bromoethyl)quinoline **44**.*

Elimination reactions associated with bromoethyl moieties appear to require base, a catalyst, or a combination of both.[265,267–269] Such conditions are similar to those reported in the literature for the formation of vinylic compounds from their corresponding sulfonate esters, as discussed previously. Interestingly, there are two reported

preparations of the pyridyl analogue, 2-(2-bromoethyl)pyridine,[265,270] and neither makes reference to any observed elimination reaction.

Our failure to prepare 2-(2-bromoethyl)quinoline **44** is presumably due to a facile elimination reaction of this molecule in which initial deprotonation is aided by the basic quinoline moiety. However, with this in mind it is unusual that the pyridine congener does not behave in a similar way. Quinoline is found to be slightly less basic in comparison to pyridine (pKa values: pyridinium ion 5.17 and quinolinium ion 4.94[271]) and therefore it would be expected that this increase in basicity would assist in the elimination reaction.

Due to the rapid formation of 2-vinylquinoline **45** and the inability to isolate pure 2-(2-bromoethyl)quinoline **44**, studies of the elimination reaction to give 2-vinylquinoline **45** could not be carried out.

It was concluded from the work described above that the addition of increasingly good leaving groups appears to increase the amount of 2-vinylquinoline **45** formed. To confirm this, the synthesis of 2-(2-iodoethyl)quinoline **115** using a classical Finkelstein reaction[272] was attempted, with a 1:5 ratio of 2-(2-chloroethyl)quinoline hydrochloride **41.HCl** and NaI being refluxed in $(CH_3)_2CO$ for 24 hours (*Scheme 41*). As the reaction proceeded, a white solid, which is presumably KCl, was observed, suggesting that the displacement of the chloride ion by the iodide was occurring. Analysis of the crude material by $^1$H NMR revealed no iodo compound **115** was present, and, as expected, **45** was the major product synthesised.

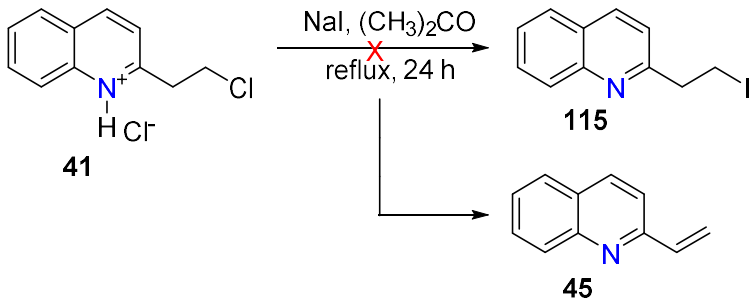


*Scheme 41. Attempted synthesis of 2-(2-iodoethyl)quinoline **115**.*

After concluding that the isolation of a 2-(2-haloethyl)quinoline compound was not feasible, our attention turned to using the elimination product, 2-vinylquinoline **45** as a starting material for quinoline-containing ligands.

### 3.3.3 The synthesis of 2-vinylquinoline (45)

2-vinylquinoline is a valuable intermediate used in many organic syntheses and appears in the literature in a range of different applications.[273–277] Established preparations include (*Scheme 42*): the $FeCl_3$-catalysed reaction between 2-methylquinoline **34** and DMF **116** (A),[219] a Wittig reaction between quinoline-2-carbaldehyde **35** and methyl triphenyl phosphonium bromide **117** (B),[278,279] a Grignard reaction between vinylmagnesium bromide **118** and N-oxyisobutyl-oxycarbonylquinolinium chloride **119** (C),[280] and a Suzuki coupling between 2-chloroquinoline **120** and vinylboronic acid pinacol ester **121** in the presence of PAPh, $K_2CO_3$ and $Pd_2(dba)_2$ (D).[264] However, these methods present a variety of potential problems including variable yields, harsh conditions, and numerous synthetic steps.

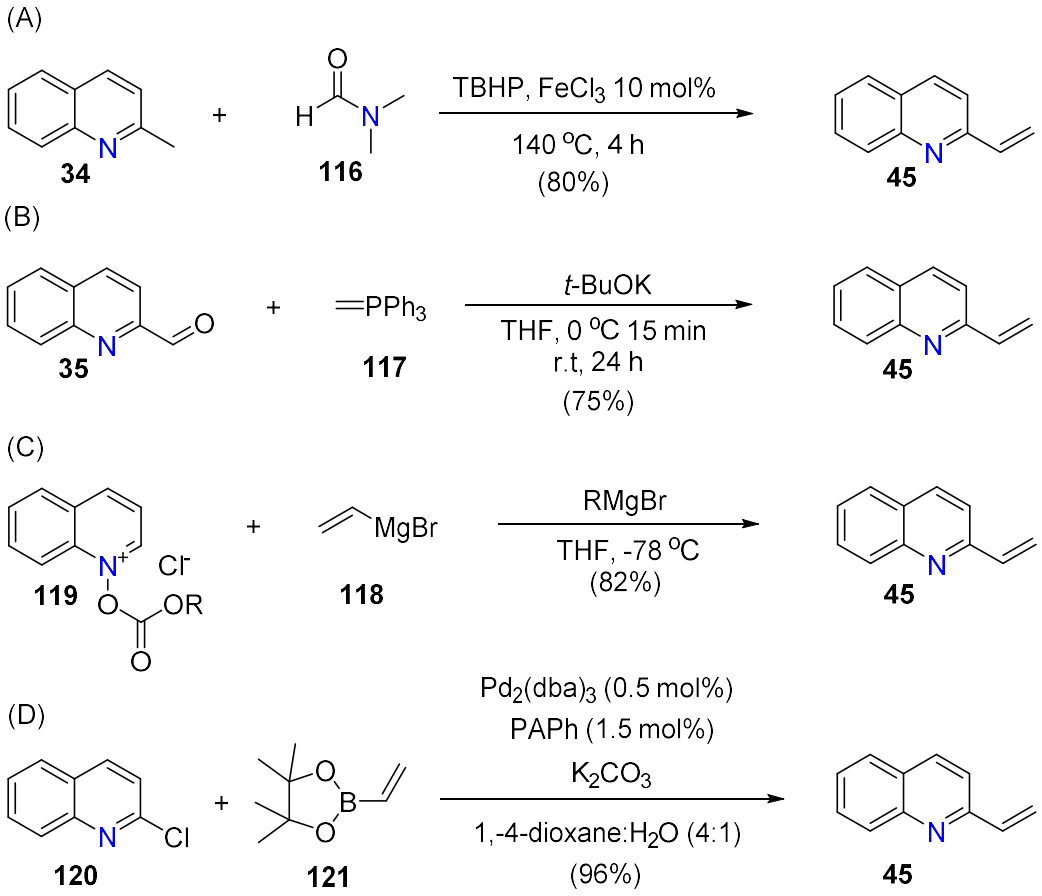


*Scheme 42. Reported methods for the synthesis of 2-vinylquinoline **45**.*

As a result, Xiao and co-workers[223] developed a one-pot synthesis for 2-vinylquinoline **45** that is simple and efficient. It should be noted, although it is not mentioned in the

paper, this method seems to be an optimisation of a previously published method by Benito *et al.* in 1989.[281]

As discussed by the authors, Mannich reactions followed by deamination[282] have been demonstrated as an efficient method for the synthesis of vinyl derivatives. Discovered by Carl Mannich, the Mannich reaction[282–284] involves a three-component condensation in which an active hydrogen-containing molecule is reacted with formaldehyde and an NH-derived amine (*Figure 64*):

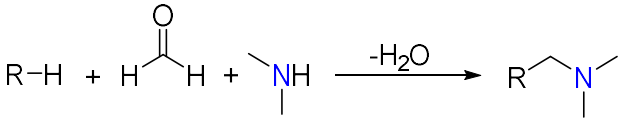


*Figure 64. General Mannich reaction.*

Deamination of the resulting product, the Mannich base, via elimination of a primary, secondary, or tertiary amine, affords the desired vinyl derivative.[282] This method has been utilised by Larsen *et al.*[285] for the synthesis of 7-chloro-2-vinylquinoline **122** prepared from a Mannich reaction of 7-chloro-2-methylquinoline **123** followed by Hofmann elimination[283] of the resulting quaternary salt **124** (*Scheme 43*).

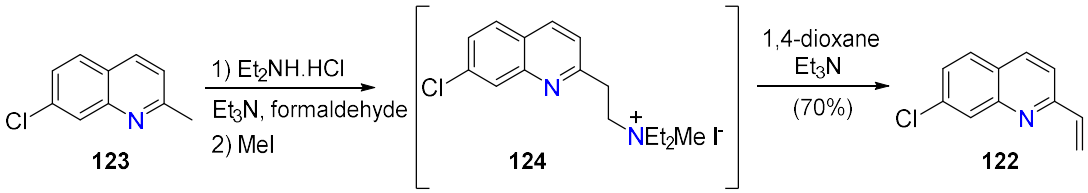


*Scheme 43. Reported synthesis of 7-chloro-2-vinylquinoline **122**.*[285]

However, when direct deamination has been used for the preparation of 2-vinylquinoline **45** in previous attempts, the yield recorded was below 2%.[286,287] The work of Xiao *et al.*[223] commenced with the synthesis of 7-chloro-2-vinylquinoline **122** from 7-chloro-2-methylquinoline **123** and was focused on increasing the yield of the reaction. The authors stated after several attempts, the reaction of 7-chloro-2-methylquinoline **123**, formaldehyde solution and diethylamine hydrochloride in the presence of 5 mol% of $Et_3N$ heated at 100 °C in 1,4-dioxane for 30 minutes afforded the desired vinyl product **122** in high yield (95%). A significant finding was the importance of the catalytic amount of $Et_3N$ present due to the observation of a substantial drop in yield (58%) in the absence of

the base. Furthermore, it was also demonstrated that accuracy in the amount of $Et_3N$ used was essential, with reduced yields observed when the addition of $Et_3N$ was above or below 5 mol%. The reaction yield and speed were decreased on decreasing the temperature, and it was shown at 25 °C, only the Mannich base was obtained in moderate yield (48%) after 48 hours. This suggests the formation of the Mannich base occurs before the formation of the desired vinyl product. Since no product and only Mannich base was formed at room temperature, the authors inferred that the energy barrier for the deamination reaction must be greater than that for the formation of the Mannich base.

In our work, following the literature procedure of Xiao *et al.*,[223] 2-methylquinoline **34**, diethylamine hydrochloride, and 30% formaldehyde solution, in the presence of $Et_3N$, were refluxed in 1,4-dioxane for 1 hour (*Scheme 44*). Following the removal of the reaction solvent, the crude material was redissolved in $CH_2Cl_2$. Following a basic work-up and purification by column chromatography, 2-vinylquinoline **45** was isolated as a light brown oil in good yield (94%).

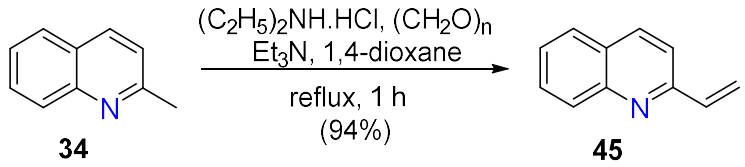


*Scheme 44. The synthesis of 2-vinylquinoline **45**.*

The identity of the product was confirmed by $^1H$ NMR spectroscopy (*Figure 65*), with the presence of the diagnostic one-proton doublet of doublets at $\delta_H$ 7.04 ppm, consistent with that previously described. Moreover, two new doublets at $\delta_H$ 6.28 and 5.67 ppm (both with $J$ = 0.9 Hz), were attributed to the desired alkene.[223] It should be noted that the authors highlighted the importance of a 5 mol% addition of $Et_3N$ (discussed above) and any deviation from this amount resulted in lower yields. However, during our work it was found that 15 mol% was necessary to obtain the title product in a high yield of 94%.

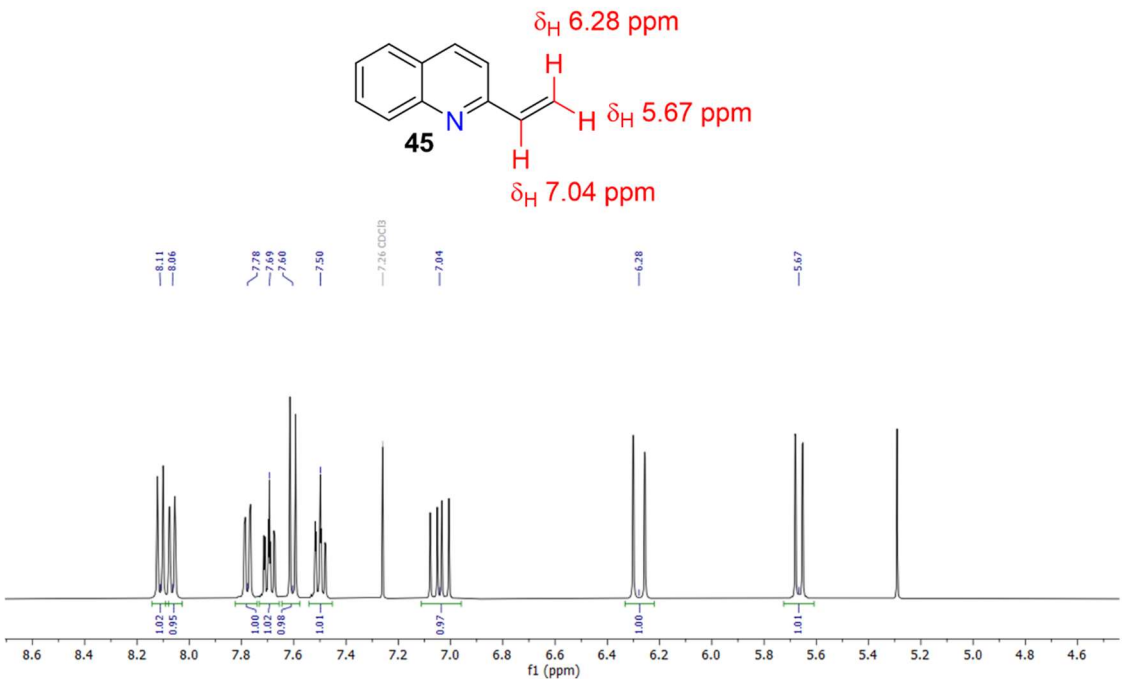


*Figure 65. $^{1}H$ NMR spectrum of 2-vinylquinoline **45** in $CDCl_3$.*

## 3.4 Investigation into the syntheses of 2-(2-chloroethyl)quinoline and 2-(2-azidoethyl)quinoline

Having established that the formation of 2-vinylquinoline **45** occurs in all of the 2-(2-haloethyl)quinoline reactions reported above, the original preparation of 2-(2-chloroethyl)quinoline **41** was reinvestigated. As described above, the literature synthesis reported this compound as a yellow solid that is soluble in $CDCl_3$; however, in our hands we obtained a sticky residue that had very poor solubility in $CDCl_3$ but good solubility in $D_2O$, strongly suggesting the isolation of the hydrochloride salt. It seems unlikely that the original authors could have obtained the free base in the absence of a basic work up due to the generation of $H^+$ during the reaction. Similarly, our attempts to convert the isolated 2-(2-chloroethyl)quinoline hydrochloride **41.HCl** to the free base form were unsuccessful; $^{1}H$ NMR ($CDCl_3$) revealed the material obtained was not 2-(2-chloroethyl)quinoline **41** but 2-vinylquinoline **45**. We propose that the formation of **45** occurs from an elimination reaction of 2-(2-chloroethyl)quinoline **42** that is assisted by the presence of an unprotonated nitrogen atom in the quinoline ring. This reaction appears to happen spontaneously; however, addition of base appears to accelerate this pathway, as was seen in our attempts at converting the hydrochloride salt of 2-(chloroethyl)quinoline hydrochloride **41.HCl** to the free base **41**.

Since the isolation of the free base **41**, as the authors claimed to have achieved, proved unsuccessful in our hands, we wanted to investigate what was driving their subsequent reactions using this compound. Huang *et al.*[250] employed the reaction between the supposed free base 2-(2-chloroethyl)quinoline **41** and sodium azide for the preparation of 2-(2-azidoethyl)quinoline **47** (*Scheme 45*).

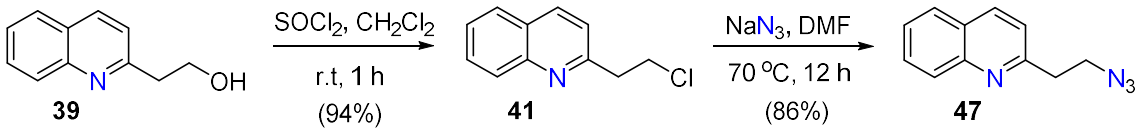


*Scheme 45. Reported synthesis of 2-(2-chloroethyl)quinoline **42** and 2-(2-azidoethyl)quinoline **47**.*[250]

Upon repeating the synthesis of 2-(2-chloroethyl)quinoline **41** following the reported literature procedure,[250] $^1$H NMR analysis ($CDCl_3$) of the crude material revealed the presence of two products, 2-(2-chloroethyl)quinoline hydrochloride **41.HCl** and 2-vinylquinoline hydrochloride **45.HCl** in approximately equal amounts, with diagnostic peaks at $\delta_H$ 4.14 ppm and 3.74 ppm corresponding to the -$CH_2CH_2$- unit of 2-(2-chloroethyl)quinoline hydrochloride, and peaks at $\delta_H$ 7.74, 6.66, and 6.10 ppm corresponding to the alkene protons of the 2-vinylquinoline hydrochloride **45.HCl**. It should be noted that from our previous work, the solubility of 2-(2-chloroethyl)quinoline hydrochloride **41.HCl** is low, therefore, there may be more of this compound present then what is observed from the integrations of the $^1$H NMR spectrum. A closer examination of the spectrum revealed a shift in the peaks observed for the 2-vinylquinoline hydrochloride **45.HCl** in comparison to that seen for free base 2-vinylquinoline **45**. In particular, the doublet of doublets usually observed at $\delta_H$ 7.04 ppm for **45**, was shifted downfield and overlapped with other aromatic signals around $\delta_H$ 7.74 ppm. It was postulated that the observed downfield shift of the **45.HCl** peaks was due to the protonation of the quinoline nitrogen resulting in the formation of the hydrochloride salt. This seemed plausible due to the acidic environment of the reaction as a result of the HCl generated. As confirmation, 2-vinylquinoline **45** was synthesised as the free base and then converted to the hydrochloride salt **45.HCl**. $^1$H NMR ($CDCl_3$) analysis of the isolated product revealed the same chemical shift in the $^1$H NMR spectrum. Figure 66 displays the $^1$H NMR spectra of both **45.HCl** and **45** highlighting the significant difference in chemical shifts of the respective compounds.

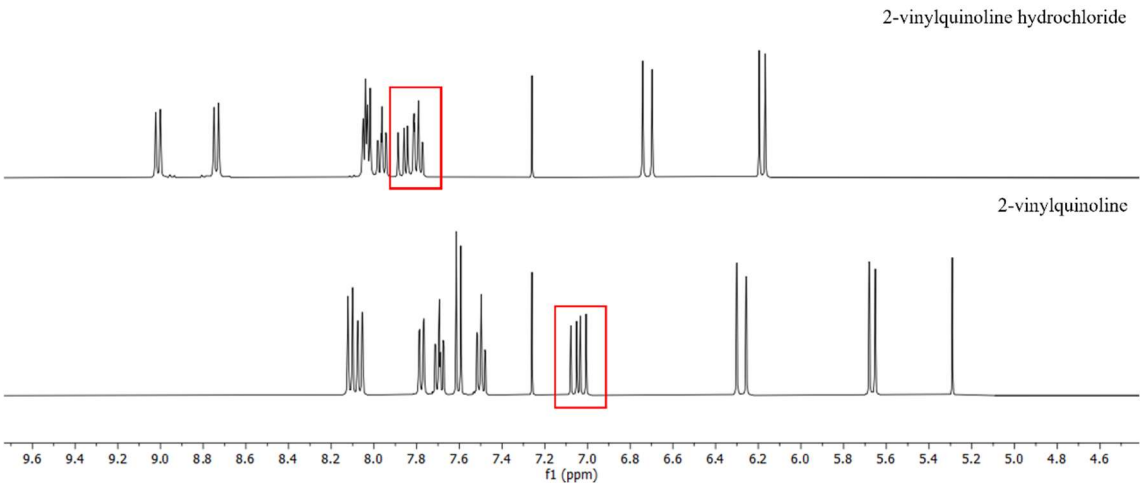


*Figure 66. $^{1}H$ NMR spectra of 2-vinylquinoline hydrochloride **45.HCl** (top) and 2-vinylquinoline **45** (bottom) in $CDCl_3$.*

Huang and co-workers referenced their synthesis described above to a paper reported by Laronze-Cochard.[288] However, this paper reports the conversion of hydroxymethyl groups to chloromethyl groups using thionyl chloride. Thus, treatment of (acridine-4,5-diyl)dimethanol **125** with $SOCl_2$ affords 4,5-bis(chloromethyl)acridine **126** in excellent yield (*Scheme 46*). The resulting bis(chloromethyl) compound is unable to undergo elimination and thus conversion of the to the vinyl analogue is not feasible. However, the same reaction with a 2-hydroxyethyl compound, will give the resulting 2-chloroethyl product, which can undergo elimination to give the vinyl derivative.

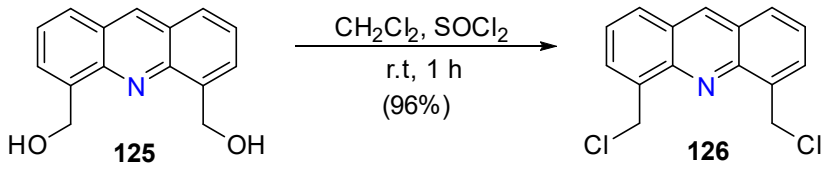


*Scheme 46. Reported synthesis of synthesis of 4,5-bis(chloromethyl)acridine **126**.*[288]

The previously isolated mixture of 2-(2-chloroethyl)quinoline hydrochloride **41.HCl** and 2-vinylquinoline hydrochloride **45.HCl** was then carried over to the synthesis of 2-(2-azidoethyl)quinoline **47**. As mentioned previously, the authors of the paper reported the isolation of 2-(2-chloroethyl)quinoline as the free base **41** in high yield ( 94%) (*Scheme 45*). The next step in their synthetic scheme was the reaction between 2-

chloroethylquinoline **41** and $NaN_3$ to afford 2-(2-azidoethyl)quinoline **47**, which according to the paper was also obtained in high yield (86%).

In our hands, the treatment of the hydrochloride salts **41.HCl** and **45.HCl** with an excess of $NaN_3$ in DMF at 70 °C afforded a 1:1 mixture of 2-vinylquinoline **45** and 2-(2-azidoethyl)quinoline **47**, as confirmed by $^1$H NMR spectroscopy. The formation of the azido product was confirmed by the change in chemical shift of the two triplets in the $^1$H NMR spectrum (*Figure 67*). Comparison of the NMR spectra before and after the reaction revealed a shift of the 2-vinylquinoline hydrochloride **45.HCl** signals back to the $^1$H chemical shifts that matched those of the free base **45**.

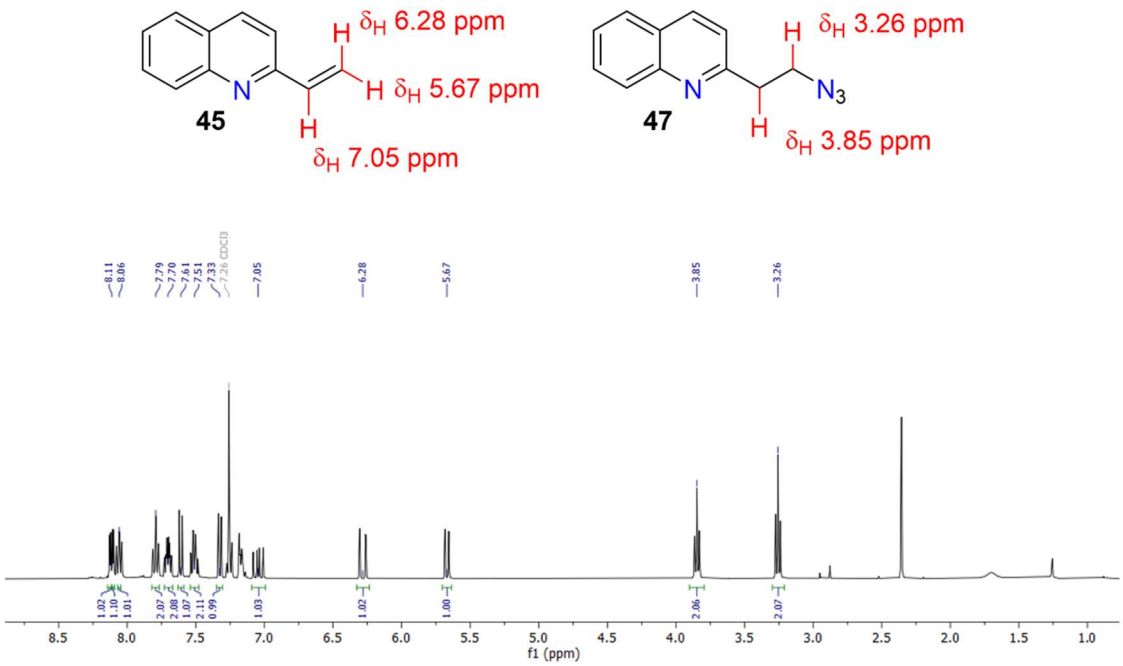


*Figure 67. $^1$H NMR spectrum of a mixture of 2-vinylquinoline **45** and 2-(2-azidoethyl)quinoline **47** in $CDCl_3$.*

Analysis of the sample was also conducted by mass spectrometry which revealed the molecular ion peak at *m/z* = 199.1 and this can be assigned to 2-(2-azidoethyl)quinoline **47** (calcd. for $C_{11}H_{11}N_4^+$ $[M+H]^+$ *m/z* = 199.09; found *m/z* = 199.1). The base peak is observed at *m/z* = 171.0 and corresponds to the loss of $N_2$ from this, a fragmentation of azide-containing compounds that has been reported previously in the literature (calcd. for $C_{11}H_{11}N_2^+$ $[M+H]^+$ *m/z* = 171.09; found *m/z* = 171.0).[289–292]

Comparison of the $^1$H NMR spectrum before and after the azide reaction revealed a shift in the chemical shifts of the 2-vinylquinoline hydrochloride **45.HCl** signals back to the

chemical shifts that match those of the free base **45**. Again, repeating the above reaction, starting with the synthesis of the reported 2-(2-chloroethyl)quinoline **41** and leaving the crude product to stand under ambient conditions for 24 hours afforded solely 2-vinylquinoline hydrochloride **45.HCl**. Further reaction of this with $NaN_3$ under the same reaction conditions as the paper reported for the synthesis of 2-(2-azidoethyl)quinoline **47**, yields a 1:1 mixture of 2-(2-azidoethyl)quinoline **47** and 2-vinylquinoline **45**, again as the free base as determined by the chemical shifts and proton integration. It is likely, therefore, that the formation of **47** proceeds from the protonated 2-vinylquinoline and not the 2-chloroethylquinoline as reported in the literature.[250]

To further confirm that 2-vinylquinoline hydrochloride **45.HCl** is the reactive species for the formation of the azido product, the free base form of 2-vinylquinoline was converted to the hydrochloride salt and reaction of this with excess $NaN_3$ under the same reaction conditions described above, afforded 2-(2-azidoethyl)quinoline and 2-vinylquinoline (1:1). In addition, 2-vinylquinoline was reacted with an excess of $NaN_3$ in DMF again following the same conditions. This reaction attempt afforded only vinyl starting material as revealed by $^1$H NMR analysis.

The authors assumed they started with pure 2-(2-chloroethyl)quinoline **41** when carrying out the synthesis of 2-(2-azidoethyl)quinoline **47**. In contrast, we have shown that, under their reaction conditions for the synthesis of **41**, an approximate 1:1 mixture of 2-(2-chloroethyl)quinoline hydrochloride **41.HCl** and 2-vinylquinoline hydrochloride **45.HCl** is formed. The authors also reported the clean isolation of the azide product; however, again in our hands we have shown this to be incorrect and in fact another approximate 1:1 mixture of 2-(2-azidoethyl)quinoline **47** and 2-vinylquinoline **45** is obtained.

The resulting free base of 2-vinylquinoline **45** that is observed in the $^1$H NMR spectrum following the azide synthesis, may have been generated via elimination of 2-(2-chloroethyl)quinoline hydrochloride **41.HCl**, from unreacted 2-vinylquinoline hydrochloride **45.HCl**, or a combination of both. Although there is evidence to suggest that both pathways could be responsible for the formation of the 2-vinylquinoline **45**, the elimination of **41.HCl** seems more plausible. The initial starting material contains an approximate 1:1 mixture of 2-(2-chloroethyl)quinoline hydrochloride **41.HCl** and 2-vinylquinoline hydrochloride **45.HCl** and the resulting product obtained also has an approximate 1:1 mixture of 2-(2-azidoethyl)quinoline **47** and 2-vinylquinoline **45**. We

suggest that the reaction is acid catalysed and 2-(2-chloroethyl)quinoline hydrochloride **41.HCl** eliminates to afford the free base of 2-vinylquinoline **45** and the protonated 2-vinylquinoline hydrochloride **45.HCl** reacts with the $NaN_3$ to form 2-(2-azidoethyl)quinoline **47**, conserving the same 1:1 ratio that is observed.

To see whether 2-(2-azidoethyl)quinoline **47** is generated from 2-(2-chloroethyl)quinoline **41**, 2-vinylquinoline **45** or both, the reaction was attempted again under the same reaction conditions using 2-vinylpyridine **51** instead of the hydrochloride salt mixture of 2-(2-chloroethyl)quinoline **41.HCl** and 2-vinylquinoline **45.HCl**. Following reaction of 2-vinylpyridine **51** and $NaN_3$ in DMF at 70 °C for 24 hours, $^1$H NMR analysis of the crude product revealed only the 2-vinylpyridine **51** starting material had been isolated. This led to the conclusion that perhaps the hydrochloride salt of the 2-vinylpyridine starting material was important for the reaction to proceed. Therefore, conversion of 2-vinylpyridine **51** to the hydrochloride salt **51.HCl** was carried out and this was then reacted with $NaN_3$ in DMF under the same reaction conditions to afford a mixture of 2-(2-azidoethyl)pyridine **52** and 2-vinylpyridine **51** (*Scheme 47*).

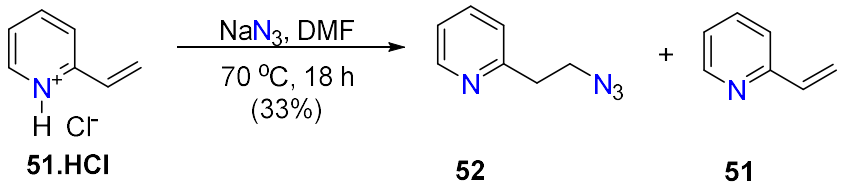


*Scheme 47. The synthesis of 2-(2-azidoethyl)quinoline **52** and 2-vinylpyridine **51**.*

Analysis of the crude material by $^1$H NMR spectroscopy revealed a $^1$H NMR spectrum (*Figure 68*) that exhibited an approximate 1:1 mixture of 2-vinylpyridine **51** and 2-(2-azidoethyl)pyridine **52**. Removal of **51** was achieved by washing the crude residue dissolved in $CH_2Cl_2$ with an aqueous solution of $NaHSO_3$ and, following the removal of the solvent (rotavap), solely 2-(2-azidoethyl)pyridine **52** was isolated. The successful isolation of **52** was confirmed by $^1$H NMR spectroscopy and LRMS. The $^1$H NMR spectrum revealed two triplets at $\delta_H$ 3.71 and 3.05 ppm that are attributed to the newly form ethyl alkyl chain. The data is consistent with the literature.[224]

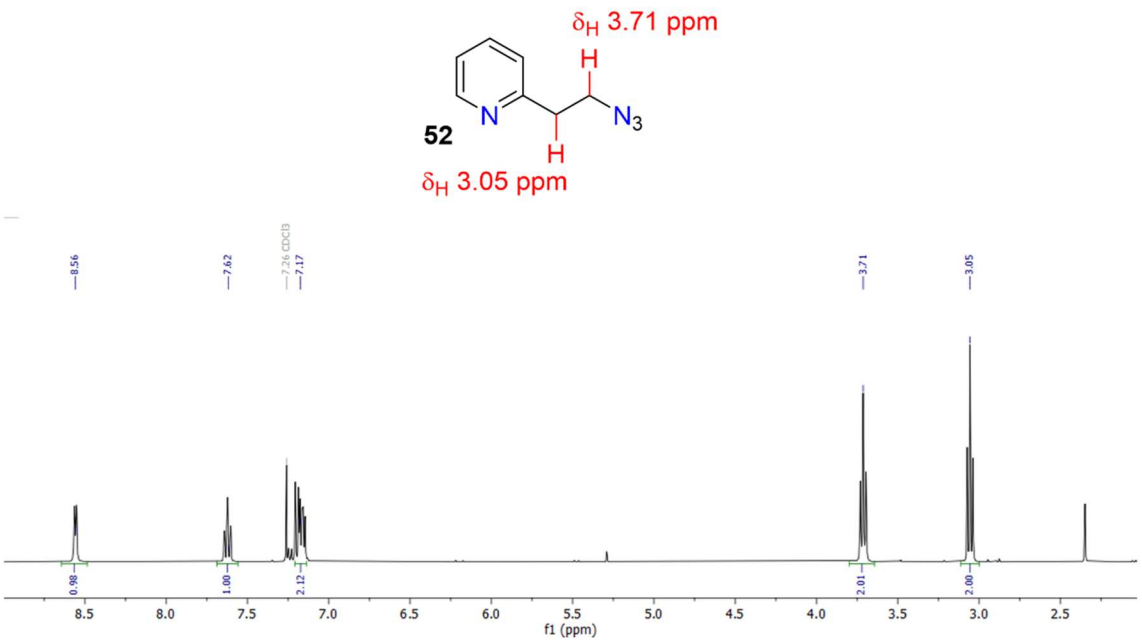


*Figure 68. $^{1}H$ NMR spectrum of 2-(2-azidoethyl)pyridine **52** in $CDCl_3$.*

### 3.4.1 The synthesis of organoazides from alkenes

The preparation of organoazides from the reaction of $NaN_3$ and an alkene is not common in the literature. Alkyl, aryl, and acyl azide derivatives[224,293–301] are most often prepared through the reaction of an azide-containing reagent with an appropriate halide,[224,250] sulfonate,[300,302] alcohol,[224,303] or amine.[304] However, only a handful of the reactions of azides with alkenes have been reported. An indirect preparation of 4-(2-azidoethyl)cyclohex-1-ene **127** starting from the diene, was reported by Proto *et al.* This involved initial conversion of the alkene **128** to the alcohol, subsequent mesylation, and then reaction of the mesyl derivative with $NaN_3$ (*Scheme 48*).[305]

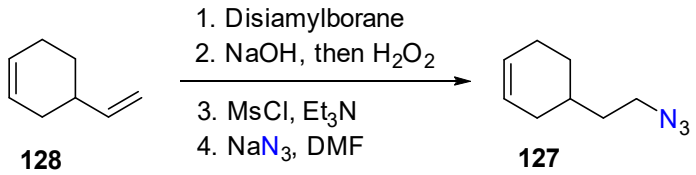


*Scheme 48. Reported synthesis of 4-(2-azidoethyl)cyclohex-1-ene **127**.*[305]

Direct formation of organic azides from an alkene can be achieved by reaction with hydrazoic acid generated *in situ* from $NaN_3$ under acidic conditions.[301,306,307] Such compounds have also been synthesised from the reaction of the appropriate alkene with $NaN_3$ in aqueous $CH_3COOH$ at temperatures ranging from 0 °C to reflux. For example,

4-(2-azidoethyl)pyridine **129** can be obtained from the reaction of 4-vinylpyridine **130** and $NaN_3$ in a $CH_3COOH$:$H_2O$ mixture at 20 °C for 32 hours (*Scheme 49*).[307]

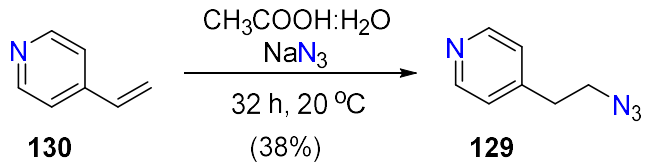


*Scheme 49. Reported synthesis of 2-(4-pyridyl)ethyl azide **129**.*[307]

An extensive study into the formation of organic azides by Hassner *et al.* demonstrates the requirement of a Lewis acid, in particular $TiCl_4$, for the reaction of alkenes bearing phenyl or two geminal alkyl substituents with azides. It was found; however, that mono- or 1,2-dialkyl akenes do not react. The authors concluded from this, and subsequent data,[301] in addition to the observed regioselectivity in these reactions, that the development of a positive charge, suggestive of a carbocation intermediate, must occur for the formation of the azide product.[303]

In 2017 Zhou *et al*. reported the synthesis of organic azides from the reaction of an alkene and trimethylsilylazide in the presence of tetrabutylammonium iodide and tert-butyl peroxybenzoate in $CH_3CN$ or $H_2O$. Similar preparations have been reported that include the use of other catalysts and solvents, with most reporting diazidation, or monoazidiation with the addition of a solvent molecule across the double bond.[308–313] The focus of Zhou's work was the diazidation of a range of different alkenes, including vinylarenes, inactivated alkenes, allene, and dienes. The authors reported a method that they claimed was applicable to a range of alkenes; it was ligand free and non-toxic and could be performed in water or organic solvents. Diazidiation was achieved in both $H_2O$ and $CH_3CN$ for all starting materials with the exception of 2-vinylpyridine **51**. The authors reported the nature of this product to be dependent on whether the reaction was performed in $CH_3CN$ or $H_2O$, where the mono- **52** or diazido **131** compound was formed, respectively (*Scheme 50*).[313]

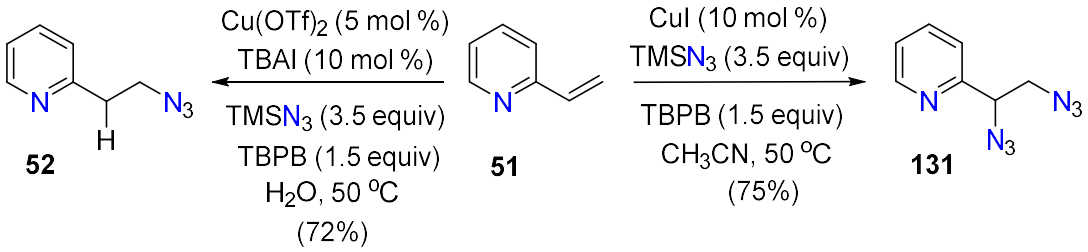


*Scheme 50. Reported synthesis of 2-(2-azidoethyl)pyridine **52** and 2-(1,2-diazidoehtyl)pyrdine **131**.*[313]

With the successful isolation of 2-(2-azidoethyl)pyridine **52** and 2-(2-azidoethyl)quinoline **47**, it was decided to investigate the chemistry of these compounds further. A SciFinder search revealed that 2-(2-azidoethyl)quinoline **47** and its derivatives are particularly rare; there is only a single report of the synthesis of 2-(2-azidoethyl)quinoline **4**,[250] and this has only been used in an amination reaction that converts **47** to 2-(2-aminoethyl)quinoline. Similarly, few substituted 2-(2-azidoethyl)quinoline **47** derivatives have been reported,[314–321] including 2-[1-(azidomethyl)butyl]quinoline **132**, 2-[1-(azidomethyl)-2-(trimethylsilyl)ethyl]-4-methylquinoline **133**[318] and methyl (β*R*)-β-azido-2-quinolinebutanoate **134**[322] (*Figure 69*). However, the chemistry of these compounds has been little explored.

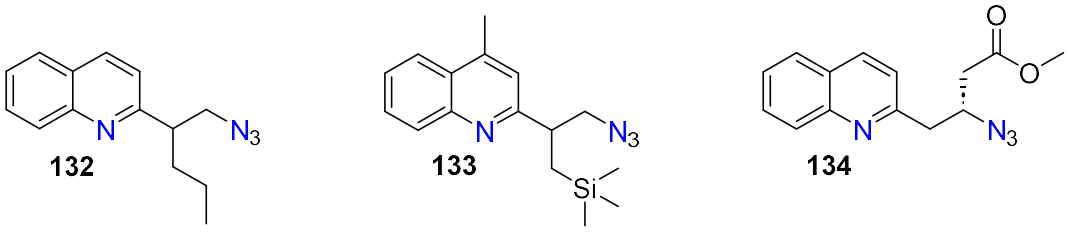


*Figure 69. Examples of substituted 2-(2-azidoethyl)quinoline in the literature. **132** (left), **133** (centre) and **134** (right).*

In contrast, 2-(azidomethyl)quinoline **135** and derivatised analogues are much more abundant in the literature.[323–328] For example, **135** can be prepared from the treatment of 2-(bromomethyl)quinoline **36** with $NaN_3$ in DMF at 40 °C,[329] or from the same reaction in $H_2O$:$(CH_3)_2CO$ (1:2) at room temperature (*Scheme 51*).[324]

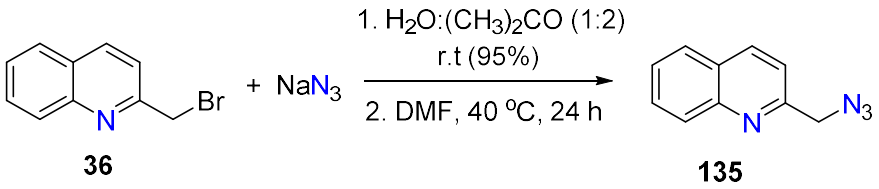


*Scheme 51. Reported synthesis of 2-(azidomethyl)quinoline **135**.*[324,329]

## 3.5 Click Chemistry

2-(Azidomethyl)quinoline **135** has been used as a starting material for the synthesis of 1-(quinolin-2-yl)methanamine **38**[238] and quinoline-2-carbaldehyde **35**,[330] in decomposition thermolysis studies,[331] and most commonly in click reactions to give 1,2,3- disubstituted triazoles.[323,324,326,328,329,332–336.] Given that we now had a simple synthesis of both 2-(2-azidoethyl)quinoline **47** and 2-(2-azidoethyl)pyridine **52**, it was decided that the click chemistry of these should be investigated

The formation of a triazole ring from the cycloaddition reaction between an azide and an alkyne was first described in the literature in the early 1960s.[337,338] Commonly referred to as the Huisgen 1,3-dipolar cycloaddition (*Figure 70*), this reaction affords a mixture of the 1,4- and 1,5- disubstituted regioisomers.[337,338]

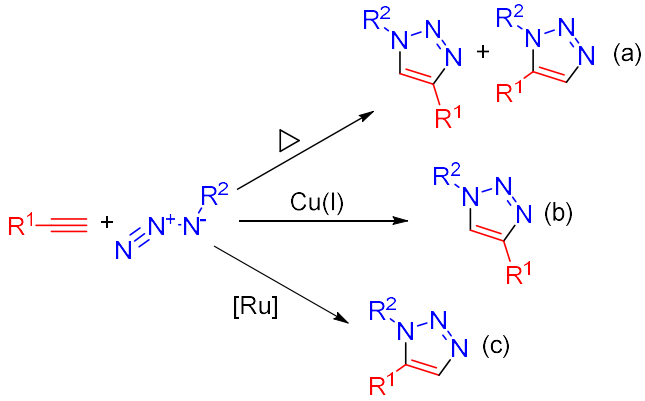


*Figure 70. Azide and alkyne cycloaddition products. (a) Huisgen 1,3-dipolar cycloaddition, 1,4- and 1,5- regioisomers; (b) Cu(I) catalysed click reaction, 1,4-isomer; (c) Ru(II) catalysed click reaction; 1,5- isomer.*

Since then, Cu(I)- or Ru(II)-catalysed click reactions have been shown to be regiospecific, affording either the 1,4-[339] or 1,5-[340] disubstituted triazole, respectively. The copper(I) catalysed azide-alkyne cycloaddition (CuAAC)[341–343] is a classical "click reaction" and

demonstrates the reaction of an azide with an alkyne affording the 1,4-disustituted 1,2,3-triazole exclusively – an analogous reaction to that of Huisgen's concerted triazole synthesis.[339] During the last several years, the CuAAC reaction and its applications have been thoroughly reviewed in the literature and, in 2022, won its discoverers a Nobel Prize.[343–345]

### 3.5.1 Quinoline triazole derivatives

The combination of the quinoline moiety and a 1,2,3-triazole is of interest due to the biological importance of both molecules. The desirable properties of quinoline have been previously discussed in *Chapter One* section 1.3. As for 1,2,3-triazoles, these molecules have been observed to play an important role in biological systems[346–350] as anticancer,[351–353] antimalarial,[354] antimicrobial,[355–357] anti-inflammatory,[358] anti-HIV,[359] and antituberculosis[360,361] agents. *Figure 71* displays the general structure of the product obtained from the click reaction of 2-(azidomethyl)quinoline **135** and an alkyne, a quinoline moiety that is coupled to a 1,2,3-triazole moiety.[324]

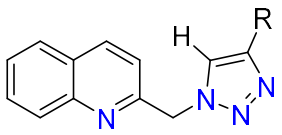


*Figure 71. General structure of a quinoline triazole hybrid.*

Kumar *et al.*[324] utilised the Cu(I)-catalysed click reaction to prepare a number of quinoline-containing compounds with appended sugars. In order to optimise the reaction conditions, the reaction of 2-(azidomethyl)quinoline **135** with the terminal alkynes propargyl alcohol **136** and phenylacetylene were first studied. For example, reaction of 2-(azidomethyl)quinoline **135** and propargyl alcohol **136** in the presence of $CuSO_4.5H_2O$ and sodium ascorbate in a 1:1 mixture of THF and $H_2O$ gave the quinoline-coupled triazole, **137** in good yield (86 %) (*Scheme 52*).[324]

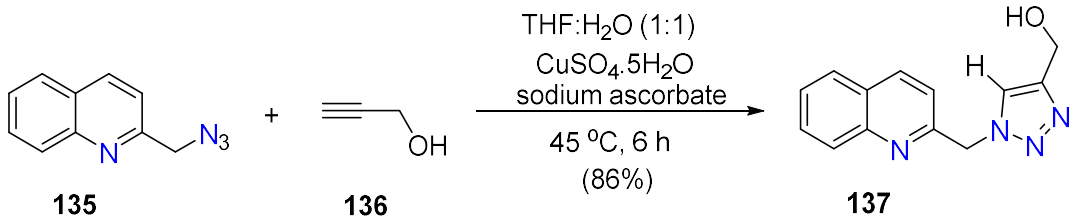


*Scheme 52. Reported synthesis of **137**.*[324]

Following this proof of concept with simple alkynes, the group introduced their chosen sugar acetylenic derivatives, such as propargyl glycosides of D-glucose, D-galactose, 4,6-*O*-ethylidene-D-glycopyranose, 4,6-*O*-butylidene-D-glycopyranose, D-mannose and D-ribose derivatives. Analogous to the above reaction, the 1,4-disubstutited triazole compounds were synthesised from the reaction of 2-(azidomethyl)quinoline **135** with the respective alkyne **138** in a mixture of THF/$H_2O$ (1:1) in the presence of $CuSO_4.5H_2O$ and sodium ascorbate to afford **139** (*Scheme 53*). This method gave a variety of quinoline triazole hybrids in yields ranging from 55% to 72%.[324]

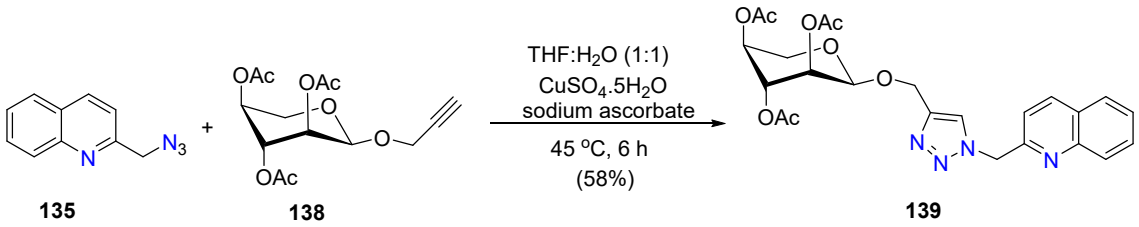


*Scheme 53. Reported synthesis of 2-(2-azidoethyl)quinoline and 2-propyn-1-yl-2,3,4,-tri-O-acetyl-β-d-ribopyranoside.*[324]

### 3.5.2 The synthesis of 2-quinolylethyl click products

Following our successful synthesis of 2-(2-azidoethyl)quinoline **47** and 2-(2-azidoethyl)pyridine **52**, we investigated the click chemistry of these ethyl azido compounds. Amalgamating the chemistry reported in *Chapter Seven*, the compounds 6-(propylamino)-2-(prop-2-yn-1-yl)-1*H*-benzo[*de*]isoquinoline-1,3(2*H*)-dione **48**[362,363] and 6-bromo-2-(prop-2-yn-1-yl)-1*H*-benzo[*f*]isoindole-1,3(2*H*)-dione **46** were the alkynes chosen for the following CuAAC reactions.

Following a reported preparation,[362] with slight modifications, a mixture of 2-vinylquinoline/2-(2-azidoethyl)quinoline **45**/**47** (isolated as a mixture from the

preparation; *vide supra*) and 6-(propylamino)-2-(prop-2-yn-1-yl)-1*H*-benzo[*de*]isoquinoline-1,3(2*H*)-dione **48** in anhydrous DMF, in the presence of CuI, was stirred at 60 °C for 24 hours (*Scheme 54*). The reaction was cooled to room temperature, filtered to remove a brown solid and the solvent was removed (rotavap). Purification by silica gel chromatography afforded the desired product **49** as an orange solid.

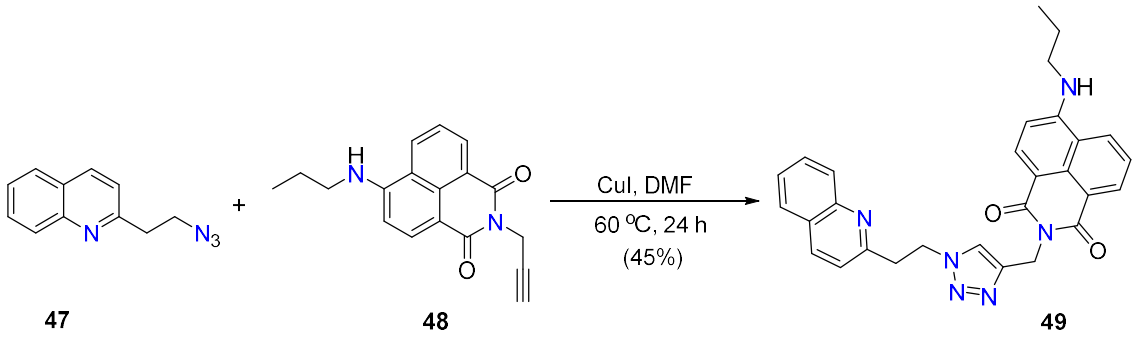


*Scheme 54. The synthesis of the click product **49**.*

Analysis by $^{1}$H NMR spectroscopy revealed the triazole peak at $\delta_H$ 7.61 ppm, in addition to the shift in the ethyl triplets of 2-(2-azidoethyl)quinoline **47** from $\delta_H$ 3.83 and 3.24 ppm to $\delta_H$ 4.92 and 3.55 ppm, reflecting the change in chemical environment of these protons resulting from the formation of the triazole ring (*Figure 72*). HRMS analysis of the material revealed a molecular ion peak at *m/z* = 513.2006 and this can be assigned to the sodiated product ion (calcd. for $C_{29}H_{26}N_6O_2Na^+$ $[M + Na]^+$ *m/z* = 513.20095; found *m/z* = 513.2006). Further confirmation of the product was obtained through the complete assignment of the structure using 2D NMR spectroscopy (HSQC, HMBC, and COSY).

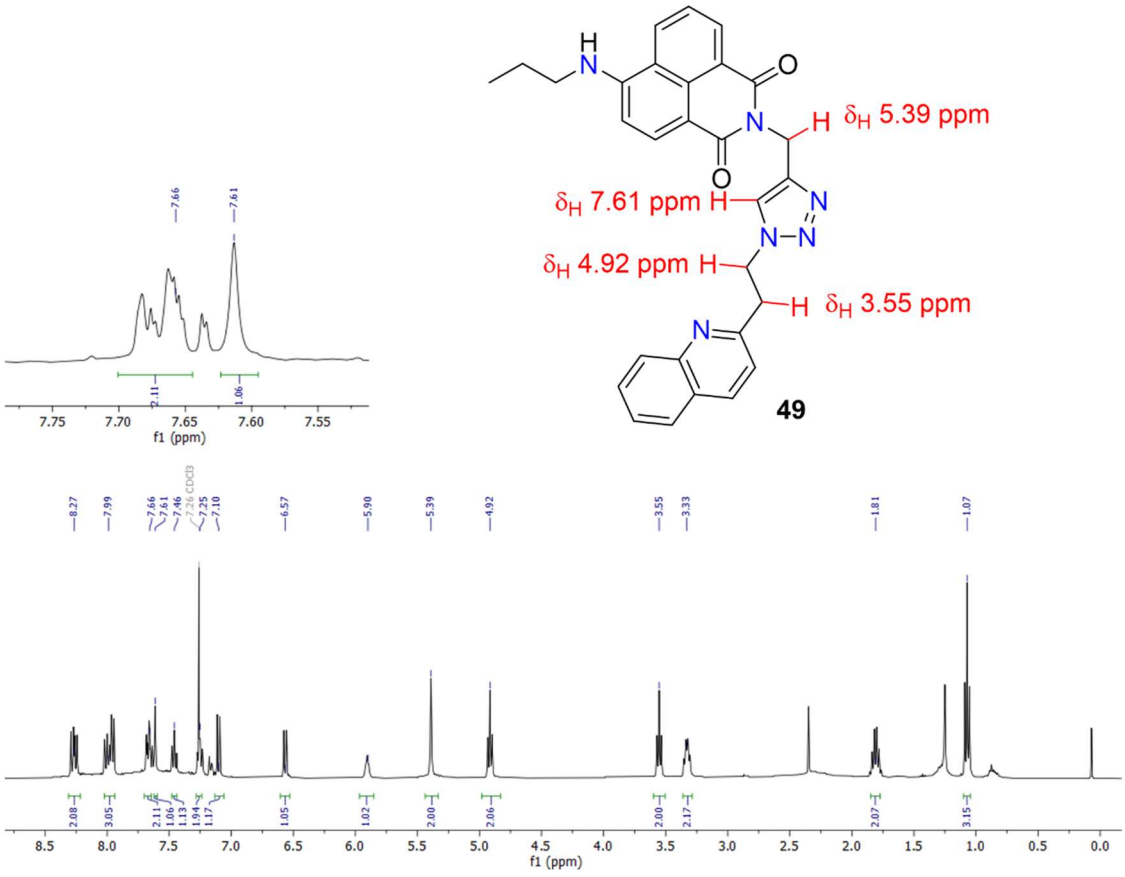


*Figure 72. $^{1}H$ NMR spectrum of the click product **49** in $CDCl_3$.*

The above method was also employed for the reaction of a mixture of 2-vinylquinoline/2-(2-azidoethyl)quinoline **45**/**47** and 6-bromo-2-(prop-2-yn-1-yl)-1*H*-benzo[*f*]isoindole-1,3(2*H*)-dione **46**, in the presence of CuI, in DMF at 60 °C for 24 hours (*Scheme 55*). Following filtration and the removal of the reaction solvent (rotavap), the desired product **50** was obtained as a grey solid following purification by silica gel column chromatography.

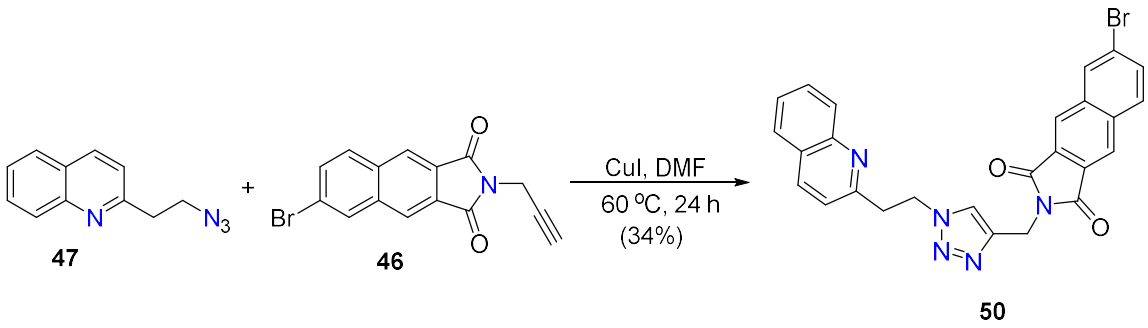


*Scheme 55. The synthesis of the click product **50**.*

The successful formation of the product was confirmed by $^{1}$H NMR spectroscopy that revealed the triazole peak at $\delta_H$ 7.58 ppm and ethylene triplets at $\delta_H$ 4.93 and 3.55 ppm, similar to the shift observed previously. In addition, the singlet at $\delta_H$ 4.97 ppm corresponds to the -$CH_2$ protons from the alkyl chain that attaches the naphthalimide and triazole rings (*Figure 73*). The HRMS spectrum revealed a molecular ion peak at *m/*z = 534.0535 and this can be assigned to the sodiated product ion (calcd. for $C_{26}H_{18}BrN_5O_2Na^+$ $[M + Na]^+$ *m/z* = 534.05361; found *m/z* = 534.0535). In addition, the product ion peak also displayed an isotope pattern that was consistent with the presence of bromine. The 2D NMR spectroscopic data obtained (HSQC, HMBC, and COSY) were consistent with the proposed product.

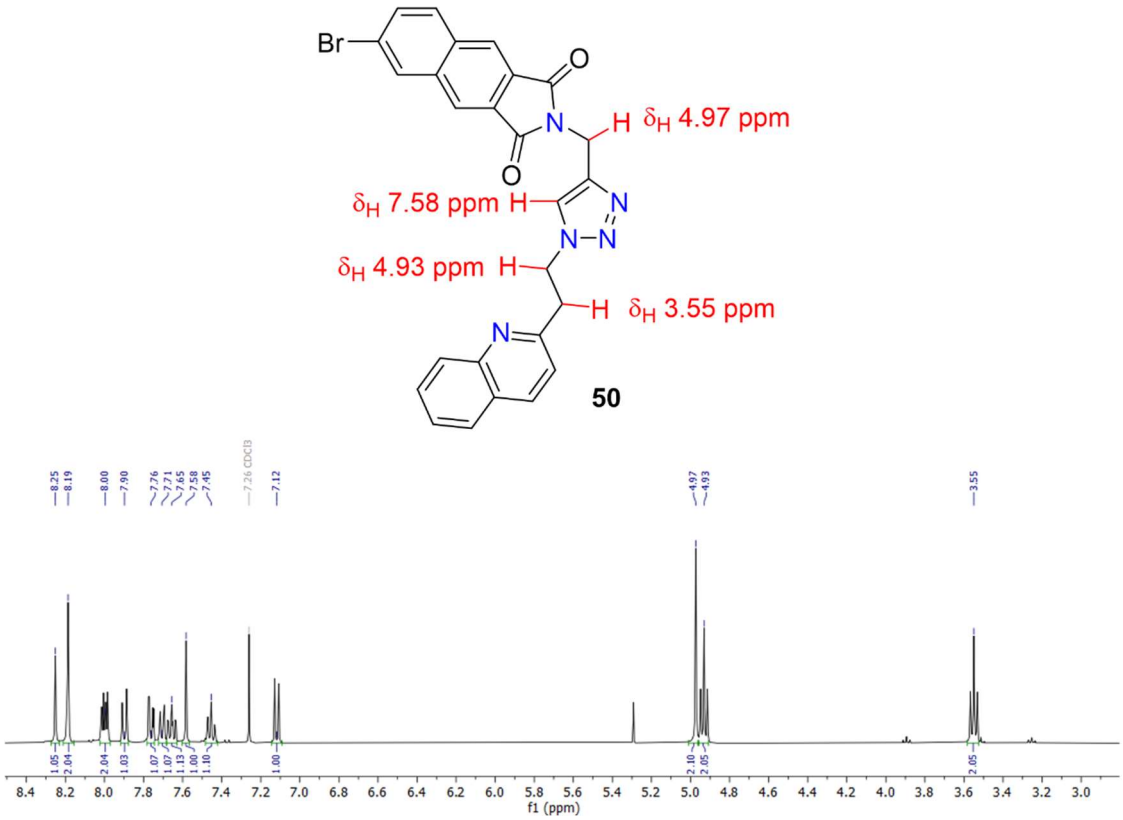


*Figure 73. $^{1}H$ NMR spectrum of the click product **50** in $CDCl_3$.*

The third click reaction attempted in this work was the reaction of 2-(2-azidoethyl)pyridine **52** and 6-(propylamino)-2-(prop-2-yn-1-yl)-1*H*-benzo[*de*]isoquinoline-1,3(2*H*)-dione **48** following the same modified methodology.[362] As reported above, **52** and **48** were stirred in DMF at 60 °C, in the presence of CuI, for 24 hours (*Scheme 56*). Subsequent to cooling, the reaction mixture was filtered to remove a solid impurity and the filtrate was concentrated (rotavap). Following purification by silica gel column chromatography, the title compound **53** was isolated as an orange solid.

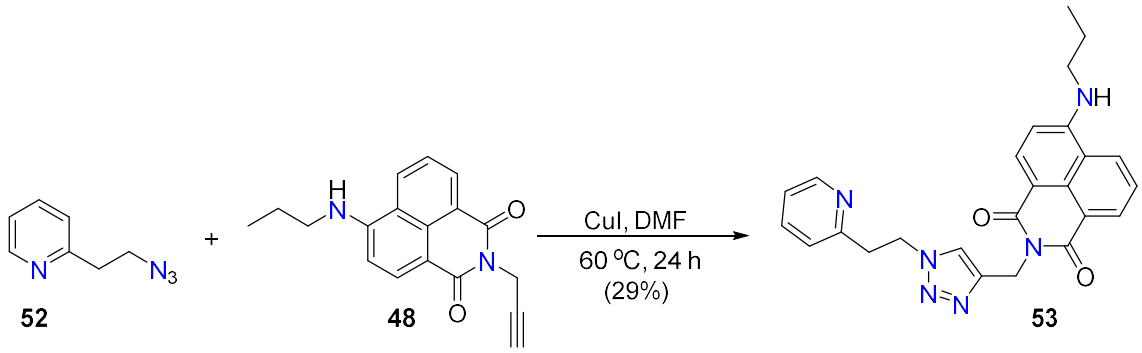


*Scheme 56. The synthesis of the click product **53**.*

The identity of the product was confirmed by NMR spectroscopy and HRMS. The $^{1}$H NMR spectrum revealed the triazole signal at $\delta_H$ 7.46 ppm and -$CH_2$-$CH_2$ peaks at $\delta_H$ 4.76 and 3.34 ppm, whilst the -$CH_2$ protons are observed at $\delta_H$ 5.40 ppm (*Figure 74*).

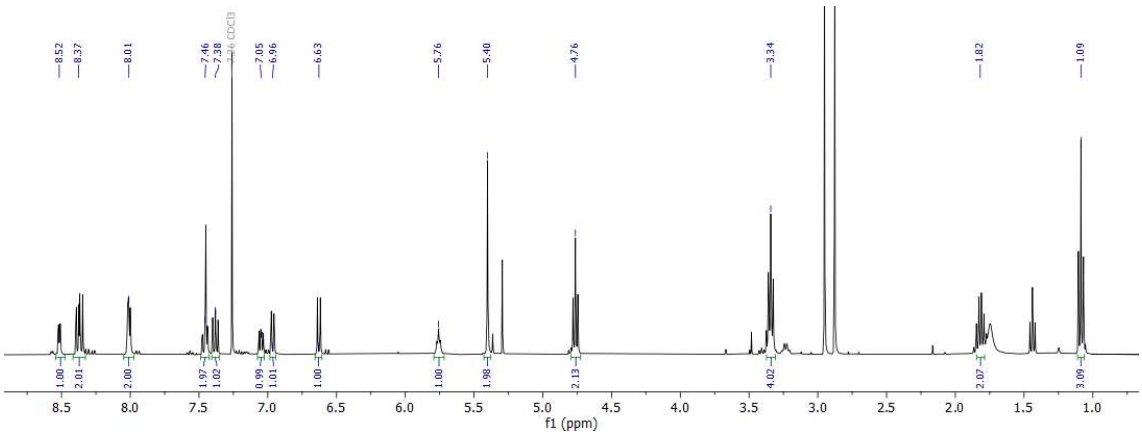


*Figure 74. $^{1}$H NMR spectrum of the click product **53** in $CDCl_3$.*

The HRMS spectrum of the material exhibited a molecular ion peak at *m/z* = 463.1850 and this can be assigned to the sodiated product ion (calcd. for $C_{25}H_{18}BrN_5O_2Na^+$ [M + Na]$^+$ *m/z* = 534.05361; found *m/z* = 534.0535). Further confirmation of the structure was obtained through assignment of the peaks using 2D NMR spectroscopy (HSQC, HMBC and COSY).

## 3.6 The synthesis of tri- and tetradentate 2-quinolylmethyl- and 2-quinolylethyl-containing ligands

With the successful synthesis and isolation of the 2-methylquinoline-derived starting materials, quinoline-2-carbaldehyde **35**, 2-(bromomethyl)quinoline **36**, 2-(quinolin-2-yl)ethan-1-ol **39** and 2-vinylquinoline **45**, the focus was shifted to the synthesis of the

corresponding ligands. While there are many reports of tridentate and tetradentate tripodal ligands that contain 2-quinolylmethyl moieties, ligands that contain 2-quinolylethyl groups are rare. Therefore, the aim of this work was to investigate the design and synthesis of tridentate and tetradentate tripodal ligands that contain both the 2-quinolylmethyl and 2-quinolylethyl moieties to afford a series of ligands.

### 3.6.1 The synthesis of the tetradentate ligands

Thus far, the majority of quinoline-derived tripodal tetraamine ligands have been prepared from either the alkylation of a haloalkylquinoline with the appropriate amine, or reductive amination. For example, **29** can be prepared from the reaction of 2-(chloromethyl)quinoline hydrochloride **41.HCl** and 1-(pyridin-2-yl)methanamine **56** in the presence of either potassium[127] or sodium carbonate (*Scheme 57*).[364]

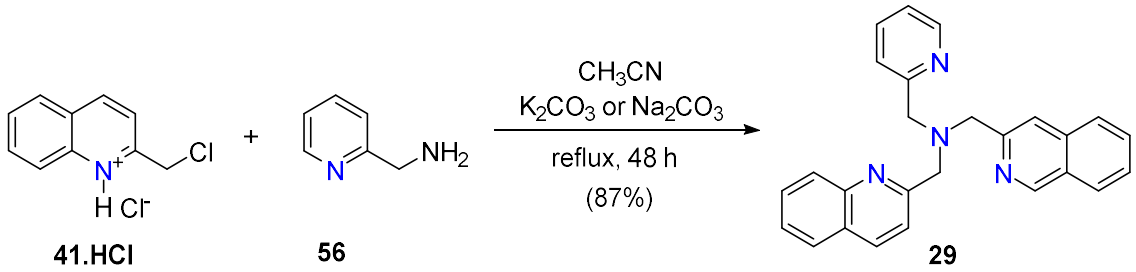


*Scheme 57. Reported synthesis of **29**.*[127,364]

With this in mind, this work commenced with the synthesis of the ligand **55**. Following a modified preparation of Wei *et al.,*[117] a solution of 2-(bromomethyl)quinoline **36** and 2-(pyridine-2-yl)ethan-1-amine **54** in THF, in the presence of *i*-$Pr_2NEt$, was stirred at room temperature for 3 days. The resulting mixture was filtered to remove a precipitate, followed by removal of the reaction solvent *in vacuo*. Following redissolution in $CH_2Cl_2$, a basic work-up and purification by column chromatography, the title compound **55** was afforded (*Scheme 58*).

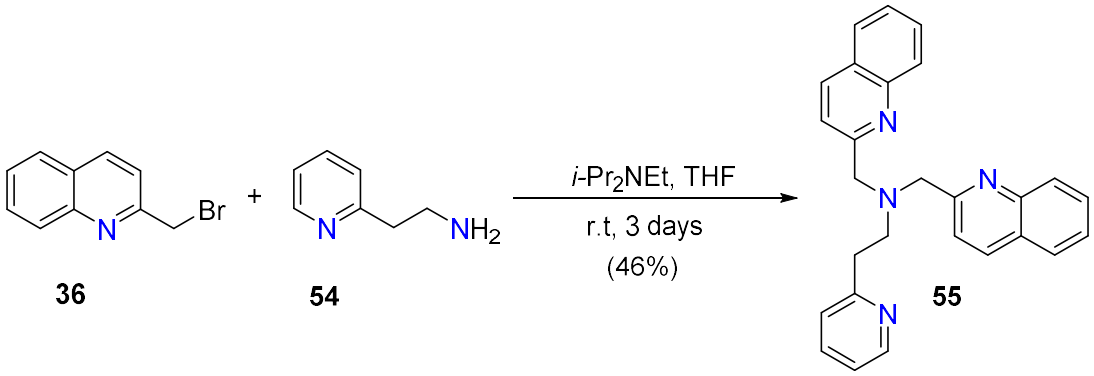


*Scheme 58. The synthesis of the ligand **55**.*

The sample was analysed by $^{1}$H NMR spectroscopy (*Figure 75*) which revealed the presence of two four proton singlets at $\delta_H$ 4.09 ppm and $\delta_H$ 3.08 ppm. The resonance appearing at $\delta_H$ 4.09 ppm can be assigned to the chemically equivalent methylene protons from each of the quinoline groups. The two sets of ethyl protons are chemically inequivalent, and therefore, vicinal coupling is expected to give two triplets in the $^{1}$H NMR spectrum. While this was not observed, the spectrum does contain a four-proton singlet appearing at $\delta_H$ 3.08 ppm. Further 2D NMR spectroscopy analysis (COSY, HSQC and HMBC) confirmed the two inequivalent $CH_2$ groups of the pyridylethyl moiety, both correlated to the singlet at $\delta_H$ 3.08 ppm. The reason for the lack of coupling is not immediately obvious.

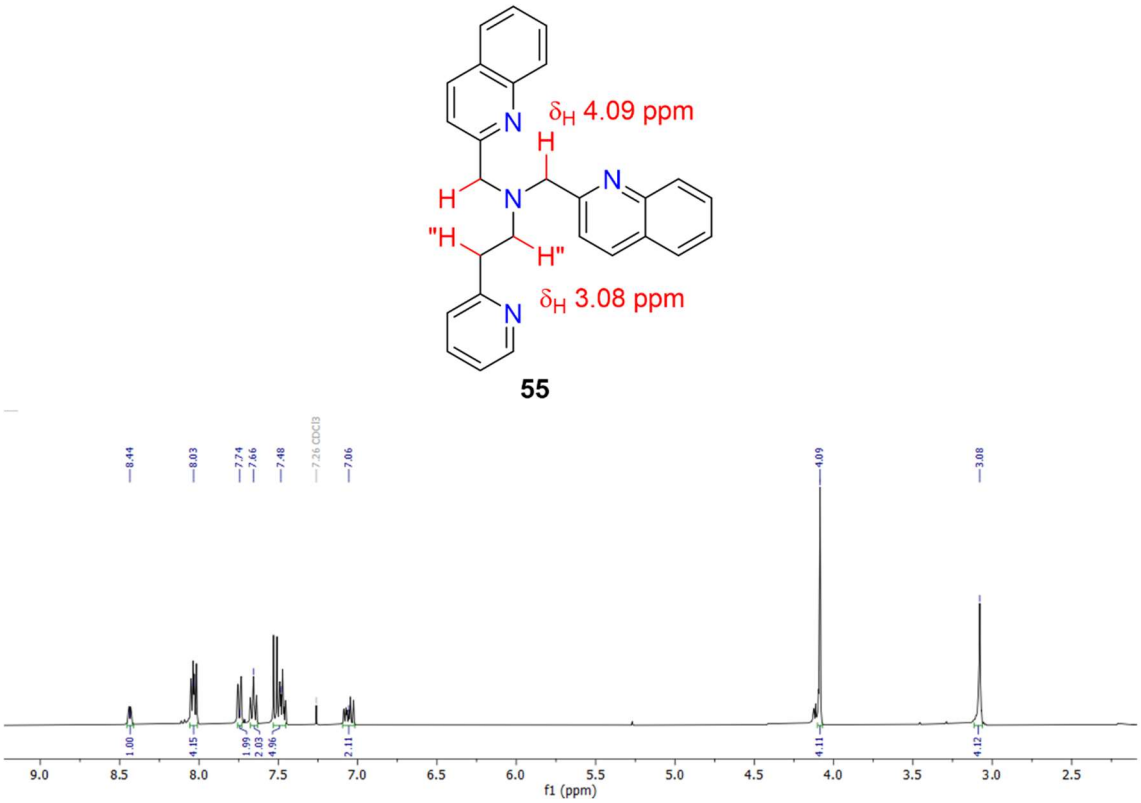


*Figure 75. $^{1}H$ NMR spectrum of **55** in $CDCl_3$.*

In addition, the $^{1}H$ NMR spectrum reveals a diagnostic doublet of doublets of doublets signal at $\delta_H$ 8.44 ppm that is attributed to the proton adjacent to the nitrogen atom of the pyridine ring (*Figure 76*). This signal appears consistently in the $^{1}H$ NMR spectra collected for the following series of ligands that contain pyridyl groups.

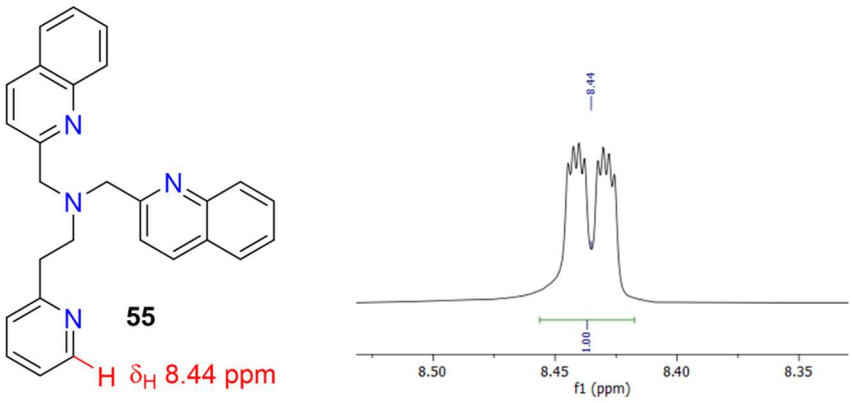


*Figure 76. Diagnostic pyridyl signal in the $^{1}H$ NMR spectrum for the ligand **55** in $CDCl_3$.*

The structure of the ligand was further confirmed by HRMS which revealed a molecular ion signal at *m/z* = 405.2076 which can be assigned to the free ligand (calcd. for $C_{27}H_{25}N_4^+$ $[M+H]^+$ *m/*z = 405.2070, found *m/z* = 405.2076).

Interestingly, a one proton singlet is observed in the $^{1}H$ NMR spectrum at $\delta_H$ 4.13 ppm that exhibits no correlation with any other proton or carbon signals, and this persisted through numerous attempts at purification by column chromatography on both alumina and silica gel (*Figure 77*). The peak was eventually removed; however, the assignment of this peak remains incomplete. Despite the persistent peak, the identity of the desired product was confirmed through NMR spectroscopy ($^{1}H$, $^{13}C$, 2D) and high-resolution mass spectrometry.

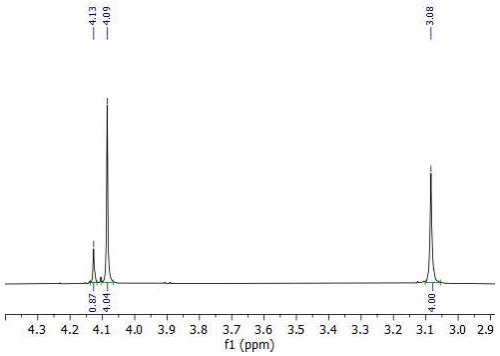


*Figure 77. Selected signals in the $^1H$ NMR spectrum of the ligand **55** over the chemical shift range $\delta_H$ = 2.9–4.4 ppm in $CDCl_3$.*

Following the isolation of the ligand with a 46% yield, a series of optimisation reactions were attempted in hopes to increase the amount of product afforded. Reviewing the literature on the synthesis of the analogous pyridine ligand, the reaction was trialled using a variety of solvents, bases, reaction times and temperatures. Mild bases such as $NaHCO_3$ and $K_2CO_3$ are commonly used bases for the synthesis of similar pyridine-containing ligands;[127,364–368] however, it appears when applied to this reaction these were not reactive enough to allow reaction to occur.

Considering the successful synthesis of **55** previously outlined, a similar synthetic approach was employed for the synthesis of **57**. Following the methodology described by Wei and coworkers,[117] with slight modifications, a solution of 2-(pyridin-2-yl)ethan-1-amine **56** and 2-(2-chloroethyl)quinoline hydrochloride **41.HCl** in THF, in the presence of *i*-$Pr_2NEt$, was stirred at room temperature for 5 days (*Scheme 59*). Subsequent aqueous work-up and purification by silica gel chromatography failed to afford the title compound **57**, as confirmed by $^1H$ NMR spectroscopy. A number of further synthetic attempts were made, which included changing the solvent, reaction time, temperature of the reaction mixture, and the identity of the base. However, no modifications to the reaction conditions resulted in formation of the desired product.

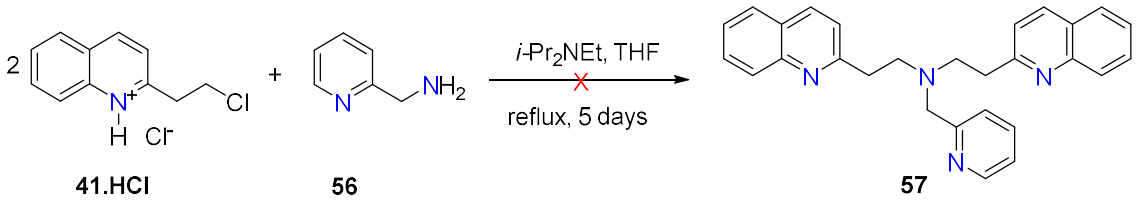


41.HCl 56 57

*Scheme 59. Attempted synthesis of the ligand **57**.*

At the time of the first attempt, it was not yet known to us that the 2-(2-chloroethyl)quinoline was isolated as the hydrochloride salt and as a result this was not considered when planning the reaction conditions. After the discovery, the above reaction was attempted again but included additional equivalents of base in attempts to neutralise the HCl salt, thereby allowing nucleophilic addition to the free amine. $^{1}$H NMR and mass spectrometry analysis revealed no corresponding peaks or signals that matched the desired ligand.

However, the $^{1}$H NMR spectrum did reveal very distinct signals typical of compounds containing a vinyl group, with diagnostic $^{1}$H NMR doublets observed at $\delta_H$ = 6.26 ppm and $\delta_H$ = 5.65 ppm corresponding to the protons on the double bond. As discussed above, we eventually identified this compound as 2-vinylquinoline (see section 3.3.3).

It is most probable that addition of the *i*-PrNEt base in the ligand synthesis results in the elimination reaction of 2-(2-chloroethyl)quinoline hydrochloride **41.HCl** proceeding at a more rapid rate than the free base 2-(2-chloroethyl)quinoline **41** can react with the amine, and therefore no ligand formation occurs.

In attempts to mitigate the elimination of 2-(2-chloroethyl)quinoline hydrochloride **41.HCl** during the reaction, the heterogeneous base $Na_2CO_3$ was employed under the same reaction conditions. Analysis of the crude material by $^{1}$H NMR spectroscopy indicated that the desired product had not been formed.

It was then decided to attempt a similar method to that used for the analogous pyridine ligand, bis[2-(2-pyridyl)ethyl]-2-[(2-pyridyl)methyl]amine **10**. Following a modified literature procedure,[30] a methanolic solution of 2-vinylquinoline **45**, 1-(pyridin-2-yl)methanamine **56** and acetic acid in the presence of $Et_3N$ was refluxed for 7 days. Following a basic work-up, $^{1}$H NMR analysis of the crude material indicated no formation of the desired product **57**.

Eventually, the ligand was successfully prepared from the reaction of 2-vinylquinoline **45** and 1-(pyridin-2-yl)methanamine **56**, in the presence of $Et_3N$, in refluxing 1,4-dioxane for 7 days (*Scheme 60*). Following a basic work-up and purification by column chromatography on alumina, the desired product **57** was isolated as a brown oil.

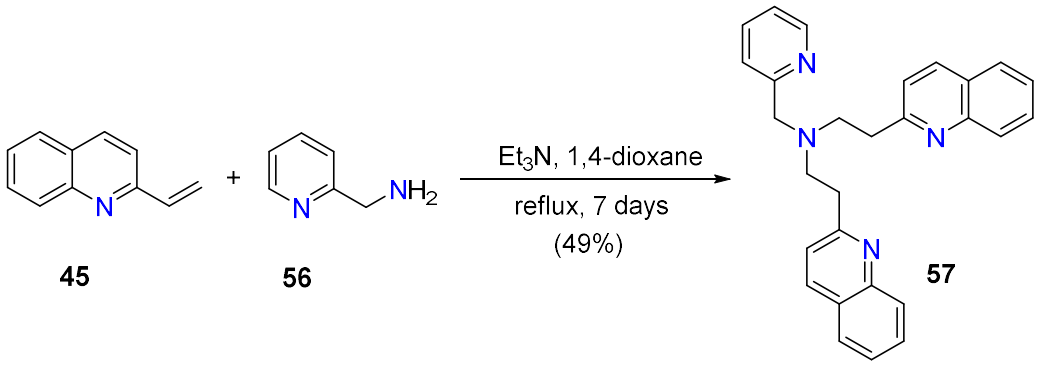


**45** **56** **57**

*Scheme 60. The synthesis of the ligand **57**.*

Analysis by $^1$H NMR spectroscopy (*Figure 78*) revealed the presence of an eight proton multiplet ranging from $\delta_H$ 3.21 ppm to $\delta_H$ 3.06 ppm, corresponding to the newly formed ethyl alkyl chains of the quinoline moieties. In addition, the -$CH_2$ protons from the pyridyl moiety are observed as a singlet at $\delta_H$ 3.91 ppm. The synthesis of **57** was further confirmed by $^{13}$C and 2D NMR (COSY, HSQC and HMBC) spectroscopy and HRMS.

The chemically inequivalent protons that make up the ethyl arm are expected to couple and hence display two triplets. However, as can be seen in *Figure 78*, this is not the case and these signals appear as a multiplet observed at $\delta_H$ 3.21 – 3.06 ppm. It is assumed that in this case the two triplets appear overlapped and as a result, a multiplet is observed. The HSQC spectrum revealed the correlation of two carbon resonances to the multiplet at $\delta_H$ 3.16 – 3.08 ppm, confirming the assignment of the quinoline ethyl protons. The multiplet could be resolved as overlapping triplets from the HSQC correlations. In conjunction with the HMBC and COSY, full assignment of the ligand was completed.

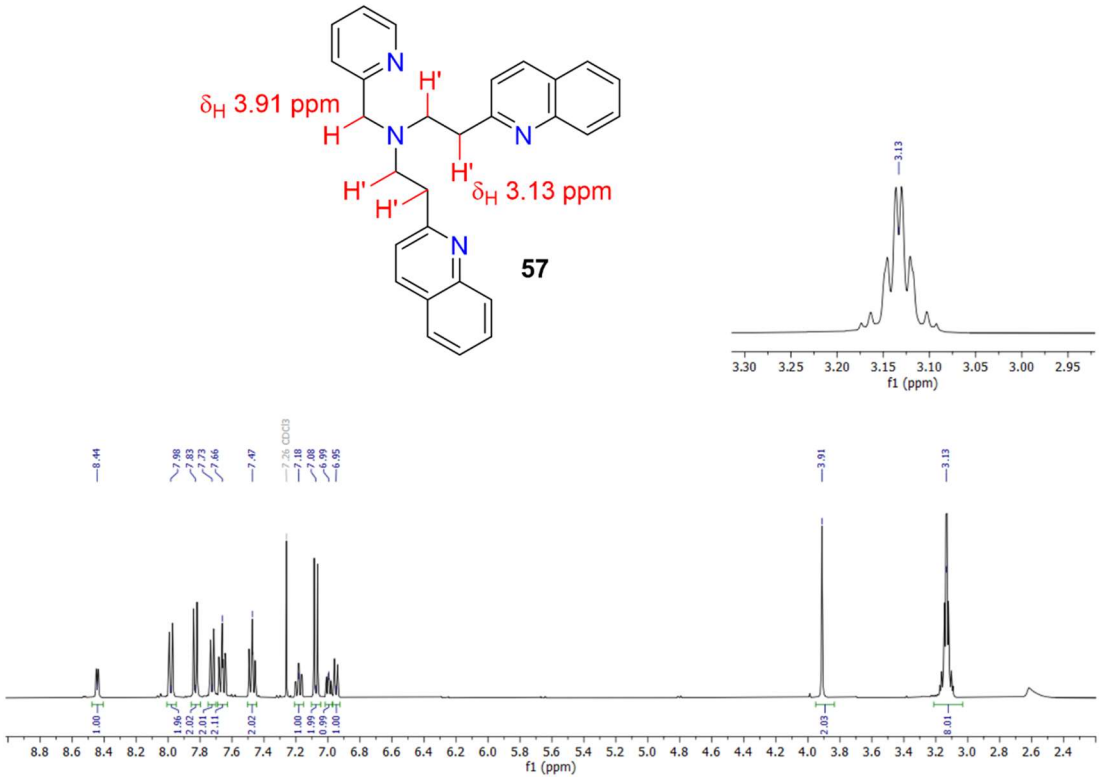


*Figure 78. $^{1}H$ NMR spectrum and key proton signal of the ligand **57** in $CDCl_3$.*

The overlapping triplet signals that correspond to the ethyl protons of the quinoline group, are also observed in similar tripodal tetraamine ligands that contain two ethyl alkyl chains. For example, $^{1}H$ NMR analysis of the pyridine congener **10** reveals an eight-proton multiplet that has been assigned to the two -$CH_2$-$CH_2$ groups.[237] The doublet of doublets of doublets (ddd) that appears at $\delta_H$ 8.44 ppm has been assigned to the proton attached to the carbon adjacent to the nitrogen atom of the pyridine. This particular peak and assignment is consistent with the ligand **55** described above and across the other pyridyl-containing ligands discussed below. A similar signal is observed for the analogous pyridyl ligands.[30,369]

The HRMS spectrum of **57** (*Figure 79*) displayed the base peak at *m/z* = 419.2228 which can be assigned to the free ligand (calcd. for $C_{28}H_{27}N_4^+$ $[M+H]^+$ *m/z* = 419.22303, found *m/z* = 419.2228). In addition, the signals at *m/z* = 441.2046 and 264.1494 were also observed and these can be assigned to the sodiated ligand, and the ligand fragment **66**, respectively (calcd. for $C_{28}H_{26}N_4Na^+$ $[M+Na]^+$ *m/z* = 441.2050; found *m/z* = 441.2046; calcd. for $C_{17}H_{18}N_3^+$ $[M+H]^+$ *m/z* = 264.1500; found *m/z* = 264.1494).

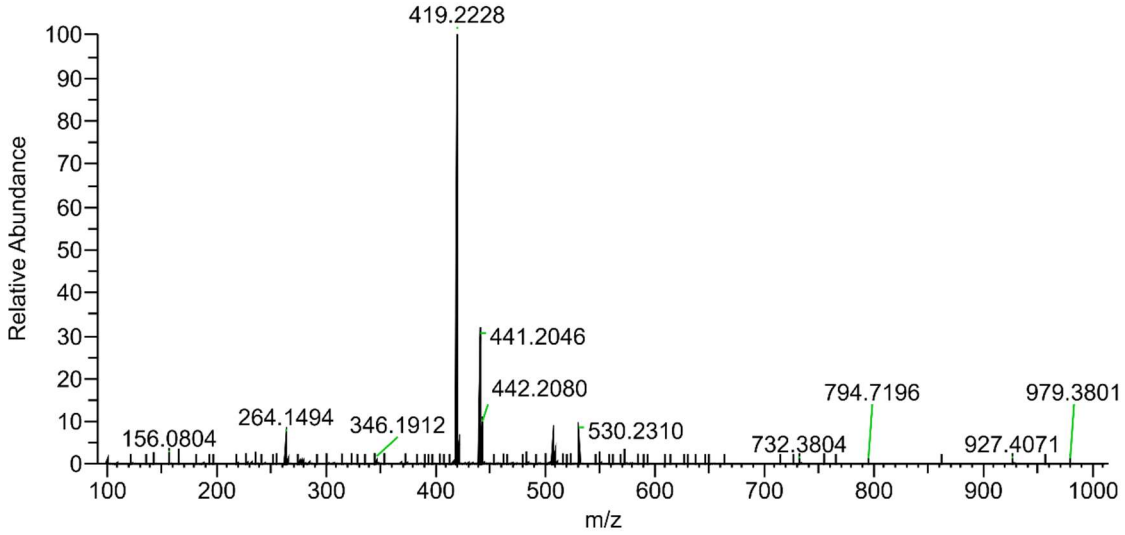


*Figure 79. The HRMS spectrum of the ligand **57**.*

Our attention was then shifted to the synthesis of the symmetrical ligand **140**. The planned synthetic pathway employed the condensation of 2-vinylquinoline **45** and ammonium chloride, based on the pyridyl congener **10** (see section 1.2.3).[28]

Following a modified literature procedure,[30] a solution of ammonium chloride in $H_2O$ was added to a solution of **45** in MeOH. The reaction mixture was heated to reflux and maintained for 7 days (*Scheme 61*). Following aqueous workup, $^1$H NMR spectroscopy and mass spectrometry revealed the formation of the title compound **140** was unsuccessful and only starting materials were observed.

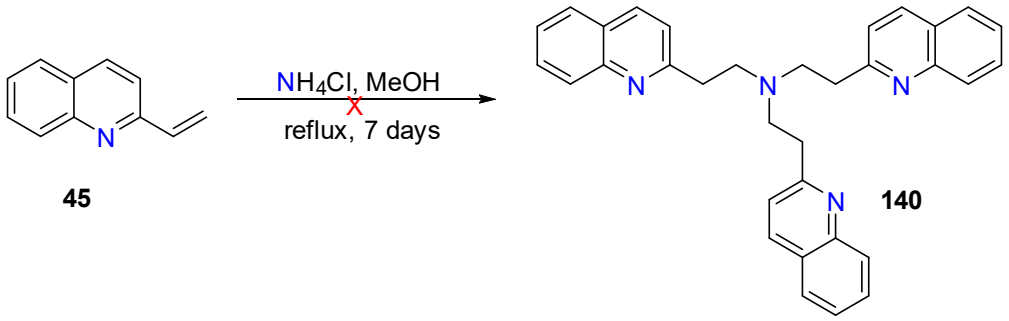


*Scheme 61. Attempted synthesis of the ligand **140**.*

The conditions were varied, including using ammonium acetate as an alternative nitrogen source, changing the solvent, reaction time and temperature. However, unfortunately none proved successful in the formation of **140**.

The ligand **58** was synthesised in a similar manner to **57** reported above from the reaction between 2-vinylquinoline **45** and 2-(pyridin-2-yl)ethan-1-amine **54** in the presence of $Et_3N$ in refluxing 1,4-dioxane for 7 days (*Scheme 62*). Following a basic work-up and purification by alumina column chromatography, the title compound **58** is afforded as a brown oil.

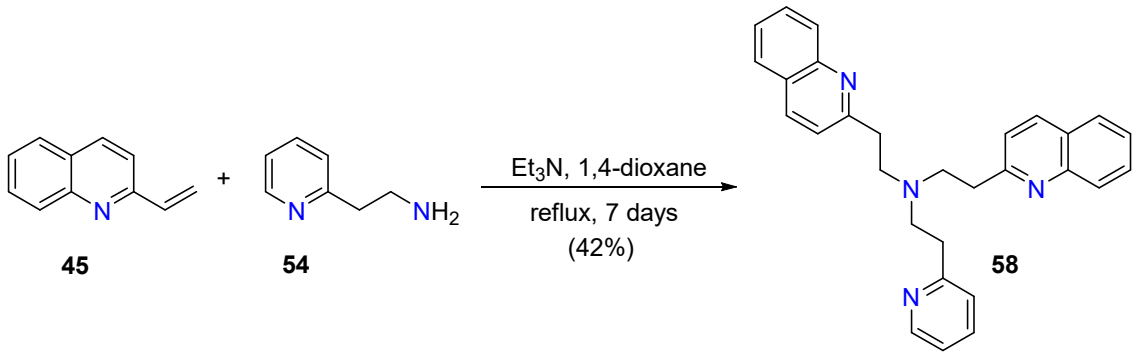


*Scheme 62. The synthesis of the ligand **58**.*

Analysis by $^1$H NMR spectroscopy (*Figure 80*) revealed the presence of an eight-proton singlet at $\delta_H$ 3.10 ppm, which is attributed to the newly formed ethyl arms of the quinoline moieties. The two triplet resonances at $\delta_H$ 3.04 and 2.91 ppm have been assigned to the ethyl -$CH_2$ protons of the pyridine moiety. The synthesis of **58** was further confirmed by $^{13}$C and 2D NMR spectroscopy and HRMS. Similar to **57**, the chemically inequivalent ethyl protons are expected to couple resulting in two four-proton triplets; however, again this is not the case. In contrast to **57**, the quinoline ethyl protons appear as one eight-proton singlet in the $^1$H NMR spectrum. This observation is similar to that found in the $^1$H NMR spectrum of **55**. The HSQC data for this ligand confirms the singlet to have correlations to two carbon signals thus confirming the assignment of the peak.

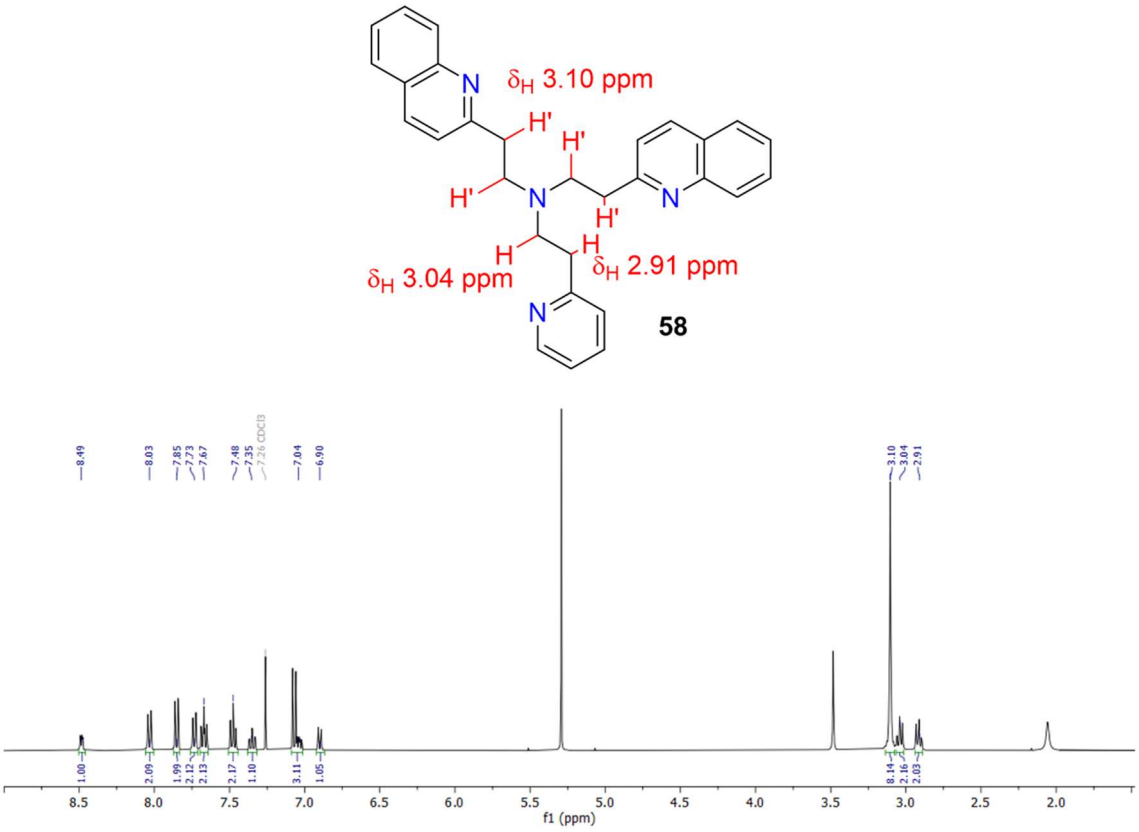


*Figure 80. $^{1}H$ NMR spectrum of the ligand **58** in $CDCl_3$.*

Analysis of **58** by HRMS afforded a spectrum that displayed a molecular ion peak at *m/*z = 433.2384 and this signal can be assigned to the free ligand (calcd. for $C_{29}H_{29}N_4^+$ $[M+H]^+$ *m/*z = 433.23867; found *m/z* = 433.2384). Fragmentation of the ligand under the conditions of the high-resolution mass spectrometer was not observed.

### 3.6.2 The synthesis of the tri- and subsequent tetradentate ligands

Having successfully prepared the tetradentate ligands, **55**, **57** and **58**, we were then interested in the synthesis of tetradentate ligands using tridentate ligands as precursors.

The synthesis of the tridentate ligand 1-(pyridin-2-yl)-*N*-[(pyridin-2-yl)methyl]methanamine **60** was achieved following a previously reported preparation.[239] A solution of 1-(pyridin-2-yl)methaneamine **56** and pyridine-2-carbaldehyde **59** were stirred at room temperature for 18 hours. After reduction with $NaBH_4$, the desired product **60** was obtained in 96% yield (*Scheme 63*). Analysis by $^{1}H$ NMR spectroscopy confirmed the successful formation of **60** with the data consistent with the literature values.[225,239]

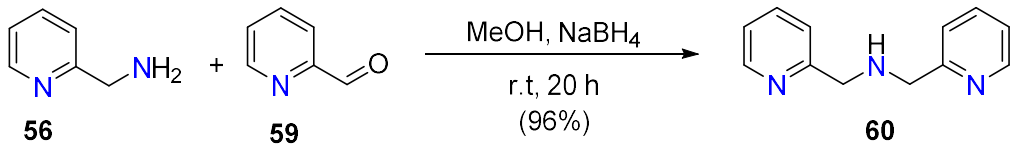


*Scheme 63. The synthesis of the ligand **60**.*

The ligand 2-(pyridin-2-yl)-*N*-[(pyridin-2-yl)ethyl]ethan-1-amine **62** was synthesised following a literature method.[226] A solution of 2-vinylpyridine **51**, 2-(pyridin-2-yl)ethan-1-amine **54** and acetic acid in MeOH were refluxed for 24 hours (*Scheme 64*). Following an aqueous work-up and purification by silica column chromatography, the desired compound **62** was obtained with a yield of 74%. The synthesis of compound **62** was confirmed by $^{1}$H NMR spectroscopy which was consistent with the literature.[226]

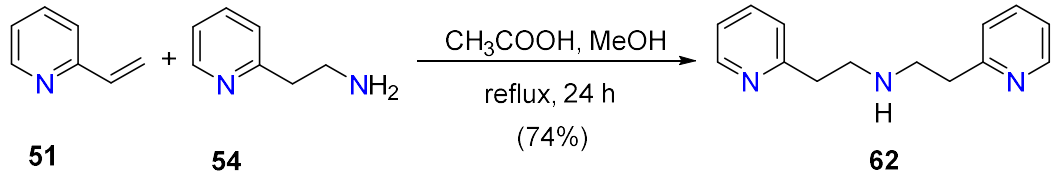


*Scheme 64. The synthesis of the ligand **62**.*

Two tridentate quinolyl-containing ligands were prepared using a modified method of Baldeau *et al*.[227] A solution of 1-(pyridin-2-yl)methaneamine **56** and quinoline-2-carbaldehyde **35** in MeOH was stirred at room temperature for 2 hours. The reaction was then cooled to 0 °C and $NaBH_4$ was added to the reaction solution slowly; this was stirred for an additional 12 hours and then refluxed for 1 hour (*Scheme 65*). Following an acid-base work-up, the title compound **67** was isolated without further purification. The structure of the desired product was confirmed by $^{1}$H NMR spectroscopy, which was consistent with previously reported data.[227]

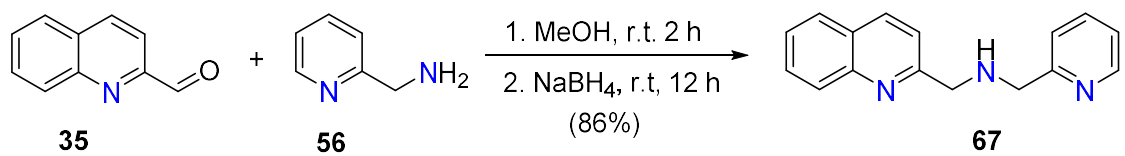


*Scheme 65. The synthesis of the ligand **67**.*

Similarly, a solution of 2-(pyridin-2-yl)ethan-1-amine **54** and quinoline-2-carbaldehyde **35** in MeOH was stirred at room temperature for 2 hours. The reaction was then cooled

to 0 °C and $NaBH_4$ was slowly added to the reaction mixture; this was then stirred for an additional 12 hours and then refluxed for 1 hour (*Scheme 66*). Following an acid-base work-up, the title compound **68** was isolated without further purification. Analysis by NMR spectroscopy ($^1H$, $^{13}C$, 2D) and HRMS revealed the successful formation of the title compound. Surprisingly, the synthesis of this ligand has not yet been reported in the literature.

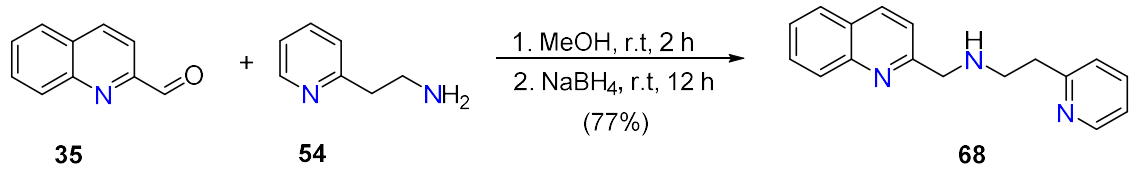


*Scheme 66. The synthesis of the ligand **68**.*

There are several tridentate ligands described in the literature that contain 2-quinolylmethyl groups;[92,94,370,371] however, the synthesis of **68** has not been reported. Interestingly, the N-methyl substituted analogue, *N*-methyl-2-(pyridin-2-yl)-*N*-[(quinolin-2-yl)methyl]ethan-1-amine **24**, is known. The synthesis of this ligand employs the reaction of *N*-methyl-2-(pyridin-2-yl)ethan-1-amine **141** and 2-(chloromethyl)quinoline hydrochloride **41.HCl** in the presence of $CsCO_3$ in refluxing THF for four days (*Scheme 67*).[242]

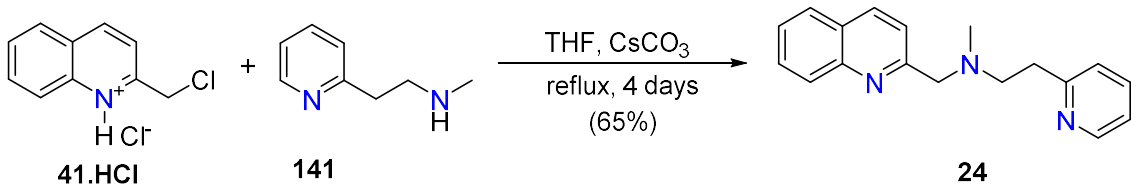


*Scheme 67. Reported synthesis of N-methyl-2-(pyridin-2-yl)-N-[(quinolin-2-yl)methyl]ethan-1-amine **24**.*

Employing a similar methodology developed for the previous ligands **57** and **58**, 1-(pyridin-2-yl)-*N*-[(pyridin-2-yl)methyl]methanamine **60** and 2-vinylquinoline **45** in the presence of $Et_3N$ were refluxed in 1,4-dioxane for 6 days (*Scheme 68*). Following a basic work-up and purification by column chromatography on alumina, the title compound **63** was isolated as a brown oil (63%).

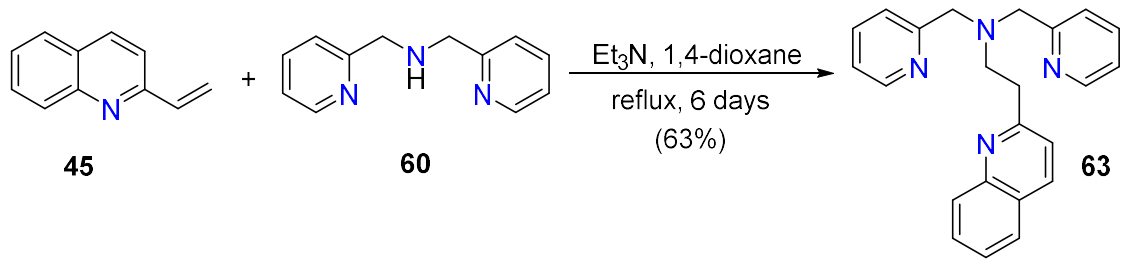


*Scheme 68. The synthesis of the ligand **63**.*

Analysis by $^{1}$H NMR spectroscopy revealed the presence of two triplets at $\delta_H$ 3.23 and 3.06 ppm, corresponding to the newly formed ethyl arm of the quinoline moiety. Furthermore, the singlet at $\delta_H$ 3.91 ppm has been assigned to the chemically equivalent -$CH_2$ protons of the two pyridine groups. The structure of **63** was further confirmed by $^{13}$C and 2D NMR spectroscopy and LRMS. In contrast to the ligands discussed above, the $^{1}$H NMR spectrum of **63** (*Figure 81*) reveals the ethyl protons of the quinoline moiety as two triplets that are not overlapping. This differs from the analogous pyridine ligand **9**, as $^{1}$H NMR analysis of this ligand displays the -$CH_2$-$CH_2$ group as a four-proton multiplet.[237]

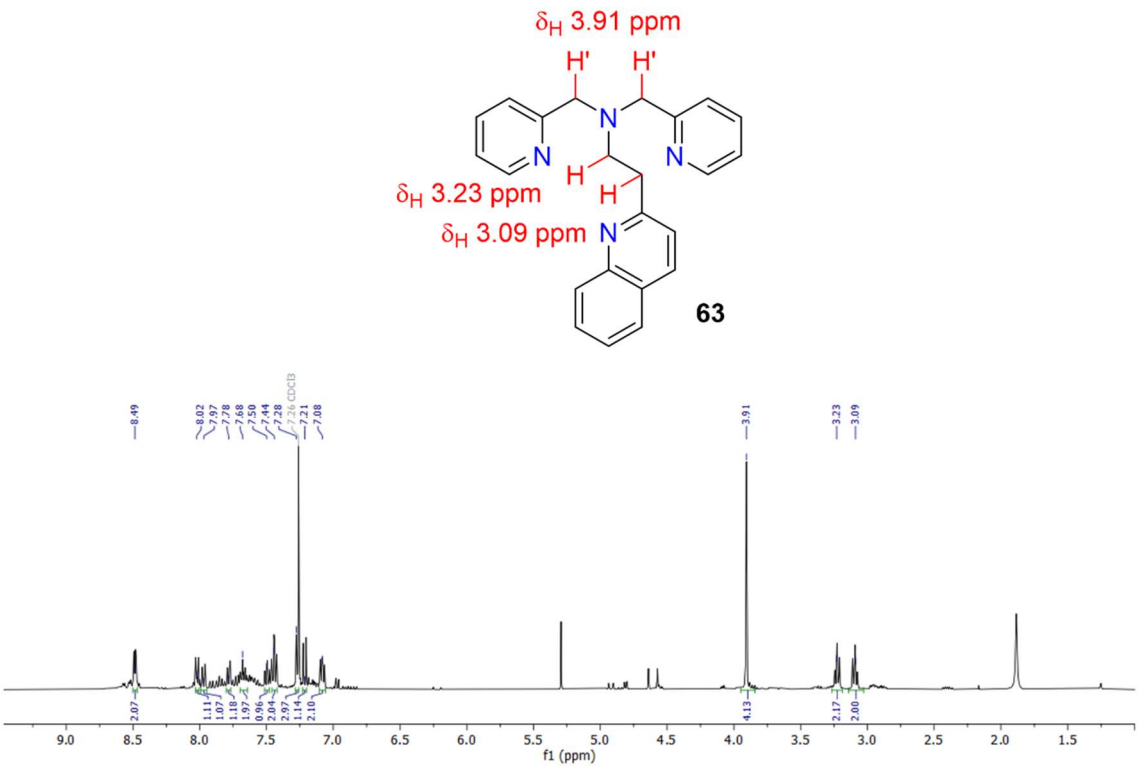


*Figure 81. $^{1}H$ NMR spectrum of the ligand **63** in $CDCl_3$.*

The ligand **64** was synthesised under the same reaction conditions as **63** from the reaction of 2-(pyridin-2-yl)-*N*-[(pyridin-2-yl)ethyl]ethan-1-amine **62** and 2-vinylquinoline **45** in the presence of $Et_3N$ in refluxing 1,4-dioxane for 6 days (*Scheme 69*). Following a basic work-up and purification by column chromatography on alumina, the title compound **64** was isolated as a brown oil (38%).

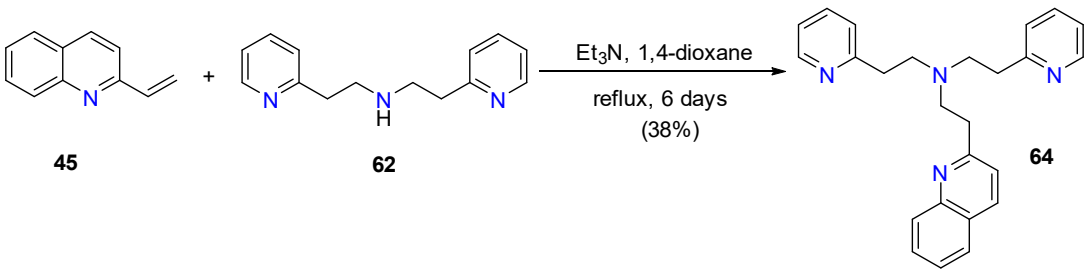


*Scheme 69. The synthesis of the ligand **64**.*

Analysis by $^{1}H$ NMR spectroscopy revealed the presence of a four-proton multiplet at $\delta_H$ 3.10 ppm, corresponding to the newly formed ethyl arm of the quinoline moiety, while the two triplet signals at $\delta_H$ 3.01 and 2.90 ppm are attributed to the chemically equivalent ethyl protons from the two pyridines (*Figure 82*). In contrast to **63**, the inequivalent ethyl

protons from the quinoline appear as a single multiplet, similar to the trend observed for **57** and **58**. The identity of this peak was confirmed in the HSQC spectrum which revealed the correlation to two carbon signals. The synthesis of **64** was further confirmed by $^{13}C$ and 2D NMR spectroscopy and HRMS.

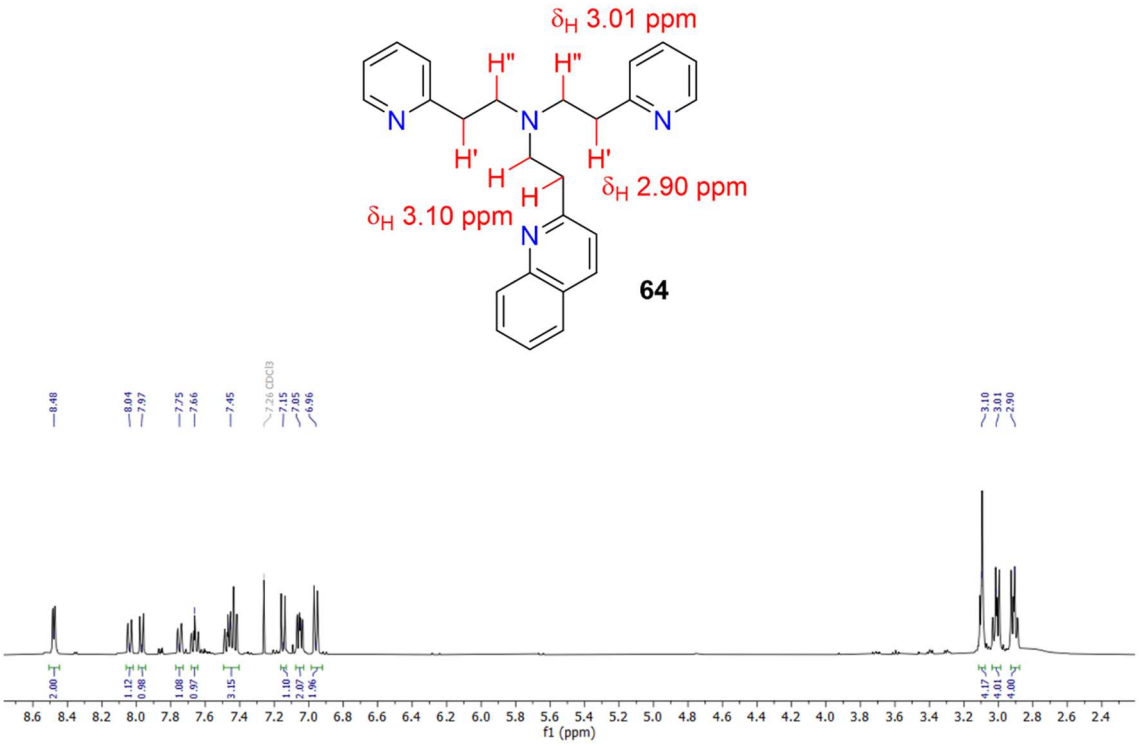


*Figure 82. $^{1}H$ NMR spectrum of the ligand **64** in $CDCl_3$.*

The asymmetric ligand **69** was synthesised from the reaction of 2-(pyridin-2-yl)-*N*-[(quinolin-2-yl)methyl]ethan-1-amine **68** and 2-vinylquinoline **45** in the presence of $Et_3N$ in 1,4-dioxane at reflux for 7 days (*Scheme 70*). Upon cooling to room temperature, the solvent was removed, and the crude material was washed with base. $^{1}H$ NMR spectroscopy and mass spectrometry of the crude material revealed the presence of the desired product; however, all purification attempts to isolate the product resulted in decomposition of **69**.

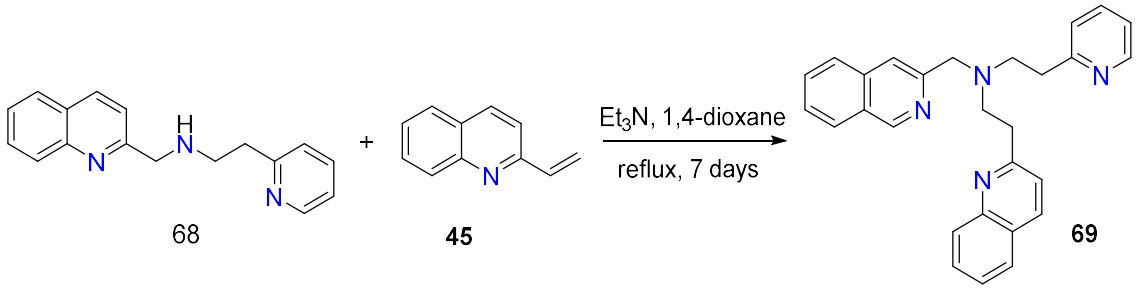


68 **45** **69**

*Scheme 70. The synthesis of the ligand **69**.*

The synthesis of the ligands **65** and **66** was achieved via an equimolar reaction of 2-vinylquinoline **45** and 1-(pyridin-2-yl)methanamine **56** or 2-(pyridin-2-yl)ethan-1-amine **54** in the presence of $Et_3N$ in refluxing dioxane for 3 days. They were also isolated as byproducts from the synthesis of their tetradentate analogues.

*N*-[(Pyridin-2-yl)methyl]-2-(quinolin-2-yl)ethan-1-amine **65** can be prepared from the reaction of **45** and 1-(pyridin-2-yl)methanamine **56** in refluxing 1,4-dioxane for 3 days with the addition of $Et_3N$ (*Scheme 71*). Following a basic workup and purification by alumina column chromatography, the title compound **65** is isolated as a brown oil.

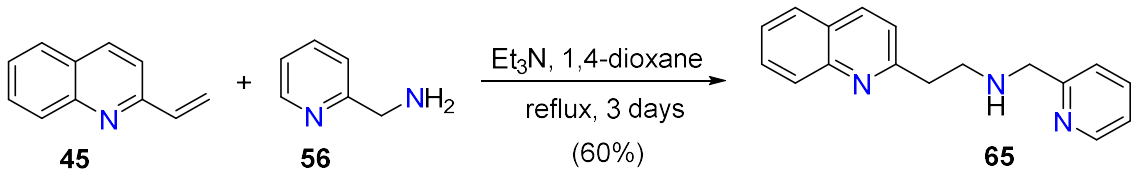


**45** **56** **65**

*Scheme 71. The synthesis of the ligand **65**.*

The structure of the tridentate ligand was confirmed by the presence of a singlet at $\delta_H$ 3.97 ppm and a multiplet signal at $\delta_H$ 3.20 ppm in $^1H$ NMR spectrum (*Figure 83*), which correlate to the newly formed -$CH_2$ and -$CH_2$-$CH_2$ alkyl arms, respectively. In addition, the characteristic doublet of doublets of doublets at $\delta_H$ 8.52 ppm which can be assigned to the proton located adjacent to the pyridine nitrogen atom is present.

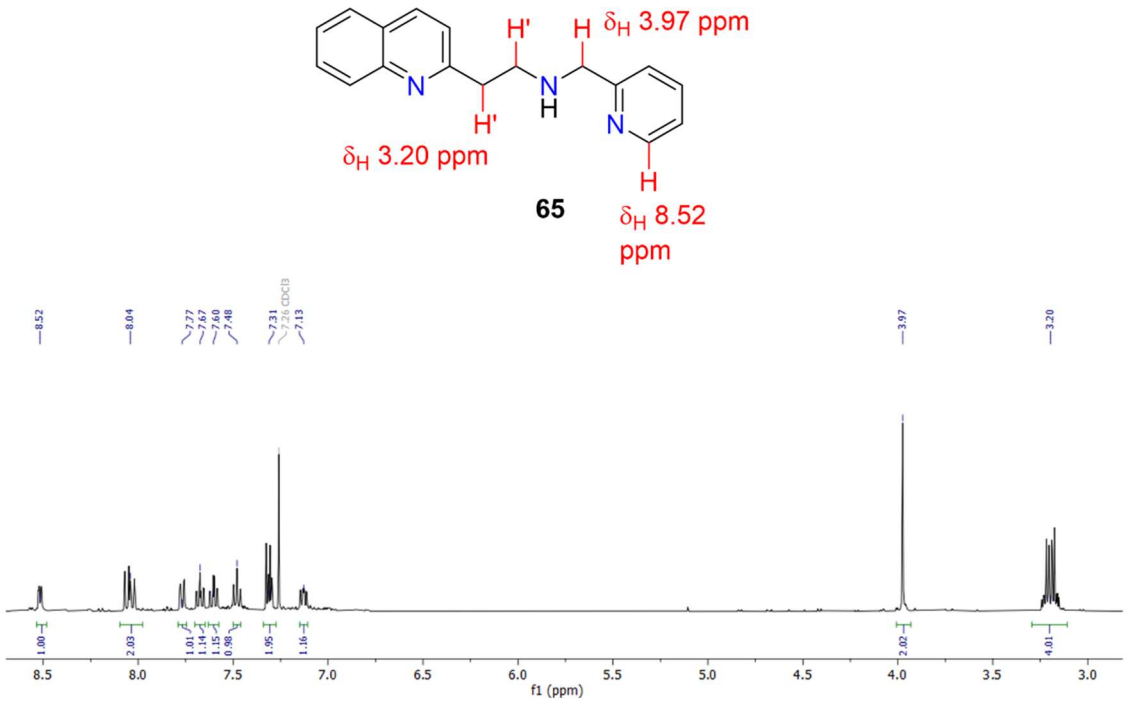


*Figure 83. $^{1}H$ NMR spectrum of the ligand **65** in $CDCl_3$.*

The HRMS spectrum revealed a molecular ion peak at *m/z* = 264.1494 and this can be assigned to the free ligand (calcd. for $C_{17}H_{18}N_3^+$ $[M+H]^+$ *m/z* = 264.14952; found *m/z* = 264.1494).

The ligand 2-(pyridin-2-yl)-*N*-[2-(quinolin-2-yl)ethyl]ethan-1-amine **66** was prepared from the reaction of **45** and 2-(pyridin-2-yl)ethan-1-amine **54**, in the presence of $Et_3N$, in 1,4-dioxane stirring at reflux for 3 days (*Scheme 72*).

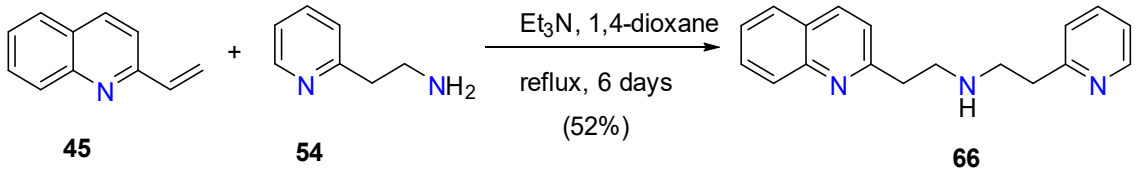


*Scheme 72. The synthesis of the ligand **66**.*

The success of this synthesis was confirmed by NMR spectroscopy and HRMS. The $^{1}H$ NMR spectrum (*Figure 84*) revealed a singlet at $\delta_H$ 3.16 ppm, attributed to the ethyl protons from the quinoline moiety, whilst the two triplets at $\delta_H$ 3.08 and 2.98 ppm can be assigned to the ethyl protons of the pyridine moiety.

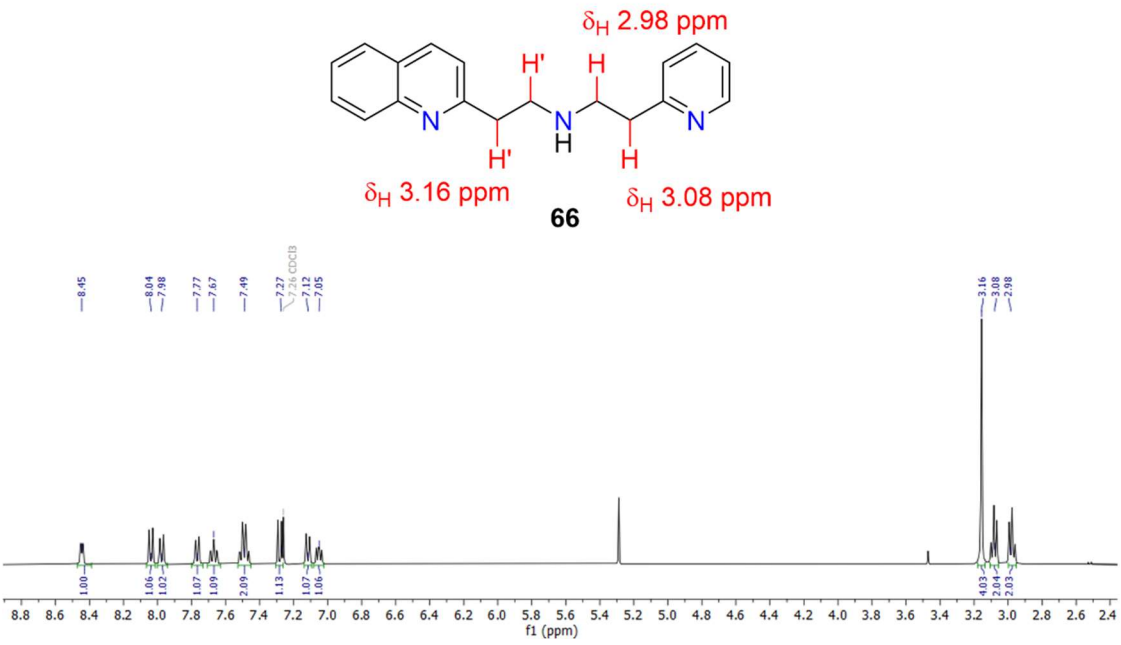


*Figure 84. $^{1}H$ NMR spectrum of the ligand **66** in $CDCl_3$.*

Furthermore, the identity of the product was confirmed by HRMS with the spectrum exhibiting a molecular ion peak at *m/z* = 278.1651 and this can be assigned to the free ligand (calcd. for $C_{18}H_{20}N_3^+$ $[M+H]^+$ *m/z* = 278.16517; found *m/z* = 278.1651).

The synthesis of **65** was also attempted using both 2-(quinolin-2-yl)ethyl methanesulfonate **42** and 2-(quinolin-2-yl)ethyl 4-methylbenzene-1-sulfonate **43** as the starting materials (see section 3.3.2). Quinoline and pyridine derivatives with mesyl or tosyl functional groups have been coupled with various amines under different reaction conditions.[372–375]

Pathway one:

A solution of previously synthesised 2-(quinolin-2-yl)ethyl methanesulfonate **42** in $CH_2Cl_2$ was cooled to 0 °C. To the solution was added 1-(pyridin-2-yl)methanamine **56** and $Et_3N$. The reaction mixture was allowed to warm to room temperature and stirred for 24 hours (*Scheme 73*). Following aqueous work-up, the crude material was analysed by $^{1}H$ NMR spectroscopy and mass spectrometry. Unfortunately, in this reaction attempt, only unreacted 1-(pyridin-2-yl)methanamine **56** and 2-vinylquinoline **45** were observed.

Pathway two:

A solution of 2-(quinolin-2-yl)ethyl 4-methylbenzene-1-sulfonate **43** in $CH_2Cl_2$ was cooled to 0 °C. To this solution was added 2-(pyridin-2-yl)ethan-1-amine **54** and $Et_3N$. The reaction mixture was allowed to warm to room temperature and stirred for 24 hours (*Scheme 73*). Following aqueous work-up, analysis by $^1H$ NMR spectroscopy and mass spectrometry of the crude material, again, revealed only unreacted 1-(pyridin-2-yl)methanamine **54** and 2-vinylquinoline **45** were observed.

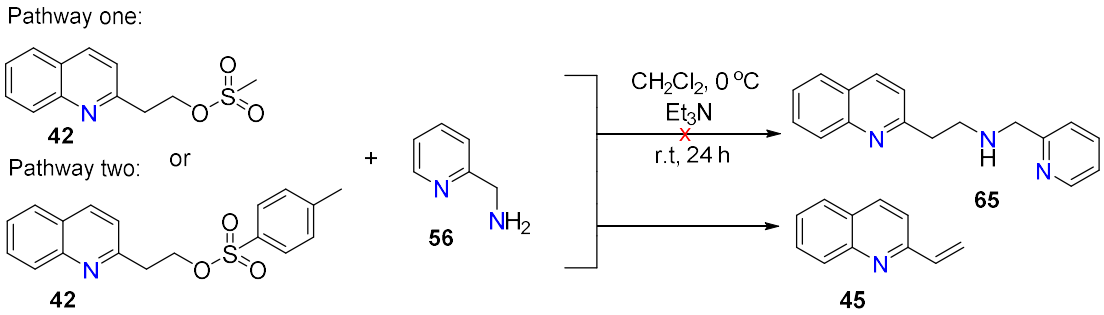


*Scheme 73. Attempted synthesis of the ligand **65**.*

The reaction conditions of both pathways appear to assist in the elimination of the sulfonate groups resulting in the generation 2-vinylquinoline **45**. However, once formed the 2-vinylquinoline **45** appears unreactive. We have previously shown that 2-vinylquinoline reacts with 1-(pyridin-2-yl)methanamine to afford the ligand **65**. However, the very different reaction conditions used are probably what lead to lack of reaction; this reaction was carried out at room temperature, whereas the synthesis of **65** was carried out at reflux (see previous discussion for the synthesis of ligand **65**), and different solvents were used ($CH_2Cl_2$ vs. 1,4-dioxane). Both reactions included the addition of $Et_3N$, however; in this reaction the base was most likely all consumed during the elimination of the sulfonate moiety, and was therefore unavailable to assist in the condensation reaction. In hindsight, the reaction conditions should have been varied, particularly the temperature and solvent; however, time constraints did not allow revisitation of this work.

To expand on the tridentate ligands that have been synthesised above, the synthesis of the unbranched tetradentate ligand **71** was investigated. Following a synthetic method detailed in the literature,[228] quinoline-2-carbaldehyde **35** and ethane-1,2-diamine **70** in EtOH were stirred at room temperature for 18 hours. Subsequent to the condensation reaction, $NaBH_4$ was added, and the solution was heated to 50 °C and maintained at this

temperature for 4 hours (*Scheme 74*). The title compound **71** was isolated as the hydrochloride salt following precipitation with concentrated HCl. The structure of the product was confirmed by means of NMR spectroscopy and mass spectrometry, results of which were consistent with literature values.[228]

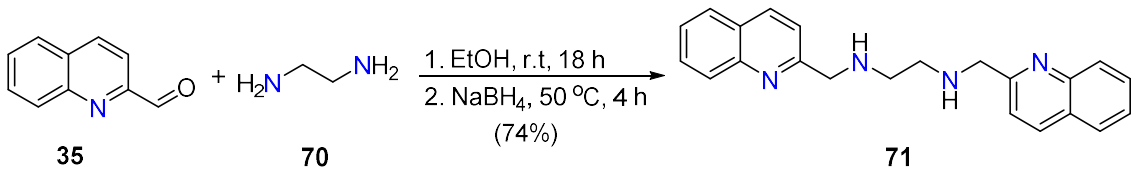


35 70 71

*Scheme 74. The synthesis of the ligand **71**.*

## 3.7 Conclusion

This chapter describes the synthesis of several quinoline-containing tri- and tetradentate ligands and the structural characterisation of each by means of NMR spectroscopy and HRMS. The new tetradentate ligands included **55**, **57**, **58**, **63**, and **64**. The interesting characterisation feature of these ligands was the observed overlapping triplet signals in the $^{1}$H NMR for the chemically inequivalent protons on the 2-quinolylethyl moiety. Rather than appearing as the expected two triplets, these protons were revealed as a singlet or multiplet. The tridentate ligands **60**, **62**, **65**, **66**, **67**, and **68** have been synthesised.

In addition, the synthesis of 2-(2-chloroethyl)quinoline **41**, 2-(2-chloroethyl)quinoline hydrochloride **41.HCl**, and 2-(2-azidoethyl)quinoline **47** have been investigated. The reported synthesis of 2-(2-chloroethyl)quinoline **41** was investigated due to some discrepancies observed between the reported method and the results we obtained. It was found that in contrast to what the authors had assumed, under their reported reaction conditions the free base of 2-(2-chloroethyl)quinoline **41** was not afforded but rather the hydrochloride salt **41.HCl**. The subsequent reaction in the same paper reported the synthesis of 2-(2-azidoethyl)quinoline **47** from the treatment of 2-(2-chloroethyl)quinoline **41** with $NaN_3$. However, again we showed this was not the case and rather the reaction of 2-vinylquinoline hydrochloride **45.HCl** (formed *in situ* from 2-(2-chloroethyl)quinoline **41**) and $NaN_3$ afforded the desired azido compound. Once 2-(2-azidoethyl)quinoline **47** was isolated, we decided to investigate this compound with two alkynes using "click" chemistry methods to afford two structures that contain a 1,2,3-triazole rings coupled to the quinoline moiety.

# Chapter Four
# Crystal structures

## 4.1 Chapter Overview

As discussed in *Chapter One*, in recent years there has been considerable interest in quinoline-based metal complexes. Characterised by their unique physiochemical, electronic, and steric properties, these complexes have found an important place in many applications across various fields, including medicinal chemistry,[376,377] material science,[378,379] enzyme modelling,[140,163,380] and catalysis.[381,382] Thus, the development of novel quinoline-based metal compounds is an area of great relevance.

Interestingly, despite the presence of several metal complexes that contain 2-quinolylethyl derived ligands, there appears to be an absence of simple unsubstituted 2-quinolylethyl-containing compounds presented in the literature. Thus, one of the main aims of this thesis was to structurally characterise metal complexes that contain 2-quinolylethyl-based ligands. This chapter reports efforts made towards structurally characterising complexes that contain the 2-quinolylethyl- and 2-quinolylmethyl-derived ligands described in *Chapter Three*.

## 4.2 Introduction

X-ray quality crystals of [Pd(**58**)Cl]Cl.x$H_2O$, [Cu(**55**)$NCCH_3$]$(ClO_4)_2$, [Zn(**55**)$NCCH_3$]$(ClO_4)_2$, [(Mn(**55**))$_2O_2$]$(ClO_4)_2$.2$CH_3CN$ and [(**62**)Co$(OH)_3$Co(**62**)]$(ClO_4)_3$.$CH_3CN$ were obtained as reported in *Chapter Two*. However, a very large number of attempts were made at obtaining crystalline materials of complexes of all ligands that were prepared in this thesis (see *Chapter Two*). Reaction conditions that were varied in attempts to obtain these crystalline materials include the following;

### 4.2.1 Solvents

The solvents used include $H_2O$, $CH_3CN$, MeOH, EtOH, $CHCl_3$, $CH_2Cl_2$, DMSO, DMF, $C_6H_{14}$, $PhCh_3$, and $(CH_3)_2CO$.

### 4.2.2 Metal salts

The starting metal salts employed include perchlorate, nitrate, chloride and sulfate.

### 4.2.3 Anions

The following salts were added to solutions of the complexes; $NaClO_4$, $NaPF_6$, $KPF_6$, $Li(N(SO_2CF_3)_2)$, $NaSbF_6$, $NaBF_4$, sodium benzoate and sodium dithionate.

### 4.2.4 Metal starting materials

The following starting materials were prepared and trialled; $[RuCl_2(DMSO)_4]$,[383] $[PdCl_2(DMSO)_2]$ and $[PtCl_2(DMSO)_2]$.[384]

### 4.2.5 Crystallisation Conditions

Several different crystallisation conditions were utilised, including slow evaporation, slow cooling, solvent layering, vapour diffusion, heating, cooling, and recrystallisation of obtained solids.

### 4.2.6 Oxidising agents

In attempts to make cobalt(III) complexes, the following oxidants were utilised; $(NH_4)_2[Ce(NO_3)_6]$, $PbO_2$, and Oxone ($2KHSO_5 \cdot KHSO_4 \cdot K_2SO_4$).[385]

Despite these many attempts, the only complexes for which we obtained X-ray quality crystals were [Pd(**58**)Cl]Cl.x$H_2O$, [Cu(**55**)$NCCH_3$]$(ClO_4)_2$, [Zn(**55**)$NCCH_3$]$(ClO_4)_2$, [(Mn(**55**))$_2O_2$]$(ClO_4)_2$.2$CH_3CN$ and [(**62**)Co$(OH)_3$Co(**62**)]$(ClO_4)_3$.$CH_3CN$. A discussion of the synthesis and characterisation of these follows.

## 4.3 Synthesis

The 2-quinolylethyl-containing ligands **58** and **64** (*Figure 85*) were reacted with the metal salts $K_2PdCl_4$ and $[Co(OH_2)_6](ClO_4)_2$, respectively, and the resulting metal complexes [Pd(**58**)Cl]Cl.x$H_2O$ and [(**62**)Co$(OH)_3$Co(**62**)]$(ClO_4)_3$.$CH_3CN$ were isolated and structurally characterised. It should be noted that the reaction between the ligand **64** and the cobalt starting material resulted in the loss of the 2-ethylquinolyl arm affording the

tridentate ligand **62**. The Cu(II), Zn(II) and Mn(III) complexes of the 2-quinolylmethyl ligand **55** (*Figure 85*) (section 3.6), [Cu(**55**)$NCCH_3$]$(ClO_4)_2$, [Zn(**55**)$NCCH_3$]$(ClO_4)_2$ and [(Mn(**55**))$_2O_2$]$(ClO_4)_2$.$2CH_3CN$ were also isolated and structurally characterised.

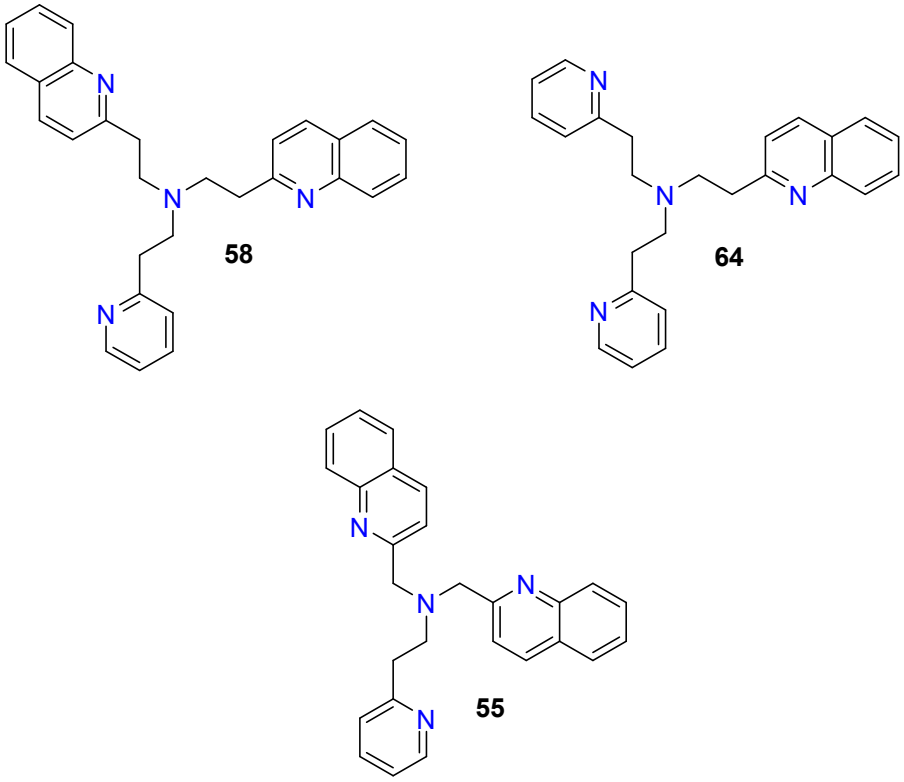


*Figure 85. Structure of the ligands **58**, **64**, and **55**.*

The palladium complex, [Pd(**58**)Cl]Cl.x$H_2O$, was prepared from the addition of a solution of **58** dissolved in $CH_3CN$ to a solution of $K_2PdCl_4$ dissolved in $H_2O$; this resulted in the formation of a fine precipitate. After stirring at room temperature for 10 minutes, the solution was heated to 70 °C for 2 hours (*Scheme 75*). Following the removal of the precipitate via vacuum filtration, the filtrate was left to stand under ambient conditions during which time crystals of X-ray quality were obtained. Crystal data for this complex are given in Table 1.

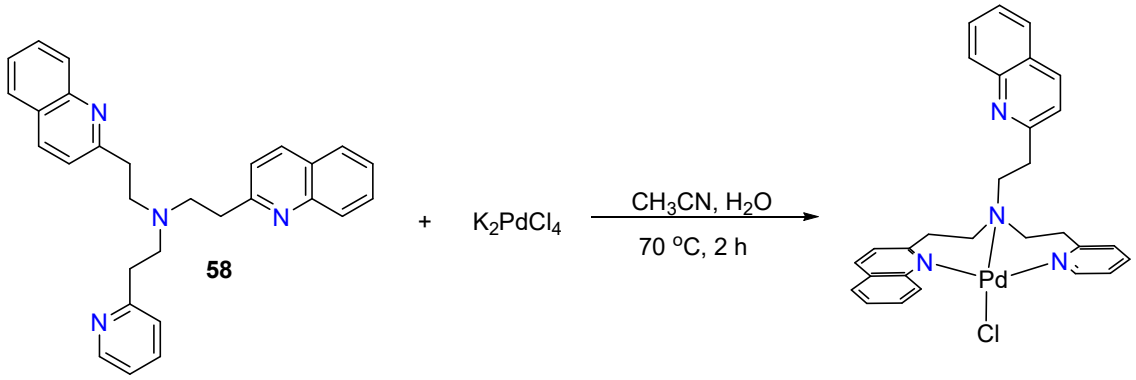


*Scheme 75. The synthesis of [Pd(**58**)Cl]Cl·xH$_2$O.*

Numerous attempts were made to obtain X-ray quality crystals of transition metal complexes containing the ligand **55**. Solutions of $[M(OH_2)_6](ClO_4)_2$ (M = Mn(II), Fe(II), Co(II), Ni(II), Cu(II)) in $CH_3CN$ were reacted with an equimolar $CH_3CN$ solution of **55** at room temperature. Upon the addition of the ligand solution to a solution of $[Fe(OH_2)_6](ClO_4)_2$ an instant rust-coloured precipitate was formed. Following the separation of the precipitate by filtration, analysis of the filtrate by mass spectrometry gave no evidence for the formation of a complex containing the ligand **55**. Following standing for 3 days under ambient conditions, no crystalline material was apparent in the $[Ni(OH_2)_6](ClO_4)_2$ solution. However, X-ray quality crystals of the new complexes [Cu(**55**)Cl]$(ClO_4)_2$, [Zn(**55**)Cl]$(ClO_4)_2$, (*Scheme 76*) and [(Mn(**55**))$_2$O$_2$]$(ClO_4)_2$.2$CH_3CN$ were obtained. Crystal data for these complexes are given in Tables 2, 3 and 4, respectively.

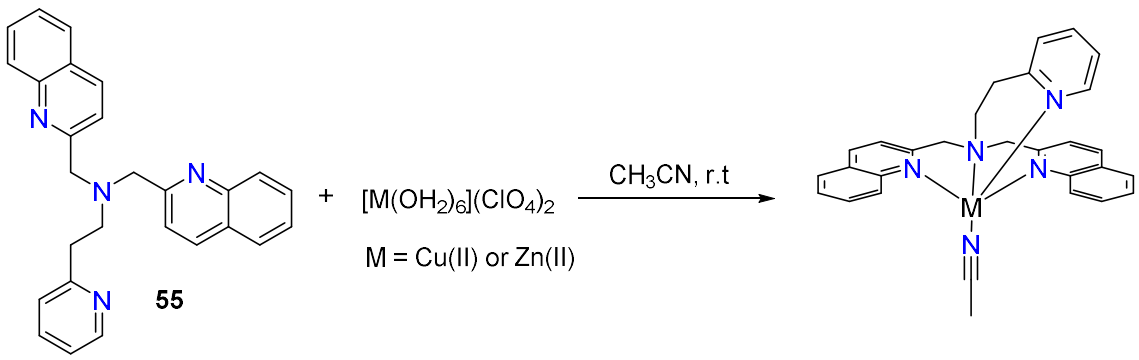


*Scheme 76. The synthesis of [Cu(**55**)Cl](ClO$_4$)$_2$ and [Zn(**55**)Cl](ClO$_4$)$_2$.*

The Co(III) complex [(**62**)Co(OH)$_3$Co(**62**)]$(ClO_4)_3$.$CH_3CN$ was prepared from the addition of a solution of **64** in $CH_3CN$ to a solution of $[Co(OH_2)_6](ClO_4)_2$ in $CH_3CN$

(*Scheme 77*). Upon standing under ambient conditions for 1 week, X-ray quality crystals were obtained. Crystal data for this complex are given in Table 5.

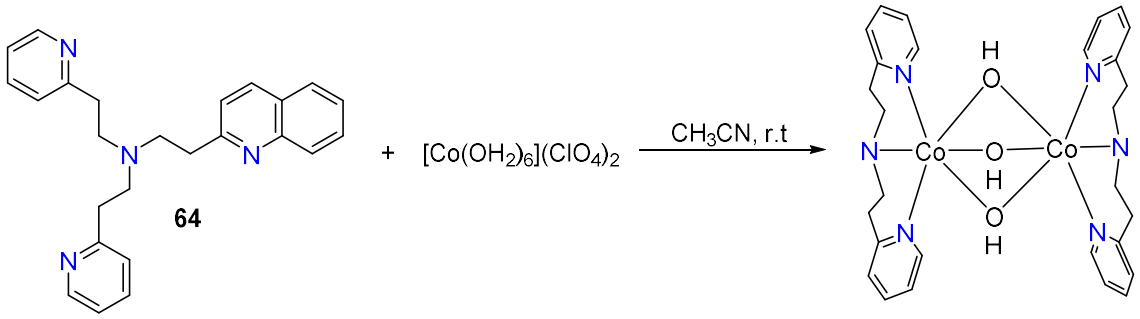


*Scheme 77. The synthesis of [(**62**)Co(OH)$_3$Co(**62**)](ClO$_4$)$_3$.CH$_3$CN.*

### 4.3.1 [Pd(58)Cl]Cl.xH$_2$O

X-ray quality crystals of the complex [Pd(**58**)Cl]Cl.xH$_2$O were obtained as described above. The complex crystallises with two [Pd(**58**)Cl]$^+$ cations in the asymmetric unit. The complex comprises a Pd(II) ion bonded to three N atoms of the ligand **58** and a chlorido ligand to give a slightly distorted square planar geometry about the metal ion ($\tau_4$ = 0.09, *Figure 86*). This is the preferred geometry of metal ions such as $Pd^{2+}$ having a $d^8$ electron configuration, and explains why one N atom of the ligand remains uncoordinated (see below) as binding of all four N atoms would not result in a square planar geometry. Considerable disorder is present in the counterions and the solvents of crystallisation, thus rendering the exact molecular formula uncertain. The ligand **58** coordinates in a hypodentate fashion, with a 2-quinolylethyl arm remaining uncoordinated to the metal ion, with a distance of 4.670 Å between the quinolyl N atom and the Pd(II) centre. The N-Pd-N bond angles are 86.89°, 86.04 °, 94.02°, 93.71°, 176.67° and 175.72°, and the N-Pd-Cl angles are 89.70°, 89.74°, 89.89°, 91.24°, 170.48° and 169.63°, close to those expected for a square planar complex. The bond distances for Pd-N$_{quinoline}$, Pd-N$_{tertiary}$, Pd-N$_{pyridine}$ and Pd-Cl are 2.036 Å and 2.038 Å, 2.099 Å and 2.107 Å, 2.040 Å and 2.056 Å, and 2.301 Å and 2.307 Å, respectively. Intermolecular π-π interactions are observed between the dangling quinoline moieties of neighbouring cations (centroid-centroid distance of 3.736 Å).

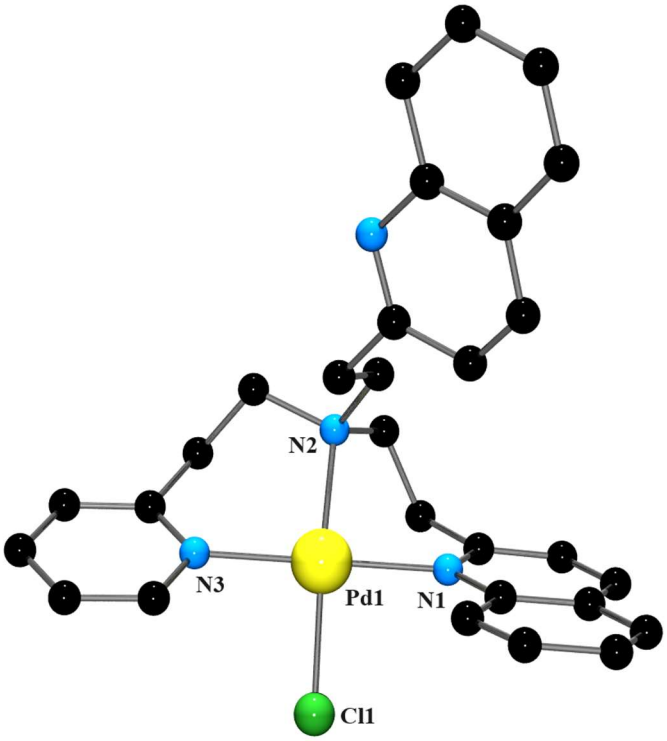


*Figure 86. Structure of the [Pd(**58**)Cl]$^{+}$ cation. H atoms have been omitted for clarity. Selected bond lengths (Å) and angles (°): Pd1-N1 2.036, Pd1-N2 2.107, Pd1-N3 2.040, Pd1-Cl1 2.301; N1-Pd1-N2 86.89, N1-Pd1-N3 176.67, N1-Pd1-Cl1 89.70, N2-Pd1-N3 94.02, N2-Pd1-Cl1 170.48, N3-Pd1-Cl1 89.89.*

**Table 1 Crystal data and structure refinement for [Pd(58)Cl]Cl.x$H_2O$**

| | |
|---|---|
| Identification code | BC296-Pd |
| Empirical formula | $C_{61}H_{77.12}Cl_{3.77}N_9O_{5.86}Pd_2$ |
| Formula weight | 1376.46 |
| Temperature/K | 119.99(10) |
| Crystal system | monoclinic |
| Space group | $P2_1/c$ |
| a/Å | 14.41317(9) |
| b/Å | 21.20131(15) |
| c/Å | 20.56448(12) |
| α/° | 90 |
| β/° | 92.1864(6) |
| γ/° | 90 |
| Volume/$Å^3$ | 6279.48(7) |
| Z | 4 |
| $\rho_{calc}g/cm^3$ | 1.456 |
| $\mu/mm^{-1}$ | 6.546 |
| F(000) | 2836.0 |
| Crystal size/$mm^3$ | 0.4 × 0.1 × 0.1 |
| Radiation | Cu Kα (λ = 1.54184) |
| 2Θ range for data collection/° | 5.99 to 145.042 |
| Index ranges | $-17 \leq h \leq 17$, $-26 \leq k \leq 25$, $-24 \leq l \leq 25$ |
| Reflections collected | 52681 |
| Independent reflections | 12108 [$R_{int}$ = 0.0373, $R_{sigma}$ = 0.0234] |
| Data/restraints/parameters | 12108/24/796 |
| Goodness-of-fit on $F^2$ | 1.021 |
| Final R indexes [I>=2σ (I)] | $R_1$ = 0.0556, $wR_2$ = 0.1577 |
| Final R indexes [all data] | $R_1$ = 0.0567, $wR_2$ = 0.1588 |
| Largest diff. peak/hole / e $Å^{-3}$ | 1.98/-0.74 |

The crystal structure confirms the presence of only one of the two possible geometric isomers; the ligand could coordinate such that both quinolines are bonded to the Pd(II) ion, or through one quinoline and one pyridine N atom. The latter is observed in the crystal structure, and $^{13}C$ NMR data are consistent with this. The $^{13}C$ NMR (*Figure 87*) spectrum revealed 23 aromatic and 6 methylene carbon signals, consistent with the isolation of one isomer. Unfortunately, in the $^{1}H$ NMR spectrum the appearance of a broad solvent signal obscures some of the proton peaks which is made evident by the COSY and HSQC spectra. Further confirmation of the characterisation of the palladium complex was obtained by HRMS (calcd. for $C_{29}H_{29}ClN_4Pd^+$ $[M]^+$ *m/z* = 574.1118, found *m/z* = 574.1115).

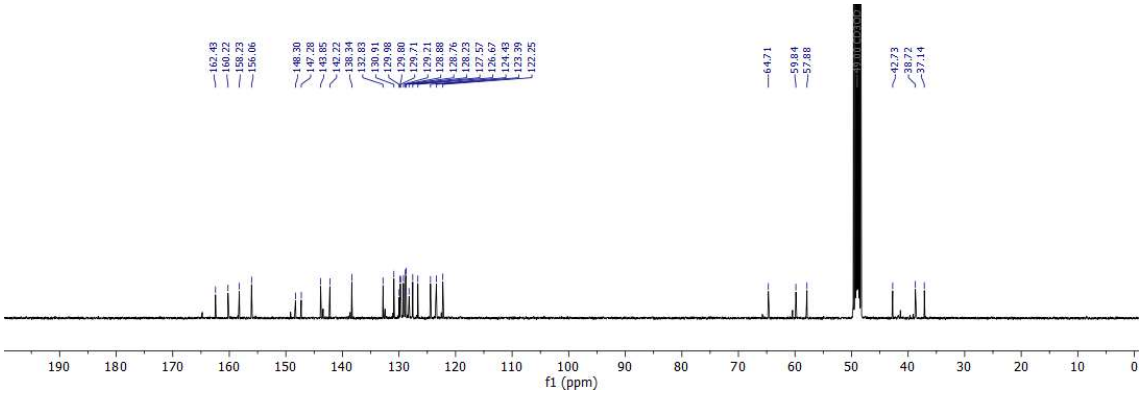


*Figure 87. $^{13}C$ NMR spectrum of the [Pd(**58**)Cl]$^+$ cation in $CD_3OD$.*

There are three closely related structurally characterised complexes present in the CSD, all of which contain tripodal tetradentate ligands, and all of which exhibit hypodentate coordination of these ligands. The complex [Pd(**9**)Cl]Cl.$H_2O$[237] contains the tetradentate tripodal ligand **9**, and, as can be seen from *Figure 88*, the metal ion is coordinated to the tertiary N atom and the two pyridylmethyl N atoms, with the pyridylethyl arm remaining uncoordinated. In contrast to the complex described above, the pyridine of the pyridylethyl arm lies above one of the coordinated pyridine rings, with a Pd-N distance of 3.076 Å, to give intracation π-π stacking with a centroid-centroid distance of 3.846 Å. A significant difference in the disposition of the quinoline moiety in the above complex relative to those of the pyridine rings in [Pd(**9**)Cl]Cl.$H_2O$ is also evident when the two structures are compared. In [Pd(**9**)Cl]Cl.$H_2O$, the mean planes of the coordinated pyridine rings are at an angle of approximately 13° to the mean plane containing the metal ion and the four donor atoms. In the above complex, this angle increases significantly to ~43° for the pyridine ring and ~62° for the quinoline ring. This is very probably due to the steric

effect of the quinoline moiety, in particular the H atom at the 8-position, which must avoid steric interactions with the chlorido ligand.

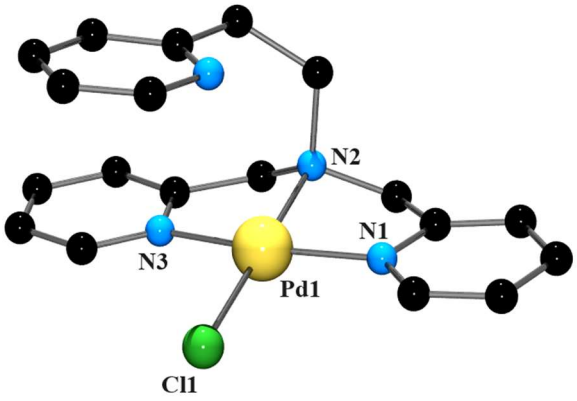


*Figure 88. Structure of the [Pd(**9**)Cl]$^+$ cation. H atoms have been omitted for clarity.*

There are two examples of the [Pd(**8**)Cl]$^+$ cation reported in the CSD, namely [Pd(**8**)Cl]Cl·2$H_2O$[237]and [Pd(**8**)Cl]($ClO_4$)[386] (*Figure 89*). In both cations, the ligand **8** is hypodentate, and again, the unbound pyridine ring lies above a coordinated pyridine ring to give intracation π-π stacking, with centroid-centroid distances of 3.507 Å and 3.817 Å, respectively. Similarly, the angle between the mean planes of the coordinated pyridine rings and the mean plane containing the metal ion and the four donor atoms are ~18° and ~10°, respectively, again, very different to those found in the [Pd(**58**)Cl]$^+$ cation.

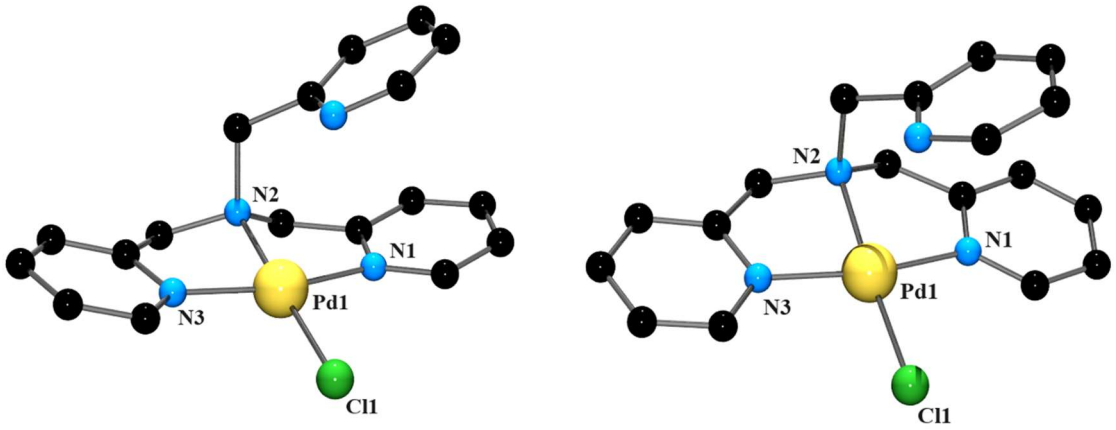


*Figure 89. Structures of the [Pd(**8**)Cl]Cl.2$H_2O$ (left) and [Pd(**8**)Cl]($ClO_4$) (right) complexes. H atoms have been omitted for clarity.*

### 4.3.2 [Cu(55)$NCCH_3$]($ClO_4$)$_2$

The metal centre in [Cu(**55**)$NCCH_3$]($ClO_4$)$_2$ (*Figure 90*) is pentacoordinate, with the Cu(II) ion bound to one acetonitrile ligand and the four nitrogen atoms of the ligand **55**. The geometry about the metal centre can be described as a distorted square-based pyramid ($\tau_5$ = 0.256).[387,388] The bond angles between the Cu(II) metal ion and the ligand (N-Cu-N) range from 82.06° to 162.95°, and the N-Cu-$N_{acetonitrile}$ angles from 93.33° to 147.59°. The ligand bond lengths are Cu-$N_{quinoline}$ 2.047 Å and 2.050 Å, Cu-$N_{pyridine}$ 2.188 Å, and Cu-$N_{tertairy}$ 2.016 Å. The bond length between the Cu(II) ion and the acetonitrile ligand is 2.004 Å. The Cu(II) ion is positioned 0.149 Å above the plane of the square base which is defined by the equatorial quinoline and tertiary nitrogen atoms of the ligand. There are π-stacking interactions[389] observed between the quinoline units of neighbouring cations, which are positioned 3.500 Å apart (centroid-centroid). The identity of the complex was further confirmed by HRMS. The mass spectrum revealed a base peak at *m/z* = 233.5643 which can be assigned to the complex formula, [Cu(**55**)]$^{2+}$ (calcd. for $CuC_{27}H_{24}N_4^{2+}$ [M]$^{2+}$ *m/z* = 233.56400; found *m/z* = 233.5643).

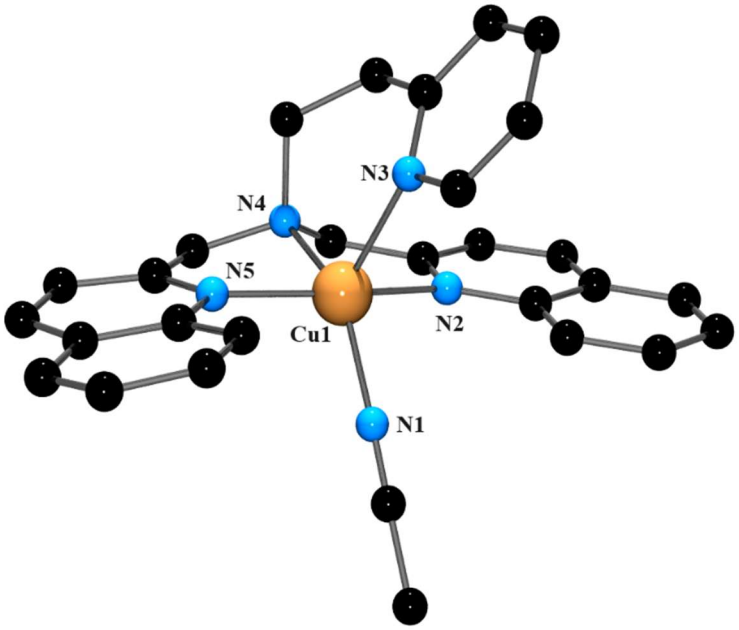


*Figure 90. Structure of the [Cu(**55**)(NCCH$_3$)]$^{2+}$cation. H atoms have been omitted for clarity. Selected bond lengths (Å) and angles (°): Cu1-N1 2.004, Cu1-N2 2.050, Cu1-N3 2.188, Cu1-N4 2.016, Cu1-N5 2.047; N1-Cu1-N2 95.78, N1-Cu1-N3 112.34, N1-Cu1-N4 147.59, N1-Cu1-N5 93.33, N2-Cu1-N3 86.46, N2-Cu1-N4 82.53, N2-Cu1-N5 162.95, N3-Cu1-N4 99.89, N3-Cu1-N5 103.34, N4-Cu1-N5 82.06.*

**Table 2 Crystal data and structure refinement for $[Cu(55)NCCH_3](ClO_4)_2$**

| | |
|---|---|
| Identification code | BC042-Cu |
| Empirical formula | $C_{29}H_{27}Cl_2CuN_5O_8$ |
| Formula weight | 707.99 |
| Temperature/K | 116.5(5) |
| Wavelength/Å | 1.54184 |
| Crystal system | Triclinic |
| Space group | P -1 |
| a/Å | 9.2839(5) |
| b/Å | 10.6305(4) |
| c/Å | 16.4412(4) |
| α/° | 100.177(2) |
| β/° | 91.169(3) |
| γ/° | 114.056(4) |
| Volume/Å$^3$ | 1450.65(11) |
| Z | 2 |
| Mg/m$^3$ | 1.621 |
| μ/mm$^{-1}$ | 3.291 |
| F(000) | 726 |
| Crystal size/mm$^3$ | 0.08 x 0.08 x 0.05 |
| Theta range for data collection | 4.652 to 74.565° |
| Index ranges | -11<=h<=11, -13<=k<=13, -17<=l<=20 |
| Reflections collected | 28062 |
| Independent reflections | 5746 [R(int) = 0.0885] |
| Completeness to theta = 67.684° | 99.9 % |
| Absorption correction | Semi-empirical from equivalents |
| Max. and min. transmission | 1.00000 and 0.86902 |
| Refinement method | Full-matrix least-squares on F2 |
| Data / restraints / parameters | 5746 / 0 / 407 |
| Goodness-of-fit on F2 | 1.028 |
| Final R indices [I>2sigma(I)] | R1 = 0.0657, wR2 = 0.1737 |
| R indices (all data) | R1 = 0.0756, wR2 = 0.1814 |
| Extinction coefficient | n/a |
| Largest diff. peak and hole | 1.532 and -1.361 e.Å-3 |

The most appropriate complexes with which to make a comparison are those that contain ligands in which the quinolines have been replaced by pyridine. However, surprisingly there are no structurally characterised copper-containing complexes containing the analogous pyridine ligand. However, there are a handful of similar copper-containing species, $[Cu(\mathbf{9})X]^{2+}$, where X = Cl ($\tau_5 = 0.12$),[233] F ($\tau_5 = 0.139$)[30] and $H_2O$ ($\tau_5 = 0.19$).[390] The value of $\tau_5$ across these compounds is smaller in comparison to the quinoline-containing species described above ($\tau_5 = 0.256$) and this can be ascribed to the additional steric interactions from the quinoline groups in **55**, specifically the H-8 protons, which results in distortion of the geometry.

A comparable complex, $[Cu(\mathbf{30})NCCH_3](ClO_4)_2$ (*Figure 91*), has been structurally characterised.[391] The Cu(II) ion is pentacoordinate, with the Cu(II) ion bound to one terminal acetonitrile ligand and the four nitrogen atoms of the ligand. The geometry about the metal centre is intermediate between square-based pyramidal and trigonal bipyramidal ($\tau_5 = 0.40$).[391] The bond angles between the Cu(II) ion and the ligand (N-Cu-N) range from 80.63° to 163.38°, and the N-Cu-$N_{acetonitrile}$ bonds are between 94.19° and 136.21°. The bond angles are similar to those observed for the $[Cu(\mathbf{55})NCCH_3]$ cation, apart from the N1-Cu1-N3 angle between the acetonitrile ligand, Cu(II), and either the axial quinoline or pyridine.

The replacement of the pyridine ring with quinoline appears to have a significant effect on the geometry about the Cu(II) centre. The geometry changes from a square-based pyramid ($\tau_5 = 0.256$) to an intermediate between square-based pyramidal and trigonal bipyramidal ($\tau_5 = 0.40$). The bond lengths are consistent with those observed in the structure of $[Cu(\mathbf{55})NCCH_3]^{2+}$. The Cu(II) cation sits virtually in the plane defined by the three equatorial nitrogen atoms of the ligand (0.051 Å), whereas in $[Cu(\mathbf{55})NCCH_3]^{2+}$ the Cu(II) ion is positioned out of the plane defined by the square-base (0.149 Å). The complex $[Cu(\mathbf{30})NCCH_3](ClO_4)_2$ also exhibits weak intermolecular π-stacking that shows a centroid-centroid distance of 3.546 Å.

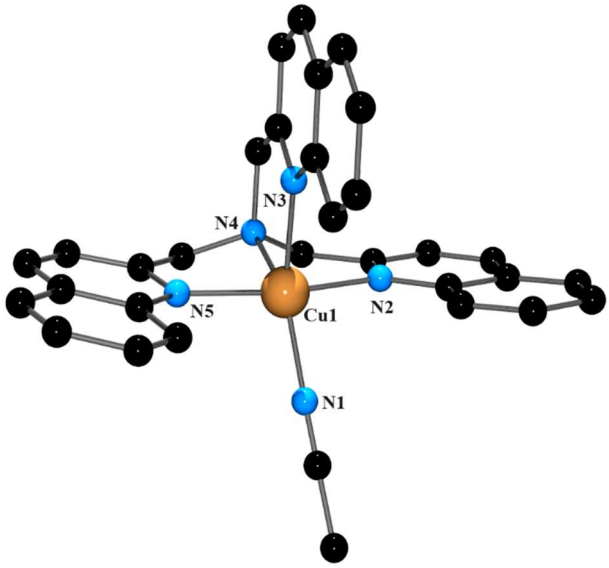


*Figure 91. Structure of the [Cu(**30**)(NCCH$_3$)]$^{2+}$cation. H atoms have been omitted for clarity.*

### 4.3.3 [Zn(55)NCCH$_3$](ClO$_4$)$_2$

The metal complexes [Cu(**55**)NCCH$_3$](ClO$_4$)$_2$ and [Zn(**55**)NCCH$_3$](ClO$_4$)$_2$ display isomorphous structures.[392] The [Zn(**55**)NCCH$_3$]$^{2+}$ cation (*Figure 92*) also exhibits a distorted square-based pyramidal N$_5$ environment about the Zn(II) centre ($\tau_5$ = 0.16). The Zn(II) centre is bound to all four nitrogen donor atoms of **55** and the fifth coordination site is occupied by a solvent acetonitrile nitrogen atom. The Zn-N bond lengths are 2.166 Å 2.182 Å for Zn-N$_{quinoline}$, 2.063 Å for Zn-N$_{pyridine}$, 2.094 Å for Zn-N$_{tertiary}$, and 2.036 Å for Zn-N$_{acetonitrile}$. The N-Zn-N and N-Zn-N$_{acetonitrile}$ bond angles range from 78.76°–156.37°, and 94.49°– 146.60°, respectively. Very weak intermolecular π-π interactions of adjacent quinoline rings of the ligand are observed, with a separation of 4.397 Å. The Zn(II) ion sits 0.233 Å above the plane of the square base formed by the equatorial quinoline and tertiary nitrogen atoms of the ligand, slightly higher than that observed for the copper complex described above.

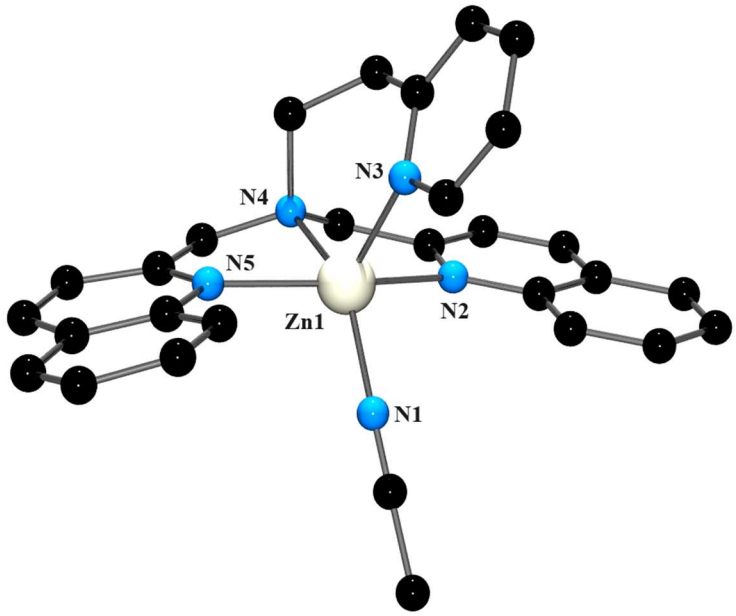


*Figure 92. Structure of the [Zn(**55**)(NCCH$_3$)]$^{2+}$cation. H atoms have been omitted for clarity. Selected bond lengths (Å) and angles (°): Zn1-N1 2.036, Zn1-N2 2.182, Zn1-N3 2.063, Zn1-N4 2.094, Zn1-N5 2.166; N1-Zn1-N2 97.80, N1-Zn1-N3 110.14, N1-Zn1-N4 146.60, N1-Zn1-N5 94.49, N2-Zn1-N3 89.89, N2-Zn1-N4 79.87, N2-Zn1-N5 156.37, N3-Zn1-N4 103.19, N3-Zn1-N5 104.71, N4-Zn1-N5 78.76.*

**Table 3 Crystal data and structure refinement for $[Zn(55)NCCH_3](ClO_4)_2$**

| | |
|---|---|
| Identification code | BC042-Zn |
| Empirical formula | $C_{29}H_{27}Cl_2ZnN_5O_8$ |
| Formula weight | 709.82 |
| Temperature/K | 115.8(23) |
| Wavelength/Å | 1.54184 |
| Crystal system | Triclinic |
| Space group | P -1 |
| a/Å | 8.91680(10) |
| b/Å | 10.7079(2) |
| c/Å | 16.9085(2) |
| α/° | 97.2950(10) |
| β/° | 91.8680(10) |
| γ/° | 113.7210(10) |
| Volume/Å$^3$ | 1459.83(4) |
| Z | 2 |
| Mg/m$^3$ | 1.615 |
| μ/mm$^{-1}$ | 3.383 |
| F(000) | 728 |
| Crystal size/mm$^3$ | 0.100 x 0.100 x 0.050 |
| Theta range for data collection | 2.646 to 74.429°. |
| Index ranges | -10<=h<=11, -13<=k<=13, -21<=l<=20 |
| Reflections collected | 41917 |
| Independent reflections | 5792 [R(int) = 0.0574] |
| Completeness to theta = 67.684° | 100.0 % |
| Absorption correction | Semi-empirical from equivalents |
| Max. and min. transmission | 1.00000 and 0.96858 |
| Refinement method | Full-matrix least-squares on F2 |
| Data / restraints / parameters | 5746 / 0 / 407 |
| Goodness-of-fit on F2 | 1.060 |
| Final R indices [I>2sigma(I)] | R1 = 0.0513, wR2 = 0.1392 |
| R indices (all data) | R1 = 0.0590, wR2 = 0.1456 |
| Extinction coefficient | n/a |
| Largest diff. peak and hole | 1.481 and -0.804 e.Å-3 |

Further analysis of the Zn(II) complex was obtained by means of NMR spectroscopy and HRMS. The $^{13}C$ NMR spectrum (Figure 93) revealed 14 aromatic and 3 methylene carbon signals, and the $^{1}H$ NMR spectrum is consistent with this. It should be noted that 23 aromatic carbon signals are expected; however, 14 signals are observed due to a number of overlapping carbons, as confirmed by 2D NMR spectra. The mass spectrum revealed a base peak at *m/z* = 234.0641 and this is consistent with the complex formula, $[Zn(\mathbf{55})]^{2+}$ (calcd. for $ZnC_{27}H_{24}N_4^{2+}$ $[M]^{2+}$ *m/z* = 234.0646; found *m/z* = 234.0641).

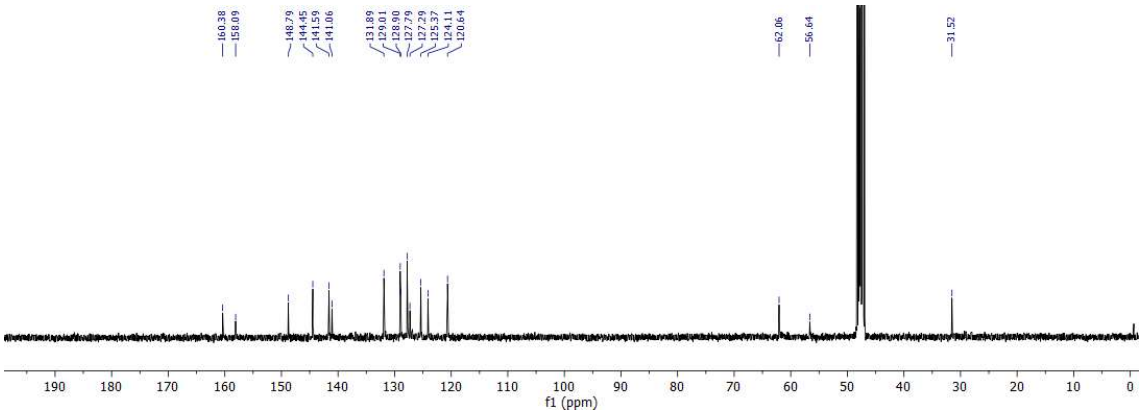


*Figure 93. $^{13}C$ spectrum of $[Zn(\mathbf{55})NCCH_3]^{2+}$ cation in $CD_3OD$.*

There are no analogous pentacoordinate Zn(II) complexes that contain the pyridine ligand congener **9**. There are a handful of the Zn(II) species that have similar structures to the $[Zn(\mathbf{55})NCCH_3]^{2+}$ cation.[158,393–396] The majority of these species have a bulky substituent on either the quinoline or pyridine moieties which result in a significant change in complex geometry with $\tau_5$ values ranging between 0.475 and 0.872.[394–396]

A single Zn(II) complex containing the ligand **55** has previously been prepared by Gan *et al.*[150] The authors have reported the structural characterisation of the Zn(II) complex, $[Zn(\mathbf{55})OH_2](ClO_4)_2.C_2H_5OH$ (*Figure 94*); however, there are no published preparations for this ligand. The cation $[Zn(\mathbf{55})OH_2]^{2+}$ is five-coordinate, with four nitrogen donors from the ligand and one monodentate aqua ligand bound to the Zn(II) metal centre, affording the complex as an intermediate between square-based pyramidal and trigonal bipyramidal geometry ($\tau_5$ = 0.39). The N-Zn-N bond angles are between 78.65° and 156.68°, and the N-Zn-O angles range from 87.45° to 132.94°. The Zn-N bond lengths are between 2.050 Å and 2.172 Å, and the Zn-O bond length is 2.004 Å. The Zn(II) ion sits 0.267 Å above the N1-N3-N4 plane. Weak intermolecular π-π interactions occur

between the quinolyl groups of neighbouring structures with a centroid-centroid distance of 3.958 Å.

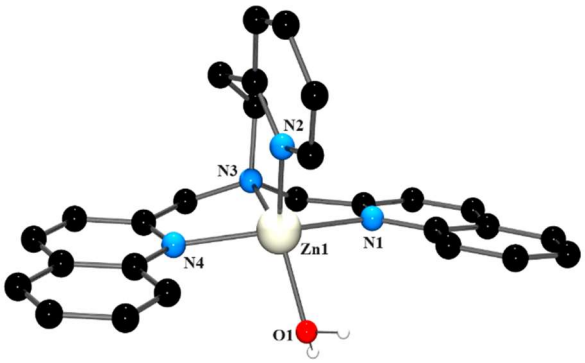


*Figure 94. Structure of the [Zn(**55**)(OH$_2$)]$^{2+}$cation. H atoms have been omitted for clarity.*

The bond lengths and angles are very similar to those observed in the [Zn(**55**)NCCH$_3$]$^{2+}$ cation. The notable difference between the two species is the geometry about the Zn(II) cation which is square-based pyramidal when the fifth coordination site is occupied by an acetonitrile ligand, and an intermediate geometry with the replacement of $H_2O$ ($\tau_5$ = 0.16 vs. $\tau_5$ = 0.39).

Another Zn(II) species that contains a ligand structurally similar to **55** illustrated in *Figure 95* is [Zn(α-MeBQPA)Cl]ClO$_4$ (α-MeBQPA = α-methyl-2-pyridylmethyl-bis(2-quinolylmethyl)amine).[397] The ligands differ by a methyl substituent that is located on the methylene carbon of the quinoline group. In contrast to [Zn(**55**)NCCH$_3$]$^{2+}$, this species has the Zn(II) metal centre positioned in a distorted trigonal bipyramidal geometry ($\tau_5$ = 0.72). There are no major differences in the bond lengths between the two species. [Zn(α-MeBQPA)Cl]$^+$ has Zn-N$_{quinoline}$ bond distances similar to those reported in [Zn(**55**)NCCH$_3$]$^{2+}$, and the Zn-N$_{pyridine}$ and Zn-N$_{tertiary}$ are slightly longer. The Zn-Cl bond length of 2.270 Å for this species is consistent with the observed literature values of similar five-coordinate Zn(II) complexes.[398–403]

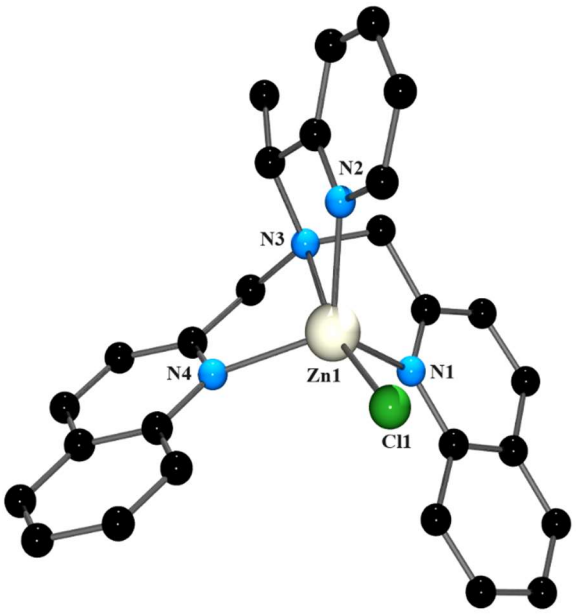


*Figure 95. Structure of the [Zn(α-MeBQPA)Cl]$^{+}$cation. H atoms have been omitted for clarity.*

### 4.3.4 [(Mn(55))$_2$O$_2$](ClO$_4$)$_2$.2CH$_3$CN

The $Mn_2$(III,III) complex, [(Mn(**55**))$_2$O$_2$](ClO$_4$)$_2$.2CH$_3$CN (*Figure 96*), has two crystallographically independent dimeric cations within the asymmetric unit, with two Mn(III) ions each bound to one **55** ligand, and bridged by a (μ-O)$_2$ core. This is unusual as bis(μ-oxo) complexes are predominantly mixed-valence Mn(III)-Mn(IV) species.[404–411]

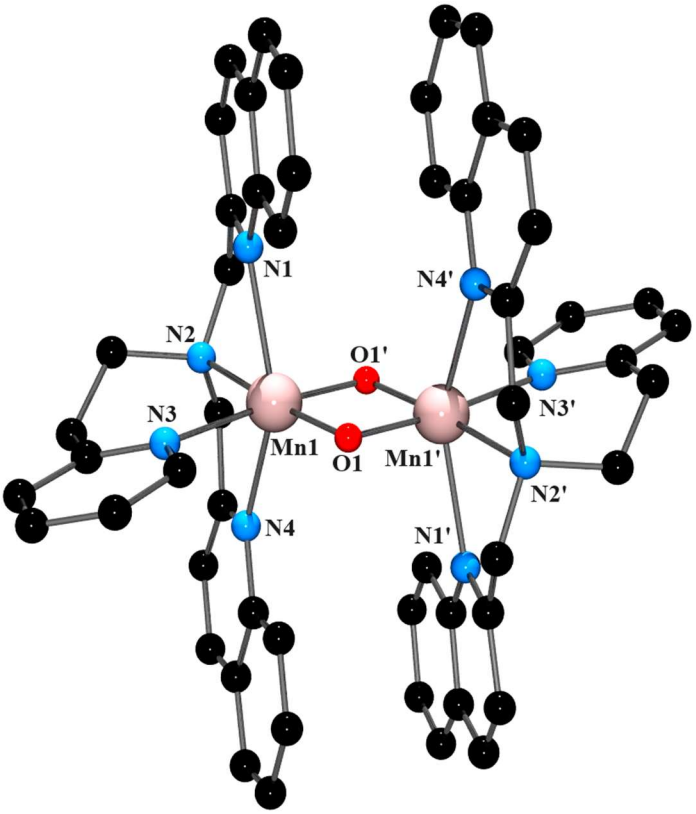


*Figure 96. Structure of the [(Mn(**55**))$_2$O$_2$]$^{2+}$cation. H atoms have been omitted for clarity. Selected bond lengths (Å) and angles (°): Mn1-N1 2.311, Mn1-N2 2.145, Mn1-N3 2.147, Mn1-N4 2.333, Mn1-O 1.827, Mn1-O1' 1.834, N1-Mn1-N2 76.53, N1-Mn1-N3 85.93, N1-Mn1-N4 150.38, N1-Mn1-O1 105.95, N1-Mn1-O1' 93.67, N2-Mn1-N3 93.10, N2-Mn1-N4 74.60, N2-Mn1-O1 174.14, N1-Mn1-O1' 89.17, N3-Mn1-N4 89.10, N3-Mn1-O1 92.38, N3-Mn1-O1' 177.54, N4-Mn1-O1 103.41, N4-Mn1-O1' 92.43, O1-Mn1-O1' 85.40.*

**Table 4 Crystal data and structure refinement for $[(Mn(55))_2O_2](ClO_4)_2.2CH_3CN$**

| | |
|---|---|
| Identification code | BC042-Mn |
| Empirical formula | $C_{58}H_{54}Cl_2Mn_2N_{10}O_{10}$ |
| Formula weight | 1231.89 |
| Temperature/K | 116.0(7) |
| Wavelength/Å | 1.54184 |
| Crystal system | Monoclinic |
| Space group | P 21/n |
| a/Å | 22.0075(3) |
| b/Å | 12.05850(10) |
| c/Å | 22.4061(3) |
| α/° | 90 |
| β/° | 112.5840(10) |
| γ/° | 90 |
| Volume/$Å^3$ | 5490.11(12) |
| Z | 4 |
| $Mg/m^3$ | 1.490 |
| $\mu/mm^{-1}$ | 5.224 |
| F(000) | 2544 |
| Crystal size/$mm^3$ | 0.16 x 0.14 x 0.14 |
| Theta range for data collection | 3.587 to 74.524°. |
| Index ranges | -27<=h<=27, -15<=k<=14, -25<=l<=27 |
| Reflections collected | 76882 |
| Independent reflections | 11063 [R(int) = 0.0664] |
| Completeness to theta = 67.684° | 100.0 % |
| Absorption correction | Semi-empirical from equivalents |
| Max. and min. transmission | 1.00000 and 0.59244 |
| Refinement method | Full-matrix least-squares on F2 |
| Data / restraints / parameters | 11063 / 0 / 741 |
| Goodness-of-fit on F2 | 1.026 |
| Final R indices [I>2sigma(I)] | R1 = 0.0453, wR2 = 0.1118 |
| R indices (all data) | R1 = 0.0522, wR2 = 0.1157 |
| Extinction coefficient | n/a |
| Largest diff. peak and hole | 1.856 and -0.576 e.Å-3 |

The Mn(III) centres display a distorted octahedral geometry. The Mn-$N_{quinoline}$ bond lengths lie between 2.298 Å and 2.396 Å, Mn-$N_{pyridine}$ from 2.247 Å and 2.155 Å, and the Mn-$N_{tertiary}$ 2.134 Å and 2.145 Å. The bridging oxygen atoms have Mn-O bond lengths of 1.826 Å and 1.834 Å. The Mn-$N_{quinoline}$ bond lengths are significantly longer than the Mn-$N_{tertiary}$, which can be attributed to the Jahn-Teller distortion that is expected for high spin $d^4$ Mn(III).[119] The Mn-Mn separation is 2.69 Å, consistent with the distances reported for similar complexes. This is unusual because Mn(III)-Mn(IV) bis(μ-oxo) dimers also predominately exhibit a Mn-Mn separation of 2.6 Å – 2.7 Å,[404,405,412–414] despite the difference in the oxidation states of the metal ions. The quinoline rings exhibit intramolecular π-π interactions with centroid-centroid distances of 3.449 Å and 3.593 Å. The *trans* X-Mn-X angles range from 149.80° to 177.54°, and the *cis* lie between 74.14° and 105.95°. The O-Mn-O angles of 85.40° and 85.13° are within the range of other reported Mn(III) complexes.[164]

The two manganese ions of each independent complex in the unit cell are bridged by two oxygen atoms and the equatorial plane is defined as containing the two O atoms, the Mn ion, and the nitrogen atoms of the pyridine ring and tertiary amine. Therefore, the quinoline groups are positioned in the axial sites. There are two geometric isomeric possibilities for six-coordinate species containing asymmetric tripodal ligands. These are the 5- and 6-isomer which refer to the size of the chelate ring in the same plane as the other donor atoms in the equatorial plane (Figure 97).[23] In this instance, the 6-isomer is present with the six-membered ring formed by the coordination of the pyridylethyl moiety to the metal centre in the defined equatorial plane. Comparing the N-Mn-N angles, it is observed that those formed by the five-membered (quinolylmethyl) rings have angles of 74.60° and 76.53°, while the six-membered (pyridylethyl) has an angle of 93.10°; indicating that the 6-isomer may be favoured on steric grounds as the acute angle is usually in the equatorial plane in other isomers.[415]

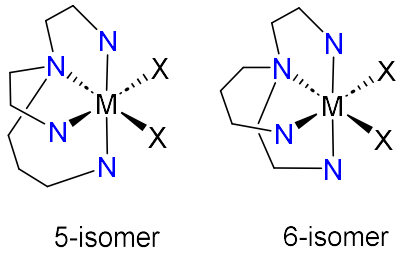


*Figure 97. The geometric 5- and 6-isomers for six-coordinate species that contain asymmetric tripodal ligands.*

The HRMS spectrum of the dinuclear manganese complex revealed a base peak at *m/z* = 475.1323. This peak is consistent with the complex formula, $[(Mn(\mathbf{55}))_2O_2]^{2+}$ (calcd. for $Mn_2C_{54}H_{48}N_8O_2^{2+}$ $[M]^{2+}$ *m/z* = 475.13300, found *m/z* = 475.1323

A manganese dimer that contains the analogous pyridine ligand **9** (Figure 98),[415] has been structurally characterised. In contrast to the III/III oxidation states observed for the manganese centres in $[(Mn(\mathbf{55}))_2O_2](ClO_4)_2.2CH_3CN$, this species exhibits Mn(III)-Mn(IV) oxidation states. Despite the different oxidation states, a similar distorted octahedral geometry is observed with each manganese cation bound to the nitrogen donors of the ligand and two bridging oxygen atoms. The two independent cations in the unit cell have *trans* X-Mn-X angles that range from 157.94° to 177.75°, and *cis* angles between 78.45° and 101.93°. The bond lengths are significantly shorter than the quinoline-containing complex above, with Mn-N and Mn-O distances of 2.080–2.119 Å and 1.806-1.822 Å, respectively. This is to be expected as the additional pyridine moieties have reduced steric hindrance compared to quinoline which allows the pyridine group to sit closer to the metal centre, and thus shorter $Mn\text{-}N_{pyridine}$ bond lengths are observed. The Mn-Mn separation is 2.69 Å which is the same distance between the Mn centres in $[(Mn(\mathbf{55}))_2O_2](ClO_4)_2.2CH_3CN$. Again, this is unusual because in contrast to $[(Mn(\mathbf{55}))_2O_2](ClO_4)_2.2CH_3CN$, the analogous pyridine dimer does not have both manganese cations in the 3+ oxidation state but rather MnIII/IV. Like the quinoline-containing complex, the pyridine congener exhibits the six-membered ring in the equatorial position.

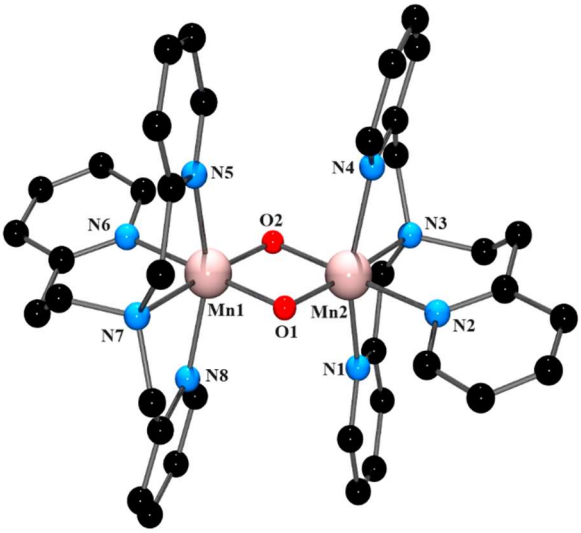


*Figure 98. Structure of the $[(Mn(\mathbf{9})_2O_2]^{3+}$ cation. H atoms have been omitted for clarity.*

Out of the 188 bis(μ-oxo) dinuclear manganese complexes that have been structurally characterised, the majority exist as $Mn_2$(III,IV) dimers.[405,416–421] On the other hand, examples of $(\mu\text{-}O)_2Mn_2$(III,III) are still rare and unusual with only 18 examples reported in the CSD.[123,163,164,203,422–431] A significant number of these $(\mu\text{-}O)_2Mn_2$(III,III) structures are quinoline-containing complexes.

One example of a bis(μ-oxo)di$Mn^{III,III}$ complex is $[Mn_2(\mathbf{30})_2(\mu\text{-}O)_2](ClO_4)_2$, containing the tetraamine tripodal quinolyl ligand **30** (*Figure 99*). The complex has been synthesised and structurally characterised as part of an investigation into the development of manganese catalase models and was found to be an approximate structural mimic of the oxidised form. A more in-depth discussion on the importance of such compounds can be found in *Chapter One*.

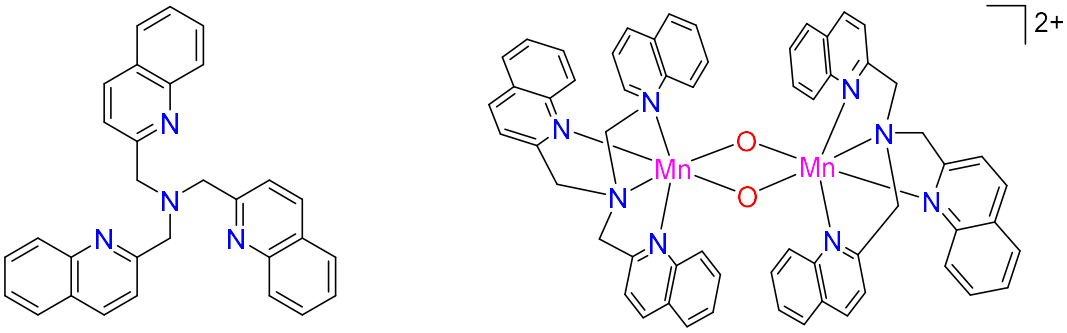


*Figure 99. Structure of the ligand **30** (right); The structure of the [Mn$_2$(**30**)$_2$(μ-O)$_2$](ClO$_4$)$_2$ complex (left).*

The Mn(III)$_2$ cation, [Mn$_2$(**30**)$_2$(μ-O)$_2$]$^{2+}$ (*Figure 100*), comprises two Mn(III) units bridged by a (μ-O)$_2$ core. The Mn-N$_{quinoline}$ bonds that lie along the Jahn-Teller axis (2.145 Å – 2.383 Å) are significantly longer than the Mn-N$_{quinoline}$ (2.145 Å) and Mn-N$_{tertiary}$ (2.114 Å) bond distances. The O-Mn-O bond lengths are 1.824 Å and 1.829 Å, similar to those reported for [(Mn(**55**))$_2$O$_2$]$^{2+}$ and [(Mn(**9**)$_2$O$_2$]$^{2+}$ described above. The distance between the two Mn(III) cations is 2.67 Å. The *cis* N-Mn-N angles lie between 74.15° and 84.40°, N-Mn-O from 89.88° to 106.7°, and the O-Mn-O angle is 85.75°. *Trans* angles are 147.36° for N-Mn-N, and 172.26° and 175.60° for the N-Mn-O angles. The manganese dimer displays intramolecular π-π interactions between quinoline groups (centroid-centroid distance of 3.681 Å).[163] Overall, this manganese dimer exhibits very similar geometry to that observed in [(Mn(**55**))$_2$O$_2$](ClO$_4$)$_2$.2CH$_3$CN.

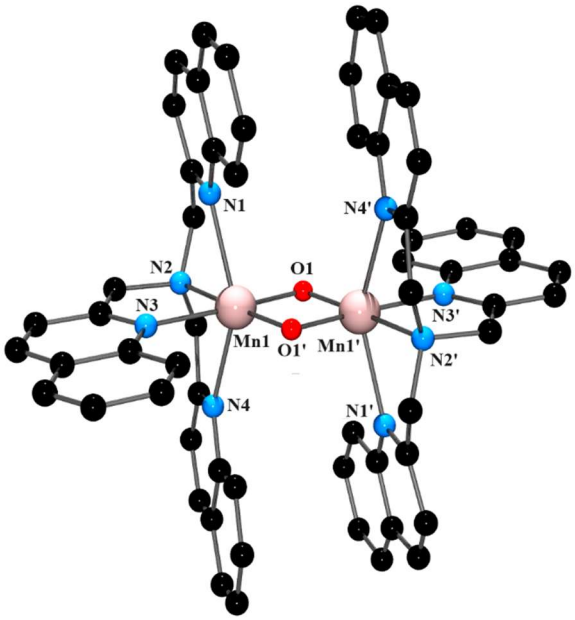


*Figure 100. Structure of the $[Mn_2(\mathbf{30})_2(\mu\text{-}O)_2]^{2+}$cation. H atoms have been omitted for clarity.*

### 4.3.5 $[(62)Co(OH)_3Co(62)](ClO_4)_3.CH_3CN$

The dimeric cobalt complex $[(\mathbf{62})Co(OH)_3Co(\mathbf{62})](ClO_4)_3.CH_3CN$ consists of two Co(III) centres that are bridged together via three hydroxido ligands. This complex was prepared from the reaction of $[Co(OH_2)_6].(ClO_4)_2$ and the ligand **64** in a solution of $CH_3CN$. X-ray quality crystals were obtained after the solution was left to stand under ambient conditions for 3 days. As shown in *Figure 101*, the 2-quinolylethyl moiety of the tripodal ligand has detached and the resulting complexed ligand is 2-(pyridin-2-yl)-*N*-[2-(pyridin-2-yl)ethyl]ethan-1-amine **62**. As to be discussed in *Chapter Five*, a significant amount of 2-vinylquinoline **45** was observed in the mass spectra obtained for the ligand-metal solutions of all the 2-quinolylethyl-containing species. Here, we have isolated the result of the 2-quinolylethyl arm detaching from the central nitrogen donor atom. Unfortunately, due to the limited amount of sample obtained, this complex has only been structurally characterised by means of X-ray crystallography.

The structure of the dinuclear complex consists of two *fac*-[Co(**62**)] units connected by three bridging hydroxido ligands. The Co(III) centres are octahedrally coordinated by three nitrogen donor atoms from the ligand and the O atoms from the bridging hydroxido ligands. The Co(III) ions are 2.595 Å apart and the Co-O bond lengths are 1.892 Å, 1.920 Å, and 1.945 Å. The Co-N bond lengths range from 1.945 Å to 1.984 Å. Bond angles

involving the metal ions and the ligand (*cis* N-Co-N) are 93.70°, 95.30°, and 96.00°, while those involving the bridging hydroxido ligands are (*trans* N-Co-O) 164.77°, 168.62°, and 173.04°, and 88.02° – 96.57° (*cis* N-Co-O). The O-Co-O angles are 77.41°, 79.58°, and 80.80°. The hydroxido ligands participate in hydrogen bonding with the perchlorate counterions with $O_{hydroxido}$-$O_{perchlorate}$ distances of approximately 2.8 Å.

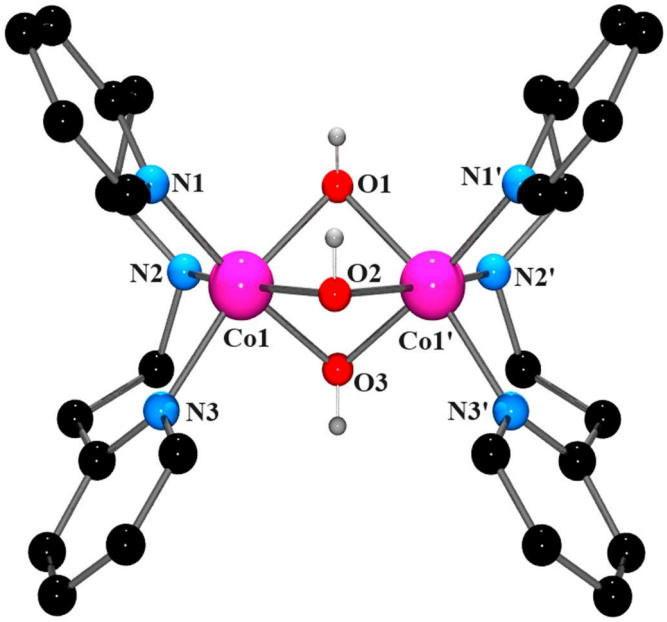


*Figure 101. Structure of the [(**62**)Co(OH)$_3$Co(**62**)]$^{3+}$cation. H atoms have been omitted for clarity. Selected bond lengths (Å) and angles (°): Co1-N1 1.984, Co1-N2 1.954, Co1-N3 1.945, Co1-O1 1.892, Co1-O2 1.945, Co1-O3 1.920; N1-Co1-N2 96.00, N1-Co1-N3 93.70, N2-Co1-N3 95.30, N1-Co1-O1 92.02, N1-Co1-O2 94.72, N1-Co1-O3 105.36, N2-Co1-O1 88.03, N2-Co1-O2 164.77, N2-Co1-O3 87.93, N3-Co1-O1 173.04, N3-Co1-O2 94.77, N3-Co1-O3 96.57, O1-Co1-O2 80.80, O1-Co1-O3 77.41, O2-Co1-O3 79.58.*

**Table 4 Crystal data and structure refinement for [(62)Co(OH)$_3$Co(62)](ClO$_4$)$_3$.CH$_3$CN**

| | |
|---|---|
| Identification code | BC255-Co |
| Empirical formula | $C_{15}H_{19.50}C_{11.50}CoN_{3.50}O_8$ |
| Formula weight | 488.94 |
| Temperature/K | 293(2) |
| Wavelength/Å | 1.54184 |
| Crystal system | Orthorhombic |
| Space group | P n m a |
| a/Å | 19.3732(3) |
| b/Å | 11.4254(2) |
| c/Å | 17.2501(3) |
| α/° | 90 |
| β/° | 90 |
| γ/° | 90 |
| Volume/Å$^3$ | 3818.25(11) |
| Z | 8 |
| Mg/m$^3$ | 1.701 |
| μ/mm$^{-1}$ | 9.462 |
| F(000) | 2004 |
| Crystal size/mm$^3$ | 0.08 x 0.04 x 0.04 |
| Theta range for data collection | 3.431 to 72.402°. |
| Index ranges | -12<=h<=23, -14<=k<=13, -20<=l<=20 |
| Reflections collected | 18769 |
| Independent reflections | 3845 [R(int) = 0.0330] |
| Completeness to theta = 67.684° | 99.9 % |
| Refinement method | Full-matrix least-squares on F2 |
| Data / restraints / parameters | 3845 / 0 / 299 |
| Goodness-of-fit on F2 | 1.018 |
| Final R indices [I>2sigma(I)] | R1 = 0.0387, wR2 = 0.1079 |
| R indices (all data) | R1 = 0.0433, wR2 = 0.1110 |
| Extinction coefficient | n/a |
| Largest diff. peak and hole | 1.026 and -1.072 e.Å-3 |

The di-cobalt(III)tris(μ-hydroxido) unit has been known since it was first identified by Werner in 1907 in the complex cation $[(NH_3)_3Co(OH)_3Co(NH_3)_3]$.[432] The bromide and iodide salts of this were structurally characterised in 1967.[433] Since this time, there have been only two entries containing this unit reported in the CSD, namely $[(dpt)Co(OH)_3Co(dpt)](ClO_4)_3$ (dpt = di(3-aminopropyl)amine)[434] and $Na[(tacn)Co(OH)_3Co(tacn)]Cl_2.(ClO_4)_2.2H_2O$ (tacn = 1,4,7-triazacyclononane).[435]

The $[(dpt)Co(OH)_3Co(dpt)]^{3+}$ and $[(tacn)Co(OH)_3Co(tacn)]^{3+}$ cations exhibit a Co-Co distance of 2.579 Å and 2.549 Å, respectively, consistent with the distance observed in $[(\mathbf{62})Co(OH)_3Co(\mathbf{62})]^{3+}$ (2.595 Å). All three cations display Co-O bond lengths of ~ 1.9 Å. A slight difference in the O-Co-O bond angles of $[(\mathbf{62})Co(OH)_3Co(\mathbf{62})]^{3+}$ (~80°) is observed compared to the O-Co-O angles of ~83° in $[(dpt)Co(OH)_3Co(dpt)]^{3+}$ and ~84° for the O-Co-O angles in $[(tacn)Co(OH)_3Co(tacn)]^{3+}$. The hydroxido ligands in both cations participate in hydrogen bonding with the chloride and perchlorate counterions with distances of approximately 2.8 Å, similar to those observed above.

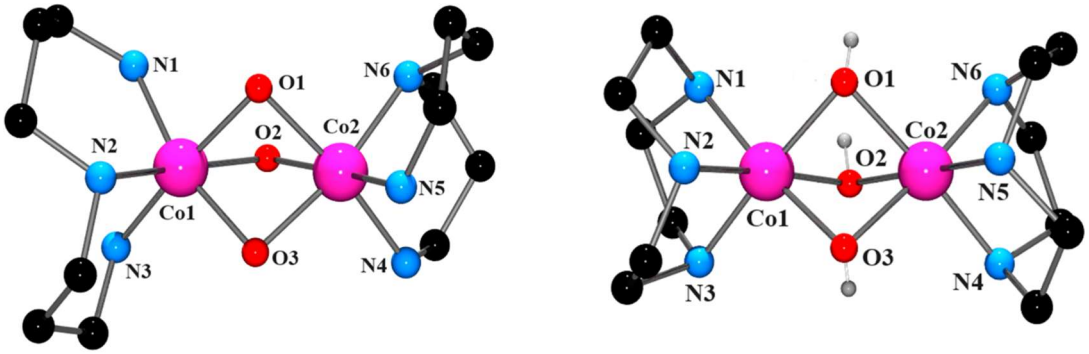


*Figure 102. Structure of the $[(dpt)Co(OH)_3Co(dpt)]^{3+}$ (right) and $[(tacn)Co(OH)_3Co(tacn)]^{3+}$ (left) cations. H atoms have been omitted for clarity. H atoms of the hydroxido ligands are not included in the reported structure of the cation $[(dpt)Co(OH)_3Co(dpt)]^{3+}$.*

## 4.4 Conclusion

This chapter has presented the synthesis and characterisation of the new complexes, $[Pd(\mathbf{58})Cl]Cl.xH_2O$, $[Cu(\mathbf{55})NCCH_3](ClO_4)_2$, $[Zn(\mathbf{55})NCCH_3](ClO_4)_2$, $[(Mn(\mathbf{55}))_2O_2](ClO_4)_2.2CH_3CN$, and $[(\mathbf{62})Co(OH)_3Co(\mathbf{62})](ClO_4)_3.CH_3CN$. The X-ray structures for each sample have been reported. $[Pd(\mathbf{58})Cl]Cl.xH_2O$ is a rare example of a metal complex that contains a 2-quinolylethyl-based ligand. Confirmation of the identity

of this complex has been obtained by means of X-ray crystallography, NMR spectroscopy and HRMS. The pentacoordinate complex cations, $[Cu(\mathbf{55})NCCH_3]^{2+}$ and $[Zn(\mathbf{55})NCCH_3]^{2+}$ are isomorphous structures. Both species have been characterised by X-ray crystallography and HRMS. In addition, $[Zn(\mathbf{55})NCCH_3]^{2+}$ has been analysed by NMR spectroscopy. The manganese cation, $[(Mn(\mathbf{55}))_2O_2]^{2+}$, is a rare example of a bis(μ-oxo) Mn(III)-Mn(III) dimer. The characterisation of this species was achieved by X-ray crystallography and HRMS. Another unusual complex isolated in this work was the dinuclear Co(III) species, $[(\mathbf{62})Co(OH)_3Co(\mathbf{62})](ClO_4)_3.CH_3CN$. This complex consists of two Co(III) ions that are connected via three bridging hydroxido ligands, a structural feature that is rare in the literature.

# *Chapter Five*
# The Characterisation of Transition Metal Complexes Containing Quinoline-Based Ligands

## 5.1 Chapter overview

This chapter describes the characterisation of transition metal complexes of the ligands described in *Chapter Two* (see sections 2.1 and 2.4). Various attempts were made to produce single-crystal samples suitable for structural analysis via single-crystal X-ray diffraction. Unfortunately, no X-ray quality crystals were obtained from the many crystallisation attempts in this work. Therefore, it was necessary to resort to alternative solution-state characterisation methods for these complexes. Foremost amongst these was mass spectrometry, which has been used in previous work[436] where similar issues were encountered. Secondly, the use of UV-visible spectroscopy was employed to obtain a series of Job plots, a method developed for the determination of mole ratios.

## 5.2 Introduction

### 5.2.1 Mass spectrometry

Electrospray ionisation mass spectrometry (ESI-MS) has been shown to be a valuable characterisation tool for the detection and identification of metal complexes.[437–439] This technique separates ions individually so that an ion containing one or more polyisotopic elements will give rise to several isotopomeric signals. Depending on both the mass and the relative abundance of the isotopes, these signals have a characteristic pattern of relative intensities and spacing. This signal grouping is known as the isotope pattern.[440] The stoichiometry of the species can potentially be determined directly from the *m/z* value, while the isotope pattern and additional MS-MS analysis can provide further confirmation.[441]

As an example of this type of characterisation, Caudle *et al.* utilised mass spectrometry to conclusively determine the binding ratio of two iron hydroxamic acid complexes. Solutions of the dihydroxamic acid ligands, $N^1$,$N^{10}$-dihydroxy-$N^1$,$N^{10}$-dimethyldecanediamide **142** and $N^1$,$N^4$-dihydroxy-$N^1$,$N^4$-dimethylbutanediamide **143** (*Figure 103*), were mixed with equimolar amounts of $FeCl_3.6H_2O$, using $CH_3CN$ as the solvent.

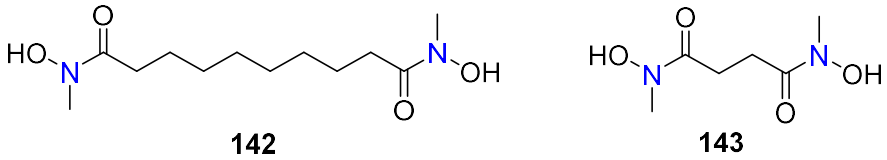


*Figure 103. Structure of the ligands **142** and **143**.*

Analysis of the Fe(III) complex containing **142**, revealed a mass spectrum that showed signals at *m/z* = 214, 314, 355, and 663. In conjunction with the expansion of the peak at *m/z* = 314, and matching the iron isotope pattern, allowed for the identification of the singly charged 1:1 $[Fe(\mathbf{142})]^+$ complex (*Figure 104*). A signal that appeared 41 mass units higher at *m/z* = 335, was concluded to be from the addition of a $CH_3CN$ ligand, $[Fe(\mathbf{142})(NCCH_3)]^+$. The chloride-containing binuclear, $[Fe_2(\mathbf{142})_2Cl]^+$, was assigned to the peak observed at *m/z* = 633, and the isotopic distribution was used for the recognition of the iron and chloride ions present.

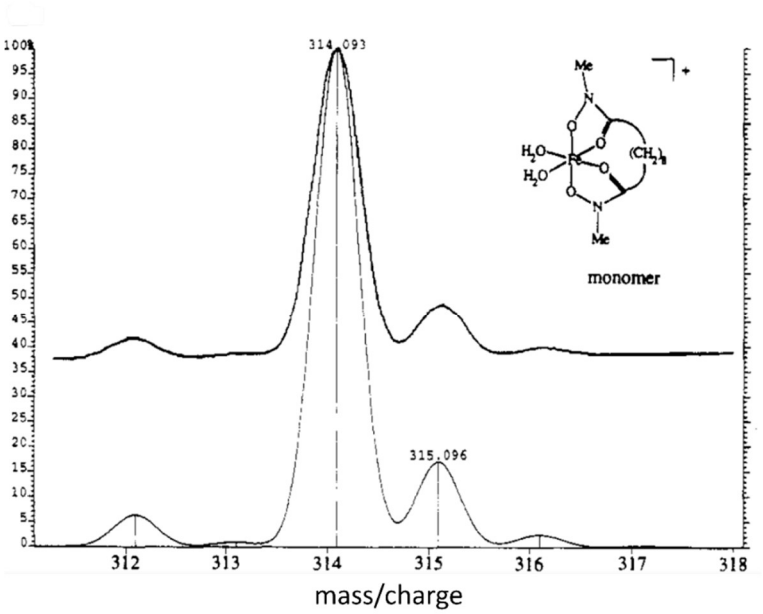


*Figure 104. The mass spectrum of a solution of **142** and $FeCl_3.6H_2O$ in $CH_3CN$ (top= experimental, bottom= calculated on the basis of isotope ratios).*[442]

The mass spectrum of the iron complex containing **143**, revealed similar features to that observed in the spectrum discussed above. A signal was observed at *m/z* = 230, consistent with a species that has a 1:1 metal-to-ligand ratio. However, according to the authors the isotope pattern of the peak could not be justified based on a singly charged entity. An isotopic distribution similar to that observed for the complex containing **142** would be expected if the corresponding species was $[Fe(\mathbf{143})]^+$. As displayed in *Figure 105*, the observed isotope pattern is consistent with an iron complex of $[Fe_2(\mathbf{143})_2]^{2+}$ with *m/z* = 230 and *z* = 2. This observation gave the authors evidence that when the alkyl chain length was *n* = 2, the short distance between the hydroxamate groups precluded the formation of the monomer due to the added ring strain and that, the 2:2 dimer was the species present in solution. The chloride-containing binuclear, $[Fe_2(\mathbf{143})_2Cl]^+$, was also observed for this ligand with a peak at *m/z* = 495 that was assigned to this complex.[442]

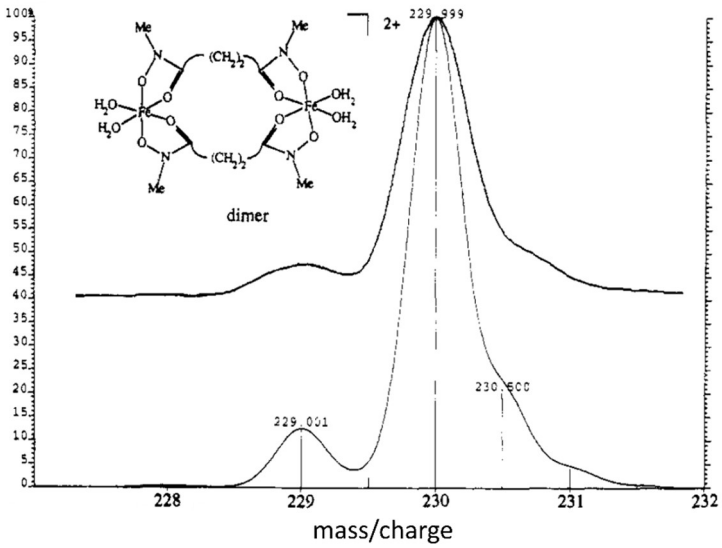


*Figure 105. The mass spectrum of a solution of **143** and $FeCl_3.6H_2O$ in $CH_3CN$ (top= experimental, bottom= calculated on the basis of the isotope ratios).*[442]

Allen *et al.* studied several complexes containing the pyridyl-based ligand **8** using ESI-MS for the characterisation of these metal species in addition to the X-ray crystallography data obtained. The selected complexes [Zn(**8**)Cl]$ClO_4$, [Zn(**8**)I]$ClO_4$ and [Cu(**8**)Br]$ClO_4$ (*Figure 106*) were prepared in MeOH and the corresponding solutions were analysed. The mass spectrum of the Zn(II) species [Zn(**8**)Cl]$ClO_4$ revealed a signal at *m/z* = 389 that was assigned to the complex ion $[Zn(\mathbf{8})Cl]^+$. The expected peak for the compound [Zn(**8**)I]$ClO_4$, to the authors surprise, was not observed in the mass spectrum and only impurity peaks were revealed. The authors speculated that this was due to the halide displacement by solvent molecules in solution. In addition, the complex [Cu(**8**)Br]$ClO_4$ was analysed and the mass spectrum revealed a signal at *m/z* = 389 that was assigned to the species $[Cu(X)Br]^+$ according to the authors. The results of this study were complementary with the solid-state X-ray data obtained.[5]

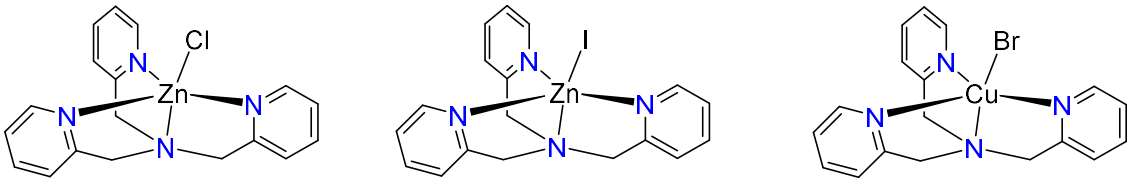


*Figure 106. The structures of the metal species [Zn(**8**)Cl]$ClO_4$, [Zn(**8**)I]$ClO_4$ and [Cu(**8**)Br]$ClO_4$.*

Hall reported the synthesis of three hexadentate ligands, *N,N'*-bis(2,2'-bipyridin-6-ylmethyl)butane-1,4-diamine **144**, *N,N'*-bis(2,2'-bipyridin-6-ylmethyl)pentane-1,5-diamine **145** and *N,N'*-bis(2,2'-bipyridin-6-ylmethyl)octane-1,8-diamine **146** (*Figure 107*) and the characterisation of the corresponding Co(III), Fe(II), Mn(II) and Ni(II) coordination complexes. The ligands can be prepared in a similar manner from the condensation of 2,2'-bipyridine-5-carbaldehyde with butane-1,4-diamine, pentane-1,5-diamine or octane-1,8-diamine, respectively, followed by the subsequent reduction.

The reaction of the ligand **144** with the first-row transition metal ions Co(III), Fe(II), Ni(II) and Mn(II) afforded X-ray quality crystals and structural characterisation confirmed the isolation of mononuclear complexes. However, crystalline material was not obtained from the reaction of the ligands **145** and **146** with the same metal ions. Thus, the identification of the complex and the metal-to-ligand ratio was determined using mass spectrometry.

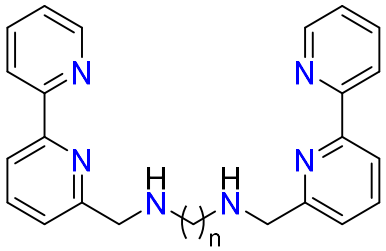


n = 4: **144**
n = 5: **145**
n = 8: **146**

*Figure 107. The general structure of the hexadentate ligands **144**, **145**, and **146**.*

The Ni(II) complex containing **145** was prepared by mixing equimolar solutions of the ligand and $[Ni(OH_2)_6](ClO_4)_2$ in $CH_3CN$. The product oiled out on standing overnight

and following the dissolution of the oil in $CH_3CN$ the solution was analysed by ESI-MS. The experimental mass spectrometry data obtained displayed a base peak at *m/z* = 596.1348 which corresponds to the complex formula, $[Ni(\mathbf{145})(ClO_4)]^+$. However, fitting the experimental data against the calculated spectra for the possible mononuclear, dinuclear and trinuclear complexes, revealed that the measured spectrum does not correspond exactly to any one of these but rather shows a presence from all three species. Comparisons between the experimental and calculated data show that the predominant species is the dinuclear complex, $[Ni_2(\mathbf{145})_2(ClO_4)_2]^{2+}$, followed by the mono- and trinuclear (*Figure 108*).

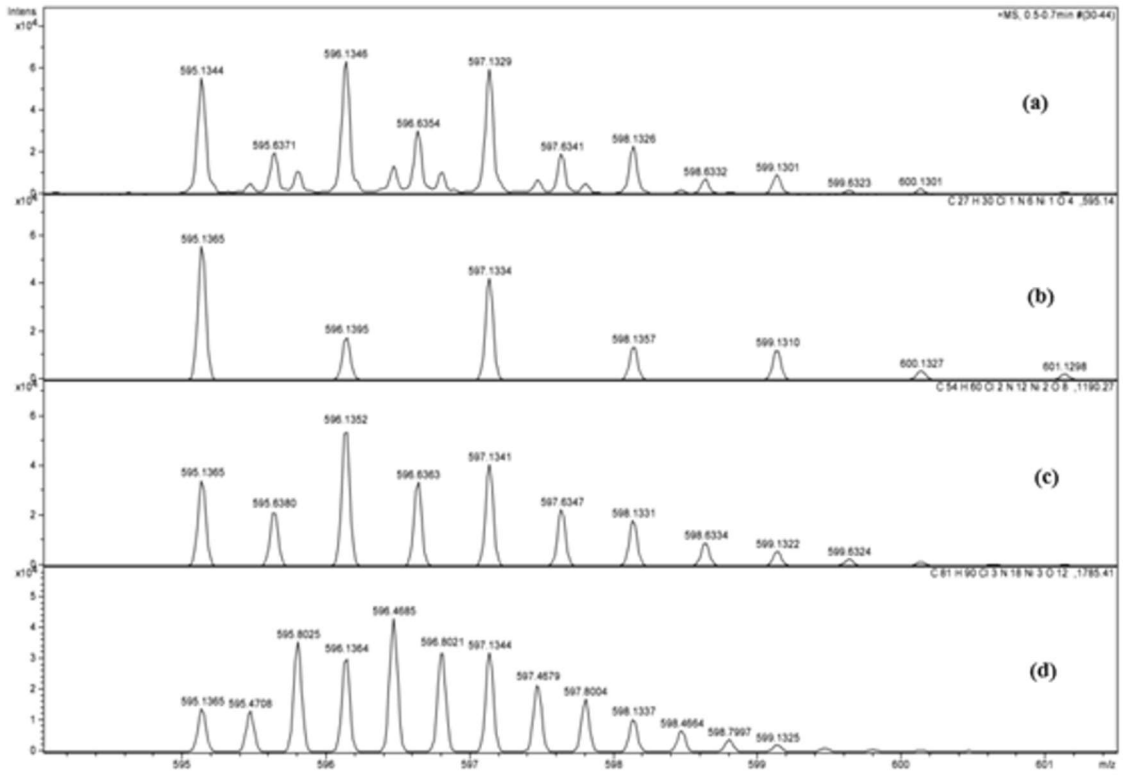


*Figure 108. The experimental mass spectrum of the Ni(II) complex containing* ***145 (a);*** *calculated spectrum of* $[Ni(\mathbf{145})(ClO_4)]^+$ *(b); calculated spectrum of* $[(Ni_2(\mathbf{145})_2(ClO_4)_2]^{2+}$ *(c); calculated spectrum of* $[(Ni_3(\mathbf{145})_3(ClO_4)_3]^{3+}$ *(d).*[443]

A solution of a Ni(II) metal complex containing the ligand **146** was prepared *in situ* by reacting 1 equivalent of the ligand with the metal perchlorate salt in $CH_3CN$ which was followed by ESI-MS analysis of the resulting solution. The obtained data displayed similar results to those seen for the ligand **145** discussed above. Again, comparisons

between the experimental and the calculated data pointed towards the presence of the mono-, di- and trinuclear species, with the dinuclear complex predominating.[443]

### 5.2.2 Job Plots

A Job plot, also known as the method of continuous variation or Job's method, is an analytical technique that can be used to determine the stoichiometry of a reaction between a transition metal ion and a ligand. Named after Paul Job who first reported the method in 1928,[444] this method has become widely used in many areas of chemistry, especially for determining the composition of complexes in solution.[445–447]

Job's method is based on the binding potential of one species (A) to another species (B) when those two species are present in a solution and is used to determine the ratio in which A and B bind.

To obtain a Job plot, aliquots of two equimolar stock solutions of metal and ligand are mixed in varying volumes such that the sum of the molar concentrations of the resulting solutions remain constant, while the metal-ligand ratio varies in each solution. UV/vis absorbance measurements of the prepared solutions are obtained and plotted against the mole fractions of the two species. The stoichiometry of the reaction is determined from the maximum of the curve, which corresponds to the maximal formation of the complex. The peak of the plot correlates to the mole fraction of the ligands bound to a metal ion. For example, *Figure 109* displays a simple Job plot that shows the absorbance maximum at a mole fraction of 0.5 indicating a metal-ligand ratio of 1:1.[448]

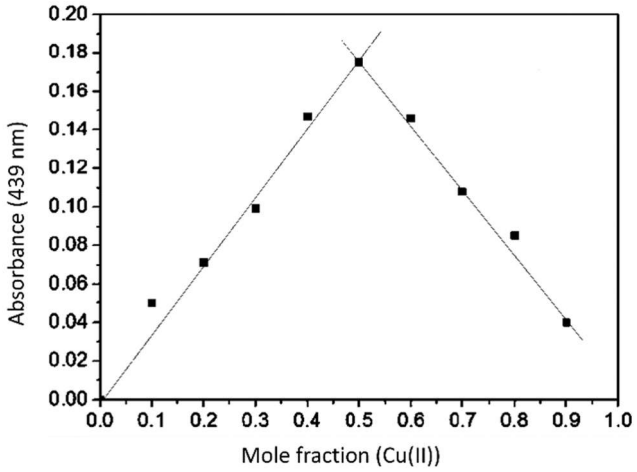


*Figure 109. A simple Job plot obtained from the addition of a pseudopeptide ligand and* $[Cu(OAc)_4(H_2O)_2]$.[448]

There are two main conditions that must be met to obtain a successful Job plot. Firstly, the system must conform to Beer's law, and secondly, there can only be one predominant complex species in solution under the experimental conditions. For instance, in the example above, the 1:1 complex predominates and there are not significant amounts of other species having different stoichiometries present.[449]

The stability of the complex formed is related to the curvature of the plotted lines. Complexes having higher formation constants afford straighter lateral segments of the curve allowing for easier determination of the position of the maximum. Two straight lines can easily be fitted, one with a positive slope due to the increase in the proportion of the complex, and the other with a negative slope due to its decreasing concentration as the stoichiometric point is exceeded. Complexes having relatively small formation constants result in more rounded plotted curves, and this can lead to more unreliable results. In this case, straight lines are plotted using the data points that are most distant from the maximum and the point at which these intersect determines the stoichiometry.[446,450,451]

A fluorescent-enhanced chemosensor has been reported for the detection of the metal ions Al(III) and Fe(III). Based on the simple naphthyridine and benzothiazole groups, the authors have synthesised the ligand *N*-(2-(2-benzothiazol-2-yl)vinyl-4-methyl-1,8-naphthyrine-7-yl)acetamide **147** (*Figure 110*). Yao *et al*. determined the binding stoichiometry of the chemosensor with the metal ions Al(III) and Fe(III). The

experimental data for the Al(III) metal ion was collected following Job's method with the absorbance of the complex solutions recorded at 377 nm. The graph obtained displayed the absorbance maximum at a mole fraction of 0.5, thus the ratio between the Al(III) metal ion and the ligand was determined to be 1:1 (*Figure 110*). The Job plot obtained for the Fe(III) samples revealed the same 1:1 binding stoichiometry between the ligand and metal ion. Further confirmation of the binding stoichiometry of both the Al(III) and Fe(III) complexes was obtained using mass spectrometry that showed a 1:1 metal-ligand ratio. In combination with the Job plots, $^{1}$H NMR spectra, ESI-MS data and DFT calculations, the binding stoichiometry was further confirmed.[452]

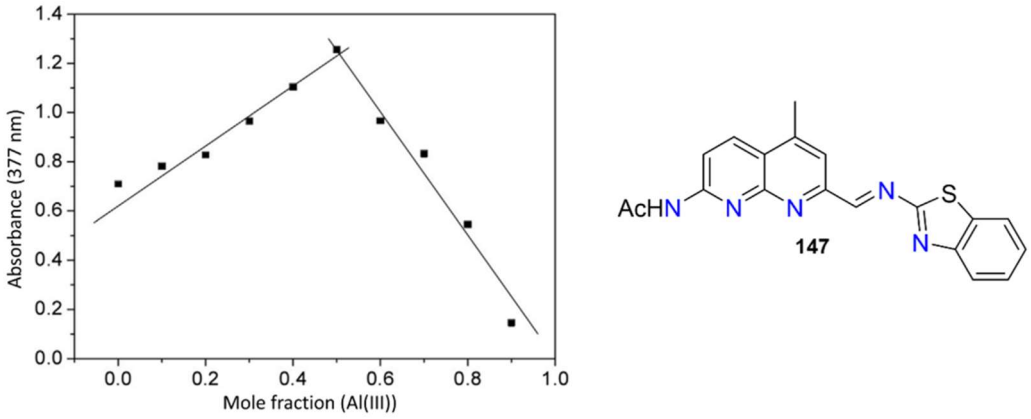


*Figure 110. Structure of the ligand **147** and corresponding Job Plot with Al(III) ions.*[452]

The recognition of Cu(II) metal ions in solution using macrocycles has utilised Job's method to study the complexation behaviours of a new cyclic derivative towards the selected metal ion. The tri-linked macrocyclic ligand **148** displayed in *Figure 111*, has been reacted with copper(II) nitrate and using Job's method the stoichiometry of the resulting complex has been determined. The experimental data affords a Job plot that shows the absorption maximum at a mole fraction of ~0.66, thus revealing the formation of a 2:1 (M:L) species in solution (*Figure 111*).[453]

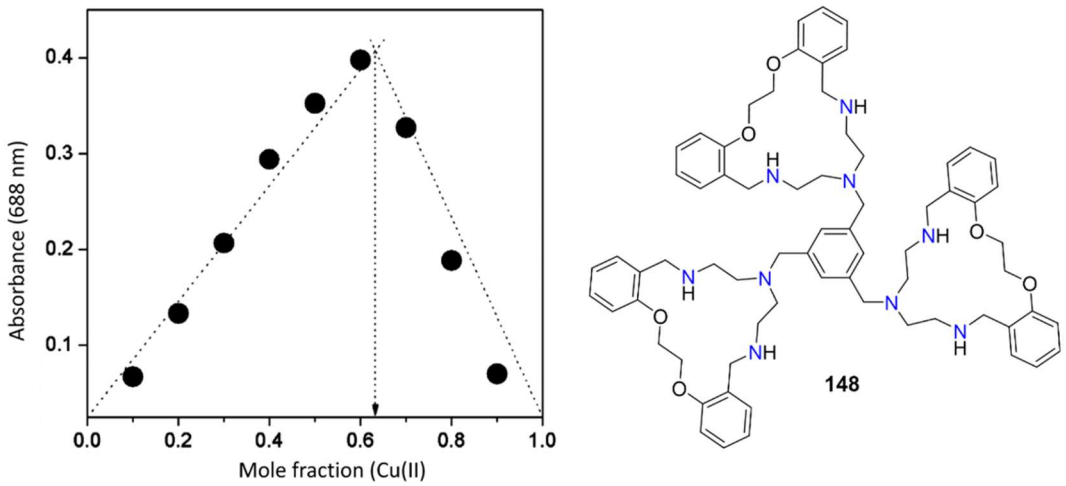


*Figure 111. Structure of the tri-linked macrocycle ligand **148** and corresponding Job plot with Cu(II) ions.*[453]

You *et al.*[454] reported the synthesis and subsequent investigation of the colourimetric sensor, (*E*)-9-(((5-mercapto-1,3,4-thiadiazol-2-yl)imino)methyl)-2,3,6,7-tetrahydro-1*H*,5*H*-pyrido[3,2,1-ij]quinolin-8-ol **149** (*Figure 112*) for the sequential detection of Cu(II) and $CN^-$ ions. A Job plot was obtained from the reaction of the sensor **149** and Cu(II), finding a 1:2 metal ion to ligand stoichiometric ratio. As can be seen in *Figure 112*, the two straight lines intersect at the absorbance maximum at the mole fraction of ~0.33, indicative of the 1:2 (M:L) ratio.

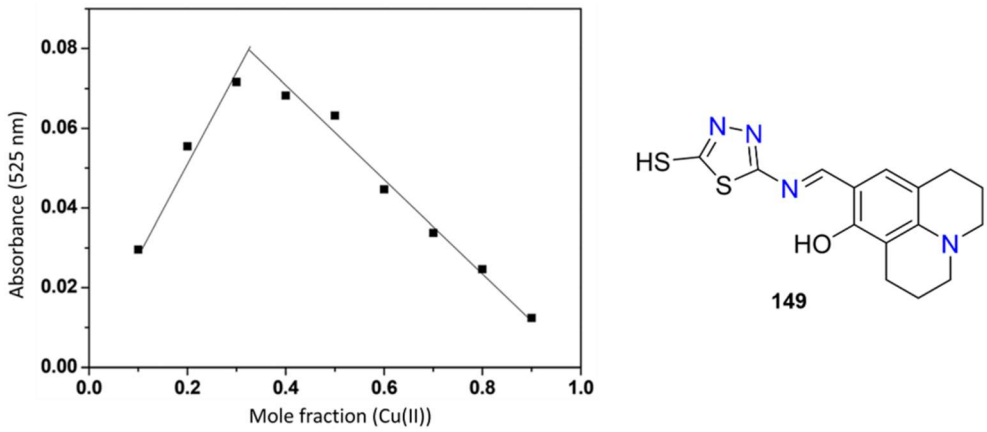


*Figure 112. Structure of the colorimetric sensor **149** and the corresponding Job plot with Cu(II) ions.*[453]

The Cu(II)-ligand solution was further reacted with the gradual addition of a solution containing $CN^-$ ions and the absorbance measurements were taken again. The Job plot

obtained demonstrated the 1:1 binding stoichiometry between the Cu(II) complex and $CN^-$ (*Figure 113*). Further analysis of this sample by negative ion mass spectrometry revealed the release of the sensor ligand and the formation of a more stable $Cu(CN)_x$ complex. The authors were able to propose the demetallation mechanism of the Cu(II) complex by $CN^-$ using both Job plot data and the mass spectrum obtained.[454]

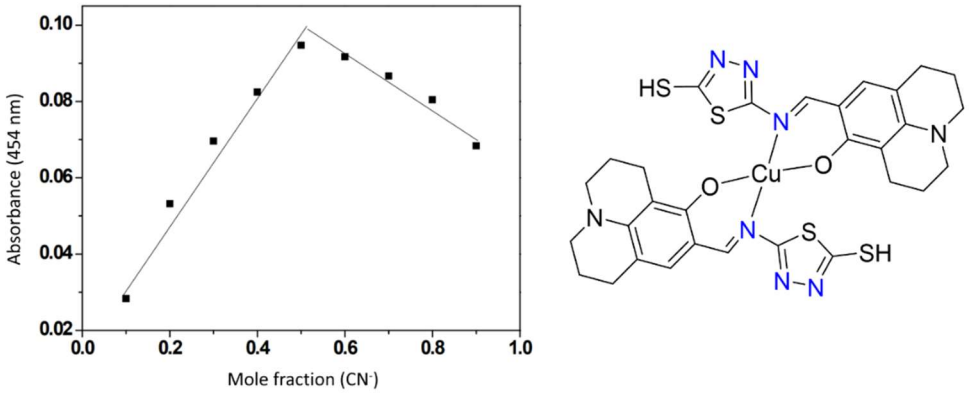


*Figure 113. Structure of the Cu(II) complex containing **149** and corresponding Job plot obtained from the addition of $CN^-$ ions.*[454]

## 5.3 Solution Studies

In the absence of X-ray crystallography data, the binding stoichiometries were determined by means of mass spectrometry and Job's method using UV-vis spectrometry. The following discussion investigates the results obtained from both analytical techniques and determines the binding stoichiometry of each ligand with several metal ions.

The solutions were made up according to the methods described in *Chapter Two*. All the experiments were conducted in $CH_3CN$. The mass spectrometry data were collected as described in section 2.3.1. Low-resolution mass spectrometry was obtained for this series of experiments. Job's method and production of the corresponding plots were carried out according to section 2.3.2. Each experiment was repeated a minimum of two times with freshly made solutions, and reproducible results were obtained.

The mass spectra were obtained from solutions that had been made up by mixing a solution of the metal ion with 1, 2 and 3 equivalents of ligand. The complex solutions were mixed and allowed to stand at room temperature for 30 minutes before each sample was directly injected into the mass spectrometer for analysis.

The observed spectrum was compared with the calculated spectrum which was obtained from Molecular Mass Calculator.[455]

The peaks that correspond to a metal ion-containing species were assigned, in part, using the specific isotope pattern of each metal ion. For example, there are two stable isotopes of copper, $^{65}Cu$ and $^{63}Cu$, with the average abundance of each being 69.17% and 30.83%, respectively.[456] As a result, the mass spectrum of a copper-containing species displays an isotope pattern of two peaks with an approximate ratio of 2:1 (*Figure 114*).[457] Zinc has five stable isotopes, $^{64}Zn$ (48.63%), $^{66}Zn$ (27.90%), $^{67}Zn$ (4.10%), $^{68}Zn$ (18.75%), and $^{70}Zn$ (0.62%).[458] The presence of this metal ion shows an isotope pattern that contains approximately five signals (*Figure 114*).[459] Nickel also has five stable isotopes, $^{58}Ni$, $^{60}Ni$, $^{61}Ni$, $^{62}Ni$, and $^{64}Ni$. The average abundances of each isotope are 67.7%, 26.2%, 1.25%, 3.66%, and 1.16% which corresponds to an isotope pattern of five signals (*Figure 114*).[460]

The isotope pattern was also used in the identification of the presence of chloride ions which are seen commonly in the following complex species as either $Cl^-$ or $ClO_4^-$ ions associated with the metal ions. Chlorine has two naturally occurring stable isotopes, $^{35}Cl$ (75.77 %) and $^{37}Cl$ (24.32 %), that have an approximate abundance ratio of 3:1.[461] The presence of chlorine in almost all the following metal complexes is confirmed by the appearance of appropriately spaced peaks in a ratio of 3:1. In some instances, the data were consistent with the presence of free chloride as determined by the isotope pattern and *m/z* values. Given there was no free chloride present in the solutions, this may be attributed to a contamination within the mass spectrometer.

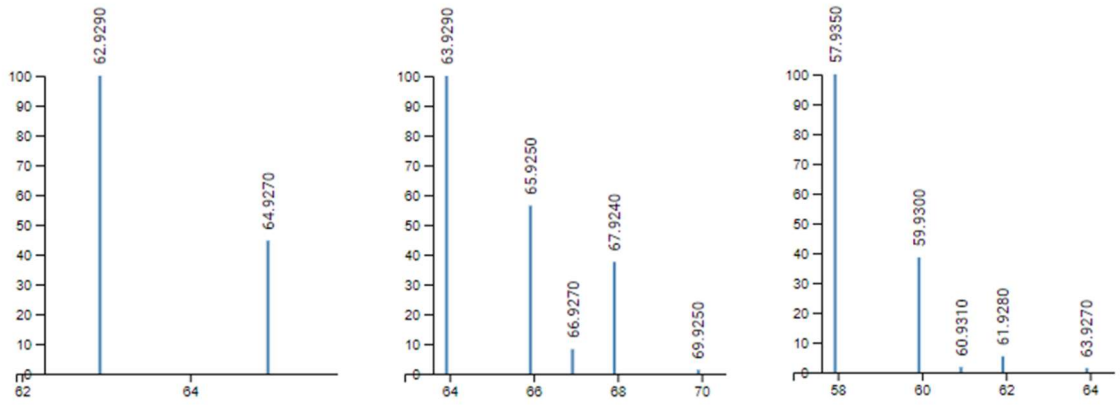


*Figure 114. Isotope patterns for the metal ions Cu (left), Zn (centre), and Ni (right).*

Determination of the ion charge from the mass spectrum was obtained using the spacing between the isotope peaks within the isotope pattern for the ion. For example, if the isotope peaks are spaced by a m/z unit of 1, the ion species is determined to have a 1+ charge.[462] For each species discussed in the following experiments, the charge of the ion was determined by the spacing between the peaks which in all cases, unless otherwise stated, were found to be $m/z = 1$, implying that $z = 1$. Reduction of the metal centre or association of a negatively charged ion affords the 1+ charge on the following species in most instances.

For the Job plots, graphs of the absorbance against the mole fraction of the metal ions Cu(II), Co(II) and Ni(II) were plotted and the intercept of the two slopes was used to determine the stoichiometry of the complexes formed in solution. The metal ions Fe(II) and Mn(II) were not investigated owing to the precipitation within the iron solutions, or very low absorbance in the case of manganese.

## 5.4 Results and Discussion

In all the mass spectra of the different quinoline-containing ligands and metal ions, a peak at $m/z = 156.0$ corresponding to 2-vinylquinoline **45**, a ligand fragment, was observed. This peak is either the most intense or the second most intense with the exception of the spectra that include Cu(II) metal ions. It appears that 2-vinylquinoline is generated by the decomposition of the ligand within the mass spectrometer during the experiment.

The reaction between the tetradentate 2-quinolylethyl-based ligands **57**, **58**, **63** and **64** and the metal ions Cu(II), Co(II), Ni(II), Zn(II) and Mn(II) has been compared to the analogous reaction with the respective pyridine congeners.

### 5.4.1 Ligand 57

**Mass spectrometry**

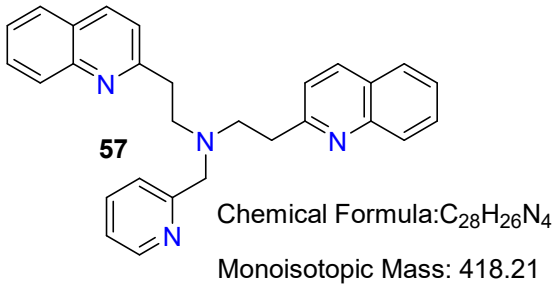


A solution of the free ligand **57** reveals a mass spectrum that displays a peak corresponding to **57** observed at an *m/z* = 419.2 (calcd. for $C_{29}H_{27}N_4^+$ $[M+H]^+$ *m/z* = 419.22, found *m/z* = 419.2) and a ligand fragment **65** (*Figure 115*) at *m/z* = 264.1 (calcd. for $C_{17}H_{18}N_3^+$ $[M+H]^+$ *m/z* = 264.15, found *m/z* = 264.1). It can be seen from this spectrum that the ligand fragments to afford a significant amount of 2-vinylquinoline **45**, observed at *m/z* = 156.0, under the conditions of this mass spectrometer.

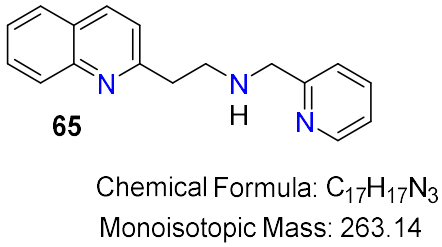


*Figure 115. Structure of the ligand fragment **65**.*

The addition of the $[Cu(OH_2)_6](ClO_4)_2$ solution to the solution of **57** (*Figure 116*) affords a mass spectrum that displays five peaks due to copper-containing species at *m/z* = 326.0, 388.0, 481.1, 526.1, and 580. In addition, signals are observed at *m/z* = 156.0, 264.1, and 419.2 which can be ascribed to 2-vinylquinoline **45**, the ligand fragment **65** and the free ligand **57**, respectively.

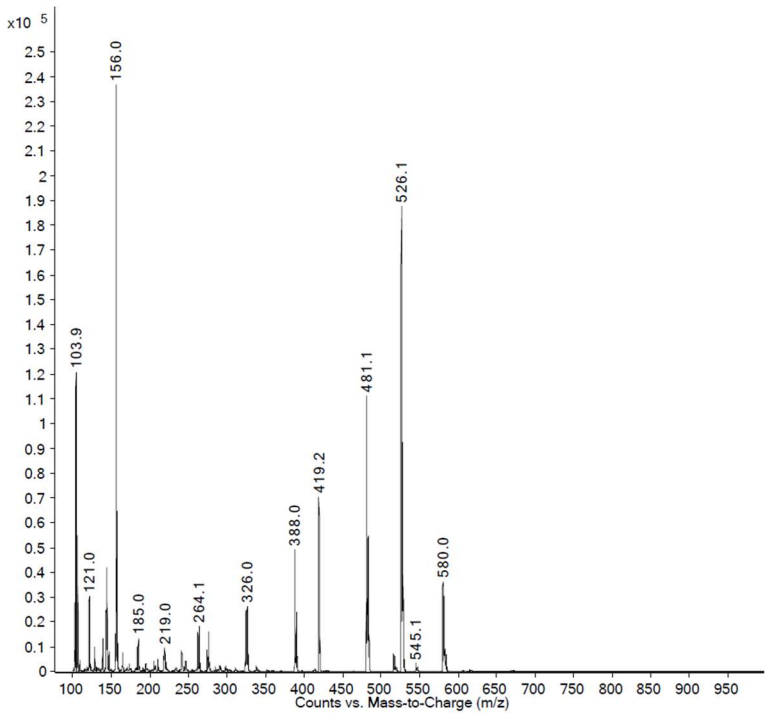


*Figure 116. The mass spectrum of an equimolar solution of **57** and $[Cu(OH_2)_6](ClO_4)_2$.*

The most intense copper-containing peak is observed at *m/z* = 526.1 which displays the expected copper ion isotope pattern and the peak spacing confirms it to be a 1+ ion. Using this reasoning, the peaks at *m/z* = 481.1, 388.0, 580.0 and 326.0 can also be assigned as resulting from 1+ ions that contain copper. On addition of a further equivalent of **57**, the copper-containing peaks decrease in intensity and the free ligand signal increases in intensity. This trend continues upon the addition of a third equivalent of ligand.

The peak at *m/z* = 526.1 is consistent with the complex formula $[Cu(\mathbf{57})(HCOO)]^+$ (calcd. for $CuC_{29}H_{27}N_4O_2^+$ $[M]^+$ *m/z* = 526.14, found *m/z* = 526.2). In this case, it appears that the Cu(II)-**57** complex has bound a negatively charged formate ion, which is used in the calibration of the mass spectrometer. The anions formate, perchlorate and chloride are frequently observed in the experimental data to follow.

The peak observed at *m/z* = 481.1 can be assigned to the mononuclear 1:1 complex, $[Cu(\mathbf{57})]^+$ (calcd. for $CuC_{28}H_{26}N_4^+$ $[M]^+$ *m/z* = 481.14, found *m/z* = 481.1). In this instance, *z* = 1, and this indicates that reduction has occurred within the mass spectrometer during the analysis of the sample to give a Cu(I) complex.

The peak observed at *m/z* = 580.0 corresponds to $[Cu(\mathbf{57})(ClO_4)]^+$ in which the 1:1 complex includes an associated perchlorate ion (calcd. for $CuC_{28}H_{26}N_4ClO_4^+$ $[M]^+$ *m/z* =

580.09, found *m/z* = 580.0). The isotope pattern is consistent with an ion containing both copper and chlorine. The 1+ charge on the ion confirms that the metal ion has not undergone reduction.

The peak at *m/z* = 326.0 is consistent with a Cu(I) complex of the neutral ligand fragment **65**, formula $[Cu(C_{17}H_{17}N_3)]^+$. The appearance of the peak at *m/z* = 326.0 is difficult to explain, this would require loss of two protons from the ligand and an oxidation state of copper of at least 2+. When the experimental data was fitted to the calculated, the isotopic ratio pattern also did not match (*Figure 117*). The assignment of this peak is not obvious at the current time.

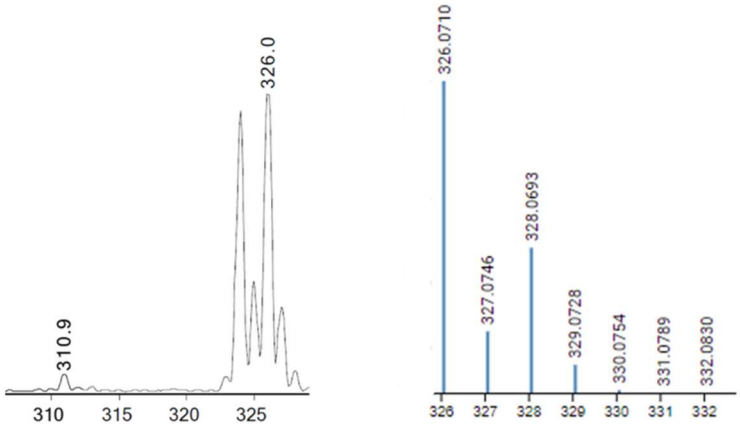


*Figure 117. Experimental peaks for $[Cu(C_{17}H_{17}N_3)]^+$(left); Calculated peaks for $[Cu(C_{17}H_{17}N_3)]^+$.*

The peak at *m/z* = 388.0 could not be assigned; however, as determined by the isotope pattern the species has a 1+ charge and contains a copper ion. The closest calculated fit was the complex species [Cu(**65**)$(NCCH_3)$(Na)]$^+$ (calcd. for $CuC_{19}H_{20}N_4Na$ *m/z* = 390.08, found *m/z* = 388.0).

The mass spectra of solutions of $[Co(OH_2)_6](ClO_4)_2$ to which 1, 2, and 3 equivalents of ligand **57** have been added show peaks at *m/z* = 156.0, 419.1 and 508.2. The latter can be assigned to the Co(II) complex ion [Co(**57**)$H_3CO]^+$ (calcd for $CoC_{29}H_{29}N_4O^+$ $[M]^+$ *m/z* = 508.16 found *m/z* = 508.2). There is a slight increase in the intensity of the complex ion peak after the addition of the second and third equivalents of the ligand **57**.

The mass spectra of solutions of $[Ni(OH_2)_6](ClO_4)_2$, $[Zn(OH_2)_6](ClO_4)_2$, and $[Mn(OH_2)_6](ClO_4)_2$ containing 1, 2, and 3 equivalents of ligand **57** display intense peaks

at *m/z* = 156.1, 419.2 and 264.1, with the only nickel-, zinc- and manganese-containing species observed being very low intensity peaks corresponding to $[M(\mathbf{57})ClO_4]^+$ in all cases. This suggests that **57** has a very low binding affinity for these metals under the conditions in the mass spectrometer.

Given the somewhat surprising results obtained for the ligand **57**, it was of interest to investigate the behaviour of the analogous pyridine ligand. This is the ligand **10**, which has three pyridine nitrogen donors, two aminoethyl and one aminomethyl alkyl chain attached to the central nitrogen atom (*Figure 118*).

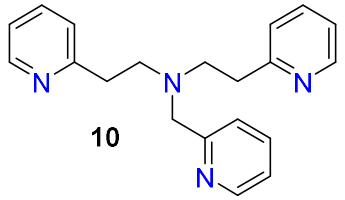


Chemical Formula: $C_{20}H_{22}N_4$

Monoisotopic Mass: 318.18

*Figure 118. Structure of the pyridyl-based ligand **10**.*

The analogous pyridine ligand, **10**, affords a molecular ion peak at *m/z* = 319.1 (calcd. for $C_{20}H_{23}N_4^+$ $[M+H]^+$ *m/z* = 319.19, found *m/z* = 319.1). The mass spectrum of an equimolar solution of $[Cu(OH_2)_6](ClO_4)_2$ and **10** shows complete reaction of the ligand and a complex ion peak at *m/z* = 426.1 corresponding to the formula $[Cu(\mathbf{10})(HCOO)]^+$ (calcd. for $CuC_{21}H_{23}N_4O_2^+$ $[M]^+$ *m/z* = 426.11, found *m/z* = 426.1). There is an additional small peak at *m/*z = 480.0 consistent with the complex ion $[Cu(\mathbf{10})(ClO_4)]^+$ (calcd. for $CuC_{20}H_{22}N_4ClO_4^+$ $[M]^+$ *m/z* = 480.06, found *m/z* = 480.0). The analogous peaks are also observed in the $[Ni(OH_2)_6](ClO_4)_2$ spectrum, with the major peak at *m/*z = 421.1 ($[Ni(\mathbf{10})(HCOO)]^+$) and the minor at *m/*z = 475.1 ($[Ni(\mathbf{10})(ClO_4)]^+$) (calcd. for $NiC_{21}H_{23}N_4O_2^+$ $[M]^+$ *m/z* = 421.11, found *m/z* = 421.1; calcd. for $NiC_{20}H_{23}N_4ClO_4^+$ $[M]^+$ *m/z* = 475.06, found *m/z* = 475.1).

An equimolar solution of $[Zn(OH_2)_6](ClO_4)_2$ and **10** gives a mass spectrum showing two zinc-containing peaks *m/z* = 427.1 and 481.0, and a peak corresponding to the free ligand **10**. The peak at *m/z* = 427.0 can be assigned to the complex ion $[Zn(\mathbf{10})(HCOO)]^+$ (calcd. for $ZnC_{21}H_{23}N_4O_2^+$ $[M]^+$ *m/z* = 427.11, found *m/z* = 427.0) and that at *m/z* = 481.0 to the $[Zn(\mathbf{10})(ClO_4)]^+$ ion (calcd. for $ZnC_{20}H_{22}N_4ClO_4^+$ $[M]^+$ *m/z* = 481.06, found *m/z* = 481.0).

The intensities of the peaks corresponding to the free ligand and the $[Zn(\mathbf{10})(HCOO)]^+$ ion increase upon the addition of the second and third equivalents of the ligand.

In contrast, the mass spectrum obtained from an equimolar solution of $[Mn(OH_2)_6](ClO_4)_2$ and **10** exhibits an intense ligand peak and a low-intensity complex ion peak at *m/z* = 472.0, assigned to $[Mn(\mathbf{10})(ClO_4)]^+$ (calcd. for $MnC_{20}H_{22}N_4ClO_4^+$ $[M]^+$ *m/z* = 472.07, found *m/z* = 472.0).

In this instance, the quinolyl-based ligand **57** and its pyridine congener display relatively similar complexation behaviour in the presence of the metal ions Cu(II), Co(II), Ni(II), Zn(II) and Mn(II). The comparable pyridine ligand **10** shows a complete reaction of the ligand and $[Cu(OH_2)_6](ClO_4)_6$ with no free ligand peak displayed, whereas the quinoline ligand **57** does not behave in this way. Both the ligands exhibit peaks that correspond to the complex formulae $[Cu(L)(ClO_4)]^+$ and $[Cu(L)(HCOO)]^+$ (L = **10** or **57**). Furthermore, the reaction of the quinolyl ligand with Cu(II) afforded an additional complex ion signal which corresponds to the mononuclear 1:1 species $[Cu(57)]^+$. Interestingly, the reaction between the pyridine congener and Cu(II) does not afford the same 1:1 complex ion signal. The reaction of **57** with the metal ions Ni(II) and Zn(II) afforded signals of very low intensity; whereas, the reaction of the pyridine congener with these metal ions afforded clear complex ion signals. Both the quinoline and pyridine ligands show one manganese complex ion of very low relative abundance and in both instances, this has been assigned to the formula $[Mn(L)(ClO_4)]^+$.

**Job Plots**

*Figure 119* shows the Job plots obtained for solutions of the ligand **57** with the metal ions Cu(II), Co(II) and Ni(II). The three plots show the maximum absorbance at a mole fraction of 0.5, indicating that the predominant complex in solution is $[M(\mathbf{57})]^{n+}$ in each case.

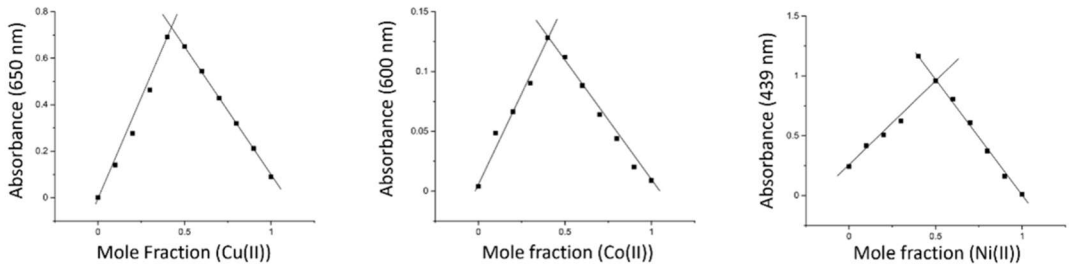


*Figure 119. The Job plots for the reaction between the ligand **57** and the metal ions Cu(II), Co(II), and Ni(II).*

While the Job plots for the Co(II) and Ni(II) complexes show that coordination of the ligand to the metal ion occurs, no evidence of their formation was observed in the mass spectrum, presumably due to the harsh conditions of the experiment, suggesting that the stability of the $[Cu(\mathbf{57})]^+$ complex is significantly greater than the Co(II) and Ni(II) congeners.

### 5.4.2 Ligand 58

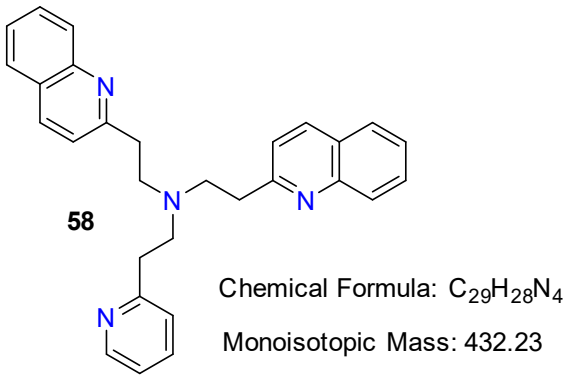


**Mass Spectrometry**

The mass spectrum of the free ligand **58** displays a peak corresponding to the free ligand at *m/z* = 433.1, while the fragment **66** gives rise to a peak at *m/z* = 278.0, as described in *Chapter Three* section 3.6.1. There is also a significant peak corresponding to the ligand fragment 2-vinylquinoline **45** (*m/z* = 156.0).

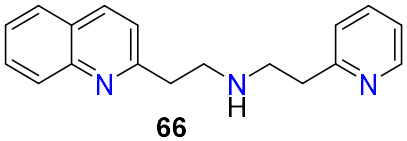


**66**

Chemical Formula: $C_{18}H_{19}N_3$

Monoisotopic Mass: 277.15

*Figure 120. Structure of the ligand fragment **66**.*

The mass spectrum obtained from the addition of 1 equivalent of the ligand to $[Cu(OH_2)_6](ClO_4)_2$ in solution exhibits an intense peak at *m/z* = 495.1 (*Figure 121*). This peak shows an isotope pattern that indicates the presence of copper and the spacing of the peaks reveals the ion to be of a 1+ charge. This can be assigned to the Cu(I) complex, $[Cu(\mathbf{58})]^+$ (calcd. for $CuC_{29}H_{28}N_4^+$ $[M]^+$ *m/z* = 495.16, found *m/z* = 495.1), where reduction of the Cu(II) ion has occurred during analysis. There are three low intensity peaks at m/z = 433.1, 278.0 and 156.0, which correspond to the free ligand **58**, a ligand fragment **66** and 2-vinylquinoline **45**, respectively. On addition of a second equivalent of the ligand, the ratio of free ligand to bound increases and there are no new peaks formed. This trend continues upon the addition of the third equivalent of **58**.

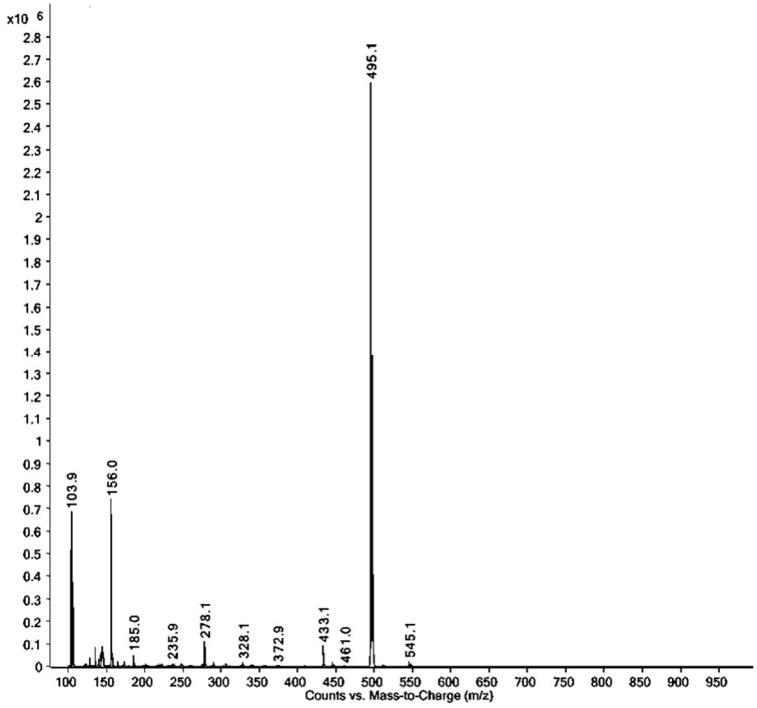


*Figure 121. The mass spectrum of an equimolar solution of the ligand **58** and $[Cu(OH_2)_6](ClO_4)_2$.*

The mass spectra obtained for solutions of Co(II), Ni(II), Mn(II) and Zn(II) containing the ligand **58** display no peaks corresponding to coordination complexes. In all cases, the 2-vinylquinoline **45** signal has a greater intensity compared to that seen in the copper experiment, and this peak increases in intensity on addition of a second and third equivalents of the ligand. For example, after the addition of Ni(II) ions to the ligand **58**, the 2-vinylquinoline fragment (*m/z* = 156.0) appears ~2.5 times greater in intensity compared to the free ligand (*m/z* = 433.1) (*Figure 122*). This is consistent across the other metal ions Co(II), Mn(II) and Zn(II). In comparison, the mass spectrum of solely the free ligand exhibits the 2-vinylquinoline **45** ion peak ~1.4 times greater in intensity compared to the free ligand peak. The absence of any complex ions in the mass spectra for these metals and the increase in the amount of 2-vinylquinoline **45** present, suggest that the addition of the metal has a catalytic effect on the decomposition of the ligand. However, despite the observed increase in 2-vinylquinoline **45**, there is no change or addition of other product ion peaks from this reaction. Lowering the cone voltage of the spectrometer could potentially minimise the fragmentation of the free ligand.[463]

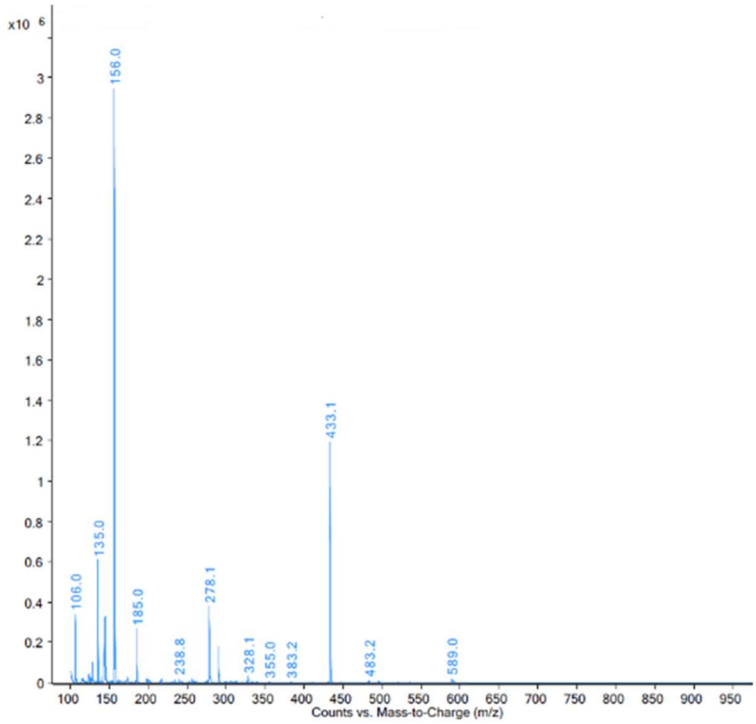


*Figure 122. The mass spectrum of a solution of the ligand **58** and $[Ni(OH_2)_6](ClO_4)_2$.*

The above experiments were repeated using the pyridine ligand congener **11** (*Figure 123*). The free ligand **11** gives rise to a molecular ion peak at *m/z* = 333.2 (calcd. for $C_{21}H_{25}N_4^+$ $[M+H]^+$ *m/z* = 333.20, found *m/z* = 333.2).

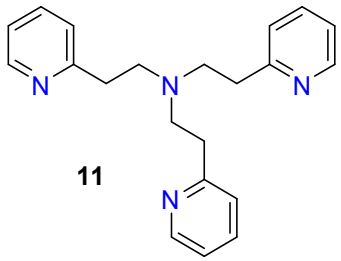


**11**

Chemical Formula: $C_{21}H_{24}N_4$
Monoisotopic Mass: 332.20

*Figure 123. Structure of the pyridyl-based ligand **11**.*

The addition of 1 equivalent of **11** to a solution of $[Cu(OH_2)_6](ClO_4)_2$ gives, in addition to the free ligand peak, three copper-containing peaks at *m/z* = 395.1, 440.1 and 494.0. The peak at *m/z* = 395.1 can be assigned to the complex ion $[Cu(\mathbf{11})]^+$, and as observed for the analogous quinoline ligand, reduction of Cu(II) to Cu(I) occurs during the experiment (calcd. for $CuC_{21}H_{24}N_4^+$ $[M]^+$ *m/z* = 395.12, found *m/z* = 395.1). The peaks at *m/z* = 440.1 and 494.0 are consistent with the formulae $[Cu(\mathbf{11})(HCOO)]^+$ and

$[Cu(\mathbf{11})(ClO_4)]^+$ (calcd. for $CuC_{22}H_{25}N_4O_2^+$ $[M]^+$ *m/z* = 440.12, found *m/z* = 440.1; $CuC_{21}H_{24}N_4ClO_4^+$ $[M]^+$ *m/z* = 494.07, found *m/z* = 494.0). Upon addition of the second and third equivalents of **11**, the free ligand peak at *m/z* = 333.2 increases in intensity.

A solution of equimolar amounts of $[Co(OH_2)_6](ClO_4)_2$ and **11** affords a mass spectrum that displays peaks that can be assigned to one cobalt-containing species and the free ligand **11**. The former at *m/z* = 490.0 can be assigned to the complex $[Co(\mathbf{11})(ClO_4)]^+$(calcd. for $CoC_{21}H_{24}N_4^+$ $[M]^+$ *m/z* = 490.08, found *m/z* = 490.0). A similar situation is observed for $[Zn(OH_2)_6](ClO_4)_2$, where a free ligand **11** peak and a peak corresponding to $[Zn(\mathbf{11})(ClO_4)]^+$ at *m/z* = 495.0 are observed. For both Co(II) and Zn(II), the intensity of the free ligand peak is much greater than that of the observed metal complex. While similar behaviour is observed for $[Mn(OH_2)_6](ClO_4)_2$, the $[Mn(\mathbf{11})(ClO_4)]^+$ complex ion is present in only trace amounts. Under the same conditions, $[Ni(OH_2)_6](ClO_4)_2$ gives a complex ion peak at *m/z* = 435.1, corresponding to the 1:1 ligand to metal complex, $[Ni(\mathbf{11})(HCOO)]^+$ (calcd. for $NiC_{22}H_{25}N_4O_2^+$ $[M]^+$ *m/z* = 435.13, found *m/z* = 435.1).

Akin to the quinoline ligand, after the addition of the pyridyl congener to a solution of $[Cu(OH_2)_6](ClO_4)_2$, the mass spectrum exhibits the 1:1 mononuclear species, $[Cu(L)]^+$ as the base peak (L = **11**). An additional complex ion peak, $[Cu(\mathbf{11})(ClO_4)]^+$, is observed in the pyridine spectrum, whereas this species is not formed during the quinoline ligand **58** reaction with Cu(II) ions. In contrast to the quinoline data which displays no peaks corresponding to any complex species for the ions Co(II), Zn(II), and Ni(II), the pyridine experiment reveals signals for all three metals. A complex ion is observed in the mass spectrum of the pyridine ligand and manganese, albeit in trace amounts.

**Job Plots**

The Job plots obtained from the reaction for ligand **58** with the metal ions Cu(II), Co(II) and Ni(II) in $CH_3CN$ are shown in *Figure 124*. All three exhibit an absorbance maximum at a mole fraction of 0.5, indicating that these metal ions have a binding stoichiometry of 1:1 with **58** in solution.

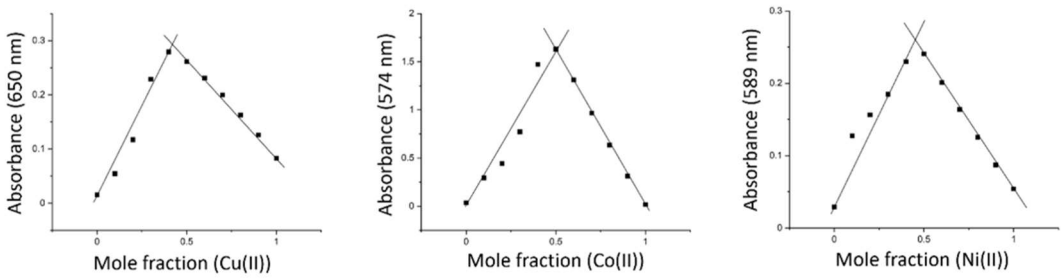


*Figure 124. The Job plots for the reaction between the ligand **58** and the metal ions Cu(II), Co(II), and Ni(II).*

### 5.4.3 Ligand 63

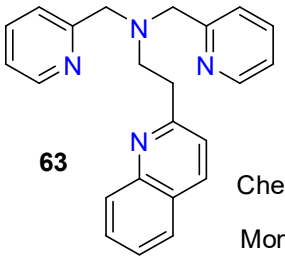

**63**

Chemical Formula: $C_{23}H_{22}N_4$

Monoisotopic Mass: 354.18

**Mass Spectrometry**

As discussed in *Chapter Three* section 3.6.1, the peak corresponding to the free ligand **63** is observed at *m/z* = 355.1, while the fragment **60** (*Figure 125*) gives rise to a peak at *m/z* = 200.1. There is also a significant peak corresponding to 2-vinylquinoline (*m/z* = 156.0).

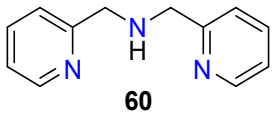

**60**

Chemical Formula: $C_{12}H_{13}N_3$

Monoisotopic Mass: 199.11

*Figure 125. Structure of the ligand fragment **60**.*

The addition of 1 equivalent of the ligand **63** to a solution of $[Cu(OH_2)_6](ClO_4)_2$ affords a spectrum that displays four copper-containing signals at *m/z* = 417.0, 452.0, 516.0, and 462.0. The signal at *m/z* = 417.0 can be assigned to the 1:1 mononuclear complex, $[Cu(\mathbf{63})]^+$ (calcd. for $CuC_{23}H_{22}N_4^+$ $[M]^+$ *m/z* = 417.11, found *m/z* = 417.0). The Cu(II) species $[Cu(\mathbf{63})Cl]^+$, $[Cu(\mathbf{63})(HCOO)]^+$, and $[Cu(\mathbf{63})(ClO_4)]^+$ can be assigned to the signals observed at *m/z* = 452.0, 462.0, and 516.0, respectively (calcd. for $CuC_{23}H_{22}N_4Cl^+$

$[M]^+$ *m/z* = 452.08, found *m/z* = 452.0; calcd. for $CuC_{24}H_{23}N_4O_2^+$ $[M]^+$ *m/z* = 462.11, found *m/z* = 462.0; calcd. for $CuC_{23}H_{22}N_4ClO_4^+$ $[M]^+$ *m/z* = 516.06, found *m/z* = 516.0). Upon the addition of a second and third equivalents of the ligand solution, a signal at *m/z* = 355.1 corresponding to the free ligand **63** was observed in addition to the four copper-containing signals.

The mass spectrum obtained from the reaction of **63** with $[Co(OH_2)_6](ClO_4)_2$ reveals three cobalt-containing signals at *m/z* = 206.5, 448.0, and 512.0, with the latter two corresponding to the complex ions $[Co(\mathbf{63})Cl]^+$ and $[Co(\mathbf{63})(ClO_4)]^+$ (calcd. for $CoC_{23}H_{22}N_4Cl^+$ $[M]^+$ *m/z* = 448.08, found *m/z* = 448.0; calcd. for $CoC_{23}H_{22}N_4ClO_4^+$ $[M]^+$ *m/z* = 512.06, found *m/z* = 512.0). The signal at *m/z* = 206.5 can be assigned to the mononuclear 1:1 2+ complex ion, $[Co(\mathbf{63})]^{2+}$ (calcd. for $CoC_{23}H_{22}N_4^{2+}$ $[M]^{2+}$ *m/z* = 206.55, found *m/z* = 206.5). A signal observed at *m/z* = 283.1, despite numerous attempts could not be assigned, with the closest fit being the Co(II) complex of the ligand fragment **60** (calcd. for $CoC_{12}H_{13}N_3Na^+$ $[M+Na]^+$ *m/z* = 281.03, found *m/z* = 283.1). A signal corresponding to the free ligand becomes present after the addition of the second equivalent and the intensity increases after the third equivalent is added.

An equimolar solution of $[Zn(OH_2)_6](ClO_4)_2$ and ligand **63** affords a mass spectrum that shows a peak due to free ligand at *m/z* = 355.1, the ligand fragment peaks at *m/z* = 200.1 (**60**) and 156.0 (**45**), and three zinc-containing signals at *m/z* = 517.0, 453.0, and 209.0. The complex, $[Zn(\mathbf{63})ClO_4]^+$, can be assigned to the peak at *m/z* = 517.0 (calcd. for $ZnC_{23}H_{22}N_4ClO_4^+$ $[M]^+$ *m/z* = 517.06, found *m/z* = 517.0). The peak at *m/z* = 453.0 can be assigned to the complex formulae $[Zn(\mathbf{63})Cl]^+$ (calcd. for $ZnC_{23}H_{22}N_4Cl^+$ $[M]^+$ *m/z* = 453.08, found *m/z* = 453.0). The signal displayed at *m/z* = 209.0 corresponds to the 2+ mononuclear 1:1 species, $[Zn(\mathbf{63})]^{2+}$ (calcd. for $ZnC_{23}H_{22}N_4^{2+}$ $[M]^{2+}$ *m/z* = 209.05, found *m/z* = 209.0). There is another signal that can be identified as a 2+ ion from the spacing of the peaks, observed at *m/z* = 285.6; however, no unequivocal assignments could be made. The addition of a second and third equivalents of the ligand reveals an increase in the intensity of the free ligand and corresponding fragments.

A solution of $[Ni(OH_2)_6](ClO_4)_2$ containing 1 equivalent of **63** affords a mass spectrum that displays three complex ion peaks at *m/z* = 206.0, 457.1, and 511.0. The signal at *m/z* = 206.0 can be assigned to the Ni(II) 2+ species $[Ni(\mathbf{63})]^{2+}$ (calcd. for $NiC_{23}H_{22}N_4^{2+}$ $[M]^{2+}$ *m/z* = 206.05, found *m/z* = 206.0). The peaks at *m/z* = 457.0 and 511.0 correspond to the

complex ions $[Ni(\mathbf{63})Cl]^+$ and $[Ni(\mathbf{63})(ClO_4)]^+$ (calcd. for $NiC_{23}H_{22}N_4Cl^+$ $[M]^+$ *m/z* = 457.11, found *m/z* = 457.1; calcd. for $NiC_{23}H_{22}N_4ClO_4^+$ $[M]^+$ *m/z* = 511.06, found *m/z* = 511.0). Similar to that observed for the zinc experiment, there is a signal displayed at *m/z* = 282.6 which from the peak spacing has been assigned as a 2+ ion. There is a mass difference of *m/z* = 76.6 between this peak and the 1:1 2+ species seen at *m/z* = 206.0. This mass difference is also observed in the zinc-containing spectrum, and again, all attempts to assign the peak have not been successful at this point in time. An increase in the intensity of the free ligand and fragment at *m/z* = 156.0 is seen after the addition of a second and third equivalents of the ligand **63**.

The addition of 1, 2, and 3 equivalents of the ligand **63** solution to a solution of $[Mn(OH_2)_6](ClO_4)_2$, reveals no signals that correspond to any manganese-containing species. This appears to be consistent with what has been observed for the other quinoline ligands discussed in this section.

The mass spectrum of the pyridine congener **9** (*Figure 126*) showed a molecular ion peak at *m/z* = 305.1 (calcd. for $C_{19}H_{21}N_4^+$ $[M+H]^+$ *m/z* = 305.17, found *m/z* = 305.1). A fragment peak is observed at *m/z* = 200.1 corresponding to the loss of the ethyl arm (calcd. for $C_{12}H_{14}N_3^+$ $[M+H]^+$ *m/z* = 200.11, found *m/z* = 200.1). Another significant fragment at *m/z* = 228.1 can be assigned to the loss of the aminomethyl pyridine moiety (calcd. for $C_{14}H_{18}N_4^+$ $[M+H]^+$ *m/z* = 228.15, found *m/z* = 228.1).

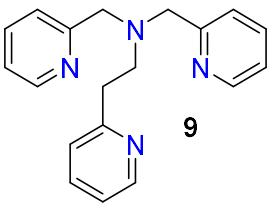


**9**

Chemical Formula: $C_{19}H_{20}N_4$
Monoisotopic Mass: 304.16

*Figure 126. Structure of the pyridyl-based ligand **9**.*

The mass spectrum of a solution of $[Cu(OH_2)_6](ClO_4)_2$ to which 1 equivalent of **9** has been added, exhibited four peaks that on the basis of the isotope patterns appeared to contain copper. The peak spacing is consistent with each of these being 1+ ions. The free ligand peak is observed in trace amounts, with its intensity increasing only slightly upon

the addition of the second and third equivalent of **9**, while the intensity of the peak at *m/z* = 412.1 increases.

The most intense signal is observed at *m/z* = 412.1. This is a 1+ ion and can be assigned to the complex $[Cu(\mathbf{9})(HCOO)]^+$ (calcd. for $CuC_{20}H_{21}N_4O_2^+$ $[M]^+$ *m/z* = 412.09, found *m/z* = 412.1). This is a Cu(II) species, with the formate ion acting as either a ligand or a counterion. Additional copper-containing peaks appear at *m/z* = 466.0, 402.0, 376.0, and 367.0. The peak at *m/z* = 367.0 can be assigned to the complex $[Cu(\mathbf{9})]^+$ (calcd. for $CuC_{19}H_{20}N_4^+$ $[M]^+$ *m/z* = 367.09, found *m/z* = 367.0), while the peaks at *m/z* = 466.0 and 402.0 are consistent with the formulae $[Cu(\mathbf{9})(ClO_4)]^+$ and $[Cu(\mathbf{9})Cl]^+$, respectively (calcd. for $CuC_{19}H_{20}N_4ClO_4^+$ $[M]^+$ *m/z* = 466.04, found *m/z* = 466.0; calcd. for $CuC_{19}H_{20}N_4Cl^+$ $[M]^+$ *m/z* = 402.06, found *m/z* = 402.0). With both Cu and Cl present, the isotope patterns for these peaks differ from those assigned as containing only Cu.

A solution of $[Co(OH_2)_6](ClO_4)_2$ containing 1 equivalent of **9** affords a mass spectrum that displays three complex ion peaks at *m/z* = 181.5, 408.1 and 462.0. The base peak at *m/z* = 181.5 can be assigned to the 2+ species, $[Co(\mathbf{9})]^{2+}$ (calcd. for $CoC_{19}H_{20}N_4^{2+}$ $[M]^{2+}$ *m/z* = 181.55, found *m/z* = 181.5). The peaks observed at *m/z* = 408.1 and 462.1 are consistent with the formulae corresponding to the Co(II) complexes $[Co(\mathbf{9})HCOO]^+$ (calcd. for $CoC_{20}H_{21}N_4O_2^+$ $[M]^+$ *m/z* = 408.09, found *m/z* = 408.1) and $[Co(\mathbf{9})ClO_4]^+$ (calcd. for $CoC_{19}H_{20}N_4ClO_4^+$ $[M]^+$ *m/z* = 462.05, found *m/z* = 462.1), respectively. The mass spectra of the following addition of the second and third equivalents of the ligand revealed no change in the peak at *m/z* = 462.1 and an increase in the intensity of the peak at *m/z* = 408.1.

Similar behaviour was observed in the spectra obtained from $[Ni(OH_2)_6](ClO_4)_2$ in the presence of 1, 2 and 3 equivalents of ligand, with three peaks shown at *m/z* = 181.0, 407.1 and 461.0. The peak at *m/z* = 181.0 is consistent with the Ni(II) 2+ species $[Ni(\mathbf{9})]^{2+}$ (calcd. for $NiC_{19}H_{20}N_4^{2+}$ $[M]^{2+}$ *m /z* = 181.05, found *m/z* = 181.0).

The Ni(II) complex ions, $[Ni(\mathbf{9})(HCOO)]^+$ and $[Ni(\mathbf{9})(ClO_4]^+$, correspond to the peaks at *m/z* = 407.1 and 461.0, respectively (calcd. for $NiC_{20}H_{21}N_4O_2^+$ $[M]^+$ *m /z* = 407.10, found *m/z* = 407.1; calcd. for $NiC_{19}H_{20}N_4ClO_4^+$ $[M]^+$ *m/z* = 461.05, found *m/z* = 461.0). The isotope patterns of both signals are consistent with the calculated data. The peaks at *m/z* = 461.0 and 421.1 decrease in intensity upon adding the second equivalent of ligand **9** and are only just visible following the addition of the third equivalent of ligand. A signal

corresponding to the free ligand **9** at *m/z* = 305.1 is also observed after the third equivalent of the ligand is added.

The most intense peak observed in the mass spectrum of a solution of **9** and $[Zn(OH_2)_6](ClO_4)_2$ is at *m/z* = 184.0, and Zn(II)-containing peaks are observed at *m/z* = 403.0, 413.0 and 467.0. These are consistent with the formulae $[Zn(\mathbf{9})Cl]^+$, $[Zn(\mathbf{9})(HCOO)]^+$ and $[Zn(\mathbf{9})(ClO_4)]^+$, respectively. The peak at *m/z* = 184.0 corresponds to the 2+ complex ion. $[Zn(\mathbf{9})]^{2+}$ (calcd. for $ZnC_{19}H_{20}N_4^{2+}$ $[M]^{2+}$ *m/z* = 184.04, found *m/z* = 184.0).

The addition of 1, 2 and 3 equivalents of **9** to a solution of $[Mn(OH_2)_6](ClO_4)_2$ revealed mass spectra that exhibited no complex ion signals and only the signal corresponding to the free ligand was observed.

The mass spectrometry data obtained for the **9** ligand in the presence of the $M^{2+}$ ions showed that all of the ligand present in the solution were either coordinated to the corresponding metal ion, or fragmented, with the exception of manganese. This is in contrasts with the analogous quinoline ligand in which the the free ligand peak was always observed. Both the quinoline and pyridine-containing ligands afforded complex ion signals when reacted with the metal ions Cu(II), Co(II), Ni(II) and Zn(II). In this instance, both the ligands **9** and **63** afforded mononuclear 1:1 2+ species with the metal ions Co(II), Ni(II) and Zn(II). No peaks corresponding to metal complexes of both the ligands with manganese were observed.

**Job Plots**

For the Job plots obtained for the ligand **63**, the graphs for the Cu(II) and Co(II) metal ions show the absorbance maximum at the mole fraction of 0.5 revealing that $[M(\mathbf{63})]^{n+}$ is the predominant complex in solution in each instance. The graph obtained for the metal ion Ni(II) shows the absorbance maximum at the mole fraction of ~ 0.3 suggesting a metal to ligand ratio of 1:2 (*Figure 127*). However, during the experiment no colour change indicative of a nickel complex was observed, which has been noted for the other quinoline ligands.

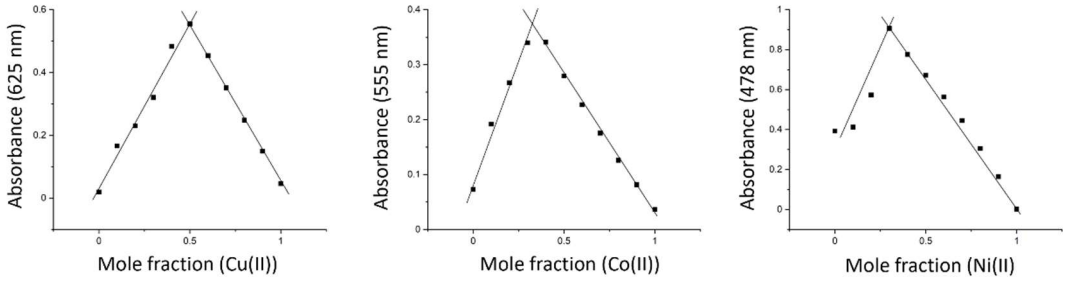


*Figure 127. The Job plots for the reaction between the ligand **63** and the metal ions Cu(II), Co(II) and Ni(II).*

### 5.4.4 Ligand 64

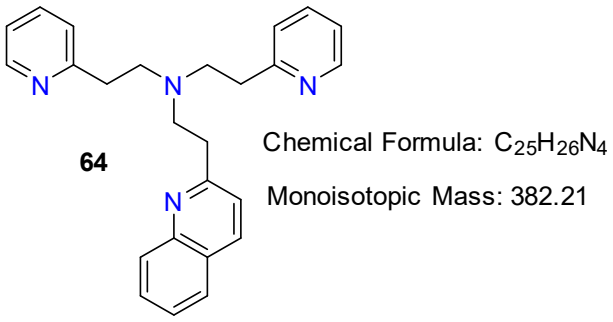


**Mass Spectrometry**

The mass spectrum obtained from a solution of **64** displayed a signal corresponding to the free base ligand at *m/z* = 383.2 (calcd. for $C_{25}H_{27}N_4^+$ $[M+H]^+$ *m/z* = 383.22, found *m/z* = 383.2). An equimolar solution of $[Cu(OH_2)_6](ClO_4)_2$ and the ligand **64** (*Figure 128*) gives rise to two copper-containing signals at *m/z* = 445.1 and 495.1, the latter being much less intense. Also present are peaks for the free ligand **64** and 2-vinylquinoline **45**. The signal at *m/z* = 445.1 can be attributed to the complex [Cu(**64**)]$^+$ (calcd. for $CuC_{25}H_{26}N_4^+$ $[M]^+$ *m/z* = 445.14, found *m/z* = 445.1) in which reduction of the Cu(II) to Cu(I) has occurred. The peak at *m/z* = 495.1, could not be assigned to any combination of copper with free ligand **64** or fragments thereof, solvent molecules or associated perchlorates. However, the isotope pattern and *m/z* value exactly resembles those seen in the [Cu(**58**)]$^+$ complex, as discussed previously in *Chapter Five* section 5.4.2. The formation of this complex may be due to several reasons such as the fragmentation of **64** which is followed by the re-formation to afford ligand **58**. Alternatively, this may be due to a contamination of a previous run leaving residual ligand behind. Upon returning to the mass spectrum of the free ligand **64**, a low-intensity peak at *m/z* = 433.1 is present that corresponds to that

of the ligand **58**. It is difficult to determine whether this contamination occurred before or during the experiment; however, $^{1}$H NMR analysis of the ligand **64** did not reveal any signals that corresponded to the other ligand **58**. This was not observed in any of the other metal ion mass spectra; however, this is likely due to the weak binding affinity of the ligand to these metal ions. The addition of a further equivalent of ligand gives essentially the same spectrum, with consistent intensity increases across all notable peaks, while addition of a third equivalent gives an increase in the intensity of the free ligand peak.

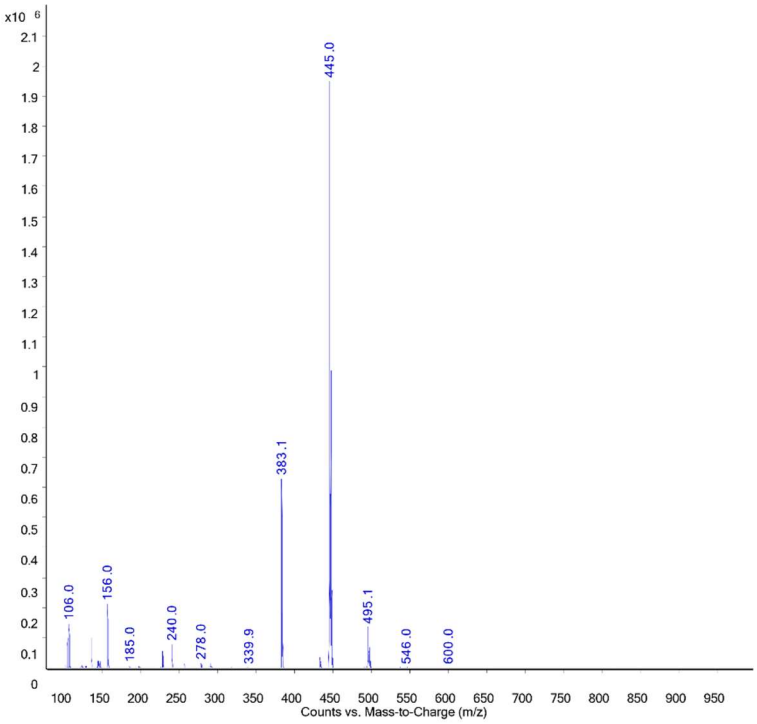


*Figure 128. The mass spectrum of an equimolar solution of the ligand **64** and $[Cu(OH_2)_6](ClO_4)_2$*

The mass spectrum of a solution of $[Co(OH_2)_6](ClO_4)_6$ and 1 equivalent of **64** displays 1+ ion peaks for the free ligand, 2-vinylquinoline **45** and a complex ion at *m/z* = 540.0. The complex species signal can be assigned to the formula $[Co(\mathbf{64})(ClO_4)]^+$ (calcd. for $CoC_{25}H_{26}N_4ClO_4^+$ $[M]^+$ *m/z* = 540.09, found *m/z* = 540.0). Addition of both a second and third equivalents of **64** gives an increase in the intensity of the free ligand and 2-vinylquinoline peaks. Similar behaviour is seen for both Mn(II) and Ni(II) experiments. Again, similar behaviour is displayed for Zn(II); however, the complex ion $[Zn(\mathbf{64})(ClO_4)]^+$ (*m/z* = 545.0, calcd. for $ZnC_{25}H_{26}N_4ClO_4^+$ $[M]^+$ *m/z* = 545.09, found *m/z* = 545.0), appears in a trace amount in comparison.

In this instance, the quinoline ligand behaves in a similar fashion to the pyridine congener **11** (see section 5.4.2) where a 1+ 1:1 copper complex ion is present and reduction of the Cu(II) to Cu(I) has occurred. The mass spectrum of **11** and the Cu(II) ions; however, does not display any other copper-containing peaks, whereas the quinoline does. Both the quinoline ligand **64** and its pyridine congener **11** display just one metal complex peak ($[M(L)(ClO_4)]^+$) (L = **11** or **64**) in each of the mass spectra for the manganese, cobalt, zinc and nickel ions. However, the quinoline ligand shows trace amounts of the complex ion with manganese and the pyridine ligand shows trace amounts of the complex peak with zinc instead.

**Job Plots**

The Job plots for the reactions of Cu(II), Co(II), and Ni(II) with the **64** ligand are given in *Figure 129*. The absorbance maximum lies at a mole fraction of 0.5 for all three ions, giving a ratio of ligand: metal ion in the complexes of 1:1.

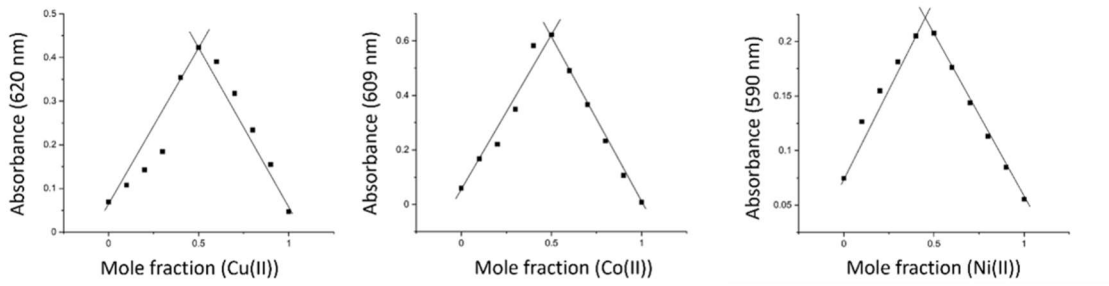


*Figure 129. The Job plots for the reaction between the ligand **64** and the metal ions Cu(II), Co(II), and Ni(II).*

## 5.4.5 Ligand 65

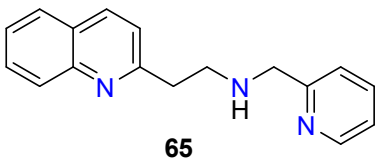


**65**

Chemical Formula: $C_{17}H_{17}N_3$

Monoisotopic Mass: 263.14

**Mass Spectrometry**

The mass spectrum of a solution of the free ligand **65** exhibited peaks at *m/z* = 264.1 and 156.0 and have been assigned to the free ligand and 2-vinylquinoline fragment, respectively.

An equimolar solution of $[Cu(OH_2)_6](ClO_4)_2$ and ligand **65** affords a mass spectrum that shows a peak due to free ligand at *m/z* = 264.1 and the ligand fragments **150** (*Figure 130*) and 2-vinylquinoline **45** at *m/z* = 205.0 and 156.0, respectively. Three copper-containing signals are observed at *m/z* = 325.0, 425.0 and 502.0.

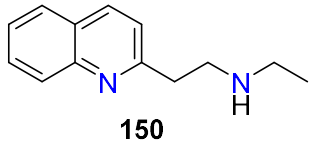


**150**

Chemical Formula: $C_{13}H_{16}N_2$
Monoisotopic Mass: 200.13

*Figure 130. Structure of the ligand fragment **150**.*

The peak at *m/z* = 325.0 can be assigned to the complex $[Cu(\mathbf{65})]^+$ (calcd. for $CuC_{17}H_{16}N_3^+$ $[M]^+$ *m/z* = 325.06, found *m/z* = 325.0), with the loss of a proton from the free ligand generating the overall 1+ charge of the complex ion. The ratio between this peak and that of the free ligand is approximately the same.

The signal observed at *m/z* = 425.0 shows an isotope pattern that is consistent with the presence of a copper ion and an associated perchlorate. This is consistent with the $[Cu(\mathbf{65})(ClO_4)]^+$ ion (calcd. for $CuC_{17}H_{17}N_3ClO_4^+$ $[M]^+$ *m/z* = 425.02, found *m/z* = 425.0). In contrast to the above, the loss of a proton is not required to match the experimental data due to the negatively charged perchlorate that is associated with the species.

The peak at *m/z* = 502.0 displays a copper isotope pattern could not be confidently assigned. A complex ion of the formula $[Cu(\mathbf{65})(NCCH_3)(H_2O)_2(ClO_4)]^+$ matches the *m/z* value calculated for $CuC_{19}H_{24}N_4ClO_4^+$ $[M]^+$ *m/z* = 502.06. However, the calculated isotope pattern does not fit that of the experimental spectrum and the reason for this remains unclear.

The mass spectrum after the addition of 2 equivalents of ligand shows an increase in the intensity of the free ligand **65** signal at *m/z* = 264.1. Upon the addition of a third

equivalent, the free ligand peak significantly increases in intensity relative to the other copper-containing signals.

Addition of 1 equivalent of **65** to $[Ni(OH_2)_6](ClO_4)_2$ affords a mass spectrum that exhibits peaks at *m/z* = 156.0, 264.1, 366.0, and 420.0. The nickel-containing complex ion, $[Ni(\mathbf{65})(HCOO)]^+$ can be assigned to the peak at *m/z* = 366.0 (calcd. for $NiC_{18}H_{18}N_3O_2^+$ $[M]^+$ *m/z* = 366.07, found *m/z* = 366.0). The peak at *m/z* = 420.0 has been assigned to the metal complex ion with the formula, $[Ni(\mathbf{65})(ClO_4)]^+$ (calcd. for $NiC_{17}H_{17}N_3ClO_4^+$ $[M]^+$ *m/z* = 420.02, found *m/z* = 420.0). The mass spectra after the addition of a second and third equivalents of ligand show only an increase in the intensity of the peaks at *m/z* = 156.0 and 264.1 corresponding to 2-vinylquinoline **45** and the free ligand **65**.

The mass spectra of solutions containing **65** and either $[Co(OH_2)_6](ClO_4)_2$, $[Ni(OH_2)_6](ClO_4)_2$, or $[Mn(OH_2)_6](ClO_4)_2$ exhibit two distinct peaks at *m/z* = 264.1 and 156.0, corresponding to the free ligand **65** and 2-vinylquinoline **45**. There are no other relevant peaks that correspond to any metal complexes.

**Job Plots**

The Job plots for the reaction of **65** with the metal ions Cu(II), Co(II) and Ni(II) in $CH_3CN$ solution are given in *Figure 131*. All three graphs show absorbance maxima at a mole fraction of approximately 0.5, thus suggesting a 1:1 ligand-to-metal ion binding ratio.

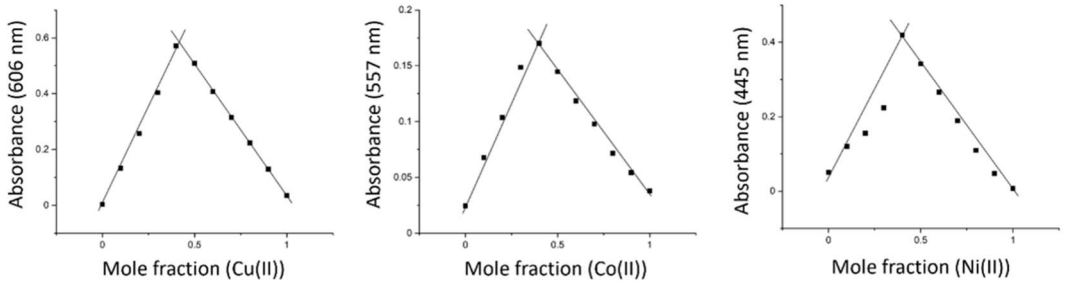


*Figure 131. The Job plots for the reaction between the ligand **65** and the metal ions Cu(II), Co(II), and Ni(II).*

### 5.4.6 Ligand 66

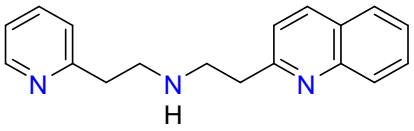


**66**

Chemical Formula: $C_{18}H_{19}N_3$

Monoisotopic Mass: 277.15

#### Mass Spectrometry

The spectrum of the free ligand **66** affords a distinct molecular ion peak at m/*z* = 278.1. The mass spectrum of an equimolar solution of $[Cu(OH_2)_6](ClO_4)_2$ and **66** displays a free ligand peak and peaks at *m/z* = 340.0 and 495.0 that contain copper ions as identified by isotopic patterns. This mass spectrum did not contain a peak of significant intensity that corresponded to 2-vinylquinoline **45** (*m/z* = 156.0).

The peak at *m/z* = 340.0 can be assigned to the 1:1 complex $[Cu(\mathbf{66})]^+$, (calcd for $CuC_{18}H_{19}N_3$ *m/z* = 340.08, found *m/z* = 340.0). The peak observed at *m/z* = 495.0 can be assigned to the complex ion $[Cu(\mathbf{58})]^+$ discussed in *Chapter Five* section 5.4.2. This peak was also observed in the mass spectrum of the reaction between the ligand **64** and $[Cu(OH_2)_6](ClO_4)_2$. In this case, the ligand **66** is a fragment of the ligand **58**, therefore, **58** may have been present in the ligand sample prior to the reaction, or the formation of the ligand could have occurred during the mass spectrometry analysis due to fragmentation and reformation. Following the addition of the second and third equivalents of **66**, there was no change in the complex ion peaks observed and only an increase in the intensity of the free ligand signal.

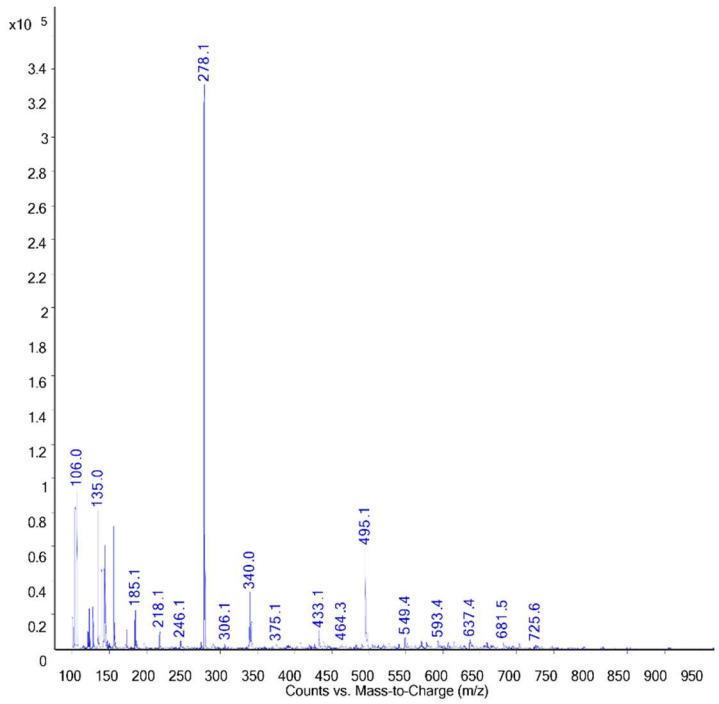


*Figure 132. The mass spectrum of an equimolar solution of the ligand **66** and $[Cu(OH_2)_6](ClO_4)_2$.*

The reaction of the metal ions Co(II), Ni(II), Zn(II) and Mn(II) with 1, 2 and 3 equivalents of ligand **66** afforded mass spectra that displayed the free ligand peak and the ligand fragment 2-vinylquinoline **45**; no peaks corresponding to metal complex ions were observed.

**Job Plots**

The reaction of Cu(II), Co(II), and Ni(II) with the **66** ligand in $CH_3CN$ afforded Job plots that are given in *Figure 133*. The absorbance maximum lies at a mole fraction of 0.5 for all three ions, giving a ratio of ligand: metal ion in the complexes of 1:1.

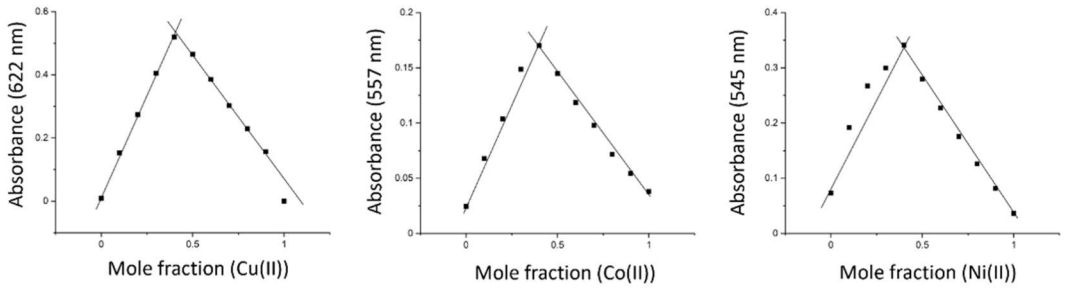


*Figure 133. The Job plots for the reaction between the ligand **66** and the metal ions Cu(II), Co(II), and Ni(II).*

## 5.5 Conclusion

In the absence of X-ray crystallography data, the use of mass spectrometry and Job plot studies strongly suggest that these quinolyl-containing ligands prefer a 1:1 (M:L) binding and in some cases this is particularly weak. The interaction between $[Cu(OH_2)_6](ClO_4)_2$ and all the ligands was demonstrated to be the strongest, with clear peaks observed in both the mass spectrometry and Job measurements. The poor quality of the data displayed in some of the Job plots may be due to the weakly binding ligands; however, further analysis is required for this to be confirmed. Conducting these experiments again under different conditions i.e. solvent, could afford better results. The metal ions Co(II), Ni(II), and Zn(II) afforded complex ions that are consistent with a 2+ charge or had a negatively bound ligand. In contrast, for Cu(II) the oxidation state was either conserved through loss of a proton, reduction of the metal ion or a negatively charged anion association. When complexation did occur between a ligand and manganese, this was consistently only in trace amounts and with a negatively charged additional ligand bound. The pyridine congeners exhibited similar behaviour when reacted with these metal ions.

# *Chapter Six*

# Synthesis of naphthalene and pyrene-containing starting materials and their corresponding bi- and tetradentate ligands

## 6.1 Chapter Overview

In *Chapter Three*, quinoline was investigated as an extension of pyridine. This chapter details the investigation into naphtho[2,3-*d*]imidazole as an extension of 1,3-benzimidazole. Only a small number of ligands containing the naphtho[2,3-*d*]imidazole moiety have been reported; these include linear and tridentate ligands and one symmetrical tripodal ligand. Thus, the synthesis of naphthalene-derived starting materials (*Scheme 78*), ligands and corresponding metal complexes is the main aim of this chapter. To further examine extended aromatic surfaces, pyrene starting materials (*Scheme 78*) and a resulting pyrene-containing ligand have also been explored.

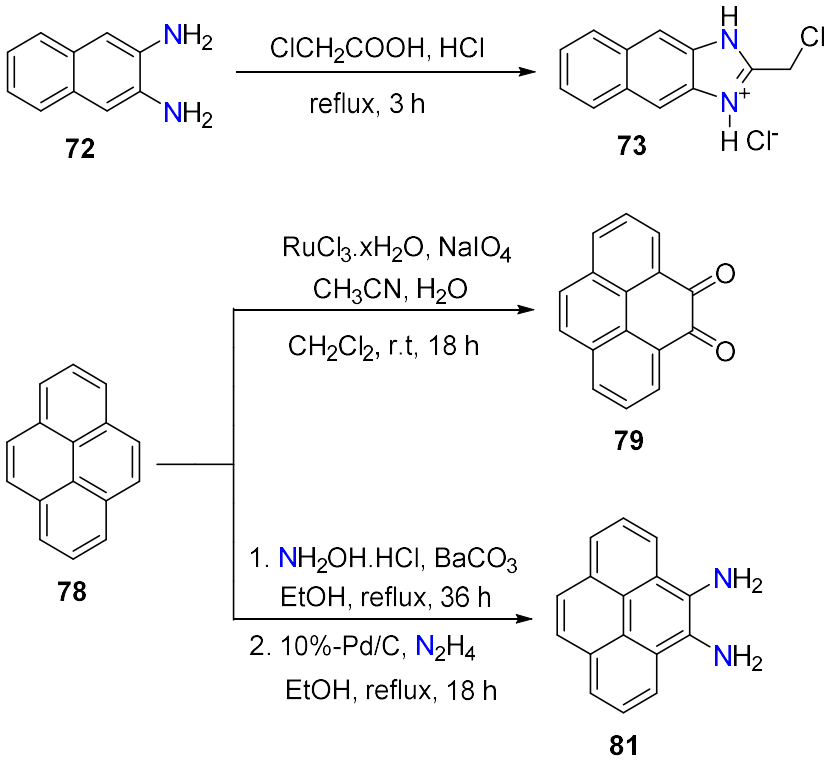


*Scheme 78. General synthetic schemes of naphthalene and pyrene starting materials derived from naphthalene-2,3-diamine and pyrene.*

## 6.2 Introduction

### 6.2.1 Naphthalene

Naphthalene, the simplest planar bicyclic aromatic molecule, was first discovered in 1819 by Alexander Garden[464] and is generally obtained from the distillation and fractionation of petroleum or coal tar.[465] Conventionally, the aromatic ring is synthesised by a Diels-Alder reaction of maleic anhydride with 1,1- diaryl ethylene, followed by decarboxylation with BaOH and copper to afford the aromatised product.[466] The cytotoxicity of naphthalene has led to extensive exploration of the compound with applications in physiology,[467] and anticancer,[468,469] antimicrobial,[470] anti-inflammatory,[469,471] antiviral,[472,473] antidepressant,[474] and anti-neurodegenerative properties,[475,476] amongst others.[335,477]

Remarkably there are no structurally characterised examples of naphthalen-2-amine acting as a monodentate ligand and there is only one such example of naphthalen-1-amine acting as a monodentate ligand. The X-ray structure of this Co(III) complex is presented in *Figure 134*; however, unfortunately the reference for this paper was unavailable.

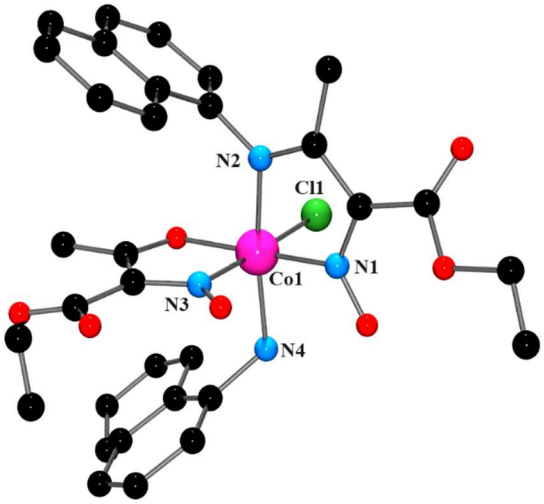


*Figure 134. Structure of the Co(III) complex that contains naphthalen-1-amine. H atoms have been omitted for clarity.*

In contrast, there are a number of examples reported of aniline acting as a monodentate ligand to several metal ions and this highlights that naphthalene has not been studied as much thus far. Therefore, it is of interest to us to incorporate the naphthalene moiety into ligand scaffolds.

Interestingly, there is also limited literature on the di-substituted naphthalene-2,3-diamine **72** acting as a bidentate ligand with only a handful of metal complexes that contain this molecule as a ligand.[478–482] One example, displayed in *Figure 135* is the cobalt complex, $[Co(\mathbf{72})_2]^{2+}$, in which two naphthalene-2,3-diamine **72** ligands are coordinated to a Co(II) centre.[479]

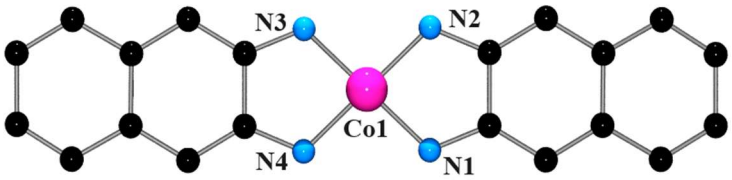


*Figure 135. Structure of the $[Co(\mathbf{72})_2]^{2+}$ complex. H atoms have been omitted for clarity.*

Again, there is only a handful of structurally characterised examples of metal complexes that contain naphthalene-1,8-diamine acting as a bidentate ligand.[99,483,484] For example, Duda and Łasocha have reported the synthesis and X-ray structure of the cadmium

complex, [CdBr(1,8-DAN)$_2$]Br, in which two naphthalene-1,8-diamine ligands are bound to the metal centre in a bidentate fashion (*Figure 136*).[484]

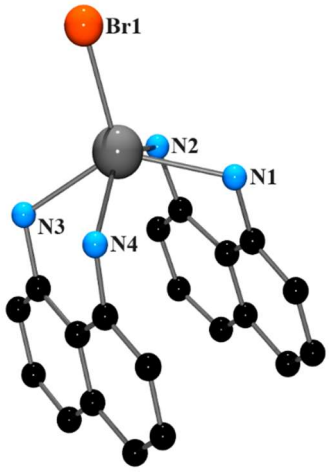


*Figure 136. Structure of the [CdBr(1,8-DAN)$_2$]$^+$ cation. H atoms have been omitted for clarity.*

Despite the paucity of examples of aminonaphthalenes acting as mono- and bidentate ligands, the naphthalene moiety has been incorporated in a number of multidentate amino ligands. In addition to naphthalene-2,3-diamine being used as a bidentate ligand, this compound can also be employed as a naphthalene scaffold for the synthesis of multidentate ligands.

Nabei *et al*. reported the synthesis of bis(*O*-vanillin)-2,3-naphthalenediimine **152**[485–487] from the reaction of naphthalene-2,3-diamine **72** and *o*-vanillin **151** (*Scheme 79*). Along with the pyridine congener, both ligands were complexed to Fe(II) ion centres and the effect of molecular packing on the occurrence of spin crossover was studied. The pyridine-based complex showed a two-step spin-crossover behaviour. In contrast to what the authors had expected, increasing the aromatic surface of the ligand with the naphthalene moiety resulted in π-stacking interactions which led to the absence of spin crossover.[487]

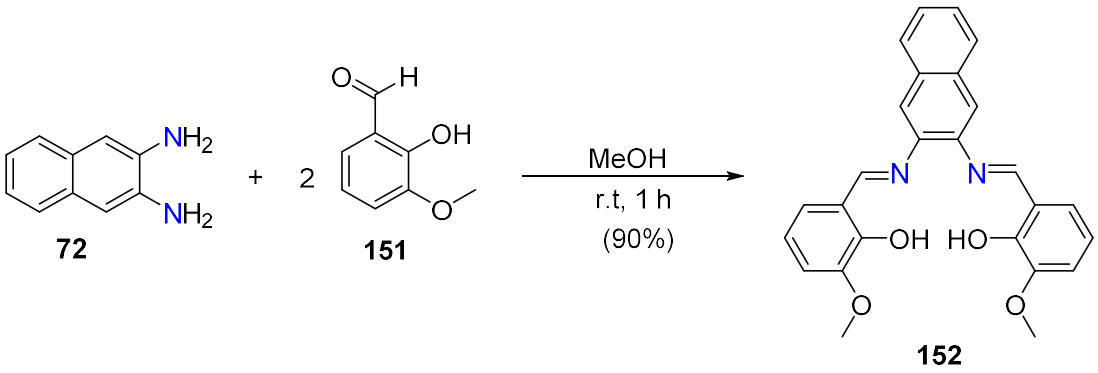


*Scheme 79. Reported synthesis of the ligand **152**.*[487]

Another example of a multidentate ligand in which the scaffold is based around naphthalene-2,3-diamine **72** is the tetradentate ligand, *N*,*N*'-naphthalene-2,3-diylbis(*N*'-methoxyurea) **154**. The synthesis of this ligand can be achieved from the reaction of naphthalene-2,3-diamine **72** and (methoxyamino)(nitro)methanone **153** in $CH_2Cl_2$, in the presence of $Et_3N$, at room temperature for 24 hours (*Scheme 80*).[488] However, to date there are no structurally characterised metal complexes that contain this naphthalene-based tetradentate ligand.

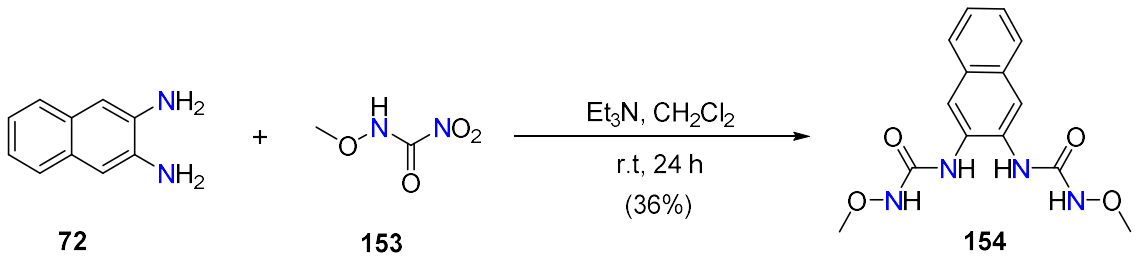


*Scheme 80. Reported synthesis of N,N'-naphthalene-2,3-diylbis(N'-methoxyurea) **154**.*[488]

Naphthalene-2,3-diamine **72** has also been shown to be an ideal starting material for the synthesis of 1*H*-naphtho[2,3-*d*]imidazole and a plethora of its derivatives. The synthesis of such compounds is simple and usually involves the reaction between naphthalene-2,3-diamine and carboxylic acids, aldehydes, and cyano-containing molecules that contain the corresponding functional group of choice. For example, the preparation of 1*H*-naphtho[2,3-*d*]imidazole **155** can be achieved from the reaction of naphthalene-2,3-

diamine **72** and formic acid (*Scheme 81*) and the compound can be isolated directly from the reaction mixture following the addition of $Na_2CO_3$.[489]

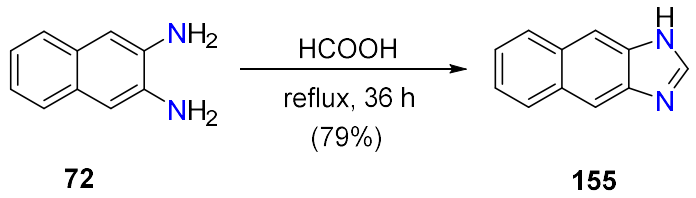


**72** **155**

*Scheme 81. Reported synthesis of **155**.*[489]

As another example, the asymmetric bidentate ligand 2-(pyrazin-2-yl)naphthoimidazole **156**, was first reported by Liu *et al*.[490] being obtained from the reaction of pyrazine-2-carbonitrile **157** with naphthalene-2,3-diamine **72** in polyphosphoric acid (*Scheme 82*). The ligand can utilise the terminal naphthyl ring to interact with calf thymus DNA via intercalation into the DNA base pairs. A Ru(II) complex of the ligand was also found to promote cleavage of plasmid DNA upon irradiation. A number of structurally similar ligands have also been reported.[491–494]

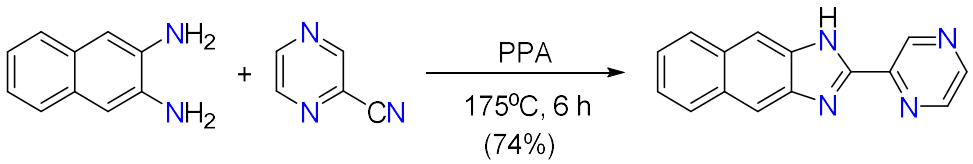


**72** **157** **156**

*Scheme 82. Synthesis of the ligand **156**.*[490]

The reaction of quinoline-2-carboxylic acid **158** and naphthalene-2,3-diamine **72** gave the quinoline derivative **159** of the ligand described above (*Scheme 83*).[493]

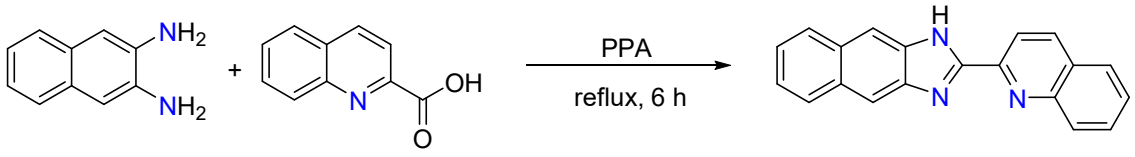


**72** **158** **159**

*Scheme 83. Reported synthesis of the ligand **159**.*[493]

This ligand was prepared as part of a series that contained pyridine, quinoline, naphtho[2,3-*d*]imidazole and 1,3-benzimidazole moieties. The heterocyclic 1,3-

benzimidazole and its derivatives have been established as significant therapeutic compounds that play an important part in various biological roles including antitumor properties. Thus, the authors decided to incorporate 1,3-benzimidazole and the naphthalene derivative into ligands and prepare Ir(III) complexes of these (*Figure 137*).[493]

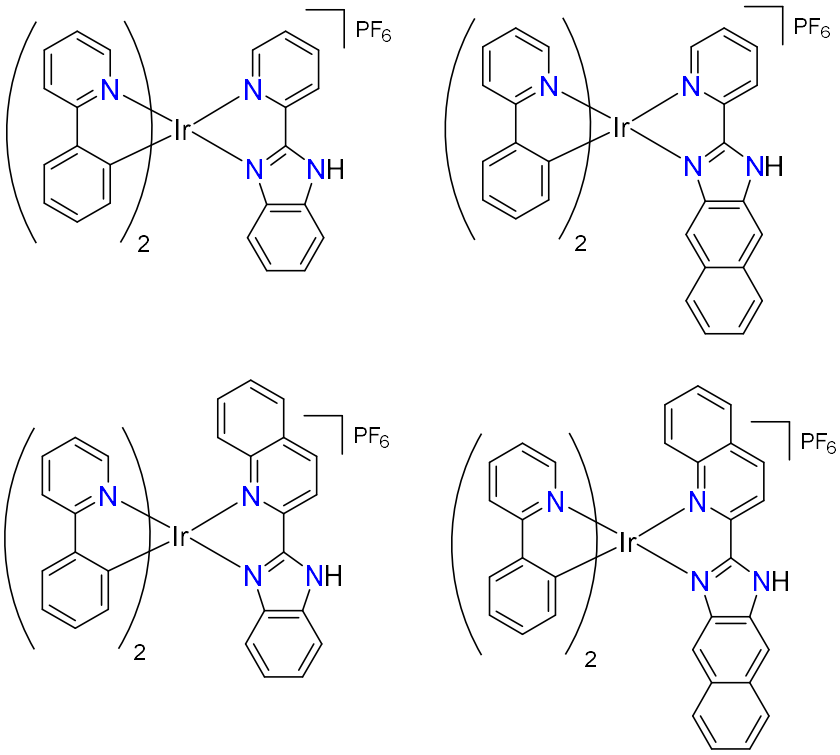


*Figure 137. Structures of the iridium complexes that contain the ligands **156** and **159**.*

### 6.2.2 Imidazole

Imidazole is a conjugated planar five-membered ring that has two nitrogen atoms at the 1- and 3-positions (*Figure 138*). One of the nitrogen atoms is protonated and behaves like a pyrrole nitrogen, and the other can be classed as more of a pyridine-type nitrogen.[271]

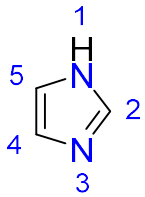


*Figure 138. The structure of imidazole.*

Imidazole is widely present in natural compounds and synthetically produced molecules and is a fundamental building block for many important compounds. The structure and

electron-rich ring of imidazole and its derivatives allow for easy binding to metal ions in a variety of enzymes and biological receptors, and such compounds can exhibit broad biological activities.[495] The structural features of the heterocycle enhance its ability to form multiple interactions with neighbouring molecules through hydrogen bonds, van der Waals interactions, and hydrophobic forces.[496] As with many heterocyclic compounds, imidazole derivatives have demonstrated importance in a variety of pharmacological applications.[497] Imidazole is included in many compounds that are of both biological and chemical interest and are part of numerous significant biomolecules (*Figure 139*). The importance of such molecules has led to an extensive body of literature that has focused on the design and synthesis of imidazole-containing ligand donors.

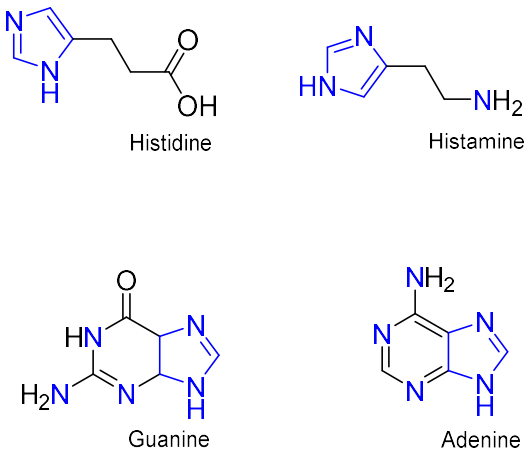


*Figure 139. Selected important imidazole-containing biological molecules.*

A commonly employed method is the Debus-Radziszewski imidazole synthesis which is a multi-component reaction between a 1,2-dicarbonyl, an aldehyde, and ammonia or a primary amine. The first stage of the reaction involves the condensation of two dicarbonyl groups and two ammonia molecules to afford the diamine analogue. A subsequent condensation reaction with an appropriate aldehyde affords the desired imidazole derivative (*Scheme 84*).[498,499]

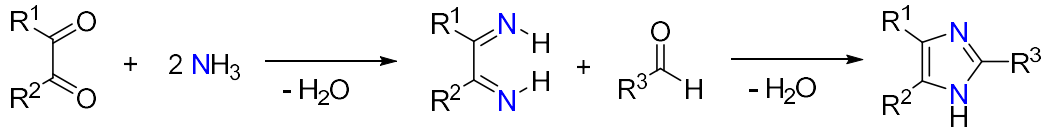

*Scheme 84. General Debus-Radziszewski imidazole synthesis.*

Modification of the general procedure by replacing one of the ammonia molecules with an appropriate primary amine affords the *N*-substituted imidazole (*Scheme 85*). [500,501]

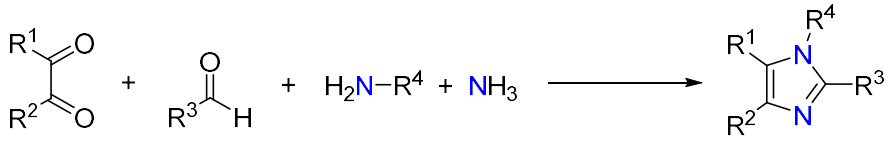

*Scheme 85. Modified Debus-Radziszewski imidazole synthesis.*

Imidazole exhibits tautomerism and exists in two equivalent tautomeric forms since each of the nitrogen atoms can be protonated. This becomes evident in unsymmetrically substituted compounds such as 4-methylimidazole (*Figure 140*).[271]

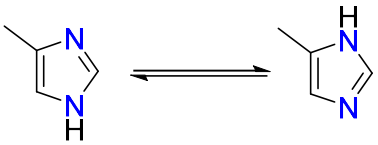

*Figure 140. Tautomerism of 4-methylimidazole.*

An example of an important imidazole-containing ligand is 2-(1*H*-imidazol-4-yl)ethanamine, commonly known as histamine. Histamine is produced by the human body in immune responses, physiological functions in the gut and as a neurotransmitter for the brain, uterus, and spinal cord. The formation of histamine is achieved through the decarboxylation of the amino acid histidine, a reaction that is catalysed by the enzyme L-histidine decarboxylase. Structurally, histamine consists of an imidazole ring with an aminoethyl side chain. Due to the imidazole moiety, histamine exists in two tautomeric forms under aqueous conditions and each form can be identified depending on which of the two nitrogen atoms is protonated (*Figure 141*). Due to the three nitrogen donor atoms present, histamine can act as a mono- or bidentate ligand and can bind to metal ions of biological interest; thus, coordination complexes of this ligand have been widely studied.

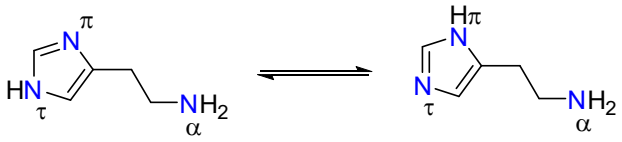


*Figure 141. The two tautomeric forms of imidazole that exist under aqueous conditions.*

For example, the Ni(II) complex of histamine (*Figure 142*) was prepared and structurally characterised in order to study the tautomeric form present. The study found that the histamine binds as a bidentate ligand and as the $N^{\tau}$-H tautomer which is the biologically active form.[502]

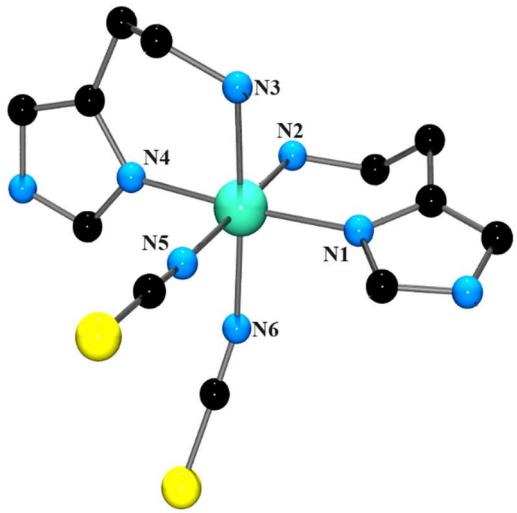


*Figure 142. Structure of the Ni(II) complex containing histamine. H atoms have been omitted for clarity.*

The basic imidazole skeleton can be categorised into three types by derivatisation products at the 1(N)-, 2-, or 4-positions, affording 1-, -2, or 4-substituted imidazole ligands, respectively. Multifunctional ligands can also be obtained from the addition of other functional groups to the imidazole moiety.[503]

In recent years imidazole has become widely studied because of the significant interest in N-heterocyclic carbene (NHC) ligands. NHC ligands are carbene species in which the carbene carbon is situated between two nitrogen atoms. Thus, it has been well established that imidazole and its derivatives make excellent NHC ligands with most ligands based on imidazole (*Figure 143*).[504]

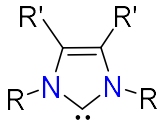

*Figure 143. General structure of imidazolylidene.*

N-substituted imidazole-containing ligands can be simple to prepare; for example, the reaction between 1,4-dibromobenzene **160** and imidazole **161** affords the rigid ligand, 1,4-di(1*H*-imidazol-4-yl)benzene **162** (*Scheme 86*).[505]

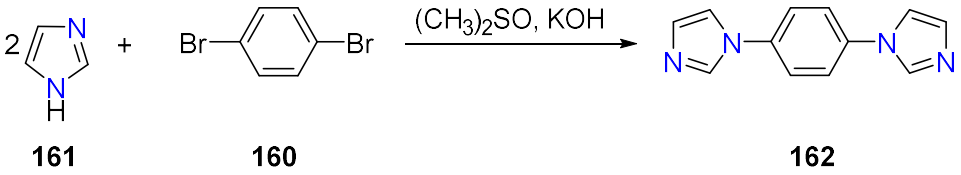


*Scheme 86. Reported synthesis of 1,4-di(1H-imidazol-4-yl)benzene **162**.*[505]

The flexible N-substituted ligand, 1,3,5-tris(imidazol-1-ylmethyl)benzene **163**, can be prepared from the reaction of 1,3,5-tris(bromomethyl)benzene **164** and 3 equivalents of imidazole **161** in the presence of KOH (*Scheme 87*).[506]

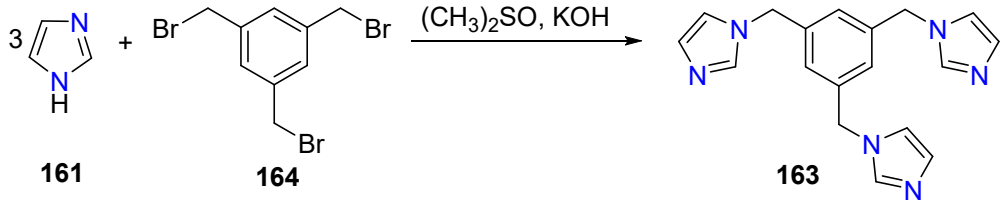


*Scheme 87. Reported synthesis of 1,3,5-tris(imidazol-1-ylmethyl)benzene **163**.*[506]

N-substituted imidazole-containing ligands can only coordinate to a metal ion through the exocyclic nitrogen atom, and this can be seen in *Figure 144*, which shows a copper coordination complex that contains the ligand 1,3,5-tris(imidazol-1-ylmethyl)benzene **163**.[507,508]

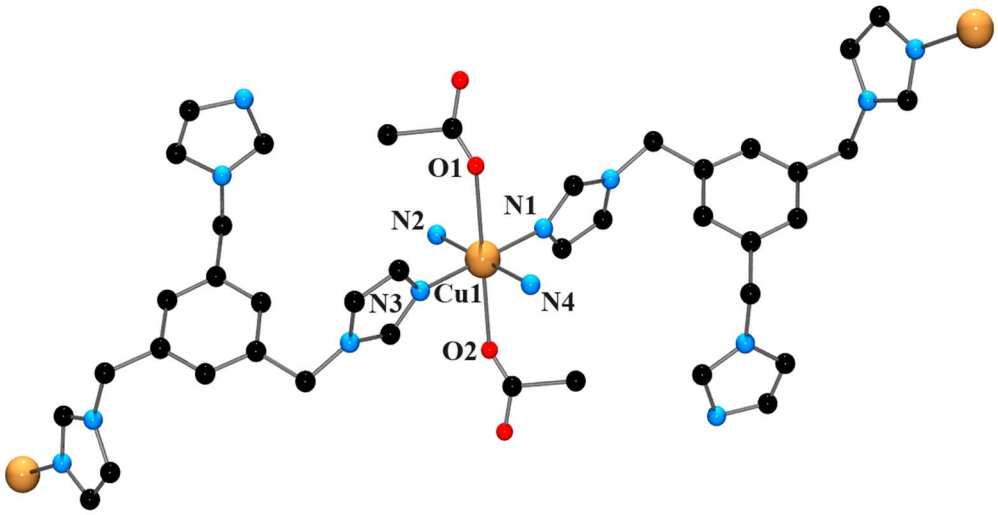


*Figure 144. Structure of a Cu(II) complex that contains the ligand **163**. H atoms have been omitted for clarity.*

In contrast to the N-substituted ligands that have one donor site, the 2- and 4-substituted imidazole-containing ligands can potentially bind to a metal ion through each of the nitrogen atoms, the imine N atom, and the amine NH atom. Another differing property is that the N-substituted imidazole are neutral and monodentate, while the 2- and 4-substituted imidazole ligands can be neutral and monodentate or anionic with the potential to bind at both the nitrogen atoms if in the deprotonated form (imidazolate anions) (*Figure 145*). Thus, ligands that contain either a 2- or 4-substituted imidazole exhibit a greater diversity of coordination modes in comparison to the N-substituted imidazole-containing ligands.

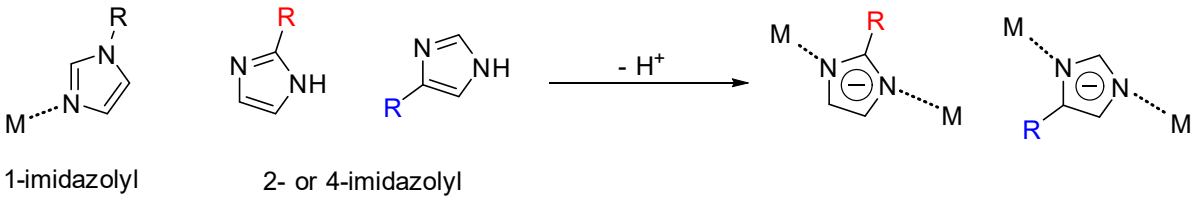


*Figure 145. Coordination modes for N-, 2-, and 4-substituted imidazole ligands.*

The synthesis of the chelating ligand, 2,2′-biimidazole **165**, can be achieved from the reaction of an aqueous solution of glyoxal **166** and ammonium acetate **167** in $H_2O$ (*Scheme 88*).[509,510]

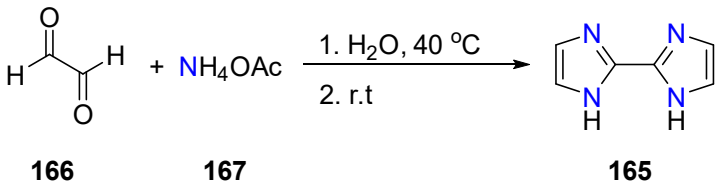


**166** **167** **165**

*Scheme 88. Reported synthesis of 2,2'-biimdazole **165**.*[509]

As mentioned above, this ligand has the potential to bind to a metal ion via both of the nitrogen donor atoms. An example of this is the Ru(II) complex, [Ru(trpy)(**165**)Cl]$PF_6$ (trpy = 2,2';6',2"-terpyridine), which displays the 2,2'-biimidazole **165** moiety acting as a bidentate ligand through which both the nitrogen atoms are bound to the metal ion centre (*Figure 146*).[511]

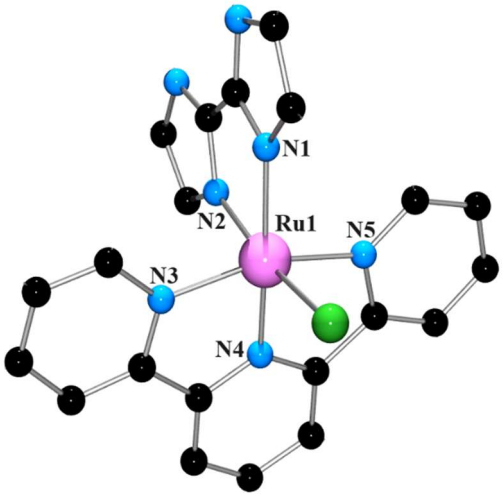


*Figure 146. Structure of the [Ru(trpy)(**165**)Cl]$^+$ cation. H atoms have been omitted for clarity.*

Of interest to this work are imidazole groups which have an extended π system, and the incorporation of these into multidentate ligands. 1,3-benzimidazole is the exemplar in this respect, with a large number of substituted derivatives known, and judicious choice of starting material allows facile incorporation of these units in multidentate ligands. For example, 2-(chloromethyl)-1*H*-1,3-benzimidazole **168**, which can react with an appropriate amine to give a multidentate ligand, can easily be prepared from the reaction of benzene-1,2-diamine **169** and chloroacetic acid **170** (*Scheme 89*). While it is not mentioned by the authors, it is assumed that the title compound was isolated as the

hydrochloride salt due to the acidic reaction conditions and absence of any basic workup.[512]

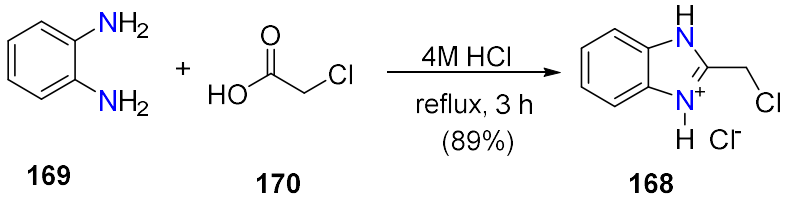


*Scheme 89. Reported synthesis of **168**.*[512]

However, imidazole appended to larger aromatic systems are uncommon, and, for example, there are relatively few naphthannulated imidazoles known. One such instance, 2-(chloromethyl)-1*H*-naphtho[2,3-*d*]imidazole hydrochloride **73.HCl**, was reported by Nobbs *et al.* from the reaction of naphthalene-2,3-diamine **72** and ethyl 2-chloroethanimidoate dihydrochloride **171**. The latter was synthesised from the reaction of chloroacetonitrile **172**, EtOH and HCl gas (*Scheme 90*).[513]

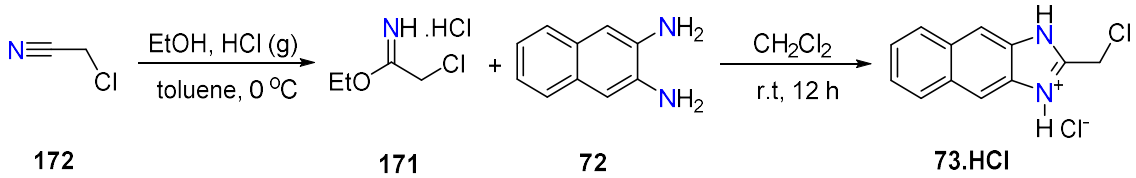


*Scheme 90. Reported synthesis of 2-(chloromethyl)-1H-naphtho[2,3-d]imidazole hydrochloride **73.HCl**.*[513]

This is a useful starting material for the synthesis of multidentate ligands. For example, reaction with 2-(*N*-methylaminomethyl)benzimidazole dihydrochloride **173.2HCl** affords the asymmetric ligand **174** (*Scheme 91*).[513]

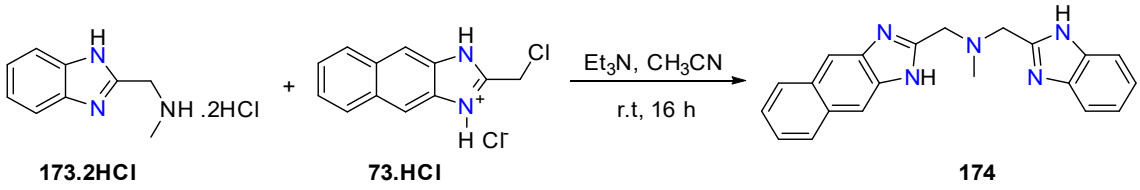


*Scheme 91. Reported synthesis of the ligand **174**.*[513]

Chromium complexes that contain the ligand **174** and its bis(benzimidazole) congener have exhibited excellent catalytic properties towards the oligomerisation of ethylene. Furthermore, studies have found that varying the substitution of these ligands affects the catalytic activity of the resulting complexes. It was found that the naphthalene-containing complex, displayed increased catalytic activity in comparison to the other asymmetric ligands synthesised; however, it was not superior to the original pyridine congener (*Figure 147*).[513]

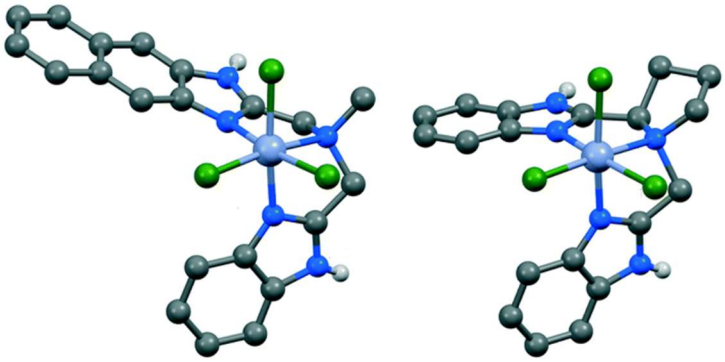

*Figure 147. Structures of the Cr(III) complexes which contain the ligand **174** (left) and the pyridine congener (right). H atoms have been omitted for clarity.*

### 6.2.3 Tripodal ligands containing naphtho[2,3-*d*]imidazole moieties

Naphthalene-2,3-diamine **72** can also be condensed with 2,2',2''-nitrilotriacetic acid **175** (*Scheme 92*)[514,515] to prepare the symmetrical tripodal tetradentate ligand **176**.[514–516]

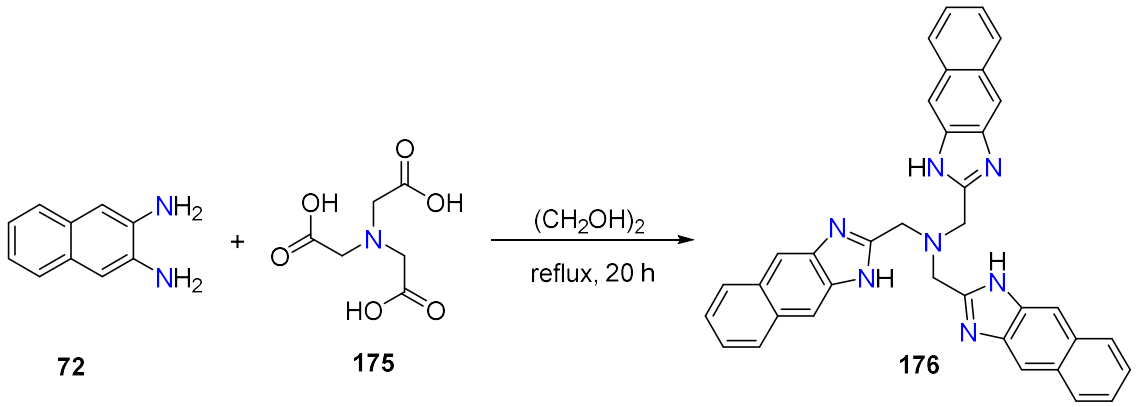


*Scheme 92. Reported synthesis of the ligand **176**.*[515]

Despite the presence of several naphtho[2,3-*d*]imidazole derived ligands in the literature, there is an absence of such tripodal tetradentate ligands, with **176** being the only one reported thus far. On the other hand, tripodal tetradentate ligands containing benzimidazole and derivatives are well known.

In 1977 Thompson *et al.* reported the first synthesis of the symmetrical tripodal ligand tris(2-benzimidazylmethyl)amine **177** (*Scheme 93*). The ligand can be prepared from the reaction of benzene-1,2-diamine **169** and 2,2',2''-nitrilotriacetonitrile **178** or alternatively from the condensation of the diamine and 2,2',2''-nitrilotriacetic acid **175**.[517]

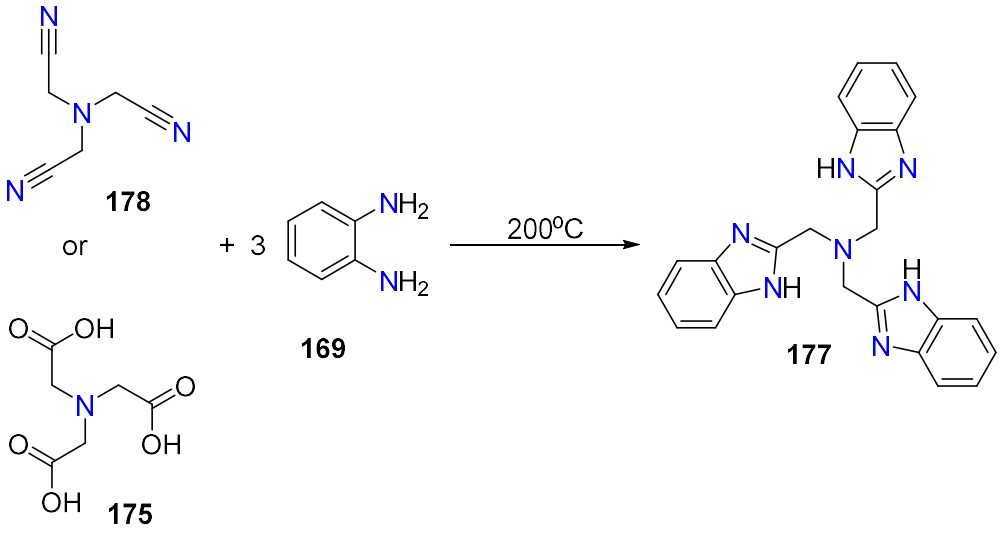


*Scheme 93. Reported synthesis of the ligand **177**.*[517]

Metal complexes of this tripodal ligand have been studied for their novel structures and properties. For example, nucleic acids are widely considered to be potential therapeutics;

however, their delivery into mammalian cells has proven to be difficult due to the environmental conditions.[518,519] As a result, the dinuclear complexes, $[Cu_2(\mathbf{177})_2Cl_2]Cl_2$ (*Figure 148*) and $[Cu_2(\mathbf{177})Cl_2(H_2O)](NO_3)_2$, have been investigated for this purpose and have shown the ability to effectively condense and transfer DNA into cells. Both the complexes exhibited extensive π-π stacking interactions between the benzimidazole groups of neighbouring molecules. The authors found the major binding mode between the Cu(II) complexes and DNA was via intercalation due to the planar aromatic surfaces from the ligand.[520–522]

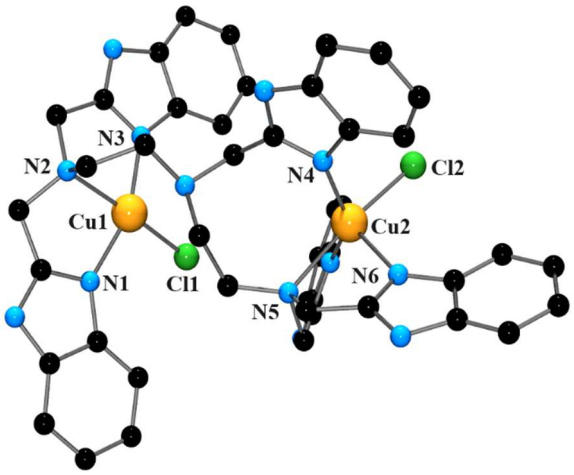


*Figure 148. Structure of the $[Cu_2(\mathbf{177})_2Cl_2]^+$ cation. H atoms have been omitted for clarity.*

Since the initial report of tri(2-benzimidazylmethyl)amine **177**,[517] a number of lower symmetry analogues have been reported. For example, as reported by Pascaly *et al.* the reaction of [(2-benzimidazolyl)methyl]amine **169** and 2-(chloromethyl)pyridine hydrochloride **84.HCl** affords the ligand **179** (*Scheme 94*).[140] Geng *et al.* subsequently reported a modified procedure from the reaction of 1-(pyridin-2-yl)-*N*-[(pyridin-2-yl)methyl]methanamine and 2-(bromomethyl)-1*H*-1,3-benzimidazole in the presence of $Na_2CO_3$ in $(CH_3)_2CO$.[523]

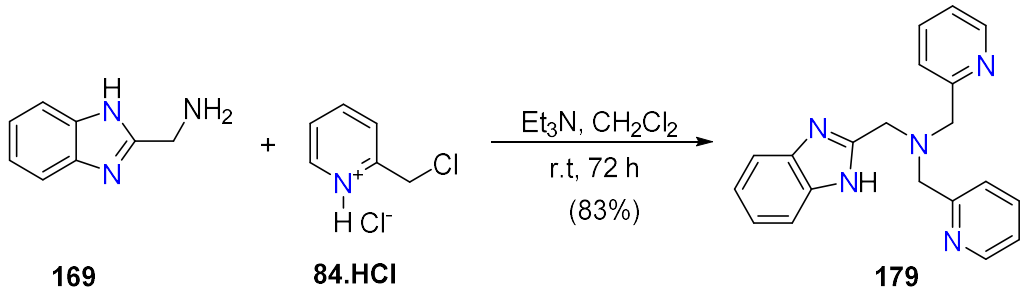


169 84.HCl 179

*Scheme 94. Reported synthesis of **179**.*[140]

The ligand **179** can also be prepared from the reductive amination reaction between 1*H*-1,3-benzimidazole-2-carbaldehyde **180** and 1-(pyridin-2-yl)-*N*-[(pyridin-2-yl)methyl]methanamine **60** in a mixture of MeOH and 1,2-dichloroethane; the resulting imine is reduced using sodium triacetoxyborohydride (*Scheme 95*).[524]

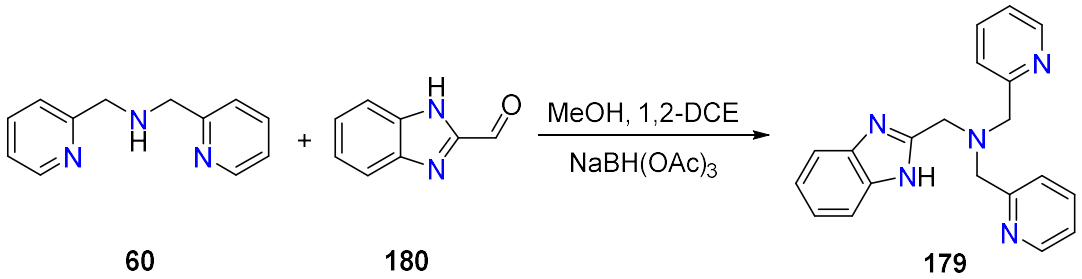


60 180 179

*Scheme 95. Reported synthesis of the ligand **179**.*[524]

This ligand **179** was used to investigate the catechol cleaving activity of iron(II)-containing model compounds for catechol 1,2-dioxygenases.[140,525] Isolated from bacteria, catechol dioxygenases are mononuclear non-heme iron enzymes that play a key role in the metabolism of aromatic compounds.[526] Of particular interest is the role of catechol dioxygenases in the metabolism process of halogenated aromatic compounds which subsequently play a vital part in the bioremediation of halogenated pollutants. *Figure 149* exhibits the X-ray structure of an Fe(II) metal centre which is bound to the ligand **179** and two oxygen atoms of a halogenated aromatic molecule.[526]

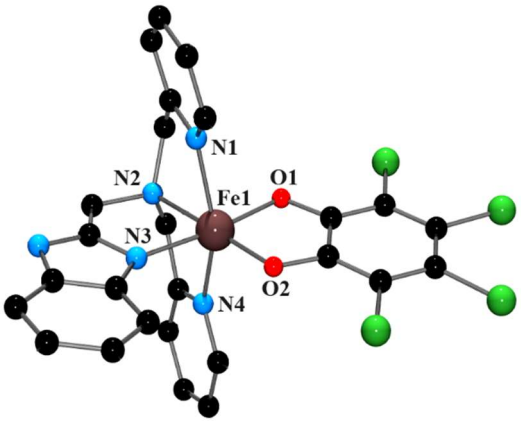


*Figure 149. Structure of a Fe(II) complex containing the ligand **179**. H atoms have been omitted for clarity.*

A feature of tripodal ligands is that the nature of the arms can be systematically varied, allowing for the synthesis of series of closely related ligands (see section 1.2.3). For example, reaction of 1-(1*H*-1,3-benzimidazol-2-yl)-*N*-[(1*H*-1,3-benzimidazol-2-yl)methyl]methanamine **181** with 2-(chloromethyl)pyridine hydrochloride **84.HCl** gives the ligand **182** (*Scheme 96*), which contains two 1,3-benzimidazole groups and one pyridine nitrogen donor.[527]

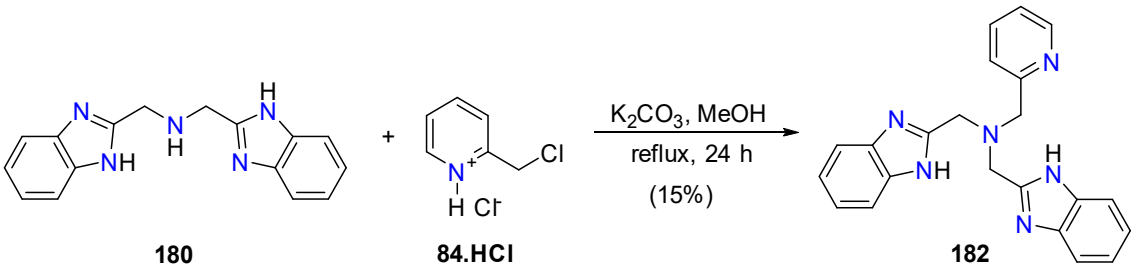


*Scheme 96. Reported synthesis of the ligand **182**.*[527]

This ligand has been coordinated to surprisingly few metal ions.[528] One such example is the Eu(III) complex depicted in Figure 35. This species was prepared as part of a study investigating luminescent lanthanide complexes and their potential use in catalysis, fluorescent imaging, and supramolecular devices within biology and medicine.[528]

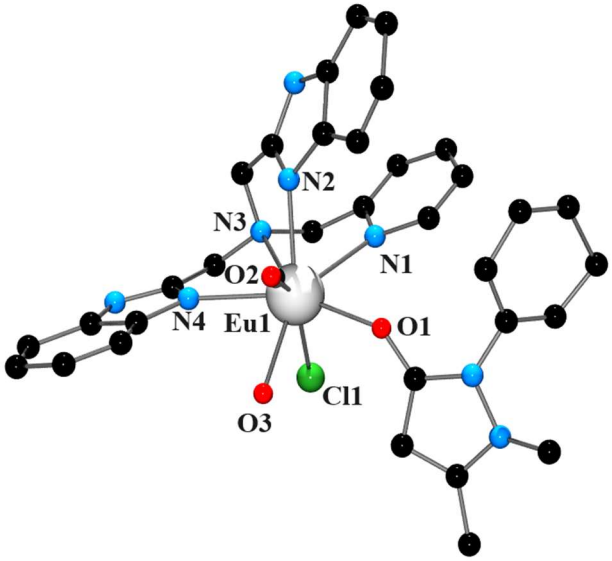


*Figure 150. Structure of the Eu(III) complex containing the ligand **182**. H atoms have been omitted for clarity.*

In light of the above discussion, our aim of this chapter is the synthesis and characterisation of a series of naphtho[2,3-*d*]imidazole-containing tripodal tetradentate ligands which contain extended π systems, in efforts to determine the effect of large planar surfaces with multidentate amine ligands.

## 6.3 Synthesis of naphthalene starting material

The ideal starting materials for incorporation of 1*H*-naphtho[2,3-*d*]imidazole units into larger multidentate ligands are either the 2-halomethyl derivatives, or the 2-aminomethyl compound. Reaction of the former with amines would allow alkylation of the amine N atom, while reaction of the latter with haloalkanes would give substitution of the amine N atom with one or two different groups. With this in mind, synthesis of 2-(chloromethyl)-1*H*-naphtho[2,3-*d*]imidazole was achieved following the methodology described by Mariappan *et al*., with slight modifications. Naphthalene-2,3-diamine **72** and chloroacetic acid **186** were refluxed in 4M hydrochloric acid for 3 hours. After cooling to room temperature, the reaction mixture was placed on ice to allow for more product to precipitate out. Following filtration, the brown solid was dried in a vacuum desiccator to afford the title product (*Scheme 97*). Analysis by $^{1}$H NMR was consistent with that reported in the literature.[512]

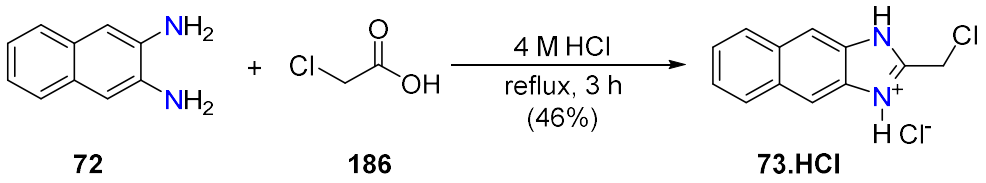


72 186 73.HCl

*Scheme 97. The synthesis of 2-(chloromethyl)-1H-naphtho[2,3-d]imidazole hydrochloride* ***73.HCl****.*

Next the synthesis of the brominated analogue was attempted, which had been prepared by an analogous method.[229] However, in our hands, reaction of naphthalene-2,3-diamine **72** and bromoacetic acid at reflux in 4 M HCl for 5 hours failed to give the desired product; analysis of the crude solid obtained by mass spectrometry revealed no signals consistent with the desired product, and in fact, a molecular ion peak at *m/z* = 217.0 corresponding to that of 2-(chloromethyl)-1*H*-naphtho[2,3-*d*]imidazole hydrochloride **73.HCl** was observed.

In addition, several attempts to prepare 1-(1*H*-naphtho[2,3-*d*]imidazol-2-yl)methanamine did not result in any product formation and analysis of the resulting solid by $^{1}$H NMR spectroscopy revealed the presence of only the starting material, naphthalene-2,3-diamine **72**. As a result, 2-(chloromethyl)-1*H*-naphtho[2,3-*d*]imidazole hydrochloride **73.HCl** was chosen as the sole naphthalene-containing starting material for the synthesis of the following tripodal ligands.

## 6.4 Synthesis of naphthalene-containing ligands

To begin with, the preparation of the tripodal tetradentate ligand **187** was attempted following the methodology employed for the synthesis of the quinoline-based ligand **55** (see section 3.6.1). This involved the reaction of 2-(chloromethyl)-1*H*-naphtho[2,3-*d*]imidazole hydrochloride **73.HCl** and 2-(pyridin-2-yl)ethan-1-amine **54**, in the presence of *i*-Pr$_2$EtN, in THF at room temperature for 4 days (*Scheme 98*). Following a basic workup, analysis of the crude material by $^{1}$H NMR revealed a spectrum with no obvious evidence of the formation of **187**. Further analysis by mass spectrometry revealed no molecular ion peaks consistent with the product. The reaction was repeated several times with different solvents, bases, and temperature conditions; however, none proved successful for the synthesis of the ligand **187**.

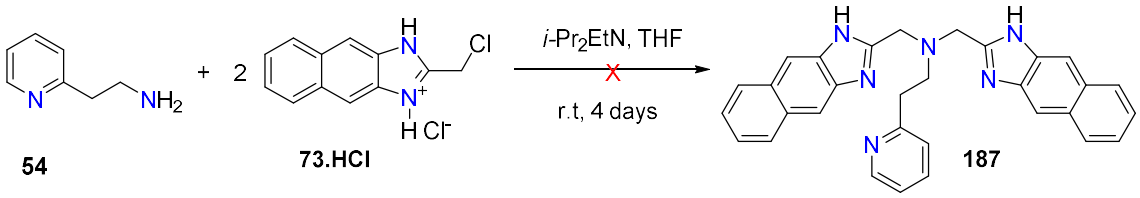


*Scheme 98. Attempted synthesis of the ligand **187**.*

Following this, 2-(chloromethyl)-1*H*-naphtho[2,3-*d*]imidazole hydrochloride **73.HCl** and 2-(pyridin-2-yl)-*N*-[2-(pyridin-2-yl)ethyl]ethan-1-amine **62** in the presence of 2 equivalents of $Et_3N$ were refluxed in 1,4-dioxane. Monitoring the reaction by TLC indicated that the complete consumption of the starting materials, even after 7 days, had not occurred and revealed a messy TLC plate. $^1H$ NMR and mass spectrometry analysis of the crude material confirmed that none of the desired product had been formed. Therefore, a series of optimisation reactions were attempted. Reviewing the literature on similar syntheses and comparable ligands, the reaction was attempted using a variety of solvents, bases, and reaction times and temperatures.

The conditions found to afford the desired product, albeit in low to moderate yields, were the addition of $Et_3N$ to a stirring mixture of 2-(chloromethyl)-1*H*-naphtho[2,3-*d*]imidazole hydrochloride **73.HCl** in $CH_2Cl_2$ followed by the addition of the corresponding tridentate ligand in $CH_2Cl_2$, and stirring at room temperature for 7 days. Following a basic work-up and removal of the solvent (rotavap), the crude residue was purified by silica gel chromatography. Purification of the compound proved difficult and required multiple columns, resulting in the isolation of the product as a brown oil (18 – 42%). The successful formation of the ligands was observed by NMR spectroscopy ($^1H$, $^{13}C$ and 2D) and mass spectrometry.

Following these conditions, the ligand **74** was successfully prepared from the reaction of 2-(chloromethyl)-1*H*-naphtho[2,3-*d*]imidazole hydrochloride **73.HCl** and 2-(pyridin-2-yl)-*N*-[2-(pyridin-2-yl)ethyl]ethan-1-amine **62** in the presence of $Et_3N$ in $CH_2Cl_2$ (*Scheme 99*). Confirmation of the desired product was obtained by $^1H$, $^{13}C$ and 2D NMR and high-resolution mass spectrometry.

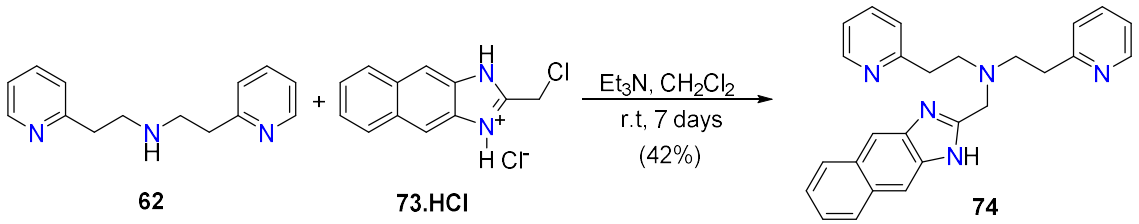


*Scheme 99. The synthesis of the ligand **74**.*

The $^{1}$H NMR spectrum of **74** revealed the presence of two four-proton triplets at $\delta_H$ 3.07 and 2.88 ppm corresponding to the ethyl protons from the pyridylethyl units, and another two-proton singlet at $\delta_H$ 4.18 ppm from the methylene protons of the naphthalene moiety. In addition, integration of the peaks observed in the aromatic region of the $^{1}$H NMR spectrum confirmed the expected number of protons. Since the ligand contains a mirror plane, this renders a number of carbon atoms chemically equivalent, and these appear as one signal, and the observation of 12 signals in the $^{13}$C NMR is consistent with this. As observed in the $^{1}$H NMR spectra of the quinolyl ligands reported in *Chapter Three* (section 3.6), the diagnostic pyridyl doublet of doublets of doublets at $\delta_H$ 8.41 ppm, corresponding to the proton adjacent to the nitrogen atom, is present (*Figure 151*).

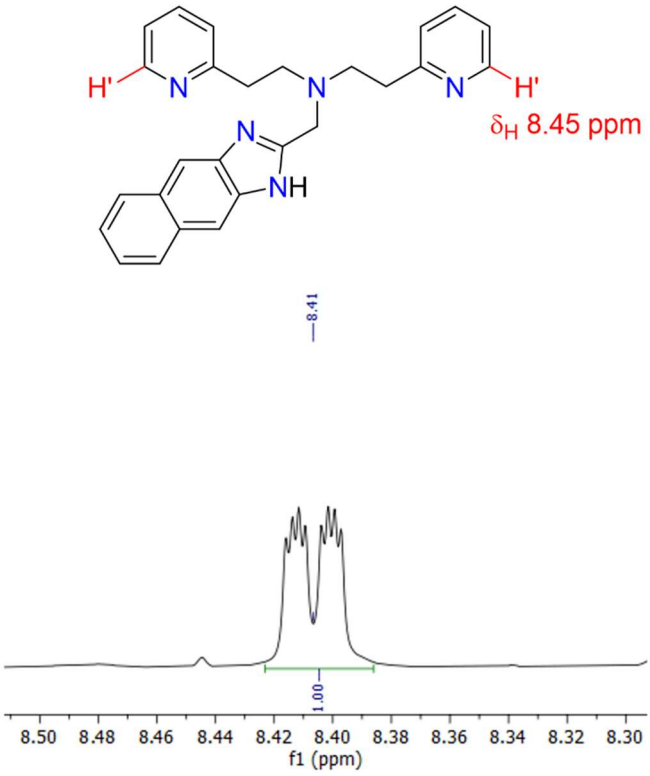


*Figure 151. Diagnostic pyridyl signal in the $^{1}H$ NMR spectrum for the ligand **74** in $CDCl_3$.*

2D NMR spectra including COSY, HSQC and HMBC were obtained allowing for the assignment of the ligand. The signal at $\delta_C$ 123.85 ppm in the $^{13}C$ NMR spectrum was confirmed to be overlapping signals, as revealed by two correlations in the HSQC spectrum to two different proton signals (*Figure 152*).

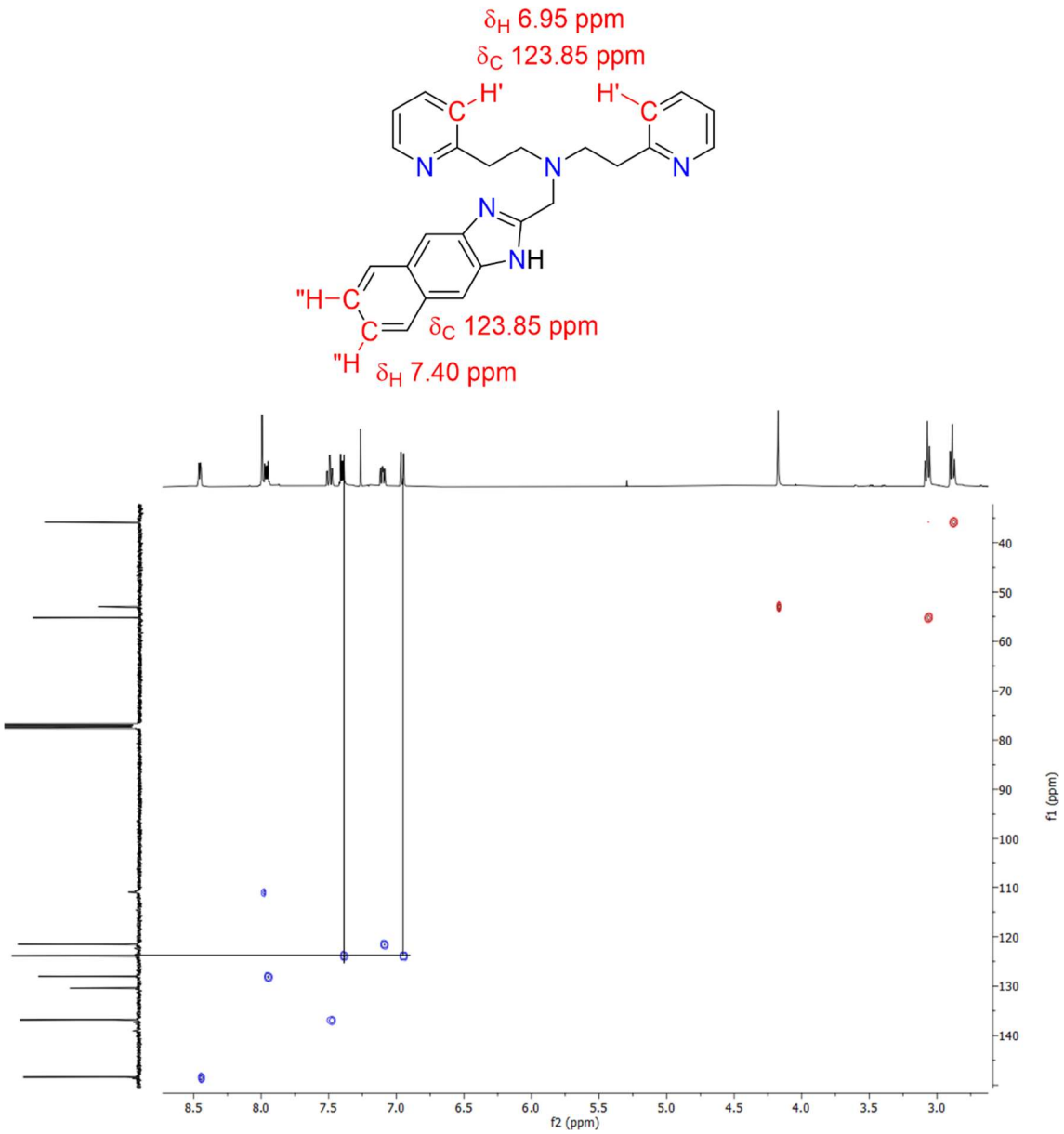


*Figure 152. Key HSQC correlations for the ligand **74** in $CDCl_3$.*

The $^{13}C$ NMR spectrum displays a small broad carbon signal occurring at $\delta_C$ 111.01 ppm that shows a correlation to a two-proton singlet at $\delta_H$ 7.99 ppm in the HSQC spectrum. Broad carbon signals are unusual; therefore, this peak was further investigated using variable temperature NMR. Recording the $^{13}C$ spectrum at 45°C resulted in the broad carbon signal disappearing (Figure 153), leaving the supposedly attached proton signal with no correlations in the HSQC. No other new carbon signals were revealed during these additional experiments. At this point in time, there are no obvious explanations for this behaviour. An additional small broad signal is observed in the $^{13}C$ NMR spectrum

taken at 25 °C at $\delta_C$ 139.01 ppm and this too disappears upon running the experiment at 45 °C.

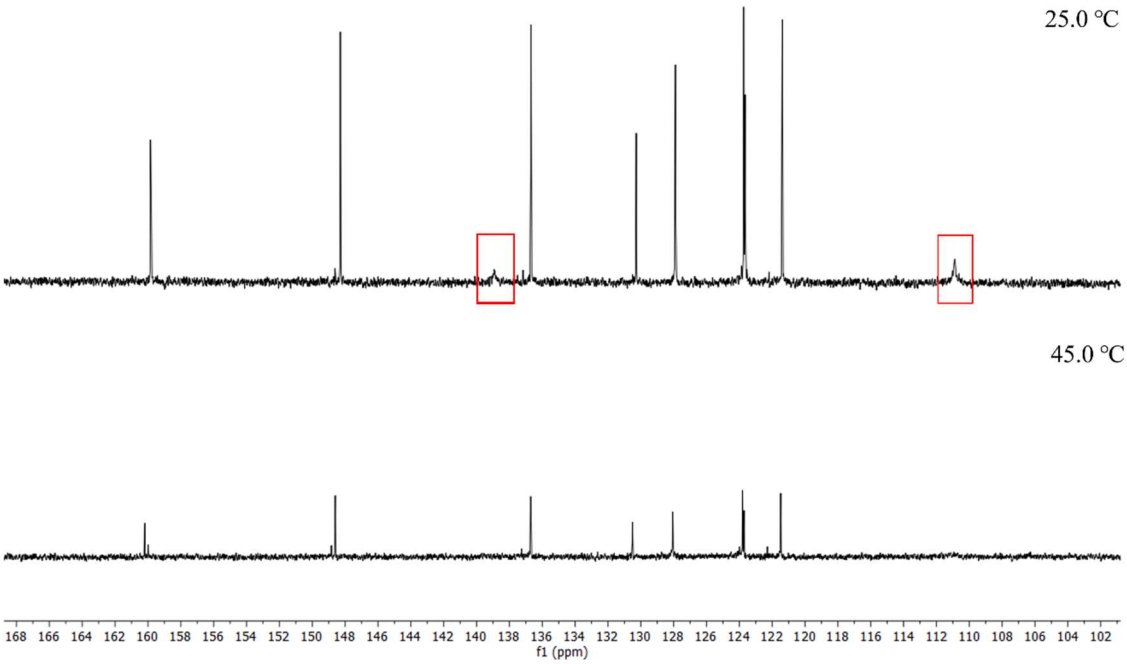


Figure 153. Variable temperature $^{13}C$ NMR spectra of the ligand **74** over the chemical shift range $\delta_C$ 100–170 ppm in $CDCl_3$.

In contrast, this peak does not show any correlations in the HSQC spectrum; however, the HMBC spectrum (*Figure 154*) does reveal a strong correlation to a signal at $\delta_H$ 7.99 ppm in the $^1H$ NMR spectrum. This correlation strongly suggests that this broad carbon signal may be a quaternary carbon atom close to this proton.

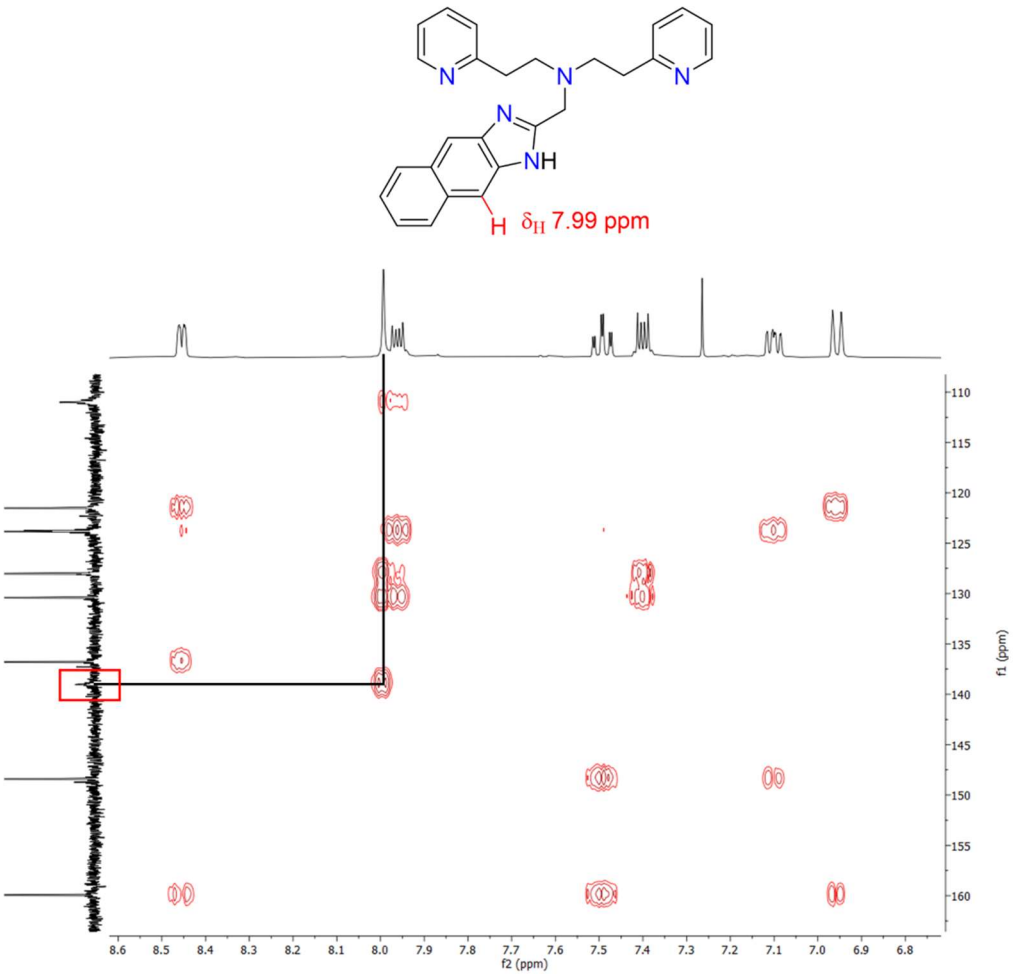


*Figure 154. Key HMBC correlations for the ligand **74** in $CDCl_3$.*

However, we are still confident in the isolation of the desired product due to the HRMS data obtained and the majority of the NMR data being consistent with the expected structure.

Mass spectrometry analysis of the material revealed a molecular ion peak at *m/z* = 408.2180 which can be assigned to the free ligand (calcd. for $C_{26}H_{26}N_5^+$ $[M+H]^+$ *m/z* = 408.21827; found *m/z* = 408.2180). An additional peak is observed at *m/z* = 430.1999 and this can be assigned to the sodiated ligand (calcd. for $C_{26}H_{25}N_5Na^+$ $[M+Na]^+$ *m/z* = 430.2000; found *m/z* = 430.1999).

The ligand **75** was synthesised under the same conditions discussed above from the reaction of 2-(chloromethyl)-1*H*-naphtho[2,3-*d*]imidazole hydrochloride **73.HCl** and 1-(pyridin-2-yl)-*N*-[(quinolin-2-yl)methyl]methanamine **67** (*Figure 155*). The title compound **75** was confirmed by NMR spectroscopy ($^1H$, $^{13}C$ and 2D) and mass spectrometry.

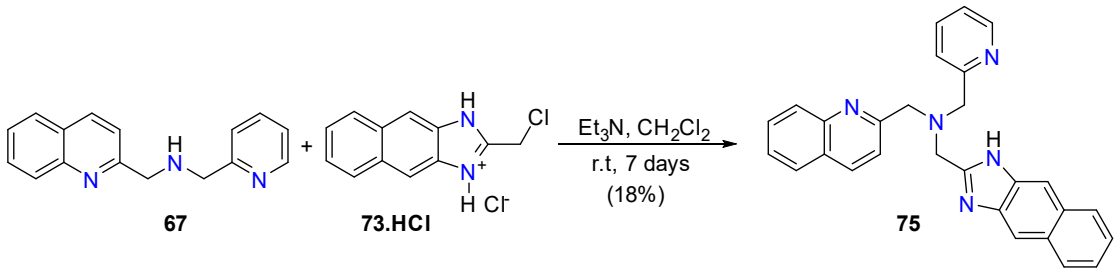


*Figure 155. The synthesis of the ligand **75**.*

The $^{1}$H NMR spectrum of **75** displayed three two-proton singlets at $\delta_H$ 4.21, 4.13, and 3.99 ppm (*Figure 156*) and from the HMBC and HSQC spectra, these correspond to the naphthalene, quinoline and pyridine -$CH_2$ protons, respectively. In addition, the diagnostic -CH proton from the pyridine group is displayed at $\delta_H$ 8.68 ppm, a signal that is observed in all the pyridine-containing ligands in this work.

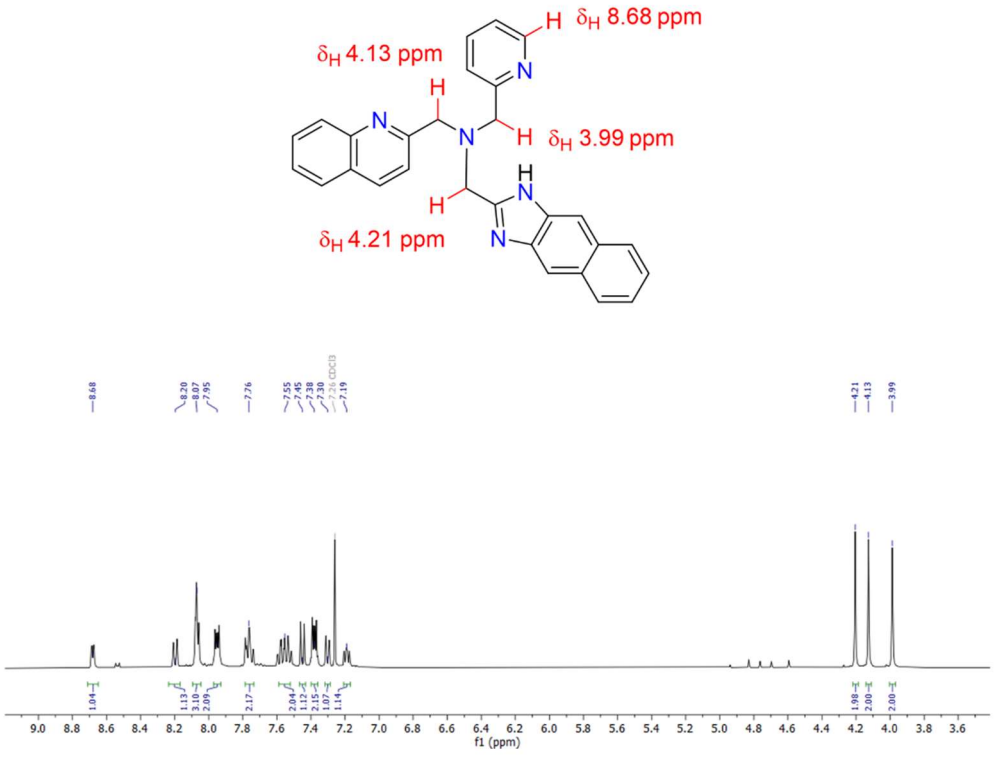


*Figure 156. $^{1}$H NMR spectrum of the ligand **75** in $CDCl_3$.*

*Figure 157* displays the aromatic region of the HSQC spectrum of **75** which shows the carbon signal at $\delta_C$ 137.05 ppm corresponding to a three-proton multiplet at $\delta_H$ 8.10 – 8.03 ppm and a one-proton multiplet at $\delta_H$ 7.63 – 7.50 ppm. In conjunction with the COSY

and HMBC spectra, this carbon signal has been identified as three coincident carbon signals, corresponding to three different protons as determined by the integrations.

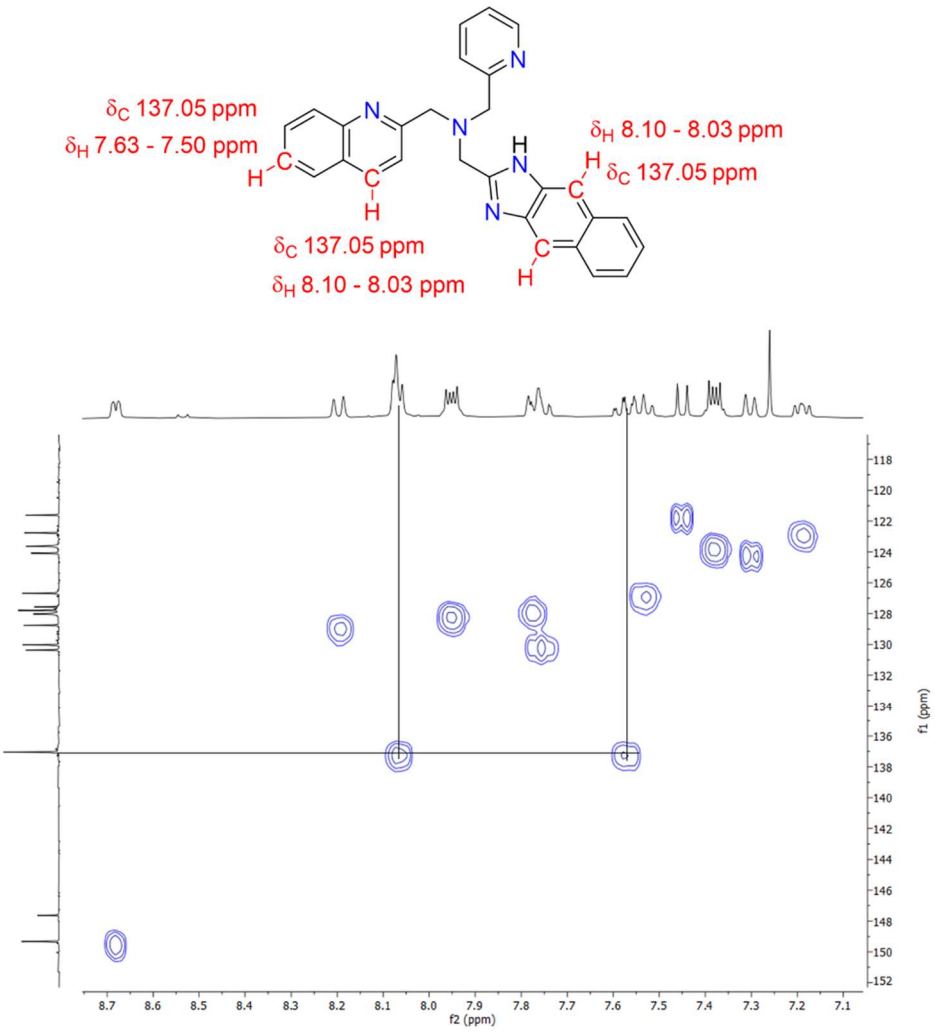


*Figure 157. Key HSQC correlations for the ligand* ***75*** *in* $CDCl_3$.

Mass spectrometry analysis of the ligand afforded a mass spectrum that displayed a molecular ion peak at *m/z* = 430.2023 that can be assigned to the free ligand (calcd. for $C_{28}H_{24}N_5$ $[M+H]^+$ 430.20262; found 430.2023). In addition, a peak at *m/z* = 452.1842 is observed and this can be assigned to the sodiated ligand (calcd. for $C_{28}H_{23}N_5Na^+$ $[M+Na]^+$ *m/*z = 452.18500; found *m/z* = 452.1842).

The **76** ligand was obtained from the reaction of 2-(chloromethyl)-1*H*-naphtho[2,3-*d*]imidazole hydrochloride **73.HCl** and 2-(pyridin-2-yl)-*N*-[(quinolin-2-yl)methyl]ethan-1-amine **68** (*Scheme 100*), following the general method described above but at a

temperature of 40 °C. Confirmation of the successful isolation of **76** was revealed by NMR spectroscopy ($^{1}H$, $^{13}C$ and 2D) and mass spectrometry.

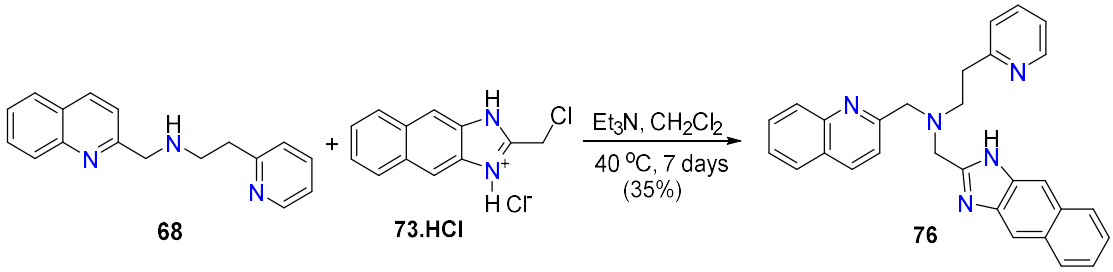


*Scheme 100. The synthesis of the ligand **76**.*

The $^{1}H$ NMR spectrum of **76** displays two singlets at $\delta_H$ 4.05 ppm (2H) $\delta_H$ 4.19 ppm (2H) that have been assigned to the -$CH_2$ protons from the methylene arm of the quinoline and naphthalene moieties, respectively. In conjunction with the HMBC and HSQC spectra, the two two-proton triplets observed in the $^{1}H$ NMR spectrum have been assigned to the -$CH_2$-$CH_2$ protons of the quinoline moiety. The triplet at $\delta_H$ 3.16 ppm corresponds to the -$CH_2$ protons closest to the central nitrogen atom, and the triplet signal at $\delta_H$ 3.05 ppm is the -$CH_2$ group adjacent to the quaternary carbon of the pyridine group (*Figure 158*).

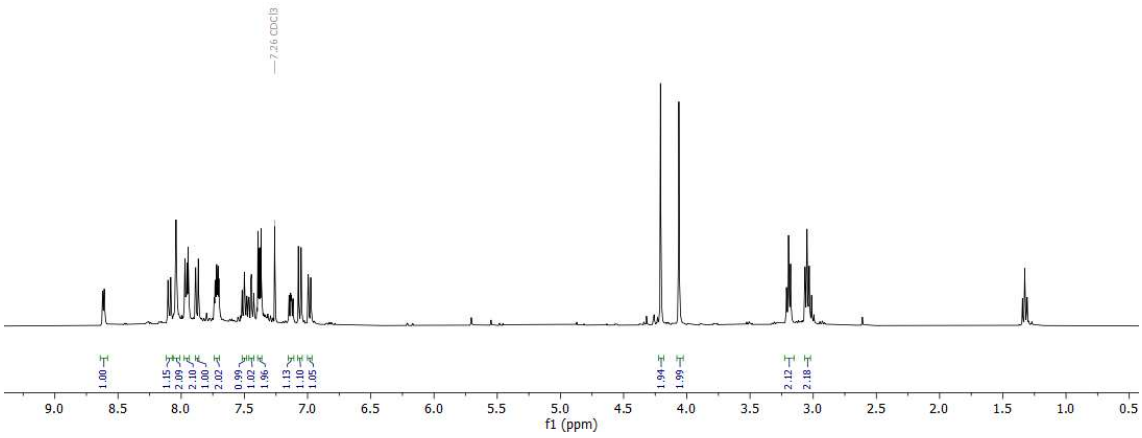


*Figure 158. $^{1}H$ NMR spectrum of the ligand **76** in $CDCl_3$.*

The NMR data obtained have been assigned as completely as possible; however, there are two very broad peaks observed at $\delta_C$ 128.12 and $\delta_C$ 123.61 ppm in the carbon spectrum that show correlation to protons in the HSQC spectrum (*Figure 159*), similar to that observed for the ligand **74**.

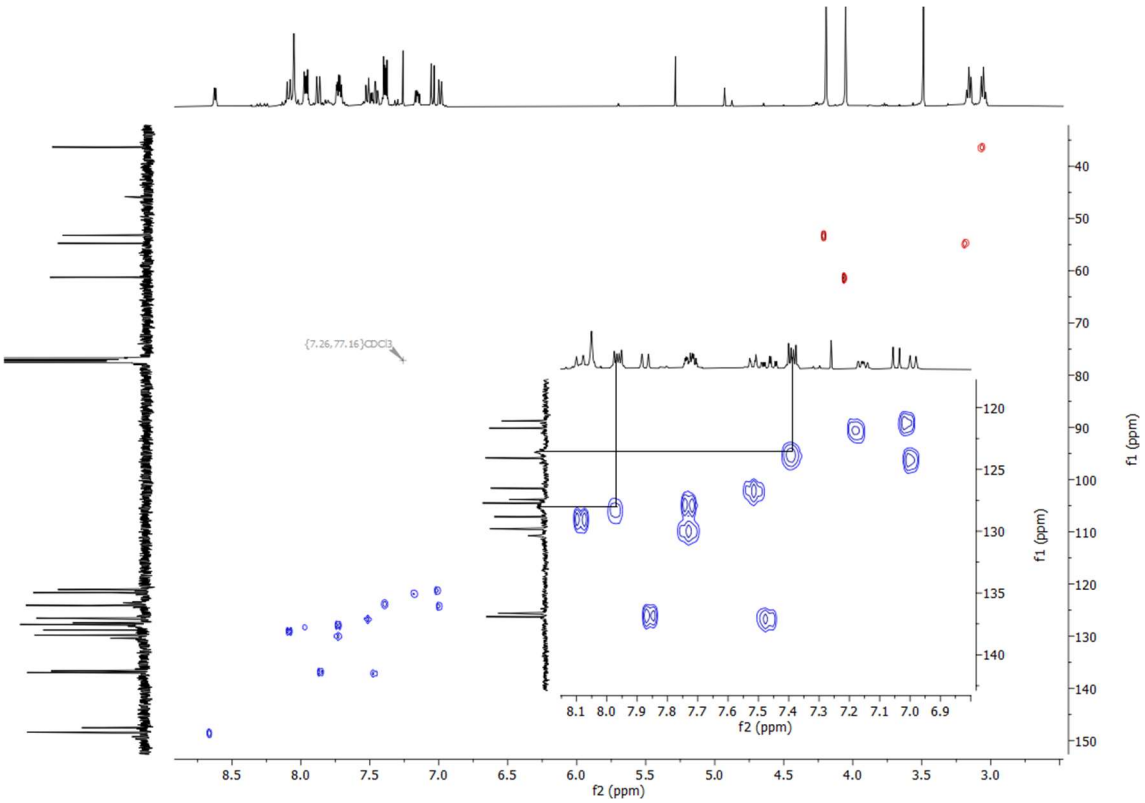


*Figure 159. Key HSQC correlations for the ligand* ***76*** *in* $CDCl_3$.

The HSQC spectrum allows for the approximate assignment of these two carbon signals and thus the corresponding proton signals as being part of the naphthalene moiety.

The observed broadness of the $^{13}C$ signals is consistent with a fluxional process occurring, and therefore the $^{13}C$ NMR was run again at 45 °C. In contrast to **74** above, this resulted in a sharpening of the two broad peaks located at $\delta_C$ 128.12 and $\delta_C$ 123.61 ppm (*Figure 160*). This strongly suggests a fluxional process that appears to only affect a particular region of the molecule. This is indeed unusual, and thus literature precedent was sought.

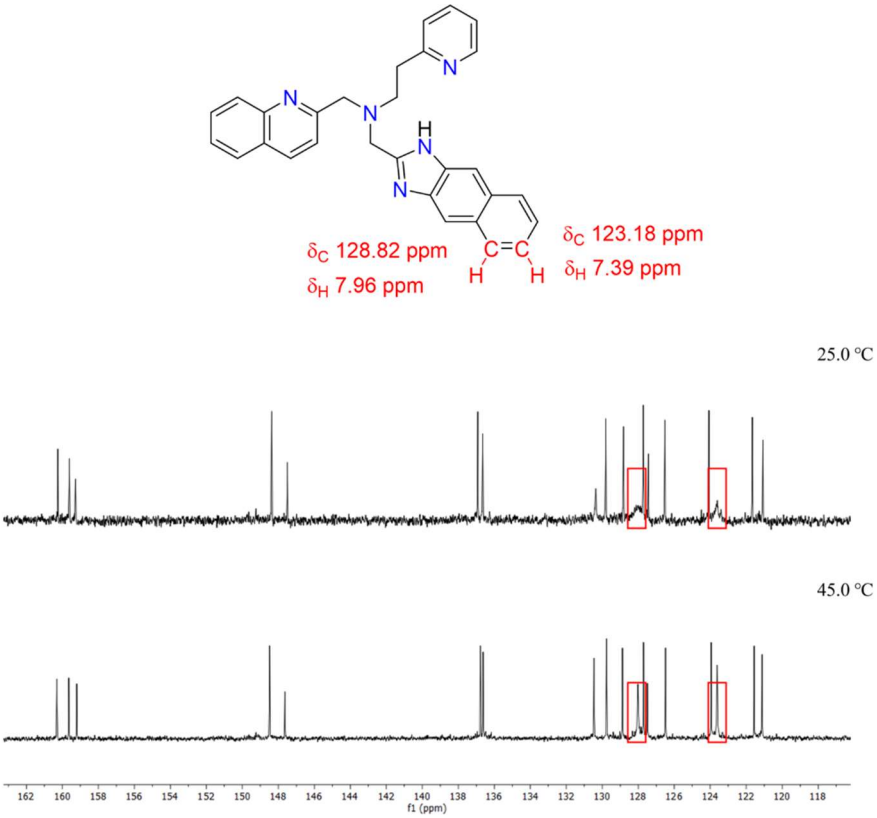


*Figure 160. Variable temperature $^{13}C$ NMR spectra of the ligand **76** over the chemical shift range $\delta_C$ 116–163 ppm in $CDCl_3$.*

The ligand **174**, appears to be one of the only structurally similar molecules to these tripodal imidazole-naphthalene ligands (*Figure 161*). However, the authors of this paper did not report any broad carbon signals in the $^{13}C$ spectrum of this molecule.[513]

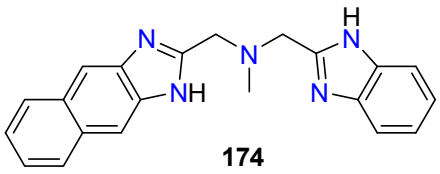

**174**

*Figure 161. Structure of the ligand **174**.*

HRMS analysis of the material revealed a molecular peak at *m/z* = 444.2180 that has been assigned to the free ligand (calcd. for $C_{29}H_{26}N_5$ $[M+H]^+$ 444.21827; found 444.2180). In addition, a peak at *m/z* = 466.1998 can be assigned to the sodiated ligand (calcd. for $C_{29}H_{25}N_5Na^+$ $[M+Na]^+$ *m/z* = 466.2000; *m/z* = found 466.1998).

The ligand **77** was synthesised following a slightly modified procedure of the general method reported above. The reaction of a solution of 2-(chloromethyl)-1*H*-naphtho[2,3-*d*]imidazole hydrochloride **73.HCl** and $Et_3N$ in $CH_2Cl_2$ and a solution of *N*-[(pyridin-2-yl)methyl]-2-(quinolin-2-yl)ethan-1-amine **66**, followed by the addition of a second equivalent of $Et_3N$, affords the title compound **77** (*Scheme 101*). During the synthesis of this naphthalene-containing ligand it was found that an increase in temperature to 40°C was required to yield any product. The structure of **77** was confirmed by NMR spectroscopy ($^1H$, $^{13}C$ and 2D) and HRMS.

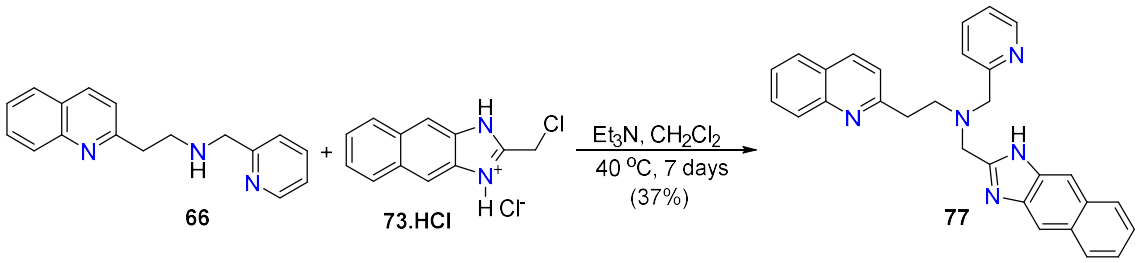


*Scheme 101. The synthesis of the ligand 77.*

The $^1H$ NMR spectrum of **77** revealed two two-proton singlets at $\delta_H$ 4.19 and 3.87 ppm that correspond to the methylene protons of the naphthalene and pyridine groups' alkyl arms, respectively. The ethyl protons from the quinoline moiety are observed in the $^1H$ NMR spectrum as a four-proton unresolved multiplet due to the overlapping triplet signals.

Analysis of **77** by 2D NMR, in particular the HMBC spectrum, revealed the presence of coincident quaternary carbon signals. Overlapping was also observed for two proton signals in the $^1H$ NMR spectrum. As can be seen in *Figure 162*, the carbon signal observed at $\delta_C$ 147.65 ppm, has two correlations to two separate proton signals in the HMBC spectrum. The multiplet at $\delta_H$ 7.95 ppm consists of overlapping signals that correspond to protons located on the naphthalene body. The multiplet at $\delta_H$ 7.74 ppm also is due to overlapping signals that have been assigned to two protons of the quinoline moiety. Thus, the two correlations suggest that a coincidence of two quaternary carbon signals has occurred.

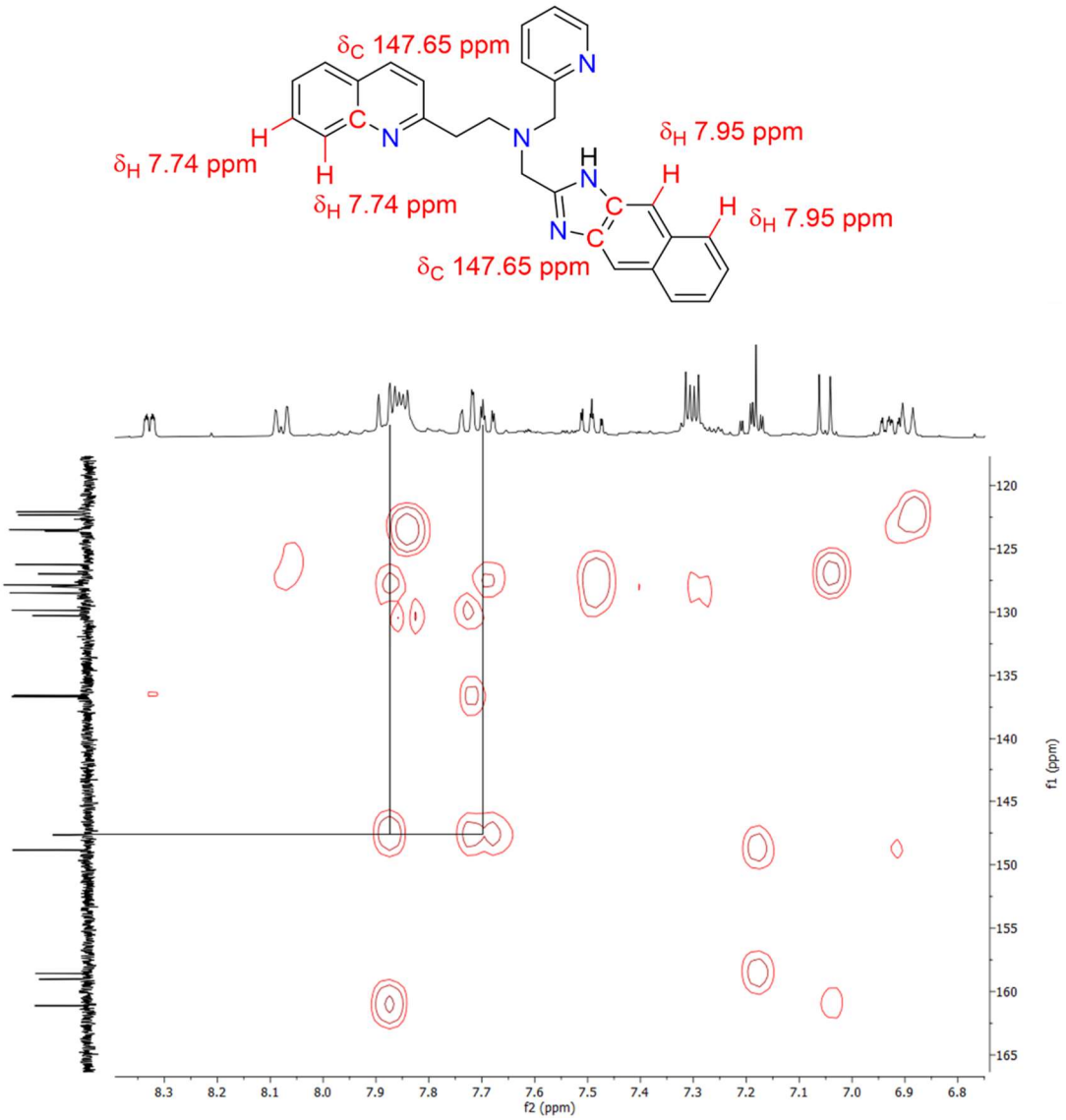


*Figure 162. Key HMBC correlations for the ligand **77** in $CDCl_3$.*

HRMS data further confirmed the successful isolation of **77** with the presence of the molecular ion peak at *m/z* = 444.2179 (calcd. for $C_{29}H_{26}N_5$ $[M+H]^+$ 444.21827; found 444.2179). A peak at *m/z* = 466.1996 is also displayed and this can be assigned to the free ligand with an associated sodium ion (calcd. for $C_{29}H_{25}N_5Na^+$ $[M+Na]^+$ *m/z* = 466.2000; *m/z* = found 466.1996).

While the synthesis of **189** was attempted several times, the desired ligand was not obtained (*Scheme 102*). Given that the quinoline-containing derivative (**63**) was successfully prepared using a similar method, the reasons for the failure of this reaction remain unclear.

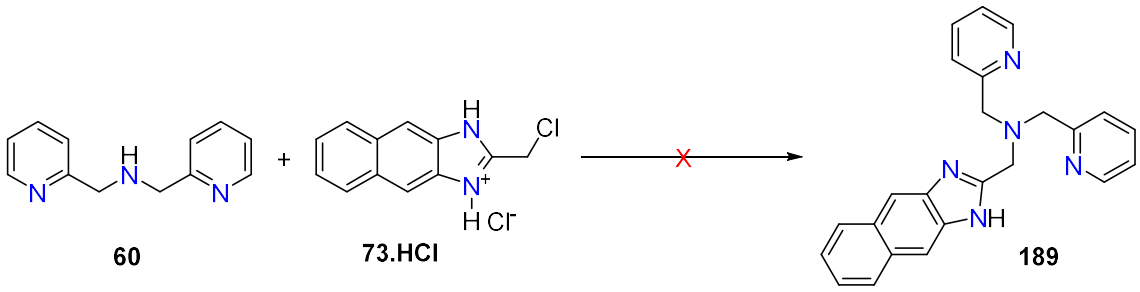


*Scheme 102. Attempted synthesis of the ligand **189**.*

## 6.5 Pyrene-based ligands

Pyrene was discovered in 1837 by Laurent from the residue collected during the distillation of coal tar.[529] Since then, this polycyclic aromatic hydrocarbon has been the subject of many investigations, primarily as a result of its unique photophysical properties, and its incorporation into a variety of ligands has been extensively studied.[530,531]

The synthesis of pyrene-containing ligand frameworks generally requires derivatisation of the molecule. Electrophilic aromatic substitution reactions of pyrene have been extensively studied and several methods for its bromination,[532] nitration,[533] acylation,[534] alkylation,[535] and formylation[536] have been reported. Although numerous preparations have been described, regioselectivity still remains a significant challenge in the substitution chemistry of pyrene.[537–539]

Electrophilic aromatic substitution reactions of pyrene usually introduce substituents at the 1-, 3-, 6-, and 8-positions of the pyrene core, owing to the increased electron density at these sites. Electrophilic substitution can also occur at the 2-, and 7-positions as, although the electron density is lower, the steric hindrance is also lower. Thus, bulkier substituents are easier to introduce here. The lowest activity is observed at the 4-, 5-, 9-, and 10-positions, also referred to as the K-region (*Figure 163*).[540,541]

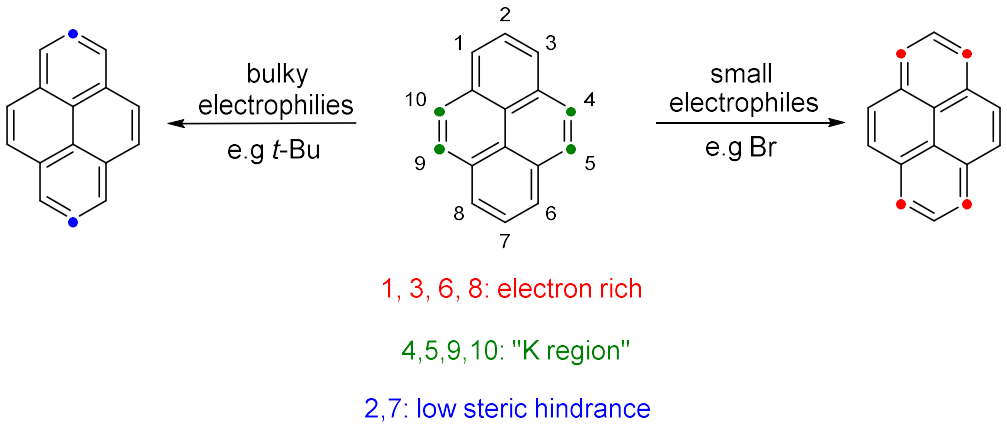


*Figure 163. Potential positions for the electrophilic substitution of pyrene.*

To achieve electrophilic substitution at these positions, the most commonly employed method starts from the Ru(III)-catalysed oxidation of pyrene to afford pyrene-4,5-dione **79**, followed by subsequent reactions for further functionalisation (*Scheme 103*).[542]

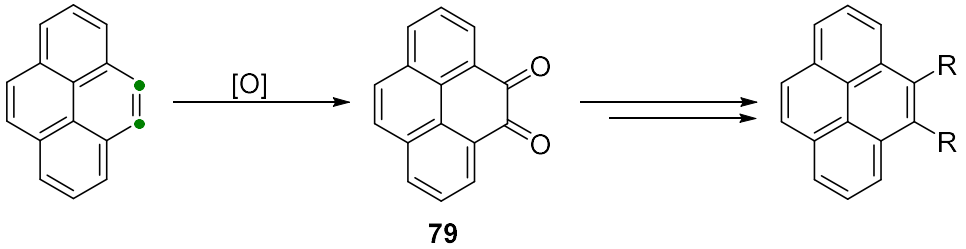


*Scheme 103. Synthetic route for 4-,5-disubstituted pyrenes.*

Pyrene-4,5-dione **79** is an ideal starting material for the synthesis of imidazole-containing pyrenes. For example, the synthesis of **183** (*Scheme 104*) demonstrates the addition of bulky substituents at both the 2- and 7-positions, and the introduction of an imidazole moiety at the 4- and 5-positions. In this instance, the bulky *tert*-butyl groups are initially introduced via a Friedel-Crafts alkylation, followed by subsequent oxidation to afford the substituted pyrene-4,5-dione **184**. The reaction of **184** with *N*-decyl-4-formylbenzamide affords the desired substituted pyreneimidazole **183**.[543]

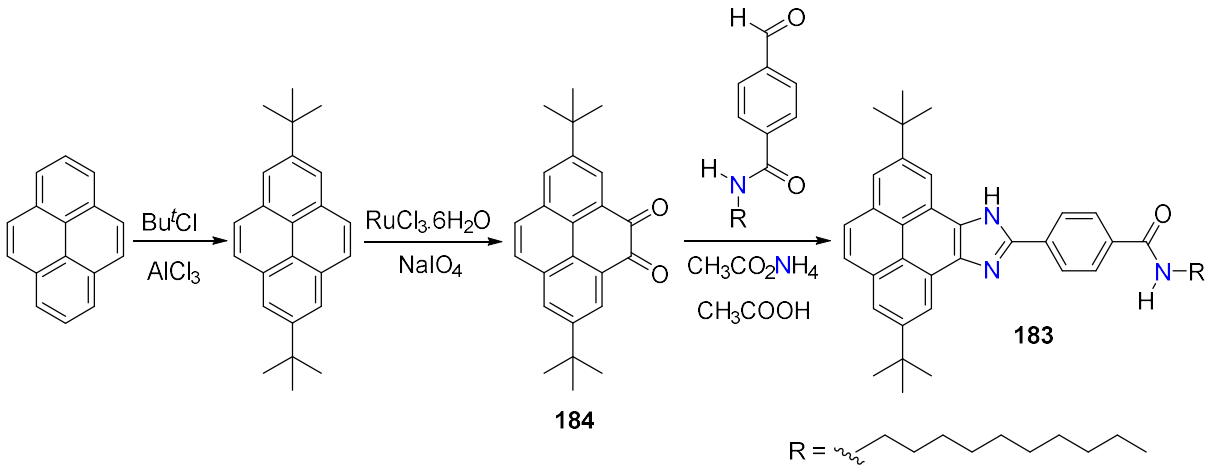


*Scheme 104. Reported synthesis of **183** via 2-,7- and 4-,5-disubstitution of pyrene.*[543]

An example of solely 4-, 5-disubstituion of pyrene is the synthesis of the ligand **185** shown in *Scheme 105*. Initial oxidation to the dione **79** is followed by reaction with pyridine-2-carbaldehyde **186**. The structure of the ligand was chosen for its rigid, conjugated, and planar geometry which provides the molecule with interesting photophysical properties.[544]

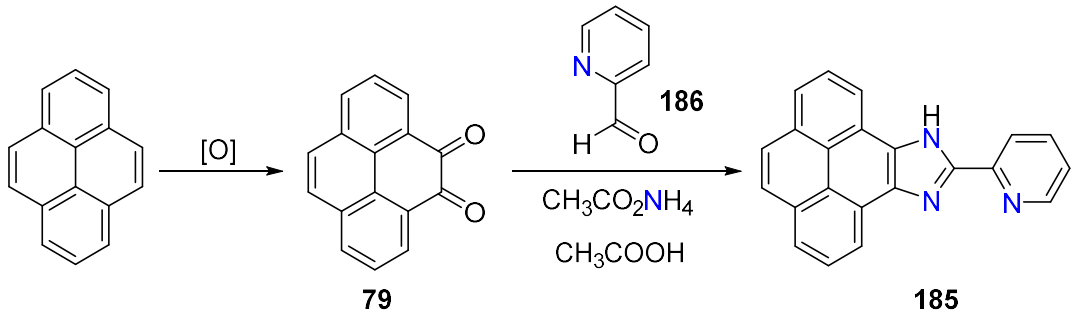


*Scheme 105. Reported synthesis of **185** via a 4-,5-disubstitution of pyrene.*[544]

Ruthenium(II) and osmium(II) complexes containing polyheterocyclic ligands have found an important place in the development of DNA-targeted drugs and sensors due to their excellent photoredox properties. Complexes that contain polycyclic ligands that are capable of DNA binding have been of particular interest due to their potential use in DNA molecule light switches, cellular imaging agents, and therapeutic cancer drugs.[545–547]

An example of this application is the use of the ligand **185** in the design and synthesis of the complex cations $[(bpy)_2M(\mathbf{185})]^{2+}$ (M = Ru, Os; bpy = 2,2'-bipyridine). The ruthenium species is exhibited in *Figure 164*. An important feature of the ligand is the

imidazole moiety, which is structurally related to the purine bases in DNA. In these complex cations, the imidazole unit has been appended to the pyrene moiety in order to investigate the influence of the extended planar surface. Techniques including absorption, emission, excited-state lifetime, circular dichroism, and thermal denaturation were used to study the binding affinities of these cations towards DNA. These experiments revealed the intercalative nature of the complexes towards DNA and also highlighted their light-switch behaviour. The complexes were studied for their anion sensing abilities through a variety of spectroscopic techniques which indicated that both compounds act as "turn-on" luminescence sensors for $H_2PO_4^-$ and "turn-off" sensors toward $F^-$ and $OAc^-$ anions. The imidazole NH plays a key role in each switch with deprotonation occurring after the addition of excess $F^-$ and $OAc^-$ anions, and hydrogen-binding interactions occurring between this proton and $H_2PO_4^-$.[548]

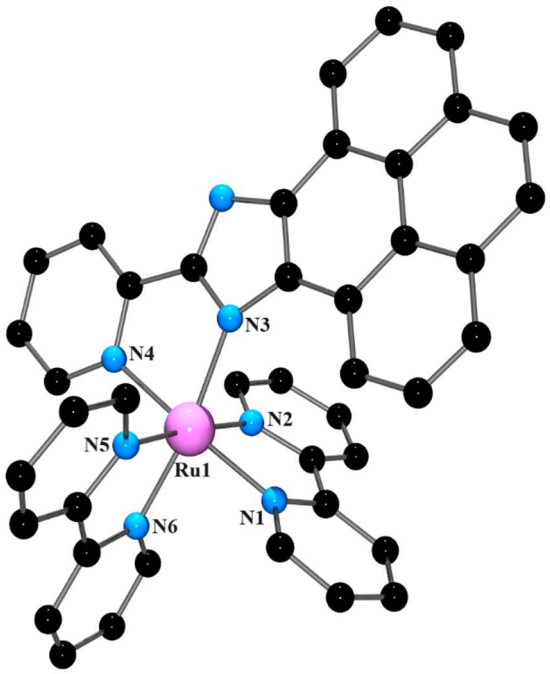


*Figure 164. Structure of the [(bpy)$_2$Ru(**185**)]$^{2+}$cation. H atoms have been omitted for clarity.*

Given the ease with which imidazole can be appended to the pyrene nucleus, we were interested in investigating the incorporation of this moiety into larger, multidentate ligands. Thus, the focus of this section was to prepare the quinoline congener of the ligand **185**.

### 6.5.1 Synthesis of pyrene starting materials and ligand

The initial goal of our studies with pyrene was to make pyrene-4,5-dione **79**, as the starting material for the synthesis of imidazole-appended pyrenes. Following the previously reported preparation,[230] the title compound **79** was prepared from the reaction of pyrene **78**, $RuCl_3.xH_2O$, and $NaIO_4$ in a mixture of $CH_3CN$, $H_2O$, and $CH_2Cl_2$ (1:1.2:1) at room temperature for 18 hours (*Scheme 106*). The mixture was filtered through celite and extracted with $CH_2Cl_2$. The combined organic phases were washed with saturated aqueous $Na_2CO_3$ and $H_2O$, dried over $MgSO_4$, and following filtration the solution was reduced to dryness. The product **79** was obtained as a bright orange solid following purification by silica gel chromatography. The identity of the product was confirmed by NMR spectroscopy and mass spectrometry; these data were consistent with the literature.[230]

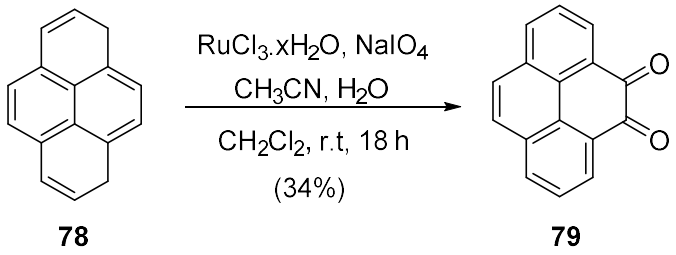


*Scheme 106. The synthesis of pyrene-4,5-dione **79**.*

With the successful isolation of pyrene-4,5-dione **79**, our attention turned to the synthesis of the new quinoline-containing bidentate ligand, **82**, using the Debus-Radziszewski imidazole synthesis (previously described in section 6.2.2), which utilises the condensation reaction between a 1,2-dicarbonyl compound, an aldehyde, and ammonia in a molar ratio of 1:1:2, respectively (*Scheme 107*). The commercial production of several imidazole derivatives employs this methodology. [549]

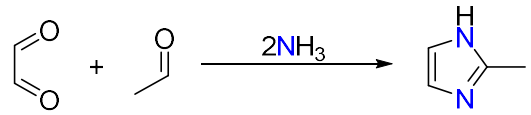


*Scheme 107. Debus-Radziszewski imidazole synthesis.*

Thus, following the slightly modified methodology of the pyridine congener,[544] pyrene-4,5-dione, quinoline-2-carbaldehyde, and ammonium acetate were stirred in refluxing

acetic acid for 6 days (*Scheme 108*). Following the purification by silica gel column chromatography, the title compound was isolated in a poor yield of 12%.

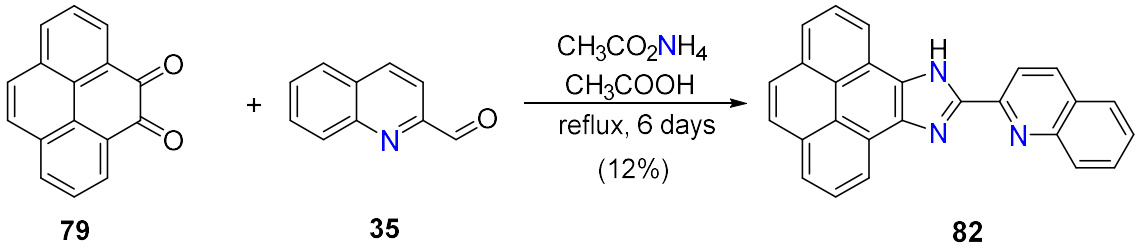


*Scheme 108. The initial synthesis of **82**.*

An alternative synthetic route of higher yield for the synthesis of **82** was therefore sought. Given that imidazole derivatives can be prepared from the reaction between a 1,2-diamine compound and an aldehyde,[550] (for example, the reaction between benzene-1,2-diamine **169** and benzaldehyde **190** affords the compound, 2-phenyl-1*H*-benzimidazole **191** (*Scheme 109*)).[551] It was envisioned that **82** could be obtained in a similar approach from the reaction of 4,5-diaminopyrene **81** and quinoline-2-carbaldehyde **35**.

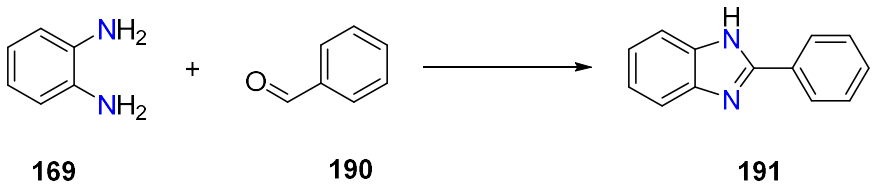


*Scheme 109. Reported synthesis of **191**.*[551]

Such an approach required the synthesis of the diamine starting material **81**. This can be prepared from **79** in two steps, the first being synthesis of **80**, and the second being reduction of this to afford the desired product.

Following a previously published method,[231] **80** was prepared from the reaction of pyrene-4,5-dione **79** and hydroxylamine hydrochloride in EtOH, in the presence of $BaCO_3$, with stirring at reflux for 36 hours (*Scheme 110*). The crude reaction mixture was reduced to dryness and 0.2 M HCl was added to the resulting solid. Filtration of the mixture and subsequent washings afforded the desired compound **80** without further purification required. Analysis by $^1$H NMR spectroscopy and mass spectrometry gave data consistent with those reported in the literature.[231]

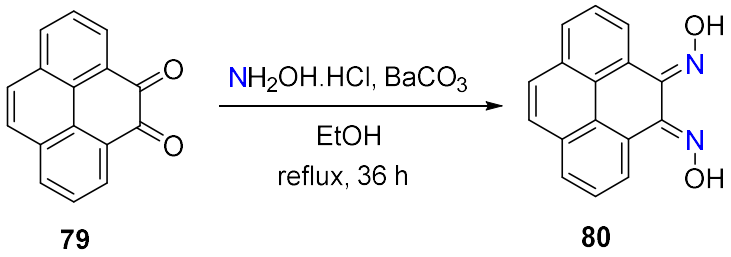


79 80

*Scheme 110. The synthesis of **80**.*

The compound **80** was then reacted with hydrazine in refluxing EtOH for 18 hours, the reaction being catalysed by 10%-Pd/C (*Scheme 111*). Following the removal of the reaction solvent (roatvap), the resulting residue was triturated in water, and following filtration, the desired product **81** was obtained as a green solid.

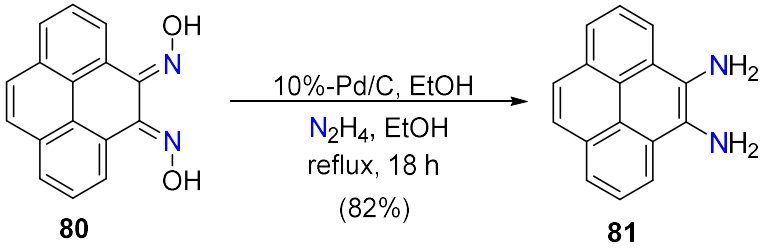


80 81

*Scheme 111. The synthesis of **81**.*

Confirmation of the structure of **81** was obtained by $^{1}$H NMR spectroscopy and mass spectrometry which gave data that are consistent with the literature.[231] As can be seen in *Figure 165*, the $^{1}$H NMR spectrum reveals a four-proton singlet at $\delta_H$ 5.21 ppm which corresponds to the newly installed -$NH_2$ groups. The synthesis of **81** was further confirmed by $^{13}$C NMR spectroscopy and mass spectrometry, with the data from both consistent with those previously described in the literature.[231]

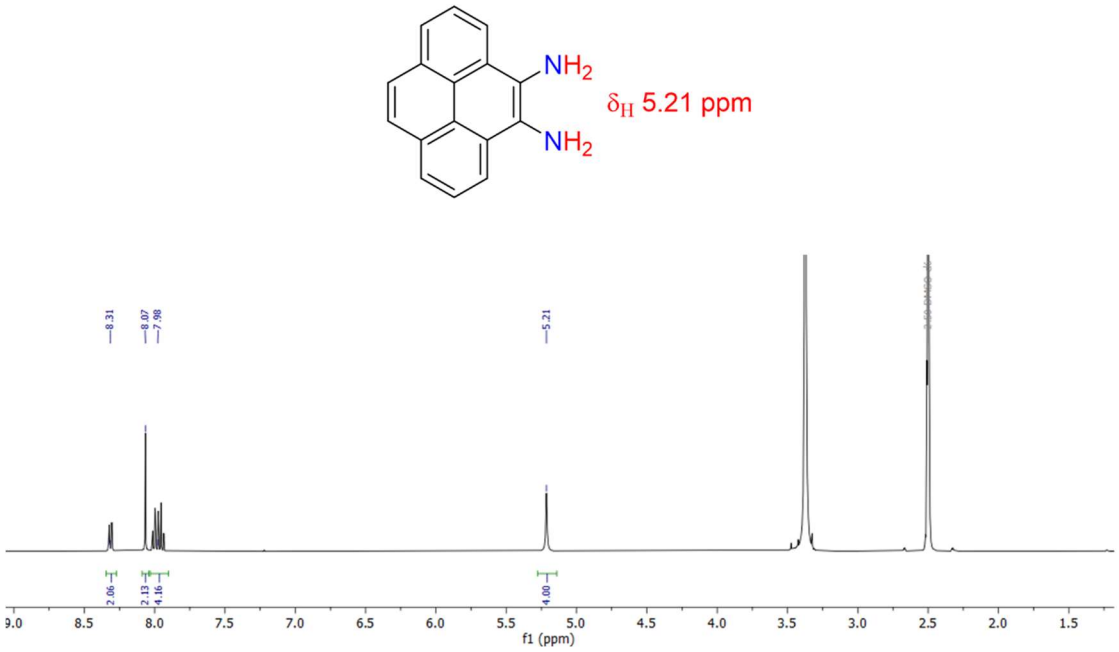


*Figure 165. $^{1}H$ NMR spectrum of **81** in $CDCl_3$.*

With the successful isolation of **81**, the next step was the reaction with quinoline-2-carbaldehyde **35** in attempts to isolate and increase the yield of the bidentate ligand (**82**).

Having this starting material in hand, we were also interested to see if the ligand **192** could be synthesised from the reaction of **81** with 2 equivalents of quinoline-2-carbaldehyde **35**, followed by the subsequent reduction with $NaBH_4$ (*Figure 166*).

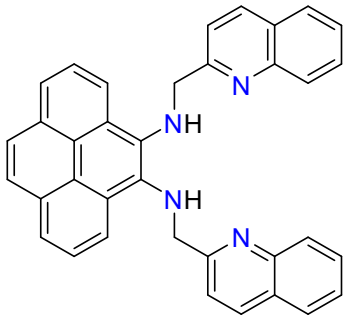


*Figure 166. Structure of **192**.*

However, from this reaction the ligand **82** was isolated instead. Therefore, from the reaction of **81** and quinoline-2-carbaldehyde **35**, followed by the addition of $NaBH_4$, in stirring in MeOH at room temperature for 16 hours, the ligand **82** was obtained in moderate yield (44%) without futher purification (*Scheme 112*).

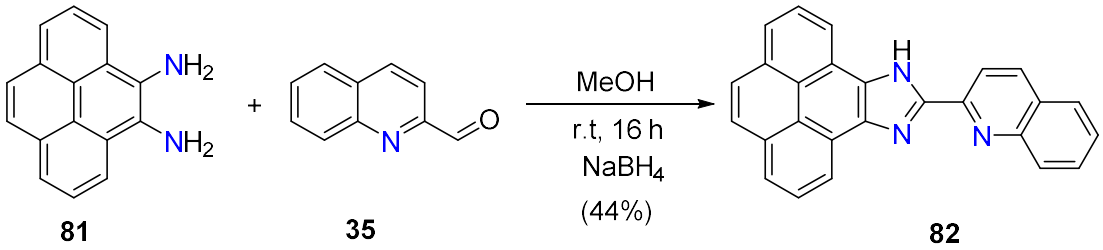


*Scheme 112. The synthesis of the ligand **82**.*

The ligand **82** was characterised by $^{1}H$ and $^{13}C$ NMR spectroscopy and high resolution mass spectrometry. Confirmation of the structure was obtained from the HRMS spectrum (*Figure 167*) which displayed a clear base peak at *m/z* = 370.1339 and this can be assigned to the free ligand (calcd. for $C_{26}H_{16}N_3^+$ $[M+H]^+$ *m/z* = 370.13387; *m/z* = found 370.1339). Another signal is present at *m/z* = 392.1159 and this can be assigned to the sodiated ligand (calcd. for $C_{26}H_{15}N_3Na^+$ $[M+Na]^+$ *m/z* = 392.1160; found *m/z* = 392.1159). In addition, a peak with approximately 7-fold less abundance in comparison to the signal at *m/z* = 370.1339, is displayed at *m/z* = 739.2601. This signal can be assigned to the protonated free ligand in which an additional ligand has become associated, presumably via π-stacking interactions (calcd. for $C_{52}H_{31}N_6^+$ $[M+H]^+$ *m/z* = 739.2600; found *m/z* = 739.2601).

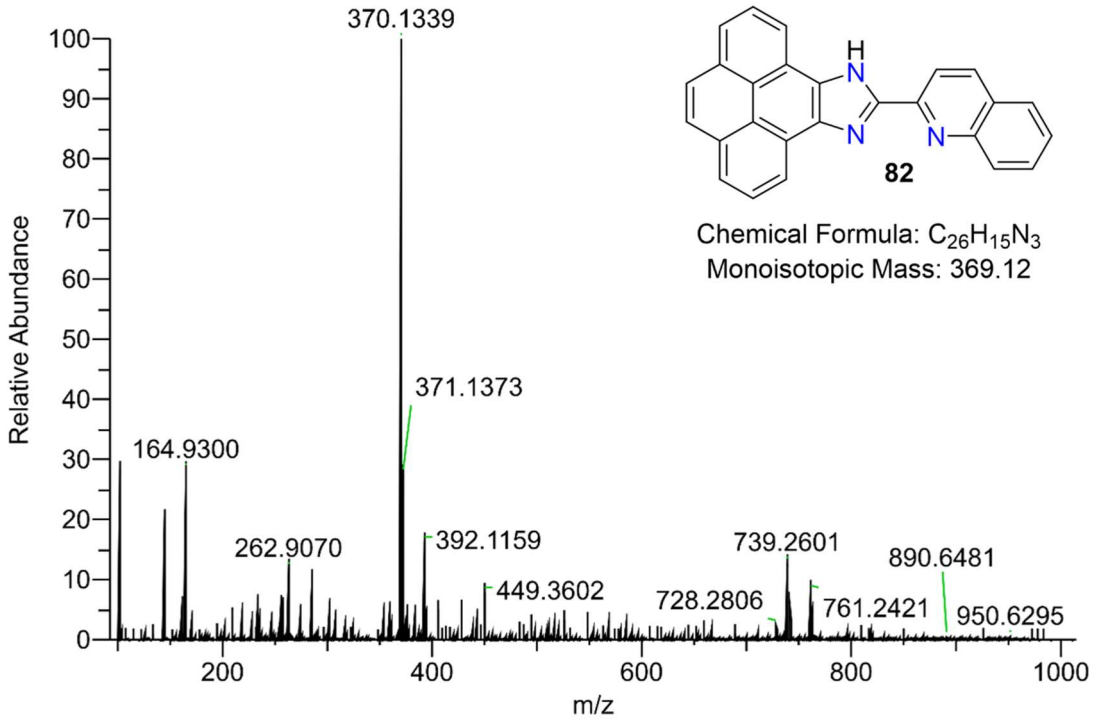


*Figure 167. HRMS spectrum of the ligand **82** recorded in $CH_3CN$.*

Unfortunately, well-resolved $^{1}H$ and $^{13}C$ NMR spectra (DMSO-$d_6$) could not be obtained, presumably partly due to the poor solubility of **82** not only in DMSO but in the majority of the deuterated solvents available. The $^{1}H$ spectrum displayed signals that integrated correctly for the expected number of protons; however, there are two very broad one-proton singlets at $\delta_H$ 9.18 and 8.91 ppm which could not be reasonably assigned (*Figure 168*). There is also a number of quaternary carbon atoms present in this molecule and their low intensity makes them difficult to observe in the $^{13}C$ NMR spectrum.

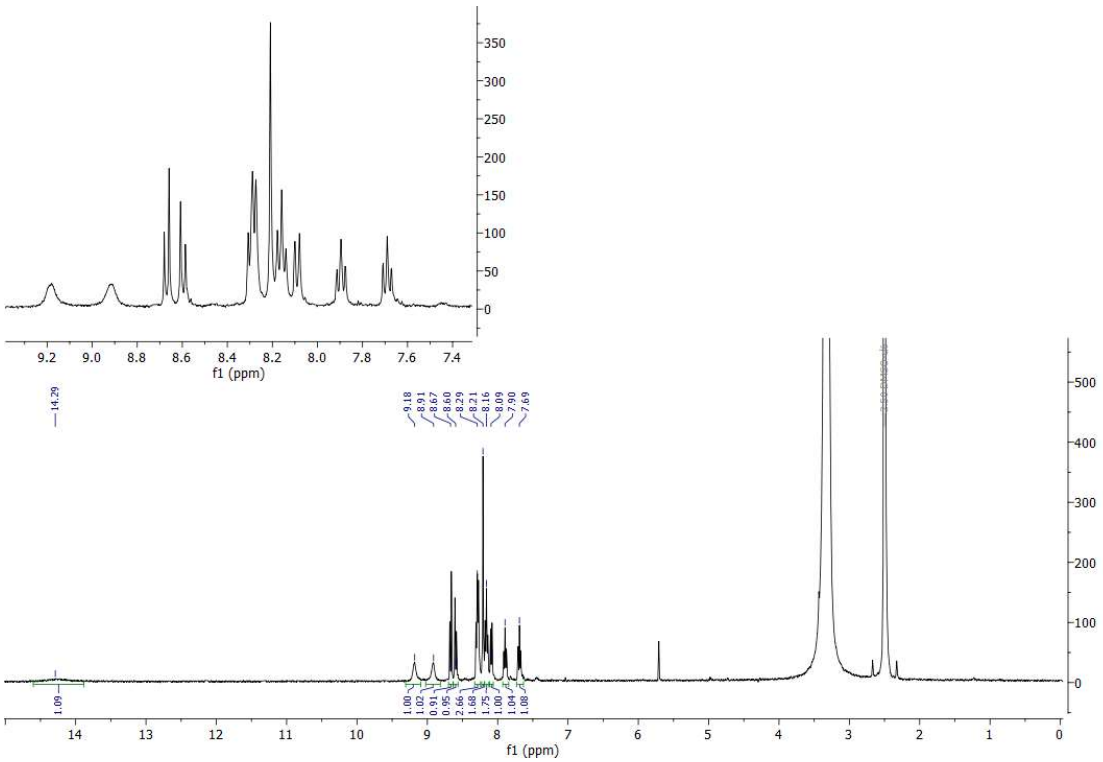


*Figure 168. $^{1}H$ NMR spectrum of the ligand **82** in DMSO-$d_6$.*

The $^{13}C$ NMR shows a relatively noisy spectrum and reveals only 11 carbon signals when 26 would be expected for this ligand. In addition, the broad singlets show no correlations in both the HSQC and HMBC spectra, and reasons for this remain unclear (*Figure 169*).

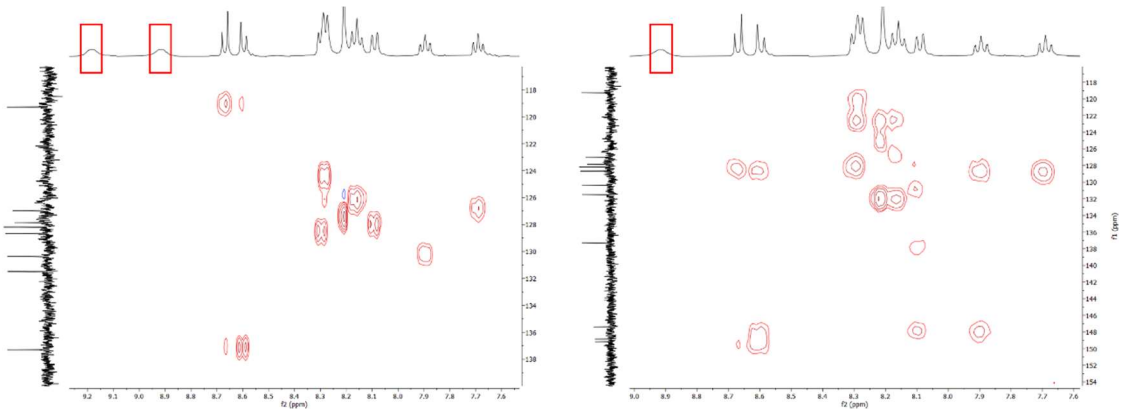

*Figure 169. Key HSQC correlations (left) and HMBC correlations (right) for the ligand **82** in DMSO-$d_6$.*

## 6.6 The characterisation of transition metal complexes containing naphthalene and pyrene-based ligands

This section describes the characterisation of transition metal complexes of the ligands discussed above. Analogous to the quinolyl-containing ligands, various attempts were made to produce single-crystal samples suitable for structural analysis via single-crystal X-ray diffraction. However, no X-ray quality crystals were obtained from the many crystallisation attempts in this work. Thus, again it was necessary to resort to alternative solution-state characterisation methods for these complexes. In this instance, mass spectrometry was utilised (see section 5.2.1).

### 6.6.1 Solution Studies

The solutions were prepared according to the methods described in *Chapter Two* section 2.3.1. All the experiments were conducted in $CH_3CN$. The mass spectrometry data were collected as described in *Chapter Two* section 2.3.1. Low resolution mass spectrometry was obtained for this series of experiments. Each experiment was repeated a minimum of two times with freshly prepared solutions, and reproducible results were obtained.

The mass spectra were obtained from solutions that had been made up by mixing a solution of the metal ion with one, two, and three equivalents of ligand. The complex solutions were mixed and allowed to stand at room temperature for 30 minutes before each sample was directly injected into the mass spectrometer for analysis.

The peaks that correspond to a metal ion-containing species were assigned, in part, using the specific isotope pattern of each metal ion (see section 5.2.1). Determination of the ion charge from the mass spectrum can be achieved using the spacing between the isotopomeric peaks within the isotope pattern for the ion (see section 5.2.1).

### 6.6.2 Naphthalene-containing ligands

**Ligand 75**

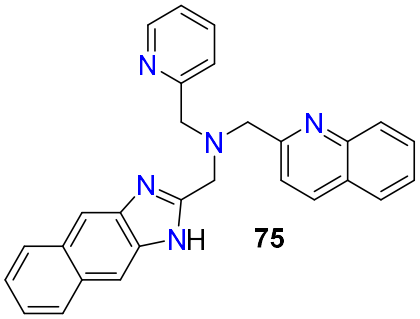


**75**

Chemical Formula: $C_{28}H_{23}N_5$
Monoisotopic Mass: 429.19

The mass spectrum of the free ligand **75** displays one product ion peak at *m/z* = 430.4. No other notable peaks corresponding to any ligand fragmentation are observed. The addition of 1 equivalent of $[Cu(OH_2)_6](ClO_4)_2$ affords a mass spectrum that displays peaks due to copper-containing species at *m/z* = 349.0, 491.0, 527.0 537.0, and 591.0.

The most intense copper-containing signal at *m/z* = 491.0 can be assigned to the mononuclear 1:1 complex $[Cu(\mathbf{75})]^+$ (calcd. for $CuC_{28}H_{22}N_5^+$ $[M–H]^+$ *m/z* = 491.11; found *m/z* = 491.0). As can be seen in *Figure 170*, the presence of copper can be confirmed from the observed isotope pattern. The observed *m/z* value is consistent with deprotonation of the imidazole N-H.

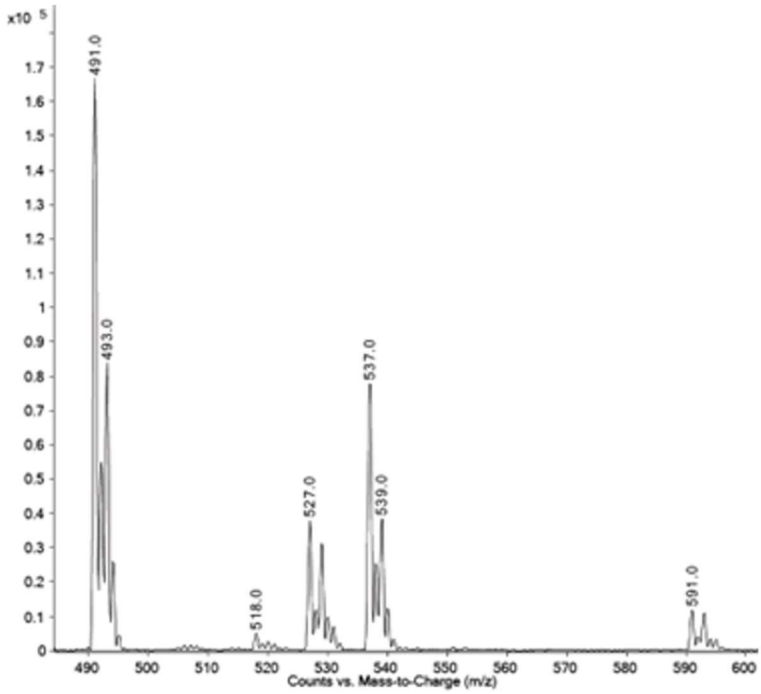


*Figure 170. Key copper-containing signals displayed in the mass spectrum of an equimolar solution of **75** and $[Cu(OH_2)_6](ClO_4)_2$.*

The signal observed at *m/z* = 527.0 corresponds to the formula $[Cu(\mathbf{75})Cl]^+$ in which the 1:1 complex includes a chloride ion (calcd. for $CuC_{28}H_{23}N_5Cl^+$ $[M]^+$ *m/z* = 527.09; found *m/z* = 527.0). With both Cu and Cl present, the isotope pattern for this signal is different from those assigned as containing only Cu. The signal at *m/z* = 537.0 can be assigned to $[Cu(\mathbf{75})(HCOO)]^+$ (calcd. for $CuC_{29}H_{24}N_5O_2^+$ $[M]^+$ *m/z* = 537.12; found *m/z* = 537.0). For this species, it appears that the Cu(II)-**75** complex has bound a negatively charged formate ion, which is used in the calibration of the instrument. The signal at *m/z* = 591.0 can be assigned to $[Cu(\mathbf{75})(ClO_4)]^+$ in which the 1:1 species has the inclusion of an associated perchlorate ion (calcd. for $CuC_{28}H_{23}N_5ClO_4^+$ $[M]^+$ *m/z* = 591.07; found *m/z* = 591.0). The observed isotope pattern is consistent with the presence of both Cu and Cl ions. The 1+ charge on the complex ion confirms that the metal centre has not undergone reduction. The addition of a second and third equivalents of ligand results in the appearance of a new signal at *m/z* = 430.1, corresponding to the free ligand **75**.

The mass spectra of a solution of $[Co(OH_2)_6](ClO_4)_2$ to which 1, 2, and 3 equivalents of ligand **75** have been added show signals at *m/z* = 244.0, 487.0, 523.0, 533.0, and 587.0. A signal observed at *m/z* = 430.0 corresponding to the free ligand is not apparent until the third equivalent of the ligand solution is added.

The peak at *m/z* = 487.0 corresponds to the mononuclear 1:1 Co(II) complex, $[Co(\mathbf{75})]^+$ (calcd. for $CoC_{28}H_{22}N_5^+$ $[M]^+$ *m/z* = 487.12; found *m/z* = 487.0). For this species, *z* = 1 and in this case, the loss of a proton, presumably from the imidazole NH, affords the overall 1+ charge. The peaks at *m/z* = 523.0, 533.0, and 587.0 can be assigned to the mononuclear 1:1 Co(II) complexes, $[Co(\mathbf{75})(X)]^+$, where X = $Cl^-$, $HCOO^-$, and $ClO_4^-$, respectively (calcd. for $CoC_{28}H_{23}N_5Cl^+$ $[M]^+$ m*/z* = 523.09; found *m/z* = 523.0; calcd. for $CoC_{29}H_{24}N_5O_2^+$ *m/z* = 533.12; found *m/z* = 533.0; calcd. for $CoC_{28}H_{23}N_5ClO_4^+$ $[M]^+$ *m/z* = 587.07, found *m/z* = 587.0). The signal observed at *m/z* = 244.0 can be assigned to the 1:1 2+ Co(II) complex, $[Co(\mathbf{75})]^{2+}$ (calcd. for $CoC_{28}H_{23}N_5^+$ $[M]^{2+}$ *m/z* = 244.06; found *m/z* = 244.0).

The most intense signal observed in the mass spectrum of an equimolar solution of **75** and $[Ni(OH_2)_6](ClO_4)_2$ (*Figure 171*) is at *m/z* = 243.5 and can be assigned to the corresponding 2+ Ni(II) species, $[Ni(\mathbf{75})]^{2+}$ (calcd. for $NiC_{28}H_{23}N_5^{2+}$ $[M]^{2+}$ *m/z* = 243.56; found *m/z* = 243.5). Two additional nickel-containing peaks are observed at *m/z* = 532.1 and 586.0 that can be assigned to the Ni(II) complexes, $[Ni(\mathbf{75})(HCOO)]^+$ and $[Ni(\mathbf{75})(ClO_4]^+$, respectively (calcd. for $NiC_{29}H_{24}N_5^+$ $[M]^+$ *m/z* = 532.12; found *m/z* = 532.1; calcd. for $NiC_{28}H_{23}N_5ClO_4^+$ $[M]^+$ *m/z* = 586.07; found *m/z* = 586.0). Upon the addition of a second and third equivalents of the ligand solution, no new peaks are revealed and an increase in the relative abundance of the present peaks is observed.

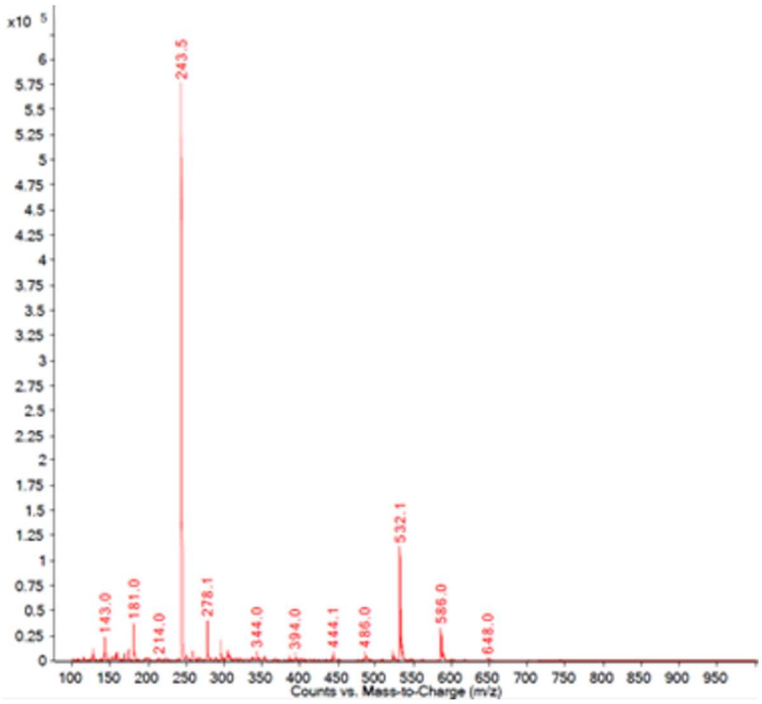


*Figure 171. The mass spectrum of an equimolar solution of **75** and $[Ni(OH_2)_6](ClO_4)_2$.*

The mass spectrum obtained from the addition of 1 equivalent of **75** to a solution $[Zn(OH_2)_6](ClO_4)_2$ exhibits an intense peak at *m/z* = 246.6. The peak shows an isotope pattern that indicates the corresponding species contains zinc and the spacing of the peaks reveals the ion to be of a 2+ charge. This can be assigned to the Zn(II) complex, $[Zn(\mathbf{75})]^{2+}$ (calcd. for $ZnC_{28}H_{23}N_5^{2+}$ $[M]^+$ *m/z* = 246.56; found *m/z* = 246.6). The peak with the second highest intensity has m*/z* = 538.0 and can be assigned to the species, $[Zn(\mathbf{75})(HCOO)]^+$ (calcd. for $ZnC_{29}H_{24}N_5O_2^+$ $[M]^+$ *m/z* = 538.12; found *m/z* = 538.0), where the 1:1 mononuclear complex includes an associated formate ion. Three other signals also display an isotope pattern that indicates the presence of zinc, and these appear at *m/z* = 492.0, 528.0, and 592.0. The signal at *m/z* = 492.0 can be assigned to the mononuclear 1:1 complex, $[Zn(\mathbf{75})]^+$ (calcd. for $ZnC_{28}H_{22}N_5^+$ $[M]^+$ *m/z* = 492.11; found *m/z* = 492.0), and indicates the loss of a proton from the ligand. The signals at *m/z* = 528.0 and 592.0 can be assigned to the Zn(II) 1:1 complexes that contain either an associated chloride or perchlorate ion, corresponding to $[Zn(\mathbf{75})(Cl)]^+$ and $[Zn(\mathbf{75})(ClO_4)]^+$, respectively (calcd. for $ZnC_{28}H_{23}N_5Cl^+$ $[M]^+$ *m/z* = 528.09; found *m/z* = 528.0; calcd. for $ZnC_{28}H_{23}N_5ClO_4^+$ $[M]^+$ *m/z* = 592.07; found *m/z* = 592.0). On addition of a second equivalent of the ligand, the ratio of free ligand to bound increases and there are no new peaks formed. This trend continues with the addition of the third equivalent of **75**.

The mass spectrum obtained from the addition of the ligand **75** to a solution of $[Mn(OH_2)_6](ClO_4)_2$ is not as clean compared to the spectra of the other metal ions (*Figure 172*). The addition of 1 equivalent of the ligand to the manganese metal ion solution reveals a spectrum that displays signals at *m/z* = 181.0, 215.6, 250.1, and the free ligand signal at 430.1. The signal at *m/z* = 215.6 can be assigned to the diprotonated free ligand species (calcd. for $C_{28}H_{25}N_5^{2+}$ $[M]^{2+}$ *m/z* = 215.60; found *m/z* = 215.6), which is not observed in any other mass spectra of this ligand **75**.

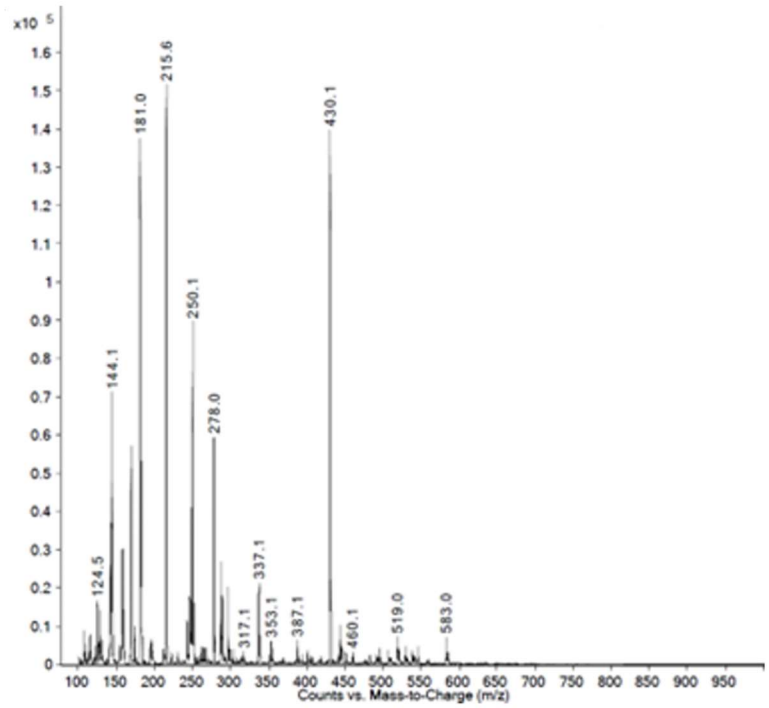


*Figure 172. The mass spectrum of an equimolar solution of **75** and $[Mn(OH_2)_6](ClO_4)_2$.*

Interestingly, the relative abundance of the signal at *m/z* = 181.0 is significant and this can be assigned to the sodiated naphthalene-2,3-diamine ligand fragment ion **72.Na** (calcd. for $C_{10}H_{10}N_2Na^+$ $[M+Na]^+$ *m/z* = 181.07; found *m/z* = 181.1). This is unusual as this ligand fragment is not seen in the mass spectrum of the free ligand suggesting that the metal ion potentially plays a role in catalysing the degradation of **75**. While this signal has been observed in the mass spectra obtained from the reaction between **75** and the other metal ions, it is of very low intensity.

**Ligand 76**

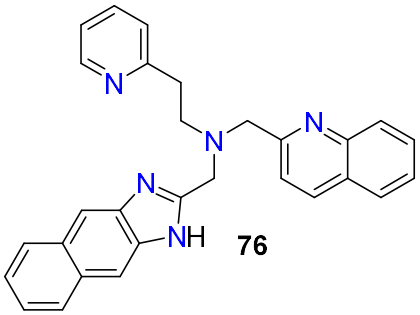


**76**

Chemical Formula: $C_{29}H_{25}N_5$
Monoisotopic Mass: 443.21

The signal that corresponds to the free ligand **76** appears at *m/z* = 444.4 in the mass spectrum obtained from a solution of **76**. The addition of 1 equivalent of ligand to a solution of $[Cu(OH_2)_6](ClO_4)_2$ affords a mass spectrum that displays three copper-containing peaks at *m/z* = 605.0, 543.0 and 505.1. The peak of the highest intensity is observed at *m/z* = 505.1 and corresponds to the 1:1 mononuclear species, $[Cu(\mathbf{76})]^+$ (calcd. for $CuC_{29}H_{24}N_5^+$ $[M]^+$ *m/z* = 505.13; found *m/z* = 505.1). The peaks at *m/z* = 605.0 and 543.0 are of significantly less intensity than the peak at *m/z* = 505.1. The signal at *m/z* = 605.0 can be assigned to the species $[Cu(\mathbf{76})(ClO_4)]^+$ (calcd. for $CuC_{29}H_{25}N_5ClO_4^+$ $[M]^+$ *m/z* = 605.08; found *m/z* = 605.0), and the signal at *m/z* = 543.0 corresponds to the 1:1 complex which includes an associated chloride ion, $[Cu(\mathbf{76})(Cl)]^+$ (calcd. for $CuC_{29}H_{25}N_5Cl^+$ $[M]^+$ *m/z* = 541.10; found *m/z* = 541.0). Upon the addition of a second and third equivalents of ligand, the signal assigned to the free ligand at *m/z* = 444.4 becomes present in the mass spectrum.

A solution of equimolar amounts of $[Co(OH_2)_6](ClO_4)_2$ and ligand **76** affords a mass spectrum that has the three most intense signals at *m/z* = 251.1, 547.1, and 601.1 in the mass spectrum (*Figure 173*). The peak at *m/z* = 251.1 can be assigned to the 1:1 mononuclear cobalt-containing species, $[Co(\mathbf{76})]^{2+}$ (calcd. for $CoC_{29}H_{25}N_5^{2+}$ $[M]^{2+}$ *m/z* = 251.07; found *m/z* = 251.1). In contrast to the analogous species observed for **75** where the complex ion has a 1+ charge, in this case there is no loss of a proton from the ligand and the metal ion remains in a 2+ oxidation state affording an overall 2+ charge on the complex ion.

The peaks at *m/z* = 547.0 and 601.1 can be assigned to the Co(II) 1:1 complexes that contain either an associated formate or perchlorate ion, corresponding to the complex

formulae $[Co(\mathbf{76})(HCOO)]^+$ and $[Co(\mathbf{76})(ClO_4)]^+$, respectively (calcd. for $CoC_{29}H_{25}N_5Cl^+$ $[M]^+$ *m/z* = 547.14; found *m/z* = 547.1; calcd. for $CoC_{29}H_{25}N_5ClO_4^+$ $[M]^+$ *m/z* = 601.09; found *m/z* = 601.1). A signal at *m/z* = 444.4 corresponding to the free ligand appears and increases in intensity upon the addition of a second and third equivalents of the ligand.

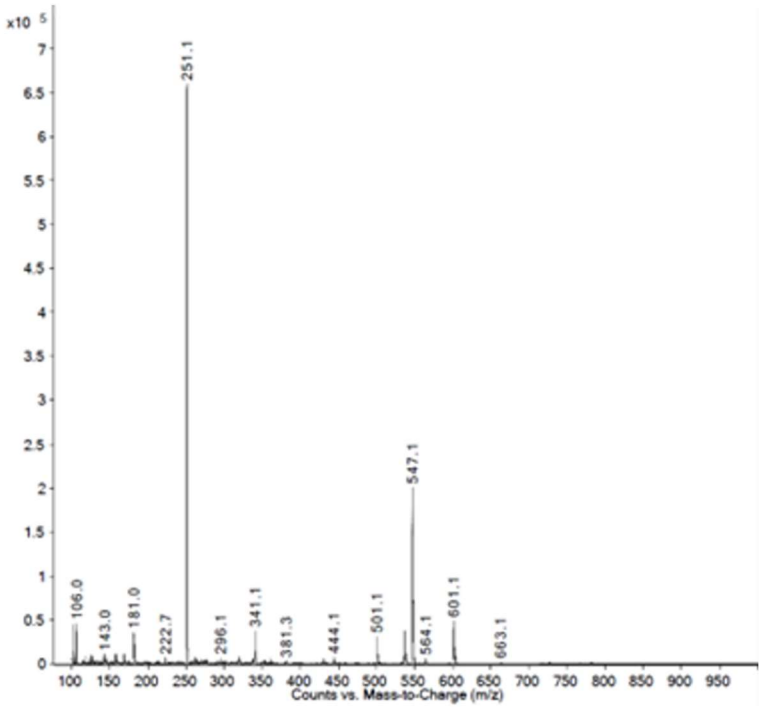


*Figure 173. The mass spectrum of an equimolar solution of the ligand **76** and $[Co(OH_2)_6](ClO_4)_2$.*

The mass spectrum of a solution of $[Ni(OH_2)_6](ClO_4)_2$ to which 1 equivalent of **76** has been added shows peaks at *m/z* = 600.0, 546.1, and 250.6. The latter can be assigned to the Ni(II) complex ion $[Ni(\mathbf{76})]^{2+}$ (calcd. for $NiC_{29}H_{25}N_5^{2+}$ $[M]^{2+}$ *m/z* = 250.57; found *m/z* = 250.6). The signals at *m/z* = 546.1 and 600.0 can be assigned to the complex species $[Ni(\mathbf{76})(HCOO)]^+$ and $[Ni(\mathbf{76})(ClO_4)]^+$ (calcd. for $NiC_{30}H_{26}N_5O_2^+$ $[M]^+$ *m/z* = 546.14; found *m/z* = 546.1; calcd. for $NiC_{29}H_{25}N_5ClO_4^+$ $[M]^+$ *m/z* = 600.09; found *m/z* = 600.0). The addition of a second and third equivalents of ligand resulted in the appearance of the free ligand peak at *m/z* = 444.4, and the increase in intensity of the 1:1 complex that has an associated formate moiety.

The mass spectra of a solution of $[Zn(OH_2)_6](ClO_4)_2$ to which 1, 2, and 3 equivalents of ligand **76** have been added reveals peaks at *m/z* = 606.0, 552.0, 542.0, 506.0, 444.1 (free ligand **76**), 339.1, 253.6, 222.6 and 181.1. The complex species $[Zn(\mathbf{76})(ClO_4)]^+$,

$[Zn(\mathbf{76})(HCOO)]^+$, and $[Zn(\mathbf{76})(Cl)]^+$ can be assigned to the signals at *m/z* = 606.0, 552.0, and 542.0, respectively (calcd. for $ZnC_{29}H_{25}N_5ClO_4^+$ $[M]^+$ *m/z* = 606.08; found *m/z* = 606.0; calcd. for $ZnC_{30}H_{26}N_5O_2^+$ $[M]^+$ *m/z* = 552.13; found *m/z* = 552.0; and calcd. for $ZnC_{29}H_{25}N_5Cl^+$ $[M]^+$ *m/z* = 542.10; found *m/z* = 542.0). The signal displayed at *m/z* = 253.6 corresponds to the 2+ Zn(II) complex ion, $[Zn(\mathbf{76})]^{2+}$ (calcd. for $ZnC_{29}H_{25}N_5^{2+}$ $[M]^{2+}$ *m/z* = 253.57; found *m/z* = 253.6). The ligand fragment that corresponds to the loss of the pyridyl group can be assigned to the signal observed at *m/z* = 339.1. The diprotonated free ligand can be assigned to the signal displayed at *m/z* = 222.6, where *z* = 2 (calcd. for $C_{29}H_{25}N_5^{2+}$ $[M+2H]^{2+}$ *m/z* = 222.10; found *m/z* = 222.6).

In addition, the signal at *m/z* = 181.0 is also observed when this ligand is reacted with $[Zn(OH_2)_6](ClO_4)_2$. Again, this signal has been identified to correspond to the sodiated naphthalene-2,3-diamine ligand fragment (calcd. for $C_{10}H_{10}N_2Na^+$ $[M+Na]^+$ *m/z* = 181.07; found *m/z* = 181.1). Unlike the ligand **75**, the peak at *m/z* = 181.1 shows a significant relative abundance in the zinc spectrum.

The mass spectrum obtained after the addition of 1 equivalent of **76** to a solution of $[Mn(OH_2)_6](ClO_4)_2$ shows peaks at *m/z* = 597.0, 535.2, 444.2 (free ligand **76**), 339.1, 222.6, and 181.1. The signal at *m/z* = 597.0 can be assigned to the 1:1 mononuclear Mn(II) complex $[Mn(\mathbf{76})(ClO_4)]^+$ (calcd. for $MnC_{29}H_{25}N_5ClO_4^+$ $[M]^+$ *m/z* = 597.09; found *m/z* = 597.0). The signal at *m/z* = 339.1 can be assigned to the same ligand fragment observed in the mass spectrum of the nickel metal ion, and the peak at *m/z* = 222.6 corresponds to the diprotonated ligand (calcd. for $C_{29}H_{25}N_5^+$ $[M+2H]^{2+}$ *m/z* = 222.10; found *m/z* = 222.6). Again, the mass spectrum reveals the signal at *m/z* = 181.0 that has been previously assigned to the sodiated ligand fragment, naphthalene-2,3-diamine **72.Na**. Upon the addition of a second and third equivalents of the ligand solution the intensity of the peak at *m/z* = 444.1 corresponding to the free ligand increases.

Unfortunately, the peak observed at *m/z* = 535.2 (*Figure 174*) could not be assigned to a corresponding fragment that matched the mass value and the isotope pattern. The complex, $[Mn(\mathbf{76})(Cl)]^+$, was found to be the closest match which is two mass units out at a *m/z* = 533.11 (calcd. for $MnC_{29}H_{25}N_5Cl^+$ $[M]^+$ *m/z* = 533.11; found *m/z* = 535.2) (*Figure 174*).

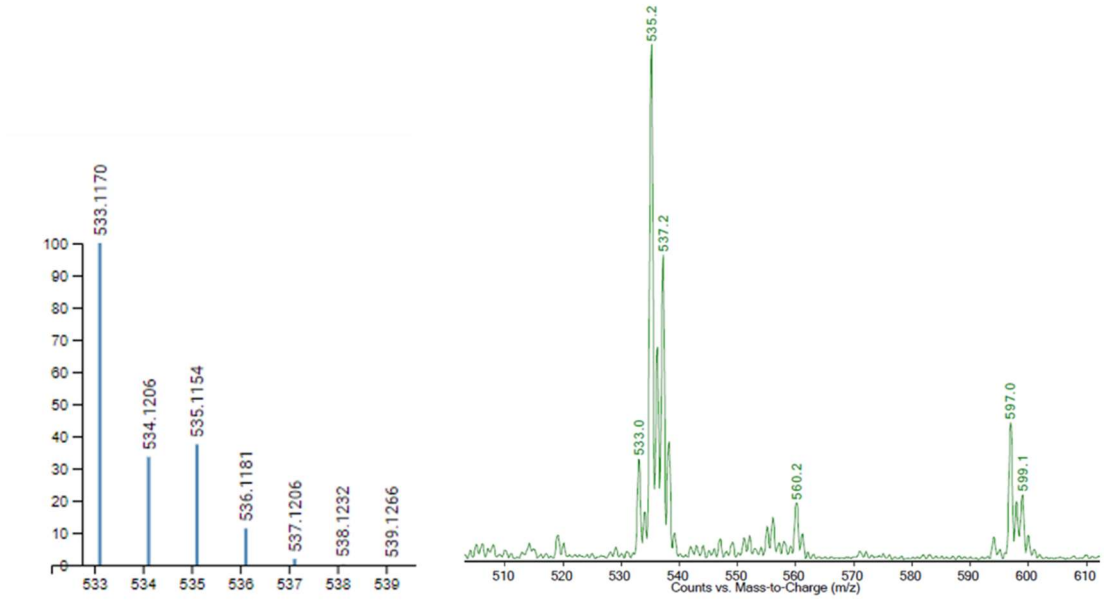


*Figure 174. Calculated data for [Mn(**76**)Cl]$^+$ m/z = 533.11 (left); experimental data showing the signal at m/z = 535.2.*

**Ligand 74**

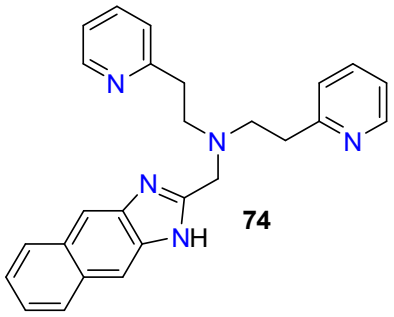


Chemical Formula: $C_{26}H_{25}N_5$
Monoisotopic Mass: 407.21

For compound **74**, the mass spectrum shows the free ligand peak at *m/z* = 408.4 (calcd. for $C_{26}H_{26}N_5^+$ $[M+H]^+$ *m/z* = 408.21; found *m/z* = 408.4) (see section 6.4). The mass spectrum obtained from the reaction of a solution of $[Cu(OH_2)_6](ClO_4)_2$ with 1 equivalent of the ligand **74** solution revealed three copper-containing signals at *m/z* = 569.0, 505.0, and 469.1. This mass spectrum showed no peak at *m/z* = 408.4 indicating the full consumption of the ligand by the Cu(II) metal ions.

The signal at *m/z* = 469.1 is of the highest intensity and can be assigned the complex, [Cu(**74**)]$^+$ (calcd. for $CuC_{26}H_{24}N_5^+$ $[M]^+$ *m/z* = 469.13; found *m/z* = 469.1). The peaks at

*m/z* = 505.0 and 569.0 correspond to the 1:1 metal complex which have an associated chloride or perchlorate anion, respectively (calcd. for $CuC_{25}H_{25}N_5Cl^+$ $[M]^+$ *m/z* = 505.10; found *m/z* = 505.0; calcd. for $CuC_{25}H_{25}N_5ClO_4^+$ $[M]^+$ *m/z* = 569.08; found *m/z* = 569.0). The addition of a second and third equivalent of the ligand solution results in increased intensity of all three copper-containing peaks and no appearance of the free ligand.

A solution of $[Co(OH_2)_6](ClO_4)_2$ containing 1 equivalent of **74** affords a mass spectrum that displays four complex ion peaks, ligand fragment ions, and the free ligand. Peaks are observed at *m/z* = 565.0, 511.1, 465.1, 233.1, 181.0 303.1 and 408.1 (free ligand **74**) (*Figure 175*).

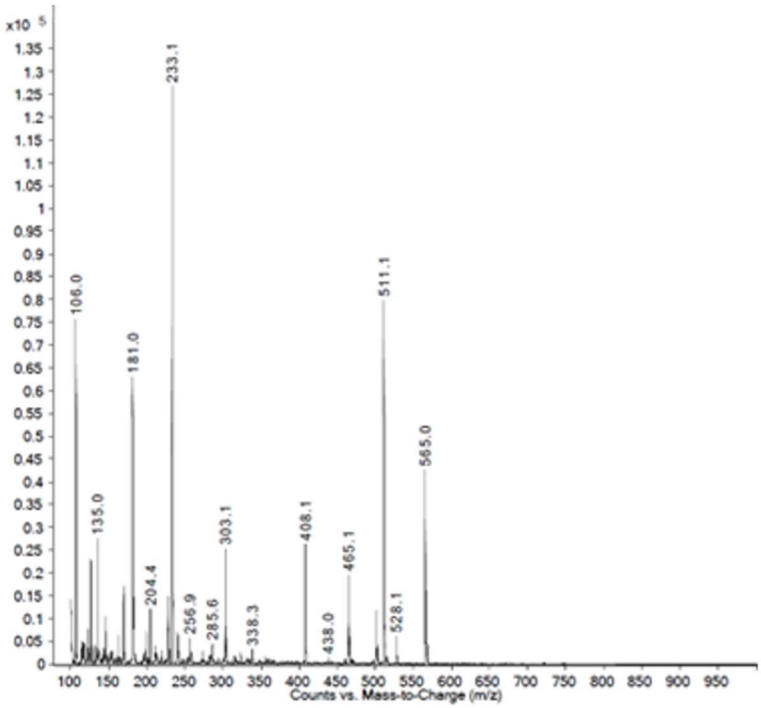


*Figure 175. The mass spectrum of an equimolar solution of **74** and $[Co(OH_2)_6](ClO_4)_2.6H_2O$.*

The signal at *m/z* = 303.1 can be assigned to the ligand fragment resulting from the loss of the naphtho[2,3-*d*]imidazole moiety (calcd. for $C_{19}H_{19}N_4^+$ $[M+H]^+$ *m/z* = 303.16; found *m/z* = 303.1). The peaks at *m/z* = 565.0 and 511.1 are consistent with the formulae corresponding to the Co(II) complexes $[Co(\mathbf{74})ClO_4]^+$ (calcd. for $CoC_{26}H_{25}N_5ClO_4^+$ $[M]^+$ *m/z* = 565.09; found *m/z* = 565.0) and $[Co(\mathbf{74})HCOO]^+$ (calcd. for $CoC_{27}H_{26}N_5O_2^+$ $[M]^+$ *m/z* = 511.14; found *m/z* = 511.1), respectively.

The signal observed at *m/z* = 465.1 is consistent with the formula $[Co(\mathbf{74})]^+$ (calcd. for $CoC_{25}H_{24}N_5^+$ $[M]^+$ *m/z* = 465.1; found *m/z* = 465.13). The peak at *m/z* = 233.1 can be assigned to the 2+ species, $[Co(\mathbf{74})]^{2+}$ (calcd. for $CoC_{26}H_{25}N_5^{2+}$ $[M]^{2+}$ *m/z* = 233.07; found *m/z* = 233.1). The mass spectra of the following addition of the second and third equivalents of the ligand solution reveal an increase in the intensities of the peaks at *m/z* = 511.1, 408.1, and 233.1, and the decrease in the intensity of the peaks at *m/z* = 565.0 and 465.1.

The mass spectrum of a solution of $[Ni(OH_2)_6](ClO_4)_2$ to which 1 equivalent of **74** has been added exhibited four signals at *m/z* = 232.5, 464.1, 510.1, and 564.0, which on the basis of the isotope patterns appear to contain nickel (*Figure 176*). The base peak at *m/z* = 510.1 can be assigned to the 1+ species, $[Ni(\mathbf{74})HCOO]^+$ (calcd. for $NiC_{27}H_{26}N_5O_2^+$ $[M]^+$ *m/z* = 510.14; found *m/z* = 510.1). The signal at *m/z* = 564.0 is consistent with the formula $[Ni(\mathbf{74})ClO_4]^+$ (calcd. for $NiC_{26}H_{25}N_5ClO_4^+$ $[M]^+$ *m/z* = 564.09; found *m/z* = 564.0). The peaks observed at *m/z* = 464.1 and 232.5 can be assigned to the mononuclear complex ion, $[Ni(\mathbf{74})]^{n+}$ with *z* = 1 (calcd. for $NiC_{26}H_{24}N_5^+$ $[M]^+$ *m/z* = 464.13; found *m/z* = 464.1) and z = 2 (calcd. for $NiC_{26}H_{25}N_5^{2+}$ $[M]^{2+}$ *m/z* = 232.57; found *m/z* = 232.5), respectively. The mass spectra obtained from the second and third equivalents of ligand addition show an increase in the intensities of all peaks and no formation of any new ones. In all three spectra no signal corresponding to the free ligand was observed.

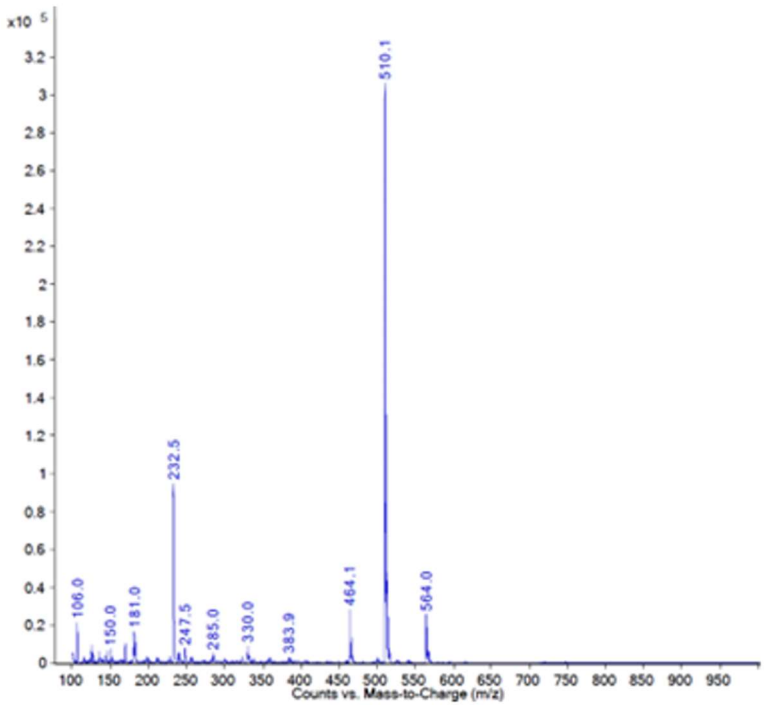


*Figure 176. The mass spectrum of an equimolar solution of **74** and $[Ni(OH_2)_6](ClO_4)_2$.*

The addition of 1 equivalent of the ligand **74** solution to the $[Zn(OH_2)_6](ClO_4)_2$ solution reveals a mass spectrum that displays the free ligand peak, three ligand fragment peaks, and three zinc-containing species observed at *m/z* = 408.1, 181.0, 228.1, 303.1, 470.0, 516.1, and 570.0, respectively (*Figure 177*).

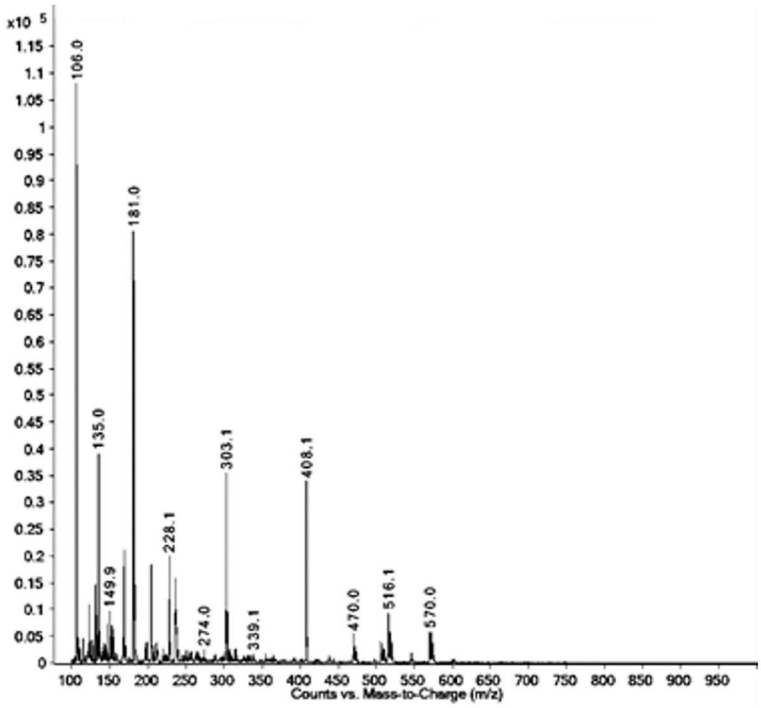


*Figure 177. The mass spectrum of an equimolar solution of **74** and $[Zn(OH_2)_6](ClO_4)_2$.*

The peak at *m/z* = 181.0 is consistent with the sodiated ligand fragment, naphthalene-2,3-diamine **72.Na**. The peaks at *m/z* = 228.1 (**62**) and 303.1 (**193**) are consistent with the ligand fragments depicted in *Figure 178* (calcd. for $C_{14}H_{18}N_3^+$ $[M+H]^+$ *m/z* = 228.15; found *m/z* = 228.1; and calcd. for $C_{19}H_{19}N_4^+$ $[M+H]^+$ *m/z* = 303.16; found *m/z* = 303.1, respectively).

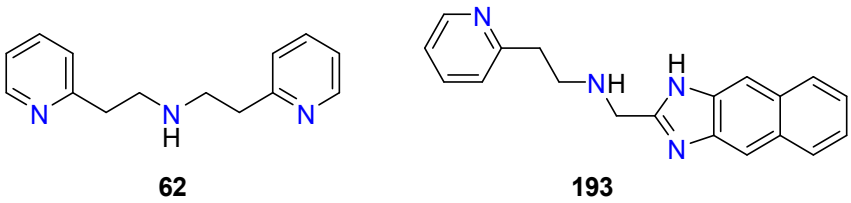


*Figure 178. The ligand fragments **62** (left) and **193** (right).*

The peak at *m/z* = 470.0 can be assigned to $[Zn(\mathbf{74})]^+$ (calcd. for $ZnC_{26}H_{24}N_5^+$ $[M]^+$ *m/z* = 470.13; found *m/z* = 470.0). The peaks observed at *m/z* = 516.1 and 570.0 are consistent with the formulae, $[Zn(\mathbf{74})HCOO]^+$ (calcd. for $ZnC_{27}H_{26}N_5O_2^+$ $[M]^+$ *m/z* = 516.13; found *m/z* = 516.1) and $[Zn(\mathbf{74})ClO_4]^+$ (calcd. for $ZnC_{26}H_{25}N_5ClO_4^+$ $[M]^+$ *m/z* = 570.08; found *m/z* = 570.0). In this case, it appears that the Zn(II)-**74** complexes have associated with

negatively charged formate and perchlorate ions, commonly observed in the other metal ion experiments discussed throughout.

The addition of a second and third equivalents of the metal solution, revealed the increase in the relative abundance of the free ligand **74** and the introduction of no new signals.

A solution of equimolar amounts of $[Mn(OH_2)_6](ClO_4)_2$ and ligand **74** yields two manganese-containing signals, albeit at very low relative abundances, at *m/z* = 497.0 and 561.0 in the mass spectrum (*Figure 179*).

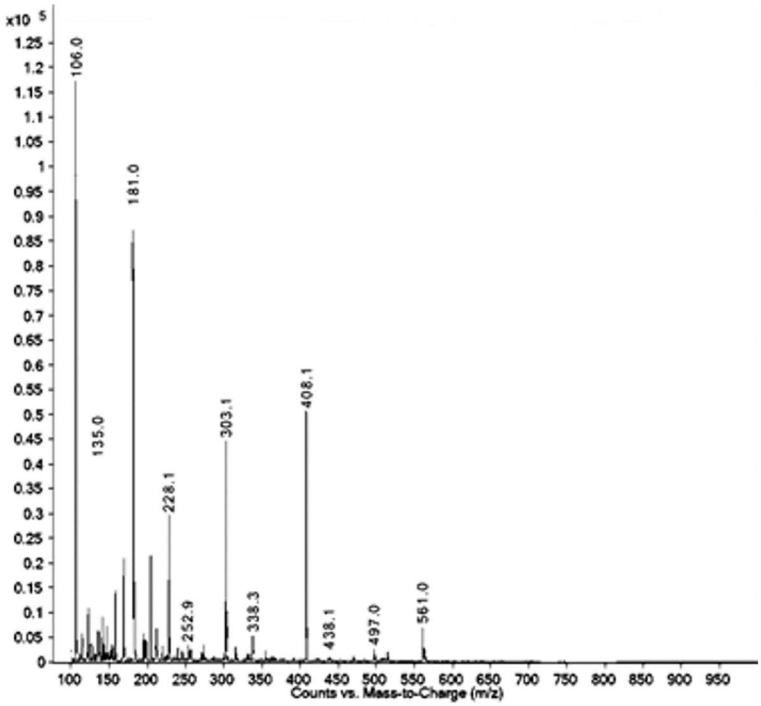


*Figure 179. The mass spectrum of an equimolar solution of **74** and $[Mn(OH_2)_6](ClO_4)_2$.*

These peaks are consistent with the formulae, $[Mn(\mathbf{74})Cl]^+$ (calcd. for $MnC_{26}H_{25}N_5Cl^+$ $[M]^+$ *m/z* = 497.11; found *m/z* = 497.0) and $[Mn(\mathbf{74})ClO_4]^+$ (calcd. for $MnC_{26}H_{25}N_5ClO_4^+$ $[M]^+$ *m/z* = 561.09; found *m/z* = 561.0). The isotope patterns observed for these two species are consistent with what is expected for chloride and perchlorate-containing species.

In addition, peaks are also observed at *m/z* = 408.1, 303.1, 228.1, and 181.0, corresponding to the free ligand **74** and fragments of, all of which have been previously assigned for this ligand.

**Ligand 77**

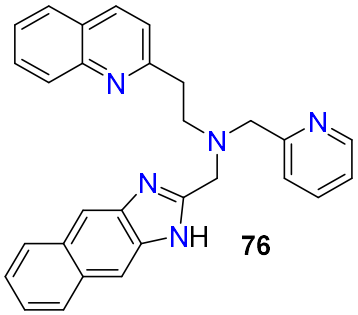


**76**

Chemical Formula: $C_{29}H_{25}N_5$
Monoisotopic Mass: 443.21

From the data given in *Chapter Six* section 6.4, the mass spectrum of the free ligand **77** displays one product ion peak at *m/z* = 444.1. The addition of 1 equivalent of $[Cu(OH_2)_6](ClO_4)_2$ affords a mass spectrum that displays peaks due to copper-containing species at *m/z* = 351.1 413.0, 505.1, 541.0, and 605.0. In addition, a signal at *m/z* = 156.0 corresponding to the 2-vinylquinoline **45** ligand fragment is present; however, there is no presence of any free ligand **77**.

Surprisingly, the most intense copper-containing signal at *m/z* = 413.0 can be assigned to the mononuclear 1:1 complex $[Cu(\mathbf{194})]^+$ in which the ligand fragment **194** is bound to a copper ion (calcd. for $CuC_{23}H_{18}N_4^+$ $[M]^+$ *m/z* = 413.08; found *m/z* = 413.0) (*Figure 180*).

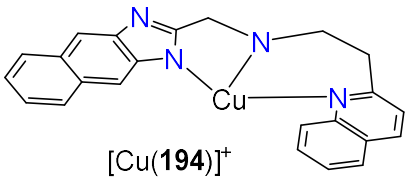


$[Cu(\mathbf{194})]^+$

*Figure 180. Suggested complex structure of the Cu(II) species for the signal observed at m/z = 413.0.*

There has been another ligand fragment copper-containing species identified in the mass spectrum at *m/z* = 351.1. This can be assigned to the complex, $[Cu(\mathbf{195})]^+$ (calcd. for $CuC_{23}H_{18}N_4^+$ $[M]^+$ *m/z* = 351.06; found *m/z* = 351.1) (*Figure 181*). In both cases, there was no free ligand **77** fragment peaks revealed in the spectrum.

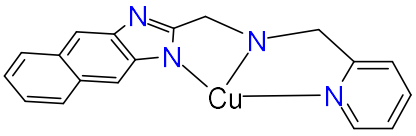


[Cu(**195**)]$^+$

*Figure 181. Suggested complex structure of the Cu(II) species for the signal observed at m/z = 351.1.*

The copper-containing signal at *m/z* = 505.1 can be assigned to the mononuclear 1:1 complex [Cu(**77**)]$^+$ (calcd. for $CuC_{29}H_{24}N_5^+$ [M]$^+$ *m/z* = 505.13; found *m/z* = 505.1). The signal observed at *m/z* = 541.0 corresponds to [Cu(**77**)Cl]$^+$ in which the 1:1 complex includes an associated chloride ion (calcd. for $CuC_{29}H_{25}N_5Cl^+$ [M]$^+$ *m/z* = 541.10; found *m/z* = 541.0). The signal at *m/z* = 605.0 can be assigned to [Cu(**77**)($ClO_4$)]$^+$ in which the 1:1 species has the inclusion of an associated perchlorate ion (calcd. for $CuC_{29}H_{25}N_5ClO_4^+$ [M]$^+$ *m/z* = 605.08; found *m/z* = 605.0). The observed isotope patterns are consistent with the presence of both Cu and Cl ions.

The addition of a second and third equivalents of the ligand **77** resulted in the increased relative abundance of all the copper-containing signals and a significant increase in the signal that corresponds to 2-vinylquinoline **45**.

The mass spectra of a solution of $[Co(OH_2)_6](ClO_4)_2$ to which 1, 2, and 3 equivalents of ligand **77** have been added show signals at *m/z* = 601.0, 537.1, 295.6, 222.6, 181.0. In addition, signals observed at *m/z* = 444.2 and 156.0 corresponding to the free ligand **77** and 2-vinylquinoline **45** ligand fragment which appear in increasing intensities upon the second and third addition of the metal ion solution.

The peaks at *m/z* = 601.0 and 537.1 can be assigned to the mononuclear 1:1 Co(II) complex, [Co(**77**)(X)]$^+$, that includes an associated anion where X = $ClO_4^-$ and $Cl^-$, respectively (calcd. for $CoC_{29}H_{25}N_5ClO_4^+$ [M]$^+$ *m/z* = 601.09; found *m/z* = 601.0; calcd. for $CoC_{29}H_{25}N_5Cl^+$ [M]$^+$ *m/z* = 537.11; found *m/z* = 537.1). The signal observed at *m/z* = 251.0 can be assigned to the 1:1 Co(II) complex, [Co(**77**)]$^{2+}$ (calcd. for $CoC_{29}H_{25}N_5^{2+}$ [M]$^{2+}$ *m/z* = 251.07; found *m/z* = 251.0). Another ion species in which *z* = 2 is the signal observed at *m/z* = 222.6 and this can be assigned to the diprotonated free ligand.

The peak at *m/z* = 181.0 is assigned to the sodiated ligand fragment, naphthalene-2,3-diamine **72.Na**. Unfortunately, at this point in time there were no plausible assignments for the signal at *m/z* = 295.6. The peak spacing suggests the species to be 2+.

The reaction of equimolar amounts of **77** and $[Ni(OH_2)_6](ClO_4)_2$, affords a mass spectrum that displays peaks at *m/z* = 600.0, 546.0, 536.0, 500.1, 295.1, 250.6, 181.0, and 156.0. In contrast to the spectra previously described for this ligand, there appears to be no ligand fragmentation other than the expected 2-vinylquionline **45** or resulting nickel complex fragments.

The Ni(II) complex ion $[Ni(\mathbf{77})]^{2+}$ can be assigned to the signal observed at *m/z* = 250.6 (calcd. for $NiC_{29}H_{25}N_5^{2+}$ $[M]^{2+}$ *m/z* = 250.57; found *m/z* = 250.6). This signal is 5-fold greater in relative abundance in comparison to the most intense 1+ nickel-containing species at *m/z* = 600.0.

The nickel-containing signal at *m/z* = 500.1, the signal with the smallest relative abundance, can be assigned to the mononuclear 1:1 complex $[Ni(\mathbf{77})]^+$ (calcd. for $NiC_{29}H_{25}N_5^+$ $[M]^+$ *m/z* = 501.14; found *m/z* = 500.1).

The signal at *m/*z = 536.0 can be assigned to the mononuclear 1:1 complex with the addition of a negatively bound chloride ion, $[Ni(\mathbf{77})Cl]^+$ (calcd. for $NiC_{29}H_{25}N_5Cl^+$ $[M]^+$ *m/z* = 536.11; found *m/z* = 536.0). The complex species $[Ni(\mathbf{77})(HCOO)]^+$ and $[Ni(\mathbf{77})(ClO_4)]^+$ can be assigned to the signals at *m/z* = 546.1 and 600.0 (calcd. for $NiC_{30}H_{26}N_5O_2^+$ $[M]^+$ *m/z* = 546.14; found *m/z* = 546.1; calcd. for $NiC_{29}H_{25}N_5ClO_4$ $[M]^+$ *m/z* = 600.09, found *m/z* = 600.0). The identity of these signals have been confirmed using both the *m/*z values and isotope patterns (*Figure 182*). The addition of a second and third equivalents of the ligand solution resulted in the increased relative abundance of the signal at *m/z* = 444.1.

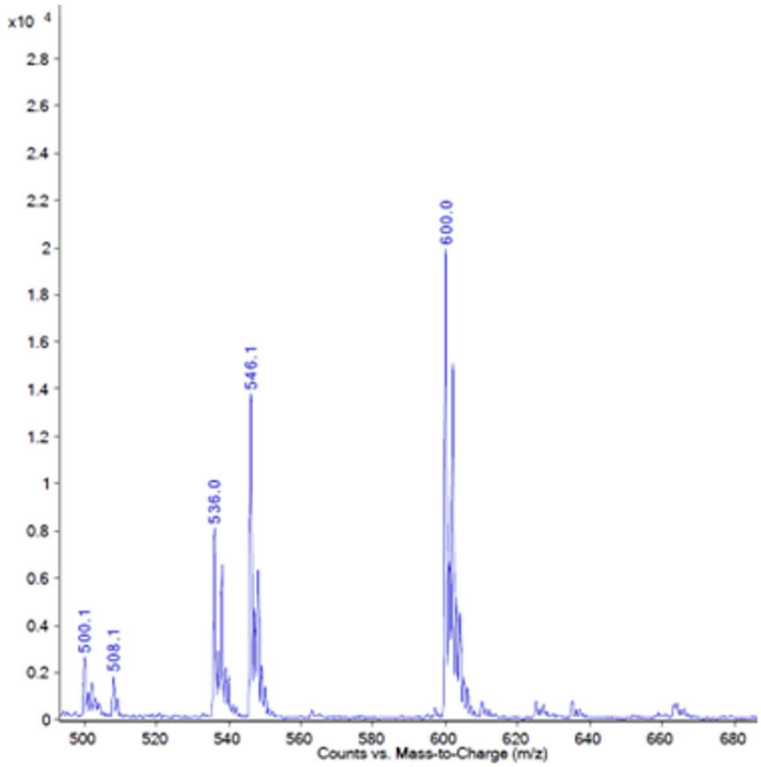


*Figure 182. Key nickel-containing signals displayed in the mass spectrum of an equimolar solution of 77 and $[Ni(OH_2)_6](ClO_4)_2$.*

The mass spectrum obtained from the addition of 1 equivalent of **77** to a solution of $[Zn(OH_2)_6](ClO_4)_2$ exhibits intense peaks at *m/z* = 156.0, 181.0, and 222.6, with the first two peaks previously assigned to ligand fragments. In this instance, the latter has *z* = 2, as determined by the peak spacing, implying a 2+ charge on the ions and can be assigned to the diprotonated free ligand.

Zinc-containing ion signals are seen at *m/z* = 253.5 and 542.0. Both of these peaks can be assigned to the mononuclear, $[Zn(\mathbf{77})]^{n+}$, Zn(II) complex. The peak at *m/z* = 253.5 can be assigned to the 2+ species $[Zn(\mathbf{77})]^{2+}$ (calcd. for $ZnC_{29}H_{25}N_5^{2+}$ $[M]^{2+}$ *m/z* = 253.57; found *m/z* = 253.5). The peak with *m/z* = 542.0 corresponds to the species, $[Zn(\mathbf{77})(Cl)]^+$ (calcd. for $ZnC_{29}H_{25}N_5Cl^+$ $[M]^+$ *m/z* = 542.10; found *m/z* = 542.0), where the 1:1 mononuclear complex includes a negatively bound chloride ion.

The mass spectrum obtained after the addition of 1 equivalent of **77** to a solution of $[Mn(OH_2)_6](ClO_4)_2$ shows peaks at *m/z* = 597.0, 444.1 (free ligand **77**), 289.1, 222.6, 181.0 (sodiated naphthalene-2,3-diamine **72**.**Na**), and 156.0 (2-vinylquinoline **45**). The signal at *m/z* = 597.0 can be assigned to the 1:1 mononuclear Mn(II) complex

$[Mn(\mathbf{77})(ClO_4)]^+$ (calcd. for $MnC_{29}H_{25}N_5ClO_4^+$ $[M]^+$ *m/z* = 597.09; found *m/z* = 597.0). The signal at *m/z* = 289.1 can be assigned to the same ligand fragment **195** described above, and the peak at *m/z* = 222.6 corresponds to the diprotonated ligand (calcd. for $C_{29}H_{25}N_5^{2+}$ $[M+2H]^{2+}$ *m/z* = 222.10; found *m/z* = 222.6). Upon the addition of a second and third equivalents of the ligand solution the peaks at *m/z* = 444.1, 289.1, 222.6, 181.0, and 156.0 increase in their relative abundance.

### 6.6.3 Pyrene-containing ligand

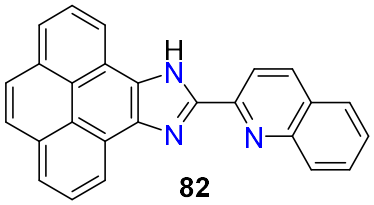


**82**

Chemical Formula: $C_{26}H_{15}N_3$
Monoisotopic Mass: 369.12

From the data given in *Chapter Six* section 6.5.1, the free ligand is observed at *m/z* = 370.1. For this ligand, and there are no other peaks that correspond to any ligand fragmentation revealed under the conditions of the experiment. The addition of 1 equivalent of $[Cu(OH_2)_6](ClO_4)_2$ affords a mass spectrum that displays peaks due to copper-containing species at *m/z* = 473.0 and 801.1. In addition, the free ligand **82** is observed at *m/z* = 370.1 (calcd. for $C_{26}H_{16}N_3^+$ $[M]^+$ *m/z* = 370.13; found *m/z* = 370.1) and the relative abundance of this peak is 3-fold and 6-fold greater than the copper-containing species at *m/z* = 473.0 and 801.1, respectively (*Figure 183*).

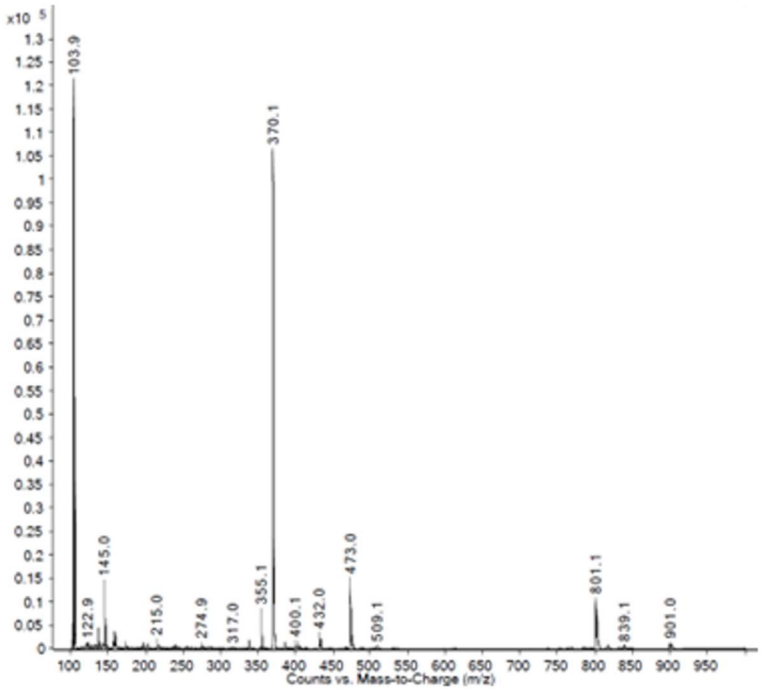


*Figure 183. The mass spectrum of an equimolar solution of* ***82*** *and* $[Cu(OH_2)_6](ClO_4)_2$.

The most intense copper-containing signal at *m/z* = 473.0 can be assigned to the complex $[Cu(\mathbf{82})NCCH_3]^+$ (calcd. for $CuC_{28}H_{18}N_4^+$ $[M]^+$ *m/z* = 473.08; found *m/z* = 473.0). The peak observed at *m/z* = 801.1 can be assigned to the complex species $[Cu(\mathbf{82})_2]^+$ in which reduction of the Cu(II) metal centre has occurred under the conditions of the mass spectrometer, affording a 1+ ion (calcd. for $CuC_{52}H_{30}N_6^+$ $[M]^+$ *m/z* = 801.18; found *m/z* = 801.1. The addition of a second and third equivalents of the ligand solution reveals an increase in the intensities of all three of the observed peaks.

Interestingly, the addition of 1, 2, and 3 equivalents of the ligand **82** solution to the metal ions Co(II), Ni(II), Zn(II), and Mn(II), afforded spectra that displayed no corresponding metal complex species and a sole molecular ion peak at *m/z* = 370.1 assigned to the free ligand. This suggests that under the conditions of the mass spectrometer, no complexation between **82** and these metal ions occur.

## 6.7 Conclusion

To conclude, the synthesis and characterisation of four 1*H*-naphtho[2,3-*d*]imidazole-containing tripodal ligands **74**, **75**, **76** and **77** have been presented. The formation of each ligand has been characterised by NMR spectroscopy and HRMS. In addition, a

pyreneimidazole-based bidentate ligand has been synthesised and characterised by means of NMR spectroscopy and HRMS.

Furthermore, the reaction of the ligands described in this chapter with the metal ions Cu(II), Co(II), Ni(II), Zn(II) and Mn(II) have been analysed using mass spectrometry. The mass spectrometry data obtained revealed a 1:1 binding stoichiometry between all four of the 1*H*-naphtho[2,3-*d*]imidazole-containing tripodal ligands and the metal ions. The pyrene derived ligand **82** exhibited both mono-ligand and diligand species when reacted with Cu(II) ions and no complex formation with the other metal ions.

# *Chapter Seven*
# Synthesis of Fluorescent 6-Amino-2,3-Naphthalimide Derivatives

## 7.1 Chapter Overview

4-Amino-1,8-naphthlimides are an important class of fluorophore that have been widely employed in a number of applications, and the synthesis of 1,8-naphthalimide derivatives have been well established in the literature. By comparison, the 6-amino-2,3-naphthlaimides have had much less attention and the chemistry of these compounds is yet to be fully understood.

The following chapter describes the progress made towards the synthesis of a variety of 6-amino-2,3-naphthalimide derivatives. It has been previously identified that the naphthalic anhydride precursor i.e. 6-bromonaphtho[2,3-*c*]furan-1,3-dione (**196**), is a key intermediate in the synthesis of these compounds. Thus, this work commences with the formation of the anhydride. With this intermediate in hand, installation of a variety of amine groups at the C-6 position on the naphthalimide ring can be achieved using a Buchwald-Hartwig cross-coupling reaction.

## 7.2 Introduction

### 7.2.1 Naphthalimides

Naphthalimides are an important class of heterocyclic compounds that are frequently researched for their unique properties with significant emphasis applied in photophysical studies. These compounds have been used in fluorescent labelling,[552] optoelectronics,[553] fluorescent probes[554,555] and enzyme inhibitors.[556,557]

There has been great interest directed towards the synthesis of various naphthalimides by the functionalisation of the naphthalene or imide moieties of the naphthalimide framework. This has driven the development of excellent chromophores, fluorophores, and potential pharmacophores.[558]

There are two isoforms, 1,8- and 2,3-naphthalimides. Typically, the framework is numbered with C-1 to C-8 assigned around the perimeter, a system analogous to that of naphthalene (*Figure 184*).

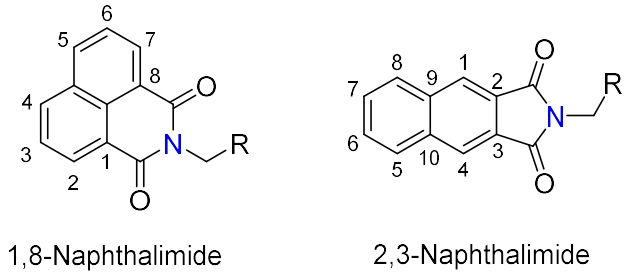


*Figure 184. The atom labelling of the 1,8- and 2,3-naphthalimides.*

### 7.2.2 4-Amino-1,8-naphthalimides

While the unsubstituted 1,8-naphthalimide core itself is weakly fluorescent ($\phi_F < 0.01$), the addition of an electron-donating substituent installed at the C-4 position significantly increases the fluorescence intensity. The fluorescence arises from the 'push-pull' based internal charge transfer (ICT) between the electron donating substituent at the 4-position of the naphthalimide ring and the electron withdrawing imide moiety (*Figure 185*).[559–561]

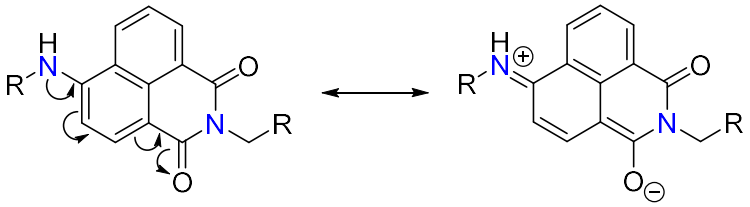

*Figure 185. The ICT in 4-amino-1,8-naphthalimide derivatives.*

As a result, this ICT mechanism affords remarkable photophysical properties including strong absorption and emission in the visible region, high fluorescence quantum yields, good photostability and large Stokes shifts. Furthermore, the photophysical properties of 4-amino-1,8-naphthalimides can be manipulated by structural modifications that alter the electron donating ability of the 4-amino group.[562–564]

There is an abundance of 4-amino-1,8-naphthalimide examples that have been reported, with several extensive reviews highlighting this area of chemistry.[560,565–567] Recently, Zeng *et al.* have reported the design and synthesis of a novel 4-amino-1,8-naphthalimide-based fluorescence probe **220** for the detection of HOCl. As displayed in *Scheme 113*, the probe is prepared over a two-step synthesis and affords the desired product in a yield of 67%. In this instance, the HOCl-reactive moiety, 2-aminoethan-1-ol **221**, is connected to the fluorophore and this can undergo a specific oxidation reaction with HOCl which results in the fluorescence switched from "ON" to "OFF".[568]

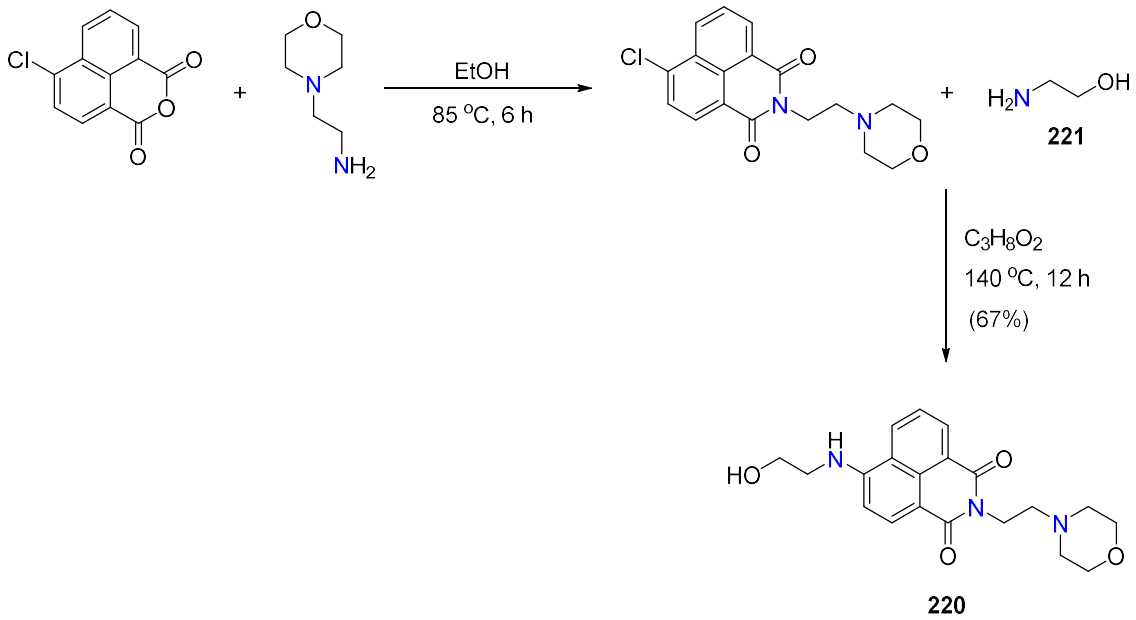


*Scheme 113. Reported synthesis of **220**.*[568]

Veale *et al.* described the synthesis and characterisation of the 4-amino-1,8-naphthalimide-based chemosensor **222** in which the tetraamine tripodal ligand *tris*(2-aminoethyl)amine **1** (see *Chapter One*, section 1.2.3) is the amino substituent located at the C-4 position. This amine group was included in the structure to act as a receptor for Cu(II) ions. The compound was prepared by heating 6-chloro-2-ethyl-1*H*-benzo[*de*]isoquinoline-1,3(2*H*)-dione **223** with an excess of *tris*(2-aminoethyl)amine **1** (*Scheme 114*).

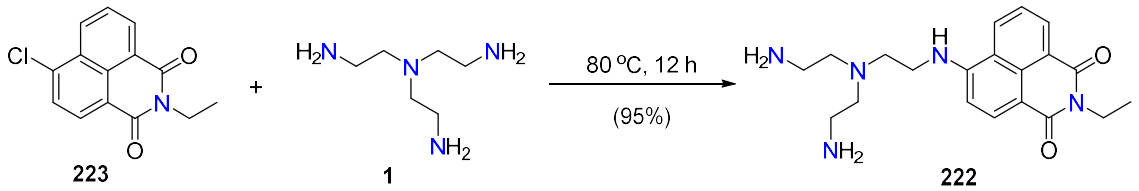


*Scheme 114. Reported synthesis of **222**.*[569]

The authors were able to successfully demonstrate that the synthesised chemosensor **222** can detect Cu(II) ions selectively at pH values of 5.6 or 7.4 over the metal ions Zn(II), Cd(II) and Hg(II). The binding at the latter pH (7.4) gives rise predominantly to the formation of a 1:1 complex species, whilst at pH 5.6 the formation of the self-assembly induced Cu(II) complex with two moieties of **222** is observed.[569]

Furthermore, Martínez-Calvo and co-workers reported four novel fluorescent sensors that are based on the 4-amino-1,8-naphthalimide framework (*Figure 186*). The synthesis of these compounds began with imide formation achieved by the treatment of 4-bromo-1,8-naphthalic anhydride with a benzylamine derivative. Subsequently, the reaction of the naphthalimide precursor with the appropriate amine group afforded the title compounds.

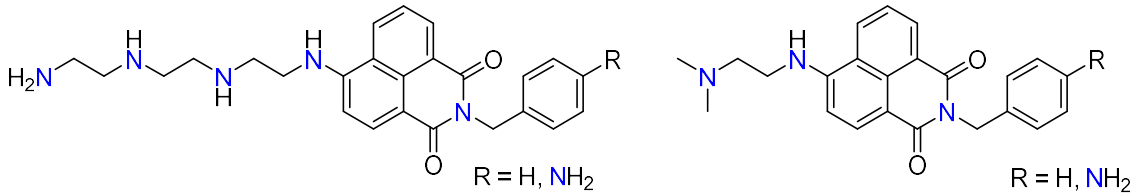


*Figure 186. The structure of the 4-amino-1,8-naphthalimide-based fluorescent sensors.*[570]

The four compounds were synthesised as pH sensors and cellular imaging agents. The pH dependence of each compound was investigated, and all demonstrated that the fluorescent emissions are highly pH dependent with the absorption being red shifted going from acidic to basic environments. Further analysis of the toxicity and localisation of these compounds within cervical cells was also performed with both tests affording promising results.[570]

### 7.2.3 6-Amino-2,3-naphthalimides

The 6-amino-2,3-naphthalimides also exhibit valuable fluorescent properties. In comparison to the numerous examples of 4-amino-1,8-naphthalimides, only a handful of 6-amino-2,3-naphthalimides are documented in the literature. With only the 6-dimethylamino and free amino derivatives available, the diversity of this class of compound is limited.

6-*N*-*N*-dimethylamino-2,3-naphthalimide **224** (*Figure 187*) was first reported in 2005 by Vázquez *et al.* and is one of the few known examples of 6-amino-2,3-naphthalimides. The formation of **224** is achieved via the functionalisation of the precursor anhydride intermediate **225** (*Figure 187*). This intermediate has the 6-amino substituent pre-installed and several synthetic steps are required for the formation of this compound. This naphthalimide has demonstrated excellent fluorescent properties including a large quantum yield and Stokes shift. The authors noted that **224** exhibits combined advantageous properties of two other environment-sensitive fluorophores, 2-propionyl-6-dimethylaminonaphthalene, PRODAN and 4-amino-1,8-naphthalimide derivatives.[554]

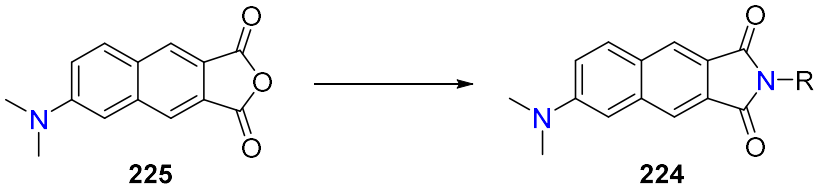


*Figure 187. The structure of **224**.*

The derivatives **226** and **227** are shown in *Figure 188* and were developed as environmentally sensitive fluorophores, which is a unique class of chromophores that have spectroscopic behaviour that is dependent on the physiochemical properties of the surrounding environment.[554,571–573]

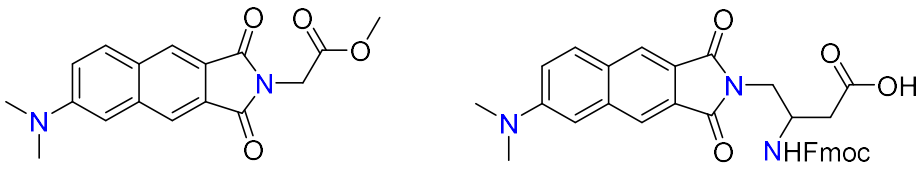


*Figure 188. The structures of **226** and **227**.*

Following the initial report of **224**, Vázquez *et al.* utilised compound **224** in the development of a novel environment-sensitive fluorescent probe in δ-opioid peptides.[554] The 6-*N,N*-(dimethylamino)-2,3-naphthalimide **224** moiety was incorporated into a larger framework that contained an amino acid-derived fragment and a pharmacophore.[552] Furthermore, the incorporation of **224** with additional peptides has been further investigated, with Sainlos and Imperiali publishing the 'building block' approach for the preparation of peptides coupled to 6-*N,N*-(dimethylamino)-2,3-naphthalimide.[574,575] In addition, this 6-amino-2,3-naphthalimide derivative has been used in the development of high-affinity binders for the treatment of celiac disease.[576]

In 2010, Baathulaa *et al.* reported the synthesis of several 6-substituted 2,3-naphthalimide derivatives including the dimethylamine, free amine, $NO_2$, Cl and I functional groups located at the 6-position (*Figure 189*). The authors studied the absorbance and fluorescence properties of each derivative in a variety of solvents. The data from this revealed an interesting feature showing these compounds are solvatochromic with unusually large Stokes shifts and appreciable quantum yields.[577] These compounds have found further application as fluorescent probes and ion sensors.[578]

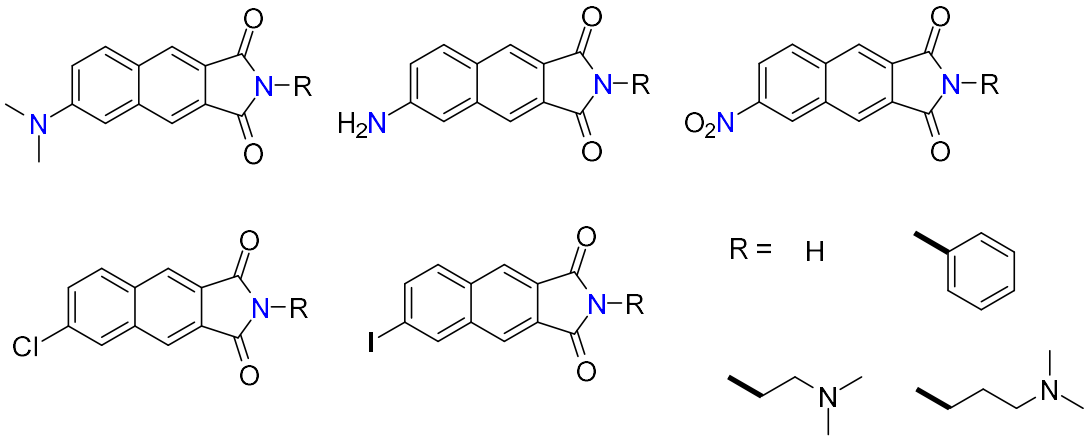


*Figure 189. Reported 6-substituted-2,3-naphthalimide derivatives.*[577]

Despite the utility of 6-amino-2,3-naphthalimides, there are very few examples reported in the literature. As such it is very difficult to grasp the effect of the nature of the 6-amino moiety on fluorescence. In turn, the structure-property relationship with this class of fluorophore is poorly understood. It is anticipated that this is the result of a lack of robust methodology to access more diverse structures.

Typically, the synthesis of 6-amino-2,3-naphthalimides is achieved over multiple steps and requires the pre-installation of the 6-amino substituent prior to the 2,3-naphthalimide formation. Using 6-*N*,*N*-dimethylamino-2,3-naphthalimide as an example, prepared from the multi-step synthesis shown below in *Scheme 115*. The first step in the synthesis is the photobromination of the commercially available 1,2-dimethyl-4-nitrobenzene (**228**), which affords 1,2-bis(dibromomethyl)-4-nitrobenzene (**229**). The treatment of **229** with maleic anhydride and KI followed by base hydrolysis affords the Diels-Alder adduct **230**. Following the successful isolation of the intermediate **230**, a reductive amination is achieved using formaldehyde solution (37%) and hydrogen in the presence of a catalytic amount of 10%-Pd/C at room temperature and 30 psi pressure, which results in the formation of the 6-amino-substituted, 6-*N,N*-(dimethylamino)-2,3-naphthalene dicarboxylic acid, in high yield (87%). Formation of the anhydride **225** is achieved following the dehydration of the previously isolated carboxylic acid in acetic anhydride under reflux for 1 hour with a high yield of 90%. With the 6-amino anhydride **225** in hand, the formation of the sequential imide is achieved from the treatment of **225** with the appropriate amine in either refluxing acetic acid or toluene, affording the desired product (*Scheme 115*).[577]

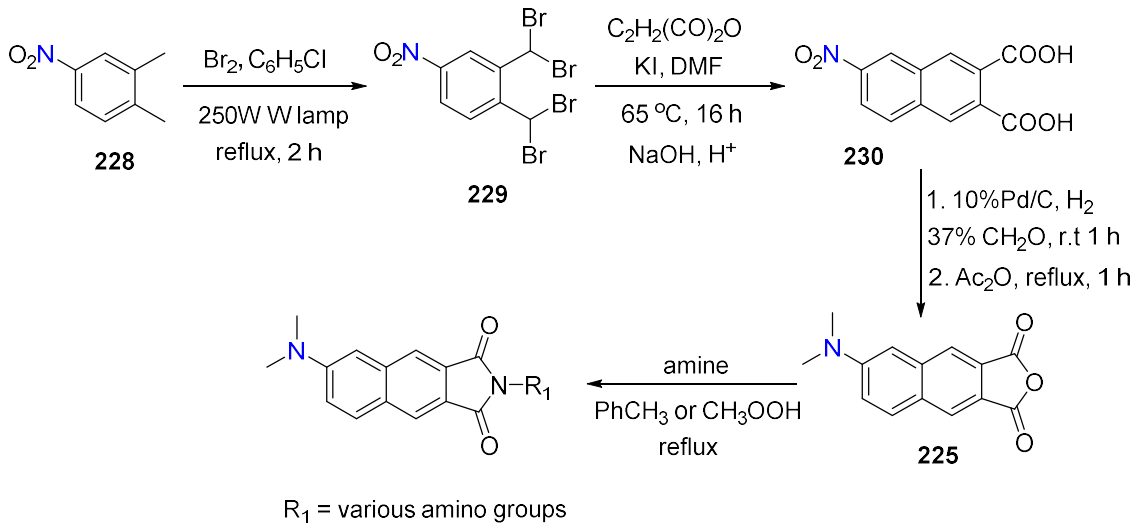


*Scheme 115. Reported synthesis of 6-N,N-dimethylaminonaphthalimide.*

The Cl- and I-substituted naphthalimide derivatives can be prepared following the same methodology described above for the isolation of the intermediate **230**. Then the reaction of this intermediate with 10%-Pd/C and a catalytic amount of hydrogen in MeOH and further diazotisation, followed by a Sandmeyer reaction affords the halogenated dicarboxylic acid **231**. Conversion of **231** is achieved by treatment of the crude material in refluxing acetic anhydride affording the desired anhydride **232**. The desired 6-substituted 2,3-naphthalimide is obtained from the condensation of **232** with the appropriate amine in acetic acid. A similar pathway is followed to obtain the free amine 6-substituted-2,3-naphthalimide **233** (*Scheme 116*). Interestingly, the authors did not appear to attempt any further functionalisation at the 6-position of the halogenated 2,3-naphthalimides.

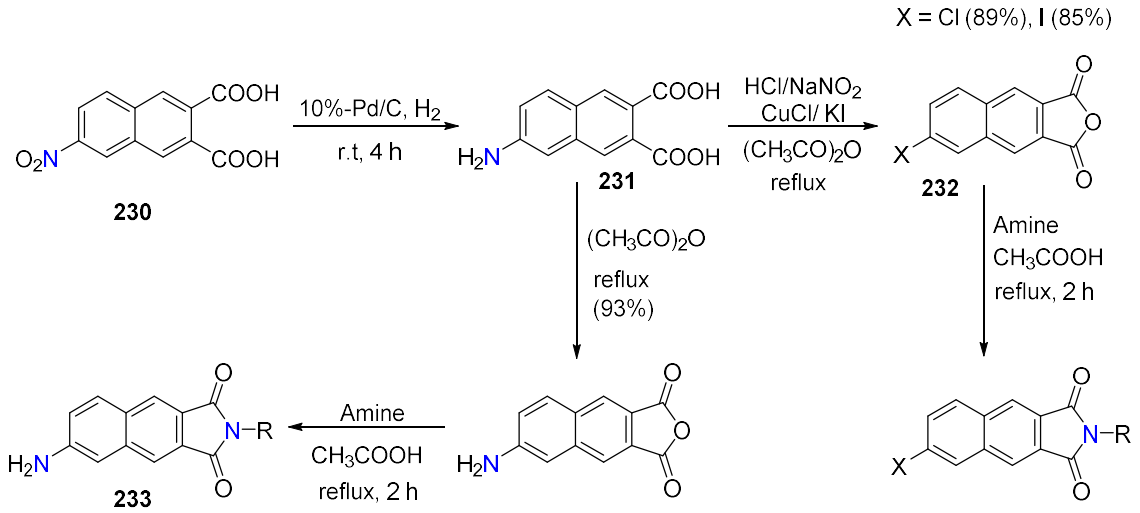


*Scheme 116. General reported synthesis for the 6-substituted 2,3-naphthalimides where C-6 = $NH_2$, Cl and I.*

### 7.2.4 Aims

In contrast to the 6-amino-2,3-naphthalimides, the chemistry for the preparation of 4-amino-1,8-naphthalimides is well established. The 4-amino-1,8-naphthalimides **234** are typically prepared in two steps from the corresponding 4-halo-1,8-naphthalic anhydride **235** starting materials, in which the imide moiety is first installed by nucleophilic acyl substitution followed by the amination at the 4-position (*Scheme 117*).[579]

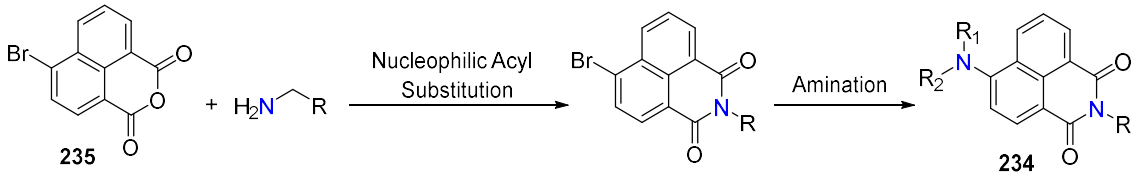


*Scheme 117. Typical synthesis of 4-amino-1,8-naphthalimides.*[579]

Thus, the synthesis of the corresponding anhydride precursor of the 2,3-naphthalimdes with a halogen group i.e. bromine, would serve as a valuable building block, allowing for the facile functionalisation of both the imide and the 6-position of the naphthalimide ring. Taking inspiration from the various methodologies available to prepare 4-amino-1,8-naphthalimides, we aimed to apply this approach to access a diverse library of 6-amino-2,3-naphthalimide derivatives.

*Scheme 118* shows the proposed synthetic pathway for the work described in this chapter. The pathway begins with the formation of the anhydride **196** obtained from the

tetrabromine starting material **197** (previously synthesised). The next step is the installation of the imide group from the reaction of **196** and the appropriate amine, followed by the introduction of the amino functionality at the 6-position of the naphthalimide ring (*Scheme 118*).

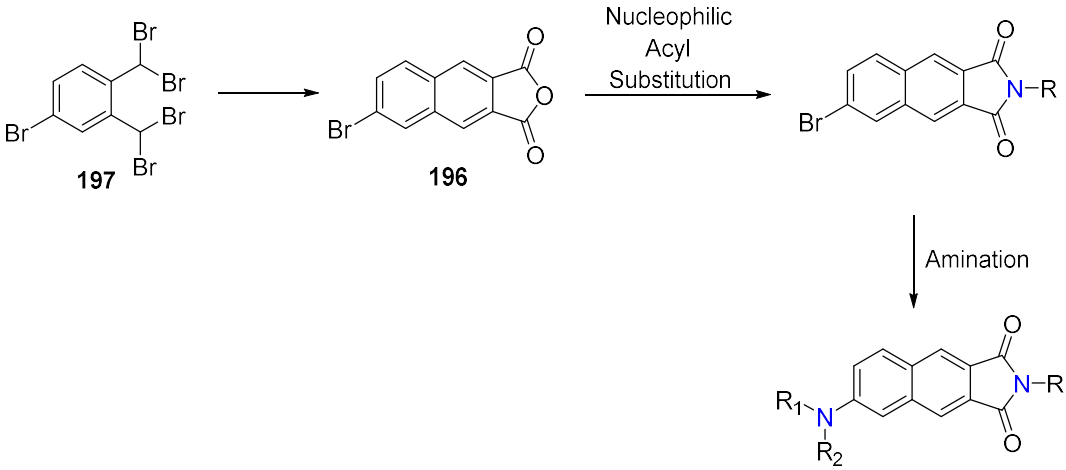


*Scheme 118. Synthetic plan for the synthesis of 6-amino-2,3-naphthalimide derivatives*

### 7.2.5 Formation of the 6-Bromo-2,3-Naphthalimide

As discussed above, these types of naphthalimides are typically accessed via the anhydride precursor. In the literature, this precursor always has the 6-position substituent pre-installed on the naphthalene ring, meaning that late-stage functionalisation to vary the amino moiety cannot be pursued. In this work, the anhydride precursor consisted of a bromo group at the 6-psotion. Thus, this work commenced with the synthesis of **196** from the treatment of 4-bromo-1,2-bis(dibromomethyl)benzene **197** with maleic anhydride and NaI in DMF stirred at 65 °C for 16 hours. After cooling to room temperature, the reaction mixture was poured into an ice/water mixture and stirred for 10 minutes (*Scheme 119*). The product was collected via vacuum filtration, and following recrystallization from acetic anhydride the desired anhydride **196** was obtained in 68% yield.

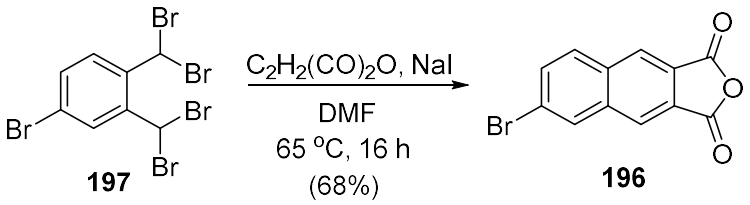


*Scheme 119. Synthesis of **196**.*

Analysis by $^{1}$H NMR spectroscopy revealed the presence of five proton signals that are attributed to the H atoms on the newly formed naphthalene ring (*Figure 190*). The synthesis of **196** was further supported by $^{13}$C NMR spectroscopy.

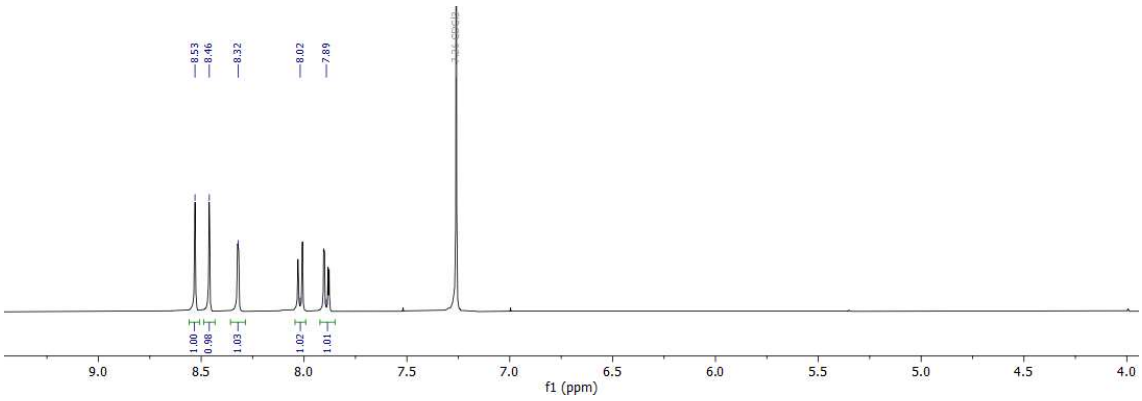


*Figure 190. $^{1}$H NMR spectrum of **196** in $CDCl_3$.*

The next step in the synthesis was the formation of the imide functional group and this was first attempted using propan-1-amine. Following the typical conditions for the formation of naphthalimides,[579] propane-1-amine was added to a mixture of **196** and $CH_3COOH$ and stirred at reflux for 48 hours (*Scheme 120*). The reaction mixture was poured onto ice and the resulting precipitate was isolated by vacuum filtration, affording the imide **199** in 90% yield. The structure of the desired imide **199** was supported by $^{1}$H NMR spectroscopy, with a new triplet at $\delta_H$ 0.98 ppm, quartet at $\delta_H$ 1.75 and a second triplet at $\delta_H$ 3.60 ppm corresponding to the introduction of the propyl group.

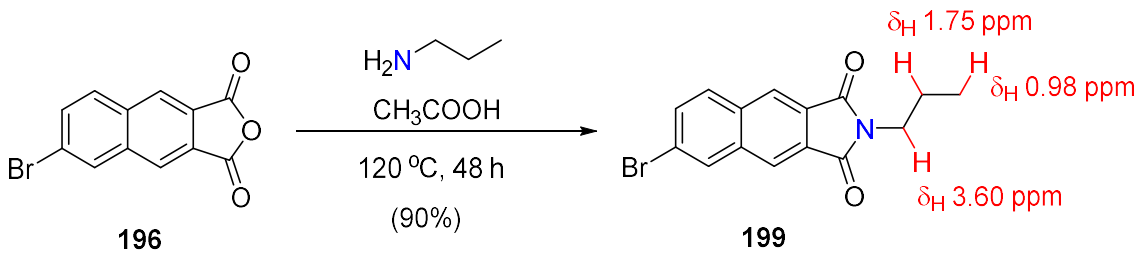


*Scheme 120. Synthesis of **199**.*

### 7.2.6 Amination at the 6-position

The chemistry typically employed for the functionalisation of the 4-position of the 1,8-naphthalimide derivatives includes either $S_NAr$ methodology or via palladium-mediated cross-coupling reactions. The former can be achieved by either heating the naphthalimide with the desired amine at temperatures greater than 100 °C[580,581] or stirring the compound with the amine in DMF.[582]

Palladium-mediated cross-coupling chemistry, specifically Buchwald-Hartwig cross-coupling, has been utilised for the amination of 1,8-naphthalimides at the 4-position.[579] Furthermore, the mild conditions relative to other amination methods, palladium-catalysed Buchwald-Hartwig cross-coupling served as a good starting point for this project.

### 7.2.7 Buchwald-Hartwig Cross-Coupling

First described in 1983 by Migita *et al.*,[583] the palladium-catalysed aryl-amine cross-coupling reaction in which bromobenzene was coupled with *N,N*-diethylaminotributyltin to afford *N,N*-diethylaminobenzene was presented. With a number of undesirable stability and toxicity features, further improvement of this methodology was of great interest.

A decade later, Buchwald and Hartwig concurrently presented a significant breakthrough in the Pd-catalysed C-N bond formation of aryl halides with amines. The simultaneous work presented exhibited a Pd-catalysed cross-coupling reaction without the undesirable conditions afforded by the original method. The Buchwald-Hartwig reaction has become a valuable tool for synthetic chemists for the synthesis of C-N bonds between aryl halides and amines (including primary/secondary, aliphatic and aromatic amines, amides and anilines).

The general catalytic cycle of the Buchwald-Hartwig amination starts with the formation of the electrophilic palladium complex **B** from the oxidative addition of the aryl halide to Pd. Subsequently, the Pd complex **B** undergoes the coordination of the amine (**C**), and deprotonation of the base affords the amido complex **D**. The product is obtained from the reductive elimination of **D** resulting in the desired amination product **E**. The catalytic cycle is complete with the regeneration of the palladium catalyst **A** (*Figure 191*).[584]

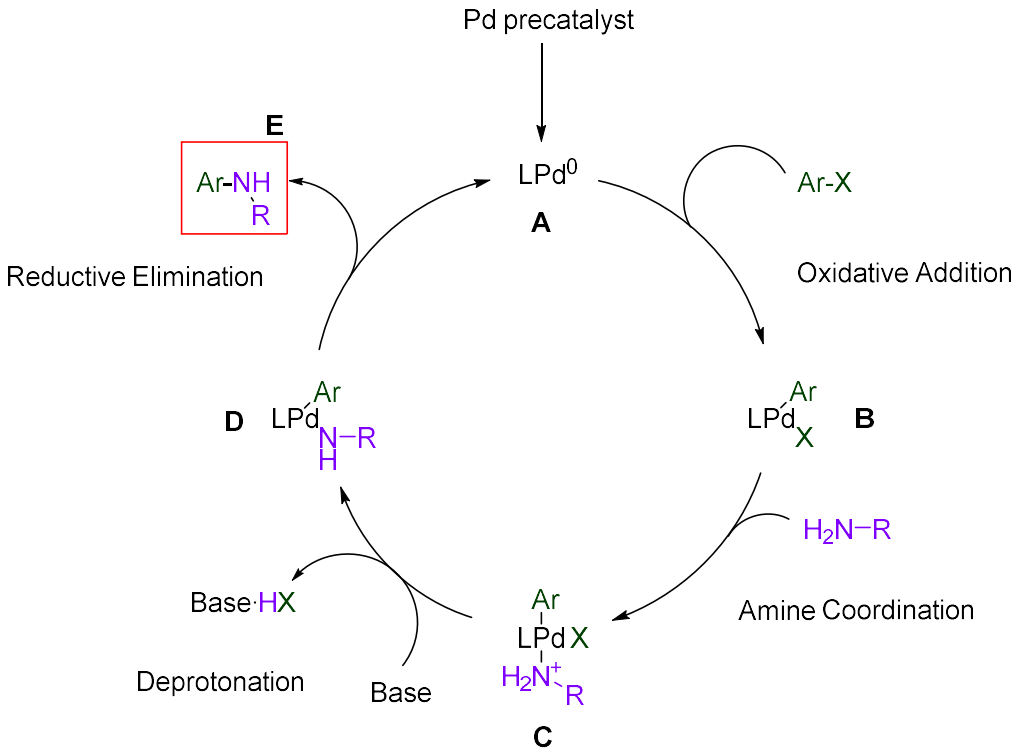


*Figure 191. General catalytic cycle for Buchwald-Hartwig cross-coupling reactions.*[585]

The key components of a Buchwald-Hartwig amination include the Pd source, ligand, base, solvent, and temperature.

The palladium source determines the efficiency of the formation of the active catalyst species, Pd(0). Due to the instability of this catalytic species, it is generally generated *in situ* from stable Pd(II) salts such as $[Pd(OAc)_2]$ and $[PdCl_2]$.[586] Phosphine ligands are typically employed for the reduction of Pd(II) to Pd(0).[585,586] For example, $[Pd(OAc)_2]$ has the Pd metal ion in a 2+ oxidation state and therefore requires a reduction step to generate the active $Pd^0$ species.[587]

There are several commercially available stable Pd(0) complexes such as $[Pd(PPh_3)_4]$, $[Pd_2(dba)_3]$ and $[Pd_2(dba)_3].CHCl_3$. These complexes are considered favourable as they eliminate the need for a reduction step to generate Pd(0).[585]

The choice of ligand is important as this depends on the substrate combination. Owing to the history of this methodology, there is a plethora of ligand structures available to choose from. The steric bulkiness of the ligand has been shown to be crucial for preventing the formation of undesirable palladium complexes that would otherwise interfere with the desired transformation.[583,588–591] The phosphine ligand p(*o*-tolyl)$_3$ **236** (*Figure 192*) has been reported in the successful coupling of aniline derivatives; however, a disadvantage of this ligand was that it was found to be unsuccessful in the cross-coupling of primary amines with aryl bromides.[588]

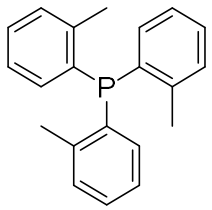


**236**

*Figure 192. Structure of P(o-tolyl)$_3$ (**236**).*

There have been several reports that have established suitable ligands for the cross-coupling reaction with primary amines and aryl bromides which led to the identification of bidentate chelating ligands such as BINAP (**237**), dppf (**238**) and Xantphos (**239**) (*Figure 193*).[588,592,593] Xantphos (**239**) was developed by van Leeuwen and co-workers,[594] and is an electron-rich chelating phosphine ligand that has been proven to be successful when employed in Pd-catalysed amination of aryl bromide transformations.[595,596]

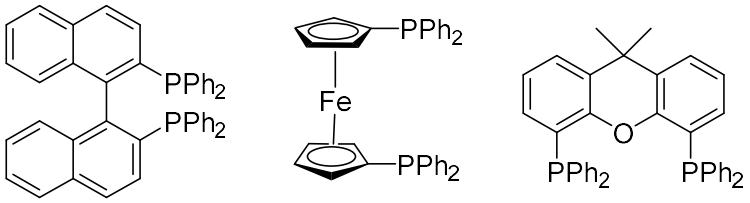


rac-BINAP **237** | dppf **238** | Xantphos **239**

*Figure 193. Bidentate chelating phosphine ligands.*

The use of a strong base i.e. NaO$^t$Bu or a weak base i.e. $Cs_2CO_3$ will have an impact on the rate, functional group tolerance and by-product formation. Alkoxide bases such as KO$^t$Bu and NaO$^t$Bu are commonly employed.[597] The solvent is important as this defines the solubility of the substrates and base. A wide variety of solvents for this transformation have been used, with 1,4-dioxane and toluene most commonly employed. Lastly, the temperature at which the reaction is carried out will influence the rate of the cross-coupling and by-product formation.[585]

As discussed above, the Buchwald-Hartwig cross-coupling reaction can be utilised under several different conditions including the source of base, solvent, and palladium and phosphine ligand source. It has been previously established that Buchwald-Hartwig methodology has been successful for the synthesis of 4-amino-1,8-naphthalimides,[579] as such the same conditions were trialled first.

In the initial reaction $[Pd_2(dba)_3]\cdot CHCl_3$ (4 mol%), Xantphos (4 mol%), 6-bromo-2-propyl-1*H*-benzo[*f*]isoindole-1,3(2*H*)-dione **199**, propane-1-amine and $Cs_2CO_3$ (3.0 equiv.) were heated in toluene for 24 hours at 60 °C (*Table 1*, Entry A). After 24 hours TLC analysis of the crude material revealed the presence of a fluorescent spot suggesting the formation of desired naphthalimide. Purification by silica gel column chromatography afforded the desired 6-amino-2,3-naphthalimide **212** in a moderate yield of 25%. In attempts to push the reaction further to completion, the reaction was repeated using an increased amount of $[Pd_2(dba)_3]\cdot CHCl_3$ (10 mol%) and Xantphos (10 mol%) and after 24 hours at 60 °C a yield of 70% was obtained following purification (*Table 1*, Entry B). It was decided next to investigate other palladium and ligand source combinations. Changing both the palladium source and phosphine ligand to $[Pd(OAc)_2]$ (2 mol%) and $PPh_3$ (4 mol%), respectively, did not result in the formation of the desired product (Entry

C). The combination of $[Pd_2(dba)_3]$ (5 mol%) and Xantphos (10 mol%) gave the desired 6-amino-2,3-naphthalimide product **212** in a 77% yield, albeit not cleanly as multiple spots were observed following TLC analysis prior to purification (Entry D). Despite the higher yield obtained for entry D, it was decided to continue using the conditions established for entry B as this reaction afforded a much cleaner mixture and hence easier purification. Next, the importance of the base was investigated, and after screening a small number of bases (entries E-I), it became clear that $CsCO_3$ gave the 6-amino-2,3-naphthalimide product in the highest yield.

*Table 1. Optimisation for the Pd-mediated amination of 6-bromo-2,3-naphthalimide* ***199*** *with propane-1-amine.*[a]

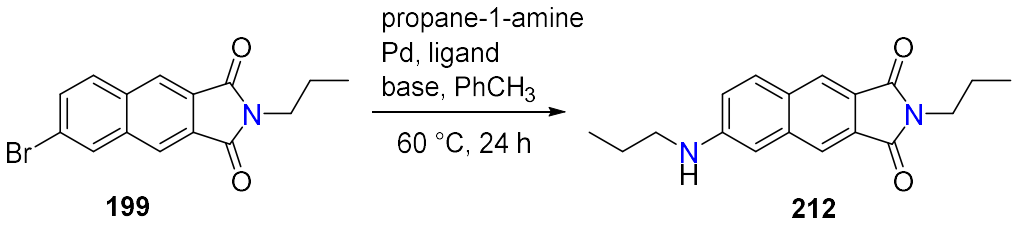


| Entry | Pd-source | mol% | Ligand | mol% | Base | Equiv | Yield(%) |
|---|---|---|---|---|---|---|---|
| A | $Pd_2(dba)_3{\cdot}CHCl_3$ | 4 | Xantphos | 4 | $Cs_2CO_3$ | 3 | 25 |
| B | $Pd_2(dba)_3{\cdot}CHCl_3$ | 10 | Xantphos | 10 | $Cs_2CO_3$ | 3 | 70 |
| C | Pd(OAc) | 2 | $PPh_3$ | 4 | $Cs_2CO_3$ | 3 | N.R |
| D | $Pd_2(dba)_3$ | 5 | Xantphos | 10 | $Cs_2CO_3$ | 3 | 77 |
| E | $Pd_2(dba)_3{\cdot}CHCl_3$ | 10 | Xantphos | 10 | $K_2CO_3$ | 3 | 20 |
| F | $Pd_2(dba)_3{\cdot}CHCl_3$ | 10 | Xantphos | 10 | $NaHCO_3$ | 3 | 7 |
| G | $Pd_2(dba)_3{\cdot}CHCl_3$ | 10 | Xantphos | 10 | $Na_2CO3$ | 3 | 20 |
| H | $Pd_2(dba)_3{\cdot}CHCl_3$ | 10 | Xantphos | 10 | K*t*OBu | 3 | N.R |
| I | $Pd_2(dba)_3{\cdot}CHCl_3$ | 10 | Xantphos | 10 | NaOH | 3 | 41 |

[a]Reagents and conditions: 6-bromo-2,3-naphthalimide (**199**, 0.157 mmol), propane-1-amine (0.785 mmol), base (3 equiv), $PhCH_3$ (5 mL), 60 °C, 24 hours.

The characterisation of the 6-amino-2,3-naphthalimide derivative was obtained by means of NMR spectroscopy and HRMS. The $^1$H NMR spectrum was useful in determining the successful instalment of the amine group which results in the characteristic upfield shift of the protons located at the 4- and 7-positions on the naphthalimide ring. This is illustrated in *Figure 194* below where the shift in these protons from $\delta_H$ 7.77 and 8.21 ppm to $\delta_H$ 6.99 and 6.91 ppm is evident between the two spectra.

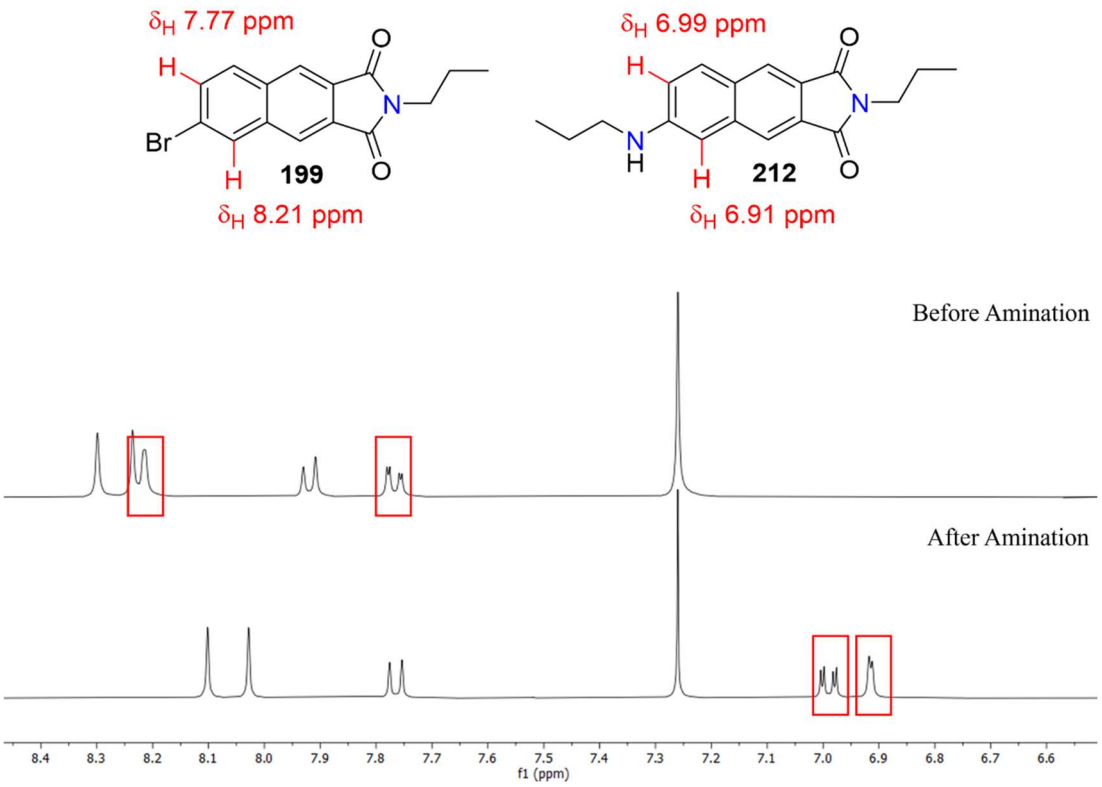


*Figure 194. $^{1}H$ NMR spectra of **199** (top) and **212** (bottom) in $CDCl_3$.*

## 7.3 The synthesis 6-substituted-2,3-naphthalimide derivatives

It was then decided to investigate the scope of this cross-coupling amination reaction with a variety of aryl and alkyl amines (including aniline, benzylamines and heterocyclic amines). Using the optimised reaction conditions described above, a family of 6-amino substituted naphthalimides were synthesised in yields ranging from 4% to 94% (*Figure 195*). The success of each reaction was determined by NMR spectroscopy and HRMS, with the characteristic upfield shift of the naphthalimide protons in the 4- and 7-position observed in the $^{1}H$ NMR spectrum.

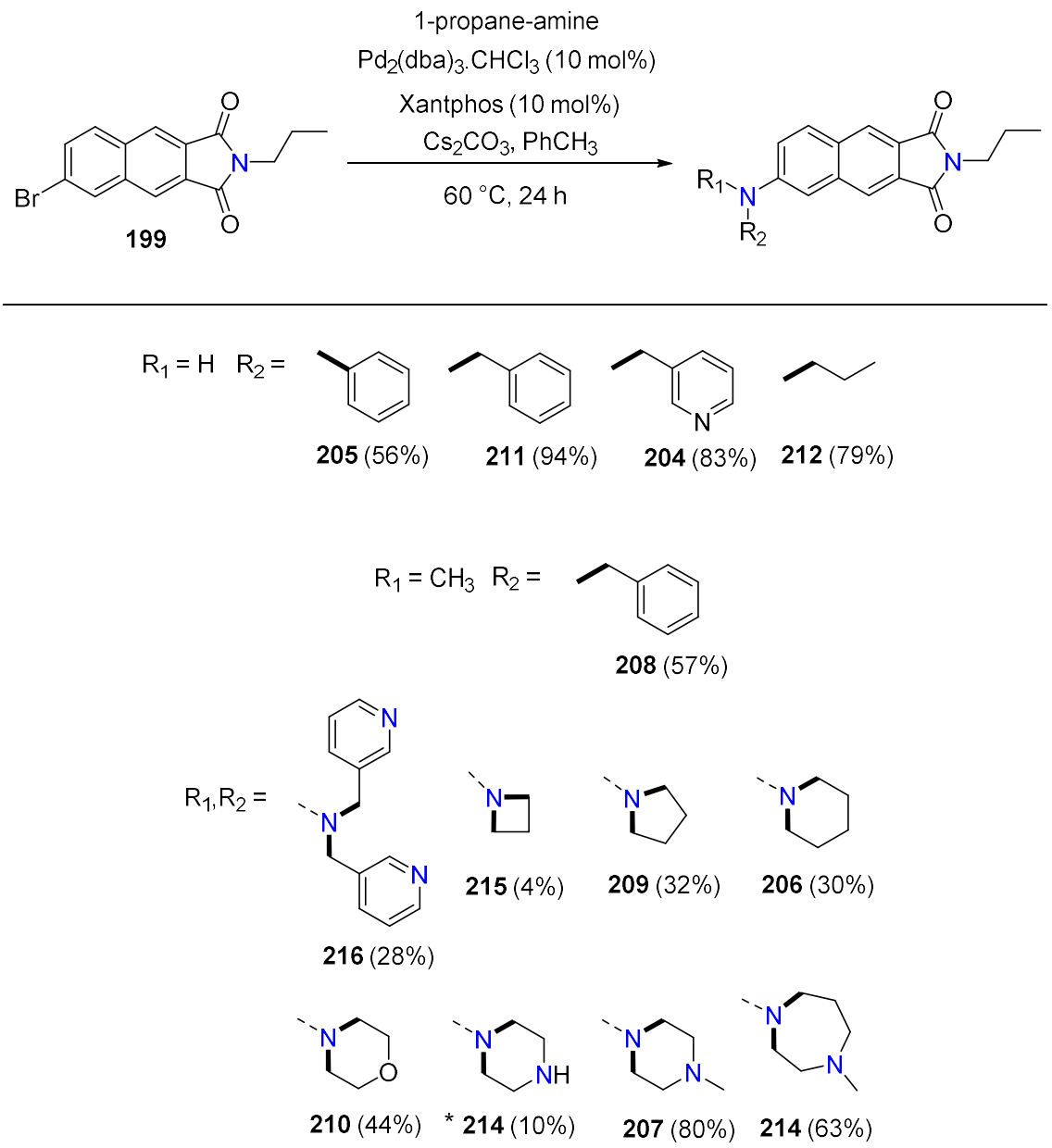


*Figure 195. Pd-mediated coupling of 6-bromo-2-propyl-1H-benzo[f]isoindole-1,3(2H)-dione **199** with various amino substrates. * Further purification required.*

The cross-coupling reactions of the aromatic amines were the most successful relative to the heterocyclic amines, with the exception of **207** and **214**. The amination reaction of 6-(benzylamino)-2-propyl-1*H*-benzo[*f*]isoindole-1,3(2*H*)-dione (**199**) and 1-phenylmethanamine afforded the highest isolated yield of 94% (**211**). The coupling product of the azetidine hydrochloride amination (**215**) resulted in the isolation of only a 4% yield, presumably due to this amine starting material being the only hydrochloride salt used. This amine and any other amine salts would require further optimisation of the reaction conditions such as the type and number of equivalents of base. Fortunately, despite the low yield, full characterisation of the compound was completed.

$^{1}$H NMR spectroscopy was utilised for the identification of the product structure. For example, the installation of the phenyl group in compound **211** was observed in the $^{1}$H NMR spectrum (*Figure 196*) which revealed the expected addition of a singlet at $\delta_H$ 4.48 ppm, and five aromatic protons observed across multiplet signals at $\delta_H$ 7.39 and 7.32 ppm. In addition, the -NH proton is revealed as a broad multiplet at $\delta_H$ 4.58 ppm. The identity of the product was further supported by $^{13}$C and 2D NMR spectroscopy and HRMS.

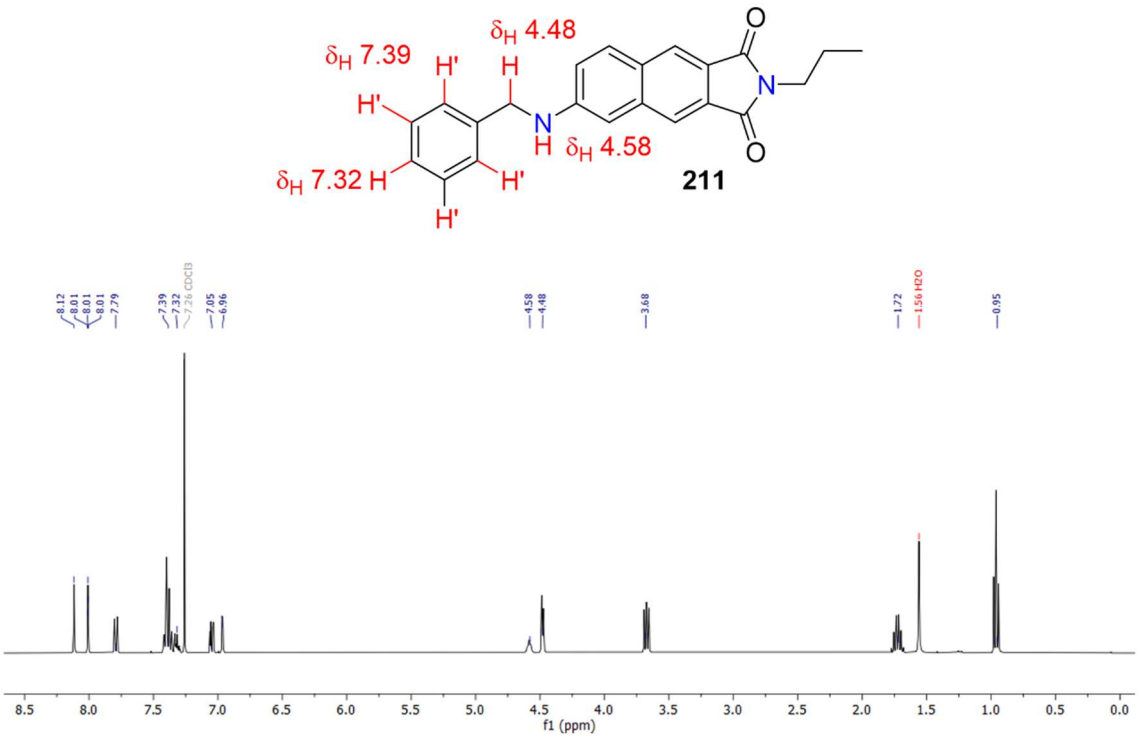


*Figure 196. $^{1}$H NMR spectrum of 6-(benzylamino)-2-propyl-1H-benzo[f]isoindole-1,3(2H)-dione (**211**) in $CDCl_3$.*

Following the development of the Pd-mediated amination methodology to access the desired 6-amino-2,3-naphthlaimide derivatives, focus turned to the functional group tolerance of the groups installed at the imide position.

A series of derivatives containing various imide groups were prepared from the reaction between 6-bromo-2-propyl-1*H*-benzo[*f*]isoindole-1,3(2*H*)-dione (**196**) and the appropriate amine in refluxing acetic acid for 48 hours (*Figure 197*). The resulting solution was poured into an ice/water mixture and the resulting precipitate was collected by filtration and dried in a vacuum desiccator to afford the desired product. As the reaction between **196** and ethanolamine in acetic acid afforded the acetylated alcohol derivative **202**, the formation of the alcohol **201** was achieved using EtOH for the solvent

in place of acetic acid. The identity of the isolated products was confirmed by NMR spectroscopy.

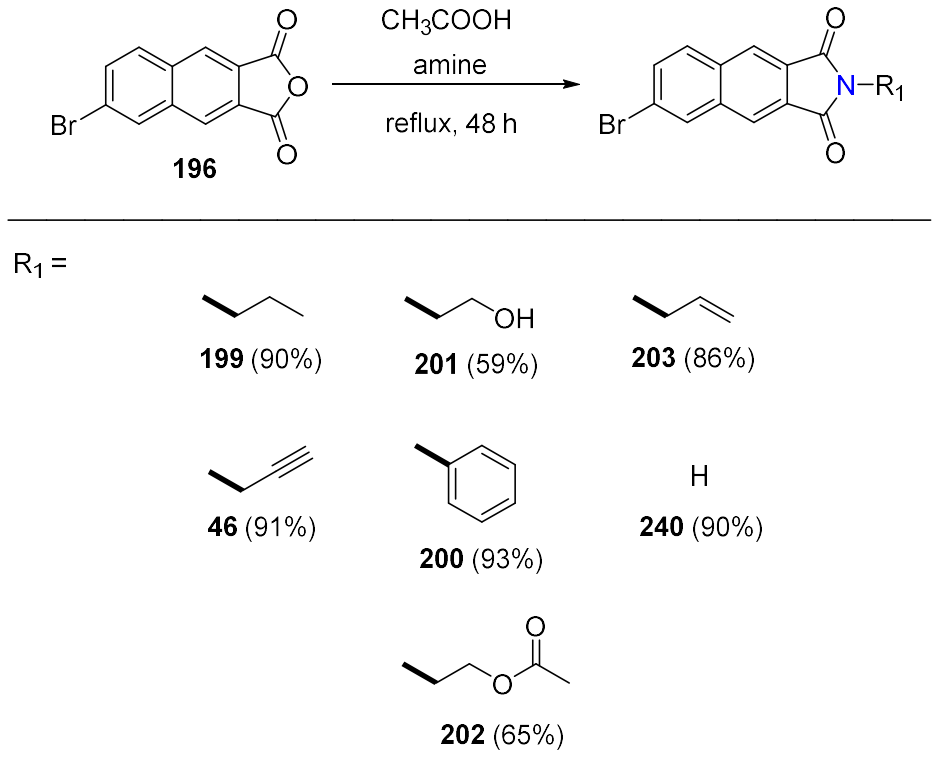


*Figure 197. Imide functionalisation of 6-bromonaphtho[2,3-c]furan-1,3-dione **196** with various amino substrates.*

The imide derivatives were all obtained in high yield (59–91%). The NMR data were readily obtained for each compound apart from **240** in which solubility was an issue and only very noisy spectra ($^{1}$H and $^{13}$C) were revealed in $D_2O$, $CD_3OD$ and DMSO-$d_6$.

In order to evaluate the functional group tolerance of the imide moiety during the amination reaction, Pd-mediated cross-couplings using the conditions established above were carried out with propane-1-amine. The imide (**202**, **203**, **46**, **200** and **240**) was treated with $Pd_2(dba)_3.CHCl_3$ (10 mol%) and Xantphos (10 mol%) in the presence of propane-1-amine (5.0 equiv) and $Cs_2CO_3$ (3.0 equiv) and the mixture was stirred at 60 °C for 24 hours. Following purification by silica gel chromatography, the 6-amino-2,3-naphthalimide derivative was obtained (*Figure 198*).

Analogous to the 6-amino-2,3-naphthlimides discussed above, the success of each reaction was determined by NMR spectroscopy and HRMS, with the characteristic upfield shift of the naphthalimide protons in the 4- and 7-position observed in the $^{1}$H NMR spectrum. In addition, observation of the two triplets and one multiplet

characteristic of the propane-1-amine moiety in the $^{1}$H NMR spectrum supported that the propyl group had been installed.

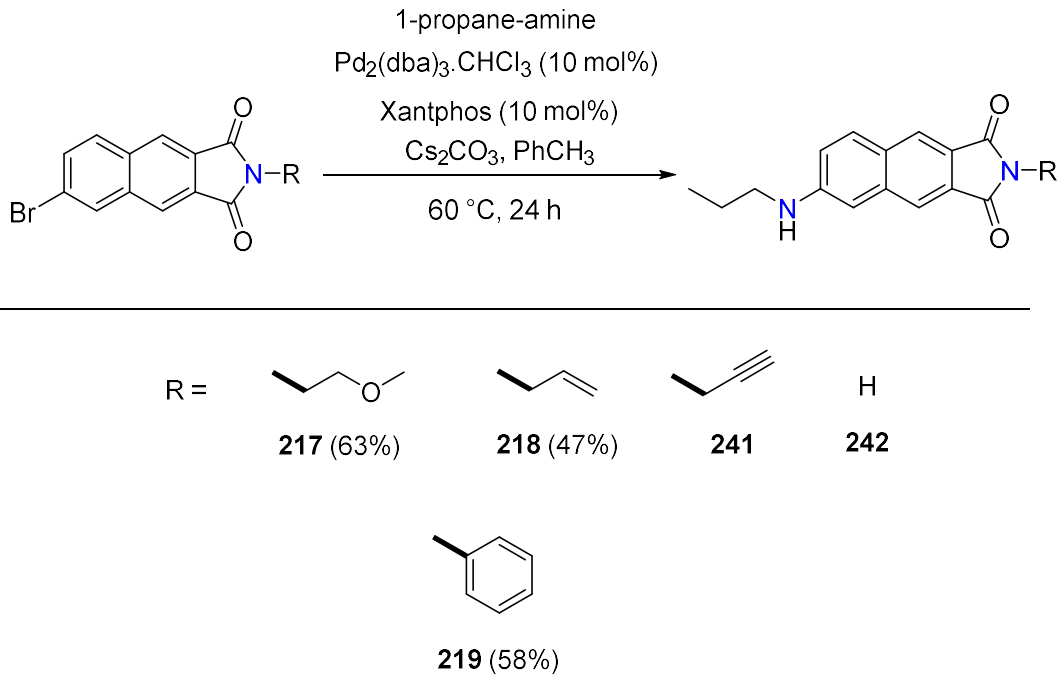


*Figure 198. Pd-mediated coupling of the imide functionalised 6-bromo-naphthalimide derivatives with 1-propane-amine.No product was obtained for compounds **241** and **242**.*

The amination reaction of compounds **217**, **218** and **219** afforded the 6-amino-2,3-naphthalimide product in respectable yields (47–63%). In contrast, **240** did not react, with the $^{1}$H NMR spectrum ($D_2O$) revealing signals that were consistent with the starting material, possibly due to the solubility issues previously encountered for this 2,3-naphthalimide. Additionally, the NH of the imide functional group may potentially coordinate to the palladium catalyst thus rendering the Pd species inactive. The formation of compound **241** was also unsuccessful and in this instance it appears that a reaction at the alkyne position predominately occurs. Interestingly, **218** which contains an alkene did not behave in this way and amination at the 6-position was successful.

## 7.4 Future Work

A future aim of this project is the optimisation of the reaction conditions for the amines that either gave very low yields of product or no formation of the desired compound. For example, a number of different bases such as $Et_3N$ and DBU could be trialled for the reaction of the azetidine hydrochloride salt, **215**.

As discussed in 0 the 6-amino-2,3-naphthalimides also exhibit valuable fluorescent properties; however, unlike the 4-amino-1,8-naphthalimides, the fluorescence of the 2,3-naphthlaimides is yet to receive such great attention. Thus, a future aim for this study includes the UV/vis absorption and fluorescence spectroscopy of the synthesised 6-amino-2,3-naphthalimide derivatives.

Since the fluorescence of 6-amino-2,3-naphthalimides is still to be completely understood, the spectroscopy studies of the 6-amino-2,3-naphthalimide derivatives presented in this chapter will contribute to this gap in the literature. Once the fluorescence has been established, areas of application for these compounds can be sought out. Preliminary studies of the photophysical properties of three selected compounds have been carried out in $CHCl_3$ and DMSO. As mentioned in *Chapter Seven* section 7.2.2 the ICT process of 4-amino-1,8-naphthalimide derivatives can be somewhat controlled by the electron donating ability of the amino group at the 4-position of the naphthalimide ring. Thus, it is of interest to analyse the photophysical properties of the 6-amino-2,3-naphthalmide to determine the influence of the different amino moieties at the C-6 position. The initial results of this study are presented in Table 2.

*Table 2. Photophysical properties of **215**, **209** and **206** in $CDCl_3$ and DMSO.*

| Compound | Solvent | $\lambda_{Abs\ max}$ (nm) | $\lambda_{Em\ max}$ (nm) | Stokes Shift (nm) |
|---|---|---|---|---|
| **215** | $CHCl_3$ | 370 | 510 | 140 |
| | DMSO | 370 | 557 | 187 |
| **209** | $CHCl_3$ | 370 | 507 | 137 |
| | DMSO | 370 | 553 | 183 |
| **206** | $CHCl_3$ | 370 | 510 | 140 |
| | DMSO | 370 | 554 | 184 |

The three compounds analysed differ by the addition of a carbon atom into the ring positioned at the C-6 carbon of the naphthalimide and exhibited similar photophysical

properties. In $CHCl_3$, the absorption maximum was 370 nm with a strong emission maxima at 507–510 nm (Stokes Shift of 187–140 nm). In DMSO, minimal changes were observed in the absorption maximum (370 nm); however, a change in the emission maxima at 553–557 nm was revealed (Stokes Shift of 183–187 nm). This is indicative of the solvatochromic behaviour of these 6-amino-2,3-naphthalimide derivatives studied. The emission and excitation spectra of **215**, **209** and **206** in $CHCl_3$ and DMSO are shown in Figure 199. Future photophysical studies on the 6-amino-2,3-naphthalimide derivatives described in this chapter would include analysing their absorbance and emission properties in other solvents of varying polarity. Furthermore, the determination of the molar extinction coefficients and quantum yields is required.

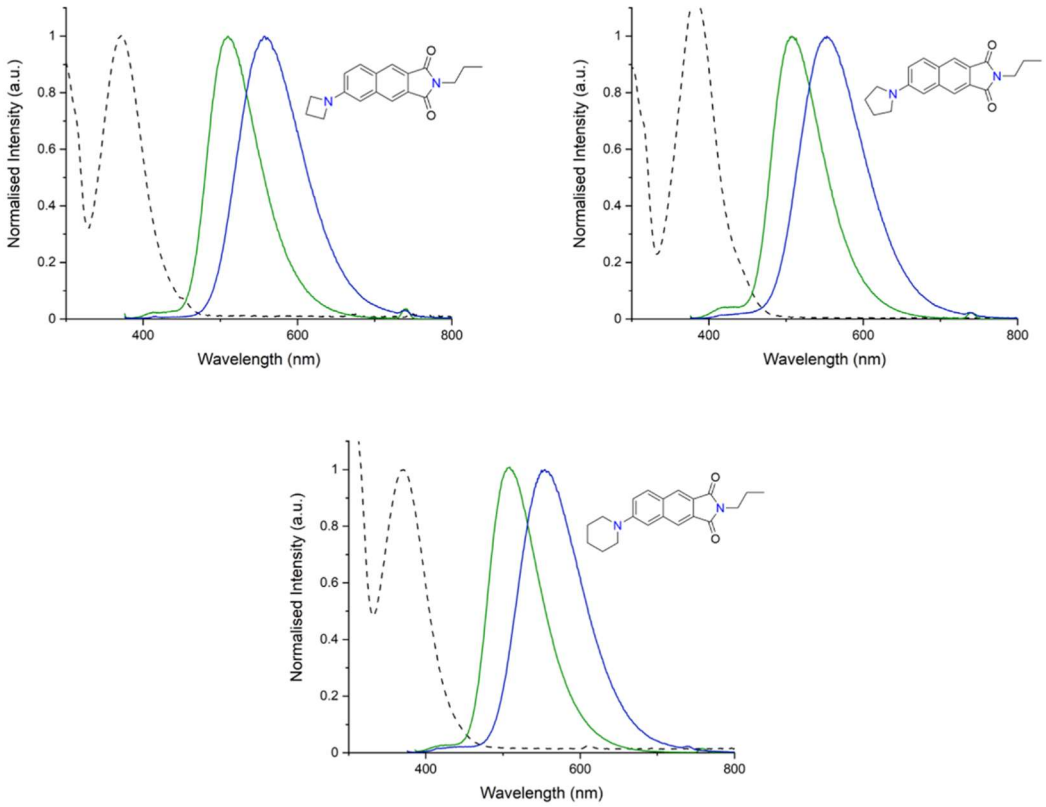


*Figure 199. (Top right) Absorption (dashed) and emission (solid) spectra of **215** in $CHCl_3$ (green) and DMSO (blue); (Top left) Absorption (dashed) and emission (solid) spectra of **209** in $CHCl_3$ (green) and DMSO (blue); (bottom) Absorption (dashed) and emission (solid) spectra of **206** in $CHCl_3$ (green) and DMSO (blue). Absorption spectra are that recorded in $CHCl_3$.*

## 7.5 Conclusion

To conclude, this chapter describes the synthesis of several 6-amino-2,3-naphthalimide derivatives including the variation of both the amine group at the 6-position of the naphthalimide ring, and variation of the imide functional group. To access these 6-amino-2,3-naphthalimide derivatives, a convenient Pd-mediated amination method that has been previously established in the literature[579] was optimised and employed for the installation of the various amine groups. This work has proven the diversity of this methodology for the coupling of a variety of primary and secondary amines including aliphatic, aromatic and heterocyclic. The introduction of the different imide functional groups to the 2,3-naphthlimide moiety afforded both successful and unsuccessful installations of the propane-1-amine group at the C-6 position of the naphthalimide ring.

## 7.6 Experimental: Chapter Seven

**6-Bromonaphtho[2,3-*c*]furan-1,3-dione (196)**

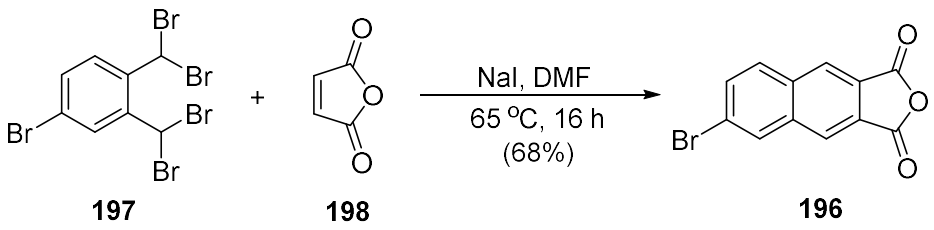


4-Bromo-1,2-bis(dibromomethyl)benzene **197** (1.098 g, 2.19 mmol) and maleic anhydride **198** (21.5 mg, 2.19 mmol) were dissolved in DMF (anhydrous, 7 mL). To this solution was added NaI (1.97 g, 13.1 mmol) and the reaction was heated at 65 °C. After 16 h, the solution was cooled to room temperature and poured into ice/water. The resulting precipitate was collected by vacuum filtration and washed with $H_2O$ to afford the title compound **196** (41.3 mg, 68%).

General procedure 1: Imine Formation

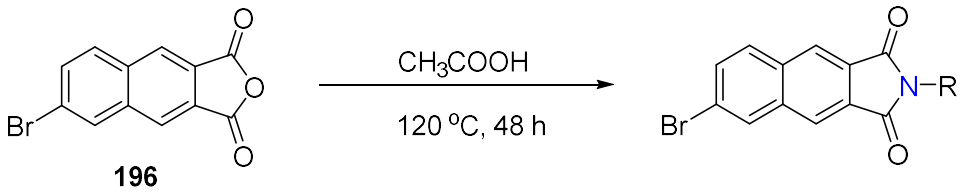


To a solution of 6-bromonaphtho[2,3-*c*]furan-1,3-dione **196** in acetic acid (5 mL) cooled to 0 °C, the amine was added. The resulting mixture was stirred at 120 °C. After 48 h, the solution was cooled to room temperature and poured into ice/water. The resulting precipitate was collected by vacuum filtration to afford the title compound.

General procedure 2: Buchwald-Hartwig Amination Reactions.

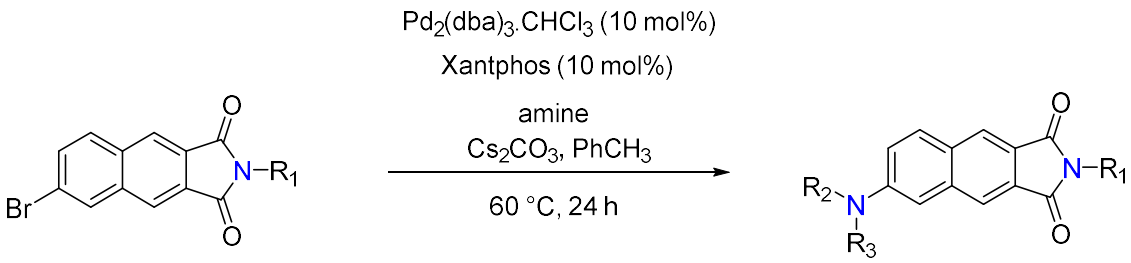


To a mixture of 6-bromo-2,3-naphthalimide, $Pd_2(dba)_3 \cdot CHCl_3$ (10 mol%), and Xantphos (10 mol%) in toluene (5 mL), amine (5 equiv.) and $Cs_2CO_3$ (3 equiv.) were added

sequentially and stirred for 24 h at 60 °C. After cooling to room temperature, an appropriate amount of $SiO_2$ was added, the solvent was removed *in vacuo* and the resulting residue dry loaded and purified by flash column chromatography.

**6-Bromo-2-propyl-1*H*-benzo[*f*]isoindole-1,3(2*H*)-dione (199)**

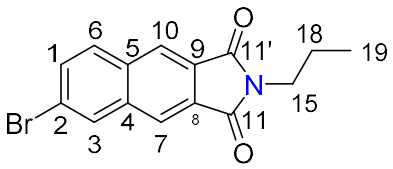


**199**

Following general procedure 1: 6-bromonaphtho[2,3-*c*]furan-1,3-dione **196** (105 mg, 0.360 mmol) and propane-1-amine (21.2 mg, 0.360 mmol) were heated in acetic acid (5 mL) at 120 °C for 48 h. The solution was poured into ice/water and the resulting precipitate was collected by vacuum filtration to afford the title compound **199** (102 g, 90%) as a white solid.

$^1$H NMR (400 MHz, $CDCl_3$) δ 8.30 (s, 1H, H-10), 8.24 (s, 1H, H-7), 8.22 (d, *J* = 2.0 Hz, 1H, H-3), 7.92 (d, *J* = 8.7 Hz, 1H, H-6), 7.76 (d, *J* = 2.0 Hz, 1H, H-1), 3.76–3.68 (m, 2H, H-15), 1.75 (h, *J* = 7.4 Hz, 2H, H-18), 0.98 (t, *J* = 7.4 Hz, 3H, H-19).

$^{13}$C NMR (101 MHz, $CDCl_3$) δ 167.96 (C-11), 167.88 (C-11'), 136.62 (C-4), 134.03 (C-5), 132.69 (C-1), 132.43 (C-3), 131.70 (C-6), 129.16 (C-8), 128.43 (C-9), 124.58 (C-10), 123.78 (C-2), 123.57 (C-7), 40.14 (C-15), 22.00 (C-18), 11.52 (C-19).

**6-Bromo-2-phenyl-1*H*-benzo[*f*]isoindole-1,3(2*H*)-dione (200)**

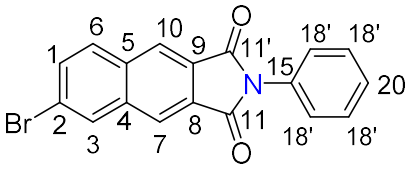


**200**

Following general procedure 1: 6-bromonaphtho[2,3-*c*]furan-1,3-dione (101 mg, 0.360 mmol) and aniline (33.6 mg, 0.360 mmol) were heated in acetic acid (5 mL) at 120 °C for 48 h. The solution was poured into ice/water and the resulting precipitate was collected by vacuum filtration to afford the title compound **200** (117 mg, 93%) a white solid.

$^{1}$H NMR (400 MHz, $CDCl_3$) δ 8.43 (s, 1H, H-10), 8.37 (s, 1H, H-7), 8.27 (d, *J* = 2.0 Hz, 1H, H-3), 7.97 (d, *J* = 8.8 Hz, 1H, H-6), 7.81 (dd, *J* = 8.7, 1.9 Hz, 1H, H-1), 7.58–7.47 (m, 4H, H-18), 7.47–7.39 (m, 1H, H-20).

$^{13}$C NMR (101 MHz, $CDCl_3$) δ 166.83 (C-11), 166.76 (C-11), 136.85 (C-2), 134.27 (C-4), 132.98 (C-1), 132.50 (C-3), 131.76 (C-6), 129.33 (C-18), 128.51 (C-20), 126.74 (C-18), 125.37 (C-10), 124.33 (C-7).

**6-Bromo-2-(2-hydroxyethyl)-1*H*-cyclopenta[*b*]naphthalene-1,3(2*H*)-dione (201)**

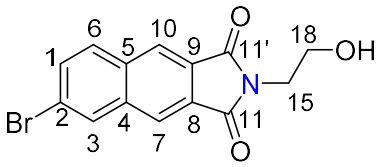


**201**

Following general procedure 1: 6-bromonaphtho[2,3-*c*]furan-1,3-dione **196** (100 mg, 0.360 mmol) and 2-aminoethan-1-ol (22.0 mg, 0.360 mmol) were heated in EtOH (5 mL) at 120 °C for 48 h. The solution was poured into ice/water and the resulting precipitate was collected by vacuum filtration to afford the title compound **201** (68 mg, 59%) a white solid.

$^{1}$H NMR (400 MHz, $CDCl_3$) δ 8.32 (s, 1H, H-10), 8.26 (s, 1H, H-7), 8.23 (m, 1H, H-3), 7.93 (d, *J* = 8.7 Hz, 1H, H-6), 7.79 (dd, *J* = 8.7, 2.0 Hz, 1H, H-1), 3.99 (m, 2H, H-18), 3.93 (m, 2H, H-15).

$^{13}$C NMR (101 MHz, $CDCl_3$) δ 167.62 (C-11), 167.54 (C-11'), 136.64 (C-4), 134.05 (C-5), 132.87 (C-1), 132.47 (C-6), 131.73 (C-3), 128.87 (C-8), 128.14 (C-9), 124.93 (C-10), 123.99 (C-2), 123.91 (C-7), 61.60 (C-18), 37.56 (C-15).

**2-(6-Bromo-1,3-dioxo-1,3-dihydro-2*H*-benzo[*f*]isoindol-2-yl)ethyl acetate (202)**

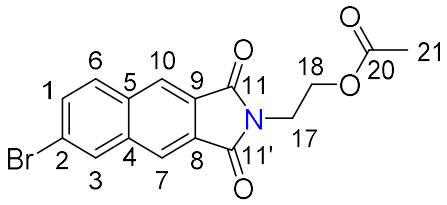


**202**

Following general procedure 1: 6-bromonaphtho[2,3-*c*]furan-1,3-dione **196** (102 mg, 0.360 mmol) and 2-aminoethan-1-ol (22.0 mg, 0.360 mmol) were heated in acetic acid (5 mL) at 120 °C for 48 h. The solution was poured into ice/water and the resulting precipitate was collected by vacuum filtration to afford the title compound **202** (84.8 mg, 65%) a white solid.

$^{1}$H NMR (400 MHz, $CDCl_3$) δ 8.33 (s, 1H, H-10), 8.26 (s, 1H, H-7), 8.23 (d, *J* = 1.9 Hz, 1H, H-3), 7.93 (d, *J* = 8.8 Hz, 1H, H-6), 7.78 (dd, *J* = 8.7, 2.0 Hz, 1H, H-1), 4.36 (t, *J* = 5.8, 4.9 Hz, 2H, H-18), 4.03 (t, *J* = 5.8, 4.9 Hz, 2H, H-17), 2.03 (s, 3H, H-21).

$^{13}$C NMR (101 MHz, $CDCl_3$) δ 171.05 (C-20), 167.62 (C-11), 167.55 (C-11'), 136.65 (C-4), 134.06 (C-5), 132.88 (C-1), 132.48 (C-6), 131.74 (C-3), 128.88 (C-8), 128.14 (C-9), 124.94 (C-10), 124.00 (C-2), 123.92 (C-7), 61.60 (C-18), 37.57 (C-17), 20.94 (C-21).

**6-Bromo-2-(prop-2-yn-1-yl)-1*H*-cyclopenta[*b*]naphthalene-1,3(2*H*)-dione (46)**

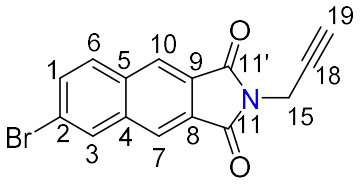


**46**

Following general procedure 1: 6-bromonaphtho[2,3-*c*]furan-1,3-dione **196** (108 mg, 0.360 mmol) and prop-2-yn-1-amine (19.8 mg, 0.360 mmol) were heated in acetic acid (5 mL) at 120 °C for 48 h. The solution was poured into ice/water and the resulting precipitate was collected by vacuum filtration to afford the title compound **46** (102 mg, 91%) as a white solid.

$^{1}$H NMR (400 MHz, $CDCl_3$) δ 8.35 (s, 1H, H-10), 8.29 (s, 1H, H-7), 8.23 (d, *J* = 2.0 Hz, 1H, H-3), 7.94 (d, *J* = 8.7 Hz, 1H, H-6), 7.79 (dd, *J* = 8.7, 2.0 Hz, 1H, H-1), 4.53 (d, *J* = 2.6 Hz, 2H, H-15), 2.25 (t, *J* = 2.5 Hz, 1H, H-19).

$^{13}$C NMR (101 MHz, $CDCl_3$) δ 166.48 (C-11), 166.42 (C-11'), 136.64 (C-4), 134.06 (C-5), 132.99 (C-1), 132.52 (C-3), 131.77 (C-6), 128.79 (C-8), 128.05 (C-9), 125.21 (C-10), 124.19 (C-7), 124.14 (C-2), 77.36 (C-18), 71.78 (C-19), 27.46 (C-15).

**6-Bromo-2-(prop-2-en-1-yl)-1*H*-benzo[*f*]isoindole-1,3(2*H*)-dione (203)**

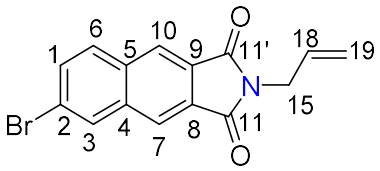


**203**

Following general procedure 1: 6-bromonaphtho[2,3-*c*]furan-1,3-dione **196** (100 mg, 0.360 mmol) and prop-2-en-1-amine (20.6 mg, 0.360 mmol) were heated in acetic acid (5 mL) at 120 ℃ for 48 h. The solution was poured into ice/water and the resulting precipitate was collected by vacuum filtration to afford the title compound **203** (97.5 mg, 86%) as a white solid.

$^{1}$H NMR (400 MHz, $CDCl_3$) δ 8.32 (s, 1H, H-10), 8.26 (s, 1H, H-7), 8.22 (d, *J* = 1.9 Hz, 1H, H-3), 7.93 (d, *J* = 8.7 Hz, 1H, H-6), 7.78 (dd, *J* = 8.7, 2.0 Hz, 1H, H-1), 5.92 (ddt, *J* = 17.1, 10.2, 5.7 Hz, 1H, H-18), 5.34–5.19 (m, 2H, H-19), 4.37 (dt, *J* = 5.7, 1.5 Hz, 2H, H-15).

$^{13}$C NMR (101 MHz, $CDCl_3$) δ 167.41 (C-11), 167.33 (C-11'), 136.63 (C-4), 134.05 (C-5), 132.79 (C-1), 132.46 (C-3), 131.72 (C-6), 131.43 (C-18), 129.04 (C-8), 128.31 (C-9), 124.81 (C-10), 123.91 (C-2), 123.79 (C-7), 118.20 (C-19), 40.57 (C-15).

**6-Bromo-1*H*-benzo[*f*]isoindole-1,3(2*H*)-dione (240)**

Following general procedure 1: 6-bromonaphtho[2,3-*c*]furan-1,3-dione **196** (102 mg, 0.360 mmol) and $NH_4OH.H_2$) (19.8 mg, 0.396 mmol) were heated in acetic acid (5 mL) at 120 ℃ for 48 h. The solution was poured into ice/water and the resulting precipitate was collected by vacuum filtration to afford the title compound **203** (89.4 mg, 90%) as a white solid.

$^{1}$H NMR (400 MHz, DMSO) δ 8.75 (d, *J* = 15.4 Hz, 2H), 8.62 (d, *J* = 2.1 Hz, 1H), 8.26 (d, *J* = 8.9 Hz, 1H), 7.86 (dd, *J* = 8.9, 2.0 Hz, 1H).

**2-Propyl-6-{[(pyridin-3-yl)methyl]amino}-1*H*-benzo[*f*]isoindole-1,3(2*H*)-dione (204)**

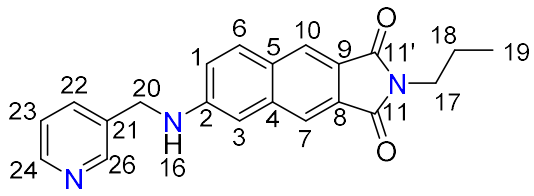


**204**

Following general procedure 2: 6-bromo-2-propyl-1*H*-benzo[*f*]isoindole-1,3(2*H*)-dione **199** (50.1 mg, 0.157 mmol), $Pd_2(dba)_3{\cdot}CHCl_3$ (16 mg, 0.157 mmol), Xantphos (9.1 mg, 0.015 mmol), 1-(pyridin-3-yl)methanamine (84.9 mg, 0.785 mmol) and $Cs_2CO_3$ (153 mg, 0.471 mmol) were heated in toluene (anhydrous, 5 mL) at 60 °C for 24 h. Purification by column chromatography (1:5 EtOAC/Hexane) afforded the title compound **204** (44.9 mg, 83%) as a yellow solid. $^1$H NMR (400 MHz, $CDCl_3$) δ 8.69 (d, *J* = 2.3 Hz, 1H, H-26), 8.57 (dd, *J* = 4.9, 1.6 Hz, 1H, H-24), 8.12 (s, 1H, H-10), 8.01 (s, 1H, H-7), 7.81 (d, *J* = 8.8 Hz, 1H, H-6), 7.73 (dt, *J* = 7.9, 2.0 Hz, 1H, H-22), 7.31 (dd, *J* = 7.8 Hz, 1H, H-23), 7.06 (dd, *J* = 8.8, 2.4 Hz, 1H, H-1), 6.95 (d, *J* = 2.4 Hz, 1H, H-3), 4.64 (t, *J* = 5.7 Hz, 1H, H-16), 4.52 (d, *J* = 5.0 Hz, 2H, H-20), 3.71–3.63 (m, 2H, H-17), 1.79–1.65 (m, 2H, H-18), 0.96 (t, *J* = 7.4 Hz, 3H, H-19).

$^{13}$C NMR (101 MHz, $CDCl_3$) δ 168.74 (C-11), 149.32 (C-26), 149.29 (C-24), 147.95 (C-2), 137.89 (C-21), 135.30 (C-22), 133.77 (C-4), 131.63 (C-6), 129.09 (C-5), 129.04 (C-9), 124.56 (C-10), 124.18 (C-8), 123.86 (C23), 122.39 (C-7), 119.96 (C-3), 107.16 (C-1), 45.62 (C-20), 39.82 (C-13), 22.06 (C-18), 11.52 (C-19). HRMS (ESI *m/z*): $C_{21}H_{20}N_3O_2$ $[M+H]^+$ 346.1550; found 346.1547.

**6-Anilino-2-propyl-1*H*-benzo[*f*]isoindole-1,3(2*H*)-dione (205)**

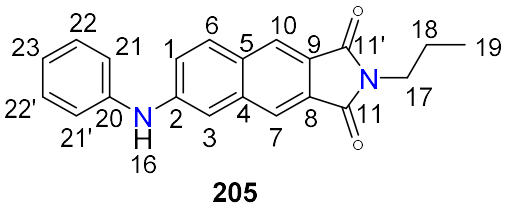


**205**

Following general procedure 2: 6-bromo-2-propyl-1*H*-benzo[*f*]isoindole-1,3(2*H*)-dione **196** (50.2 mg, 0.157 mmol), $Pd_2(dba)_3{\cdot}CHCl_3$ (16 mg, 0.157 mmol), Xantphos (9.1 mg, 0.015 mmol), aniline (73.1 mg, 0.785 mmol) and $Cs_2CO_3$ (153 mg, 0.471 mmol) were

heated in toluene (anhydrous, 5 mL) at 60 °C. Purification by column chromatography (1:5 EtOAC/Hexane) afforded the title compound **205** (28.8 mg, 56%) as a yellow solid.

$^{1}$H NMR (400 MHz, $CDCl_3$) δ 8.15 (s, 1H, H-10), 8.03 (s, 1H, H-7), 7.86 (d, *J* = 8.9 Hz, 1H, H-6), 7.49 (d, *J* = 2.4 Hz, 1H, H-3), 7.43–7.30 (m, 3H, H-1, H-21), 7.28–7.20 (m, 2H, H-22), 7.11 (td, *J* = 7.3, 1.2 Hz, 1H, H-23), 6.22 (s, 1H, H-16), 3.72–3.64 (m, 2H, H-17), 1.74 (m, *J* = 7.4 Hz, 2H, H-18), 0.96 (t, *J* = 7.4 Hz, 3H, H-19).

$^{13}$C NMR (101 MHz, $CDCl_3$) δ 168.65 (C-11), 168.62 (C-11'), 144.80 (C-20), 141.03 (C-2), 137.52 (C-4), 131.67 (C-6), 130.04 (C-5), 129.79 (C-21), 128.95 (C-9), 124.84 (C-8), 124.47 (C-10), 123.47 (C-23), 122.73 (C-7), 121.29 (C-3), 120.43 (C-22), 111.44 (C-1), 39.85 (C-17), 22.05 (C-18), 11.52 (C-19). HRMS (ESI *m/z*): $C_{21}H_{18}N_2O_2Na$ $[M+Na]^+$ 353.1261; found 353.1257.

**6-(Cyclohexylamino)-2-propyl-1*H*-benzo[*f*]isoindole-1,3(2*H*)-dione (206)**

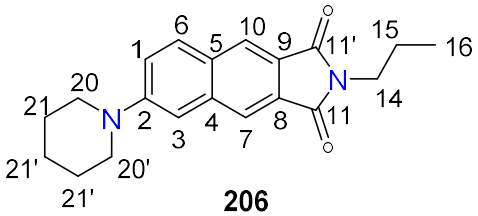


**206**

Following general procedure 2: 6-bromo-2-propyl-1*H*-benzo[*f*]isoindole-1,3(2*H*)-dione **199** (51.0 mg, 0.157 mmol), $Pd_2(dba)_3{\cdot}CHCl_3$ (16 mg, 0.157 mmol), Xantphos (9.1 mg, 0.015 mmol), piperidine (66.8 mg, 0.785 mmol) and $Cs_2CO_3$ (153 mg, 0.471 mmol) were heated in toluene (anhydrous, 5 mL) at 60 °C. Purification by column chromatography (1:5 EtOAC/Hexane) afforded the title compound **206** (15.3 mg, 30%) as a yellow solid. $^{1}$H NMR (400 MHz, $CDCl_3$) δ 8.15 (s, 1H, H-10), 8.10 (s, 1H, H-7), 7.87 (d, *J* = 9.1 Hz, 1H, H-6), 7.39 (dd, *J* = 9.1, 2.6 Hz, 1H, H-1), 7.23 (d, *J* = 2.5 Hz, 1H, H-3), 3.73–3.64 (m, 2H, H-14), 3.46–3.39 (m, 4H, H-20), 2.64 (dd, *J* = 6.3, 3.8 Hz, 6H, H-21), 1.80–1.67 (m, 2H, H-15), 0.97 (t, *J* = 7.4 Hz, 3H, H-16).

$^{13}$C NMR (101 MHz, $CDCl_3$) δ 168.82 (C-11), 168.77 (C-11'), 151.86 (C-2), 137.64 (C-4), 131.07 (C-6), 128.89 (C-5), 128.73 (C-9), 124.38 (C-8), 124.29 (C-10), 122.88 (C-7), 121.09 (C-3), 111.31 (C-1), 49.66 (C-20), 39.79 (C-14), 25.67 (C-21), 24.42 (C-15), 22.06 (C-21'), 11.53 (C-16). HRMS (ESI *m/z*): $C_{20}H_{23}N_2O_2$ $[M+H]^+$ 323.1754; found 323.1753.

**6-(4-Methylpiperazin-1-yl)-2-propyl-1*H*-benzo[*f*]isoindole-1,3(2*H*)-dione (207)**

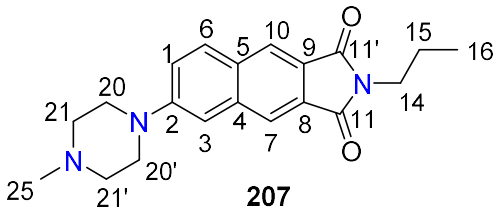


**207**

Following general procedure 2: 6-bromo-2-propyl-1*H*-benzo[*f*]isoindole-1,3(2*H*)-dione **196** (50.1 mg, 0.157 mmol), $Pd_2(dba)_3 \cdot CHCl_3$ (16 mg, 0.157 mmol), Xantphos (9.1 mg, 0.015 mmol), 1-methylpiperazine (89.6 mg, 0.785 mmol) and $Cs_2CO_3$ (153 mg, 0.471 mmol) were heated in toluene (anhydrous, 5 mL) at 60 °C for 24 h. Purification by column chromatography (1:5 EtOAC/Hexane) afforded the title compound **207** (42.2 mg, 80%) as a yellow solid.

$^1$H NMR (400 MHz, $CDCl_3$) δ 8.15 (s, 1H, H-10), 8.09 (s, 1H, H-7), 7.87 (d, *J* = 9.1 Hz, 1H, H-6), 7.39 (dd, *J* = 9.1, 2.5 Hz, 1H, H-1), 7.23 (d, *J* = 2.5 Hz, 1H, H-3), 3.72–3.64 (m, 2H, H-14), 3.46–3.39 (m, 4H, H-20), 2.63 (dd, *J* = 6.2, 4.0 Hz, 4H, H-21), 2.39 (s, 3H, H-25), 1.80–1.66 (m, 2H, H-15), 0.96 (t, *J* = 7.4 Hz, 3H, H-16).

$^{13}$C NMR (101 MHz, $CDCl_3$) δ 168.58 (C-11), 168.55 (C-11'), 151.14 (C-2), 137.34 (C-4), 131.05 (C-6), 129.23 (C-5), 128.71 (C-9), 124.75 (C-8), 124.17 (C-10), 122.95 (C-7), 120.62 (C-1), 111.41 (C3), 54.83 (C-21), 48.16 (C-20), 46.12 (C-25), 39.71 (C-14), 21.94 (C-15), 11.40 (C-16). HRMS (ESI *m/z*): $C_{20}H_{24}N_3O_2$ $[M+H]^+$ 338.1863; found 338.1859.

**6-[Benzyl(methyl)amino]-2-propyl-1*H*-benzo[*f*]isoindole-1,3(2*H*)-dione (208)**

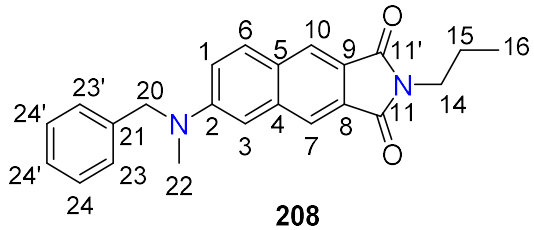


**208**

Following general procedure 2: 6-bromo-2-propyl-1*H*-benzo[*f*]isoindole-1,3(2*H*)-dione **199** (50.0 mg, 0.157 mmol), $Pd_2(dba)_3 \cdot CHCl_3$ (16 mg, 0.015 mmol), Xantphos (9.1 mg, 0.015 mmol), *N*-methyl-1-phenylmethanamine (84.9 mg, 0.785 mmol) and $Cs_2CO_3$ (154 mg, 0.471 mmol) were heated in toluene (anhydrous, 5 mL) at 60 °C for 24 h. Purification by column chromatography (1:5 EtOAC/Hexane) afforded the title compound **208** (31.9 mg, 57%) as a yellow solid.

$^{1}$H NMR (400 MHz, $CDCl_3$) δ 8.11 (s, 1H, H-10), 8.03 (s, 1H, H-7), 7.82 (d, *J* = 9.1 Hz, 1H, H-6), 7.37–7.30 (m, 2H, H-23), 7.30–7.19 (m, 4H, H-24, H-1), 7.07 (d, *J* = 2.6 Hz, 1H, H-3), 4.72 (s, 2H, H-20), 3.72–3.64 (m, 2H, H-14), 3.21 (s, 3H, H-22), 1.80–1.66 (m, 2H, H-15), 0.96 (t, *J* = 7.4 Hz, 3H, H-16).

$^{13}$C NMR (101 MHz, $CDCl_3$) δ 168.75 (C-11), 149.74 (C-2), 137.70 (C-21), 137.64 (C-4), 131.37 (C-6), 128.87 (C-23), 128.77 (C-5), 127.56 (C-9), 127.35 (C-3), 126.49 (C-24), 124.39 (C-10), 123.36 (C-8), 122.46 (C-7), 117.70 (C-23'), 107.97 (C-1), 56.29 (C-20), 39.65 (C-14), 38.95 (C-22), 21.95 (C-15), 11.40 (C-16). HRMS (ESI *m/z*): $C_{23}H_{23}N_2O_2$ $[M+H]^+$ 359.1754; found 359.1751.

**2-Propyl-6-(pyrrolidin-1-yl)-1*H*-benzo[*f*]isoindole-1,3(2*H*)-dione (209)**

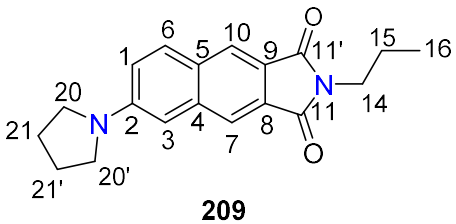


**209**

Following general procedure 2: 6-bromo-2-propyl-1*H*-benzo[*f*]isoindole-1,3(2*H*)-dione **199** (50.2 mg, 0.157 mmol), $Pd_2(dba)_3{\cdot}CHCl_3$ (16 mg, 0.157 mmol), Xantphos (9.1 mg, 0.015 mmol), pyrrolidine (55.8 mg, 0.785 mmol) and $Cs_2CO_3$ (153 mg, 0.471 mmol) were heated in toluene (anhydrous, 5.0 mL) at 60 °C for 24 h. Purification by column chromatography (1:5 EtOAC/Hexane) afforded the title compound **209** (15.5 mg, 32%) as a yellow solid.

$^{1}$H NMR (400 MHz, $CDCl_3$) δ 8.11 (s, 1H, H-10), 8.03 (s, 1H, H-7), 7.82 (d, *J* = 9.0 Hz, 1H, H-6), 7.07 (m, 1H, H-1), 6.86 (d, *J* = 2.4 Hz, 1H, H-3), 3.71–3.63 (m, 2H, H-14), 3.45 (td, *J* = 5.2, 2.1 Hz, 4H, H-20), 2.15–2.03 (m, 4H, H-21), 1.80–1.66 (m, 2H, H-15), 0.97 (t, *J* = 7.4 Hz, 3H, H-16).

$^{13}$C NMR (101 MHz, $CDCl_3$) δ 169.02 (C-11), 168.93 (C-11), 148.04 (C-2), 137.89 (C-4), 131.48 (C-6), 128.91 (C-5), 127.12 (C-9), 124.80 (C-10), 122.65 (C-8), 122.21 (C-7), 117.85 (C-1), 107.26 (C-3), 47.89 (C-20), 39.73 (C-14), 25.67 (C-21), 22.10 (C-15), 11.55 (C-16). HRMS (ESI *m/z*): $C_{19}H_{21}N_2O_2$ $[M+H]^+$ 309.1598; found 309.1596.

**6-(Morpholin-4-yl)-2-propyl-1*H*-benzo[*f*]isoindole-1,3(2*H*)-dione (210)**

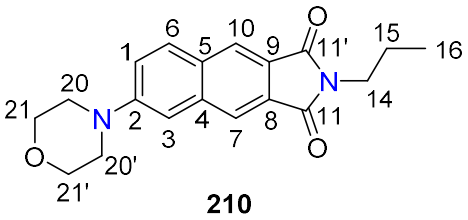


**210**

Following general procedure 2: 6-bromo-2-propyl-1*H*-benzo[*f*]isoindole-1,3(2*H*)-dione **199** (50.1 mg, 0.157 mmol), $Pd_2(dba)_3 \cdot CHCl_3$ (16 mg, 0.157 mmol), Xantphos (9.1 mg, 0.015 mmol), morpholine (68.3 mg, 0.785 mmol) and $Cs_2CO_3$ (153 mg, 0.471 mmol) were heated in toluene (anhydrous, 5 mL) at 60 °C for 24 h. Purification by column chromatography (1:5 EtOAC/Hexane) afforded the title compound **210** (44.4 mg, 44%) as a yellow solid.

$^1$H NMR (400 MHz, $CDCl_3$) δ 8.16 (s, 1H, H- 10), 8.10 (s, 1H, H-7), 7.89 (d, *J* = 9.1 Hz, 1H, H-6), 7.38 (dd, *J* = 9.1, 2.5 Hz, 1H, H-1), 7.23 (d, *J* = 2.5 Hz, 1H, H-3), 3.95–3.88 (m, 4H, H-21), 3.72–3.64 (m, 2H, H-14), 3.39–3.32 (m, 4H, H-20), 1.85–1.70 (m, 2H, H-15), 0.97 (t, *J* = 7.4 Hz, 3H, H-16).

$^{13}$C NMR (101 MHz, $CDCl_3$) δ 168.64 (C-11), 168.60 (C-11'), 151.34 (C-2), 137.36 (C-4), 131.27 (C-6), 129.63 (C-5), 128.89 (C-9), 125.12 (C-8), 124.31 (C-10), 123.06 (C-7), 120.30 (C-1), 111.44 (C-3), 66.80 (C-21), 48.58 (C-20), 39.85 (C-14), 22.05 (C-15), 11.52 (C-16). HRMS (ESI *m/z*): $C_{19}H_{21}N_2O_3$ $[M+H]^+$ 325.1547; found 325.1545.

**6-(Benzylamino)-2-propyl-1*H*-benzo[*f*]isoindole-1,3(2*H*)-dione (211)**

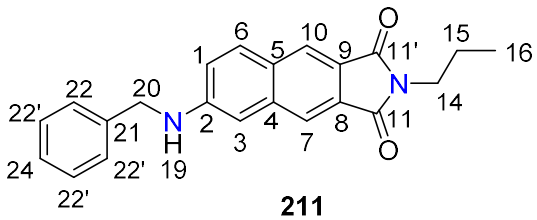


**211**

Following general procedure 2: 6-bromo-2-propyl-1*H*-benzo[*f*]isoindole-1,3(2*H*)-dione **199** (50.1 mg, 0.157 mmol), $Pd_2(dba)_3 \cdot CHCl_3$ (16 mg, 0.157 mmol), Xantphos (9.1 mg, 0.015 mmol), 1-phenylmethanamine (84.1 mg, 0.785 mmol) and $Cs_2CO_3$ (153 mg, 0.471 mmol) were heated in toluene (anhydrous, 5 mL) at 60 °C for 24 h. Purification by column chromatography (1:5 EtOAC/Hexane) afforded the title compound **211** (50.8 mg, 94%) as a yellow solid.

$^{1}$H NMR (400 MHz, $CDCl_3$) δ 8.12 (s, 1H, H-10), 8.01 (s, 1H, H-7) 7.79 (dd, *J* = 8.8, 0.7 Hz, 1H, H-6), 7.46–7.35 (m, 4H, H-22), 7.34–7.29 (m, 1H, H-24), 7.05 (dd, *J* = 8.8, 2.4 Hz, 1H, H-1), 6.96 (d, *J* = 2.4 Hz, 1H, H-3), 4.58 (d, *J* = 5.6 Hz, 1H, H-19), 4.48 (d, *J* = 5.2 Hz, 2H, H-20), 3.73–3.63 (m, 2H, H-14), 1.80–1.66 (m, 2H, H-15), 0.96 (t, *J* = 7.4 Hz, 3H, H-16).

$^{13}$C NMR (101 MHz, $CDCl_3$) δ 168.86 (C-11), 168.83 (C-11'), 148.45 (C-2), 138.21 (C-21), 138.03 (C-4), 131.48 (C-6), 129.04 (C-22), 129.01 (C-5), 128.79 (C-9), 127.86 (C-24), 127.68 (C-22'), 124.58 (C-10), 123.83 (C-8), 122.37 (C-7), 120.02 (C-1), 106.96 (C-3), 48.11 (C-20), 39.79 (C-14), 22.08 (C-15), 11.53 (C-16). HRMS (ESI *m/z*): $C_{22}H_{21}N_2O_2$ $[M+H]^+$ 345.1598; found 345.1596.

**2-Propyl-6-(propylamino)-1*H*-benzo[*f*]isoindole-1,3(2*H*)-dione (212)**

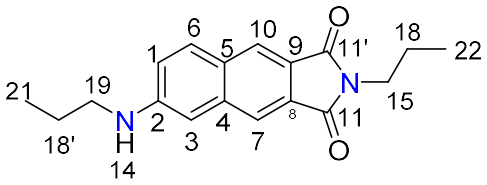


**212**

Following general procedure 2: 6-bromo-2-propyl-1*H*-benzo[*f*]isoindole-1,3(2*H*)-dione **199** (50.1 mg, 0.157 mmol), $Pd_2(dba)_3{\cdot}CHCl_3$ (16 mg, 0.157 mmol), Xantphos (9.1 mg, 0.015 mmol), propane-1-amine (46.4 mg, 0.785 mmol) and $Cs_2CO_3$ (153 mg, 0.471 mmol) were heated in toluene (anhydrous, 5 mL) at 60 °C for 24 h. Purification by column chromatography (1:5 EtOAC/Hexane) afforded the title compound **212** (36.8 mg, 79%) as a yellow solid.

$^{1}$H NMR (400 MHz, $CDCl_3$) δ 8.10 (s, 1H, H-10), 8.03 (s, 1H, H-7), 7.77 (d, *J* = 8.8 Hz, 1H, H-6), 6.99 (dd, *J* = 8.8, 2.4 Hz, 1H, H-1), 6.92 (d, *J* = 2.3 Hz, 1H, H-3), 4.19 (s, 1H, H-14), 3.72–3.64 (m, 2H, H-15), 3.23 (t, *J* = 7.1 Hz, 2H, H-19), 1.81–1.66 (m, 4H, H-18), 1.06 (t, *J* = 7.4 Hz, 3H, H-21), 0.97 (t, *J* = 7.4 Hz, 3H, H-22).

$^{13}$C NMR (101 MHz, $CDCl_3$) δ 168.95 (C-11), 168.89 (C-11'), 148.87 (C-2), 138.19 (C-4), 131.40 (C-6), 129.01 (C-5), 128.49 (C-9), 124.61 (C-10), 123.48 (C-8), 122.22 (C-7), 120.05 (C-3), 106.33 (C-1), 45.50 (C-19), 39.77 (C-15), 22.60 (C-18), 22.09 (C-18'), 11.78 (C21), 11.54 (C-22).

**6-(Piperazin-1-yl)-2-propyl-1*H*-benzo[*f*]isoindole-1,3(2*H*)-dione (213)**

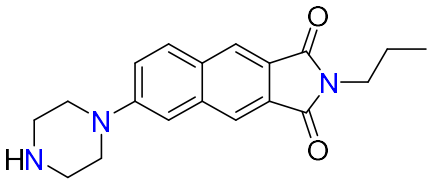

Following general procedure 2: 6-bromo-2-propyl-1*H*-benzo[*f*]isoindole-1,3(2*H*)-dione **199** (50.3 mg, 0.157 mmol), $Pd_2(dba)_3 \cdot CHCl_3$ (16 mg, 0.157 mmol), Xantphos (9.1 mg, 0.015 mmol), piperazine (67.6 mg, 0.785 mmol) and $Cs_2CO_3$ (153 mg, 0.471 mmol) were heated in toluene (anhydrous, 5 mL) at 60 °C for 24 h. Purification by column chromatography (1:5 EtOAC/Hexane) afforded the title compound **213** (53 mg, 10%) as a yellow solid. Further purification is required.

**6-(1-Methyl-1,4-diazepane)-2-propyl-1*H*-benzo[*f*]isoindole-1,3(2*H*)-dione (214)**

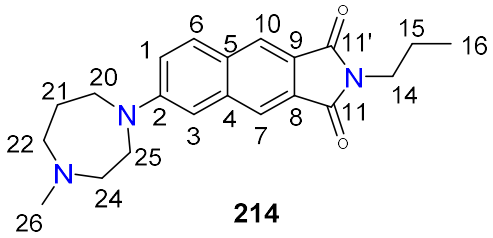


**214**

Following general procedure 2: 6-bromo-2-propyl-1*H*-benzo[*f*]isoindole-1,3(2*H*)-dione **199** (50.1 mg, 0.157 mmol), $Pd_2(dba)_3 \cdot CHCl_3$ (16 mg, 0.157 mmol), Xantphos (9.1 mg, 0.015 mmol), 1-methyl-1,4-diazepane (89.6 mg, 0.785 mmol) and $Cs_2CO_3$ (153 mg, 0.471 mmol) were heated in toluene (anhydrous, 5 mL) at 60 °C for 24 h. Purification by column chromatography (1:5 EtOAC/Hexane) afforded the title compound **214** (34.7 mg, 63%) as a yellow solid.

$^1$H NMR (400 MHz, $CDCl_3$) δ 8.11 (s, 1H, H-10), 8.04 (s, 1H, H-7), 7.84 (d, $J$ = 9.1 Hz, 1H, H-6), 7.20 (dd, $J$ = 9.2, 2.7 Hz, 1H, H-1), 7.02 (d, $J$ = 2.6 Hz, 1H, H-3), 3.81–3.74 (m, 2H, H-20), 3.72–3.62 (m, 4H, H-14, H-21), 2.88 (s, 2H, H-22), 2.71 (s, 2H, H-24), 2.48 (s, 3H, H-26), 2.20–2.13 (m, 2H, H-25), 1.80–1.65 (m, 2H, H-15), 0.97 (t, $J$ = 7.4 Hz, 3H, H-16).

$^{13}$C NMR (101 MHz, $CDCl_3$) δ 168.88 (C-11), 168.83 (C-11'), 149.39 (C-2), 137.89 (C-4), 131.64 (C-6), 128.99 (C-5), 127.57 (C-9), 124.52 (C-10), 123.43 (C-8), 122.48 (C-7), 117.35 (C-1), 107.63 (C-3), 57.95 (C-22), 57.10 (C-24), 48.38 (C-20), 46.59 (C-26),

29.85 (C-14), 27.17 (C-25), 22.09 (C-15), 11.54 (C-16). HRMS (ESI *m/z*): $C_{20}H_{24}N_3O_2$ $[M+H]^+$ 338.1863; found 338.1859.

**6-(Azetidin-1-yl)-2-propyl-1*H*-benzo[*f*]isoindole-1,3(2*H*)-dione (215)**

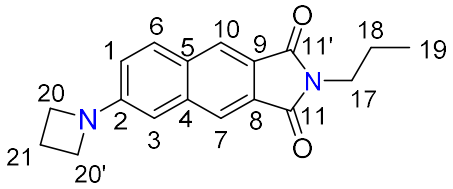


**215**

Following general procedure 2: 6-bromo-2-propyl-1*H*-benzo[*f*]isoindole-1,3(2*H*)-dione **199** (50.1 mg, 0.157 mmol), $Pd_2(dba)_3{\cdot}CHCl_3$ (16 mg, 0.157 mmol), Xantphos (9.1 mg, 0.015 mmol), azetidine (73.4 mg, 0.785 mmol) and $Cs_2CO_3$ (153 mg, 0.471 mmol) were heated in toluene (anhydrous, 5 mL) at 60 °C for 24 h. Purification by column chromatography (1:5 EtOAC/Hexane) afforded the title compound **215** (1.9 mg, 4%) as a yellow solid.

$^1$H NMR (400 MHz, $CDCl_3$) δ 8.12 (s, 1H, H-10), 8.03 (s, 1H, H-7), 7.82 (dd, *J* = 8.9, 0.7 Hz, 1H, H-6), 6.87 (dd, *J* = 8.8, 2.4 Hz, 1H, H-1), 6.73 (d, *J* = 2.3 Hz, 1H, H-3), 4.07 (t, *J* = 7.3 Hz, 4H, H-20), 3.72–3.64 (m, 2H, H-17), 2.48 (tt, *J* = 7.9, 6.9 Hz, 2H, H-21), 1.80–1.66 (m, 2H, H-18), 0.96 (t, *J* = 7.4 Hz, 3H, H-19).

$^{13}$C NMR (101 MHz, $CDCl_3$) δ 168.91 (C-11), 168.85 (C-11'), 151.62 (C-2), 137.50 (C-4), 131.43 (C-6), 128.96 (C-5), 128.04 (C-9), 124.87 (C-10), 123.41 (C-8), 122.22 (C-7), 116.44 (C-1), 106.61 (C-3), 52.09 (C-20), 39.78 (C-17), 22.08 (C-18), 16.82 (C-21), 11.54 (C-19). HRMS (ESI *m/z*): $C_{18}H_{19}N_2O_2$ $[M+H]^+$ 295.1441; found 295.1440.

**6-(Dipyridin-3-yl)methyl)-2-propyl-1*H*-benzo[*f*]isoindole-1,3(2*H*)-dione (216)**

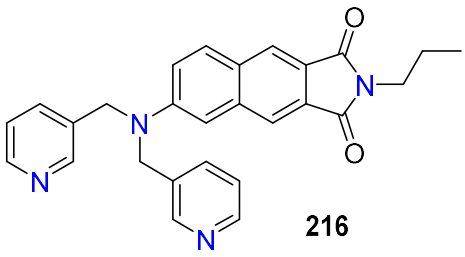


**216**

Following general procedure 2: 6-bromo-2-propyl-1*H*-benzo[*f*]isoindole-1,3(2*H*)-dione **199** (50.0 mg, 0.157 mmol), $Pd_2(dba)_3{\cdot}CHCl_3$ (16 mg, 0.157 mmol), Xantphos (9.1 mg, 0.015 mmol), 1-(pyridin-3-yl)-*N*-[(pyridin-3-yl)methyl]methanamine (156 mg, 0.785

mmol) and $Cs_2CO_3$ (153 mg, 0.471 mmol) were heated in toluene (anhydrous, 5 mL) at 60 °C for 24 h. Purification by column chromatography (1:5 EtOAC/Hexane) afforded the title compound **216** (19.4 mg, 28%) as a brown oil. Further purification is required. HRMS (ESI *m/z*): $C_{27}H_{25}N_4O_2$ $[M+H]^+$ 437.19720; found 437.1969.

**2-(2-Hydroxyethyl)-6-(propylamino)-1*H*-benzo[*f*]isoindole-1,3(2*H*)-dione (217)**

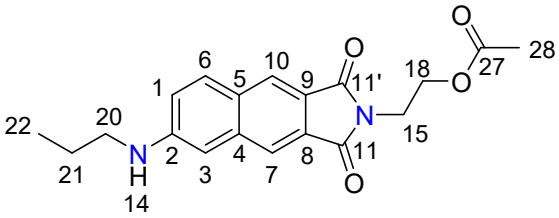


**217**

Following general procedure 2: 6-bromo-2-(2-hydroxyethyl)-1*H*-benzo[*f*]isoindole-1,3(2*H*)-dione **201** (50.5 mg, 0.156 mmol), $Pd_2(dba)_3{\cdot}CHCl_3$ (16 mg, 0.015 mmol), Xantphos (9.1 mg, 0.015 mmol), propane-1-amine (46.1 mg, 0.781 mmol) and $Cs_2CO_3$ (152 mg, 0.469 mmol) were heated in toluene (anhydrous, 5 mL) at 60 °C for 24 h. Purification by column chromatography (1:5 EtOAC/Hexane) afforded the title compound **217** (29.3 mg, 63%) as a yellow solid.

$^1$H NMR (400 MHz, $CDCl_3$) δ 8.11 (s, 1H, H-7), 8.04 (d, *J* = 0.7 Hz, 1H, H-10), 7.76 (dd, *J* = 8.8, 0.7 Hz, 1H, H-6), 6.99 (dd, *J* = 8.8, 2.4 Hz, 1H, H-1), 6.90 (d, *J* = 2.3 Hz, 1H, H-3), 4.33 (dd, *J* = 5.8, 5.0 Hz, 2H, H-18), 4.25 (s, 1H, H-14), 3.98 (dd, *J* = 5.8, 5.0 Hz, 2H, H-15), 3.23 (t, *J* = 7.1 Hz, 2H, H-20), 2.03 (s, 1H, H-28) 1.73 (h, *J* = 7.4 Hz, 2H, H-21), 1.06 (t, *J* = 7.4 Hz, 3H, H-22).

$^{13}$C NMR (101 MHz, $CDCl_3$) δ 171.08 (C-27), 168.57 (C-11), 168.47 (C-11'), 149.00 (C-2), 138.24 (C-4), 131.43 (C-1), 128.70 (C-5), 128.48 (C-9), 124.93 (C-7), 123.08 (C-8), 122.48 (C-10), 120.21 (C-3), 106.25 (C-1), 61.77 (C-19), 45.45 (C-20), 37.10 (C-15), 22.56 (C-21), 20.96 (C-28) 11.77 (C-22). HRMS (ESI *m/z*): $C_{17}H_{18}N_2O_3$ $[M+H]^+$ 298.1310; found 297.1595.

**2-(Prop-2-en-1-yl)-6-(propylamino)-1*H*-cyclopenta[*b*]naphthalene-1,3(2*H*)-dione (218)**

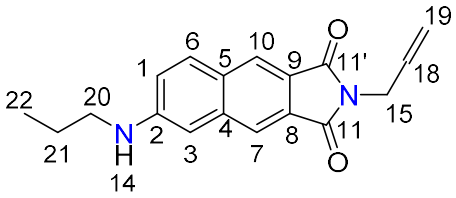


**218**

Following general procedure 2: 6-bromo-2-(prop-2-en-1-yl)-1*H*-benzo[*f*]isoindole-1,3(2*H*)-dione **203** (50.1 mg, 0.158 mmol), $Pd_2(dba)_3 \cdot CHCl_3$ (16 mg, 0.015 mmol), Xantphos (9.1 mg, 0.015 mmol), propane-1-amine (46.6 mg, 0.790 mmol) and $Cs_2CO_3$ (154 mg, 0.474 mmol) were heated in toluene (anhydrous, 5 mL) at 60 °C for 24 h. Purification by column chromatography (1:5 EtOAC/Hexane) afforded the title compound **218** (21.9 mg, 47%) as a yellow solid.

$^1$H NMR (400 MHz, $CDCl_3$) δ 8.11 (s, 1H, H-10), 8.04 (s, 1H, H-7), 7.76 (d, *J* = 8.8 Hz, 1H, H-6), 6.99 (dd, *J* = 8.8, 2.4 Hz, 1H, H-1), 6.91 (d, *J* = 2.3 Hz, 1H, H-3), 5.92 (ddt, *J* = 17.2, 10.3, 5.6 Hz, 1H, H-18), 5.31–5.15 (m, 2H, H-19), 4.32 (dt, *J* = 5.6, 1.5 Hz, 2H, H-15), 4.23 (s, 1H, H-14), 3.23 (t, *J* = 7.1 Hz, 2H, H-20), 1.74 (h, *J* = 7.3 Hz, 2H, H-21), 1.06 (t, *J* = 7.4 Hz, 3H, H-22).

$^{13}$C NMR (101 MHz, $CDCl_3$) δ 168.39 (C-11), 168.32 (C-11'), 148.95 (C-2), 138.22 (C-4), 131.97 (C-18), 131.42 (C-3), 128.88 (C-5), 128.48 (C-9), 124.82 (C10), 123.29 (C-8), 122.40 (C-7), 120.13 (C-6), 117.56 (C-19), 106.30 (C-1), 45.47 (C-20), 40.21 (C-15), 22.57 (C-21), 11.77 (C-22). HRMS (ESI *m/z*): $C_{18}H_{19}N_2O_2$ $[M+H]^+$ 295.1441; found 295.1439.

**2-Phenyl-6-(propylamino)-1*H*-benzo[*f*]isoindole-1,3(2*H*)-dione (219)**

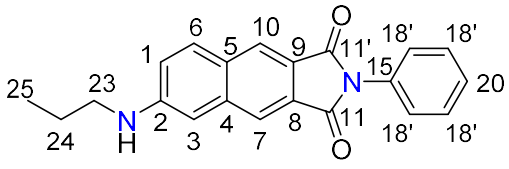


**219**

Following general procedure 2: 6-bromo-2-phenyl-1*H*-benzo[*f*]isoindole-1,3(2*H*)-dione **200** (50.3 mg, 0.141 mmol), $Pd_2(dba)_3 \cdot CHCl_3$ (16 mg, 0.014 mmol), Xantphos (9.1 mg,

0.014 mmol), propane-1-amine (41.9 mg, 0.709 mmol) and $Cs_2CO_3$ (137 mg, 0.423 mmol) were heated in toluene (anhydrous, 5 mL) at 60 ℃ for 24 h. Purification by column chromatography (1:5 EtOAC/Hexane) afforded the title compound **219** (27.2 mg, 58%) as a yellow solid.

$^1$H NMR (400 MHz, $CDCl_3$) δ 8.21 (s, 1H, H-10), 8.13 (s, 1H, H-7), 7.79 (d, *J* = 8.9 Hz, 1H, H-6), 7.56–7.45 (m, 4H, H-18), 7.45–7.33 (m, 1H, H-20), 7.02 (dd, *J* = 8.8, 2.4 Hz, 1H, H-1), 6.94 (d, *J* = 2.4 Hz, 1H, H-3), 3.24 (t, *J* = 7.1 Hz, 2H, H-23), 1.73 (h, *J* = 7.3 Hz, 2H, H-24), 1.07 (t, *J* = 7.4 Hz, 3H, H-25).

$^{13}$C NMR (101 MHz, $CDCl_3$) δ 167.76 (C-11), 167.68 (C-11'), 149.08 (C-2), 138.49 (C-4), 132.35 (C-5), 131.45 (C-6), 129.14 (C-18), 128.74 (C-9), 128.48 (C-8), 128.02 (C-20), 126.80 (C-19), 126.78 (C-18), 125.36 (C-10), 122.81 (C-7), 120.37 (C-1), 106.16 (C-3), 45.44, 22.54, 11.77. HRMS (ESI *m/z*): $C_{21}H_{19}N_2O_2$ $[M+H]^+$ 331.1441; found 331.1440.

# *Chapter Eight*
# Conclusion and Future Work

## 8.1 Conclusion

This thesis has presented an investigation into the synthesis and characterisation of ligands that contain extended aromatic surfaces and the resulting coordination chemistry. Of particular interest was the incorporation of quinoline and naphthalene scaffolds into multidentate ligands. To this end, the synthesis and characterisation of the tetradentate tripodal 2-quinolylmethyl ligand **55** and tridentate 2-quinolulemthyl ligand **68**, and the tri- and tetradentate 2-quinolylethyl-based ligands **57**, **58**, **63**, **64** and **66** was achieved. Each ligand was characterised by means of NMR spectroscopy ($^{1}$H, $^{13}$C, COSY, HSQC and HMBC) and HRMS.

During the synthesis of the quinoline starting materials, we obtained results that differed from the literature methodology. This work was based on the synthesis of 2-(2-chloroethyl)quinoline which in our hands was obtained as the hydrochloride salt, unlike the reported procedure. The further reaction of this with $NaN_3$ was also investigated. This led to the isolation of 2-(2-azidoethyl)quinoline and subsequent 'click chemistry' between this molecule and two different 1,8- and 2,3-naphthalimide derivatives.

The copper, zinc and manganese complexes of **55** were isolated and structurally characterised. The Cu and Zn complexes are isomorphous in which both metal ions are five coordinate with the metal ion bound by all four nitrogen donor atoms of the ligand and the fifth position occupied by a coordinating $CH_3CN$ ligand. The reaction of **55** and Mn(II) afforded a rare bis(μ-oxo) diMn(III) species that has potential applications in modelling the enzyme involved in the oxygen-evolving complex of Photosystem II.

A Pd(II) complex of the 2-quinolylethyl ligand **58** has been isolated and characterised. The cation displays a square planar geometry with one of the quinolyl arms remaining

uncoordinated. X-ray crystallography and NMR spectroscopy data confirm the isolation of a single geometric isomer of this species. The reaction of the 2-quinolylethyl-containing ligand **64** with Co(II) afforded the dimer [(**62**)Co(OH)$_3$Co(**62**)](ClO$_4$)$_3$.CH$_3$CN, in which the 2-quinolylethyl arm has detached from the ligand. The dinuclear species is a rare example of a complex in which two Co(III) metal centres are bridged together via three hydroxido ligands. There are only two other examples of structurally characterised cobalt complexes that contain this ligand coordination environment.[434,435] Despite our numerous efforts, no crystalline material was obtained for any other coordination complexes of other metal ions or 2-quinolylethyl-containing ligands. Thus, alternative solution state characterisation methods including mass spectrometry and Job's method were utilised. The results of these studies revealed a 1:1 binding stoichiometry of all the metal ions and ligands analysed, regardless of the starting mole ratios of ligand to metal. Furthermore, the weak binding affinity of the majority of the ligands to the metal ions Co(II), Ni(II), Zn(II) and Mn(II) was revealed.

In addition, the incorporation of the naphthalene moiety as an extension of benzimidazole was studied. This work included the synthesis of four tetradentate tripodal ligands that contain a 2-methyl-1*H*-naphtho[2,3-*d*]imidazole group, namely **74**, **75**, **76** and **77**. Each of the four ligands was characterised by means of NMR spectroscopy ($^1$H, $^{13}$C, COSY, HSQC and HMBC) and HRMS. Interestingly, these ligands also did not afford any crystalline material upon the reaction with several metal ions. Therefore, solution state characterisation methods were also employed to analyse the resulting metal complexes. In this instance, only mass spectrometry studies of the reaction between the naphthalene-containing ligands and metal ions were conducted.

To round off our investigation into the incorporation of planar aromatic moieties into amino ligands, pyrene was examined, and the synthesis of a pyrene and quinoline-based bidentate ligand **82** is presented.

The final chapter presents a separate project carried out under the supervision of Dr. Cassandra Fleming. This work entailed the synthesis of a series of 6-amino-2,3-naphthalimide derivatives in which the functionalisation at the imide group and C-6 position on the naphthalimide ring was varied, and an investigation into the fluorescent properties of the resulting 6-amino-2,3-naphthalimide derivatives was conducted.

## 8.2 Future Work

There is a wide scope for future research building on the results presented in this thesis. Firstly, with only a few quinolylethyl-based ligands known, and, to date, no reports of tripodal tetradentate ligands containing unsubstituted 2-quinolylethyl moieties, there are still a large number of possible quinoline ligands that could be synthesised. Of particular interest is the further investigation into the synthesis of 1-(quinolin-2-yl)methanamine and 2-(quinolin-2-yl)ethan-1-amine starting materials as these compounds would provide the central nitrogen source in place of the pyridyl units used in this work.

The photophysical properties of quinoline derivatives have been well established and remains an active area of research. Quinoline is of interest as the molecule exhibits low initial fluorescence but can form highly fluorescent complexes with various metal ions.[598] There has been a number of recent studies that have utilised quinoline-derived compounds as a fluorescent probe for several applications including bioimaging[599,600] and metal ion sensing.[601] Therefore, it would be of interest to investigate the photophysical properties of the quinoline-containing ligands and corresponding metal complexes that have been presented in this work.

A small section of this thesis described the synthesis of 2-(2-azidoethyl)quinoline and the sequential click chemistry of this molecule. This work only presented the synthesis and each compound was only analysed by NMR spectroscopy and HRMS. Further characterisation of these compounds including the photophysical properties would be interesting and may reveal potential applications.

A significant aspect of our work was the lack of crystalline material obtained for structural characterisation. Although a number of conditions and techniques were trialled, more work is required to fully analyse the coordination chemistry of these ligands.

An interesting result was obtained during the characterisation of the naphthalene-containing ligands and this was the indication of a fluxional process occurring. This was indicated by the broad naphthalene carbon signals revealed in the $^{13}C$ NMR spectra. Additional investigation into this feature is required to fully understand what is influencing this process.

Overall, the ligands described in this thesis have expanded the field of multidentate tripodal chemistry and future work will hopefully reveal a number of interesting applications.

# References


1. Kumar, R. *et al.* Quinoline-based metal complexes: Synthesis and applications. *Coord Chem Rev* **499**, 215453 (2024).
2. Blackman, A., Bottle, S., Schmid, S., Mocerino, M. & Wille, U. Transition metal chemistry. in *Chemistry* 551–556 (John Wiley & Sons Australia, 2015).
3. Royappa, A. T. *et al.* Copper(I) oxalate complexes: Synthesis, structures and surprises. *Polyhedron* **119**, 563–574 (2016).
4. Chieh, P. C. Crystal and molecular structure of aquobis-(2,2′-bipyridyl)palladium dinitrate. *J. Chem. Soc., Dalton Trans.* 1643–1646 (1972) doi:10.1039/DT9720001643.
5. Allen, C. S., Chuang, C.-L., Cornebise, M. & Canary, J. W. Electrospray mass spectrometry and X-ray crystallography studies of divalent metal ion complexes of tris (2-pyridylmethyl) amine. *Inorganica Chim Acta* **239**, 29–37 (1995).
6. Ouellette, R. J. & Rawn, J. D. Alkanes and Cycloalkanes: Structures and Reactions. in *Organic Chemistry* 87–133 (Elsevier, 2018). doi:10.1016/B978-0-12-812838-1.50004-9.
7. Gordon, M. S. Ring strain in cyclopropane, cyclopropene, silacyclopropane, and silacyclopropene. *J Am Chem Soc* **102**, 7419–7422 (1980).
8. Irving, H., Williams, R. J. P., Ferrett, D. J. & Williams, A. E. The influence of ring size upon the stability of metal chelates. *Journal of the Chemical Society (Resumed)* 3494 (1954) doi:10.1039/jr9540003494.
9. Lundin, N. J., Hamilton, I. G. & Blackman, A. G. Synthesis and hypodentate Cu(II) complexes of new tripodal tetraamine ligands incorporating a long pendant arm. *Polyhedron* **23**, 97–102 (2004).
10. β β’ β"-Triaminotriethylamine and its complex metallic compounds. *Proceedings of the Royal Society of London. Series A, Containing Papers of a Mathematical and Physical Character* **109**, 444–458 (1925).
11. Ristenpart, E. Ueber die Einwirkung von Ammoniak und Alkylaminen auf Bromäthylphtalimid. *Berichte der deutschen chemischen Gesellschaft* **29**, 2526–2533 (1896).
12. Geue, R., Sargeson, A. & Wijesekera, R. Metal Ion Promoted Hydrolysis of Polyphosphates. *Aust J Chem* **46**, 1021 (1993).
13. Vasil’eva, V. F., Lavrova, O. Y., Dyatlova, M. N. & Yashunskii Zh. Obshch. Khim, V. G. Vasileva, V. F., et al. ‘Synthesis and complex-forming properties of N’-(beta-carboxyethyl)-diethylenetetramine-*N*,*N*,*N*’’’,*N*’’-tetraacetic acid’. *Journal of General Chemistry* **36**, 688 (1966).
14. Dittler-Klingemann, A. M. & Hahn, F. E. Trigonal-Bipyramidal Copper(II) Complexes with Symmetric and Unsymmetric Tripodal Tetramine Ligands. *Inorg Chem* **35**, 1996–1999 (1996).
15. Fanshawe, R. L. & Blackman, A. G. Synthesis of the New Asymmetric Tripodal Amine Ligand abap: Crystal Structure of $[Co(abap)(O_2NO)](ClO_4)_2$ and Stability

and Reactivity of $[Co(abap)(OH_2)_2]^{3+}$ toward Phosphate Esters. *Inorg Chem* **34**, 421–423 (1995).
16. Streater, M., Taylor, P. D., Hider, R. C. & Porter, J. Novel 3-hydroxy-2(1H)-pyridinones. Synthesis, iron(III)-chelating properties and biological activity. *J Med Chem* **33**, 1749–1755 (1990).
17. Keypour, H. & Stotter, D. A. Macrocycle synthesis. CR-type complexes displaying pendant ligation and N3S coordination. *Inorganica Chim Acta* **33**, L149–L150 (1979).
18. Mann, F. G. & Pope, W. J. LXIII.–γγ′γ″-Triaminotripropylamine and its complex compounds with nickel. *J. Chem. Soc.* **129**, 489–493 (1926).
19. Blackman, A. G. The coordination chemistry of tripodal tetraamine ligands. (2004) doi:10.1016/j.poly.2004.10.012.
20. Leibold, M. *et al.* Effect of Chelate Ring Size in Iron(II) Isothiocyanato Complexes with Tetradentate Tripyridyl-alkylamine Ligands on Spin Crossover Properties. (2016) doi:10.1002/zaac.201500684.
21. Cavigliasso, G. *et al.* A computational study of the electronic structure, bonding, and spectral properties of tripodal tetraamine Co(III) carbonate complexes. *Dalton Transactions* 2433–2441 (2008) doi:10.1039/B717619H.
22. Mcclintock, L. F., Cavigliasso, G., Stranger, R. & Blackman, A. G. The donor ability of the chelated carbonate ligand: protonation and metallation of $[(L)Co(O_2CO)]^+$ complexes in aqueous solution. (2008) doi:10.1039/b806981f.
23. Jaffray, P. M., Mcclintock, L. F., Baxter, K. E. & Blackman, A. G. Cobalt(III) Carbonate and Bicarbonate Chelate Complexes of Tripodal Tetraamine Ligands Containing Pyridyl Donors: The Steric Basis for the Stability of Chelated Bicarbonate Complexes. (2005) doi:10.1021/ic0482537.
24. Mann, F. G. & Pope, W. J. B B' B" - Triaminotriethylamine and its Complexes Metallic Compounds. *Proceedings of the Royal Society* (1925).
25. Canary, J. W., Wang, Y., Roy, R., Lawrence Que & Miyake, H. Tris[(2-Pyridyl)Methyl] Amine (TPA) and (+)-Bis[(2-Pyridyl)methyl]-1-(2-Pyridyl)-Ethylamine (α-Metpa). in 70–75 (2007). doi:10.1002/9780470132630.ch11.
26. Anderegg, G. & Wenk, F. Pyridinderivate als Komplexbildner VIII Die Herstellung je eines neuen vier- und sechszähnigen Liganden. *Helv Chim Acta* **50**, 2330–2332 (1967).
27. Brownstein, S. K., Plouffe, P.-Y., Bensimon, C. & Tse, J. Complexes of Tris((2-pyridyl)alkyl)amines with Lithium and Sodium Salts+. *Inorg. Chem* **33**, 354–358 (1994).
28. Karlin, K. D., Hayes, J. C., Hutchinson, J. P., Hyde, J. R. & Zubieta, J. Synthesis and x-ray structural characterization of Cu(I) and Cu(II) derivatives of a new symmetric tripodal ligand $N(CH_2CH_2\text{-}py)_3$, (py = 2-pyridyl). *Inorganica Chim Acta* **64**, L219–L220 (1982).
29. Tooze, R. P. *et al.* Anal. Caled for. *J. Chem. Soc., Chem. Commun* **112**, 883 (1990).
30. Schatz, M. *et al.* Copper(I) Complexes, Copper(I)/$O_2$ Reactivity, and Copper(II) Complex Adducts, with a Series of Tetradentate Tripyridylalkylamine Tripodal Ligands. (2001) doi:10.1021/ic000924n.
31. Blackman, A. G. Tripodal Tetraamine Ligands Containing Three Pyridine Units: The other Polypyridyl Ligands. (2008) doi:10.1002/ejic.200800115.
32. Jain, S. *et al.* Comprehensive review on current developments of quinoline-based anticancer agents. *Arabian Journal of Chemistry* **12**, 4920–4946 (2019).
33. Ginsburg, S. & Wilson, I. B. Oximes of the Pyridine Series. *J Am Chem Soc* **79**, 481–485 (1957).

34. Suliphuldevara Matada, B., Pattanashettar, R. & Gunavanthrao Yernale, N. A comprehensive review on the biological interest of quinoline and its derivatives. *Bioorg. Med. Chem* **32**, 115973 (2021).
35. Ray, R. L. Alkaloids—The world's pain killers. *J Chem Educ* **37**, 451–454 (1960).
36. Mohasin, Md. *et al.* A Review on Synthesis and Biological Applications of Quinoline Derivative as Fused Aromatic Compounds. *Polycycl Aromat Compd* 1–30 (2023) doi:10.1080/10406638.2023.2270118.
37. Elebiju, O. F., Ajani, O. O., Oduselu, G. O., Ogunnupebi, T. A. & Adebiyi, E. Recent advances in functionalized quinoline scaffolds and hybrids—Exceptional pharmacophore in therapeutic medicine. *Front Chem* **10**, (2023).
38. Weyesa, A. & Mulugeta, E. Recent advances in the synthesis of biologically and pharmaceutically active quinoline and its analogues: a review. *RSC Adv* **10**, 20784–20793 (2020).
39. Mittal, R. K., Aggarwal, M., Khatana, K. & Purohit, P. Quinoline: Synthesis to Application. *Med Chem (Los Angeles)* **19**, 31–46 (2023).
40. Bissani Gasparin, C. & Pilger, D. A. 8-Hydroxyquinoline, Derivatives and Metal-Complexes: A Review of Antileukemia Activities. *ChemistrySelect* **8**, (2023).
41. Sonkar, C., Sarkar, S. & Mukhopadhyay, S. Ruthenium(ii)–arene complexes as anti-metastatic agents, and related techniques. *RSC Med Chem* **13**, 22–38 (2022).
42. Gupta, R., Luxami, V. & Paul, K. Insights of 8-hydroxyquinolines: A novel target in medicinal chemistry. *Bioorg Chem* **108**, 104633 (2021).
43. Joaquim, A. R. *et al.* Novel Antimicrobial 8-Hydroxyquinoline-Based Agents: Current Development, Structure–Activity Relationships, and Perspectives. *J Med Chem* **64**, 16349–16379 (2021).
44. Tang, C. W. & VanSlyke, S. A. Organic electroluminescent diodes. *Appl Phys Lett* **51**, 913–915 (1987).
45. Southcott, L. & Orvig, C. Inorganic radiopharmaceutical chemistry of oxine. *Dalton Transactions* **50**, 16451–16458 (2021).
46. Kurebayashi, Y., Choyke, P. L. & Sato, N. Imaging of cell-based therapy using 89Zr-oxine ex vivo cell labeling for positron emission tomography. *Nanotheranostics* **5**, 27–35 (2021).
47. Lewis, D. F. & Fay, R. C. X-Ray crystal structure of tetrakis(8-quinolinolato)zirconium(IV), a dodecahedral M(AB)4 system. *J Chem Soc Chem Commun* 1046 (1974) doi:10.1039/c39740001046.
48. Kathirgamanathan, P. *et al.* Discovery of two new phases of zirconium tetrakis(8-hydroxyquinolinolate): synthesis, crystal structure and their electron transporting characteristics in organic light emitting diodes (OLEDs). *J. Mater. Chem.* **21**, 1762–1771 (2011).
49. Massicano, A. V. F. *et al.* Production of [89Zr]Oxinate\4 and cell radiolabeling for human use. *J Labelled Comp Radiopharm* **64**, 209–216 (2021).
50. Cuza, E. *et al.* Coordination isomerism in spin crossover (SCO) materials. *J Appl Phys* **129**, (2021).
51. Mirzaei, M. *et al.* Rationalization of Noncovalent Interactions within Six New MII/8-Aminoquinoline Supramolecular Complexes (MII = Mn, Cu, and Cd): A Combined Experimental and Theoretical DFT Study. *Cryst Growth Des* **15**, 1351–1361 (2015).
52. Sureshbabu, P., Varghese, B., Sujitha, E. & Sabiah, S. Syntheses, structure, DNA docking and antimicrobial studies of copper(II) complexes with diethylenetriamine and N-bidentate ligands. *Inorganica Chim Acta* **536**, 120898 (2022).
53. Niu, C. *et al.* Two cadmium(II) 1-D coordination polymers, {[$Cd_2$(μ-Cl)$_4$$Cl_2$($CH_3OH$)($H_2O$)]·(H-aql)$_2$}n and [Cd(μ-Cl)$_2$ (aql)]n : synthesis, crystal structures and fluorescent properties. *J Coord Chem* **61**, 1997–2007 (2008).

54. Setifi, F. *et al.* Crystal structure of bis(azido-κN)bis(quinolin-8-amine-$\kappa_2$N,N′)iron(II). *Acta Crystallogr E Crystallogr Commun* **72**, 1488–1491 (2016).
55. Yang, F.-L. *et al.* Spin switching in tris(8-aminoquinoline)iron(ii)$(BPh_4)_2$: quantitative guest-losing dependent spin crossover properties and single-crystal-to-single-crystal transformation. *Dalton Transactions* **48**, 231–241 (2019).
56. Mirzaei, M. *et al.* Influence of accompanying anions on supramolecular assembly and coordination geometry in HgII complexes with 8-aminoquinoline: experimental and theoretical studies. *CrystEngComm* **15**, 1404 (2013).
57. Luque, A. *et al.* Iridium catalysts featuring amine-containing ligands for the dehydrogenation of formic acid. *J Organomet Chem* **916**, 121259 (2020).
58. Baruah, A. M., Karmakar, A. & Baruah, J. B. Steric effects in controlling co-ordination environment in zinc 2-nitrobenzoate complexes. *Inorganica Chim Acta* **361**, 2777–2784 (2008).
59. Habashy, D. A. *et al.* Cytotoxicity of fac-$Mn(CO)_3$ complexes with a bidentate quinoline ligand towards triple negative breast cancer. *Dalton Transactions* **51**, 14041–14048 (2022).
60. Kabir, E., Noyon, M. R. O. K. & Hossain, Md. A. Synthesis, biological and medicinal impacts of metallodrugs: A study. *Results Chem* **5**, 100935 (2023).
61. Fernández-Bachiller, M. I. *et al.* Novel Tacrine−8-Hydroxyquinoline Hybrids as Multifunctional Agents for the Treatment of Alzheimer's Disease, with Neuroprotective, Cholinergic, Antioxidant, and Copper-Complexing Properties. *J Med Chem* **53**, 4927–4937 (2010).
62. Huang, W. *et al.* Development of the "hidden" multifunctional agents for Alzheimer's disease. *Eur J Med Chem* **177**, 247–258 (2019).
63. Wang, Z. *et al.* Design, Synthesis, and Evaluation of Multitarget-Directed Selenium-Containing Clioquinol Derivatives for the Treatment of Alzheimer's Disease. *ACS Chem Neurosci* **5**, 952–962 (2014).
64. Gomes, L. M. F. *et al.* 8-Hydroxyquinoline Schiff-base compounds as antioxidants and modulators of copper-mediated Aβ peptide aggregation. *J Inorg Biochem* **139**, 106–116 (2014).
65. Chand, K., Alsoghier, H. M., Chaves, S. & Santos, M. A. Tacrine-(hydroxybenzoyl-pyridone) hybrids as potential multifunctional anti-Alzheimer's agents: AChE inhibition, antioxidant activity and metal chelating capacity. *J Inorg Biochem* **163**, 266–277 (2016).
66. Bareggi, S. R. & Cornelli, U. Clioquinol: Review of its Mechanisms of Action and Clinical Uses in Neurodegenerative Disorders. *CNS Neurosci Ther* **18**, 41–46 (2012).
67. Lazarević, T., Rilak, A. & Bugarčić, Ž. D. Platinum, palladium, gold and ruthenium complexes as anticancer agents: Current clinical uses, cytotoxicity studies and future perspectives. *Eur J Med Chem* **142**, 8–31 (2017).
68. Zhang, C., Xu, C., Gao, X. & Yao, Q. Platinum-based drugs for cancer therapy and anti-tumor strategies. *Theranostics* **12**, 2115–2132 (2022).
69. Czarnomysy, R., Radomska, D., Szewczyk, O. K., Roszczenko, P. & Bielawski, K. Platinum and Palladium Complexes as Promising Sources for Antitumor Treatments. *Int J Mol Sci* **22**, 8271 (2021).
70. Wang, F.-Y. *et al.* New Platinum(II) agent induces bimodal death of apoptosis and autophagy against A549 cancer cell. *Free Radic Biol Med* **129**, 418–429 (2018).
71. Pavlidis, N. *et al.* Synthesis, characterization and pharmacological evaluation of quinoline derivatives and their complexes with copper(II) in in vitro cell models of Alzheimer's disease. *J Inorg Biochem* **217**, 111393 (2021).

72. Diao, D., Simaan, A. J., Martinez, A. & Colomban, C. Bioinspired complexes confined in well-defined capsules: getting closer to metalloenzyme functionalities. *Chemical Communications* **59**, 4288–4299 (2023).
73. Zhang, Y., Muhammad, F. & Wei, H. Inorganic Enzyme Mimics. *ChemBioChem* **22**, 1496–1498 (2021).
74. Cox, N. *et al.* Electronic structure of the oxygen-evolving complex in photosystem II prior to O-O bond formation. *Science (1979)* **345**, 804–808 (2014).
75. Mukhopadhyay, S., Mandal, S. K., Bhaduri, S. & Armstrong, W. H. Manganese Clusters with Relevance to Photosystem II. *Chem Rev* **104**, 3981–4026 (2004).
76. Mandal, D., Roychowdhury, S., Biswas, J. P., Maiti, S. & Maiti, D. Transition-metal-catalyzed C–H bond alkylation using olefins: recent advances and mechanistic aspects. *Chem Soc Rev* **51**, 7358–7426 (2022).
77. Knowles, W. S. & Sabacky, M. J. Catalytic asymmetric hydrogenation employing a soluble, optically active, rhodium complex. *Chemical Communications (London)* 1445 (1968) doi:10.1039/c19680001445.
78. Grau, B. W., Neuhauser, A., Aghazada, S., Meyer, K. & Tsogoeva, S. B. Iron-Catalyzed Olefin Metathesis: Recent Theoretical and Experimental Advances. *Chemistry – A European Journal* **28**, (2022).
79. Docherty, J. H. *et al.* Transition-Metal-Catalyzed C–H Bond Activation for the Formation of C–C Bonds in Complex Molecules. *Chem Rev* **123**, 7692–7760 (2023).
80. Jana, R., Pathak, T. P. & Sigman, M. S. Advances in Transition Metal (Pd,Ni,Fe)-Catalyzed Cross-Coupling Reactions Using Alkyl-organometallics as Reaction Partners. *Chem Rev* **111**, 1417–1492 (2011).
81. Geier, S. J., Vogels, C. M., Melanson, J. A. & Westcott, S. A. The transition metal-catalysed hydroboration reaction. *Chem Soc Rev* **51**, 8877–8922 (2022).
82. Yorimitsu, H., Kotora, M. & Patil, N. T. Special Issue: Recent Advances in Transition-Metal Catalysis. *The Chemical Record* **21**, 3335–3337 (2021).
83. Malapit, C. A. *et al.* Advances on the Merger of Electrochemistry and Transition Metal Catalysis for Organic Synthesis. *Chem Rev* **122**, 3180–3218 (2022).
84. Chan, A. Y. *et al.* Metallaphotoredox: The Merger of Photoredox and Transition Metal Catalysis. *Chem Rev* **122**, 1485–1542 (2022).
85. Rehman, F. *et al.* Zn(II) Complexes with Quinoline Supported Amidate Ligands: Synthesis, Fluorescence, and Catalytic Activity. *Russ J Gen Chem* **89**, 2516–2521 (2019).
86. Drury, W. J. *et al.* Synthesis of Versatile Chiral N,P Ligands Derived from Pyridine and Quinoline. *Angewandte Chemie International Edition* **43**, 70–74 (2004).
87. Zhang, D., Zhang, Y., Hou, W., Guan, Z. & Huang, Z. Phosphine-Iminoquinoline Iron Complexes for Ethylene Polymerization and Copolymerization. *Organometallics* **36**, 3758–3764 (2017).
88. Sangtrirutnugul, P., Stradiotto, M. & Tilley, T. D. Rhodium Complexes Containing a Tridentate Bis(8-quinolyl)methylsilyl Ligand: Synthesis and Reactivity. *Organometallics* **25**, 1607–1617 (2006).
89. Gangwar, M. K., Dahiya, P., Emayavaramban, B. & Sundararaju, B. Cp*CoIII-Catalyzed Efficient Dehydrogenation of Secondary Alcohols. *Chem Asian J* **13**, 2445–2448 (2018).
90. Patel, U. N., Pandey, D. K., Gonnade, R. G. & Punji, B. Synthesis of Quinoline-Based NNN-Pincer Nickel(II) Complexes: A Robust and Improved Catalyst System for C–H Bond Alkylation of Azoles with Alkyl Halides. *Organometallics* **35**, 1785–1793 (2016).
91. Hsu, C. *et al.* Pyrazolo[4,3-h]quinoline Ligand-Based Iridium(III) Complexes for Electrochemiluminescence. *Chem Asian J* **12**, 1649–1658 (2017).

92. Häfliger, P. *et al.* Structure, stability, and biodistribution of cationic $[M(CO)_3]^+$ (M = Re, $^{99}Tc$, $^{99m}Tc$) complexes with tridentate amine ligands. *Synthesis and Reactivity in Inorganic, Metal-Organic and Nano-Metal Chemistry* **35**, 27–34 (2005).
93. Gusev, D. G. Dehydrogenative Coupling of Ethanol and Ester Hydrogenation Catalyzed by Pincer-Type YNP Complexes. *ACS Catal* **6**, 6967–6981 (2016).
94. Massoud, S. S. *et al.* Mononuclear, dinuclear and polymeric 1D thiocyanato- and dicyanamido–copper(II) complexes based on tridentate coligands. *Polyhedron* **54**, 26–33 (2013).
95. Mautner, F. A. *et al.* One-Dimensional Cadmium Polymers with Alternative di(EO/EE) and di(EO/EO/EO/EE) Bridged Azide Bonding Modes. *Cryst Growth Des* **13**, 4518–4525 (2013).
96. Dhanalakshmi, T., Suresh, E., Stoeckli-Evans, H. & Palaniandavar, M. New Copper(II) Complexes as Efficient Catalysts for Olefin Aziridination: The Effect of Ligand Steric Hindrance on Reactivity. *Eur J Inorg Chem* **2006**, 4687–4695 (2006).
97. Muthuramalingam, S., Velusamy, M. & Mayilmurugan, R. Fixation of atmospheric $CO_2$ as C1-feedstock by nickel(ii) complexes. *Dalton Transactions* **50**, 7984–7994 (2021).
98. Dhanalakshmi, T., Loganathan, R., Suresh, E., Stoeckli-Evans, H. & Palaniandavar, M. Interaction of copper(II) complexes with bis(p-nitrophenyl)phosphate: Structural and spectral studies. *Inorganica Chim Acta* **372**, 237–242 (2011).
99. Mautner, F. A. *et al.* Coordination Polymers in Dicyanamido-Cadmium(II) with Diverse Network Dimensionalities. *Crystals (Basel)* **11**, 181 (2021).
100. Kryatov, S. V *et al.* Dioxygen Binding to Complexes with Fe $II_2(\mu\text{-}OH)_2$ Cores: Steric Control of Activation Barriers and $O_2$-Adduct Formation. (2005) doi:10.1021/ic0485312.
101. Li, J.-L. *et al.* Significant differences in the biological activity of mononuclear Cu(ii) and Ni(ii) complexes with the polyquinolinyl ligand. *New Journal of Chemistry* **39**, 529–538 (2015).
102. Kim, H., Kang, J., Kim, K. B., Song, E. J. & Kim, C. A highly selective quinoline-based fluorescent sensor for Zn(II). *Spectrochim Acta A Mol Biomol Spectrosc* **118**, 883–887 (2014).
103. Li, J.-L. *et al.* Self-activated DNA cleavage of a water-soluble mononuclear Cu(II) complex with polyquinolinyl ligand. *J Coord Chem* **67**, 3598–3612 (2014).
104. Bhattacharyya, A. *et al.* BODIPY appended copper(ii) complexes for cellular imaging and singlet oxygen mediated anticancer activity in visible light. *RSC Adv* **6**, 104474–104482 (2016).
105. Carr, B., Fleming, C. L. & Blackman, A. G. Syntheses and structures of transition metal complexes of quinoline-containing multidentate amine ligands. *Coord Chem Rev* **502**, 215599 (2024).
106. Zhang, J. *et al.* Derivatization, complexation, and absolute configurational assignment of chiral primary amines: Application of exciton-coupled circular dichroism. *Chirality* **15**, 180–189 (2003).
107. Osako, T., Nagatomo, S., Kitagawa, T., Cramer, C. J. & Itoh, S. Kinetics and DFT studies on the reaction of copper(II) complexes and $H_2O_2$. *JBIC Journal of Biological Inorganic Chemistry* **10**, 581–590 (2005).
108. Škalamera, Đ. *et al.* Synthesis and characterization of ML and $ML_2$ metal complexes with amino acid substituted bis(2-picolyl)amine ligands. *Dalton Transactions* **45**, 2845–2858 (2016).

109. Zhou, Y.-H. *et al.* p-Nitrophenyl acetate hydrolysis promoted by Zn(II) and Co(II) complexes with the tripodal ligand of N,N′-bis(2-quinolinylmethyl)amantadine. *J Coord Chem* **70**, 177–188 (2017).
110. Zhou, Y.-H. *et al.* Synthesis, structure and superoxide dismutase-like activity of copper(II) complexes based on N,N′-bis(2-quinolinylmethyl)amantadine. *Polyhedron* **85**, 849–856 (2015).
111. Zahn, S. & Canary, J. W. Absolute Configurations of N,N -Dialkyl α-Amino Acids and β-Amino Alcohols from Exciton-Coupled Circular Dichroism Spectra of Cu(II) Complexes. *Org Lett* **1**, 861–864 (1999).
112. Mesquita, L. M. *et al.* Dinuclear Zinc(II) Macrocyclic Complex as Receptor for Selective Fluorescence Sensing of Pyrophosphate. *Inorg Chem* **55**, 2212–2219 (2016).
113. Saga, M., Sakane, G., Yamazaki, S. & Saito, K. Fluorescent ligand design for mononuclear copper(I) complex fluorescence in aqueous solution. *Inorganica Chim Acta* **502**, 119368 (2020).
114. Saravanan, N., Sankaralingam, M. & Palaniandavar, M. Manganese(ii) complexes of tetradentate 4N ligands with diazepane backbones for catalytic olefin epoxidation: effect of nucleophilicity of peroxo complexes on reactivity. *RSC Adv.* **4**, 12000–12011 (2014).
115. Mameli, M. *et al.* Synthesis and Coordination Properties of Quinoline Pendant Arm Derivatives of [9]aneN(3) and [9]aneN(2)S as Fluorescent Zinc Sensors. *Inorg Chem* **48**, 9236–9249 (2009).
116. Lo, W. K. C., McAdam, C. J., Blackman, A. G., Crowley, J. D. & McMorran, D. A. The pentadentate ligands 2PyN2Q and N4Py, and their Cu(II) and Zn(II) complexes: A synthetic, spectroscopic and crystallographic structural study. *Inorganica Chim Acta* **426**, 183–194 (2015).
117. Wei, N., Murthy, N. N., Chen, Q., Zubieta, J. & Karlin, K. D. Copper(I)/Dioxygen Reactivity of Mononuclear Complexes with Pyridyl and Quinolyl Tripodal Tetradentate Ligands: Reversible Formation of Cu:$O_2$ =1:1 and 2:1 Adducts. *Inorg. Chem* **33**, 1953–1965 (1994).
118. Amendola, V. *et al.* Electrochemically Controlled Assembling/Disassembling Processes with a Bis-imine Bis-quinoline Ligand and the CuII/CuI Couple. *Chemistry - A European Journal* **5**, 3679–3688 (1999).
119. Mikata, Y. *et al.* Quinoline-based tetradendate nitrogen ligands stabilize the bis(μ-oxo) dinuclear manganese(iii,iii) core. *Dalton Transactions* 3330 (2007) doi:10.1039/b705080a.
120. Rieger, B., Abu-Surrah, A. S., Fawzi, R. & Steiman, M. Synthesis of chiral and C2-symmetric iron(II) and cobalt(II) complexes bearing a new tetradentate amine ligand system. *J Organomet Chem* **497**, 73–79 (1995).
121. Saga, M., Anamushi, T., Miyahara, W., Yamazaki, S. & Saito, K. Fluorescent Character of Cu(I/II) Complexes with Bisquinoline-based Ligands and Fluorometric Detection of Reductants. *Analytical Sciences* **31**, 185–189 (2015).
122. Suzuki, K., Oldenburg, P. D. & Que, L. Iron-Catalyzed Asymmetric Olefin cis-Dihydroxylation with 97 % Enantiomeric Excess. *Angewandte Chemie International Edition* **47**, 1887–1889 (2008).
123. Mikata, Y. *et al.* Structure and electrochemical properties of (μ-O)$_2$Mn$_2$(iii,iii) and (μ-O)$_2$Mn$_2$(iii,iv) complexes supported by pyridine-, quinoline-, isoquinoline- and quinoxaline-based tetranitrogen ligands. *Dalton Transactions* **50**, 4133–4144 (2021).
124. Mayilmurugan, R., Stoeckli-Evans, H. & Palaniandavar, M. Novel Iron(III) Complexes of Sterically Hindered 4N Ligands: Regioselectivity in Biomimetic Extradiol Cleavage of Catechols. *Inorg Chem* **47**, 6645–6658 (2008).

125. Wei, N., Murthy, N. N. & Karlin, K. D. Chemistry of Pentacoordinate $[LCu_n\text{-}Cl]^+$ Complexes with Quinolyl Containing Tripodal Tetradentate Ligands L. *Inorg. Chem* **33**, 6093–6100 (1994).
126. Karlin, K. D. *et al.* Kinetics and Thermodynamics of Formation of Copper-Dioxygen Adducts: Oxygenation of Mononuclear Copper(I) Complexes Containing Tripodal Tetradentate Ligands. *J. Am. Chem. Soc* **115**, 9506–9514 (1993).
127. Massoud, S. S. *et al.* Efficient hydrolytic cleavage of plasmid DNA by chloro-cobalt(II) complexes based on sterically hindered pyridyl tripod tetraamine ligands: synthesis, crystal structure and DNA cleavage. *Dalton Trans* **43**, 10086–10103 (2014).
128. Adhikari, S., Mandal, S., Ghosh, A., Das, P. & Das, D. Strategically Modified Rhodamine-Quinoline Conjugate as a CHEF-Assisted FRET Probe for $Au^{3+}$: DFT and Living Cell Imaging Studies. *Journal of Organic Chemistry* **80**, 8530–8538 (2015).
129. Mikata, Y., Nodomi, Y., Ohnishi, R., Kizu, A. & Konno, H. Tris(8-methoxy-2-quinolylmethyl)amine (8-MeOTQA) as a highly fluorescent $Zn^{2+}$ probe prepared by convenient C3-symmetric tripodal amine synthesis. *Dalton Transactions* **44**, 8021–8030 (2015).
130. Saga, M., Sakane, G., Yamazaki, S. & Saito, K. Fluorescent ligand design for mononuclear copper(I) complex fluorescence in aqueous solution. (2019) doi:10.1016/j.ica.2019.119368.
131. Guo, X. *et al.* Polypyridyl Co complex-based water reduction catalysts: why replace a pyridine group with isoquinoline rather than quinoline? *Dalton Transactions* **50**, 2042–2049 (2021).
132. Su, Y., Yang, W., Yang, X., Zhang, R. & Zhao, J. Visible Light-Induced CO-Release Reactivity of a Series of ZnII–Flavonolate Complexes. *Aust J Chem* **71**, 549 (2018).
133. Yu, F. Magnetic properties of a mononuclear iron(II) complex with a typical $FeN_6$ coordination octahedron. *Acta Crystallogr C* **68**, m287–m290 (2012).
134. Wang, J. *et al.* Electrocatalytic and Photocatalytic Reduction of $CO_2$ to CO by Cobalt(II) Tripodal Complexes: Low Overpotentials, High Efficiency and Selectivity. *ChemSusChem* **11**, 1025–1031 (2018).
135. Massoud, S. S. *et al.* Copper(ii) complexes based on tripodal pyridyl amine derivatives as efficient anticancer agents. *New Journal of Chemistry* **43**, 6186–6196 (2019).
136. Chen, K. & Que, L. Stereospecific Alkane Hydroxylation by Non-Heme Iron Catalysts: Mechanistic Evidence for an $Fe^{V}O$ Active Species. *J Am Chem Soc* **123**, 6327–6337 (2001).
137. Li, B. *et al.* Side-effect of ancillary ligand on electron transfer and photodynamics of a dinuclear valence tautomeric complex. *Chemical Communications* 2269 (2008) doi:10.1039/b801171k.
138. Wu, D. Y., Sato, O. & Duan, C. Y. A mixed-spin Fe(II) tetranuclear cluster: Preparation, structure and magnetic property. *Inorg Chem Commun* **12**, 325–327 (2009).
139. Lucas, H. R., Meyer, G. J. & Karlin, K. D. CO and $O_2$ Binding to Pseudo-tetradentate Ligand−Copper(I) Complexes with a Variable N-Donor Moiety: Kinetic/Thermodynamic Investigation Reveals Ligand-Induced Changes in Reaction Mechanism. *J Am Chem Soc* **132**, 12927–12940 (2010).
140. Pascaly, M. *et al.* The systematic influence of tripodal ligands on the catechol cleaving activity of iron(III) containing model compounds for catechol 1,2-dioxygenases. *J. Chem. Soc., Dalton Trans* 828–837 (2001) doi:10.1039/b0085111.

141. Parkand, H. & Lee, D. Ligand Taxonomy for Bioinorganic Modeling of Dioxygen-Activating Non-HemeI ron Enzymes Chemistry-A European Journal. *Chem. Eur.J* **2020**, 5916–5926.
142. Suenaga, Y., Mibu, T., Okubo, T., Maekawa, M. & Kuroda-Sowa, T. Syntheses, structure and properties of dinuclear Co complexes with bis(catecholate) ligands – Effect of a quinoline ring in the terminal group. *Polyhedron* **171**, 480–485 (2019).
143. Suenaga, Y. *et al.* Dinuclear cobalt complexes with a redox active biphenyl bridging ligand $[Co_2(BP)(tqa)_2](PF_6)_2$($H_4BP$ = 4,4′-bis(3- tert-butyl-1,2-catechol), tqa = tris(2-quinolylmethyl)amine): structure and magnetic properties. *Dalton Transactions* **50**, 9833–9841 (2021).
144. Mibu, T. *et al.* Syntheses and properties of mononuclear cobalt-dioxolene complexes with the ancillary ligand containing bulky quinoline rings – Electronic state manipulation of the complexes by steric effect. *Inorganica Chim Acta* **527**, (2021).
145. Takahashi, N. *et al.* Dinuclear cobalt complexes with an asymmetric biphenyl bridging ligand, $[Co_2(LFBu)(bpqa)_2](PF_6)_2$ ($H_4LFBu$ = 5-fluoro-5′-tert-butyl-3,3′,4,4′-tetrahydroxybiphenyl, bpqa = bis(2-pyridylmethyl)(2-quinolylmethyl)amine): Spectroscopic, electrochemical and magnetic characterization. *Inorganica Chim Acta* **541**, 121095 (2022).
146. Mibu, T., Suenaga, Y., Okubo, T., Maekawa, M. & Kuroda-Sowa, T. Spectroscopic characterization of valence tautomeric behavior in a cobalt-dioxolene complex using an ancillary ligand containing quinoline groups. *Inorg Chem Commun* **114**, 107826 (2020).
147. Kieber-Emmons, M. T. *et al.* Observation of a $CuII_2$(μ-1,2-peroxo)/$CuIII_2$(μ-oxo)$_2$ Equilibrium and its Implications for Copper–Dioxygen Reactivity. *Angewandte Chemie International Edition* **53**, 4935–4939 (2014).
148. Fry, H. C., Lucas, H. R., Narducci Sarjeant, A. A., Karlin, K. D. & Meyer, G. J. Carbon Monoxide Coordination and Reversible Photodissociation in Copper(I) Pyridylalkylamine Compounds. *Inorg Chem* **47**, 241–256 (2008).
149. Kataoka, Y., Paul, D., Miyake, H., Shinoda, S. & Tsukube, H. A Cl- anion-responsive luminescent $Eu^{3+}$ complex with a chiral tripod: ligand substituent effects on ternary complex stoichiometry and anion sensing selectivity. *Dalton Transactions* 2784 (2007) doi:10.1039/b703944a.
150. Gan, W., Jones, S. B., Reibenspies, J. H. & Hancock, R. D. A fluorescent ligand rationally designed to be selective for zinc(II) over larger metal ions. The structures of the zinc(II) and cadmium(II) complexes of *N*,*N*-bis(2-methylquinoline)-2-(2-aminoethyl)pyridine. *Inorganica Chim Acta* **358**, 3958–3966 (2005).
151. Tzedakis, T. Electrochemical study of binuclear manganese complexes as catalysts in Kraft pulp bleaching. *Electrochim Acta* **46**, 99–109 (2000).
152. Mialane, P., Tchertanov, L., Banse, F., Sainton, J. & Girerd, J.-J. Aminopyridine Iron Catecholate Complexes as Models for Intradiol Catechol Dioxygenases. Synthesis, Structure, Reactivity, and Spectroscopic Studies. *Inorg Chem* **39**, 2440–2444 (2000).
153. Mibu, T., Suenaga, Y., Okubo, T., Maekawa, M. & Kuroda-Sowa, T. Crystal Structure of a Dinuclear Co Complex with Doubly Bridged Fluorides: Di-μ-fluoride Bis{(2-pyridylmethyl)bis(2-quinolylmethyl)amine} Dicobalt(II) Bis(tetrafluoroborate). *X-ray Structure Analysis Online* **35**, 61–62 (2019).
154. Mikata, Y. *et al.* Isoquinoline-derivatized tris(2-pyridylmethyl)amines as fluorescent zinc sensors with strict $Zn^{2+}$/$Cd^{2+}$ selectivity. *Dalton Transactions* **43**, 10751 (2014).

155. Zheng, H., Zang, Y., Dong, Y., Young, V. G. & Que, L. Complexes with $FeIII_2$ (μ-O)(μ-OH), $FeIII_2(\mu\text{-}O)_2$, and $[FeIII_3(\mu_2\text{-}O)_3]$ Cores: Structures, Spectroscopy, and Core Interconversions. *J Am Chem Soc* **121**, 2226–2235 (1999).
156. Zhang, J., Siu, K., Lin, C. H. & Canary, J. W. Conformational dynamics of Cu(i) complexes of tripodal ligands: steric control of molecular motion. *New Journal of Chemistry* **29**, 1147 (2005).
157. Yamaguchi, M. *et al.* Syntheses, Characterization, and Catalytic Ability in Alkane Oxygenation of Chloro(dimethyl sulfoxide)ruthenium(II) Complexes with Tris(2-pyridylmethyl)amine and Its Derivatives. *Inorg Chem* **45**, 8342–8354 (2006).
158. Williams, N. J., Gan, W., Reibenspies, J. H. & Hancock, R. D. Possible Steric Control of the Relative Strength of Chelation Enhanced Fluorescence for Zinc(II) Compared to Cadmium(II): Metal Ion Complexing Properties of Tris(2-quinolylmethyl)amine, a Crystallographic, UV−Visible, and Fluorometric Study. *Inorg Chem* **48**, 1407–1415 (2009).
159. Biswas, A. N. *et al.* Modeling TauD-J: A High-Spin Nonheme Oxoiron(IV) Complex with High Reactivity toward C–H Bonds. *J Am Chem Soc* **137**, 2428–2431 (2015).
160. Bae, S. H. *et al.* Mononuclear Nonheme High-Spin (S=2) versus Intermediate-Spin (S=1) Iron(IV)–Oxo Complexes in Oxidation Reactions. *Angewandte Chemie International Edition* **55**, 8027–8031 (2016).
161. Lee, N. Y. *et al.* Structure and spin state of nonheme FeIVO complexes depending on temperature: predictive insights from DFT calculations and experiments. *Chem Sci* **8**, 5460–5467 (2017).
162. Gü, P. *et al.* Biological activity of manganese(I) tricarbonyl complexes on multidrug-resistant Gram-negative bacteria: From functional studies to in vivo activity in Galleria mellonella. *Metallomics* **11**, 2033 (2019).
163. Biswas, S., Das, P., Rasaily, S., Pariyar, A. & Biswas, A. N. Synthesis, structures and catalase activities of bis(μ-oxo)diMnIII,III and bis(μ-acetato)diMnII,II complexes bearing a quinolyl donor tripod ligand. *Inorganica Chim Acta* **492**, 76–82 (2019).
164. Mikata, Y. *et al.* Conversion of $(\mu\text{-}OH)_2Mn_2$(II,II) complex to $(\mu\text{-}O)_2Mn_2$(III,III) core supported by a quinoxaline-based tetranitrogen ligand. *Inorganica Chim Acta* **509**, 119688 (2020).
165. Mikata, Y. Quinoline- and isoquinoline-derived ligand design on TQEN (*N,N,N′,N′*-tetrakis(2-quinolylmethyl)ethylenediamine) platform for fluorescent sensing of specific metal ions and phosphate species. *Dalton Transactions* **49**, 17494–17504 (2020).
166. Rath, N. P., Holt, E. M. & tanimura, K. Fluorescent copper(I) complexes: correlation of structural and emission characteristics of $[\{CuI(quin)_2\}_2]$ and $[Cu_4I_4(quin)_4]$(quin = quinoline). *Journal of the Chemical Society, Dalton Transactions* 2303 (1986) doi:10.1039/dt9860002303.
167. Bukowska-Strzyżewska, M., Skoweranda, J., Heyduk, E. & Mroziński, J. Crystal structure and magnetic properties of tetrakis(μ-crotonato)bis(quinoline)dicopper(II). *Inorganica Chim Acta* **73**, 207–213 (1983).
168. Faizi, Md. S. H. & Sen, P. [Bis(quinolin-2-ylcarbonyl)amido-κ3 *N,N′,N″*]bromido(*N,N*-dimethylformamide-κO)copper(II). *Acta Crystallogr Sect E Struct Rep Online* **70**, m206–m207 (2014).
169. Moulton, B. *et al.* A new 65.8 topology and a distorted 65.8 $CdSO_4$ topology: two new supramolecular isomers of $[M_2(bdc)_2(L)_2]$n coordination polymers. *Chemical Communications* 1342 (2003) doi:10.1039/b301221b.
170. Wei, L., Babich, J. W., Ouellette, W. & Zubieta, J. Developing the $\{M(CO)_3\}$+ Core for Fluorescence Applications: Rhenium Tricarbonyl Core Complexes with

Benzimidazole, Quinoline, and Tryptophan Derivatives. *Inorg Chem* **45**, 3057–3066 (2006).
171. Muthuramalingam, S., Sankaralingam, M., Velusamy, M. & Mayilmurugan, R. Catalytic Conversion of Atmospheric $CO_2$ into Organic Carbonates by Nickel(II) Complexes of Diazepane-Based N4 Ligands. *Inorg Chem* **58**, 12975–12985 (2019).
172. Mikata, Y., Kizu, A. & Konno, H. TQPHEN (*N,N,N′,N′*-tetrakis(2-quinolylmethyl)-1,2-phenylenediamine) derivatives as highly selective fluorescent probes for Cd2+. *Dalton Transactions* **44**, 104–109 (2015).
173. Mikata, Y. *et al.* Quinoline-based fluorescent zinc sensors with enhanced fluorescence intensity, Zn/Cd selectivity and metal binding affinity by conformational restriction. *Dalton Transactions* **42**, 9688 (2013).
174. Adams, H. *et al.* Dinuclear zinc(II) complexes of a Robson macrocycle. *Journal of the Chemical Society, Dalton Transactions* 275 (1995) doi:10.1039/dt9950000275.
175. Alcock, N. W., Benniston, A. C., Moore, P., Pike, G. A. & Rawle, S. C. Macrocyclic ligands designed to impose tetrahedral coordination: [1-(3-dimethylaminopropyl)-1,5,9-triazacyclododecane], L1, [1{2-(pyrrolidin-1-yl)ethyl}-1,5,9-triazacyclododecane], L2, and their zinc(II) complexes. *J Chem Soc Chem Commun* 706 (1991) doi:10.1039/c39910000706.
176. Rawle, S. C., Clarke, A. J., Moore, P. & Alcock, N. W. Ligands designed to impose tetrahedral co-ordination: a convenient route to aminoethyl and aminopropyl pendant arm derivatives of 1,5,9-triazacyclododecane. *Journal of the Chemical Society, Dalton Transactions* 2755 (1992) doi:10.1039/dt9920002755.
177. Lui, X. *et al.* Synthesis, crystal structure, activity and quantum chemistry of trinuclear complex of bis(2-benzimidazolylmethyl)amine. *Acta Chimi Sin* **57**, 1185 (1999).
178. Marandi, F., Soudi, A. A., Morsali, A. & Kempe, R. Zinc(II) and Cadmium(II) Complexes of the 3-(2-Pyridyl)-5,6-diphenyl-1,2,4-triazine (PDPT) Ligand, Structural Studies of $[Zn(PDPT)_2\ Cl(ClO_4)]$ and $[Cd(PDPT)_2(NO_3)(ClO_4)]$. *Z Anorg Allg Chem* **631**, 3070–3073 (2005).
179. Scheidt, W. R., Cheng, B., Venugopal Reddy, K. & Brancato, K. E. Alternant Bond Distances in Octaethylporphyrin π-Cation Radicals. *J Porphyr Phthalocyanines* **21**, 273–286 (2017).
180. da Rocha, J. C. *et al.* Crystallographic evidence of metal scrambling in an N4O2-tetraiminodiphenolate macrocyclic complex. *J Mol Struct* **1072**, 69–76 (2014).
181. Saga, M., Sakane, G., Yamazaki, S. & Saito, K. Crystal Structure of a Copper(II) Complex with N,N'-Bis(2-methylquinolyl)-dimethyl-1,3-propanediamine. *X-ray Structure Analysis Online* **31**, 41–42 (2015).
182. Chen, X.-Q., Cai, Y.-D., Ye, Y.-S., Tong, M.-L. & Bao, X. Investigation of SCO property–structural relationships in a family of mononuclear Fe(ii) complexes. *Inorg Chem Front* **6**, 2194–2199 (2019).
183. Legros, J.-Y., Primault, G., Toffano, M., Rivière, M.-A. & Fiaud, J.-C. Reactivity of Quinoline- and Isoquinoline-Based Heteroaromatic Substrates in Palladium(0)-Catalyzed Benzylic Nucleophilic Substitution. *Org Lett* **2**, 433–436 (2000).
184. Singh, N., Niklas, J., Poluektov, O., Van Heuvelen, K. M. & Mukherjee, A. Mononuclear nickel (II) and copper (II) coordination complexes supported by bispicen ligand derivatives: Experimental and computational studies. *Inorganica Chim Acta* **455**, 221–230 (2017).
185. Mikata, Y. *et al.* Bisquinoline-based fluorescent zinc sensors. *Dalton Transactions* 3800 (2009) doi:10.1039/b820763a.

186. Morris, L. S. *et al.* Epoxidation of alkenes bearing a carboxylic acid group by iron complexes of the tetradentate ligand *N,N′*-dimethyl-*N,N′*-bis(2-pyridylmethyl)-1,2-diaminoethane and its derivatives. *Inorganica Chim Acta* **413**, 149–159 (2014).
187. Chen, J. & Klein Gebbink, R. J. M. Deuterated N2Py2 Ligands: Building More Robust Non-Heme Iron Oxidation Catalysts. *ACS Catal* **9**, 3564–3575 (2019).
188. Govor, E. V. *et al.* Anion Tuning of Cu(II)/4,4′-Bi-1,2,4-Triazole Coordination Polymers. *Z Anorg Allg Chem* **636**, 209–217 (2010).
189. Chatterjee, A., Seikh, Md. M., Chowdhury, S. & Ghosh, R. Catecholase and catechol cleavage activities of a dinuclear phenoxobridged Cu(II) complex: Synthesis, structure and magnetostructural studies. *Inorganica Chim Acta* **521**, 120345 (2021).
190. Inci, D., Aydin, R. & Zorlu, Y. Affinity of a new copper(II) complex to DNA/BSA and antioxidant/radical scavenging activities: crystal structure of [Cu(4,7-diphenyl-1,10-phenanthroline)(leucine)($NO_3$)($H_2O$)]. *J Coord Chem* **69**, 2677–2696 (2016).
191. Marino, N. *et al.* Synthesis, Structure, and Magnetic Properties of Regular Alternating μ-bpm/di-μ-X Copper(II) Chains (bpm = 2,2′-bipyrimidine; X = OH, F). *Inorg Chem* **51**, 4323–4334 (2012).
192. Derrick, J. S. *et al.* Stereochemistry of metal tetramethylcyclam complexes directed by an unexpected anion effect. *Dalton Transactions* **46**, 13166–13170 (2017).
193. Richaud, A. *et al.* Electrophilic Modulation of the Superoxide Anion Radical Scavenging Ability of Copper(II) Complexes with 4-Methyl Imidazole. *J Phys Chem A* **125**, 2394–2401 (2021).
194. Usman, M. *et al.* Coumarin centered copper(ii) complex with appended-imidazole as cancer chemotherapeutic agents against lung cancer: molecular insight via DFT-based vibrational analysis. *RSC Adv* **7**, 36056–36071 (2017).
195. Rasheed, W. *et al.* Crystallographic Evidence for a Sterically Induced Ferryl Tilt in a Non-Heme Oxoiron(IV) Complex that Makes it a Better Oxidant. *Angewandte Chemie International Edition* **57**, 9387–9391 (2018).
196. Park, G.-S. Zn(II) Complex of Tachquin, *N,N',N''*-Tris(2-quinolinylmethyl)-*cis,cis*-1,3,5-triaminocyclohexane); Synthesis and X-ray Structure of [Zn(tachquin)]($ClO_4$)$_2$.$H_2O$. *Bull Korean Chem Soc* **26**, 1849–1852 (2005).
197. Hazell, A., Mønsted, O., Rasmussen, J. C. & Toftlund, H. Three overcrowded zinc(II) complexes with potentially hexadentate polypyridyl ligands. *Acta Crystallogr C* **64**, m185–m189 (2008).
198. Munshi, S. *et al.* Hydrogen-atom and oxygen-atom transfer reactivities of iron(iv)-oxo complexes of quinoline-substituted pentadentate ligands. *Dalton Transactions* **51**, 870–884 (2022).
199. Biswas, J. P. *et al.* Effect of the Ligand Backbone on the Reactivity and Mechanistic Paradigm of Non-Heme Iron(IV)-Oxo during Olefin Epoxidation. *Angewandte Chemie International Edition* **60**, 14030–14039 (2021).
200. Ramírez, E. *et al.* Oxygen Transfer from Trimethylamine N-Oxide to Cu I Complexes Supported by Pentanitrogen Ligands. *Eur J Inorg Chem* **2020**, 2798–2808 (2020).
201. Rana, S. *et al.* Selective C–H halogenation over hydroxylation by non-heme iron(iv)-oxo. *Chem Sci* **9**, 7843–7858 (2018).
202. Massie, A. A. *et al.* Equatorial Ligand Perturbations Influence the Reactivity of Manganese(IV)-Oxo Complexes. *Angewandte Chemie International Edition* **56**, 4178–4182 (2017).

203. Hitomi, Y. *et al.* Aerobic Catechol Oxidation Catalyzed by a Bis(μ-oxo)dimanganese(III,III) Complex via a Manganese(II)−Semiquinonate Complex. *Inorg Chem* **44**, 3473–3478 (2005).
204. Dubois, L. *et al.* Carboxylate Ligands Drastically Enhance the Rates of Oxo Exchange and Hydrogen Peroxide Disproportionation by Oxo Manganese Compounds of Potential Biological Significance. *Chemistry – A European Journal* **14**, 3013–3025 (2008).
205. Park, G., Ye, N., Rogers, R. D., Brechbiel, M. W. & Planalp, R. P. Effect of metal size on coordination geometry of *N,N′,N″*-tris(2-pyridylmethyl)-*cis,cis*-1,3,5-triaminocyclohexane: synthesis and structure of $[M^{II}L](ClO_4)_2$ (M=Zn, Cd and Hg). *Polyhedron* **19**, 1155–1161 (2000).
206. Matyuska, F. *et al.* Tailoring the local environment around metal ions: a solution chemical and structural study of some multidentate tripodal ligands. *Dalton Transactions* **46**, 8626–8642 (2017).
207. Li, Y. *et al.* X-Ray diffraction structure of Cu(II) and Zn(II) complexes of 8-aminoquinoline derivatives (TDMQ), related to the activity of these chelators as potential drugs against Alzheimer's disease. *J Mol Struct* **1251**, 132078 (2022).
208. Machura, B., Małecki, J. G., Świtlicka, A., Nawrot, I. & Kruszynski, R. Copper(II) complexes of bis(pyrazol-1-yl)methane – Synthesis, spectroscopic characterization, X-ray structure and DFT calculations. *Polyhedron* **30**, 864–872 (2011).
209. Comba, P., Lampeka, Y. D., Nazarenko, A. Y., Prikhod'ko, A. I. & Pritzkow, H. Interactions between Copper(II) Complexes of Mono-, Bis-, and Tris(macrocyclic) Ligands and Inorganic or Organic Guests. *Eur J Inorg Chem* **2002**, 1464–1474 (2002).
210. Mykhalichko, B., Lavrenyuk, H. & Mykhalichko, O. A flame retardant-hardener for epoxy resins: Synthesis, structural, and DFT studies of the $[Cu(H_2NC_2H_4NH_2)_2(H_2O)Cl]Cl$ complex. *Turk J Chem* **45**, (2021).
211. Elsegood, M. R. J. & Redshaw, C. Alkylzinc Hydrazides: Self-Assembly of Hexanuclear Ring Systems in Acetonitrile. *Chemistry – A European Journal* **14**, 3530–3534 (2008).
212. Khan, M. A. & Tuck, D. G. The structure of (2,2'-bipyridine)dichlorozinc(II), Zn(C10H8N2)Cl2. *Acta Crystallogr C* **40**, 60–62 (1984).
213. Hamada, T., Manabe, K. & Kobayashi, S. Enantio- and Diastereoselective, Stereospecific Mannich-Type Reactions in Water. *J Am Chem Soc* **126**, 7768–7769 (2004).
214. Zhang, W. *et al.* Preparation of Tetradentate Copper Chelators as Potential Anti-Alzheimer Agents. *ChemMedChem* **13**, 684–704 (2018).
215. Romero, E. A. *et al.* Understanding the Activity and Enantioselectivity of Acetyl-Protected Aminoethyl Quinoline Ligands in Palladium-Catalyzed β-C(sp3)–H Bond Arylation Reactions. *J Am Chem Soc* **141**, 16726–16733 (2019).
216. Zhao, Q., Liu, S., Li, Y. & Wang, Q. Design, Synthesis, and Biological Activities of Novel 2-Cyanoacrylates Containing Oxazole, Oxadiazole, or Quinoline Moieties. *J Agric Food Chem* **57**, 2849–2855 (2009).
217. Wang, L. *et al.* Design, synthesis and preliminary bioactivity evaluations of substituted quinoline hydroxamic acid derivatives as novel histone deacetylase (HDAC) inhibitors. (2015) doi:10.1016/j.bmc.2015.06.024.
218. Comba, P. *et al.* The Mechanism of the (Bispidine)copper(II)-Catalyzed Aziridination of Styrene: A Combined Experimental and Theoretical Study. *Chemistry – A European Journal* **14**, 5313–5328 (2008).

219. Li, Y., Guo, F., Zha, Z. & Wang, Z. Iron-Catalyzed Synthesis of 2-Vinylquinolines via sp3 C-H Functionalization and Subsequent C-N Cleavage. doi:10.1002/asia.201201039.
220. Yang, T. *et al.* Discovery of a Teraryl Oxazolidinone Compound (S)-N-((3-(3-Fluoro-4-(4-(pyridin-2-yl)-1H-pyrazol-1-yl)phenyl)-2-oxooxazolidin-5-yl)methyl)acetamide Phosphate as a Novel Antimicrobial Agent with Enhanced Safety Profile and Efficacies. *J Med Chem* **58**, 6389–6409 (2015).
221. Zore, M. *et al.* Synthesis and Biological Evaluation of Fingolimod Derivatives as Antibacterial Agents. **6**, 18465–18486 (2021).
222. Fukata, G., O'Brien, C. & O'Ferrall, R. A. M. Enamine–imine tautomerism of benzyl- and phenacyl-quinolines. *Journal of the Chemical Society, Perkin Transactions 2* 792–795 (1979) doi:10.1039/P29790000792.
223. Xiao, J., Huang, Y., Song, Z. & Feng, W. Facile catalyst-free synthesis of 2-vinylquinolines via a direct deamination reaction occurring during Mannich synthesis. *RSC Adv* **5**, 99095–99098 (2015).
224. Suzuki, T. *et al.* Rapid Discovery of Highly Potent and Selective Inhibitors of Histone Deacetylase 8 Using Click Chemistry to Generate Candidate Libraries. (2012) doi:10.1021/jm300837y.
225. Bhattacharya, S., Snehalatha, K. & Praveen Kumar, V. Synthesis of New Cu(II)-Chelating Ligand Amphiphiles and Their Esterolytic Properties in Cationic Micelles. (2003) doi:10.1021/jo026323q.
226. Krishnamurthy, D. *et al.* Mononuclear, Dinuclear, and Pentanuclear [{N,S(thiolate)}Iron(II)] Complexes: Nuclearity Control, Incorporation of Hydroxide Bridging Ligands, and Magnetic Behavior. *Chemistry - A European Journal* **11**, 7328–7341 (2005).
227. Baldeau, S. M., Slinn, C. H., Krebs, B. & Rompel, A. Five manganese(II) complexes with seven- or eight-coordinated Mn(II), revealing different coordination modes for the nitrato ligands. *Inorganica Chim Acta* **357**, 3295–3303 (2004).
228. Shiraishi, Y., Ichimura, C. & Hirai, T. A quinoline-polyamine conjugate as a fluorescent chemosensor for quantitative detection of Zn(II) in water. (2007) doi:10.1016/j.tetlet.2007.09.032.
229. Khalifa, M. E. *et al.* Synthesis and Pharmacological Investigations of Novel Pyrazolyl and Hydrazonoyl Cyanide Benzimidazole Entities. *J Heterocycl Chem* **56**, 1426–1436 (2019).
230. Merz, J. *et al.* Synthesis, Photophysical and Electronic Properties of New Red-to-NIR Emitting Donor–Acceptor Pyrene Derivatives. *Chemistry – A European Journal* **26**, 438–453 (2020).
231. Mamada, M. *et al.* Benzimidazole Derivatives: Synthesis, Physical Properties, and n-Type Semiconducting Properties. *Chemistry – A European Journal* **20**, 11835–11846 (2014).
232. Masferrer-Rius, E., Hopman, R. M., van der Kleij, J., Lutz, M. & Klein Gebbink, R. J. M. On the Ability of Nickel Complexes Derived from Tripodal Aminopyridine Ligands to Catalyze Arene Hydroxylations. *Chimia (Aarau)* **74**, 489–494 (2020).
233. Jopp, M. *et al.* Anticancer activity of a series of copper(II) complexes with tripodal ligands. (2017) doi:10.1016/j.ejmech.2017.03.019.
234. Ambundo, E. A. *et al.* Influence of Coordination Geometry upon Copper(II/I) Redox Potentials. Physical Parameters for Twelve Copper Tripodal Ligand Complexes. 1 (1999) doi:10.1021/ic990334t.
235. Che, C.-M., Yam, V. W.-W. & Mak, T. C. W. A Novel Monooxoruthenium(V) Complex Containing a Polydentate Pyridyl Amine Ligand. Syntheses, Reactivities,

and X-ray Crystal Structure of [Ru(II)($N_4O$)($H_20$)]($ClO_4$)$_2$. *Journal of American Chemical Society* **112**, 2284–2291 (1990).
236. Brownstein, S. K., Plouffe, P.-Y., Bensimon, C. & Tse, J. Complexes of Tris((2-pyridyl)alkyl)amines with Lithium and Sodium Salts. *Inorg. Chem* **33**, 354–358 (1994).
237. Lonnon, D. G., Craig, D. C. & Colbran, S. B. Rhodium, palladium and platinum complexes of tris(pyridylalkyl)amine and tris(benzimidazolylmethyl)amine N4-tripodal ligands. *Dalton Transactions* 3785–3797 (2006) doi:10.1039/B602556K.
238. Zahn, S. & Canary, J. W. Cu(I/II) Redox Control of Molecular Conformation and Shape in Chiral Tripodal Ligands: Binary Exciton-Coupled Circular Dichroic States. (2002) doi:10.1021/ja0120429.
239. Wong, Y.-L., Mak, C.-Y., Kwan, S. & Lee, H. K. Mononuclear iron(III) complexes supported by tripodal N 3 O ligands: Synthesis, structure and reactivity towards DNA cleavage. *Inorganica Chim Acta* **363**, 1246–1253 (2009).
240. Rojas, D. *et al.* Binuclear copper(II) oxidation products from copper(I) complexes with tridentate ligands. Magnetostructural characterization. *Inorg Chem* **43**, 6324–6330 (2004).
241. Sams, C. K., Somoza, F., Bernal, I. & Toftlund, H. Coordination chemistry of transition metal complexes of a novel pentadentate ligand. *Inorganica Chim Acta* **318**, 45–52 (2001).
242. Mautner, F. A. *et al.* One-dimensional cadmium polymers with alternative di(EO/EE) and di(EO/EO/EO/EE) bridged azide bonding modes. *Cryst Growth Des* **13**, 4518–4525 (2013).
243. Vartak, A. P., Gabriela Deaciuc, A., Dwoskin, L. P. & Crooks, P. A. Quinlobelane: A water-soluble lobelane analogue and inhibitor of VMAT2. *Bioorg Med Chem Lett* **20**, 3584–3587 (2010).
244. Ding, D., Dwoskin, L. P. & Crooks, P. A. Efficient synthesis of cis-2,6-di-(2-quinolylpiperidine). *Tetrahedron Lett* **54**, 5211–5213 (2013).
245. Ding, D., Nickell, J. R., Dwoskin, L. P. & Crooks, P. A. Quinolyl analogues of norlobelane: Novel potent inhibitors of [3H]dihydrotetrabenazine binding and [3H]dopamine uptake at the vesicular monoamine transporter-2. *Bioorg Med Chem Lett* **25**, 2613–2616 (2015).
246. Chen, G. *et al.* Ligand-accelerated enantioselective methylene C(sp3)–H bond activation. *Science (1979)* **353**, 1023–1027 (2016).
247. Yang, Y., aobing Wang, H. & Haiyan Ma, nd. Unprecedented Reaction Pathway of Sterically Crowded Calcium Complexes: Sequential C-N Bond Cleavage Reactions Induced by C-H Bond Activations. doi:10.1002/asia.201601497.
248. Sahu, R., Kumar Padhi, S., Sekhar Jena, H. & Manivannan, V. Conversion of 2-(aminomethyl) substituted pyridine and quinoline to their dicarbonyldiimides using copper(II) acetate. (2010) doi:10.1016/j.ica.2010.01.028.
249. Banfi, L., Guanti, G., Mugnoli, A. & Riva, R. Lipase catalyzed asymmetrization of quinolyl substituted 1,3-propanediols. *Tetrahedron Asymmetry* **9**, 2481–2492 (1998).
250. Huang, Y.-Y. *et al.* Validation of Phosphodiesterase-10 as a Novel Target for Pulmonary Arterial Hypertension via Highly Selective and Subnanomolar Inhibitors. (2019) doi:10.1021/acs.jmedchem.9b00224.
251. Bonney, K. J. & Braddock, D. C. A unifying stereochemical analysis for the formation of halogenated C 15-acetogenin medium-ring ethers from laurencia species via intramolecular bromonium ion assisted epoxide ring-opening and experimental corroboration with a model epoxide. *Journal of Organic Chemistry* **77**, 9574–9584 (2012).

252. Lutteke, G. *et al.* Intramolecular Butenolide Allene Photocycloadditions and Ensuing Retro-Ene Reactions of Some Photoadducts. *European J Org Chem* **2011**, 3146–3155 (2011).
253. Olefins in the Allylic Position reducing entry alcohol allylic halide % yield agent/solvent olefin.
254. Ashby, E. C. & Welder, C. O. Reactions of Saturated and Unsaturated Tertiary Alkyl Halides and Saturated Secondary Alkyl Iodides with Lithium Aluminum Deuteride. Convincing Evidence for a Single-Electron-Transfer Pathway. (1998) doi:10.1021/jo9807058.
255. Jyoti Das, P. An Efficient Conversion of Alcohols to alkyl bromides Using Pyridinium based Liquids: A green alternative to Appel Reaction Asian Journal Of Chemistry Asian Journal Of Chemistry. *Article in Asian Journal of Chemistry* (2018) doi:10.14233/ajchem.2018.21086.
256. Nicolai, S., Sedigh-Zadeh, R. & Waser, J. Pd(0)-catalyzed alkene oxy- and aminoalkynylation with aliphatic bromoacetylenes. *Journal of Organic Chemistry* **78**, 3783–3801 (2013).
257. Midgley, G. & Thomas, C. B. Selectivity of radical formation in the reaction of carbonyl compounds with manganese(III) acetate. *Journal of the Chemical Society, Perkin Transactions 2* 1103–1108 (1987) doi:10.1039/P29870001103.
258. Abou-Gharbia, M. *et al.* Antipsychotic Activity of Substituted -Carbolines. *J Med Chem* **30**, 1818–1823 (1987).
259. Hardouin, C. *et al.* Multikilogram Synthesis of a Potent Dual Bcl-2/Bcl-xL Antagonist. 1. Manufacture of the Acid Moiety and Development of Some Key Reactions. *Org Process Res Dev* **24**, 652–669 (2020).
260. Maj, A. M., Suisse, I., Hardouin, C. & Agbossou-Niedercorn, F. Synthesis of new chiral 2-functionalized-1,2,3,4-tetrahydroquinoline derivatives via asymmetric hydrogenation of substituted quinolines. *Tetrahedron* **69**, 9322–9328 (2013).
261. Dalko, P. *et al.* Stimuli - or bio - responsive copolymers, the polymers comprising the same and their use in drug delivery. (2021).
262. Schnopp, M. & Haberhauer, G. Highly Selective Recognition of α-Chiral Primary Organoammonium Ions by C3-Symmetric Peptide Receptors. *European J Org Chem* **2009**, 4458–4467 (2009).
263. Albanese, D., Ghidoli, C. & Zenoni, M. Concise Synthesis of Vinylheterocycles through-Elimination under Solventless Phase Transfer Catalysis Conditions Scheme 1 a. *Org Process Res Dev* **48**, 736–739 (2005).
264. Sharland, J. C. *et al.* Asymmetric synthesis of pharmaceutically relevant 1-aryl-2-heteroaryl-and 1,2-diheteroarylcyclopropane-1-carboxylates. (2021) doi:10.1039/d1sc02474d.
265. Alunni, S., De Angelis, F., Ottavi, L., Papavasileiou, M. & Tarantelli, F. Evidence of a borderline region between E1cb and E2 elimination reaction mechanisms: A combined experimental and theoretical study of systems activated by the pyridine ring. *J Am Chem Soc* **127**, 15151–15160 (2005).
266. Wenkert, E., Ferreira, V., Michelotti, E. & Tingoli, M. Synthesis of acyclic, cis olefinic pheromones by way of nickel-catalyzed Grignard reactions. *J Org Chem* **50**, 719–721 (1985).
267. Chidambaram, M., Sonavane, S. U., de la Zerda, J. & Sasson, Y. Didecyldimethylammonium bromide (DDAB): a universal, robust, and highly potent phase-transfer catalyst for diverse organic transformations. *Tetrahedron* **63**, 7696–7701 (2007).
268. Nicolas, M., Fabre, B., Pilard, J. F. & Simonet, J. A new efficient route to 3-vinylthiophene. *J Heterocycl Chem* **36**, 1105–1106 (1999).

269. Fokin, A. A. *et al.* Preparative Synthesis of Vinyl Diamondoids. *Synth Commun* **43**, 1772–1777 (2013).
270. Chakrabarti, K., Mishra, A., Panja, D., Paul, B. & Kundu, S. Selective synthesis of mono- and di-methylated amines using methanol and sodium azide as C1 and N1 sources. *Green Chemistry* **20**, 3339–3345 (2018).
271. Joule, J. A. & Smith, G. F. *Heterocyclic Chemistry*. (Van Nostrand Reinhold, 1972).
272. Finkelstein, H. Darstellung organischer Jodide aus den entsprechenden Bromiden und Chloriden. *Berichte der deutschen chemischen Gesellschaft* **43**, 1528–1532 (1910).
273. Nonogaki, S. & Hatano, Y. Photopolymer imaging using epoxy and bromine containing ethylenically unsaturated compounds. (1981).
274. Kalivretenos, A., Reichel, L. & Gluckman, J. Molecularly imprinted polymers for extraction of cannabinoids and uses thereof. (2020).
275. Mignon, M. & Pourille, C. Anhydrous solid composition for dyeing keratin fibres comprising a polymer comprising at least one heterocyclic vinyl monomer. (2018).
276. Hou, X., Wu, Z. & Wang, D. Microwave irradiation technique: Green potent energy source for sustainable applications (1300) doi:10.1088/1742-6596/1378/4/042029.
277. Fakhfakh, M. A. *et al.* Synthesis and Biological Evaluation of Substituted Quinolines: Potential Treatment of Protozoal and Retroviral Co-infections. doi:10.1016/j.bmc.2003.09.007.
278. Flores-Noria, R. *et al.* Synthesis and optoelectronic properties of phenylenevinylenequinoline macromolecules. *New Journal of Chemistry* **38**, 974 (2014).
279. Mclean, L. A. *et al.* Asymmetric Synthesis of Heterocyclic Chloroamines and Aziridines by Enantioselective Protonation of Catalytically Generated Enamines. (2022) doi:10.33774/chemrxiv-2021-d41h5.
280. Fakhfakh, M. A., Franck, X., Fournet, A., Hocquemiller, R. & Figadère, B. Expeditious preparation of 2-substituted quinolines. *Tetrahedron Lett* **42**, 3847–3850 (2001).
281. Benito, Y., Rodriguez, J. G., Baeza, J. G., Fernandez-Sanchez, C. & Gomez-Anton, M. R. Synthesis and polymerization of 2-vinylquinoline and 2-vinylnaphthalene with $AlEt_3$-$VCl_3$: Influence of pyridine as donor ligand. *Eur Polym J* **26**, 689–693 (1990).
282. Tramontini, M. & Angiolini, L. *Mannich Bases Chemistry and Uses*. (CRC Press, 1994).
283. March, J. *Advanced Organic Chemistry: Reactions, Mechanisms, and Structure*. (JOHN WILEY & SONS, US, 1992).
284. Heravi, M. M. & Zadsirjan, V. Recent advances in applications of Mannich reaction in total synthesis of alkaloids. in *Recent Applications of Selected Name Reactions in the Total Synthesis of Alkaloids* 153–190 (Elsevier, 2021). doi:10.1016/B978-0-12-824021-2.00007-8.
285. Larsen, R. D. *et al.* Practical route to a new class of $LTD_4$ receptor antagonists. *Journal of Organic Chemistry* **61**, 3398–3405 (1996).
286. Boekelheide, V. & Sieg1, A. L. A Synthesis Of 1-Vinylisoquinoline And Related Derivatives.
287. Sieff, D., Institute, R., Boekelheide, V. & Marinetti, G. A Study of the Alkylation of Active Methylene.
288. Laronze-Cochard, M. *et al.* Synthesis and biological evaluation of novel 4,5-bis(dialkylaminoalkyl)-substituted acridines as potent telomeric G-quadruplex ligands. *Eur J Med Chem* **44**, 3880–3888 (2009).

289. Li, Y., Hoskins, J. N., Sreerama, S. G. & Grayson, S. M. MALDI-TOF Mass Spectral Characterization of Polymers Containing an Azide Group: Evidence of Metastable Ions. (2010) doi:10.1021/ma100599n.
290. Xiao, Q., Ju, Y., Yang, X. & Zhao, Y. F. Electrospray ionization mass spectrometry of AZT H-phosphonates conjugated with steroids. *Rapid Communications in Mass Spectrometry* **17**, 1405–1410 (2003).
291. Abramovitch, R. A., Kyba, E. P. & Scriven, E. F. V. Mass Spectrometry of Aryl Azides. *Journal of Organic Chemistry* **36**, 3796–3803 (1971).
292. Oliveira, A. M. *et al.* Mass Spectrometry of Aliphatic Azides Electron impact (EI) mass spectra of $N_3C_2COOH$, $N_3CH_2COCH$. *Communications In Mass Spectrometry Rapid Commun. Mass Spectrom* **13**, 559–561 (1999).
293. Farmer, J. *et al.* The macrocyclic compounds and methods of making and using the same. (2005).
294. Righi, G., D'achille, C., Pescatore, G. & Bonini, C. New stereoselective synthesis of the peptidic aminopeptidase inhibitors bestatin, phebestin and probestin. *Tetrahedron Lett* **44**, 6999–7002 (2003).
295. Bräse, S., Gil, C., Knepper, K. & Zimmermann, V. Organic Azides: An Exploding Diversity of a Unique Class of Compounds. *Angewandte Chemie International Edition* **44**, 5188–5240 (2005).
296. Martínez, L. E., Leighton, J. L., Carsten, D. H. & Jacobsen, E. N. Highly Enantioselective Ring Opening of Epoxides Catalyzed by (salen)Cr(III) Complexes. *J Am Chem Soc* **117**, 5897–5898 (1995).
297. Sabitha, G., Babu, R. S., Rajkumar, M. & Yadav, J. S. Cerium(III) chloride promoted highly regioselective ring opening of epoxides and aziridines using $NaN_3$ in acetonitrile: A facile synthesis of 1,2-azidoalcohols and 1,2-azidoamines. *Org Lett* **4**, 343–345 (2002).
298. Titz, A., Radic, Z., Schwardt, O. & Ernst, B. A safe and convenient method for the preparation of triflyl azide, and its use in diazo transfer reactions to primary amines. *Tetrahedron Lett* **47**, 2383–2385 (2006).
299. Rô Me Waser, J., Gaspar, B., Nambu, H. & Carreira, E. M. Hydrazines and Azides via the Metal-Catalyzed Hydrohydrazination and Hydroazidation of Olefins. (2006) doi:10.1021/JA062355.
300. Meng, G. *et al.* Modular click chemistry libraries for functional screens using a diazotizing reagent. *Nature 2019 574:7776* **574**, 86–89 (2019).
301. Scriven, E. F. V. & Turnbull, K. Azides: Their Preparation and Synthetic Uses. *Chem Rev* **88**, 297–368 (1988).
302. Bevilacqua, V. *et al.* Copper-Chelating Azides for Efficient Click Conjugation Reactions in Complex Media. *Angewandte Chemie International Edition* **53**, 5872–5876 (2014).
303. Hassner, A., Fibiger, R. & Andisik, D. Lewis Acid Catalyzed Conversion of Alkenes and Alcohols to Azides1. *J Org Chem* **49**, 4237–4244 (1984).
304. Katritzky, A. R., El Khatib, M., Bolshakov, O., Khelashvili, L. & Steel, P. J. Benzotriazol-1-yl-sulfonyl azide for diazotransfer and preparation of azidoacylbenzotriazoles. *Journal of Organic Chemistry* **75**, 6532–6539 (2010).
305. Proto, S. *et al.* Model Studies on the Synthesis of Madangamine Alkaloids. Assembly of the Macrocyclic Rings. *Org Lett* **14**, 3916–3919 (2012).
306. Boyer, J. H. Addition of Hydrazoic Acid to Conjugated Systems. *J. Amer. Chem. Soc.,* **73**, 5248-5252, (1951).
307. Katritzky, A., Takahashi, I., Marson, C. & Scriven, E. The synthesis of 1,2,3-triazoles and aziridines using 2-(4-pyridyl)ethyl azide. *Chem Scr* **28**, 149–155 (1987).

308. Xu, L., Chen, J. & Chu, L. Solvent-tuned chemoselective carboazidation and diazidation of alkenes via iron catalysis. *Cite this: Org. Chem. Front* **6**, 512 (2019).
309. Peng, H., Yuan, Z., Chen, P. & Liu, G. Palladium-Catalyzed Intermolecular Oxidative Diazidation of Alkenes. *Chin J Chem* **35**, 876–880 (2017).
310. Cai, C.-Y., Zheng, Y.-T., Li, J.-F. & Xu, H.-C. Cu-Electrocatalytic Diazidation of Alkenes at ppm Catalyst Loading. *Cite This: J. Am. Chem. Soc* **2022**, 11980–11985 (2022).
311. Fumagalli, G., Rabet, P. T. G., Boyd, S. & Greaney, M. F. Three-Component Azidation of Styrene-Type Double Bonds: Light-Switchable Behavior of a Copper Photoredox Catalyst. *Angewandte Chemie - International Edition* **54**, 11481–11484 (2015).
312. Lu, M.-Z., Wang, C.-Q. & Loh, T.-P. Copper-Catalyzed Vicinal Oxyazidation and Diazidation of Styrenes under Mild Conditions: Access to Alkyl Azides. (2015) doi:10.1021/acs.orglett.5b03130.
313. Zhou, H. *et al.* Copper-Catalyzed Ligand-Free Diazidation of Olefins with $TMSN_3$ in $CH_3CN$ or in $H_2O$. (2017) doi:10.1021/acs.orglett.7b02982.
314. Geneste, H. *et al.* Novel Inhibitor Compounds of Phosphodiesterase Type 10a. (2013).
315. Deprez Poulain, R. *et al.* 5-Membered Heteroaryl Compounds Containing a Hydroxamate Moiety And Their Use. (2020).
316. Iwao, M. & Kuraishi, T. Synthesis and thermolysis of N-heteroarylacetylazides and α-oximino-α-(N-heteroaryl)acetylazides. *J Heterocycl Chem* **16**, 689–698 (1979).
317. Wang, W., Qin, Z., Zhang, X., Zhao, W. & Yang, W. Catalyst-free C(sp3)–H functionalization of methyl azaarenes with heteroaromatic trifluoromethyl ketone hydrates: "all-water" synthesis of α-trifluoromethyl tertiary alcohols. *Org Biomol Chem* **21**, 4304–4308 (2023).
318. Liu, Z. & Liu, Z.-Q. An Intermolecular Azidoheteroarylation of Simple Alkenes via Free-Radical Multicomponent Cascade Reactions Scheme 1. Design a Multicomponent Minisci Reaction through Radical Polar Reversal. *Org. Lett* **19**, 5649–5652 (2017).
319. Rigby, J. H. & Danca, D. M. Vinyl isocyanates in alkaloid synthesis. Camptothecin model studies. *Tetrahedron Lett* **38**, 4969–4972 (1997).
320. Lear, J. M. *et al.* Multi-component heteroarene couplings via polarity-reversed radical cascades †. *Chem. Commun* **55**, 8820 (2019).
321. Shen, J. *et al.* Photoinitiated multicomponent cascade reaction of N-heteroarenes with unactivated alkenes and trimethylsilyl azide. (2022) doi:10.1016/j.mcat.2022.112330.
322. Deprez Poulain, R. *et al.* Preparation of triazoles and related 5-membered heteroaryl compounds containing a hydroxamate moiety useful as sensitizers for chemotherapy of malignant tumors. (2020).
323. Su, C.-L. *et al.* Using gene expression database to uncover biology functions of 1,4-disubstituted 1,2,3-triazole analogues synthesized via a copper (I)-catalyzed reaction. (2017) doi:10.1016/j.ejmech.2017.03.034.
324. Karthik Kumar, K., Seenivasan, S. P., Kumar, V. & Das, T. M. Synthesis of quinoline coupled [1,2,3]-triazoles as a promising class of anti-tuberculosis agents. (2011) doi:10.1016/j.carres.2011.06.028.
325. Michaels, H. A., Simmons, J. T., Clark, R. J. & Zhu, L. Fused Polycyclic Compounds via Cycloaddition of 4-(1′-Cyclohexenyl)-5-iodo-1,2,3-triazoles with 4-Phenyl-1,2,4-triazoline-3,5-dione: The Importance of a Sacrificial Iodide Leaving Group. *J. Org. Chem* **78**, 15 (2013).

326. Kuang, G.-C. *et al.* Experimental Investigation on the Mechanism of Chelation-Assisted, Copper(II) Acetate-Accelerated Azide-Alkyne Cycloaddition. *J. Am. Chem. Soc* **133**, 13984–14001 (2011).
327. Paul, S., Roy, P., Saha Sardar, P. & Majhi, A. Design, Synthesis, and Biophysical Studies of Novel 1,2,3-Triazole-Based Quinoline and Coumarin Compounds. (2019) doi:10.1021/acsomega.9b00414.
328. Brotherton, W. S. *et al.* Apparent Copper(II)-Accelerated Azide−Alkyne Cycloaddition. *Org Lett* **11**, 4954–4957 (2009).
329. Wu, Z. G. *et al.* Visible-Light-Mediated Click Chemistry for Highly Regioselective Azide–Alkyne Cycloaddition by a Photoredox Electron-Transfer Strategy. *Chemistry – A European Journal* **26**, 5694–5700 (2020).
330. Qinglan, H., Zhiqiang, T., Changjiang, Y., Xiaoming, Z. & Liuyong, W. Research for the t-BuOK-Catalyzed Synthesis of Aromatic Aldehydes and Ketone from Arylmethyl Azides. *Chinese Journal of Organic Chemistry* **37**, (2017).
331. Garner, B. R., Mullock, E. B., Suschitzky, H., Xiii, P. & Garner, R. Structure and Mechanism in Organic Chemistry. *J. Chem. Ed* **38**, 621 (1966).
332. Kuang, G. C., Michaels, H. A., Simmons, J. T., Clark, R. J. & Zhu, L. Chelation-assisted, copper(II)-acetate-accelerated azide-alkyne cycloaddition. *Journal of Organic Chemistry* **75**, 6540–6548 (2010).
333. Miyake, Y. *et al.* Metalloprotein-Catalyzed Click Reaction for in Situ Generation of a Potent Inhibitor. *ACS Catal* **10**, 5383–5392 (2020).
334. Li, Z. *et al.* Design, synthesis, and biological evaluation of triazole-pyrimidine-methylbenzonitrile derivatives as dual A 2A /A 2B adenosine receptor antagonists. *J Enzyme Inhib Med Chem* **37**, 1514–1526 (2022).
335. Michaels, H. A., Simmons, J. T., Clark, R. J. & Zhu, L. Fused polycyclic compounds via Cycloaddition of 4-(1′-Cyclohexenyl)- 5-iodo-1,2,3-triazoles with 4-phenyl-1,2,4-triazoline-3,5-dione: The importance of a sacrificial iodide leaving group. *Journal of Organic Chemistry* **78**, 5038–5044 (2013).
336. Brandhofer, T., Özdemir, A., Gini, A. & Mancheño, O. G. Double Cu-Catalyzed Direct Csp3−H Azidation/CuAAC Reaction: A Direct Approach towards Demanding Triazole Conjugates. *Chemistry – A European Journal* **25**, 4077–4086 (2019).
337. Breugst, M. & Reissig, H. U. The Huisgen Reaction: Milestones of the 1,3-Dipolar Cycloaddition. *Angewandte Chemie - International Edition* **59**, 12293–12307 (2020).
338. Huisgen, R. 1,3-Dipolar Cycloadditions. *Proceedings of Chemical Society* 357–396 (1961).
339. Rostovestev, V. V., Green, L. G. & Fokin, V. V. A Stepwise Huisgen Cycloaddition Process: Copper(I)-Catalyzed Regioselective "Ligation" of Azides and Terminal Alkynes. *Angewandte Chemie International Edition* **41**, 2596–2599 (2002).
340. Zhang, L. *et al.* Ruthenium-catalyzed cycloaddition of alkynes and organic azides. *J Am Chem Soc* **127**, 15998–15999 (2005).
341. Kolb, H. C. & Sharpless, K. B. The growing impact of click chemistry on drug discovery. *Drug Discov Today* **8**, 1128–1137 (2003).
342. Rostovtsev, V. V., Green, L. G., Fokin, V. V. & Sharpless, K. B. ChemInform Abstract: A Stepwise Huisgen Cycloaddition Process: Copper(I)-Catalyzed Regioselective "Ligation" of Azides and Terminal Alkynes. *ChemInform* **33**, no-no (2010).
343. Liang, L. & Astruc, D. The copper(I)-catalyzed alkyne-azide cycloaddition (CuAAC) 'click' reaction and its applications. An overview. *Coord Chem Rev* **255**, 2933–2945 (2011).

344. Moses, J. E. & Moorhouse, A. D. The growing applications of click chemistry. doi:10.1039/b613014n.
345. Tron, G. C. *et al.* Click Chemistry Reactions in Medicinal Chemistry: Applications of the 1,3-dipolar Cycloaddition Between Azides and Alkynes. *Med Res Rev* **28**, 278–308 (2007).
346. Celik, F., Unver, Y., Barut, B., Ozel, A. & Sancak, K. Synthesis, Characterization and Biological Activities of New Symmetric Bis-1,2,3-Triazoles with Click Chemistry. *Med Chem (Los Angeles)* **14**, 230–241 (2018).
347. Matin, M. M. *et al.* Triazoles and Their Derivatives: Chemistry, Synthesis, and Therapeutic Applications. *Front Mol Biosci* **9**, (2022).
348. Dheer, D., Singh, V. & Shankar, R. Medicinal attributes of 1,2,3-triazoles: Current developments. *Bioorg Chem* **71**, 30–54 (2017).
349. Vala, D. P., Vala, R. M. & Patel, H. M. Versatile Synthetic Platform for 1,2,3-Triazole Chemistry. *ACS Omega* **7**, 36945–36987 (2022).
350. Agalave, S. G., Maujan, S. R. & Pore, V. S. Click chemistry: 1,2,3-triazoles as pharmacophores. *Chem Asian J* **6**, 2696–2718 (2011).
351. Yu, W. *et al.* The Hsp90 inhibitor 17-allylamide-17-demethoxygeldanamycin induces apoptosis and differentiation of Kasumi-1 harboring the Asn822Lys KIT mutation and down-regulates KIT protein level. *Leuk Res* **30**, 575–582 (2006).
352. Peterson, L. B. & Blagg, B. S. J. Click chemistry to probe Hsp90: Synthesis and evaluation of a series of triazole-containing novobiocin analogues. (2010) doi:10.1016/j.bmcl.2010.04.140.
353. Doiron, J. *et al.* Synthesis and structure activity relationship of 1-and 2-substituted-1,2,3-triazole letrozole-based analogues as aromatase inhibitors. (2011) doi:10.1016/j.ejmech.2011.05.074.
354. Batra, N. *et al.* Synthesis and Antimalarial Evaluation of [1, 2,3]-Triazole-Tethered Sulfonamide-Berberine Hybrids. *ChemistrySelect* **3**, 9790–9793 (2018).
355. Ulusoy, N., Gürsoy, A. & Otuk, G. Synthesis and antimicrobial activity of some 1,2,4-triazole-3-mercaptoacetic acid derivatives. *Il Farmaco* **56**, 947–952 (2001).
356. Abdel-Wahab, B. F., Mohamed, H. A. & Awad, G. E. A. Synthesis And Biological Activity Of Some New 1,2,3-Triazole Hydrazone Derivatives. *Chem. Bull* **4**, 106–109 (2015).
357. Vatmurge, N. S. *et al.* Synthesis and antimicrobial activity of β-lactam–bile acid conjugates linked via triazole. *Bioorg Med Chem Lett* **18**, 2043–2047 (2008).
358. Shu, H., Izenwasser, S., Wade, D., Stevens, E. D. & Trudell, M. L. Synthesis and CB1 cannabinoid receptor affinity of 4-alkoxycarbonyl-1,5-diaryl-1,2,3-triazoles. *Bioorg Med Chem Lett* **19**, 891–893 (2009).
359. Da Silva, F. D. C. *et al.* Synthesis, HIV-RT inhibitory activity and SAR of 1-benzyl-1H-1,2,3-triazole derivatives of carbohydrates. (2008) doi:10.1016/j.ejmech.2008.02.047.
360. Somu, R. V. *et al.* Rationally-designed nucleoside antibiotics that inhibit siderophore biosynthesis of Mycobacterium tuberculosis. *J Med Chem* **49**, 31–34 (2006).
361. Costa, M. S. *et al.* Synthesis, tuberculosis inhibitory activity, and SAR study of N-substituted-phenyl-1,2,3-triazole derivatives. *Bioorg Med Chem* **14**, 8644–8653 (2006).
362. Yu, J., Xiao, S., Chen, F., Li, L. & Xu, G. Cyclodextrin mediated efficient energy transfer between 4-amido-1,8-naphthalimide and porphyrin. *Dyes and Pigments* **180**, 108518 (2020).
363. Lizzul-Jurse, A. *et al.* Readily functionalizable phosphonium-tagged fluorescent coumarins for enhanced detection of conjugates by mass spectrometry. *Org Biomol Chem* **14**, 7777–7791 (2016).

364. Mialane, P., Tchertanov, L., Banse, F., Sainton, J. & Girerd, J.-J. In Iron Carriers and Iron Proteins. *Angew. Chem., Int. Ed. Engl* **28**, 2440–2444 (1992).
365. Seo, H. *et al.* Evaluating Metal−Ligand Interactions of Metal-Binding Isosteres Using Model Complexes. (2023) doi:10.1021/acs.inorgchem.1c02433.
366. Britovsek, G. J. P., England, J. & White, A. J. P. Non-heme Iron(II) Complexes Containing Tripodal Tetradentate Nitrogen Ligands and Their Application in Alkane Oxidation Catalysis. (2005) doi:10.1021/ic0509229.
367. Beni, A., Dei, A., Laschi, S., Rizzitano, M. & Sorace, L. Tuning the Charge Distribution and Photoswitchable Properties of Cobalt–Dioxolene Complexes by Using Molecular Techniques. *Chemistry – A European Journal* **14**, 1804–1813 (2008).
368. Gransbury, G. K. *et al.* Understanding the Origin of One-or Two-Step Valence Tautomeric Transitions in Bis(dioxolene)-Bridged Dinuclear Cobalt Complexes. *J. Am. Chem. Soc* **142**, 10692–10704 (2020).
369. Tyeklar, Z. *et al.* Reversible reaction of dioxygen (and carbon monoxide) with a copper(I) complex. X-ray structures of relevant mononuclear Cu(I) precursor adducts and the trans-(.mu.-1,2-peroxo)dicopper(II) product. *J Am Chem Soc* **115**, 2677–2689 (1993).
370. Lin, C.-Y., Giuliano, M. W., Ellis, B. D., Miller, S. J. & Anslyn, E. V. From substituent effects to applications: enhancing the optical response of a four-component assembly for reporting ee values. *Chem Sci* **7**, 4085–4090 (2016).
371. Dhanalakshmi, T., Suresh, E. & Palaniandavar, M. Olefin aziridination by copper(II) complexes: Effect of redox potential on catalytic activity. *Inorganica Chim Acta* **365**, 143–151 (2011).
372. Cui, T., Ye, C. X., Thelemann, J., Jenisch, D. & Meggers, E. Enantioselective and Enantioconvergent Iron-Catalyzed C(sp3)-H Aminations to Chiral 2-Imidazolidinones. *Chin J Chem* **41**, 2065–2070 (2023).
373. Nersesian, D. L. *et al.* In vitro SAR of pyrrolidine-containing histamine H3 receptor antagonists: Trends across multiple chemical series. *Bioorg Med Chem Lett* **18**, 355–359 (2008).
374. Mathieu, G., Patel, H. & Lebel, H. Convenient Continuous Flow Synthesis of N-Methyl Secondary Amines from Alkyl Mesylates and Epoxides. *Org Process Res Dev* **24**, 2157–2168 (2020).
375. Archer, J. *et al.* Substituted thienyl-hydroxamic acids as histone deacetylase inhibitors. (2004).
376. Sonawane, H. R., Vibhute, B. T., Aghav, B. D., Deore, J. V. & Patil, S. K. Versatile applications of transition metal incorporating quinoline Schiff base metal complexes: An overview. *Eur J Med Chem* **258**, 115549 (2023).
377. Yang, Y. *et al.* Platinum(II) 5-substituted-8-hydroxyquinoline coordination compounds induces mitophagy-mediated apoptosis in A549/DDP cancer cells. *J Inorg Biochem* **241**, 112152 (2023).
378. Gole, M. T. *et al.* Synthesis and electronic properties of transition metal complexes containing sulfonamidoquinoline ligands. *Polyhedron* **205**, 115269 (2021).
379. Lewinska, G., Sanetra, J. & Marszalek, K. W. Application of quinoline derivatives in third-generation photovoltaics. *Journal of Materials Science: Materials in Electronics* **32**, 18451–18465 (2021).
380. Yatabe, T. *et al.* A model for the water-oxidation and recovery systems of the oxygen-evolving complex. *Dalton Trans.* **43**, 3063–3071 (2014).
381. To, C. T. & Chan, K. S. Carbon–Carbon Bond Activation by Group 9 Metal Complexes. *European J Org Chem* **2019**, 6581–6591 (2019).
382. Sinha, S. K. *et al.* Toolbox for Distal C–H Bond Functionalizations in Organic Molecules. *Chem Rev* **122**, 5682–5841 (2022).

383. Bratsos, I. & Alessio, E. Ruthenium Complexes. in *Inorganic Syntheses* vol. 35 148–163 (2010).
384. Price, J. H., Williamson, A. N., Schramm, R. F. & Wayland, B. B. Palladium(II) and platinum(II) alkyl sulfoxide complexes. Examples of sulfur-bonded, mixed sulfur- and oxygen-bonded, and totally oxygen-bonded complexes. *Inorg Chem* **11**, 1280–1284 (1972).
385. Mohabeer, P. K. *et al.* Synthesis, structure and fluxionality of Co(III) complexes containing chelated sulfate. *Polyhedron* **176**, 114303 (2020).
386. Hui Zhang, Z., He Bu, X., Ang Zhu, Z. & Ti Chen, Y. Synthesis, crystal structure and spectroscopic characterization of the complex of palladium(II) with tris(2-pyridylmethyl)amine. *Polyhedron* **15**, 2787–2792 (1996).
387. Blackman, A. G., Schenk, E. B., Jelley, R. E., Krenske, E. H. & Gahan, L. R. Five-coordinate transition metal complexes and the value of τ5: observations and caveats. *Dalton Transactions* **49**, 14798–14806 (2020).
388. Addison, A. W., Rao, T. N., Reedijk, J., van Rijn, J. & Verschoor, G. C. Synthesis, structure, and spectroscopic properties of copper(II) compounds containing nitrogen–sulphur donor ligands; the crystal and molecular structure of aqua[1,7-bis(N-methylbenzimidazol-2′-yl)-2,6-dithiaheptane]copper(II) perchlorate. *J. Chem. Soc., Dalton Trans.* 1349–1356 (1984) doi:10.1039/DT9840001349.
389. Hunter, C. A. & Sanders, J. K. M. The nature of pi-pi interactions. *J Am Chem Soc* **112**, 5525–5534 (1990).
390. Choi, K.-Y. Synthesis, Properties, and X-ray Crystal Structure of Copper(II) Complex with Bis[(2-pyridyl)methyl]-2-(2-pyridyl)ethylamine. *Journal of the Korean Chemical Society* **51**, 31–35 (2007).
391. Moore, C. M. & Szymczak, N. K. A tris(2-quinolylmethyl)amine scaffold that promotes hydrogen bonding within the secondary coordination sphere. *Dalton Transactions* **41**, 7886 (2012).
392. Nespolo, M. & Souvignier, B. Point groups in crystallography. *Zeitschrift für Kristallographie* **224**, (2009).
393. Chen, X.-Y. *et al.* Two-Photon Fluorescent Probes of Biological Zn(II) Derived from 7-Hydroxyquinoline. *Org Lett* **11**, 4426–4429 (2009).
394. Eccles, N. *et al.* Remote conformational responses to enantiomeric excess in carboxylate-binding dynamic foldamers. *Chemical Communications* **55**, 9331–9334 (2019).
395. Xue, L., Wang, H.-H., Wang, X.-J. & Jiang, H. Modulating Affinities of Di-2-picolylamine (DPA)-Substituted Quinoline Sensors for Zinc Ions by Varying Pendant Ligands. *Inorg Chem* **47**, 4310–4318 (2008).
396. Meng, X., Wang, S., Li, Y., Zhu, M. & Guo, Q. 6-Substituted quinoline-based ratiometric two-photon fluorescent probes for biological $Zn^{2+}$ detection. *Chemical Communications* **48**, 4196 (2012).
397. Canary, J. W., Allen, C. S., Castagnetto, J. M. & Wang, Y. Conformationally Driven, Propeller-like Chirality in Labile Coordination Complexes. *J Am Chem Soc* **117**, 8484–8485 (1995).
398. Mikata, Y. *et al.* Effect of methoxy substituents on fluorescent $Zn^{2+}$ $Cd^{2+}$ selectivity of bisquinoline derivatives with *a N,N′*-dimethylalkanediamine skeleton. *Dalton Transactions* **52**, 7411–7420 (2023).
399. Fritsch, J. M., Thoreson, K. A. & McNeill, K. Synthesis and structures of acyclic monoanionic tetradentate aza β-diketiminate complexes of magnesium, zinc, and cadmium. *Dalton Trans.* 4814–4820 (2006) doi:10.1039/B609616F.
400. Xiang, J. & Mei, P. The reactivity of hydrazones in the presence of Zn(II) ion: Oxidative coupling of hydrazones with alcohol and oxidative cyclization of hydrazones. *Inorg Chem Commun* **24**, 162–165 (2012).

401. Pang, X. *et al.* Coordination assemblies of rigid–flexible 1,3-bis(5-(pyridine-2-yl)-1,2,4-triazole-3-yl)propane ligands with $MCl_2$ (M = Fe, Co, Cu or Zn): structural diversity and mass spectra. *Transition Metal Chemistry* **42**, 533–542 (2017).
402. Duboc, C. *et al.* High-field EPR investigation of a series of mononuclear Mn(II) complexes doped into Zn(II) hosts. *Polyhedron* **26**, 5243–5249 (2007).
403. Shen, K. *et al.* Aerobic oxygenation catalyzed by first row transition metal complexes coordinated by tetradentate mono-carbon bridged bis-phenanthroline ligands: intra-versus intermolecular carbon–hydrogen bond activation. *Dalton Transactions* **48**, 6396–6407 (2019).
404. Triller, M. U., Hsieh, W.-Y., Pecoraro, V. L., Rompel, A. & Krebs, B. Preparation of Highly Efficient Manganese Catalase Mimics. *Inorg Chem* **41**, 5544–5554 (2002).
405. Yamazaki, H., Igarashi, S., Nagata, T. & Yagi, M. Substituent Effects on Core Structures and Heterogeneous Catalytic Activities of MnIII(μ-O)$_2$MnIV Dimers with 2,2′-6′,2″-Terpyridine Derivative Ligands for Water Oxidation. *Inorg Chem* **51**, 1530–1539 (2012).
406. Hureau, C., Blondin, G., Cesario, M. & Un, S. Direct Measurement of the Hyperfine and g-Tensors of a Mn(III)−Mn(IV) Complex in Polycrystalline and Frozen Solution Samples by High-Field EPR. *J Am Chem Soc* **125**, 11637–11645 (2003).
407. Nielsen, A., McKenzie, C. J. & Bond, A. D. Di-μ-oxido-bis{bis[N,N ′-bis(2-pyridylmethyl)ethane-1,2-diamine]manganese(III,IV)} tris(perchlorate) hexahydrate: clarification of an order–disorder phase transition. *Acta Crystallogr C* **65**, 447–450 (2009).
408. Hill, J. P. *et al.* Decomposition of Dinuclear Manganese Complexes for the Preparation of Nanostructured Oxide Materials. *Inorg Chem* **47**, 8306–8314 (2008).
409. Stebler, M., Ludi, A. & Buergi, H. B. [(phen)$_2$Mn$^{IV}$(μ-O)$_2$](PF$_6$)$_3$.CH$_3$CN and [(phen)$_2$Mn$^{IV}$(μ-O)$_2$](ClO$_4$)$_4$.CH$_3$CN (phen = 1,10-phenanthroline): crystal structure analyses at 100 K, interpretation of disorder, and optical, magnetic, and electrochemical results. *Inorg Chem* **25**, 4743–4750 (1986).
410. Schindler, S., Walter, O., Pedersen, J. Z. & Toftlund, H. Synthesis and characterization of a new dinuclear bis(μ-oxo)manganese(III)/manganese(IV) complex. *Inorganica Chim Acta* **303**, 215–219 (2000).
411. Suzuki, M., Senda, H., Kobayashi, Y., Oshio, H. & Uehara, A. Synthesis and Characterization of the Di(μ-oxo)Dimanganese(III,IV) Complex with Carboxylato Groups as a Terminal Ligand. *Chem Lett* **17**, 1763–1766 (1988).
412. Lennartson, A. & McKenzie, C. J. Oxidation of a dinuclear manganese(II) complex to an oxide-bridged dimanganese(IV) complex. *Acta Crystallogr C* **68**, m347–m352 (2012).
413. Goodson, P. A., Glerup, J., Hodgson, D. J., Michelsen, K. & Weihe, H. Syntheses and characterization of binuclear manganese(III,IV) and -(IV,IV) complexes with ligands related to *N,N'*-bis(2-pyridylmethyl)-1,2-ethanediamine. *Inorg Chem* **30**, 4909–4914 (1991).
414. Frapart, Y.-M. *et al.* Chemical Modeling of the Oxygen-Evolving Center in Plants. Synthesis, Structure, and Electronic and Redox Properties of a New Mixed Valence Mn−Oxo Cluster: [Mn $_2^{III,IV}$O$_2$ (bisimMe$_2$en)$_2$ ]$^{3+}$ (bisimMe$_2$en = *N*,*N*‘-Dimethyl- *N*,*N*‘-bis(imidazol-4-ylmethyl)ethane-1,2-diamine). EPR Detection of an Imidazole Radical Induced by UV Irradiation at Low Temperature. *J Am Chem Soc* **118**, 2669–2678 (1996).

415. Oki, A. R., Glerup, J. & Hodgson, D. J. Syntheses and characterization of binuclear manganese(III,IV) and -(IV,IV) complexes with ligands related to tris(2-pyridylmethyl)amine. *Inorg Chem* **29**, 2435–2441 (1990).
416. Nielsen, A., McKenzie, C. J. & Bond, A. D. Di-μ-oxido-bis{bis[N ,N′-bis(2-pyridylmethyl)ethane-1,2-diamine]manganese(III,IV)} tris(perchlorate) hexahydrate: clarification of an order–disorder phase transition. *Acta Crystallogr C* **65**, m447–m450 (2009).
417. Plaksin, P. M., Stoufer, R. C., Mathew, M. & Palenik, G. J. Novel antiferromagnetic oxo-bridged manganese complex. *J Am Chem Soc* **94**, 2121–2122 (1972).
418. Baffert, C. *et al.* Two New Terpyridine Dimanganese Complexes: A Manganese(III,III) Complex with a Single Unsupported Oxo Bridge and a Manganese(III,IV) Complex with a Dioxo Bridge. Synthesis, Structure, and Redox Properties. *Inorg Chem* **41**, 1404–1411 (2002).
419. Fujisawa, K., Sakuma, S., Ikarugi, R., Jose, A. & Solomon, E. I. Thermally stable manganese(III) peroxido complexes with hindered $N_3$ tripodal ligands: Structures and their physicochemical properties. *J Inorg Biochem* **225**, 111597 (2021).
420. Levaton, B. B. & Olmstead, M. M. Incorporation of $\mu_3$-$CO_3$ into an MnIIIMnIVMn12 cluster: {[(cyclam)MnIV(μ-O)$_2$MnIII ($H_2O$)(μ-OH)]$_6$($\mu_3$-$CO_3$) 2}$Cl_8$·24$H_2O$. *Acta Crystallogr Sect E Struct Rep Online* **66**, m1226–m1227 (2010).
421. Jensen, A. F., Su, Z., Hansen, N. K. & Larsen, F. K. X-Ray Diffraction Study of the Correlation between Electrostatic Potential and K-Absorption Edge Energy in a Bis(.mu.-oxo) Mn(III)-Mn(IV) Dimer. *Inorg Chem* **34**, 4244–4252 (1995).
422. Glerup, J. *et al.* Synthesis and Characterization of Bis(.mu.-oxo)dimanganese(III,III), -(III,IV), and -(IV,IV) Complexes with Ligands Related to N,N'-Bis(2-pyridylmethyl)-1,2-ethanediamine (Bispicen). *Inorg Chem* **33**, 4105–4111 (1994).
423. Goodson, P. A. & Hodgson, D. J. Synthesis and characterization of a bis(oxo)-bridged MN(III)Mn(III) complex, bis(.mu.-oxo)bis[N,N'-bis((6-methylpyrid-2-yl)methyl)ethane-1,2-diamine]dimanganese(III) perchlorate. *Inorg Chem* **28**, 3606–3608 (1989).
424. Al-Juaid, S. S. *et al.* Attachment to manganese or cobalt of a bulky tri(organosilyl)methyl ligand containing an $NMe_2$ or an OMe donor group. *J Organomet Chem* **649**, 121–127 (2002).
425. Fohlmeister, L. & Jones, C. Stabilisation of carbonyl free amidinato-manganese(ii) hydride complexes: "masked" sources of manganese(i) in organometallic synthesis. *Dalton Transactions* **45**, 1436–1442 (2016).
426. Gultneh, Y., Yisgedu, T. B., Tesema, Y. T. & Butcher, R. J. Dioxo-Bridged Dinuclear Manganese(III) and -(IV) Complexes of Pyridyl Donor Tripod Ligands: Combined Effects of Steric Substitution and Chelate Ring Size Variations on Structural, Spectroscopic, and Electrochemical Properties. *Inorg Chem* **42**, 1857–1867 (2003).
427. Chai, J. *et al.* Synthesis and Reaction of [{HC(CMeNAr)$_2$}Mn]$_2$ (Ar = 2,6- iii $Pr_2C_6H_3$): The Complex Containing Three-Coordinate Manganese(I) with a Mn−Mn Bond Exhibiting Unusual Magnetic Properties and Electronic Structure. *J Am Chem Soc* **127**, 9201–9206 (2005).
428. Goodson, P. A., Oki, A. R., Glerup, J. & Hodgson, D. J. Design, synthesis, and characterization of bis(.mu.-oxo)dimanganese(III,III) complexes. Steric and electronic control of redox potentials. *J Am Chem Soc* **112**, 6248–6254 (1990).

429. Pal, S., Gohdes, J. W., Wilisch, W. C. A. & Armstrong, W. H. Synthesis, structure, and properties of a [manganese] complex that consists of an $\{Mn_2O_2(O_2CCH_3)\}^{2+}$ core and a spanning hexadentate ligand. *Inorg Chem* **31**, 713–716 (1992).
430. Neuba, A., Seewald, O., Flörke, U. & Henkel, G. Di-μ-oxido-bis{[1,3-bis(tetramethylguanidino)propane-$\kappa_2$ *N,N′*]bromidomanganese(III)}. *Acta Crystallogr Sect E Struct Rep Online* **63**, m2099–m2100 (2007).
431. Vincent, J. B. *et al.* Models of the manganese catalase enzymes. Dinuclear manganese(III) complexes with the $[Mn_2(\mu\text{-}O)(\mu\text{-}O_2CR)_2]^{2+}$ core and terminal monodentate ligands: preparation and properties of $[Mn_2O(O_2CR)_2X_2(bpy)_2]$ (X = chloride, azide, water). *J Am Chem Soc* **115**, 12353–12361 (1993).
432. Kauffman, G. B. Alfred Werner's research on polynuclear coordination compounds. *Coord Chem Rev* **9**, 339–363 (1973).
433. Andersen, P. *et al.* The Crystal Structures of Tri-mu-hydroxo-bis[triammine cobalt(III)] Bromide and Iodide. *Acta Chem Scand* **21**, 243–256 (1967).
434. Searle, G. & Hambley, T. The preparation and characterization of mer-Bis[di(3-aminopropyl)amine]cobalt(III) perchlorate, and the crystal structure of its hydrolysis product Bis[di(3-aminopropyl)amine]tri-μ-hydroxo-dicobat(III) perchlorate. *Aust J Chem* **35**, 1297 (1982).
435. Larsen, E. *et al.* Base Hydrolysis of (1,4,7-Triazacyclononane)(3-thiapentane-1,5-diamine)cobalt(III) and the Crystal and Molecular Structure of Sodium Tri-mu-hydroxobis{1,4,7-triazacyclononanecobalt(III)} Dichloride Diperchlorate Dihydrate Isolated from the Reaction. *Acta Chem Scand* **48**, 107–112 (1994).
436. Hall, N. A. Synthesis and Characterisation of Complexes Derived from a Series of Polyamine Ligansd. (University of Otago, 2009).
437. Arakawa, R. Application of Mass Spectrometry to Coordination Chemistry. *Journal of Mass Spectrometry Society of Japan* **56**, 247–262 (2008).
438. Tsednee, M., Huang, Y. C., Chen, Y. R. & Yeh, K. C. Identification of metal species by ESI-MS/MS through release of free metals from the corresponding metal-ligand complexes. *Scientific Reports 2016 6:1* **6**, 1–13 (2016).
439. Belkhir-Talbi, D. *et al.* Synthesis, characterization, theoretical studies, ADMET and drug-Likeness analysis: Electrochemical and biological activities of metal complexes of 3-(2-hydroxybenzoyl)-*2H*-chromen-2-one. (2018) doi:10.1016/j.molstruc.2018.11.035.
440. Henderson, W. & McIndoe, J. S. Fundamentals. in *Mass Spectrometry of Inorganic, Coordination and Organometallic Compounds* 1–21 (Wiley, 2005). doi:10.1002/0470014318.ch1.
441. Marco, V. B. Di & Bombi, G. G. Electrospray Mass Spectrometry (Esi-Ms) In The Study Of Metal-Ligand Solution Equilibria. (2005) doi:10.1002/mas.20070.
442. Caudle, T., Stevens, R. D. & Crumbliss, A. L. Electrospray Mass Spectrometry Study of 1:1 Ferric Dihydroxamates. *Inorg. Chim. Acta* **33**, 2189.
443. Hall, N. A., Duboc, C., Collomb, M.-N., Deronzier, A. & Blackman, A. G. Factors influencing mononuclear versus multinuclear coordination in a series of potentially hexadentate acyclic N6 ligands: the roles of flexibility and chelate ring size. *Dalton Transactions* **40**, 12075 (2011).
444. Job, P. Formation and Stability of Inorganic Complexes in Solution. *Annales de Chimie Science des Matériaux* **9**, 113–203 (1928).
445. Olson, E. J. & Bühlmann, P. Getting More out of a Job Plot: Determination of Reactant to Product Stoichiometry in Cases of Displacement Reactions and n:n Complex Formation. *J Org Chem* **76**, 8406–8412 (2011).
446. Renny, J. S., Tomasevich, L. L., Tallmadge, E. H. & Collum, D. B. Method of Continuous Variations: Applications of Job Plots to the Study of Molecular

Associations in Organometallic Chemistry. *Angewandte Chemie International Edition* **52**, 11998–12013 (2013).
447. Valéria, A., Simionato, C., Cantú, M. D. & Carrilho, E. Characterization of metal-deferoxamine complexes by continuous variation method: A new approach using capillary zone electrophoresis. (2006) doi:10.1016/j.microc.2006.01.018.
448. Blasco, S. *et al.* Coordination of $Cu^{2+}$ Ions to C2 Symmetric Pseudopeptides Derived from Valine. *Inorg Chem* **49**, 7841–7852 (2010).
449. Hill, Z. D. & MacCarthy, P. Novel approach to Job's method: An undergraduate experiment. *J Chem Educ* **63**, 162–167 (1986).
450. Bosque-Sendra, J. M., Almansa-Lopez, E., Garcia-Campana, A. M. & Cuadros-Rodriguez, L. Data Analysis in the Determination of Stoichiometries andStability Constants of Complexes. *Analytical Sciences* **19**, (2003).
451. Mabrouk, M., Hammaad, S. F., Abdelaz, M. A. & Mansour, F. R. Ligand exchange method for determination of mole ratios of relatively weak metal complexes: a comparative study. *Chem Cent J* **12**, 1–7 (2018).
452. Yao, D., Huang, X., Guo, F. & Xie, P. A new fluorescent enhancement chemosensor for $Al^{3+}$ and $Fe^{3+}$ based on naphthyridine and benzothiazole groups. *Sens Actuators B Chem* **256**, 276–281 (2018).
453. Seo, J., Park, S., Lee, S. S., Fainerman-Melnikova, M. & Lindoy, L. F. Copper(II) Interaction with Mono-, Bis- and Tris-Ring $N_3O_2$ Macrocycles: Synthetic, X-ray, Competitive Membrane Transport, and Hypochromic Shift Studies. *Inorg Chem* **48**, 2770–2779 (2009).
454. You, G. R., Park, G. J., Lee, J. J. & Kim, C. A colorimetric sensor for the sequential detection of $Cu^{2+}$ and $CN^-$ in fully aqueous media: practical performance of $Cu^{2+}$. *Dalton Transactions* **44**, 9120–9129 (2015).
455. Chen, T. https://sci-massspec.aut.ac.nz/#/MassCalculator.
456. Shields, W. R., Murphy, T. J. & Garner, E. L. Absolute Isotopic Abundance Ratio and the Atomic Weight of a Reference Sample of Copper. *Journal Of Research of the National Bureau of Standards-A. Physics and Chemistry* **68A**, 589–592 (1964).
457. Eaton, G. R. & Eaton, S. S. Electron Paramagnetic Resonance Spectroscopy. in *Comprehensive Coordination Chemistry II* 37–48 (Elsevier, 2003). doi:10.1016/B0-08-043748-6/01105-1.
458. Rosman, K. J. R. A survey of the isotopic and elemental abundance of zinc. *Geochim Cosmochim Acta* **36**, 801–819 (1972).
459. Maréchal, C. N., Télouk, P. & Albarède, F. Precise analysis of copper and zinc isotopic compositions by plasma-source mass spectrometry. *Chem Geol* **156**, 251–273 (1999).
460. Brosi, A. R. Metal Oxide-Isotopes of Nickel. *Ind Eng Chem* **44**, 955–956 (1952).
461. Owen, H. R. & Schaeffer, O. A. The Isotope Abundances of Chlorine from Various Sources 1. *J Am Chem Soc* **77**, 898–899 (1955).
462. Tabb, D. L. *et al.* Determination of peptide and protein ion charge states by fourier transformation of isotope-resolved mass spectra. *J Am Soc Mass Spectrom* **17**, 903–915 (2006).
463. Cai, S. S., Hanold, K. A. & Syage, J. A. Comparison of Atmospheric Pressure Photoionization and Atmospheric Pressure Chemical Ionization for Normal-Phase LC/MS Chiral Analysis of Pharmaceuticals. *Anal Chem* **79**, 2491–2498 (2007).
464. Franck, H.-G. & Stadelhofer, J. W. Naphthalene — production and uses. in *Industrial Aromatic Chemistry* 298–299 (Springer, Berlin, 1988).
465. Schreiner, C. A. Genetic Toxicity of Naphthalene: A Review. *J Toxicol Environ Health B Crit Rev* **6**, 161–183 (2003).

466. Sibff, D., Bergmann, F., Szmuszkowicz1, J. & Fawaz, G. Condensation of 1,1-Diarylethylenes with Maleic Anhydride Contribution from the 'The Condensation of 1,1-Diarylethylenes with maleic Anhydride'. (1947).
467. Kapraun, D. F. *et al.* A Physiologically Based Pharmacokinetic Model for Naphthalene With Inhalation and Skin Routes of Exposure. *Toxicol Sci* **177**, 377 (2020).
468. Luo, L. *et al.* Synthesis and anticancer activity evaluation of naphthalene-substituted triazole spirodienones. *Eur J Med Chem* **213**, (2021).
469. Abozeid, M. A. *et al.* Synthesis of novel naphthalene-heterocycle hybrids with potent antitumor, anti-inflammatory and antituberculosis activities. *RSC Adv* **10**, 42998–43009 (2020).
470. Kalariya, R. *et al.* Synthesis, biological evaluation and molecular docking study of novel amide-coupled naphthalene scaffolds as potent inhibitors of bacterial recombinase A. *European Journal of Medicinal Chemistry Reports* **6**, 100078 (2022).
471. Sharma, S., Srivastava, V. K. & Kumar, A. Anti-inflammatory activity of some novel α-amino naphthalene derivatives. *Arzneimittel-Forschung/Drug Research* **53**, 44–52 (2003).
472. Perrone, R. *et al.* Synthesis, Binding and Antiviral Properties of Potent Core-Extended Naphthalene Diimides Targeting the HIV-1 Long Terminal Repeat Promoter G-Quadruplexes. *J Med Chem* **58**, 9639–9652 (2015).
473. Soylu-Eter, Ö. *et al.* Antiviral activity and molecular modeling studies on 1H-indole-2,3-diones carrying a naphthalene moiety. *J Mol Struct* **1281**, 135100 (2023).
474. Ang, W. *et al.* Synthesis and biological evaluation of novel naphthalene compounds as potential antidepressant agents. (2014) doi:10.1016/j.ejmech.2014.05.061.
475. Rivera-Marrero, S. *et al.* A new naphthalene derivative with anti-amyloidogenic activity as potential therapeutic agent for Alzheimer's disease. (2020) doi:10.1016/j.bmc.2020.115700.
476. Umar, T. *et al.* Naphthalene-triazolopyrimidine hybrid compounds as potential multifunctional anti-Alzheimer's agents. *Bioorg Med Chem* **27**, 3156–3166 (2019).
477. Makar, S., Saha, T. & Singh, S. K. Naphthalene, a versatile platform in medicinal chemistry: Sky-high perspective. *Eur J Med Chem* **161**, 252–276 (2019).
478. Takemoto, S., Oshio, S., Shiromoto, T. & Matsuzaka, H. Dinuclear Ruthenium(II) K 2-Diamido/η 6-Naphthalene Complexes Featuring a Coordinatively Unsaturated yet Highly π-Basic (η 5-C 5 Me 5 )Ru Diamide Fragment Scheme 1. *J. Chem. Soc., Chem. Commun* **111**, 801–804 (1989).
479. Der-shin, L., Peng, Sh. M., Chern, Shing & Sheu, S. C. Structure of the 1:2 complex of cobalt(II) with 2,3-naphthosemiquinone diimine anion. *Acta Crystallographica Section C* **42**, 402–404 (1986).
480. Reinhardt, M. *et al.* Molecular and thin film properties of cobalt half-sandwich compounds for optoelectronic application. *Physical Chemistry Chemical Physics* **19**, 6768–6776 (2017).
481. Takemoto, S. *et al.* A Dinuclear Ruthenium(II) Chelating Amido Complex: Synthesis, Characterization, and Coupling Reaction with Carbon Monoxide. *Organometallics* **23**, 3587–3589 (2004).
482. Matsuzaka, H. *et al.* Synthesis and Molecular Structure of the Amido-Bridged Dinuclear Rhodium Complex [Cp*Rh{$\mu_2$-$(NH)_2C_{10}H_6$-2,3}($\mu_2$-Cl)RhCp*][$PF_6$] (Cp* = η 5-$C_5$Me5). *Molecular Crystals and Liquid Crystals Science and Technology. Section A. Molecular Crystals and Liquid Crystals* **342**, 1–6 (2000).

483. Nachtigal, C., Al-Gharabli, S., Eichele, K., Lindner, E. & Mayer, H. A. Structural Studies of an Array of Mixed Diamine Phosphine Ruthenium(II) Complexes [1]. *Organometallics* **21**, 105–112 (2002).
484. Duda, M., Oszajca, M. & Łasocha, W. New complexes of Zn(II) and Cd(II) halides with 1,8-diaminonaphthalene: Synthesis, structure, and thermal stability. *J Mol Struct* **1273**, 134263 (2023).
485. Ansari, K. I. *et al.* Manganese(III)-salens induce tumor selective apoptosis in human cells. *J Inorg Biochem* **103**, 818–826 (2009).
486. Ansari, K. I., Grant, J. D., Woldemariam, G. A., Kasiri, S. & Mandal, S. S. Iron(III)-salen complexes with less DNA cleavage activity exhibit more efficient apoptosis in MCF7 cells. *Org Biomol Chem* **7**, 926 (2009).
487. Nabei, A., Kuroda-Sowa, T., Okubo, T., Maekawa, M. & Munakata, M. The effect of molecular packing on the occurrence of spin crossover phenomena in one-dimensional Fe(II)-bis-Schiff base complexes. (2008) doi:10.1016/j.ica.2008.02.065.
488. Saha, D., Taily, I. M., Naik, S. & Banerjee, P. Electrochemical access to benzimidazolone and quinazolinone derivatives via in situ generation of isocyanates. *Chemical Communications* **57**, 631–634 (2021).
489. Grobler, I., Smith, V. J., Bhatt, P. M., Herbert, S. A. & Barbour, L. J. Tunable Anisotropic Thermal Expansion of a Porous Zinc(II) Metal–Organic Framework. *J Am Chem Soc* **135**, 6411–6414 (2013).
490. Liu, Y.-J. *et al.* Ruthenium(II) complexes containing asymmetric 2-(pyrazin-2-yl)naphthoimidazole: syntheses, characterization, DNA-binding and photocleavage studies. (2005) doi:10.1016/j.ica.2004.12.037.
491. Sogame, S. *et al.* Discovery of a benzimidazole series of ADAMTS-5 (aggrecanase-2) inhibitors by scaffold hopping. (2013) doi:10.1016/j.ejmech.2013.10.075.
492. Grella, G. E., Cabras, M. C., Murineddu, G., Pau, A. & Pinna, G. A. Synthesis and cytotoxicity of substituted 2-benzylnaphth[2,3-d]imidazoles. *European Journal of Pharmaceutical Sciences* **20**, 267–272 (2003).
493. Wang, F.-X. *et al.* Dual Functions of Cyclometalated Iridium(III) Complexes: Anti-Metastasis and Lysosome-Damaged Photodynamic Therapy. (2017) doi:10.1021/acsami.7b10258.
494. Reeves, G. T., Addison, A. W. & Zeller, M. Ruthenium(II) complexes of the tetradentate polypyridyl thioether 1,2-bis[3 ‘-(2”-pyridyl)-1 0-thiapropyl]benzene. doi:10.1016/j.poly.2020.114367.
495. Zhang, L., Peng, X.-M., Damu, G. L. V., Geng, R.-X. & Zhou, C.-H. Comprehensive Review in Current Developments of Imidazole-Based Medicinal Chemistry. *Med Res Rev* **34**, 340–437 (2014).
496. Molina, P., Tárraga, A. & Otón, F. Imidazole derivatives: A comprehensive survey of their recognition properties. *Org Biomol Chem* **10**, 1711–1724 (2012).
497. Alghamdi, S. S., Suliman, R. S., Almutairi, K., Kahtani, K. & Aljatli, D. Imidazole as a promising medicinal scaffold: Current status and future direction. *Drug Des Devel Ther* **15**, 3289–3312 (2021).
498. Debus, H. Ueber die Einwirkung des Ammoniaks auf Glyoxal. *Justus Liebigs Ann Chem* **107**, 199–208 (1858).
499. Radzisewski, Br. Ueber Glyoxalin und seine Homologe. *Berichte der deutschen chemischen Gesellschaft* **15**, 2706–2708 (1882).
500. Gelens, E. *et al.* Efficient library synthesis of imidazoles using a multicomponent reaction and microwave irradiation. *Mol Divers* **10**, 17–22 (2006).

501. Saxer, S., Marestin, C., Mercier, R. & Dupuy, J. The multicomponent Debus–Radziszewski reaction in macromolecular chemistry. *Polym Chem* **9**, 1927–1933 (2018).
502. Wojtczak, A., Jaskólski, M. & Kosturkiewicz, Z. ab,cf-Bis[4-(2-aminoethyl)imidazole-$N^3$,$N^8$]-*de*-bis(isothiocyanato)nickel(II). *Acta Crystallogr C* **41**, 1752–1755 (1985).
503. Chen, S.-S. The roles of imidazole ligands in coordination supramolecular systems. *CrystEngComm* **18**, 6543–6565 (2016).
504. *N-Heterocyclic Carbenes in Synthesis*. (Wiley, 2006). doi:10.1002/9783527609451.
505. Chen, S.-S. *et al.* Synthesis and Characterization of Metal Complexes with Mixed 4-Imidazole-Containing Tripodal Ligand and Varied Dicarboxylic Acid. *Cryst Growth Des* **12**, 2315–2326 (2012).
506. Liu, H.-K., Sun, W.-Y., Ma, D.-J., Tang, W.-X. & Yu, K.-B. The first X-ray structurally characterized M3L2 cage-like complex with tetrahedral metal centres and its encapsulation of a neutral guest molecule. *Chemical Communications* **84**, 591–592 (2000).
507. Chen, S.-S. *et al.* Temperature dependent selective gas sorption of the microporous metal-imidazolate framework [Cu(L)] [$H_2L$ = 1,4-di(1H-imidazol-4-yl)benzene]. *Chem. Commun.* **47**, 752–754 (2011).
508. Liu, H.-K. *et al.* Assembly of supermolecular complexes with tripodal ligand titmb and tib: a 2D rhombic grid network assembled from 2-connected tib. (2002) doi:10.1039/b201446g.
509. Xiao, J.-C. & Shreeve, J. M. Synthesis of 2,2‘-Biimidazolium-Based Ionic Liquids: Use as a New Reaction Medium and Ligand for Palladium-Catalyzed Suzuki Cross-Coupling Reactions. *J Org Chem* **70**, 3072–3078 (2005).
510. Feng, M., Zhao, G., Gao, H. & Zhang, S. Tetracarboxyl-Functionalized Ionic Liquid: Synthesis and Catalytic Properties. *Aust J Chem* **68**, 1513 (2015).
511. Okamura, M. *et al.* A mononuclear ruthenium complex showing multiple proton-coupled electron transfer toward multi-electron transfer reactions. *Dalton Transactions* **41**, 13081 (2012).
512. Mariappan, G. *et al.* Synthesis and biological evaluation of 2-substituted benzimidazole derivatives. (2011) doi:10.1016/j.arabjc.2011.11.008.
513. Nobbs, J. D., Tomov, A. K., Young, C. T., White, A. J. P. & Britovsek, G. J. P. From alternating to selective distributions in chromium-catalysed ethylene oligomerisation with asymmetric BIMA ligands. *Catal Sci Technol* **8**, 1314–1321 (2018).
514. Rodionov, V. O., Presolski, S. I., Gardinier, S., Lim, Y.-H. & Finn, M. G. Benzimidazole and Related Ligands for Cu-Catalyzed Azide-Alkyne Cycloaddition. (2007) doi:10.1021/ja072678l.
515. Li, S. *et al.* A 2D metal-organic framework interpenetrated by a 2D supramolecular framework assembled by CH/π interactions. *Inorg Chem Commun* **130**, 108705 (2021).
516. Chen, T. *et al.* Iodine uptake enhanced electrical conductivity by a metal-organic framework bearing nanotube array of π-stacked columns. *J Mol Struct* **1289**, 135858 (2023).
517. Thompson, L. K., Ramaswamy, B. S. & Seymour, E. A. Cobalt (II) and zinc(II) complexes of the tripod’ ligand tris(2-benzimidazylmethyl)amine. Some five-coordinate derivatives and some with mixed stereochemistries. *Canadian Journal of Chemistry* **55**, 878 (1977).
518. Gewirtz, A. M., Sokol, D. L. & Ratajczak, M. Z. Nucleic Acid Therapeutics: State of the Art and Future Prospects. *Blood* **92**, 712–736 (1998).

519. Opalinska, J. B. & Gewirtz, A. M. Nucleic-acid therapeutics: basic principles and recent applications. *Nat Rev Drug Discov* **1**, 503–514 (2002).
520. Liu, L. *et al.* Dinuclear metal(II) complexes of polybenzimidazole ligands as carriers for DNA delivery. *Biomaterials* **31**, 1380–1391 (2010).
521. Meng, X., Liu, L., Zhou, C., Wang, L. & Liu, C. Dinuclear Copper(II) Complexes of a Polybenzimidazole Ligand: Their Structures and Inductive Roles in DNA Condensation. *Inorg Chem* **47**, 6572–6574 (2008).
522. Meng, X., Liu, L., Zhang, H., Luo, Y. & Liu, C. Tris(benzimidazolyl)amine-Cu(ii) coordination units bridged by carboxylates: structures and DNA-condensing property. *Dalton Transactions* **40**, 12846 (2011).
523. Geng, Q.-X., Cong, H., Tao, Z., Lindoy, L. F. & Wei, G. Cucurbit[7]uril-improved recognition by a fluorescent sensor for cadmium and zinc cations. *Supramol Chem* **28**, 784–791 (2016).
524. Presolski, S. I., Mamidyala, S. K., Manzenrieder, F. & Finn, M. G. Resin-supported catalysts for CuAAC click reactions in aqueous or organic solvents. *ACS Comb Sci* **14**, 527–530 (2012).
525. Pascaly, M. *et al.* Structures and Properties of Novel Mononuclear Iron(III) Complexes with Benzimidazole Containing Tripodal Tetradentate Ligands doi:10.1002/(SICI)1521-3749(200001)626:1<50::AID-ZAAC50>3.0.CO;2-Y.
526. Broderick, J. B. Catechol dioxygenases. *Essays Biochem* **34**, 173–189 (1999).
527. Yang, X.-P. *et al.* Studies on lanthanide complexes of the tripodal ligand bis(2-benzimidazolylmethyl)(2-pyridylmethyl)amine. Crystal structures and luminescence properties †. *J. Chem. Soc., Dalton Trans* 3253–3260 (2000) doi:10.1039/b003566l.
528. Yang, X.-P., Kang, B.-S., Wong, W.-K., Su, C.-Y. & Liu, H.-Q. Syntheses, Crystal Structures, and Luminescent Properties of Lanthanide Complexes with Tripodal Ligands Bearing Benzimidazole and Pyridine Groups. *Inorg Chem* **42**, 169–179 (2003).
529. Wisniak, J. Auguste Laurent. Radical and radicals. *Educación Química* **20**, 166–175 (2009).
530. Kinik, F. P., Ortega-Guerrero, A., Ongari, D., Ireland, C. P. & Smit, B. Pyrene-based metal organic frameworks: from synthesis to applications. *Chem Soc Rev* **50**, 3143–3177 (2021).
531. Figueira-Duarte, T. M. & Müllen, K. Pyrene-Based Materials for Organic Electronics. *Chem Rev* **111**, 7260–7314 (2011).
532. Schulze, M., Scherer, A., Diner, C. & Tykwinski, R. R. Synthesis of 1-Bromopyrene and 1-Pyrenecarbaldehyde. in *Organic Syntheses* 100–114 (Wiley, 2017). doi:10.1002/0471264229.os093.09.
533. Ross, D. S., Hum, G. P. & Schmitt, R. J. Nitration of Pyrene by $NO_2$ and $N_2O_4$. in 155–168 (1987). doi:10.1021/ba-1988-0217.ch009.
534. Jousselin-Oba, T. *et al.* Novel Fluorophores based on Regioselective Intramolecular Friedel–Crafts Acylation of the Pyrene Ring Using Triflic Acid. *Chemistry – A European Journal* **23**, 16184–16188 (2017).
535. Ciechańska, M., Wrona-Piotrowicz, A., Makal, A. & Zakrzewski, J. Alkylation of the K-Region in a Sterically Hindered Pyrene Carboxamide via Directed Reaction with Alkyllithiums under Air. *J Org Chem* **83**, 12793–12797 (2018).
536. Dmytrejchuk, A. M., Jackson, S. N., Meudom, R., Gorden, J. D. & Merner, B. L. Regioselective Synthesis of Unsymmetric Tetra- and Pentasubstituted Pyrenes with a Strategy for Primary C-Alkylation at the 2-Position. *J Org Chem* **83**, 10660–10667 (2018).

537. Dewar, M. J. S. & Dennington, R. D. DEWAR-PI study of electrophilic substitution in selected polycyclic fluoranthene hydrocarbons. *J Am Chem Soc* **111**, 3804–3808 (1989).
538. Altschuler, L. & Berliner, E. Rates of Bromination of Polynuclear Aromatic Hydrocarbons . *J Am Chem Soc* **88**, 5837–5845 (1966).
539. Vollmann, H., Becker, H., Corell, M. & Streeck, H. Beiträge zur Kenntnis des Pyrens und seiner Derivate. *Justus Liebigs Ann Chem* **531**, 1–159 (1937).
540. Casas-Solvas, J. M., Howgego, J. D. & Davis, A. P. Synthesis of substituted pyrenes by indirect methods. *Org. Biomol. Chem.* **12**, 212–232 (2014).
541. Shahrokhi, F., Fazli Estabragh, R. & Zhao, Y. Synthesis and comparative studies of K-region functionalized pyrene derivatives. *New Journal of Chemistry* **44**, 16786–16794 (2020).
542. Qian, C.-G. & Xiao, B. 4,5-Disubstituted pyrenes from phenangermoles. *Organic Chemistry Frontiers* **10**, 640–644 (2023).
543. Valera, J. S., Calbo, J., Gómez, R., Ortí, E. & Sánchez, L. Blue-emitting pyrene-based aggregates. *Chemical Communications* **51**, 10142–10145 (2015).
544. Mardanya, S., Karmakar, S., Das, S. & Baitalik, S. Anion and cation triggered modulation of optical properties of a pyridyl-imidazole receptor rigidly linked to pyrene and construction of INHIBIT, OR and XOR molecular logic gates: A combined experimental and DFT/TD-DFT investigation. *Sens Actuators B Chem* **206**, 701–713 (2015).
545. Troian-Gautier, L. & Moucheron, C. RutheniumII Complexes bearing Fused Polycyclic Ligands: From Fundamental Aspects to Potential Applications. *Molecules* **19**, 5028–5087 (2014).
546. Chen, X. *et al.* Effects of intercalative ligands on the DNA binding, DNA topoisomerase II and DNA transcription inhibition of polypyridyl ruthenium(II) complexes. *Inorganica Chim Acta* **378**, 140–147 (2011).
547. Wolfe, A., Shimer, G. H. & Meehan, T. Polycyclic aromatic hydrocarbons physically intercalate into duplex regions of denatured DNA. *Biochemistry* **26**, 6392–6396 (1987).
548. Mardanya, S., Karmakar, S., Maity, D. & Baitalik, S. Ruthenium(II) and Osmium(II) Mixed Chelates Based on Pyrenyl–Pyridylimidazole and 2,2′-Bipyridine Ligands as Efficient DNA Intercalators and Anion Sensors. *Inorg Chem* **54**, 513–526 (2015).
549. Ebel, K., Koehler, H., Gamer, A. O. & Jäckh, R. Imidazole and Derivatives. in *Ullmann's Encyclopedia of Industrial Chemistry* 638 (Wiley, 2000). doi:10.1002/14356007.a13_661.
550. Elumalai, V. & Hansen, J. H. A Green, Scalable, One-Minute Synthesis of Benzimidazoles. *Synlett* **31**, 547–552 (2020).
551. Lee, Y.-S. *et al.* Significant facilitation of metal-free aerobic oxidative cyclization of imines with water in synthesis of benzimidazoles. *Tetrahedron* **71**, 532–538 (2015).
552. Vázquez, M. E. *et al.* 6- N,N-Dimethylamino-2,3-naphthalimide: A New Environment-Sensitive Fluorescent Probe in δ- and μ-Selective Opioid Peptides. *J Med Chem* **49**, 3653–3658 (2006).
553. Li, J., Lin, H., Huang, J. & Yin, J. Dicyano-substituted 2,3-naphthalimide: Synthesis and optoelectronic properties. *Dyes and Pigments* **170**, 107564 (2019).
554. Vázquez, M. E., Blanco, J. B. & Imperiali, B. Photophysics and Biological Applications of the Environment-Sensitive Fluorophore 6-N,N-Dimethylamino-2,3-naphthalimide. *J Am Chem Soc* **127**, 1300–1306 (2005).

555. Nandhikonda, P. & Heagy, M. D. Dual Fluorescent N-Aryl-2,3- naphthalimides: Applications in Ratiometric DNA Detection and White Organic Light-Emitting Devices. *Org Lett* **12**, 4796–4799 (2010).
556. Korycka-Machala, M. *et al.* Naphthalimides Selectively Inhibit the Activity of Bacterial, Replicative DNA Ligases and Display Bactericidal Effects against Tubercle Bacilli. *Molecules* **22**, 154 (2017).
557. Wang, X. *et al.* Naphthalimides exhibit in vitro antiproliferative and antiangiogenic activities by inhibiting both topoisomerase II (topo II) and receptor tyrosine kinases (RTKs). *Eur J Med Chem* **65**, 477–486 (2013).
558. Gopala, L., Cha, Y. & Lee, M. H. Versatile naphthalimides: Their optical and biological behavior and applications from sensing to therapeutic purposes. *Dyes and Pigments* **201**, 110195 (2022).
559. Banerjee, S., Kitchen, J. A., Gunnlaugsson, T. & Kelly, J. M. The effect of the 4-amino functionality on the photophysical and DNA binding properties of alkyl-pyridinium derived 1,8-naphthalimides. *Org Biomol Chem* **11**, 5642 (2013).
560. Duke, R. M., Veale, E. B., Pfeffer, F. M., Kruger, P. E. & Gunnlaugsson, T. Colorimetric and fluorescent anion sensors: an overview of recent developments in the use of 1,8-naphthalimide-based chemosensors. *Chem Soc Rev* **39**, 3936 (2010).
561. Panchenko, P. A., Fedorov, Y. V., Fedorova, O. A. & Jonusauskas, G. Comparative analysis of the PET and ICT sensor properties of 1,8-naphthalimides containing aza-15-crown-5 ether moiety. *Dyes and Pigments* **98**, 347–357 (2013).
562. Izawa, H. *et al.* Unique Photophysical Properties of 1,8-Naphthalimide Derivatives: Generation of Semi-stable Radical Anion Species by Photo-Induced Electron Transfer from a Carboxy Group. *ACS Omega* **6**, 13456–13465 (2021).
563. Pardo, A., Poyato, J. M. L. & Martin, E. Photophysical properties of 1,8-naphthalimide derivatives. *Journal of Photochemistry* **36**, 323–329 (1987).
564. Uesaka, T. *et al.* Synthesis and photophysical properties of photostable 1,8-naphthalimide dyes incorporating benzotriazole-based UV absorbers. *RSC Adv* **12**, 17350–17361 (2022).
565. Gudeika, D. A review of investigation on 4-substituted 1,8-naphthalimide derivatives. *Synth Met* **262**, 116328 (2020).
566. Qian, X. *et al.* "Alive" dyes as fluorescent sensors: fluorophore, mechanism, receptor and images in living cells. *Chemical Communications* **46**, 6418 (2010).
567. Mohan, B., Kunhumon, N. M. & Shanmugaraju, S. Fluorescence sensing and bioimaging of Cu(ii) ions using amino-1,8-naphthalimide-based small-molecule chemosensors. *Sensors & Diagnostics* **2**, 1158–1175 (2023).
568. Zeng, X., Chen, J., Yu, S., Liu, Z. & Ma, M. The Development of a 4-aminonaphthalimide-based Highly Selective Fluorescent Probe for Rapid Detection of HOCl. *J Fluoresc* **32**, 1843–1849 (2022).
569. Veale, E. B., Kitchen, J. A. & Gunnlaugsson, T. Fluorescent tren -based 4-amino-1,8-naphthalimide sensor for Cu(II) based on the use of the (fluorophore–spacer–receptor) photoinduced electron transfer (PET) principle. *Supramol Chem* **25**, 101–108 (2013).
570. Martínez-Calvo, M. *et al.* 4-Amino-1,8-naphthalimide based fluorescent photoinduced electron transfer (PET) pH sensors as liposomal cellular imaging agents: The effect of substituent patterns on PET directional quenching. *Front Chem Sci Eng* **14**, 61–75 (2020).
571. Fuller, A. A., Seidl, F. J., Bruno, P. A., Plescia, M. A. & Palla, K. S. Use of the environmentally sensitive fluorophore 4-*N,N*-dimethylamino-1,8-naphthalimide to study peptoid helix structures. *Peptide Science* **96**, 627–638 (2011).

572. Choulier, L. & Enander, K. Environmentally Sensitive Fluorescent Sensors Based on Synthetic Peptides. *Sensors* **10**, 3126–3144 (2010).
573. Miao, R. *et al.* A General Method to Develop Highly Environmentally Sensitive Fluorescent Probes and AIEgens. *Advanced Science* **9**, (2022).
574. Sainlos, M. & Imperiali, B. Tools for investigating peptide–protein interactions: peptide incorporation of environment-sensitive fluorophores through SPPS-based 'building block' approach. *Nat Protoc* **2**, 3210–3218 (2007).
575. Venkatraman, P. *et al.* Fluorogenic probes for monitoring peptide binding to class II MHC proteins in living cells. *Nat Chem Biol* **3**, 222–228 (2007).
576. Kapoerchan, V. V. *et al.* Design, synthesis and evaluation of high-affinity binders for the celiac disease associated HLA-$DQ_2$ molecule. *Mol Immunol* **47**, 1091–1097 (2010).
577. Baathulaa, K., Xu, Y. & Qian, X. Unusual large Stokes shift and solvatochromic fluorophore: Synthesis, spectra, and solvent effect of 6-substituted 2,3-naphthalimide. *J Photochem Photobiol A Chem* **216**, 24–34 (2010).
578. Loredo, A., Wang, L., Wang, S. & Xiao, H. Single-atom switching as a general approach to designing colorimetric and fluorogenic probes for mercury ions. *Dyes and Pigments* **186**, 109014 (2021).
579. Fleming, C. L., Ashton, T. D. & Pfeffer, F. M. Synthesis of 4-amino substituted 1,8-naphthalimide derivatives using palladium-mediated amination. *Dyes and Pigments* **109**, 135–143 (2014).
580. Gudeika, D. *et al.* Hydrazones containing electron-accepting and electron-donating moieties. *Dyes and Pigments* **91**, 13–19 (2011).
581. Wu, A., Xu, Y., Qian, X., Wang, J. & Liu, J. Novel naphthalimide derivatives as potential apoptosis-inducing agents: Design, synthesis and biological evaluation. *Eur J Med Chem* **44**, 4674–4680 (2009).
582. Grabchev, I., Moneva, I., Bojinov, V. & Guittonneau, S. Synthesis and properties of fluorescent 1,8-naphthalimide dyes for application in liquid crystal displays. *J Mater Chem* **10**, 1291–1296 (2000).
583. Kosugi, M., Kameyama, M. & Migita, T. Palladium-Catalyzed Aromatic Amination Of Aryl Bromides With N,N-Di-Ethylamino-Tributyltin. *Chem Lett* **12**, 927–928 (1983).
584. Forero-Cortés, P. A. & Haydl, A. M. The 25th Anniversary of the Buchwald–Hartwig Amination: Development, Applications, and Outlook. *Org Process Res Dev* **23**, 1478–1483 (2019).
585. Surry, D. S. & Buchwald, S. L. Dialkylbiaryl phosphines in Pd-catalyzed amination: a user's guide. *Chem. Sci.* **2**, 27–50 (2011).
586. The Basic Chemistry of Organopalladium Compounds. in *Palladium Reagents and Catalysts* 1–26 (Wiley, 2004). doi:10.1002/0470021209.ch1.
587. Rio, J. *et al.* We Already Know Everything about Oxidative Addition to Pd(0): Do We? *ACS Catal* **13**, 11399–11421 (2023).
588. Wolfe, J. P., Wagaw, S. & Buchwald, S. L. An Improved Catalyst System for Aromatic Carbon−Nitrogen Bond Formation: The Possible Involvement of Bis(Phosphine) Palladium Complexes as Key Intermediates. *J Am Chem Soc* **118**, 7215–7216 (1996).
589. Surry, D. S. & Buchwald, S. L. Biaryl Phosphane Ligands in Palladium-Catalyzed Amination. *Angewandte Chemie International Edition* **47**, 6338–6361 (2008).
590. Louie, J. & Hartwig, J. F. Palladium-catalyzed synthesis of arylamines from aryl halides. Mechanistic studies lead to coupling in the absence of tin reagents. *Tetrahedron Lett* **36**, 3609–3612 (1995).

591. Guram, A. S., Rennels, R. A. & Buchwald, S. L. A Simple Catalytic Method for the Conversion of Aryl Bromides to Arylamines. *Angewandte Chemie International Edition in English* **34**, 1348–1350 (1995).
592. Driver, M. S. & Hartwig, J. F. A Second-Generation Catalyst for Aryl Halide Amination: Mixed Secondary Amines from Aryl Halides and Primary Amines Catalyzed by (DPPF)$PdCl_2$. *J Am Chem Soc* **118**, 7217–7218 (1996).
593. Louie, J., Driver, M. S., Hamann, B. C. & Hartwig, J. F. Palladium-Catalyzed Amination of Aryl Triflates and Importance of Triflate Addition Rate. *J Org Chem* **62**, 1268–1273 (1997).
594. Guari, Y., van Es, D. S., Reek, J. N. H., Kamer, P. C. J. & van Leeuwen, P. W. N. M. An efficient, palladium-catalysed, amination of aryl bromides. *Tetrahedron Lett* **40**, 3789–3790 (1999).
595. Martinelli, J. R., Watson, D. A., Freckmann, D. M. M., Barder, T. E. & Buchwald, S. L. Palladium-Catalyzed Carbonylation Reactions of Aryl Bromides at Atmospheric Pressure: A General System Based on Xantphos. *J Org Chem* **73**, 7102–7107 (2008).
596. Yin, J. & Buchwald, S. L. Pd-Catalyzed Intermolecular Amidation of Aryl Halides: The Discovery that Xantphos Can Be Trans-Chelating in a Palladium Complex. *J Am Chem Soc* **124**, 6043–6048 (2002).
597. Sunesson, Y., Limé, E., Nilsson Lill, S. O., Meadows, R. E. & Norrby, P.-O. Role of the Base in Buchwald–Hartwig Amination. *J Org Chem* **79**, 11961–11969 (2014).
598. Boonkitpatarakul, K. *et al.* An 8-aminoquinoline derivative as a molecular platform for fluorescent sensors for Zn(II) and Cd(II) ions. *J Lumin* **198**, 59–67 (2018).
599. Muthusamy, S. *et al.* Development of a quinoline-derived turn-on fluorescent probe for real time detection of hydrazine and its applications in environment and bioimaging. *Dyes and Pigments* **206**, 110618 (2022).
600. Frederickson, C. J., Kasarskis, E. J., Ringo, D. & Frederickson, R. E. A quinoline fluorescence method for visualizing and assaying the histochemically reactive zinc (bouton zinc) in the brain. *J Neurosci Methods* **20**, 91–103 (1987).
601. Mohamad, N. S. *et al.* The Role of 8-Amidoquinoline Derivatives as Fluorescent Probes for Zinc Ion Determination. *Sensors* **21**, 311 (2021).